UNIVERSIDAD DE BURGOS

DEPARTAMENTO DE QUÍMICA

FACULTAD DE CIENCIAS

Materiales sensores fluorogénicos derivados de perilenodiimidas: Aplicaciones medioambientales y en bioimagen

TESIS DOCTORAL

Patricia Calvo Gredilla

2017

UNIVERSIDAD DE BURGOS

DEPARTAMENTO DE QUÍMICA

FACULTAD DE CIENCIAS

D. Tomás Torroba Pérez, Catedrático del Área de Química Orgánica del Departamento de Química de la Universidad de Burgos,

Certifica:

Que el trabajo de investigación aquí presentado: "**Materiales sensores fluorogénicos derivados de perilenodiimidas: Aplicaciones medioambientales y en bioimagen"** por la licenciada Dª Patricia Calvo Gredilla para aspirar al título de Doctor en Química por la Universidad de Burgos, ha sido realizado bajo su dirección y autoriza la presentación como Tesis Doctoral.

Burgos a 30 de Julio de 2017

Fdo: Tomás Torroba Pérez

Agradecimientos

Cuando comencé esta tesis no era consciente de lo que realizarla suponía, de cuanto iba a disfrutar, de lo emocionante que sería y, de hecho, considero que la línea temporal debe ser en ese orden. El conocimiento científico y personal que he adquirido en esta aventura me ha hecho ser capaz de apreciar lo importante y de crecer como químico.

En este caso, esta aventura se emprendió gracias a Tomás Torroba Pérez. Al hacer una valoración de estos años, lo más destacable es su preocupación diaria por los avances, su implicación para conseguir colaboraciones y el mejor material para trabajar. Aparte de mi director, José García Calvo, mi compañero de laboratorio, ha sido la persona con quien he hablado, discutido y aprendido no sólo de perilenos o fluorescencia sino de su perspectiva sobre la investigación. La dedicación a la investigación, las charlas de ciencia y el tiempo compartido con mis compañeros de laboratorio Daisy. C. Romero Velásquez y Víctor García Calvo nunca los olvidaré. Del trato diario en el laboratorio me llevo un muy buen recuerdo, ya que la convivencia con diferentes personas te hace convertirte en mejor ser humano. Éstas personas son las ya nombradas, las siguientes: Jorge.B, Sergio.D, Alicia.S, Sandra.E, Andrea.S, Elsa.H, Pablo.P, Pablo.P, Israel.C, Sandra.D, Marcin.M y de forma muy destacada Münü.D, Clara.A, Nerea.J, Miriam.M y Marcos.I. Además, he de dar las gracias en especial a dos personas más: Alberto Diez de la Varga por la dedicación a la espectrometría de masas de mi tesis y a Laura Asturias Arribas por sus sugerencias del inglés de ésta. No se me debe olvidar agradecer al equipo de I+D+i de la Universidad de Burgos: Jacinto.D, Pilar.C y Marta.M y al equipo de I+D+i de la Universidad de Valladolid por su tiempo, así como, a todas las personas con las que hemos colaborado a lo largo de estos años y que serán citadas en el capítulo correspondiente.

Y para finalizar, cada persona coexiste con varias facetas simultáneamente y por tanto, dar las gracias a mi familia: Ángela, Víctor, Raúl, César, Marcela y a mis colegas, que me han apoyado durante estos años, es imprescindible.

1. Abbreviations.

AcOEt: Ethyl acetate.
CBR: Chemical Biological Radiological.
$CDCl_3$: Deuterated chloroform.
$CHCl_3$: Chloroform.
CH_3HSO_3: methanesulfonic acid.
CNT: Carbon Nanotubes.
$\mathbf{C_q}$: Quaternary Carbon.
D_2O: Deuterated water.
DABCO: 1,4-Diazabicyclo[2.2.2]octane.
1,2-DCE: 1,2-dichloroethane.
DCM: Dichloromethane.
DIPEA: N,N-Diisopropylethylamine.
DMAP: 4-Dimethylaminopyridine.
DMPA: 2,2-Dimethoxy-2-phenylacetophenone.
DMF: N,N'-Dimethylformamide.
DMSO: Dimethyl sulfoxide.
DIPEA: N,N'-Diisopropylethylamine.
EDG: electron donating group.
EWG: electron withdrawing group.
EtOAc: Ethyl acetate.
ERS: Electron Spin Resonance.
EtOH: Ethanol.
FAM: 6-carboxyfluorescein.
FBS: fetal bovine serum in cell culture.
FRET: Fluorescence Resonance Energy Transfer.
HCl (37 %): Hydrochloric acid.
HNO_3 (60 %): Nitric acid.
H_2O: water
H_2O_2 (30 %): oxide peroxide.
H_2SO_4 (97 %) Sulphuric acid.
IR: Infrared.
KBr: Potassium bromide.
KOH: Potasium hydroxide.
MCPB: 3-Chloroperoxybenzoic acid.
MeCN: Acetonitrile.
MeOH: Methanol.
MeOD: Deuterated methanol.
MTS: 3-(4,5-dimethylthiazol-2-yl)-5-(3-carboxymethoxyphenyl)-2-(4-sulfophenyl)-2H-tetrazolium
MTT: 3-(4, 5-dimethylthiazolyl-2)-2, 5-diphenyltetrazolium bromide.
MWCNT: MultiWalled Carbon Nanotubes.
NaOH: Sodium hydroxide.
NBS: N-bromosuccinimide.
NIS: N-iodosuccinimide.
NMP: N-methylpyrrolidone.
NMR: Nuclear Magnetic Resonance.
NEt_3: Triethylamine.
PBS: Phosphate buffer solution.
PDA: Perylenedianhydride.
PDI: Perylenediimide.

PhCl: Chlorobenzene.
$pTsOH \cdot H_2O$: p-Toluenesulfonic acid.
PyBOP: benzotriazol-1-yl-oxytripyrrolidinophosphonium hexafluorophosphate.
Silica: silica gel.
TATP: Triperoxide Triacetone.
TBTA: Tris[(1-benzyl-1H-1,2,3-triazol-4-yl)methyl]amine.
TFA: Trifluoroacetic acid.
TAMRA: Tetramethylrhodamine.
THF: tetrahydrofurane.
UV-Vis: Ultraviolet- Visible.

2. Techniques.

^{1}H NMR: Proton Nuclear Magnetic Resonance.
^{13}C NMR: Carbon Nuclear Magnetic Resonance.
^{19}F NMR: Fluorine Nuclear Magnetic Resonance
FT-IR: Fourier Transform Infrared Spectroscopy.
HRMS.EI: High Resolution Mass Spectroscopy. Electron Ionization.
HRMS.MALDI: Matrix-Assisted Laser Desorption/Ionization.
HRMS.MALDI.DCTB: Trans-2-[3-(4-tert-Butylphenyl)-2-methyl-2-propenylidene]malononitrile.
HRMS. MALDI.DIT: Dithranol.
HRMS. MALDI-TOF: Time-of-Flight.
HMBC: Heteronuclear Multiple Bond Correlation.
HMQC: Heteronuclear Multiple-Quantum Correlation.
COSY: Correlation Spectroscopy.
NOESY: Nuclear Overhauser SpectroscopY.
DEPT: Distortionless Enhancement by Polarization Transfer.
HPLC: High-Performance Liquid Chromatography.
TLC: Thin Layer Chromathography.

INDEX

Introduction and Objectives

Chapter 1. Detection of home-made explosives with fluorescent devices based on perylenediimides

Chapter 2A. Water-soluble fluorescent perylenediimides

Chapter 2B. Targeting G-quadruplex structures with water-soluble fluorescent perylenediimides

Chapter 2C. Detection of proteins through molecular recognition mediated by perylenediimides

Chapter 3. Synthesis, characterization and cellular imaging of fluorescent carbon nanotubes

Synthesis and characterization: Chapter 1

Synthesis and characterization: Chapter 2

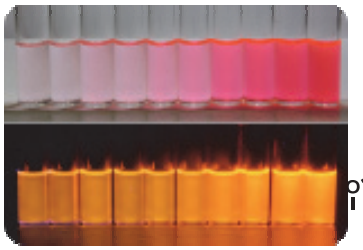

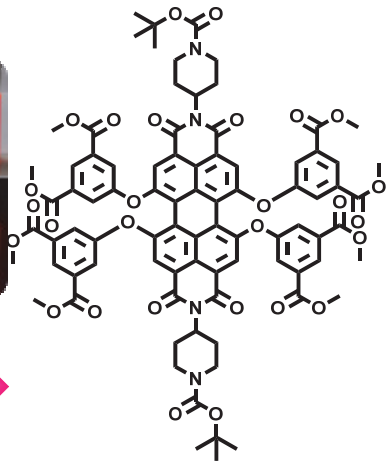

[PC51]

INTRODUCTION AND OBJECTIVES

PATRICIA CALVO GREDILLA Ph. D. THESIS

SUMMARY

A summary of concepts of luminescence and chemical probes as well as the projects in which the work is involved is presented as introduction of the Ph.D. Thesis; it will be followed by a description of the objectives of the Ph.D. Thesis.

1. INTRODUCTION.

The main purpose of the research in the group is the design and development of detection devices, capable of rapid, on-site detection of multiple kinds of agents and CBR agents (Chemical, Biological and Radiological) with high sensitivity and specificity. The work of the group will address new sensor devices that shall be used for the detection of hazardous CBR agents within many stages of normal life. The sensor devices to be developed are characterized by their portability, easiness to use and reusability. Another important feature of the new devices will be their modular design combined through generalized and standardized protocols. The aforementioned objective of the work will be directed to achieve the final goal of providing means of countermeasure to mitigate a possible incident of CBR health hazardous agents and to increase the security in normal life. Therefore, the main objectives of the work of the group are listed as follows:

- Obtainment of the specifications and requirements of new sensors for the targets selected from pathogens and toxins that could be able to detect.
- Create library of luminescent and colorimetric probes for labelled detection of target species (toxins, proteins or cells).
- Functionalization of alkyl-silanes in order to be used as monomers in the preparation of new chemical sensors.
- Synthesis of functionalized metabolites as possible probes for specific enzymatic activities.
- Development of the sensors' subsystems, both for acquisition and detection of the pathogens.

The research work corresponding to this purpose was divided into tasks, each specific for each of the development phases of the projected sensors.

1 - Design and synthesis of fluorescent labels and functionalization of alkyl-silanes: This task addresses the design and synthesis of a reasonable numbers of fluorescent and colorimetric probes with easiness of bonding to a given target species or to metabolites for selective detection and functionalization of the synthesized fluorescent probes to be used in the preparation of supported sensors. Thus, the fluorescent probes and their silica-supported derivatizations will be tailored for the development of the sensors in order to reach the maximum selectivity and sensitivity for the selected targets. The main objectives to obtain from the sensors specifications are:

- High Specificity – the fluorescent probes must be able to assure a minimum number of false positives as possible for every enzyme or metabolite targeted.
- High Sensitivity – the fluorescent probes must therefore be able to detect the selected substances under the appropriate experimental conditions.

The aim of this part of the work is the preparation of activatable imaging agents targeted through different mechanisms to identify the analytes required at every stage of the development of the work. Their detection is based on a change in optical properties brought about by the target on specific probes. The advantage of activatable probes is that probe signal to noise ratio is not limited by targeting efficiency. Measuring an increase in probe emission intensity will be the common measurement parameter, and also change in emission or excitation ratio by using optical agents composed of a Förster resonance energy transfer (FRET) pair. These detection agents will allow previously unperformed visualizations of diverse biomolecules and metabolites and will be designed to be robust in an *in-vivo* environment.

2 - Sensor development: The development of the sensors to be utilized in the sensor devices will be designed to obtain sensors with:

- High Specificity – the sensor must be able to assure a minimum number of false positives as possible, since that any false detection of an analyte may ramify into a series of unnecessary containment events, which must be avoided to not increase the cost of the food supply chain security.
- High Sensitivity – the sensor must therefore present a high aptitude to detect the selected substances within a selected environment.
- Low cost per operation.
- Cheap maintenance capabilities.

3 - Laboratory Testing: This work will address the performance of the response produced by the novel sensor against the selected target. The outcome of this task will be the preliminary laboratory testing of the sensors and the performance results with respect to validation criteria. At the development stage, sensor performance will be assessed for the following criteria:

- accuracy
- precision
- linearity
- specificity
- sensitivity
- operating range (lower and upper limit of detection)
- matrices effects
- robustness

The outcome of this work will be used to validate the functional requirements of the sensor and will provide preliminary results towards analytical validation.

In this way, the Ph.D. Thesis will contribute to the development of novel fluorescent and colorimetric probes that can be used in the labelled detection of toxins and CBR agents, in connection to the main purpose of the research work. The study will be performed by the synthesis of small-molecule “switchable” fluorescent probes, which will induce changes in the fluorescence properties (intensity and/or wavelength) only at the intended target to allow sensitive and specific detection with high target-to-background ratios. The probes for proteins will be fluorogenic substrates that will allow the monitoring of specific toxins by either turn-on fluorescence or fluorescence resonance energy transfer (FRET) in which the fluorescence switching of this type of probe will be based on the modification of the environment of the molecule by the target toxin. Switchable probes for protein targets and selected metabolites will involve the incorporation of solvatochromic fluorophores to ligands specific to the target protein or metabolite and the chemical bonding to surfaces for their reusability. These processes will be refined to increase the reliability and redundancy of sensor readings.

4 - Fluorescence and colorimetric based sensors: Fluorescence and colorimetric probes are widely used as sensitive elements in the determination of molecules, enzymes or bacteria. They can be used alone or as array. However, none of these methods already mentioned are 100 % effective, and more important: difficulties with references are not totally overcome yet. The early detection of many human threats is crucial if they are to be prevented successfully, thus, the development of imaging techniques that can facilitate early detection of chemical threats is of high importance. Changes in the levels of protein expression are known to occur in many diseases, making their accurate detection at low concentrations an area of considerable active research. Fluorescent probes that can be activated show immense promise in this area. If properly designed they should exhibit no signal until they interact with their target analyte, reducing the level of background fluorescence and potentially endowing them with greater sensitivity. The mechanisms of fluorescence changes in activating probes vary, depending on their mechanisms of action and the *in-vitro* or *in-vivo* settings in which they have been employed. Current optical imaging probe applications are hampered by poor sensitivity and specificity to the target, but molecular-level fluorescent signal activation strategies can efficiently overcome these limitations.

2. CONCEPT OF LUMINESCENCE.

Luminescence is the emission of light by a substance after electromagnetic excitation. It is divided in two categories, fluorescence and phosphorescence, depending on the nature of the excited state explained in the Jablonski diagram. When a quantum of light (a single photon) goes through a solution, it can be absorbed (Figure 1) generating a higher excited state that relaxes quickly to the lower vibrational excited state and thereby loses energy. When the electron returns to the ground state, the remaining energy is dissipated by the emission of a photon with longer wavelength, fluorescence emission (Figure 1). If an intersystem crossing is produced in the excited state and therefore, spins of electrons in the singlet state are exchanged by the triple state, phosphoresce emission will be generated instead of fluorescence emission (Figure 1).[1]

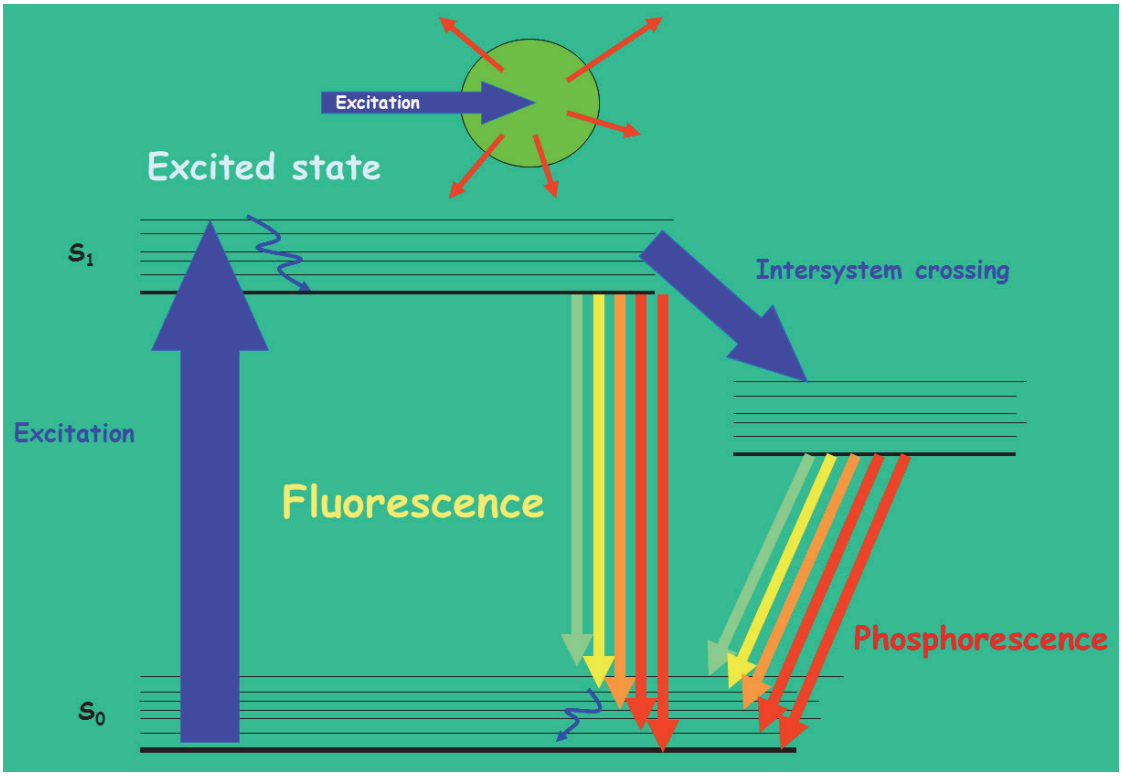

Figure 1. The Jablonski energy diagram.

To sum up, the fluorescence is a phenomenon in which a susceptible substance absorbs light to reemit light (photons) from excited electronically states after a given time. This phenomenon displays a number of general rules.[2] In the Stokes shift, the fluorescence typically occurs at lower energies or longer wavelengths. On the contrary, in phenomena that involve two photons (called anti-Stokes) the fluorescence occurs at shorter wavelengths.

- Emission spectra are typically independent of the excitation spectra, because the relaxation occurs in about 10^{-12} s.
- Emission spectra is normally a specular image of absorption spectra, this rule is namely mirror-image. Exceptions to this rule are related to variations of chemical environment, complex formation or occurrence of a reaction.

[1] H. C. Ishikawa, R. Ankerhold, G. P. C. Drummen, *Molecules*, **2012**, *17*, 4047-4132.
[2] J. R. Lakowicz, *Principles of Fluorescence Spectroscopy*, 3ª Edition Springer, San Diego, **2006**.

Fluorescence is affected by polarity and viscosity of the solvent, pH, pressure, temperature, presence of quenchers and/or ions in solution and the formation of hydrogen bonds. This solvent-dependence is known as solvathocromic effect. It consists in the change of the frequency and intensity of absorption-luminescence bands in UV-Vis, IR, NMR or ERS spectroscopies due to a variety of dynamic processes that occur after light absorption.

In accordance with the Jablonski diagram (Figure 2a), when the electron is in the excited state (S1) the polar solvent molecules stabilize this state (normally with larger dipole moment). Consequently, as the solvent polarity is increased this effect becomes larger, resulting in emission at lower energies (bathochromic shift). In general, only fluorophores that are themselves polar display a large sensitivity to solvent polarity. Absorption spectra are less sensitive than emission spectra because of time for absorption is much less than for emission and the environment around ground and excited states is different. In some cases, solvent polarity can have a dramatic effect on emission spectra, as it is shown in Figure 2b.

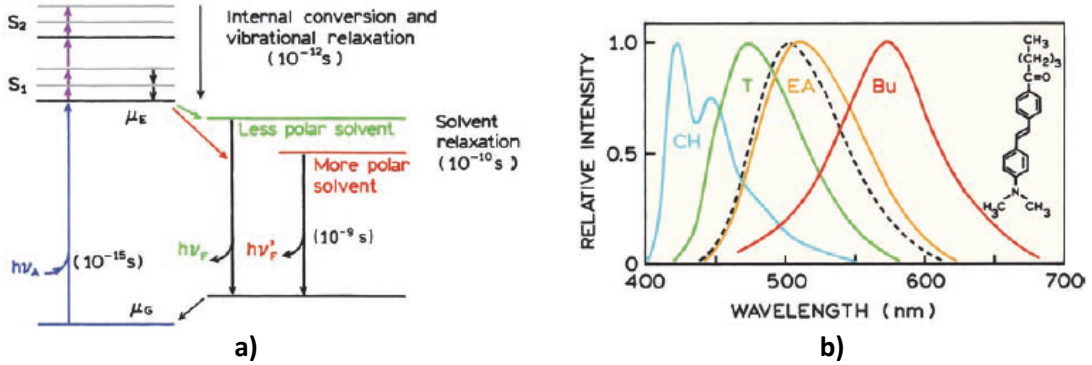

Figure 2. a) Jablonski diagram for fluorescence with solvent relaxation. b) Example of strong emission dependence with solvent polarity (CH: cyclohexane, T:toluene, EA: ethyl acetate, Bu: butanol).

Moreover, each fluorophore is characterized by two important characteristics: quantum yields and fluorescence lifetimes.

- The **quantum Yield (Φ)** is the number of emitted photons relative to the number of absorbed photons. Its value varies between 0 and 1; 1 means that each photon absorbed is emitted and 0 no emission. This property serves to classify the luminescence intensity of each fluorophore. Herein, the quantum yield is determined by comparison with a reference, employing the general equation:

$$\Phi = \Phi_R \frac{n^2}{n_R^2} \frac{A_R}{A} \frac{F}{F_R}$$

Where

- Φ is the quantum yield.
- *n* represents the refractive index of the solvent.
- *A* is the absorbance.
- *F* is the fluorescence intensity.
- *R* means that the parameter is associated to a reference sample.

- The **fluorescence lifetime (τ_i)** determines the time available for the fluorophore to interact with or diffuse in its environment. The theoretical fluorescence decay is modelled as a sum of exponentials:

$$F(t) = \sum_i A_i e^{-\frac{t}{\tau_i}}$$

where A_i is the weighted amplitude (fractional value between 0 and 1) and τ_i is the lifetime of the *i*-th fluorescent component. Instrument Response Function (IRF) is recorded from a reference scattering sample that does not fluoresce (in this case LUDOX dispersion). Both *F(t)* and IRF are recorded at a sampling rate adapted to the repetition rate of the pulsed source in order to avoid non-linear effects in the acquisition. The convolution of *F(t)* is fitted to the experimental decay curve, *I(t)*, by iterative change of the amplitude and lifetime parameters, using the least-squares method to optimize the fitting parameters. The quality of the fit is determined by ensuring that the *χ2* statistical parameter is between 0 and 1 and there are no deviations or tendencies in the residues.

3. FLUOROGENIC SENSORS.

Fluorogenic sensors have a high economic and social impact in the everyday life. Overall, a sensor is a device that converts a chemical-physical phenomenon into a measurable response, commonly electric signal. The parameters that define a sensor include intensity, decay time, anisotropy, quenching efficiency and luminescence energy transfer. Their design implies the specific recognition of particular chemical species from a reversible manner and in trace amounts. The reversibility is an essential requisite for the *in-vivo* or continuous monitoring of analytes but for individual measurements it is not necessary. Besides, within the most recent period, the detection of an isolated analyte has been overcome by new systems that are able to detect diverse classes or mixtures of compounds in a similar manner that nature has used in the development of human senses of smell and taste. Although the sensor design is a complex process, it is counteracted by the advantages of luminescent signalling systems.

The luminescent measurements present several advantages with respect to other detection methods. They are normally very sensitive (usually achieving submicromolar detection limits),[3] cheap, easily performed, very versatile, high specificity and offer the possibility of real-time monitoring due to their fast response times.[4] These entire make that the fluorescence is one of the most frequently exploited phenomenon for chemical sensors and biosensors. Particularly, fluorescence chemosensors are convenient to image physiologically important ions or small-molecules by in situ methods. To date, an enormous amount of work has been developed for the rational design of fluorescent chemosensors for ions and neutral analytes.[5] Several analytical methods are available for obtaining information about transmission in living cells, including absorption spectrometry, fluorescence spectrometry, electrochemical methods, chemical luminescence and isotope-based methods.

These luminescent devices are composed of two subunits: a receptor and a signalling unit. The binding site possess geometrical and bonding features for specific interaction (hydrogen bonds, coordinative, electrostatic or π interactions) with chemical species, in this way, that change is transformed by the signalling unit into a fluorescent signal (Figure 3).[6] Consequently, luminescent chemical sensors play a relevant role in key sectors such as industrial detection, therapeutic or medical diagnosis in medicine and environmental impact assessments in several types of contaminants monitoring.[7]

---

[3] O. S. Wolfbeis, *Fluorescence methods and applications; Spectroscopy, Imaging and Probes*, Wiley-Blackwell, New York Academy of Sciences, New York, USA, **2008**.

[4] Y. Suzuki, K. Yokoyama, *Biosensors* **2015**, *5*, 337-363.

[5] H. Jia, M. Yang, Q. Meng, G. He, Y. Wang, Z. Hu, R. Zhang, Z. Zhang, *Sensors*, **2016**, *16*, 79.

[6] L. Fabbrizzi, A. Poggi, *Chem. Soc. Rev.*, **1995**, 197-202.

[7] a) A. P. Demchenko, *Introduction to Fluorescence Sensing*, Springer Science + Business Media B.V., Berlin, **2009**; b) P. Hänninen, H. Härma, *Lanthanide Luminescence, Photophysical, Analytical and Biological Aspects*, *Springer Series on Fluorescence*, Springer-Verlag, Berlin, Heidelberg, **2011**.

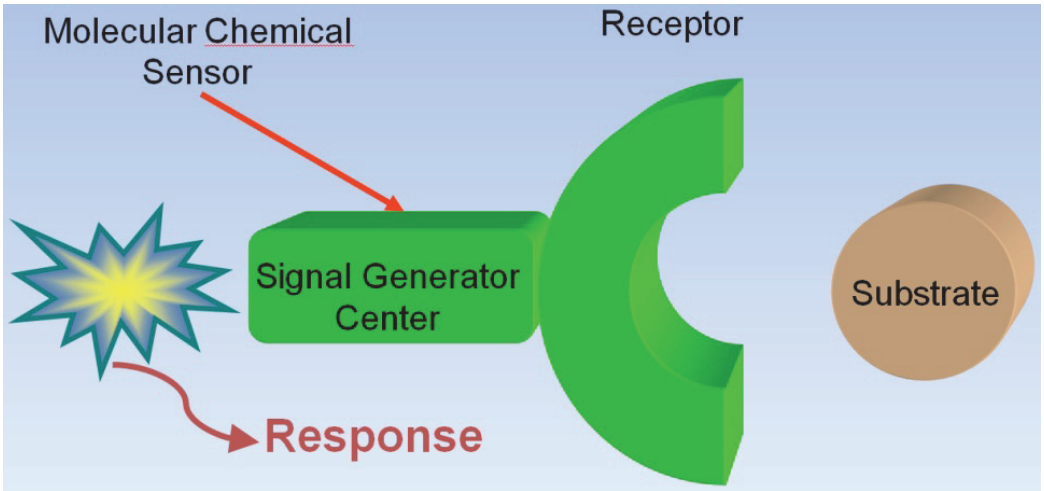

Figure 3. The design of the construction of a fluorescent sensor.

Being the molecular nanotechnology the most advanced frontier of research in many scientific branches, it is not surprising that this was the frame of evolution and development of molecular sensors. Since nanotechnology is yet a young science and it still presents safety problems in the production and use, it is increasingly necessary to perform new research to separate the real from the suspected risk. This is particularly important for nanoparticles due to not only own the highest number of industrial applications but also because dimensions and width are controllable as well as the surface derivatization. This is why combining nanotechnology and luminescent signalling may give rise to unique materials and large improvements in the chemical sensors prospect.[8]

With the war against terrorism,[9] the necessity of precise and reliable chemical and biological sensors, working in real time, has vastly increased.[10] The chemical detection permits the study and control of processes from the laboratory to the industrial scale and plays an important role in the food industry for the control of quality and safety of food. There are many types of organic molecules of high importance for which there are no chemical sensors for their detection, so to expand the field of analytes that can be detected and quantified is a very important issue. In the case of biomolecules, nature give a high number of specific interactions that can be used for the generation of biosensors, notwithstanding there is a high number of molecules that are not easily detectable, therefore the design of new specific fluorogenic probes is required.

The photoluminescent mechanisms that participate in the detection of analytes can be studied from different types of fluorogenic probes. The intrinsic fluorogenic probes where the transduction signalling mechanism is based on the perturbation of the photoinduced charge transfer from the donor to the acceptor group, being both a part of the π-conjugated system of the fluorophore. Instead, many other are based on extrinsic fluorogenic probes, in which the receptor moiety and the fluorophore are covalently bonded but electronically independent. In this case, it is possible to synthesize different receptors that are further connected to the fluorophore to construct the signalling probe. Usually receptor and signalling unit are spatially close so the interaction of the analyte with the receptor induces a change in the environment of the fluorophore, therefore inducing a luminescence change (Figure 4).

[8] A. P. Demchenko, Ed., *Advanced Fluorescence Reporters in Chemistry and Biology I-III,* Springer Series on Fluorescence 8-10, (Series Ed. O. S. Wolfbeis), Springer-Verlag, Berlin, Heidelberg, **2010**-**2011.**
[9] S. Mikhalovsky, A. Khajibaev, Eds., *Biodefence: Advanced Materials and Methods for Health Protection, NATO Science for Peace and Security Series*, Springer, Dordrecht, The Netherlands, **2011**.
[10] L. M. Eubanks, T. J. Dickerson, K. D. Janda, *Chem. Soc. Rev.* **2007**, *36*, 458–470.

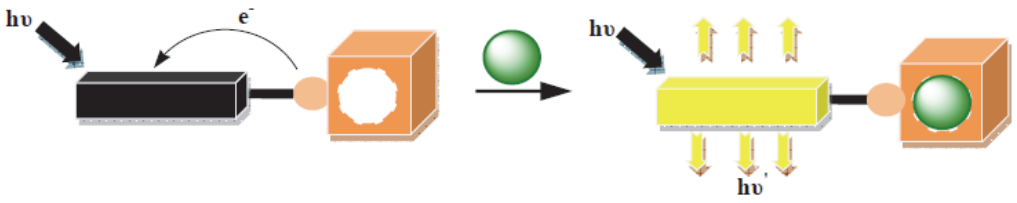

Figure 4. Extrinsic fluorogenic probes.

Sometimes the fluorogenic probe contains two fluorophore groups and the distance between them is affected by the complexation of an analyte. In that case, the recognition of the analyte is based on the difference of luminescence between the monomer and the excimer (Figure 5).

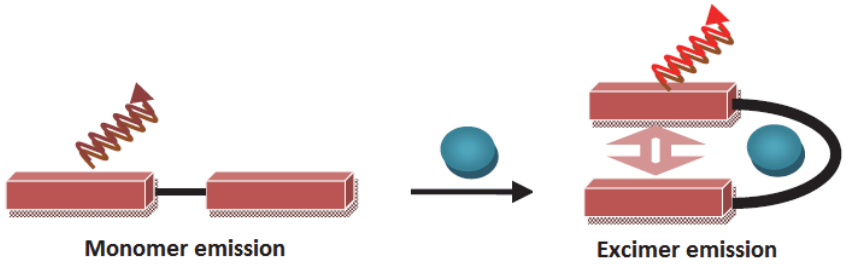

Figure 5. Chemosensor based on excimer emission.

There are strategies where the analyte displaces a fluorophore from an ensemble fluorophore-receptor, or alternatively bonds to the fluorogenic reagent hence triggering a luminescence response as in the chemical dosimeters (Figure 6).

Figure 6. A chemical dosimeter.

After the production of a fluorogenic indicator, it is normally incorporated to a solid support for the preparation of an indicator material such as silica nanoparticles,[11] polymers, among them supports.[12] Whereas if the analyte under study is an ion, the probes will be used in solution. Some examples related to these ideas have already been developed by our group, as indicated below.

[11] H. Mader, X. Li, S. Saleh, M. Link, P. Kele, O. S. Wolfbeis, *Ann. N. Y. Acad. Sci.* **2008**, *1130*, 218–223.
[12] R. B. Thompson, Ed., *Fluorescence Sensors and Biosensors,* CRC Press, Taylor & Francis Group, Boca Raton, Florida, USA, **2006**.

4. BIBLIOGRAPHICAL PRECEDENTS OF THE RESEARCH GROUP.

A modified indene chromogenic sensor with an electron donor moiety that was subsequently silylated to be supported on silica-gel was developed by our research group in 2005. This ensemble was able to detect and discriminate amines in aqueous solution according to the length of the alkyl chain joined to the amine (Figure 7).[13]

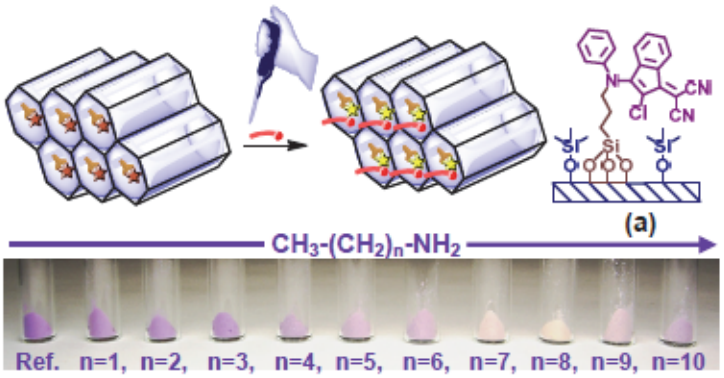

Figure 7. Colour change of chemical probe (a) in the presence of primary aliphatic amines, from left to right: no amine to *n*-dodecylamine.

Four years later, a similar idea of a sensor in solution was improved not only as chromogenic probe but also as a turn-on fluorogenic probe for copper(II) detection in water-acetonitrile 1:1 solution.[14] The quinolone-indene derivative suffers a hypochromic shift in the presence of Cu^{2+} cations (Figure 8).

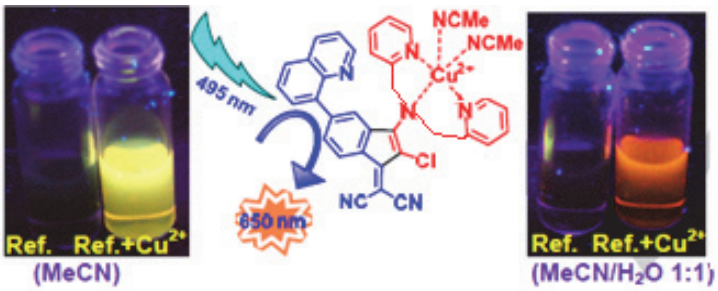

Figure 8. A quinoline-indene selective off-on fluorogenic probe for Cu^{2+}.

From that moment, the adopted line was the development of fluorogenic probes. The Figure 9 shows a bis-diarylurea receptor tagged with two units of an aminoindene (solvatochromic fluorescent indicator) suitable for the selective fluorescent discrimination of *ω*-aminoacids. The probe behaves as a molecular ruler due to the changing from yellow emission to blue, as a function of the distance between the terminal ammonium and the carboxylate group into the *ω*-aminoacids.[15]

[13] S. Basurto, T. Torroba, M. Comes, R. Martínez-Máñez, F. Sancenón, L. Villaescusa, P. Amorós, *Org. Lett.*, **2005**, *7*, 5469-5472.
[14] E. Ballesteros, D. Moreno, T. Gómez, T. Rodríguez, J. Rojo, M. García-Valverde, T. Torroba, *Org. Lett.*, **2009**, *11*, 1269-1272.
[15] D. Moreno, J. V. Cuevas, G. García-Herbosa, T. Torroba, *Chem. Commun.*, **2011**, *47*, 3183-3185.

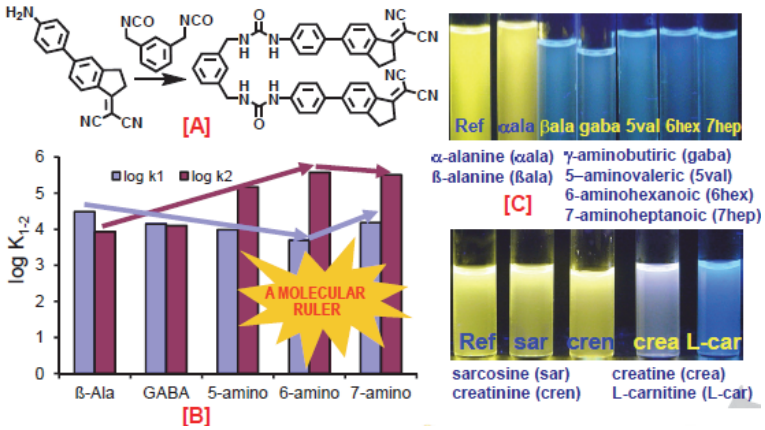

Figure 9. [A]: Synthesis of the fluorescent probe. [B]: Plot of log K_{1-2} for 2:1 complexes of *ω*-aminoacids and the fluorescent probe. [C]: Effect of the addition of an amount of aminoacids or their metabolites in water to solutions of probe in DMSO: *ω*-aminoacids under a UV light, 366 nm.

Along the same synthetic line as before, a turn-on fluorogenic probe for the detection of cyanide anion from natural sources was developed. The detection is selective toward the cyanide anion (Figure 10) in an organic and biological compatible solvent, with a good limit of detection around micromolar concentrations.[16]

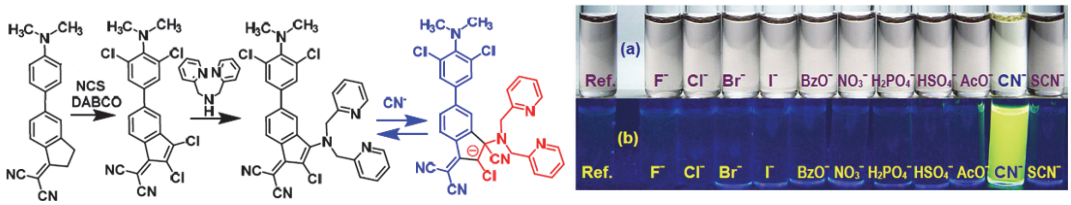

Figure 10. Colour and fluorescent changes by the addition of several anions to solutions of probe under (a) white light and (b) UV light, 366 nm.

Afterwards, dicyanomethylene derivatives were synthesized to interact in different ways with Hg^{2+} and $MeHg^{+}$. From the comparison of the results provided by the two probes (Figure 11), the concentration of each analyte was obtained and this was useful for chemical speciation of Hg(II) in live cells.[17]

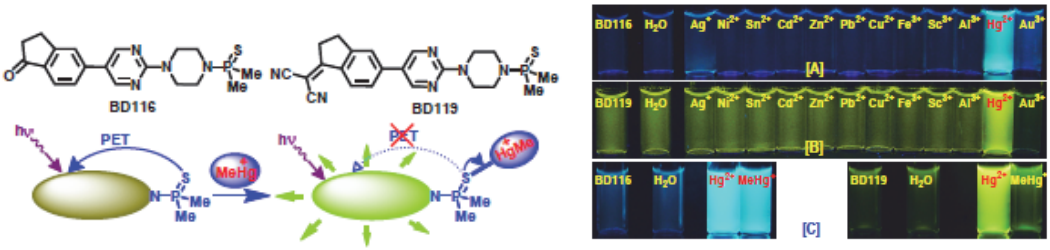

Figure 11. Two fluorogenic probes (BD116-A or BD119-B) under 366 nm UV light and a scheme of their way of action. A, B, and C show the sensitivity of each probe to Hg^{2+} and $MeHg^{+}$.

[16] T. Gómez, D. Moreno, B. D. de Greñu, A. C. Fernández, T. Rodríguez, J. Rojo, J. V. Cuevas, T. Torroba, *Chem. Asian J.*, **2012**, *8*, 1271-1278.

[17] B. D. de Greñu, J. García-Calvo, J. Cuevas, G. García-Herbosa, B. García, N. Busto, S. Ibeas, T. Torroba, B. Torroba, A. Herrera, S. Pons, *Chem. Sci.*, **2015**, *6*, 3757-3764.

In 2014, our group prepared a family of fluorogenic indene derivatives that were able to discriminate among nerve agents sarin, soman, tabun, VX and their mimics, in water or organic solvents (Figure 12). By qualitative fluorescence patterns and quantitative multivariate analysis, a complete differentiation between Chemical Warfare Agents (CWA) and their mimics was obtained, suitable for the accurate in-the-field detection of nerve agents.[18]

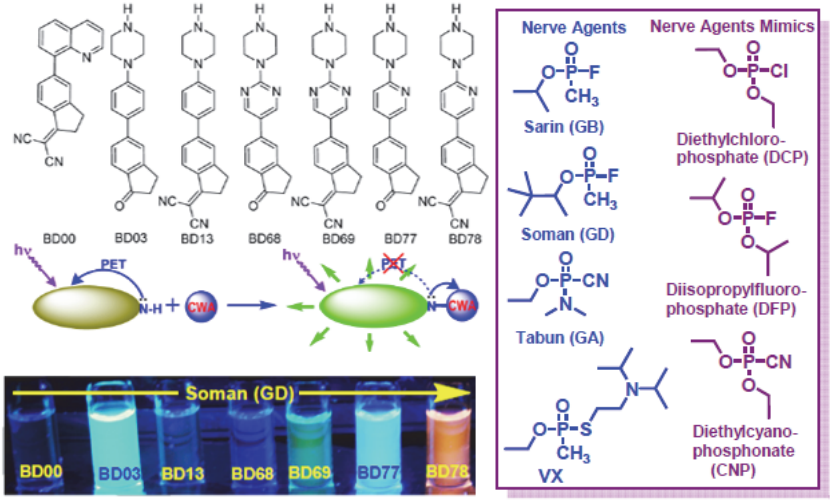

Figure 12. Fluorescent indicators for nerve agents and their mode of action. Inset box: structures of nerve agents and their mimics. Photograph: Samples containing Soman in MeCN mixed with each of the seven probes in DMSO.

5. PROJECTS IN WHICH THE GROUP IS INVOLVED.

Although some problems of biosecurity or biodetection have already been solved, a large majority of cases remains unresolved. Therefore, the efforts of our research group were oriented to the preparation of fluorogenic probes for the detection of contaminants of high environmental impact that currently have no easy solutions, such as CBR agents or explosives. Regarding to biosecurity, our group was included in an international project called SNIFFER FP7-SEC-2012-312411 (sensory devices network for food supply chain security), funded under the seventh framework programme. At the same time, we were also involved in a bioimaging national project called FLUOTOXIN BU051U16 (“Desarrollo de materiales fluorogénicos nanoestructurados para la detección de toxinas agroalimentarias de origen bacteriano y estudio de su acción celular”), provided by Junta de Castilla y León. Our latest proyect was ("Desarrollo de nuevos dispositivos moleculares fluorogénicos para la deteccion rápida de agentes de origen químico o biológico de alto riesgo"), FLUOROMOL, supported by the Ministerio de Economía y competitividad (Spain). In the text below, SNIFFER project will be explained and, briefly, FLUOTOXIN and FLUOROMOL.

5.1. SNIFFER project.

The SNIFFER project was intended for the detection of chemical threats (which may result from accidental, intentioned or natural release of CBR agents) in one or more stages of the food supply chain, which could cause damaging or even death to humans and animals as well as great economic losses. Natural releases of pathogens have provoked many incidents, some of them extremely serious. For these reasons, high reliability, portability and ease to operate devices are intended to design to act in the appropriate stages of the chain decreasing the risk.

[18] B. D. de Greñu, D. Moreno, T. Torroba, A. Berg, J. Gunnars, T. Nilsson, R. Nyman, M. Persson, J. Pettersson, I. Eklind, P. Wästerby, *J. Am. Chem. Soc.*, **2014**, *136*, 4125-4128.

Current portable detection devices present serious drawbacks such as, low sensitivity and specificity, insufficient detection capacity and time-consuming analysis; moreover, the fixed apparatus need large sample preparation. In order to overcome these weaknesses, SNIFFER project proposed a combination between the available detection devices for CBR and novel technology in a network environment. The envisioned network can potentially cover the entire food supply chain in which various detection devices that will be spread through the more vulnerable points (such as cow grazing, milk farm, cheese factory, transport hubs, etc). The detection devices will be devoted to the detection of CBR agents within the food supply chain, transmitting the information to a command and control centre, from where an operator may remotely or wirelessly control the detection devices and receive all their information pertaining to their analysis, through an intuitive user interface (Figure 13).

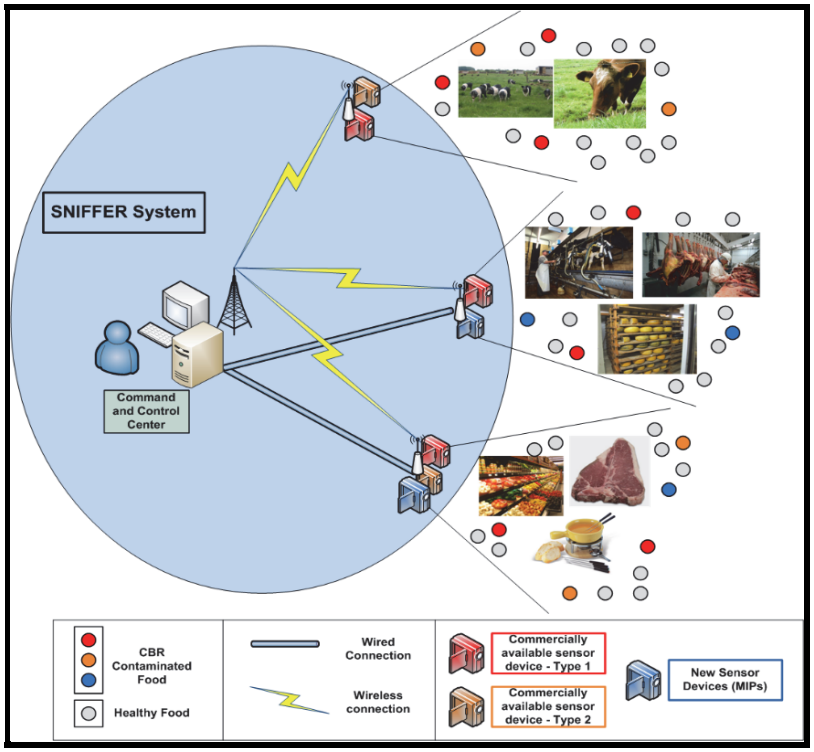

Figure 13. Representative scheme of the SNIFFER system.

5.2. FLUOTOXIN project.

The focus of this project is on basic and translational research in the field of chemical and biological defence by a multi-disciplinary approach with the aim to develop new fluorogenic molecular devices for the fast detection of chemical agents and bioterrorism/contamination-related toxins from pathogens that seriously affect humans or animals.

5.3. FLUOROMOL project.

The purpose of this project is divided in two topics. The first one is related to the design and synthesis of fluorogenic probes for the detection of home-made explosives. The second one tries to employ several synthetic materials for the study of *in-vivo* cells, specifically in bioimagen.

6. ELECTION OF PERYLENEDIIMIDES AS FLUOROGENIC PROBES.

As it was previously explained, at the University of Burgos we have synthesized several fluorescent probes for analytical applications. These probes are well suited for the fast detection of several toxic metabolites. We have developed new receptors tagged with one or two units of a few highly solvatochromic fluorescent indicators. In this way, the selective fluorescent discrimination of highly toxic analytes can be performed by comparative results from arrays of different fluorescent probes. In many cases, the rate of generation, intensity and duration of the fluorescence was different in every case by the naked eye, an effect that we have deeply studied in order to discriminate diverse toxic analytes. Because of the easy functionalization of the fluorescent probes, it is possible to make a solid array containing a range of fluorescent tags bonded to selective receptors for the selected metabolite, thus permitting its fast detection. In these fluorescent sensors, the indenes on the periphery will act as solvatochromic indicators. Selective excitation of the fluorophore permits the report of the fluorescence of the ensemble in the presence of an interfering metabolite. Further functionalization of the periphery of the silica support may adapt the chemical environment to the best reception of the selected metabolite to be detected. The system is flexible enough to be adapted to very specialized environments. Following this chemistry, the group was asked to participate in the SNIFFER project to provide for the requisite fluorescent probes that combined to molecularly imprinted polymers should give rise to the desired new dual-nature sensors. Soon we realized that albeit our fluorescent probes were extremely selective and powerful they did not accomplish the requisite stability against prolonged exposition to light and air that was necessary for the purposes of the project. So we moved to a new class of fluorescent materials that provided for the requisite chemical stability and at the same time were easily functionalized according to the required objectives. Perylenediimides (PDIs) have received significant attention due to their potential applications in molecular optoelectronic devices[19] and building blocks to construct supramolecular or artificial photosynthetic systems,[20] but have been scarcely used in the search of chemical sensors.[21] The perylene-3,4,9,10-tetracarboxylic diimide (commonly known as perylenediimides and abbreviated in this thesis as PDIs) exhibit outstanding chemical, thermal and photochemical stability. Moreover, they exhibit a high absorption coefficient and are electron-accepting materials.[22,23] These coloured compounds are highly fluorescent and tend to form aggregates in solution. The colour and the luminescence are related to the concentration and the temperature.[24] The carbon atoms likely to be modified in the chemical structure of PDI are peri or imide, ortho and bay positions (Figure 14). Therefore, PDIs are highly promising materials for applications in organic solar cells, photovoltaic devices, and for laser dyes.[25]

[19] P. Samori, A. Fechtenkötter, E. Reuther, M. D. Watson, N. Severin, K. Müllen, J. P. Rabe, *Adv. Mater.,* **2006**, *18*, 1317–1321.

[20] E. J. Alexy, J. M. Yuen, V. Chandrashaker, J. R. Diers, C. Kirmaier, D. F. Bocian, D. Holten, J. S. Lindsey, *Chem. Commun.,* **2014**, *50*, 14512-14515.

[21] X. Lu, Z. Guo, M. Feng, W. Zhu, *ACS Appl. Mater. Interfaces,* **2012**, *4*, 3657−3662.

[22] E. Kozma, M. Catellani, *Dyes Pigm.*, **2013**, *98*, 160-179.

[23] Y. Nagao, T. Naito, Y. Abe, T. Misono, *Dyes Pigm.*, **1996**, *32*, 71-83.

[24] S. Suzuki, M. Kozaki, K. Nozaki, K. Okada, *J. Photochem. Photobiol. C*, **2011**, *12*, 269-292.

[25] S. Asir, *The Synthesis of Chiral Perylene and Naphthalene Diimides***,** Ph.D. Thesis, Eastern Mediterranean University, Turskish, **2009**.

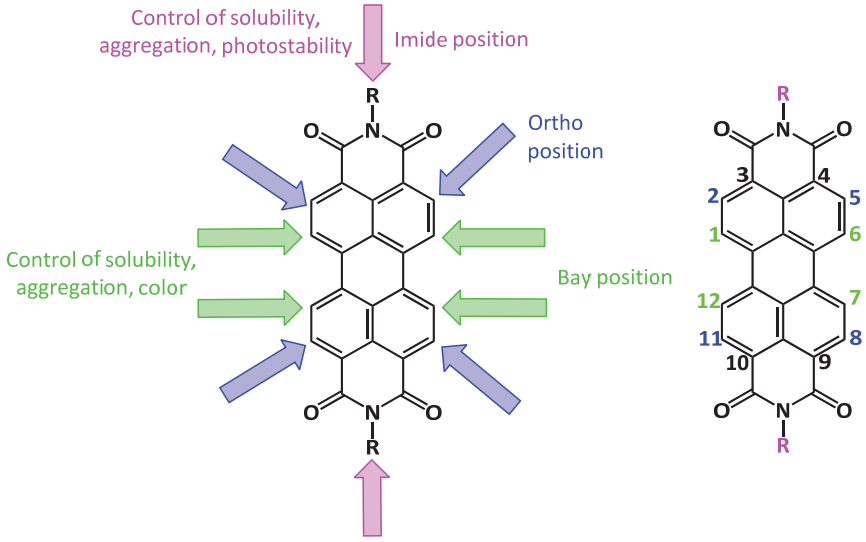

Figure 14. Left. Functional sites of perylenediimides. Right. A generic PDI showing the numbering of the positions in the ring system.

The perylenediimide synthesis in solution is limited by their strong predisposition to aggregate via π-π interaction among them. In the same way, the parent compound, perylene tetracarboxylic dianhydride (shortly named PDA) present a total insolubility in organic solvents.[26] However, for the preparation of soluble perylenediimides, there are three different proved strategies to solubilize them:

Langhals *et al.*,[28] who added steric bulk groups at the imide position decreases intermolecular aggregation of the perylene planar core by decreasing propensity of π-π stacking, was the first one in developing this strategy. The optical or electronic properties are unchanged with the modification of the imide substituents but the bulky groups in these positions can be used to affect aggregation, solubility, etc.[27] The condensation reaction could be performed symmetrically and unsymmetrically with respect to the substitution in the imide positions.

The symmetrical reaction of PDA with reactive primary aliphatic amines can be carried out without any problems, for example in DMF or another aprotic solvent. For less reactive aliphatic or aromatic amines the solvents quinoline or molten imidazole are useful. Zinc salts like zinc acetate or zinc chloride are essential catalyst for the reaction. The role of the zinc salts is not clear - they are denoted as dehydrating reagents or might help solubilizing by complexation of the anhydride.[28]

There are two main ways to prepare unsymmetrical PDIs: the recipe of Nagao[29] and Misono in 1981 that PDI was treated with sulfuric acid to reach perylene monoimide monoanhydride (valid just for aliphatic amines because the aromatic amines could be sulphonated) and the recipe of Tröster[30] in 1983 that proposed to start with PDA.

[26] N. V. Handa, L. D. Shirtcliff, B. K. Lavine, D. R. Powell, D. K. Berlin, *Phosphorus, Sulfur Silicon Relat. Elem.*, **2014**, *189*, 738-752.
[27] C. Huang, S. Barlow, S. R. Marder, *J. Org. Chem.*, **2011**, *76*, 2386-2407.
[28] H. Langhals, *Heterocycles,* **1995**, *40*, 477–500.
[29] N. Yukinori, M. Takahisa, *Bulletin of the Chemical Society of Japan* **1981**, *54*, 1269-1270.
[30] H. Langhals, *Helv. Chim. Acta*, **2005**, *88*, 1309-1343.

Seybold *et al.* at BASF[31] first mastered the second synthetically more elaborate strategy. This approach consists on introducing a π-donor and acceptor group at the bay-positions (1, 6, 7, and 12 positions of the perylene core) which enabled them not only to increase their solubility, but also to tune their optical and electronic properties at the same time. With respect to the structural properties, the parent perylenediimide exhibits flat π-systems as confirmed by X-ray diffraction of several single crystal examples. Nevertheless, by introducing bulky groups in bay-positions the planarity of the perylenediimide disappears and the steric strain generated can lead to a propeller-like twisting of the two naphthalene units. This case was demonstrated crystallographically for two perylenediimides.[27]

The third stage involves the functionalization of the ortho-positions of the perylene core (2, 5, 8 and 11 positions), which mainly helped in retaining the planarity of the PDI core upon chemical modification. [32,33]

The aggregation effects and the substituents attaching in the different positions of the perylenediimides have vividly outcomes in the physical properties of PDIs related to absorption and luminescence. When these effects are not present, a mirror image of the absorption and emission spectrum in common organic solvents and small Stokes shift are observed, while a core substitution can significantly affect both properties. As indicated in the Figure 15, there are noteworthy HOMO and LUMO coefficients on the bay positions.

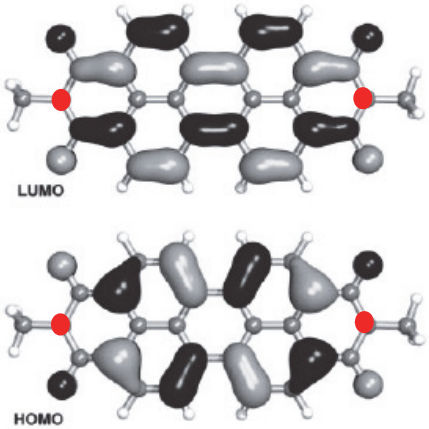

Figure 15. Frontier orbitals HOMO and LUMO of an example of perylenediimides (*N,N'*-dimethyl-PDI) according to DFT calculations. The frontier orbitals exhibit nodes at the imide positions highlighted in red.

Accordingly, the HOMO is expected to be destabilized by π-donor substituents and the LUMO stabilized by π-acceptors leading to bathochromic shifts of the spectra in either case. Substitution at the imide position negligibly affects absorption and emission properties because nodes in the HOMO and LUMO (Figure 15) at the imide nitrogen reduce the coupling between the perylenediimide units and the imide substituents to a minimum,[34] and just affects to the solid-state colour of PDIs.[35]

[31] G. Seybold, G. Wagenblast, *Dyes Pigm.*, **1988**, *11*, 303-317.

[32] R. K. Dubey, *Synthesis and Function of Photoactive Donor-Acceptor Systems of Bay-Functionalized Perylene Diimide Dyes in View of 1,7- and 1,6-Regioisomers*, Ph.D. Thesis, Tampere University of Technology, Tampere, **2013**.

[33] G. Battagliarin, C. Li, V. Enkelmann, K. Müllen*, Org. Lett.*, **2011**, *13*, 3012–3015.

[34] F. Würthner, *Chem. Commun.*, **2004**, 1564-1579.

[35] P. M. Kazmaier, R. Hoffmannt, *J. Am. Chem. Soc.,* **1994**, *116*, 9684-9691.

In contrast, substituents on the aromatic core bay-positions show a much more obvious effect on the absorption and emission spectra of PDIs as expected, due to the stronger electronic coupling between the π-orbitals of PDIs and the substituents on the aromatic bay region.

Compound	λ_{ex} (nm)	λ_{em} (nm)	Luminescence
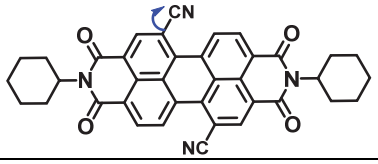	530	545	Green
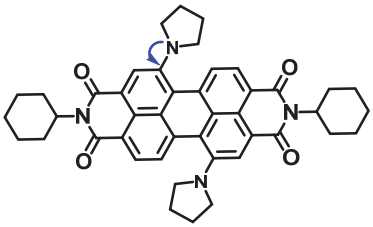	686	721	Deep red

Table 1. Optical properties of selected perylenediimides.

A bathochromic shift would be expected when electron withdrawing groups, as occur in the Table 1 to bay-substituted perylenediimides.[32]

Therefore, the preparation of highly fluorescent substituted perylenediimides constitutes a useful pathway for the preparation of stable dyes for use in water or solvents, thus giving rise to new chemical sensors required for the purposes of the projects. The fluorescent compounds can be tested with no risk of decomposition on the way to develop and validate new fluorescent sensors. At the same time, it is possible to develop new synthetic methodologies for the preparation of PDIs that will permit a large chemical flexibility in the design of new structural motifs containing fluorescent as well as fluorogenic PDIs useful for the development of new fluorogenic molecular devices for the fast detection of highly harmful chemical and biological agents intended for bacterial toxins, homemade explosives and harmful metabolites, which complement the existing methodologies. The work will be intended for the development of fast methods for orphan analytes, those analytes that have no easy method to quickly detect them.

7. OBJECTIVES.

The objectives to perform this doctoral thesis are based on some requirements demanded by the projects in which this work is involved. These projects are SNIFFER, FLUOTOXIN and FLUOROMOL, explained in detail in the introduction. The present thesis deals with the general objective of the synthesis and characterization of two families of fluorogenic sensors based on functionalized perylenediimides and their subsequent applications in bioimagen and environmental detection. These two families of compounds are obtained by:

- introduction of cyclic amines in peri position and Suzuki-coupling with different boronic esters in bay positions: **Family I**.
- inclusion of amines with functionalizable groups in peri-positions and nucleophilic substitution of chlorines on aromatic carbon positions with different water-solubilizing phenol groups in bay position: **Family II**.

Every one of the three chapters has been defined by one general objective and every one of them has been divided into several specific objectives that will be included in the following work planning.

In the first chapter, the perylenediimides from **family I** will be synthesized and then anchored to polymers and silica and used for two functions: the *in-situ* detection of home-made explosives by fluorescence and the formation of gold and palladium nanoparticles for different purposes.

- **General Objective of Chapter 1**: Development of different solid materials to detect and discriminate home-made explosives in comparison to classic oxidants.
  - To synthesize perylenediimides bearing donor groups.
  - To perform fluorescent titrations in organic-aqueous mixtures in the presence of some oxygen-based oxidizing reagents.
  - To prepare polymer conjugates with perylenediimides bearing donor groups.
  - To check the sensitivity of these modified polymers to gaseous traces of home-made explosives.
  - To anchor perylenediimides bearing donor groups on silica supports.
  - To test the sensitivity of these modified silicas to gaseous traces of home-made explosives.

The second chapter is divided in three chapters: A, B and C, because the **family II** composed by water-soluble and fluorescent perylenediimides are used for three goals.

In the chapter 2A, charged organic molecules capable of stabilizing G-quadruplex DNA in peri-positions are anchored to the **family II**, with the aim of studying their biological effects and their potential use as biomarkers for bioimaging.

- **General Objective of Chapter 2A**: Design of new water-soluble fluorogenic probes and their study in cellular bioimaging.

- To obtain potentially water-soluble fluorescent tetra-substituted perylenediimides.
- To synthesize tetra-substituted perylenediimides with biological molecules in peri positions: biotin and testosterone.

In the chapter 2B, organic groups are anchored in peri-positions to the **family II**, with the aim of studying their biological effects and their potential use in stabilizing G-quadruplex DNA.

➢ **General Objective of Chapter 2B**: The study water-soluble fluorogenic probes in cellular environments and in G-quadruplex binding.

- To study cell internalization, biocompatibility and cytotoxicity of tetra-substituted perylenediimides in living cells.
- To analyse the activity of the synthesized materials against DNA strands of quadruple helix.

In the chapter 2C, the fluorogenic detection of proteins will be developed on the route to the synthesis of a triisaccharide bonded to perylenediimides of the **family II**.

➢ **General Objective of Chapter 2C:** Development of fluorogenic probes for proteins and toxins detection.

- To perform preliminary fluorescent titrations of the biotinylated derivatives in the presence of avidin.
- To carry out fluorogenic assays with the complex avidin-biotinylated derivatives in the presence of graphene oxide.
- To obtain modified globotriaosyl derivatives with a long chain linkable to other functional groups.
- To synthesize globotriaosyl conjugates with tetra-substituted perylenediimides.

In the third chapter, the **family II** has been anchored to carbon nanotubes and subsequently solubilized in water. These fluorophores will be applied in cell bioimaging.

➢ **General Objective of Chapter 3**: Functionalization of carbon nanotubes for their study in cell bioimaging.

- To design and perform different pathways for the CNT-functionalization.
- To check the efficiency of differently functionalized CNT in cell bioimaging.

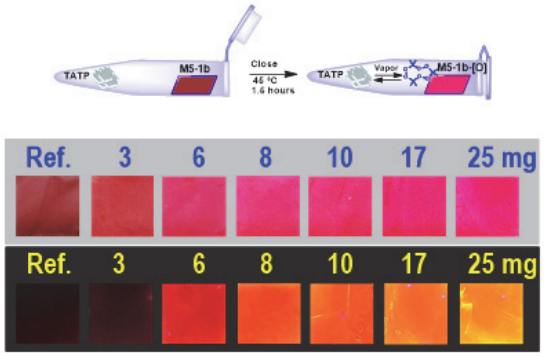

CHAPTER 1: DETECTION OF HOME-MADE EXPLOSIVES WITH FLUORESCENT DEVICES BASED ON PERYLENEDIIMIDES

PATRICIA CALVO GREDILLA Ph. D. THESIS

SUMMARY

A new synthesis of perylenediimide (PDI) based devices, which exhibit high fluorescence in the presence of TATP (triacetone triperoxide) gas has been carried out.

1. INTRODUCTION OF EXPLOSIVES.

An explosive is a solid or a liquid (or a mixture of both) that, by chemical reaction, could emit gases at such temperature, pressure and speed in which could cause physical effects, affecting its surroundings.[1] These substances are divided into two categories, low and high explosives, based on the type of chemical reaction that takes place and the speed at which it proceeds. Low explosives will deflagrate, or burn rapidly at intense temperatures, but they do not detonate,[2] while high ones will do it. The detonation is a process by which the energetic material decomposes giving place a shockwave, whose temperatures can reach from 3000 to 4500 K.[3] The detonation velocity covers an approximate range from 1500 to 10000 m/s, since slower explosive reactions, which are propagated by thermal conduction and radiation, are known as deflagration.[4] The speed of the reaction and the temperature are factors that contribute to categorize the material. Therefore, high explosives are then further classified by their use as either primary or secondary explosives (Figure 1).[5]

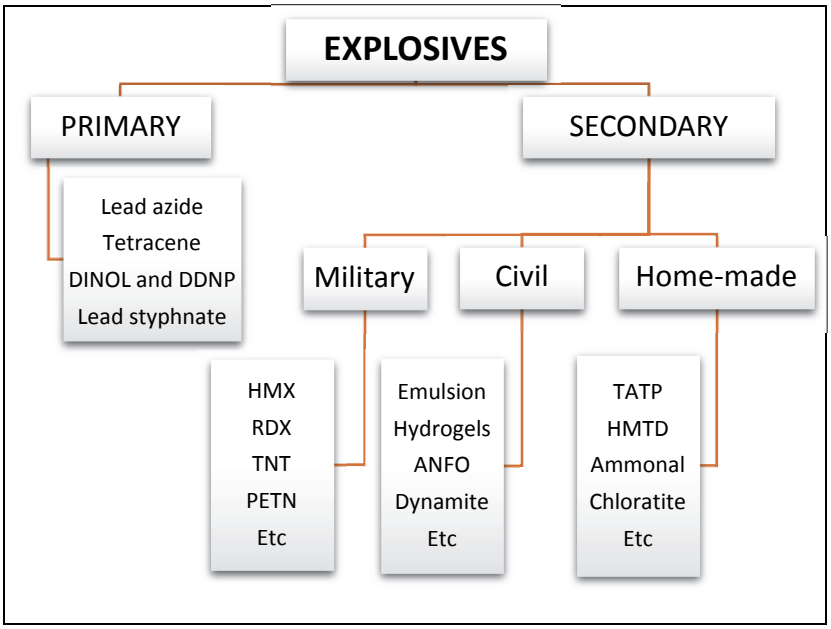

Figure 1. Classification of the most emblematic explosives according to the susceptibility of ignition (ease to start the reaction of decomposition).

Primary explosives are the most sensitive to spark, impact or flame, for this reason, they are used to initiate secondary ones. The primary safety considerations in the formulation, manufacture and use of explosives are that they must explode when it is only desired. The insensitive main charge (normally the secondary explosives) has to be initiated by a minimum amount of a more sensitive explosive. These, at the same time, are divided considering their military, civil and home-made applications. The military explosives are manufactured by their standards. The civil explosives are designed, produced and used for commercial and industrial applications. Finally, home-made explosives (or improvised explosive devices, IEDs), which

[1] REAL DECRETO 230/1998, de 16 de febrero, por el que se aprueba el Reglamento de explosivos.
[2] S. Fordham, *High Explosives and Propellants*, Pergamon international library: Oxford, **1980**.
[3] R. L. Woodfin, *Trace Chemical Sensing of Explosives*, Wiley-Interscience: New Jersey, **2007**,
[4] R. Meyer, J. Köhler, A. Homburg, *Explosives*, Wiley-VCH Verlag GmbH & Co. KGaA, Weinheim, **2007**.
[5] J. Yinon, S. Zitrin, *Modern Methods and Applications in Analysis of Explosives*, West Sussex: Wiley, Chinchester, **1993**.

have become popular among terrorists, can be employed for numerous combinations of high and low explosives.[6]

Triacetone triperoxide (TATP) belongs to a group called peroxide-based explosives, characterized by the unstable peroxide bonds (-O-O-), giving its explosive and oxidant features. Analogue structures to TATP are diacetone diperoxide (DADP) and hexamethylene triperoxide diamine (HMTD), as it could be seen in the Figure 2. In order to frame TATP in the explosive world, it is compared to the strength of trinitrotoluene (TNT). TATP and HMTD are about 88% and 60% more powerful than TNT.[2] Trinitrotoluene has a detonation velocity of 6900 m/s, while the detonation velocity of TATP is 5300 m/s.[7] Oxley *et al*. determined that the vapour pressure of TATP at 25 °C is about 7 Pa (it sublimes at the rate of 0.9% w/w per hour[8]), which is higher than TNT around $5 \cdot 10^{-4}$ Pa. Consequently, TATP is very difficult to safely handle, reasons why terrorists dubbed it *''the Mother of Satan''*.[9] TATP could be considered for military uses, however due to its heat, impact and friction sensitivity, it is not employed in this field.

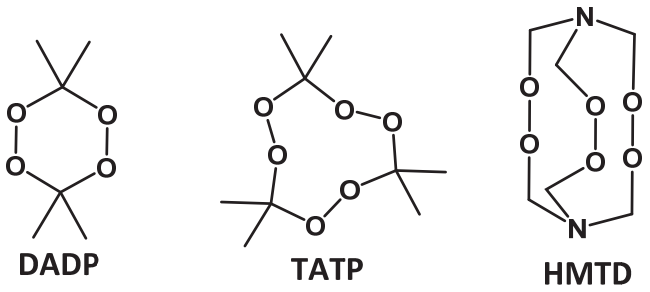

Figure 2. Chemical structures of DADP, TATP and HMTD.

2. PROBLEMS IN TATP DETECTION.

TATP is easily prepared from acetone and hydrogen peroxide under acidic catalysis. The TATP formation properly works in the presence of catalysts such as hydrochloric acid, tin (IV) chloride, or nitric acid. However, in presence of methanesulfonic, perchloric or sulphuric acid, isolated TATP has been found to undergo spontaneous gradual transformation to DADP.[10] The melting point for pure TATP is in the range of 95 – 98.5 °C, but impurities present in the sample will lead to a decreased melting point as low as 73 – 79 °C, hence existing a dependence with the synthesis method used. The majority of publications coincide in the synthesis (Figure 3), but in the decomposition products of TATP, in which are based the majority of detection systems, are not reach an agreement.

Keinan *et al*.[11] and Oxley *et al*.[8] agree that the main decomposition products of TATP are acetone and ozone, and others like dioxygen, methyl acetate, ethane, and carbon dioxide.

[6] La Seguridad frente a artefactos explosivos. Ministerio de Defensa Español, **2009**.

[7] P. W. Cooper, *Explosives Engineering*, Wiley-VCH, New York, **1996**.

[8] J. C. Oxley, J. L. Smith, H. Chen, *Propellants Explos. Pyrotech.*, **2002**, *27*, 197-246.

[9] http://thefutureofthings.com/3035-tatp-countering-the-mother-of-satan/, accessed in August, 14, **2015**.

[10] R. Matyas, J. Pachman, H.-G. Ang, *Propellants Explos. Pyrotech.*, **2008**, *33*, 89-91. b) K. Betlz, *The development of calibrants through characterization of volatile organic compounds from peroxide based explosives and a non-target chemical calibration compound*, Ph.D. Thesis, Florida International University, **2013**.

[11] F. Dubnikova, R. Kosloff, J. Almog, Y. Zeiri, R. Boese, H. Itzhaky, A. Alt, E. Keinan, *J. Am. Chem. Soc.*, **2005**, *127*, 1146-1159.

Whereas Hiyoshi and Nakamura have shown that the rapid heating degradation of TATP takes place mainly in the gas phase, producing mostly carbon dioxide and water.[12]

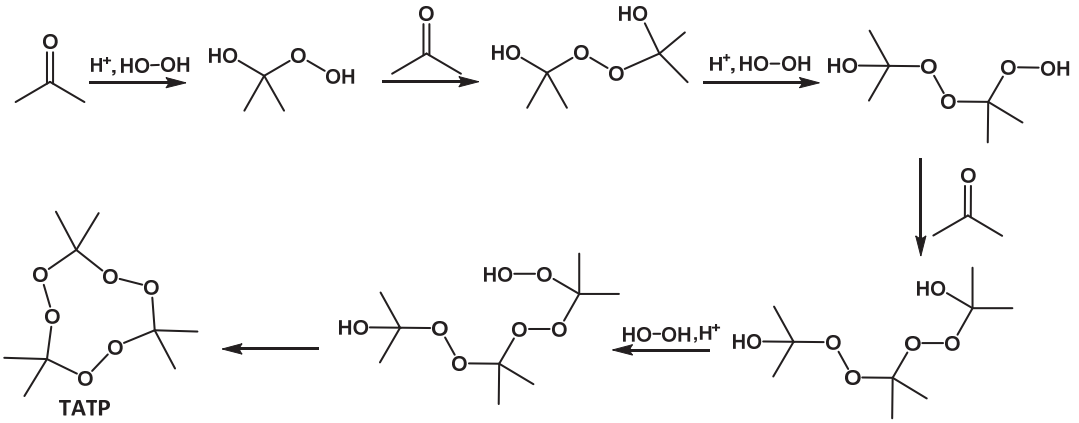

Figure 3. Supposed mechanism of TATP formation.

The lack of significant absorption in the UV-visible range or luminescence bands, the high degradability and careful handling of TATP make it difficult the selection of its detection method. Consequently, the reliable detection of TATP using a portable and small footprint sensor continues to draw interest; however, scientists have carried out some experiments in this area of research. Several studies have been published for the direct detection of TATP including Gas Chromatography-Mass Spectrometry (GC-MS),[13] Ion Mobility Spectrometry (IMS),[14,15,16] tetraherz absorption spectroscopy[17] and Molecular Imprinted Polymers (MIPs).[18] Moreover, this explosive has been indirectly identified by the detection of hydrogen peroxide after acidic cleavage,[19] UV irradiation,[20] DESI-MS,[21] IR and Raman spectrometry.[22] Nevertheless, these detection methods present noteworthy limitations such as time consuming, expensive instrumentation, trained operators and they are not applicable for on-site analyses.

Besides, portable devices like metal oxide based gas sensors[23] have been extensively studied, but they have been criticized for their lack of long term stability and poor selectivity.

[12] R. I. Hiyoshi, J. Nakamura, *Propellants Explos. Pyrotech.*, **2007**, *32*, 127-134.
[13] R.-M. Räsänen, M. Nousiainen, K. Peräkorpi, M. Sillanpää, L. Polari, O. Anttalainen, M. Utriainen, *Anal. Chim. Acta*, **2008**, *623*, 59-65.
[14] G. A. Buttigieg, A. K. Knight, S. Denson, C. Pommier, M. Bonner-Denton, *Forensic Sci. Int.*, **2003**, *135*, 53-59.
[15] J. Kozole, J. Tomlinson-Phillips, J. R. Stairs, J. D.Harper, S. R.Lukow, R. T.Lareau, H. Boudries, H. Lai, C. S. Brauer, *Talanta*, **2012**, *99*, 799–810.
[16] J. C. Oxley, J. L. Smith, K. Shinde, J. Moran, *Propellants Explos. Pyrotech.*, **2005**, *30*, 127-130.
[17] J. Wilkinsona, C. T. Koneka, J. S. Morana, E. M. Witkob, T. M. Korterb, *Chem. Phys. Lett.*, **2009**, *478*, 172-174.
[18] S. Kassahun-Mamo, J. Gonzalez-Rodriguez, *Sensors*, **2014**, *14*, 23269-23282.
[19] a) M. E. Germain, M. J. Knapp, *Inorg. Chem.*, **2008**, *47*, 9748-9750.; b) H. Lin, K. S. Suslick, *J. Am. Chem. Soc.*, **2010**, *132*, 15519-15521.; c) R. Schulte-Ladbeck, U. Karst, *Anal. Chim. Acta*, **2003**, *482*, 183-188.; d) S. Girotti, E. Ferri, E. Maiolini, L. Bolelli, M. D'Elia, D. Coppe, F. S. Romolo, *Anal. Bioanal. Chem.*, **2011**, *400*, 313-320.
[20] a) S. Malashikhin, N. S. Finney, *J. Am. Chem. Soc.*, **2008**, *130*, 12846–12847.; b) R. Schulte-Ladbeck, P. Kollab, U. Karst, *Analyst*, **2002**, *127*, 1152-1154.
[21] I. Cotte-Rodríguez, H. Hernández-Soto, H. Chen, R. G. Cooks, *Anal. Chem.*, **2008**, *80*, 1512-1519.
[22] L. Jensen, P. M. Mortensen, R. Trane, P. Harris, R. W. Berg, *Appl. Spectrosc.*, **2009**, *63*, 92-97.
[23] W.-H. Zhang, W.-D. Zhang, L.-Y. Chen, *Nanotechnology*, **2010**, *21*, 315502.

Moreover, immunosensor platforms for the detection of TATP have been developed with polyclonal antibodies, instead of monoclonal ones, giving a nonspecific response.[24] Dogs are strikingly a good identification method, but their olfactory system become saturated after a large period of working time.

The most recent detection portable device has been designed by O. Gregory *et al*. [25] It is based on a thin film with inorganic microheaters and electrodes, that detects explosives in gas phase with a limit of detection in the ppb range (Figure 4. Left). ACRO Security Technologies (a company founded by Keinan) has created a disposable marker-size "peroxide explosives tester or ACRO-P.E.T", whose LOD is about µg. This company has developed a unique patented technology for identifying peroxide-based explosives, [26] such as TATP (Figure 4. Right).

Figure 4. Novel devices to detect TATP. Left) Small footprint of thin film microheaters. Right) ACRO-P.E.T. – a simple to use pen like device.

3. THE IMPORTANCE OF TATP EXPLOSIVE DETECTION.

Home-made explosives can be easily prepared on board in an airplane, which have given rise to restrictions on carrying liquids in hand luggage,[27] and the careful monitoring of luggage and people at airports.[28] TATP is frequently used in suicide terrorist attacks, as a failed shoe bomb attempt in an American Airlines airplane in 2001,[29] London subways bomb attacks in 2005 and more recently, the bomb attacks in Paris (2015) and in Brussels (2016).[30] Therefore, this explosive constitutes a threat in public transport or mass events where prevention of indiscriminate attacks with explosives is a major concern.[31]

[24] M. A. Walter, U. Panne, M. G. Weller, *Biosensors*, **2011**, *1*, 93-106.
[25] Z. C. Caron, V. N. Patel, D. J. Meekins, M. J. Platek, O. J. Gregory, *Nano. Synth.*, **2016**, *1*, 1531-1537.
[26] http://news.thomasnet.com/companystory/acro-announces-new-and-enhanced-version-of-innovative-peroxide-explosive-tester-519941
[27] EU Aviation Security Regulations and Screening of Liquids, Aerosols and Gels (LAGS), Rapiscan Systems, OSI Systems, Inc., www.rapiscansystems.com, accessed in August, 14, **2015**.
[28] See for example: Communiqué, Airport Business, Winter **2011**, pp. 27-28, Winter **2012**, pp. 34-36, Winter **2013**, pp. 29-31 and Winter **2014**, p. 28, Airports Council International, European Region, 6 Square de Meeûs, B-1000 Brussels, Belgium, and PPS Publications Ltd, 3a Gatwick Metro Centre, Balcombe Road, Horley, Surrey RH6 9GA, United Kingdom, **2011-2014**.
[29] F. Dubnikova, R. Kosloff, Y. Zeiri, Z. Karpas, *J. Phys. Chem. A*, **2002**, *106*, 4951-4956.
[30] http://cen.acs.org/articles/94/web/2016/03/Explosive-used-Brussels-isnt-hard.html
[31] M. Ranstorp, M. Normark, *Understanding Terrorism Innovation and Learning: Al-Qaeda and Beyond*, **2015** – Routledge, Taylor & Francis Group LLC, 7625 Empire Drive, Florence, Kentucky 41042-2919, USA, Chapter 1, pp. 1-15 and references therein.

4. AIM OF THIS CHAPTER.

As it has been previously explained, the importance of TATP detection resides in the ease with which this kind of substances is prepared by anybody. No large chemistry knowledge is needed and the reagents for the fabrication of the explosive could be bought anywhere without arousing suspicions. Moreover, there are very few available portable detection devices on the market and those have poor LOD. Consequently, this chapter is focused on the synthesis and characterization of several fluorogenic perylenediimides, subsequently anchoring to solid supports, polymers and silica, for the easy, rapid and in-situ gas phase detection of TATP.

The first part of this chapter has been accomplished in collaboration with DYSMOL Research Group of Miguel Hernandez University (UHM). Nathalie Zink Lorre (a doctorate student of DYSMOL group) synthetized a family of perylenediimides under direction of Tomás Torroba Pérez first in the University of Burgos and then in the University Miguel Hernandez in Elche. Then, our group performed the optical measurements, established the linkage to polymers and developed a detection method of TATP.[32] In this sense, the Polymer Research Group of Burgos University supplied the used membranes.

[32] P. Calvo-Gredilla, J. García-Calvo, J. V. Cuevas, T. Torroba, J.-L. Pablos, F. C. García, J.-M. García, N. Zink-Lorre, E. Font-Sanchis, A. Sastre-Santos, F. Fernández-Lázaro, *Chem. Eur. J.*, **2017**, published online 21 July 2017, DOI: 10.1002/chem.201702412.

5. RESULTS AND DISCUSSION.

The general purpose is to bond to a fluorogenic perylenediimide a group susceptible to undergo an oxidation process and, therefore, to be oxidized in the presence of TATP explosive, promoting a structural change in the fluorophore, transduced in a luminescence signal. The proposed synthetic route consists of four consecutive stages:

- An imidization process in peri-positions to solubilize the PDIs avoiding the aggregation among them.
- Bromination process in bay-positions.
- Subsequent Suzuki coupling with three boronic esters. These three boronates will be in charge of undergoing a further oxidation process.
- Deprotection of the BOC groups on the piperazine amines.

5.1. Synthesis and characterization of the perylenediimides for use as chemosensors.

According to the literature, small and linear alkyl chains lead to quite insoluble PDIs in organic solvents, although bulky amines forced out of the molecular plane of the PDI, thereby hampering the face-to-face π-π stacking of the perylenediimides.[33] Cyclohexylamine was the best option to work since there were many examples in the literature[34] with good results. Other checked amines such as norbornane amine and cyclododecylamine gave poor yields or products with low solubility. Firstly, fine-tuning of the method for the synthesis was developed in order to achieve the best reaction conditions, because this was the first time our group worked with this kind of compounds. A family of dyes have been synthesised based on the functionalization in bay positions of the perylenediimide with three different boronic esters. Twelve dyes were made considering that there are two types of bay positions, those from monobrominated and dibrominated compounds. From now on, the dyes from monobrominated PDIs will be called PDIs with one branch (Scheme 3) and those coming from dibrominated ones PDIs with two branches (Scheme 3). Based on the reaction conditions obtained from the preliminary experiments, the imidization and bromination processes were taken into account to prepare the series of cyclohexylamine derivatives (Scheme 1).

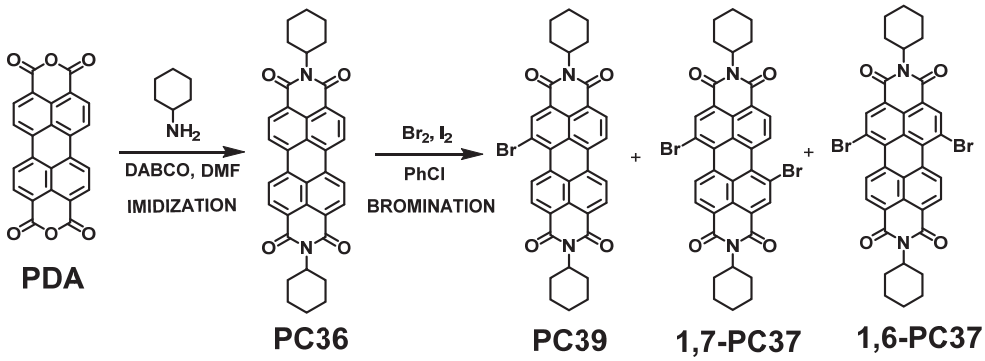

Scheme 1. Preparation and bromination of perylenediimides.

[33] a) R. K. Dubey, *Synthesis and Function of Photoactive Donor-Acceptor Systems of Bay-Functionalized Perylene Diimide Dyes in View of 1,7- and 1,6-Regioisomers*, Ph.D. Thesis, Tampere University of Technology, Tampere, **2013**. b) C. Huang, *Perylene diimide-based materials for organic electronic and optical limiting applications*, Ph.D. Thesis, Georgia Institute of technology, EE.UU, **2010**.

[34] a) M. Yong-Shan, W. Chen-Hui, Z. Ying-Jie, Y. Ying, H. Ci-Xiang, Q. Xin-Jian, S. Zhiqiang, *Supramol. Chem.*, **2004**, *19*, 141-149.; b) M. Supur, M. E. El-Khouly, J. H. Seok, J. H. Kim, K.-Y. Kay, S. Fukuzumi, *J. Phys. Chem. C*, **2010**, *114*, 10969-10977.

The imidization reaction: The main problem of the imidization reaction is the low solubility of PDA in any solvent; therefore, it is necessary to tune the reaction conditions (Table 1) in order to reach a balance between the reaction time and the yield. Several polar solvents with high boiling point were checked like *N*,*N*'-dimethylformamide (DMF), imidazole, *N*-methylpyrrolidone (NMP) and chlorobenzene (PhCl), but the best results were obtained with DMF. Once selected the solvent, the relationship between the amount of amine and the yield was studied (entries 1 and 2). There are not significant differences in the yield varying the amount of amine under equal reaction conditions. Even, a solvent-free reaction was warmed by maximizing the amount of amine (entry 3), due to the cyclohexylamine is a liquid and has basic character, but the results were not satisfactory at conventional heating. With the addition of a base (entry 4) was tried to discover if it would improve the yield under reflux, but it did not occur. Given the many similar yield, the heating method was changed to microwave-assisted heating. The conditions employed in the entries 5 and 6 reflect that the reaction rate was reduced 24 times. However, the yield of the reaction is remained constant by increasing the temperature and by changing the heating system. According to the results gained in the entry 7, when introducing six equivalents of the base DABCO (whose pK_b = 5.2 and it is more basic than cyclohexylamine, whose pK_b = 3.3) the yield increases 20 per cent, because the basic media improves the nucleophilicity of amine.

	Eq of PDA:Amine	Eq of Base	Solvent, mL	T, °C	Heating	Time, h	Yield*, %
Entry 1	1:5	-	40 DMF	111	Reflux	24	38
Entry 2	1:3	-	40 DMF	111	Reflux	24	32
Entry 3	1:68	-	-	136	Reflux	24	< 10
Entry 4	1:5	2,5 DABCO	40 DMF	130	Reflux	24	40
Entry 5	1:3	-	2 DMF	130	MW	1	41
Entry 6	1:5	-	20 DMF	200	MW	1	45
Entry 7	1:2.5	6 DABCO	20 DMF	200	MW	1	66

Table 1. Reaction conditions for the imidization reaction. 300 mg of PDA were used in all entries. * The yields were calculated after the purification by chromatographic column.

The bromination reaction: First, bromine was employed as brominating agent in high concentration with respect the perylenediimide (**PC36**) in dichloromethane (DCM) as solvent and iodine as catalyst.[35] Two products were achieved in the bromination reaction, the monobromo- and dibromo perylenediimides. The entries 1 and 2 show very poor yields. The reaction in chloroform gave some increase of the yield of the dibromo derivative (entry 3). By increasing the boiling point of the solvent to 1,2-dichloroethane (DCE) (entry 4, bp = 83 °C) and chlorobenzene (PhCl) (entry 5, bp = 132 °C), decreasing of volume of solvent, and heating by microwave oven (Biotage Initiator Classic) the amount of dibrominated compound increased. Therefore, good reaction conditions to synthesise the dibrominated compound were achieved (Table 2), whereas the yield of the monobrominated compound did not increase from 25 %.

[35] P. Rajasingh, R. Cohen, E. Shirman, L. J. W. Shimon, B. Rybtchinski, *J. Org. Chem.*, **2007**, *72*, 5973-5979.

	Eq of PC36:Bromine	Eq Iodine	ml of Solvent	T, °C	Heating	Time, days	Yield*: Di/Mono/PDI
Entry 1	1:70	-	40 DCM	23	-	5	10/16/74
Entry 2	1:60	spatula tip	40 DCM	41	reflux	2	15/10/75
Entry 3	1:60	spatula tip	40 $CHCl_3$	61	reflux	5	40/17/43
Entry 4	1:60	spatula tip	4 1,2-DCE	83	MW	1 h	50/25/25
Entry 5	1:60	spatula tip	4 PhCl	132	MW	1 h	87/11/2

Table 2. Reaction conditions for the bromination reaction. 50 mg of **PC36** were used in all entries. *The yields were calculated after the purification by chromatographic column.

In order to improve the yield of monobromination process, some reaction conditions were experienced (Table 3). In this case, *N*-bromosuccinimide was used as a bromine source and *N*-iodosuccinimide and $AuCl_3$ were employed as catalyst. Unfortunately, no entry reflect an improvement of the yield of monobrominated yield. As a consequence, appropriate reaction conditions for selectively obtaining monobrominated compounds have not been achieved.

	Eq of PC36:NBS	Eq NIS/ $AuCl_3$	ml of Solvent	T, °C	Heating	Time, days	Yield*: Di/Mono/PDI
Entry 1	1:1	-/spatula tip	1.5 1,2-DCE	84	reflux	2	7/4/81
Entry 2	1:10	-/spatula tip	4.5 1,2-DCE	84	reflux	2	80/1/19
Entry 3	1:1	1/-	15 1,2-DCE	84	reflux	2	2/0/98
Entry 4	1:1	1/-	4.5 PhCl	131	MW	2h	18/2/80

Table 3. Reaction conditions for the bromination reaction changing the formula. 30 mg of **PC36** were used in all entries. * The yields were calculated after the purification by chromatographic column.

Würthner published in 2004 that the dibromination reaction was not regioselective.[36] The synthetic procedure for the preparation of the 1,7-bay functionalized PDIs produced the corresponding 1,6-bay-functionalized derivative (so-called 1,6-regiosiomer) in 25-30 % quantity as a side product. The removal, as well as the characterization of the 1,6-regioisomer was very difficult. This problem is reflected in the NMR spectra of brominated compounds, the aliphatic signals were not affected by the regioisomer compounds, but the aromatic signals are split into two, as seen in Figure 5. The Figure 5 shows the purification process of regioisomerically pure 1,7-dibrominated[37] by NMR. The pure 1,7-regioisomer was possible to obtain, but the 1,6-regioisomer was always isolated as a mixture of 1,6 and 1,7-regioisomers.

[36] F. Würthner, *Chem. Commun.*, **2004**, 1564-1579.

[37] S. Sengupta, R. K. Dubey, R. W. M. Hoek, S. P. P. v. Eeden, D. D. Gunbas, F. C. Grozema, E. J. R. Sudhölter, W. F. Jager, *J. Org. Chem.*, **2014**, *79*, 6655-6662.

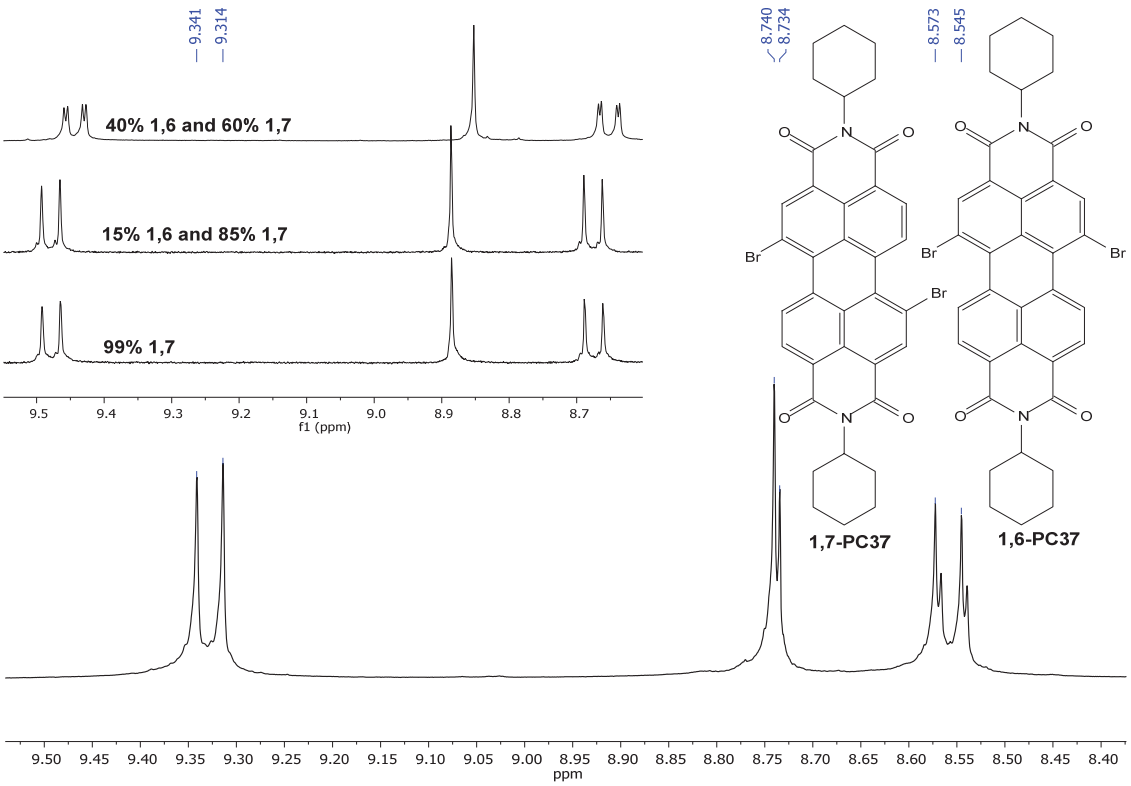

Figure 5. Aromatic part of ^{1}H-NMR spectrum of dibrominated-PDI. In the upper left corner, the stacking spectrum represents the different proportions during the purification process of the regioisomers.

The Suzuki reaction: The monobromo-compound **PC39** was then used as substrate for the corresponding Suzuki reactions with three different boronic esters catalysed by palladium(0). Then, the fourth step of the Scheme 3 is an acid deprotection of the Suzuki products to acquire the desired dyes called **PC117**, **PC63d** and **PC119**. For the Suzuki reaction, general conditions were employed: 4-[4-(*N*''-*tert*-Butoxycarbonyl)piperazin-1-yl]arylboronic acid pinacol ester (1 equivalent), cesium carbonate (0.5 mmol) and a catalytic amount of tetrakis(triphenylphosphine)palladium(0) were added under nitrogen to *N,N'*-dicyclohexyl-1-bromoperylene-3,4,9,10-tetracarboxylic diimide (1 equivalent) dissolved in THF:H_2O (20:2). The mixture was heated at reflux for 24 hours and extracted with DCM, the combined organic extracts were dried over anhydrous sodium sulphate, filtered and evaporated under reduced pressure. Purification was carried out by silica gel flash chromatography using DCM:MeCN (90:10) as eluent to give compounds **PC53**, **PC63** and **PC64** as a deep purple solids in 60-65 % yields.

The deprotection reaction: For the deprotection reaction, general conditions were employed: Trifluoroacetic acid (1 equivalent) was added dropwise to *N,N'*-bis(cyclohexyl)-1-(4-[4-(*N*''-*tert*-butoxycarbonyl)piperazin-1-yl]aryl)perylene-3,4,9,10-tetracarboxylic diimide (1 equivalent) dissolved in DCM. The mixture was stirred at room temperature for 2 hours, then NaOH was added until pH = 6-8 and the mixture was extracted with DCM, the combined organic extracts were dried over anhydrous sodium sulphate, filtered and evaporated under reduced pressure to obtain black solids in almost quantitative yield of **PC117**, **PC63d** and **PC119** (Scheme 2).

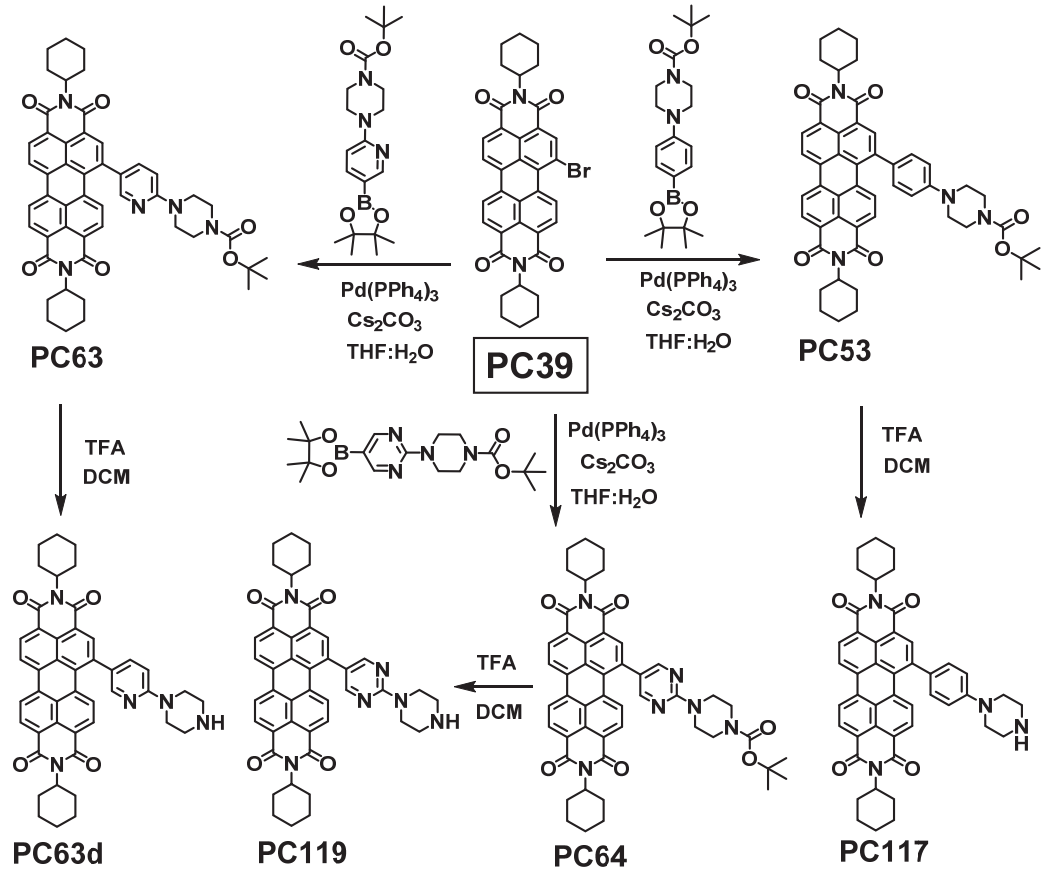

Scheme 2. General synthesis of perylenediimide dyes with one branch.

Then, a mixture of regioisomers of **PC37** were used as starting materials for the Suzuki reactions with three boronic esters, catalysed by palladium(0). For the Suzuki reaction, general conditions were employed as in previous cases: 4-[4-(*N*''-*tert*-butoxycarbonyl)piperazin-1-yl]arylboronic acid pinacol ester (2 equivalents), cesium carbonate (1 mmol) and a catalytic amount of tetrakis(triphenylphosphine)palladium (0) were added under nitrogen to *N,N'*-bis(cyclohexyl)-1,6- and 1,7-dibromoperylene-3,4,9,10-tetracarboxylic diimide (220 mg, 0.31 mmol) dissolved in THF:H_2O (40:4). The mixture was heated at reflux for 24 hours and extracted with DCM, the combined organic extracts were dried over anhydrous sodium sulphate, filtered and evaporated under reduced pressure. Purification was carried out by silica gel flash chromatography using DCM:MeCN (80:20) as a mixture of 1,6- and 1,7-PC54 in 60-65 % yields. To separate the resulting compound of the Suzuki reaction (1,7-compound from 1,6-), several chromatographic columns were necessary (silica, DCM:MeCN (80:20)) to separate pure **1,7-PC54**, **1,7-PC57** and **1,7-PC60**. For the deprotection reaction, general conditions were also employed: Trifluoroacetic acid (1 equivalent) was added dropwise to *N,N'*-bis(cyclohexyl)-1,7-bis-((4-[4-(*N*''-tert-butoxycarbonyl)piperazin-1-yl]aryl))perylene-3,4,9,10-tetracarboxylic diimide (2 equivalents) dissolved in DCM. The mixture was stirred at room temperature for 2 hours, then NaOH was added until pH = 6-8 and the mixture was extracted with DCM, the combined organic extracts were dried over anhydrous sodium sulphate, filtered and evaporated under reduced pressure to obtain black solids in almost quantitative yield of **1,7-PC114**, **1,7-PC115** and **1,7-PC116** (Scheme 3).

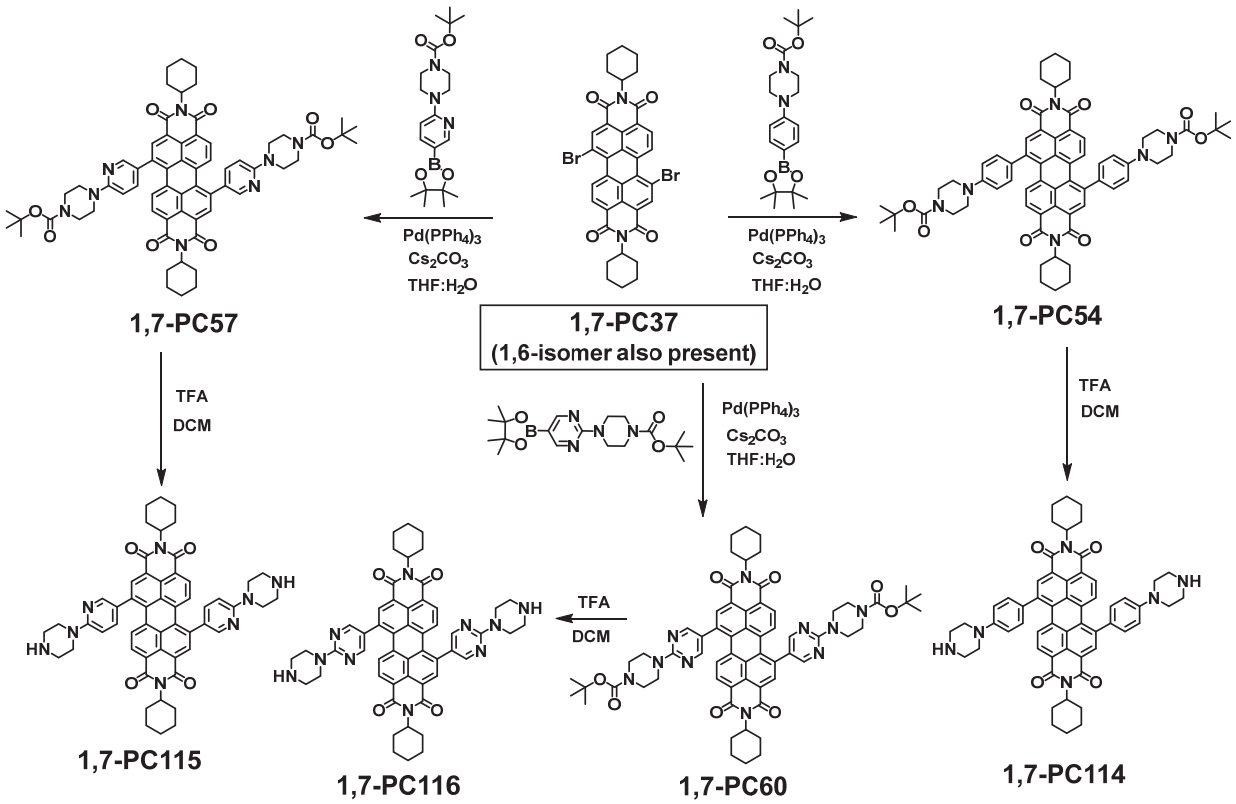

Scheme 3. General synthesis of perylenediimide dyes with two branches.

In all cases, products were characterized by using the usual physical and spectroscopic methodologies: mp, IR, ^{1}H, ^{13}C-NMR, DEPT, COSY, NOESY, HMBC and HMQC spectroscopy, MS and HRMS spectrometry, and UV-visible and fluorescence spectroscopy when required, until satisfactory data were obtained. All data are contained in the experimental chapter.

5.2. TATP detection with a perylenediimide anchored to a film.

This section was carried out in collaboration with DYSMOL Research Group of Miguel Hernandez University (UMH) of Elche. They provided us with the perylenediimides, called **NZ20-33**, explained in the **¡Error! No se encuentra el origen de la referencia.** and Scheme 5. With them, some qualitative studies for TATP and for acids and oxidants were performed. Herein, the solvent, the work concentration and the excitation wavelength will be explained. And then, qualitative and quantitative studies for TATP and for acids and oxidants were accomplished.

5.2.1. Synthetic scheme of perylenediimides.

The ideal probe to reach the aim of this chapter of the thesis should have a strongly fluorescent reporter and a quenching group easily oxidizable by a mild oxidizing reagent in the absence of any solvent. Perylenediimides bear an electron poor π-conjugated aromatic core, suitable for multiple chemical modifications and optical sensing.[38] Our approach consisted of a modification of the fluorescent PDI core with one or two electron donor aryl groups by the classic carbon-carbon Suzuki coupling chemistry.[39] The expected regioisomers can be easily separated as described.[40] The starting *mono*- and *di*-bromo-PDIs were carefully selected from the bibliography because of their easy availability and usefulness.[41] They can be submitted to Suzuki reactions with boronic acid derivatives under classical conditions,[42] to obtain compounds with the required characteristics as fluorogenic sensors of the home-made explosive TATP. The phenylpiperazine group was the appropriate group to attach the probe to polymers, therefore a family of PDIs was synthetized, by using the reactions previously explained, in collaboration with the members of DYSMOL. The synthesis of the starting materials was performed by Nathalie Zink Lorre, first during a one-month stay in the University of Burgos, then at the DYSMOL lab in the UMH. Monofunctionalized and difunctionalized PDIs may undergo different electronic effects;[43] consequently, we prepared PDIs having one and two *p*-aminophenyl groups to study their physicochemical characteristics, their sensitivity to oxidants and their covalent anchoring to polymers (Scheme 4 and Scheme 5). To modulate the electron donor-acceptor effect, we used N-Boc-substituted piperazinylphenylboronic acid derivatives, which we previously employed to modify the fluorescence of fluorogenic probes.[44] In this way, a Suzuki coupling was carried between mono-bromo-PDI or di-bromo-PDI with the phenylboronic acid pinacol ester. Compounds **NZ29-NZ31** and **NZ26**-**NZ33** were purple and

[38] a) S. Seifert, D. Schmidt, F. Würthner, *Chem. Sci*. **2015**, *6*, 1663-1667; b) D. Jänsch, C. Li, L. Chen, M. Wagner, K. Müllen, *Angew. Chem. Int. Ed*. **2015**, *54*, 2285–2289; c) L. You, D. Zha, E. V. Anslyn, *Chem. Rev*. **2015**, *115*, 7840–7892; d) W. Ma, L. Qin, Y. Gao, W. Zhang, Z. Xie, B. Yang, L. Liua, Y. Ma, *Chem. Commun*. **2016**, *52*, 13600–13603.

[39] C. Huang, S. Barlow, S. R. Marder, *J. Org. Chem*. **2011**, *76*, 2386–2407.

[40] A. Keerthi, S. Valiyaveettil, *J. Phys. Chem. B*, **2012**, *116*, 4603–4614.

[41] C. D. Schmidt, N. Lang, N. Jux, A. Hirsch, *Chem. Eur. J.*, **2011**, *17*, 5289–5299.

[42] R. R. Reghu, H. K. Bisoyi, J. V. Grazulevicius, P. Anjukandi, V. Gaidelis, V. Jankauskas*, J. Mater. Chem*. **2011**, *21*, 7811–7819.

[43] a) M. Barrejón, S. Pla, I. Berlanga, M. J. Gómez-Escalonilla, L. Martín-Gomis, J. L. G. Fierro, M. Zhang, M. Yudasaka, S. Iijima, H. B. Gobeze, F. D'Souza, A. Sastre-Santos, F. Langa, *J. Mater. Chem. C*, **2015**, *3*, 4960–4969; b) L. Martín-Gomis, G. Rotas, K. Ohkubo, F. Fernández-Lázaro, S. Fukuzumi, N. Tagmatarchis, A. Sastre-Santos, *Nanoscale*, **2015**, *7*, 7437–7444; c) V. M. Blas-Ferrando, J. Ortiz, K. Ohkubo, S. Fukuzumi, F. Fernández-Lázaro, A. Sastre-Santos, *Chem. Sci.*, **2014**, *5*, 4785–4793.

[44] a) B. Díaz de Greñu, D. Moreno, T. Torroba, A. Berg, J. Gunnars, T. Nilsson, R. Nyman, M. Persson, J. Pettersson, I. Eklind, P. Wästerby, *J. Am. Chem. Soc*. **2014**, *136*, 4125–4128; b) B. Díaz de Greñu, J. García-Calvo, J. Cuevas, G. García-Herbosa, B. García, N. Busto, S. Ibeas, T. Torroba, B. Torroba, A. Herrera, S. Pons, *Chem. Sci.* **2015**, *6*, 3757–3764; c) J. García-Calvo, P. Calvo-Gredilla, M. Ibáñez-Llorente, T. Rodríguez, T. Torroba, *Chem. Rec*. **2016**, *16*, 810–824.

green non-fluorescent compounds, respectively in common solvents (Schemes 4 and Scheme 5).

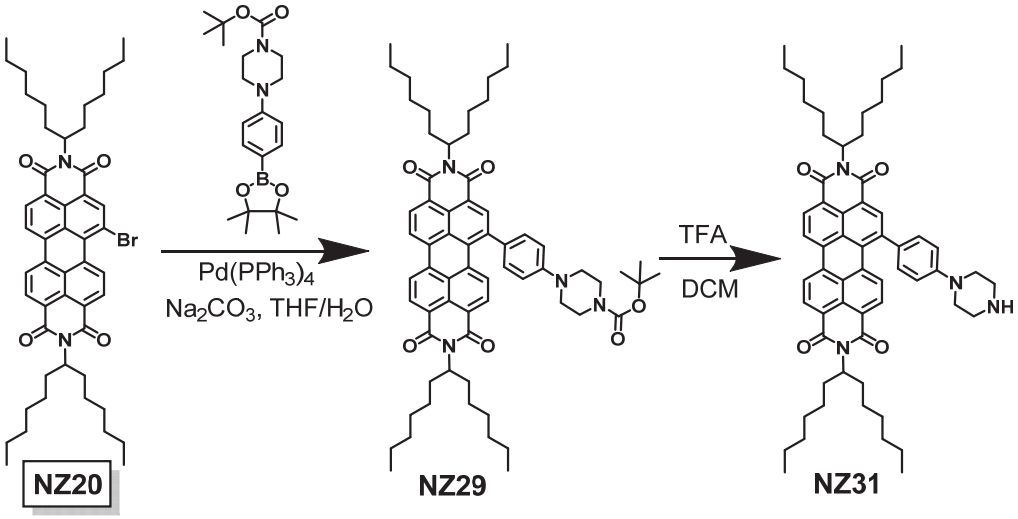

Scheme 4. Synthesis of the perylenediimides (PDIs) used in the study with one branch.

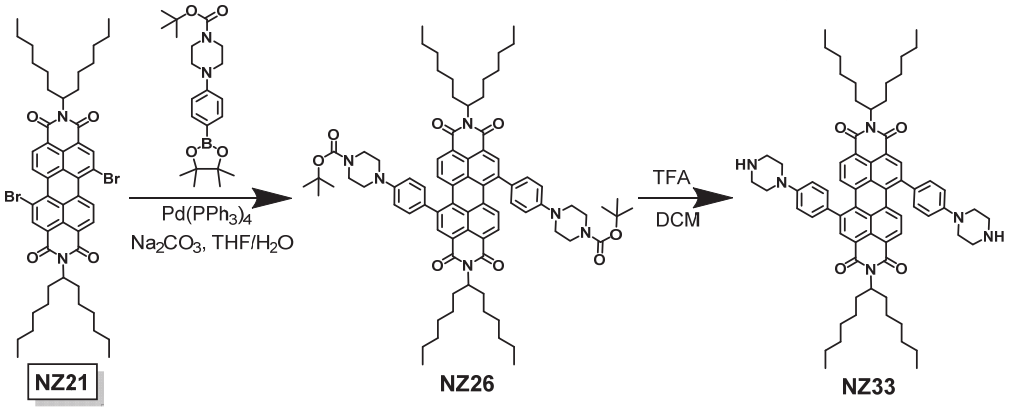

Scheme 5. Synthesis of the perylenediimides (PDIs) used in the study with two branches.

5.2.2. Determination of the solvent, the work concentration and the excitation wavelength.

Once synthesized the compounds **NZ29-NZ31** and **NZ26**-**NZ33**, a selection of solvent, concentration and excitation wavelength was performed. The solvent was selected after performing a study of the solvatochromism of **NZ31** and **NZ29** (10 µM) in solvents: 1. acetone, 2. acetonitrile, 3. methanol, 4. dichloromethane, 5. N,N-dimethylformamide, 6. dimethylsulfoxide, 7. diethyl ether, 8. hexane, 9. tetrahydrofuran (Figure 6 and Figure 7).

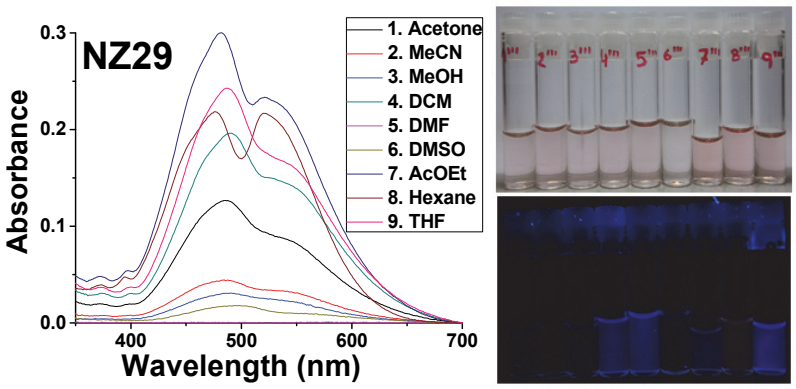

Figure 6. UV/Vis spectra of **NZ29** in some organic solvents.

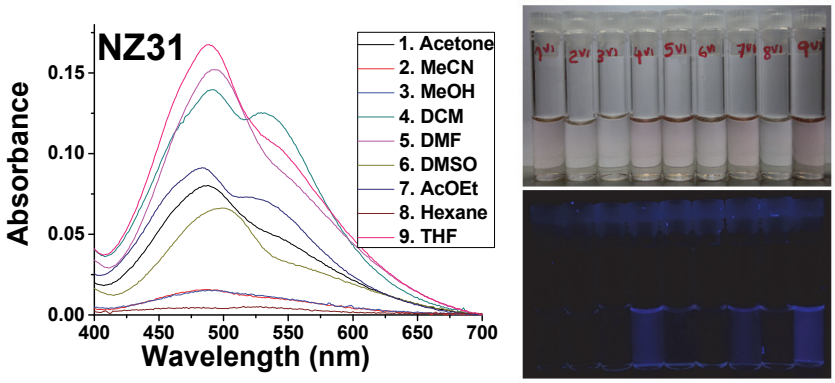

Figure 7. UV/Vis spectra of **NZ31** in some organic solvents.

The greater absorbance was in Et_2O, THF, DMF and DCM. However, Et_2O was too volatile, whereas, DMSO and DMF were hard to evaporate. THF could lead to secondary reactions with peroxides. Finally, DCM showed good solubility, but it was too volatile. As a consequence, the selected solvent was $CHCl_3$, in order to solve the peroxides it was necessary to add a second solvent, in this case 10 % of methanol was adequate.

In order to choose an optimum work concentration, the absorbance of the probe **NZ29** was checked to be linear around the maximum at 486 nm, therefore nine solutions of **NZ29** were prepared and measured. The fluorescence was almost negligible in all cases and the selected working concentration was 5 µM, based on the absorbance (Figure 8).

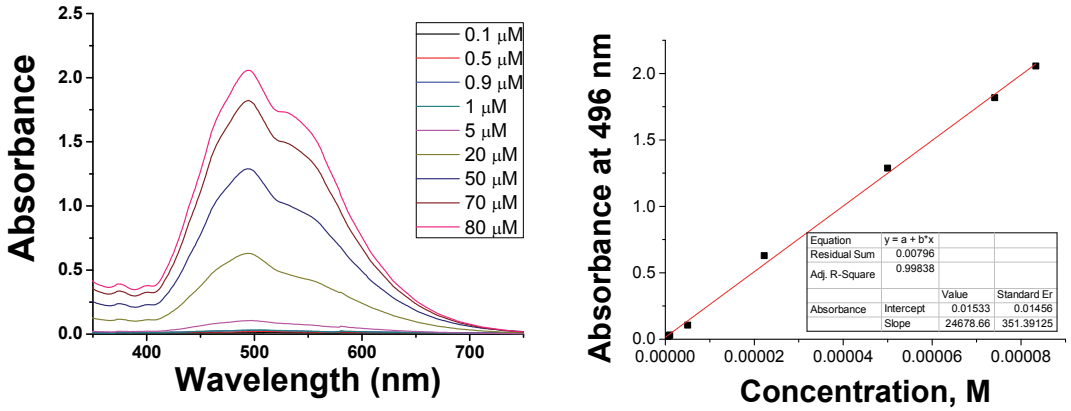

Figure 8. UV-Vis spectra of **NZ29** in $CHCl_3$:MeOH 9:1 v/v at some concentrations.

The excitation wavelength (maximum of absorbance) was performed in the same conditions than previous tests, $CHCl_3$:MeOH 9:1 v/v, 5 µM (Figure 9):

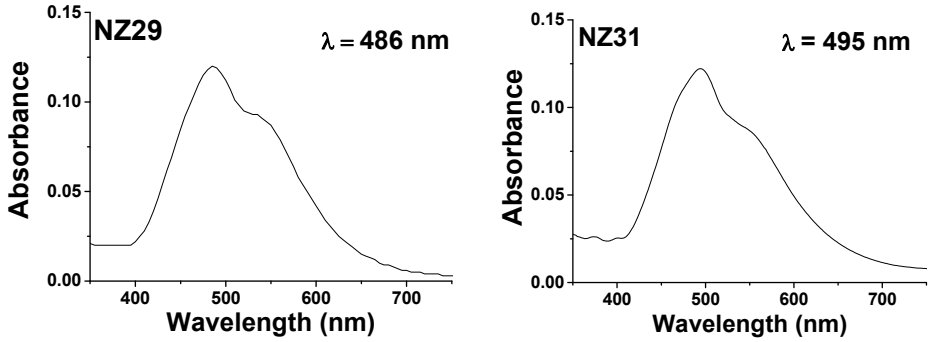

Figure 9. UV/Vis spectra of **NZ29** and **NZ31** in $CHCl_3$:MeOH 9:1 v/v, 5 µM.

5.2.3. Qualitative study of the probes NZ29-NZ31 and NZ26-NZ33.

With this information, the qualitative changes of colour and fluorescence of solutions of compounds **NZ29-NZ31** and **NZ26**-**NZ33**, in the presence of the most common organic and mineral acids and oxidants in several solvents, were tested.

Except for a common sensitivity to concentrated acids, seen as an increase in fluorescence emission, which disappears under addition of aqueous base or buffer (HEPES pH = 8) to the sample (See synthesis and characterization section), the most remarkable finding was a dramatic increase in the fluorescence emission of **NZ29-NZ31** and **NZ26**-**NZ33** in the presence of *m*-chloroperbenzoic (MCPB) acid, a widespread oxidant used in organic solvents, and a somewhat similar increase in the fluorescence emission of **NZ31** and **NZ33** in the presence of oxone, a useful oxidant and precursor of organic peroxides. Benzoyl peroxide or hydrogen peroxide (30 %) did not show similar changes under the same conditions (5 µM concentration of the probe in $CHCl_3$:MeOH 9:1 v/v, 0.05 to 50 equivalents of oxidant).

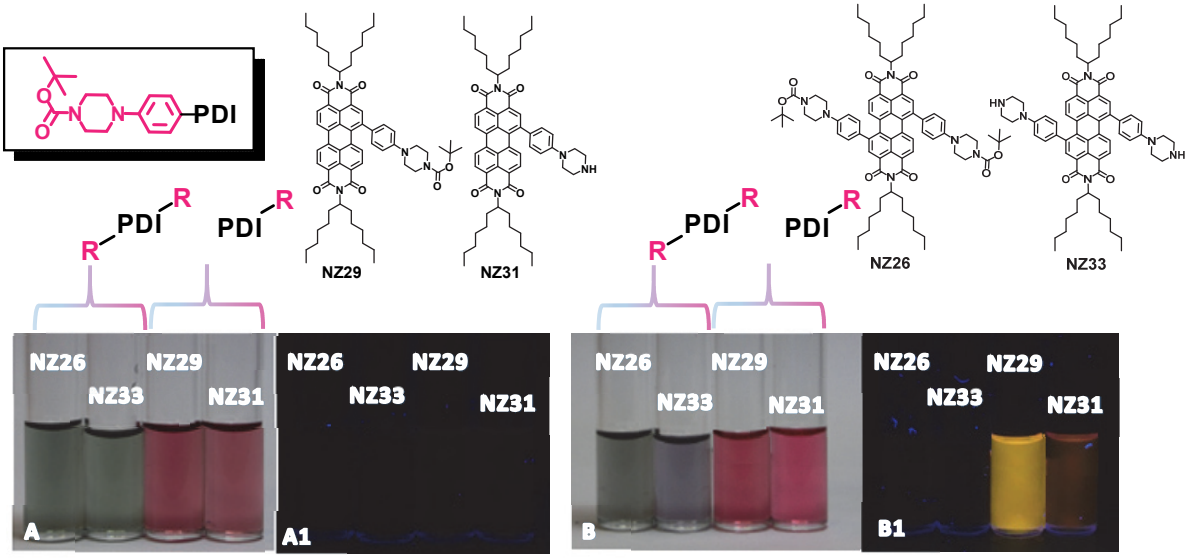

Figure 10. All the probes were dissolved in $CHCl_3$:MeOH 9:1 v/v, 10 µM (0.5 ml) before (**A**, A**1**) and after (**B**, **B1**) addition of 10 mg of TATP (**A**, **B**, under white light and **B**, **B1**, under UV light, 366 nm).

Then, the fluorescence changes in the presence of TATP was verified. The fluorescence of **NZ29** increased intensely, but the fluorescence of **NZ31** increased very little under the same conditions (Figure 10). Compounds **NZ26**-**NZ33** only showed colour changes under the same conditions. Apart of a common sensitivity of the four compounds to MCPB acid, the best suited for the detection of TATP was undoubtedly compound **NZ29**.

5.2.4. Quantitative study of the probes NZ29-NZ31.

In this sense, quantitative point to point titrations of **NZ29** and TATP were carried out in the same solvent and concentration than in qualitative tests. The UV-Visible titration shows a new band at 525 nm apart from 487 nm. Besides, this colour change in visible was reinforced by the appearance of an emission band at 563 nm, with a 140 fold overall increase of the fluorescence emission after addition of excess TATP (Figure 11).

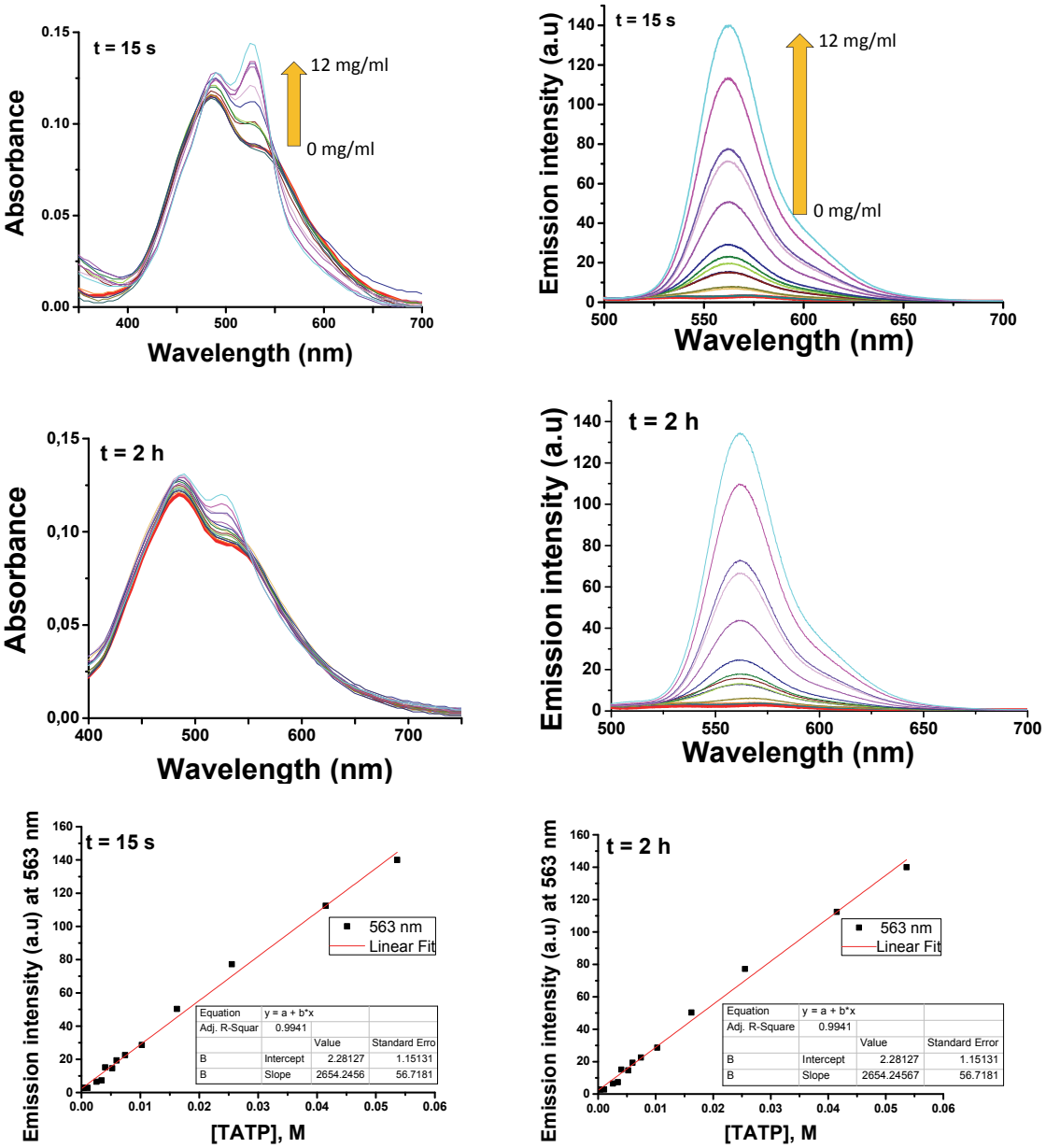

Figure 11. ***Upper graphics.*** UV-Vis and Fluorescence titration curves (left) and titration plot (right) of **NZ29** with TATP (5 µM **NZ29**, $CHCl_3$:MeOH 9:1 v/v, 0 to 12 mg/mL TATP) at 15 seconds. ***Medium graphics.*** The same titrations than above after 2 hours. ***Lower graphics.*** Fluorescence titrations plots at 563 nm of **NZ29** after 15 seconds and after 2 hours for LOD determination.

The increase of emission did not depend on time, because the titration curve obtained after measuring every point within 15 seconds of preparation was exactly the same to the plot obtained when we measured every point after two hours. The plot at the maximum emission intensity (563 nm) could be fitted to a straight line with no sign of asymptotic maximum after addition of a large excess of TATP (Figure 11). From the fluorescent titration we got a detection limit of 3.3×10^{-3} M (0.7 mg/mL) for TATP in solution, suitable for detection of small amounts of TATP in improvised explosives. To determinate the limit of detection was adjusted to minimum squares linear regression. The limit of detection (LOD) for TATP was 0.73 mg/mL ($3.3 \cdot 10^{-3}$ M) in a 5 µM solution of the **NZ29**, within 15 seconds after addition measurements (Figure 12).

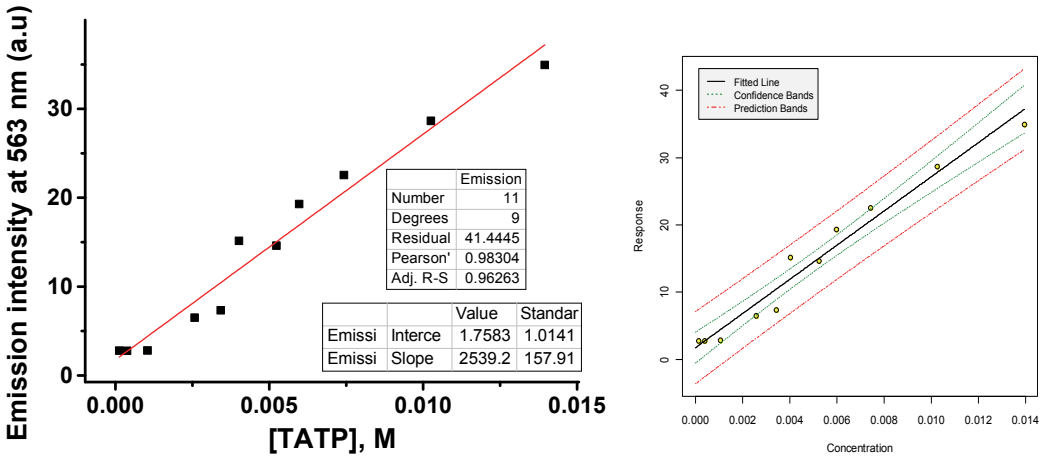

Figure 12. Fluorescence calibration plot of **NZ29** and TATP in $CHCl_3$:MeOH 9:1 v/v, 5 µM **NZ29**, after 15 seconds (left), fitted line, confidence bands and prediction bands (right) for LOD determination.

The fact that compound **NZ29** is only sensitive to TATP and organic oxidants makes the system a complementary detection method for known methodologies, which depend on the detection of decomposition products such as hydrogen peroxide or acetone.

Moreover, the *N*-Boc protected compound **NZ29** worked better than the unprotected compound **NZ31**, because the *p*-aminophenyl moiety as the functional group necessary for the sensing process, being the piperazine group unnecessary for the process. Therefore, the secondary amino group constituted a perfect handle for the anchoring of the chemical probe **NZ31** to a solid support.

5.3. Detection of TATP with a membrane supporting NZ31.

For that purpose, an acyl chloride functionalized polymer, suitable for the surface linking of the chemical probe having excellent thermal and mechanical performance, was selected and prepared by Jesús-Luis Pablos Lagartos, from the Polymers Group of the University of Burgos.[45] The membrane was prepared as a film by the radical polymerization of the corresponding co-monomers, 1-vinyl-2-pyrrolidone (VP), butyl acrylate (A4), and methacryloyl chloride (MCl), the cross-linking agent ethylene glycol dimethacrylate (EGDMA), and the radical photo-initiator 2,2-dimethoxy-2-phenylacetophenone (DMPA). Two examples were prepared, **M2**, prepared with 2 % of EGDMMA, and **M5**, prepared with 5 % of EGDMMA as the cross-linking agent affording membranes **M2-NZ31** and **M5-NZ31**. The first series of experiments gave a better performance for the membrane **M5-NZ31**, therefore we report only the results with that film (Scheme 6). Membrane **M5-NZ31** was not fluorescent, in analogy to compounds **NZ29-NZ31**. **M5-NZ31** showed a slight colour and fluorescence change by exposing the film to HCl vapour, but the colour and the fluorescence faded by addition of HEPES, pH = 8, solution. On the other hand, the film showed a change in colour but no change in fluorescence was seen in the presence of HNO_3 vapour.

[45] a) B. Redondo-Foj, M. Carsi, P. Ortiz-Serna, M. J. Sanchis, S. Vallejos, F. García, J. M. García, *Macromolecules,* **2014**, *47*, 5334–5346; b) B. Redondo-Foj, M. Carsi, P. Ortiz-Serna, M. J. Sanchis, F. García, J. M. García, *J. Phys. D: Appl. Phys.,* **2013**, *46*, 295304. c) S. Fernandez-Alonso, T. Corrales, J.L. Pablos, F. Catalina, *Polymer* **2017**, *124*, 139-150.

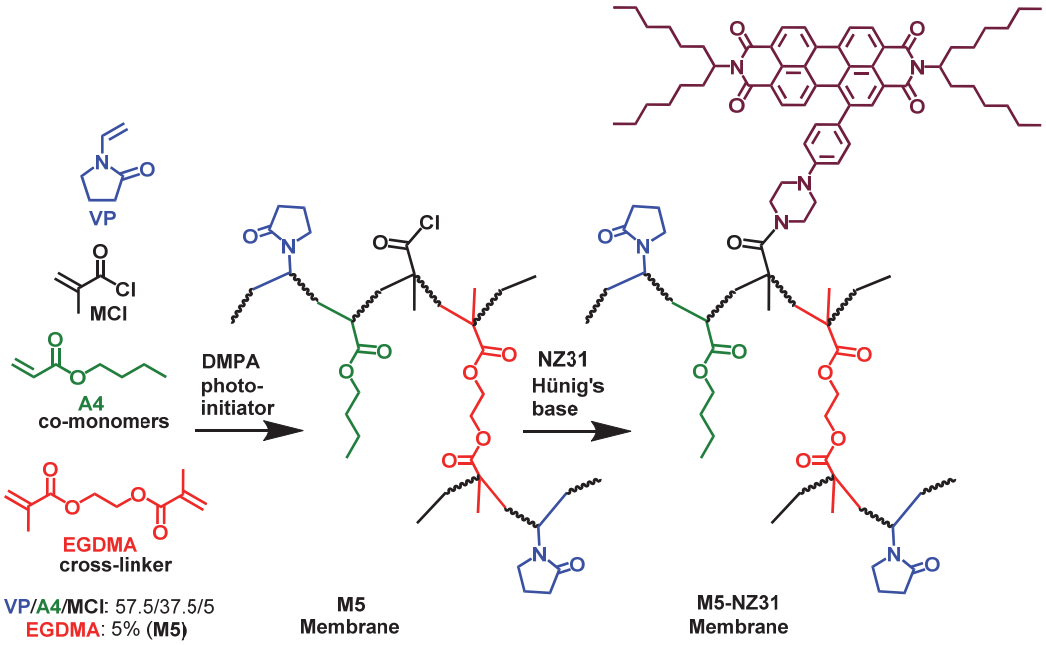

Scheme 6. A representation of the random polymeric structure of membrane **M5-NZ31**.

The most vivid changes were shown by dipping the film in a 5×10^{-2} M $CHCl_3$ solution of MCPB acid, or in a 30% H_2O_2 solution, or by keeping the film in a Teflon sealed tube (13 mL volume) with 25 mg TATP at 50 °C for 1.5 hours. In that case, the colour or the fluorescence of the treated film did not change by dipping the film in HEPES, pH = 8, solution (Figure 13). The colour and fluorescence changes experienced by the film in the presence of MCPB acid, H_2O_2 and TATP remained unchanged after 24 hours standing on the bench. There was no leaking of the colorant from the film to water or organic solvent, therefore the oxidation happened without detachment of the dye from the supporting film.

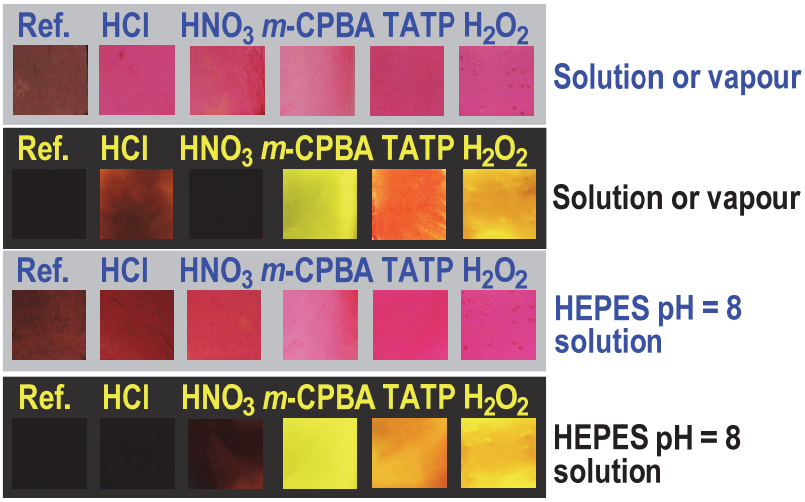

Figure 13. Colour and fluorescence changes of membrane **M5-NZ31** with some acids and oxidants. ***Upper row***: **Ref.**: pristine **M5-NZ31**; **HCl**: **M5-NZ31** in the presence of the vapours of a drop of HCl 35%; **HNO_3**: **M5-NZ31** in the presence of the vapours of a drop of HNO_3 65%; ***m*-CPBA**: addition of MCPB acid (5×10^{-2} M in $CHCl_3$, 500 µL); **TATP**: **M5-NZ31** in the presence of the vapours of 25 mg of solid TATP for 1.5 hours at 50 °C in a Teflon vial; **H_2O_2**: addition of H_2O_2 30% (500 µL); *left*: under with light; *right*: under a UV lamp, 254 nm. ***Lower row***: **Ref.**: pristine **M5-NZ31**; **HCl**: **M5-NZ31** in the presence of the vapours of a drop of HCl 35% and then addition of HEPES pH = 8, 500µL; **HNO_3**: **M5-NZ31** in the presence of the vapours of a drop of HNO_3 65% and then addition of HEPES pH = 8, 500 µL; ***m*-CPBA**: addition of MCPB acid (5×10^{-2} M in $CHCl_3$, 500 µL); **TATP**: **M5-NZ31** in the presence of 25 mg of solid TATP for 1 hour at 63 °C in a Teflon vial and then addition of HEPES pH = 8, 500 µL; **H_2O_2**: addition of H_2O_2 30% (500 µL); *left*: under white light; *right*: under a UV lamp, 366 nm.

Subsequently, the ability of the membrane **M5-NZ31** to detect minute amounts of solid TATP by submitting the membrane to different amounts of TATP in similar conditions to previous experiment was tested with the aim to find the detection limit of the method. The experiment consisted of charging a Teflon vial (13 mL) with TATP at the bottom of the vial and a small square of the membrane at the top of the vial, the vial was then sealed and slowly heated until 45-50 ºC for 1 to 1.5 hours to homogenize the temperature inside the vial (Figure 14). After that, the vial was cooled to room temperature, opened and the membrane was measured in the spectrofluorometer and then registered a photograph in every case, because the polymer piece adquiered strong orange fluorescence and pink colour. The TATP sublimed in the Teflon tube was observed, so it was found crystallized along the inside wall of the vial.

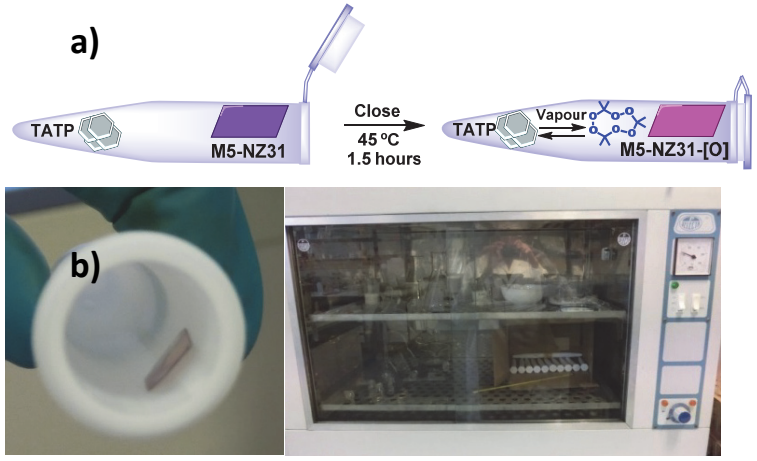

Figure 14. a) Scheme of the experiment of solvent-free detection of TATP. b) Sublimation experiment of **M5-NZ31** and TATP in the heating oven.

A comparison of the qualitative effect of increasing amounts of TATP on the membranes (Figure 15) and the quantitative titration is shown in Figure 16. Exposing the film to increasing amounts of solid TATP afforded clear pink colour and fluorescence changes, thus the colour change could be appreciated by the naked eye. The increase in the fluorescence was more intense, so it could be followed under the UV light of 366 nm. The brightness of the fluorescence under the UV light resulted to be proportional to the amount of TATP, likewise which could be appreciated by the naked eye. The effect was cumulative in respect of different expositions of the film to TATP amounts giving the signal of a single exposition to the sum of TATP amounts.

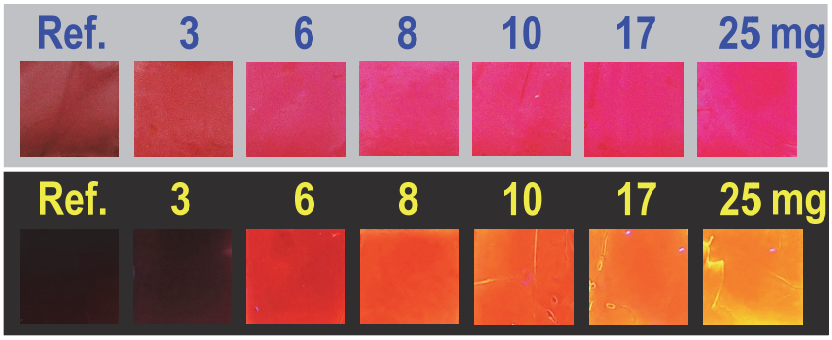

Figure 15. The qualitative effect of exposing the **M5-NZ31** membrane to increasing amounts of TATP vapour (A) under white light and (B) under UV light (366 nm).

Quantitative measurements of the fluorescence of the membrane in the fluorometer clearly confirmed that the resulting fluorescence was a function of the amount of TATP to which it was exposed in the experiment. Also, but in a lesser extension, the colour change

increased with the amount of TATP. In that case, from the UV-Vis spectra we noticed that in addition to the initial absorbance band at 487 nm, a new absorption band at 525 nm appeared in the film when exposed to increasing amounts of TATP. From the fluorescence spectra of the films exposed to solid TATP, the appearance of an emission band at 574 nm that increased as a function of the amount of TATP was noticed. The titration spectra at 574 nm could be fitted to a straight line from which the detection limit was calculated to be the exposition to 3 mg of solid TATP under these conditions (Figure 16).

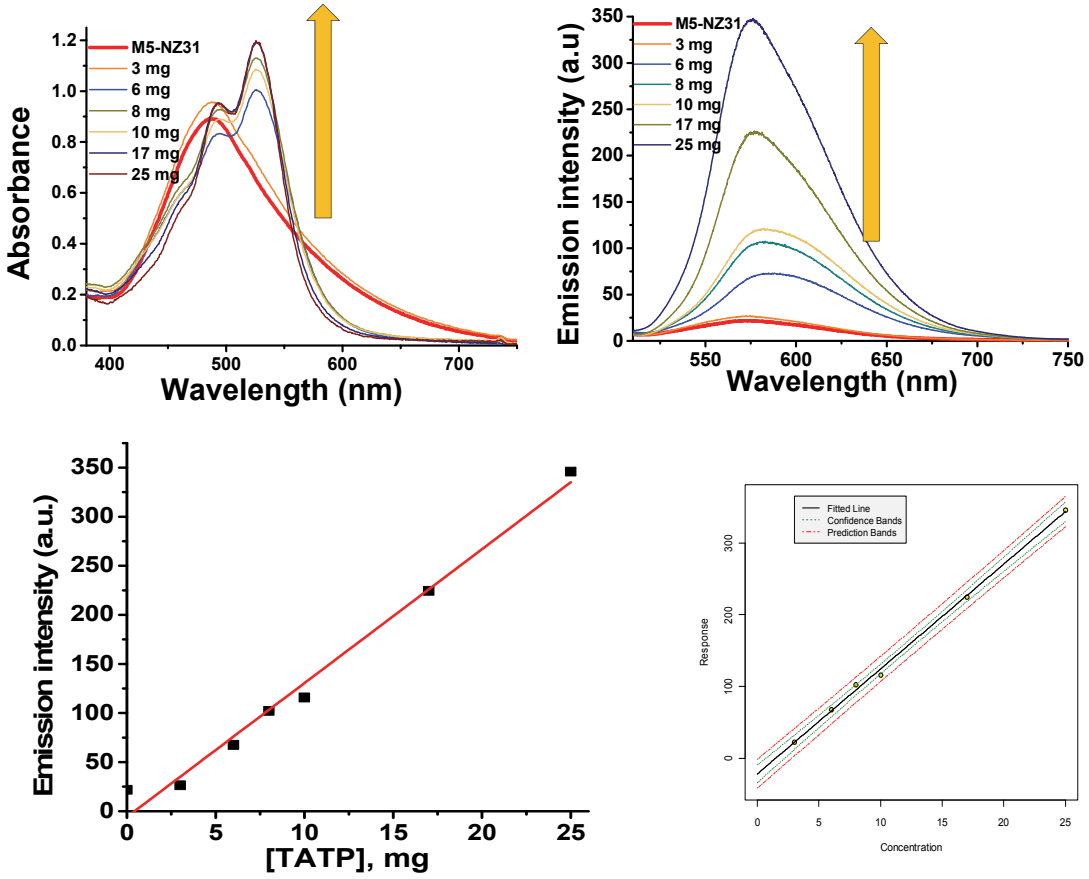

Figure 16. ***Upper***. UV-Vis and fluorescence titration curves obtained by exposing the **M5-NZ31** membrane to increasing amounts of TATP vapour. ***Lower. Left*** Fluorescence titration plot of **M5-NZ31** and TATP vapour. ***Right***. Fitted line, confidence and prediction bands for the fluorescent titration plot of **M5-NZ31** and TATP in the gas phase for LOD determination.

5.4. Quantitative titrations and kinetics of NZ29 with MCPB, oxone and H2O2.

To corroborate the oxidant response of **NZ29** and **M5-NZ31** with TATP, several kinetic and titration experiments were realized with three different oxidants: oxone, MCPB acid, H_2O_2. The titrations with oxone in solution were performed with sixteen solutions of **NZ29** (5 μM) in $CHCl_3$:MeOH 9:1. Then, the concentration of oxone was adjusted from 0 – 1.74 mM in every solution, being an excitation wavelength: 515 nm. The spectra were registered 15 seconds after the addition at 25 ºC. Moreover, the limit of detection for oxone was 31 μM, or 0.01 mg/mL (10 mg/l) within 15 seconds measurements (Figure 17).

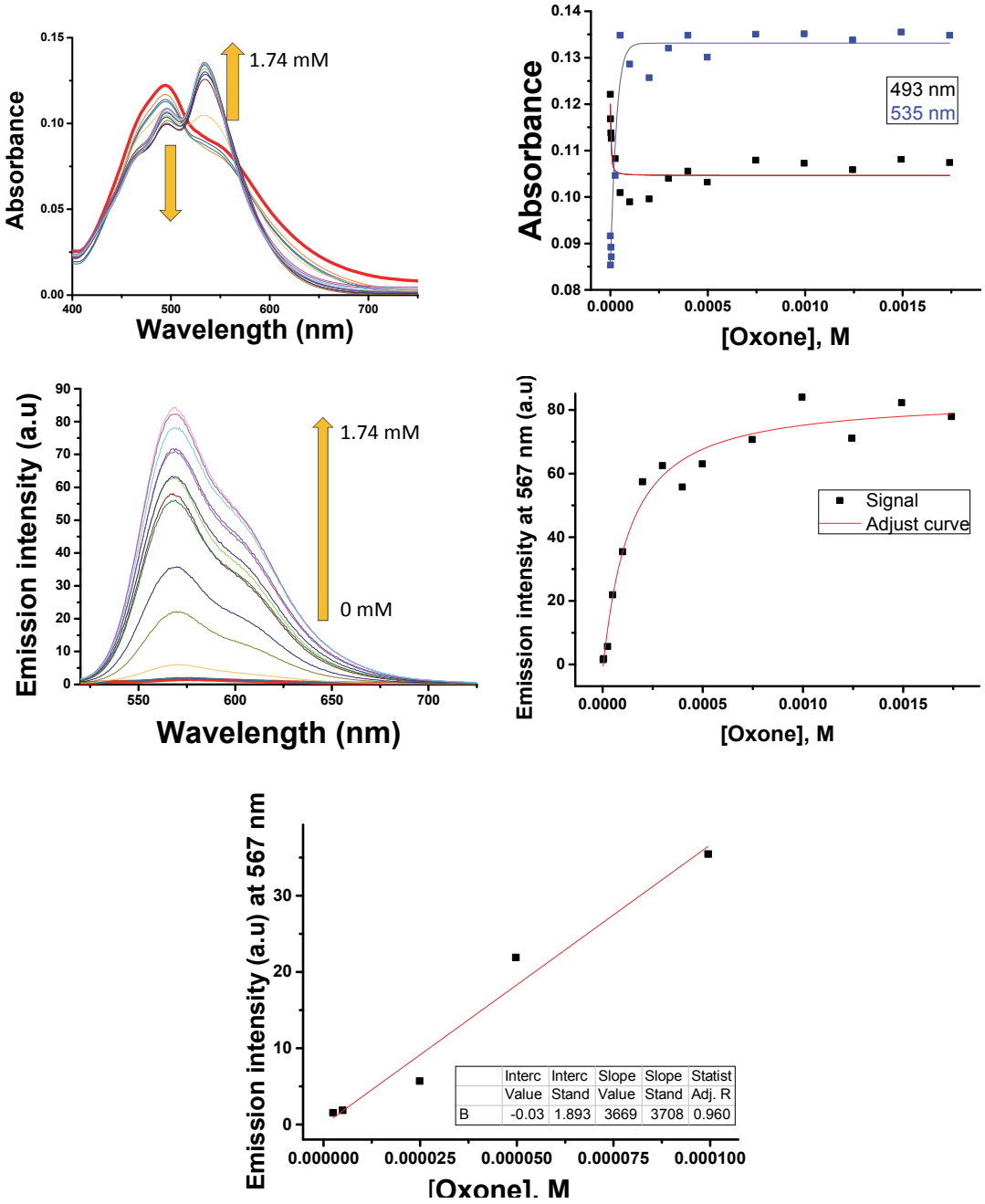

Figure 17. ***Upper graphics. Left.*** UV-Vis titration spectra of **NZ29** and oxone in $CHCl_3$:MeOH 9:1 v/v, 5 μM **NZ29** after 15 seconds. ***Right.*** UV-Vis titration plot of **NZ29** and oxone in $CHCl_3$:MeOH 9:1 v/v, 5 μM **NZ29** after 15 seconds at 493 nm and 535 nm. ***Upper-medium graphics. Left.*** Fluorescence titration spectra of **NZ29** and oxone in $CHCl_3$:MeOH 9:1 v/v, 5 μM **NZ29** after 15 seconds, λ_{exc} = 515 nm. ***Right.*** Fluorescence titration plot of **NZ29** and oxone in $CHCl_3$:MeOH 9:1 v/v, 5 μM **NZ29** after 15 seconds. ***Lower graphics***. Fluorescence titration plot of **NZ29** and oxone in $CHCl_3$:MeOH 9:1 v/v, 5 μM **NZ29**, after 15 seconds for LOD determination.

A kinetic study of **NZ29** and oxone in solution was executed. Two solutions of **NZ29** (50 μM) in $CHCl_3$:MeOH 9:1 v/v were prepared. A solution of oxone was added over each one of them to reach a molar proportion of 1:2 and 1:10, respectively (Figure 18.).

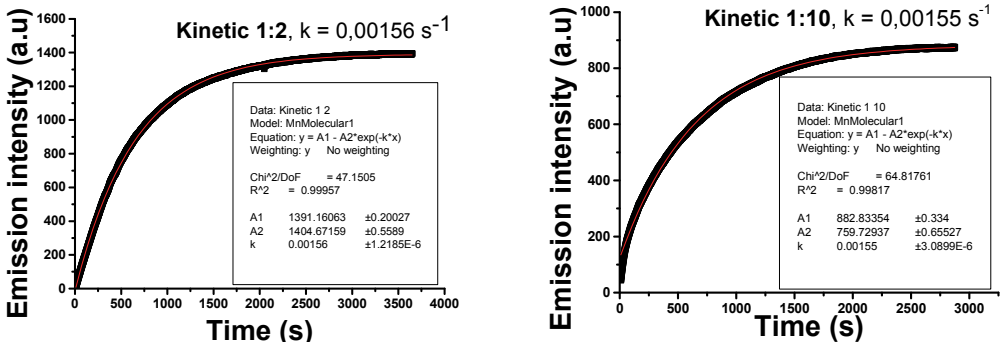

Figure 18. Kinetics experiments of **NZ29** with oxone.

The titrations with MCPB in solution were performed with 18 solutions of **NZ29** (5 μM) in $CHCl_3$:MeOH 9:1. The concentration of MCPB was adjusted from 0.05 to 50 equivalents in the titration, the excitation wavelength was 518 nm. The spectra were registered 15 seconds after the addition and then after 2 hours, in order to study the changes on time at 25 ºC. The limit of detection for MCPB was 2×10^{-4} M, or 0.017 mg/mL (170 mg/L) within 15 seconds (Figure 19.).

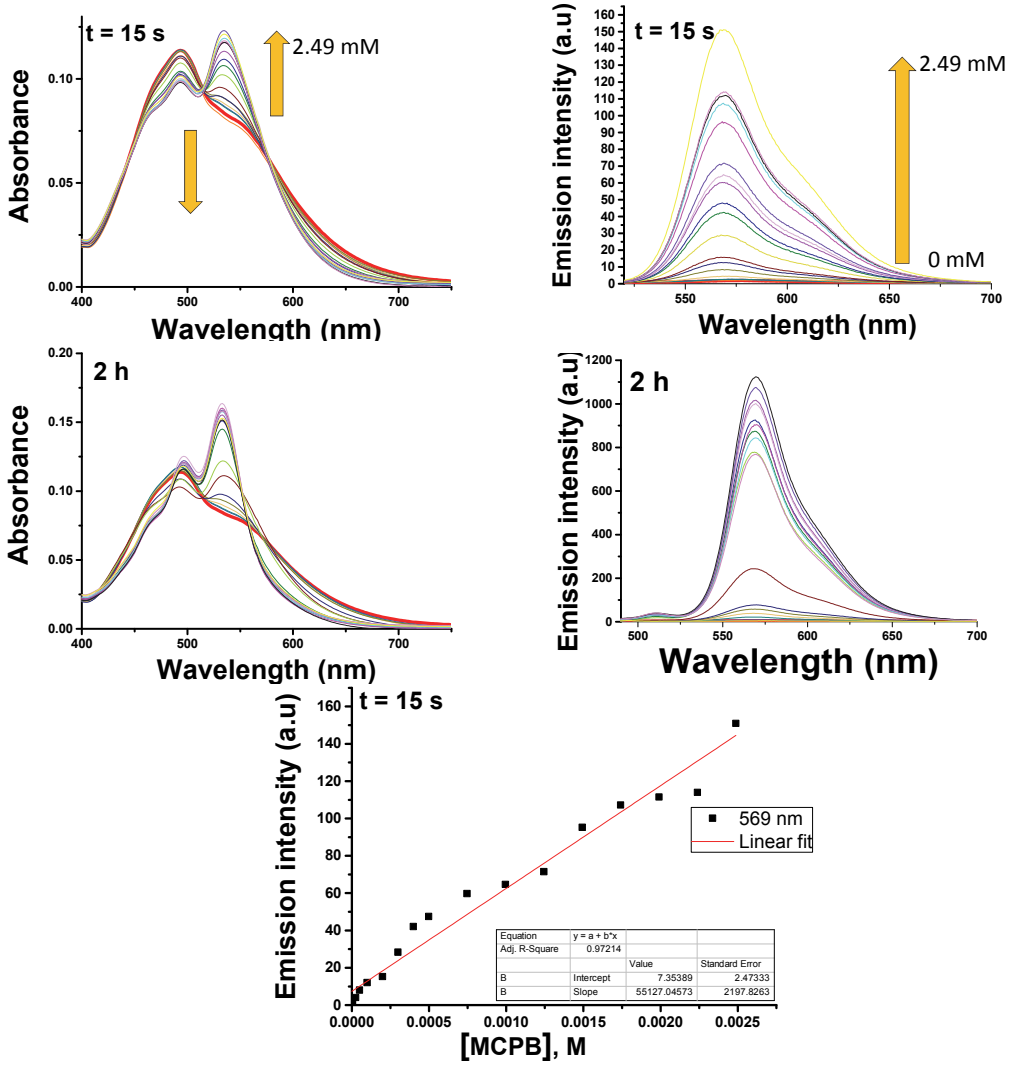

Figure 19. ***Upper Left.*** UV-Vis titration spectra of **NZ29** and MCPB in $CHCl_3$:MeOH 9:1 v/v, 5 μM **NZ29** after 15 seconds. ***Right.*** UV-Vis titration plot of **NZ29** and MCPB in $CHCl_3$:MeOH 9:1 v/v, 5 μM **NZ29** after 15 seconds at 493 nm and 535 nm. ***Medium Left.*** Fluorescence titration spectra of **NZ29** and MCPB in $CHCl_3$:MeOH 9:1 v/v, 5 μM **NZ29** after 15 seconds, λ_{exc} = 515 nm. ***Right graphics.*** Fluorescence titration plot of **NZ29** and MCPB in $CHCl_3$:MeOH 9:1 v/v, 5 μM **NZ29** after 15 seconds. ***Lower.*** Fluorescence LOD determination of **NZ29** and MCPB in $CHCl_3$:MeOH 9:1 v/v, 5 μM **NZ29**, after 15 seconds.

By comparison of the response of **NZ29** vs TATP with the response of **NZ29** with oxone and MCPB and H_2O_2, we noticed that the response was faster for oxone and MCPB and slower for H_2O_2 (Figure 21.lower graphics). The titration curves in fluorescence were of the same type, but the differences in absorbance titration curves of **NZ29** permitted discrimination between TATP and the rest of oxidants, as demonstrated in the Figure 17 for oxone and in the Figure 19 for MCPB.

In this way, the same study was established to **M5-NZ31**. Fifteen pieces of membrane **M5-NZ31** (1×1 cm) were submerged in solutions of MCPB of increasing concentrations from 0.01 to 70 mM, in $CHCl_3$:MeOH 7:3 (2 mL) for 30 minutes and then the UV-Visible and fluorescent spectra was registered (Figure 20).

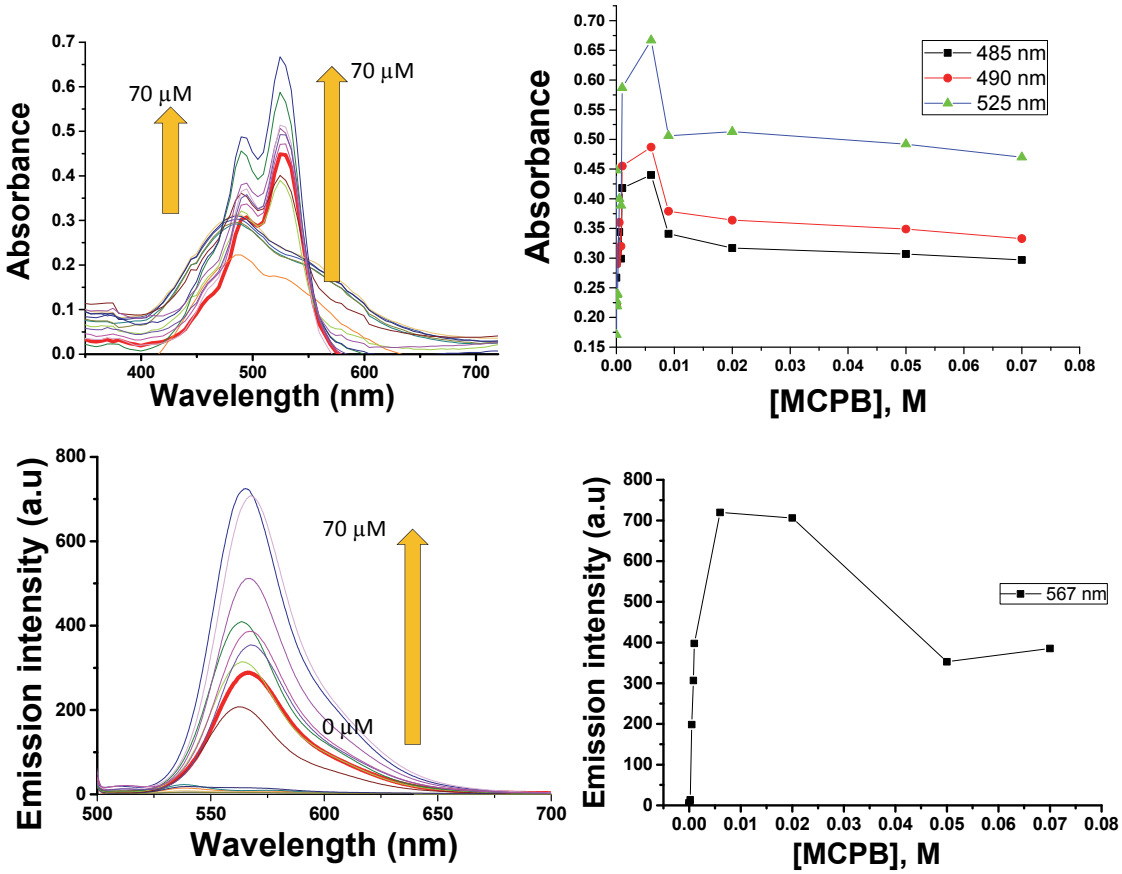

Figure 20. ***Upper graphics.*** UV-Vis titration spectra of **M5-NZ31** and MCPB in solution (left) and titration plots of **M5-NZ31** MCPB in solution at 485, 490 and 525 nm (right). ***Lower graphics.*** Fluorescence titration spectra of **M5-NZ31** and MCPB in solution (left) and titration plot of **M5-NZ31** and MCPB in solution (right), λ_{exc} = 492 nm, λ_{em} = 567 nm.

A kinetic study of **M5-NZ31** in the presence of MCPB and H_2O_2 in solution was carried out. The conditions of the measurements were 3×10^{-3} M of MCPB in $CHCl_3$:MeOH 7:3 v/v for 1.5 hours or aqueous H_2O_2 30 % for 9 hours. The excitation wavelength was 485 or 487 nm and the temperature was 25 ºC. On one hand, the membrane was submerged in a solution of MCPB 3 mM in $CHCl_3$:MeOH 7:3 v/v for 1.5 hours, being the excitation wavelength 485 nm. On the other hand, the membrane was submerged in an aqueous solution of H_2O_2 30 % w/v for 9 hours, being the excitation wavelength 487 nm and the emission wavelength 575 nm (Figure 21).

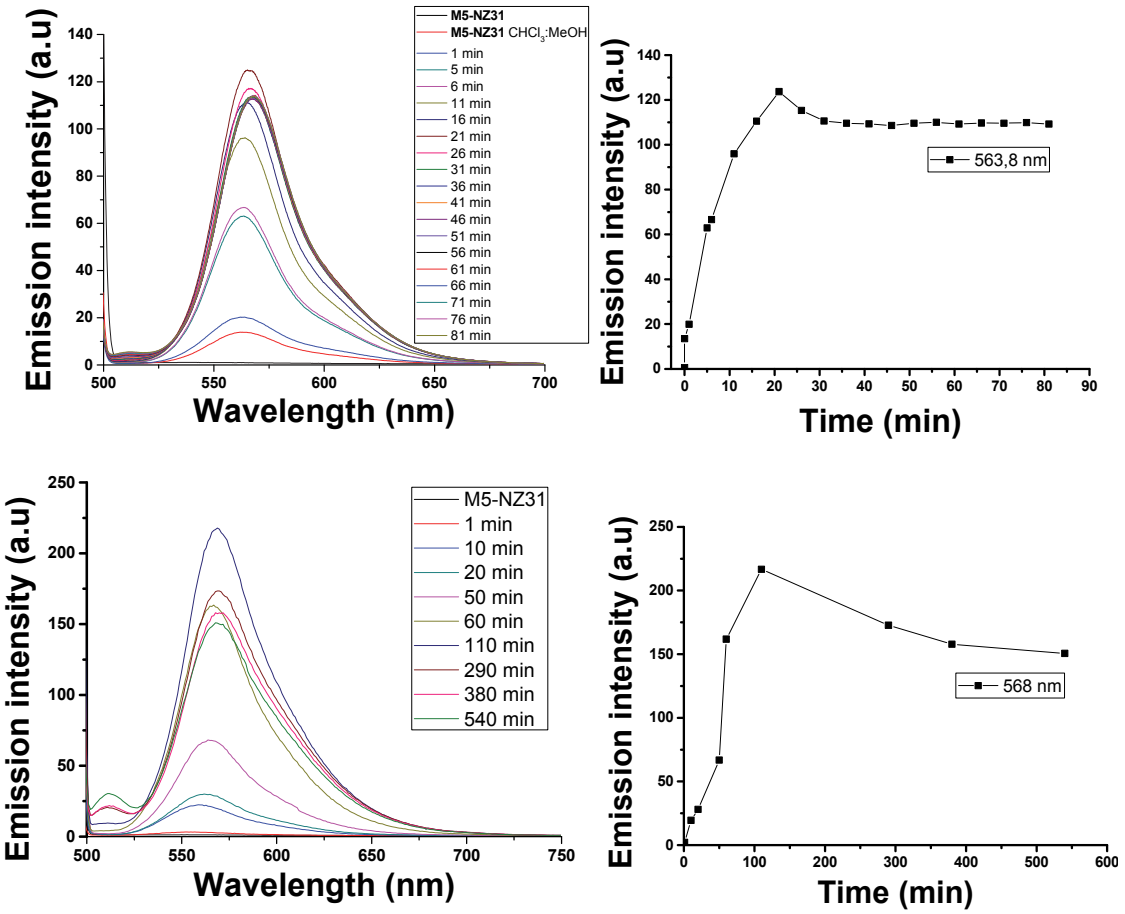

Figure 21. ***Upper graphics.*** Fluorescence spectra corresponding to the kinetic experiment of **M5-NZ31** and MCPB in solution, λ_{exc} = 485 nm, λ_{em} = 567 nm. ***Lower graphics.*** Fluorescence spectra corresponding to the kinetic experiment of **M5-NZ31** and H_2O_2 in solution, λ_{exc} = 485 nm, λ_{em} = 568 nm.

In this case, the film reached a maximum of the fluorescent emission at 568 nm after 110 minutes and then slowly decreased until a constant value. The results confirmed an oxidative process of the film by the oxidants, with related titration curves in absorbance and fluorescence, albeit the titration plots are different in each case, depending on the oxidative power of every reagent, and the physical state, gas phase or dissolved, and the organic or aqueous solvent used in the experiments. From these experiments, we concluded that the mechanism of detection of TATP in the gas phase by the membrane was similar to the observed in solution, apparently by oxidation of the colorant.

5.5. The oxidation mechanism and DFT calculations to support it.

After **M5-NZ31** was exposed to TATP vapour, a 1.7 % increase in the oxygen content of the polymer, measured by energy-dispersive X-ray spectroscopy (EDS) on SEM (see synthesis and characterization section), would be compatible with the oxidation of the piperazine nitrogen of the PDI, hence triggering the fluorescent response (Scheme 7).

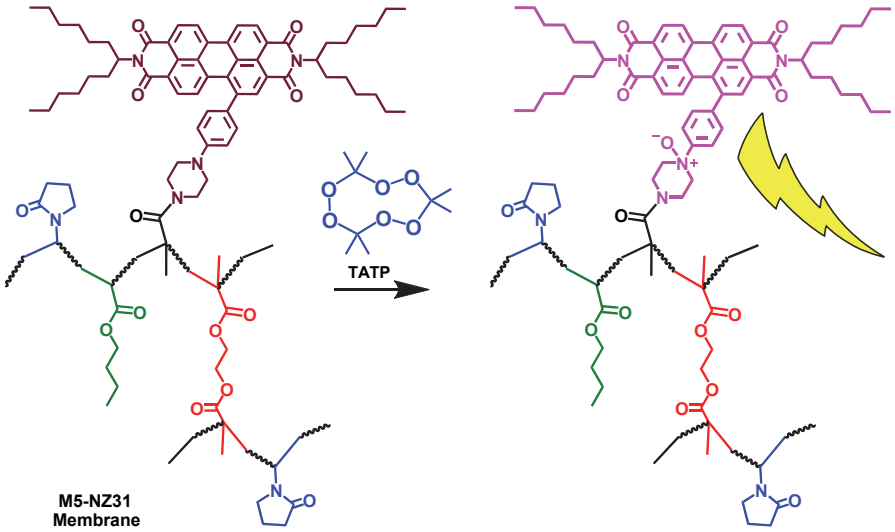

Scheme 7. Proposed mechanism for the oxidation of the polymer sensor in the presence of TATP.

To confirm the proposed mechanism in Scheme 7, DFT calculations of a unsubstituted 1-[p-(piperazin-*N*-yl)phenyl]-3,4,9,10-perylenetetracarboxy diimide **NZ31**-model compound and the corresponding *N*-oxide were performed. The HOMO of the model compound showed an extended orbital system including the bay aniline group and the perylenediimide core whilst the HOMO of the *N*-oxide showed an orbital system centred on the N-oxide moiety (Figure 22). In both cases, the LUMO was centred only on the perylene core. Therefore, *N*-oxidation of **NZ31** interrupts the initial conjugation between the perylenediimide core and the bay aniline group, so the original fluorescence of the perylenediimide core is restored.

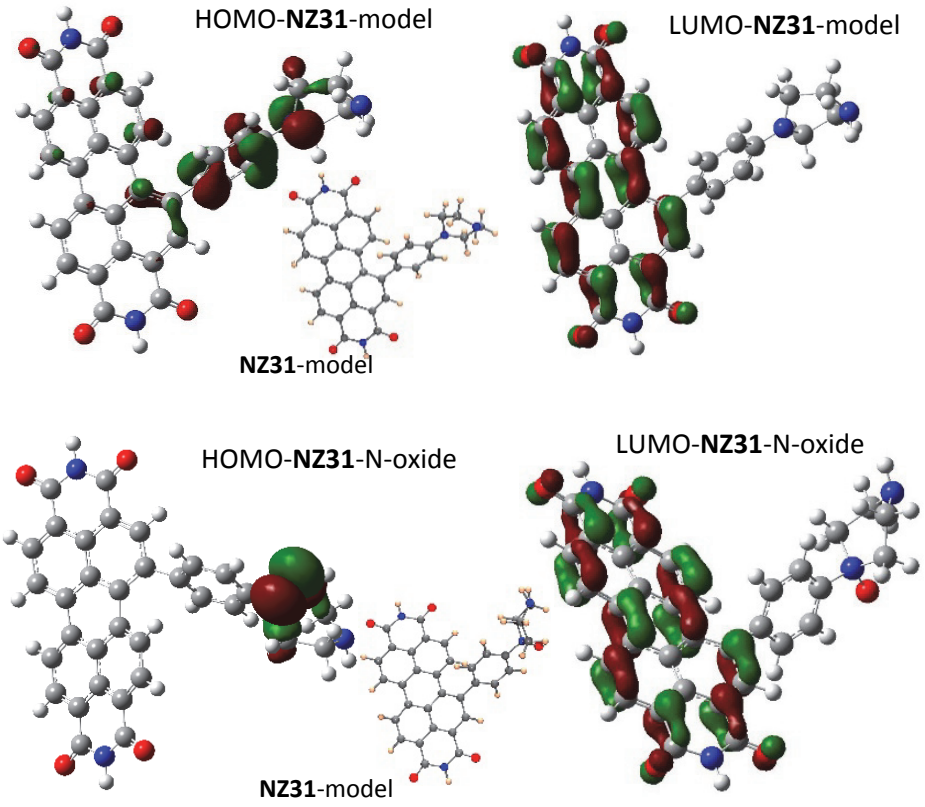

Figure 22. DFT calculations on model compounds **NZ31** and **NZ31**-N-oxide.

The quenching of the fluorescence in substituted PDIs, in which electron-rich aryl groups are bounded to the perylene core, was already observed,[46] and this behaviour should have an electronic explanation. The LUMO has a very similar shape in both compounds and it is spread over the perylene core displaying a π^* nature. In compound **NZ31**, the HOMO is mainly centred on the phenyl substituent on the bay region with π^* interaction with the nitrogen atom of the piperazine fragment and small contribution of the perylene core. In the product of N-oxidation the HOMO does not display any participation of the perylene core and is localized on the piperazine N-oxide group in which the oxygen atom establishes a π^* interaction with the nitrogen atom. Apparently, *N*-oxidation of **NZ31** interferes the photoinduced electron transfer between the bay phenylpiperazine group and the perylenediimide core, so the original fluorescence of the perylenediimide core is restored. This fact should explain the different luminescent behaviour observed in compound **NZ31** and its oxidation product. On the other hand, to confirm the oxidation of the probe, a small sample of **NZ29** to reaction with excess TATP in dichloromethane at room temperature for 1 hour was subjected. Later, the residue was sent to MALDI-TOF mass spectrometry, from which a peak at m/z 1030, corresponding to the N-oxide of **NZ29**, was clearly seen.

[46] a) W. Qiu, S. Chen, X. Sun, Y. Liu, D. Zhu, *Org. Lett.,* **2006**, *8*, 867–870; b) S. Nakazono, S. Easwaramoorthi, D. Kim, H. Shinokubo, A. Osuka, *Org. Lett.* **2009**, *11*, 5426–5429; c) C-C. Chao, M. Leung, Y. O. Su, K-Y. Chiu, T-H. Lin, S.-J. Shieh, S-C. Lin, *J. Org. Chem.,* **2005**, *70*, 4323–4331.

5.6. TATP detection with a chemosensor anchored to silica support.

From the possible chemosensors summarized in the scheme 2 and Scheme 3, the behaviour with respect to different oxidants was studied. A qualitative test with TATP was carried out to get the best probe and solvent. Then, the selection of work concentration, the qualitative and quantitative study for the oxidant TATP was performed.

5.6.1. Qualitative study for TATP and solvent selection.

The best mixture for the study is $CHCl_3$:MeOH 9:1. A study with TATP is given in Figure 23.

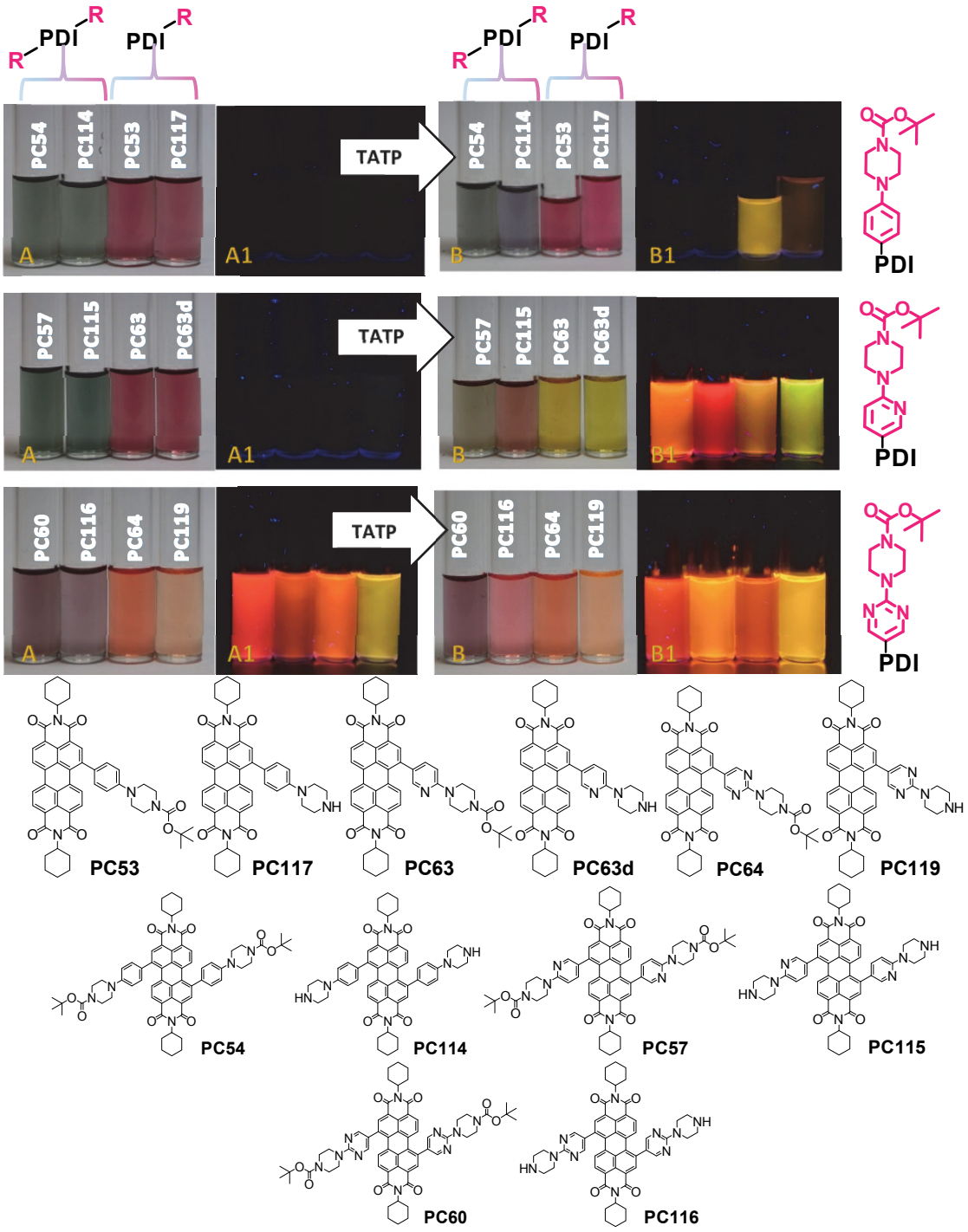

Figure 23. 10 mg of TATP were added to possible probes (50 μM, in $CHCl_3$:MeOH 9:1 v/v), whose lateral groups are described on the right. Photos **A** and **A1** are done under white light and photos **B** and **B1** are done under 366 nm light. Structures are given below.

$CHCl_3$ is an adequate solvent due to its moderate boiling point and proper solubility for all solvents and MeOH meets the requirements of solubilisation of peroxides compounds with 10 % is an acceptable proportion. The idea was to select a pair of compounds with the same lateral groups, protected and deprotected, which exhibited an OFF-ON luminescence process. The OFF-ON process is more selective to the desired product than the ON-OFF due to discard the fluorescence deactivation by substances or elements present in the media. Therefore, the discussion was reduced to **PC63**-**PC63d**. Based on the same behaviour; **PC57**-**PC115** was excluded because the luminescence interpretation will be more complicated because these compounds have two branches, so two oxidizable groups. The compound **PC63**-**PC63d** was suitable to be anchored to silica, consequently it was subjected to further study.

5.6.2. Selection of work concentration.

With the intention of choosing an optimum concentration for the quantitative studio, **PC63** absorbance was checked to be linear while concentration changes are small, so seven solutions were prepared in $CHCl_3$:MeOH 9:1 v/v at 25 ^oC. The fluorescence was not registered due to the value was near to the ground and the chosen working concentration was 2.5 µM, based on the absorbance (Figure 24).

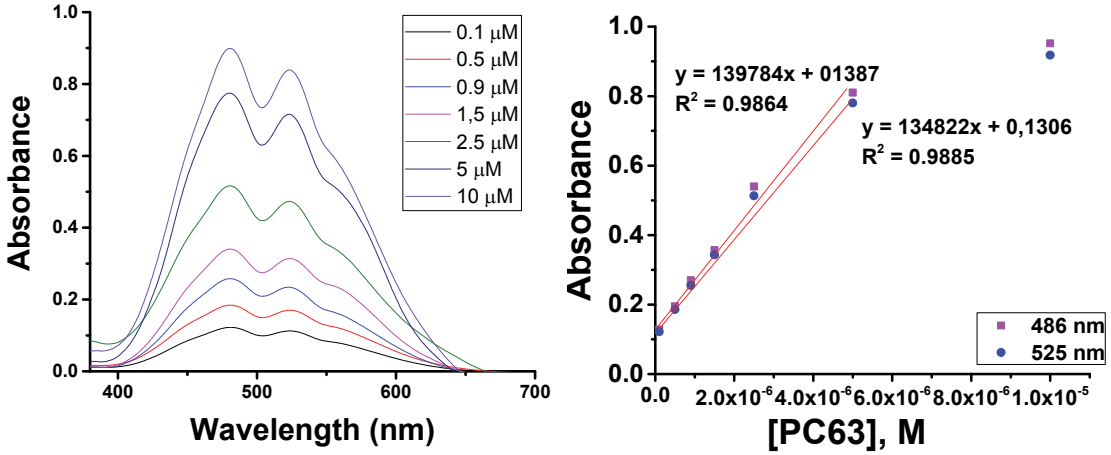

Figure 24. UV-Vis spectra of **PC63** in $CHCl_3$:MeOH 9:1 v/v at some concentrations.

5.6.3. Qualitative and quantitative study for acids and oxidants.

Hydrochloric acid and hydrogen peroxide are the mainly compounds that are used as the starting materials of the TATP formation. Therefore, a qualitative and quantitative study of **PC63** versus the oxidants and acids is required. The Figure 25 shows how the quantity of hydrochloric acid and different oxidants affect to the luminescence of the probe **PC63**. This compound is able to draw a distinction among acids and oxidants. Several oxidants present certain acid character, such as methachloroperbozoic acid (MCPB) and oxone, so HEPES buffer was introduced to eliminate this parameter. After addition the HEPES buffer, the luminescence of **PC63** generated by adding acids was deactivated, therefore, it could be attributable to an acid-base process. Whereas, the luminescence created by the oxidants was maintained even after treatment with the buffer, so it is not an acid-base reaction.

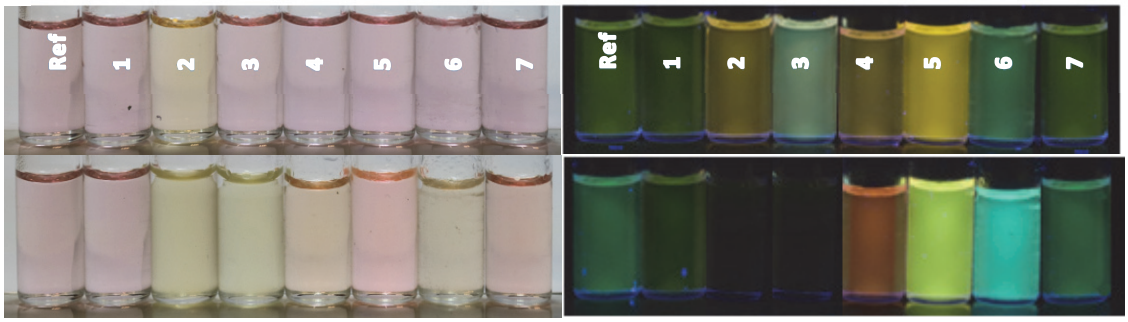

Figure 25. 500 µL solutions of **PC63** were prepared in $CHCl_3$:MeOH 9:1 v/v, 10^{-5} M, left: under white light and right: under 366 nm light. Upper row: **PC63** in the presence of 1. 10 µL of HEPES (0.5 M in water), 2. HCl (0.1 M in water), 3. HCl (0.01 M in water), 4. TATP (0.2 M in $CHCl_3$), 5. MCPB (0.2 M in $CHCl_3$), 6. oxone (0.2 M in water) and 7. H_2O_2 (0.89 M, 30 % v/v). Lower row: **PC63** in the presence of 1, 2, 3, 4, 5, 6, 7 adding 10 µL of HEPES (pH = 8).

The luminescence of **PC63** in the presence of MCPB, oxone and TATP showed changes. Two quantitative titrations with TATP and MCPB, used as reference of classic oxidant, were performed. Point to point quantitative titrations of **PC63** were accomplished (Figure 26), in order to perceive the response of **PC63** with TATP, dissolved in $CHCl_3$:MeOH 9:1 v/v, 2.5 µM at 25 °C. The limit of detection (LOD) was 4.8 mM or 2.1 mg in a 2.5 ml solution.

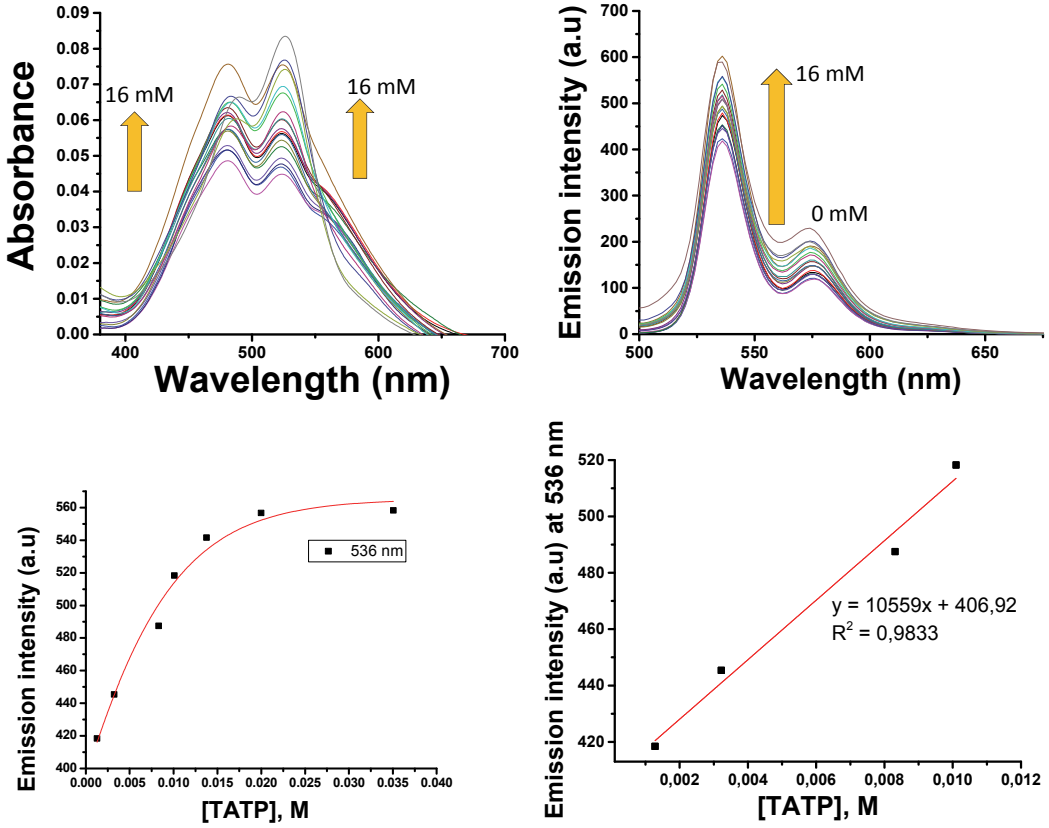

Figure 26. ***Upper graphics.*** UV-Vis and fluorescence titration spectra of **PC63** and TATP in solution λ_{exc} = 484 nm, λ_{em} = 536 and 580 nm. ***Lower graphics.*** Left: Fluorescence titration plot of **PC63** and TATP in solution. Right: Fluorescence titration plot of **PC63** and TATP in solution for determination limit of detection.

Quantum yield (QY) was determined by its general equation (explained in the introduction of the thesis). This parameter allow to know how to vary the luminescence in the presence of

TATP. The process was repeated three times to obtain the media and a confidence interval, keeping in mind that the error associated to the method is usually 1 %.

- Φ PC63 ($CHCl_3$) = 0.27 ± 0.01
- Φ PC63 + TATP ($CHCl_3$) = 0.36 ± 0.01

The quantum yield of **PC63** with TATP is higher than in its absence. In other words, the solutions of **PC63** with TATP in chloroform are around 33% brighter than **PC63** in the same solvent.

In order to observe the absorbance and fluorescence tendency of **PC63** with MCPB dissolved in $CHCl_3$:MeOH 9:1 v/v, 2.5 µM at 25 ºC, a quantitative titration of **PC63** with MCPB was performed. The obtained limit of detection was 3.2 mM or 1.4 mg in a 2.5 ml solution. There are two fluorescent responses for the increase of methachloroperbenzoic acid concentration, between 3 mM to 32 mM the increase is at 557 nm, then the fluorescence increases at 501 nm, appearing a new band (Figure 27).

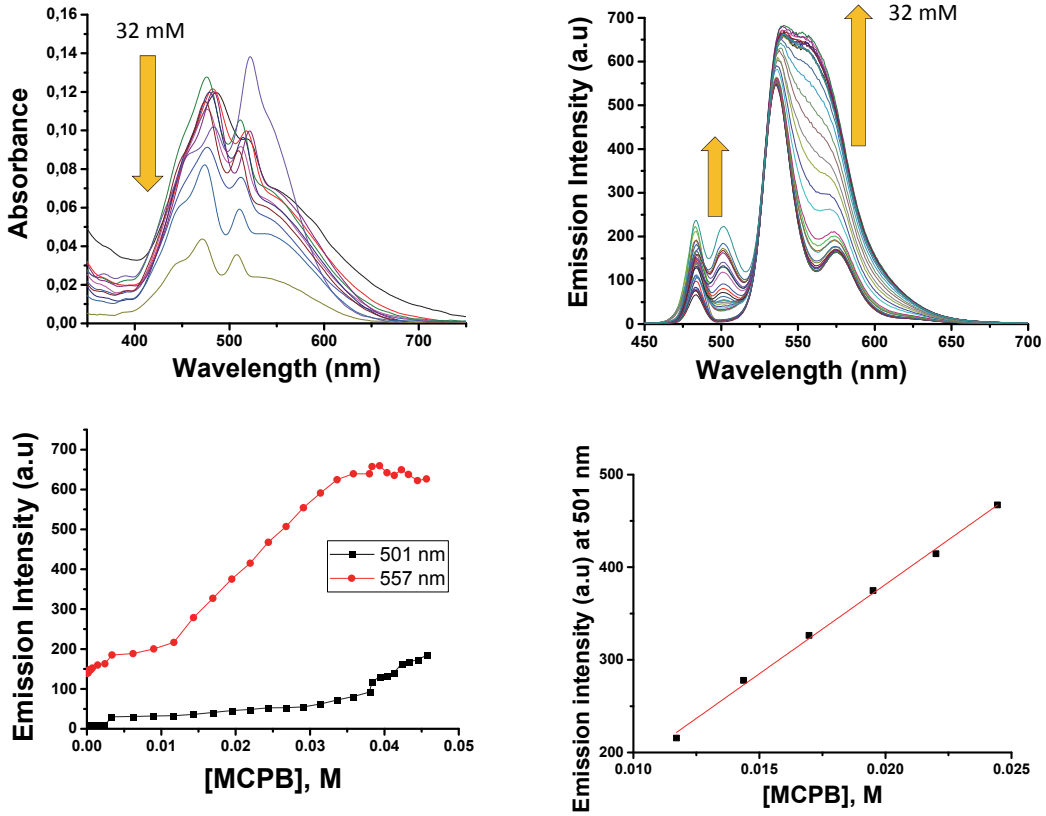

Figure 27. ***Upper graphics.*** UV-Vis and fluorescence titration spectra of **PC63** and MCPB in solution λ_{exc} = 485 nm, λ_{em} = 503 and 540 nm. ***Lower graphics.*** Left: Fluorescence titration plot of **PC63** and MCPB in solution and Right: Fluorescence titration plot of **PC63** and MCPB in solution for determination of the limit of detection.

The comparison between the UV-Vis and fluorescence titration spectra of **PC63** with TATP and with MCPB reveals several differences. In both UV-Vis and fluorescence titration spectrum of **PC63** with TATP or with MCPB, the bands increase when the TATP or MCPB concentration increases. However, the UV-Vis titration spectrum of **PC63** in the presence of MCPB decreases with increasing concentrations of MCPB, a behaviour different of the one showed for TATP. According to the fluorescence spectra, **PC63** in the presence of TATP exhibits two characteristic fluorescent bands: 536 and 580 nm but in the presence of MCPB appears a new

band at 503 nm, until a total of three bands. A higher amount of MCPB in comparison to TATP was necessary to reach the equilibrium. This fact could be due to the different nature of both oxidants, MCPB and TATP. Therefore, **PC63** is capable of distinguishing between two different oxidants. The limit of detection of TATP (4.8 mM) is higher than the LOD of MCPB (3.2 mM), as might be expected, because MCPB is better oxidant than TATP.

5.7. TATP detection with silica supported probes.

Two perylenediimides were used in this part; one of them was already done: **PC63** and the other one was prepared according to the achieved results: **PC63ds**. **PC63ds** was synthetized from **PC63d**, which reacted with an isocyanatopropylsilane to form a silane of carboxamide-PDI (Scheme 8). Thus, three kind of TATP detectors have been developed:

A: 4 mg of **PC63ds** were heated in toluene:water 500:10 µL with 500 mg of silica nanoparticles (silicon dioxide 10-20 nm) to obtain modified silica-probe called **nPC63ds**.

B: 0.5 mg of **PC63ds** were heated in toluene:water 500:10 µL with 5x10 cm layer silica gel 60 to obtain modified supported silica-probe called **pPC63ds**.

C: 0.5 mg of **PC63** were stirred in $CHCl_3$ with 5x10 cm layer silica gel 60 to obtain absorbed silica-probe, called **pPC63**.

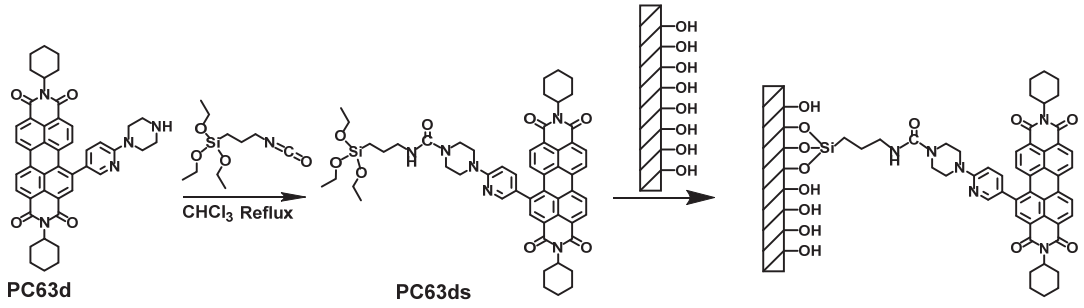

Scheme 8. Anchoring of the fluorogenic probe to silica.

The aspect of these materials and the thermogravimetric analysis (TGA) are shown in the Figure 28. The TGA of **nPC63ds** displays a loss of 6-7 % weight corresponding to the presence of organic matter, the PDI. Moreover, the silica nanoparticles were characterized by excitation and emission spectra (Figure 29).

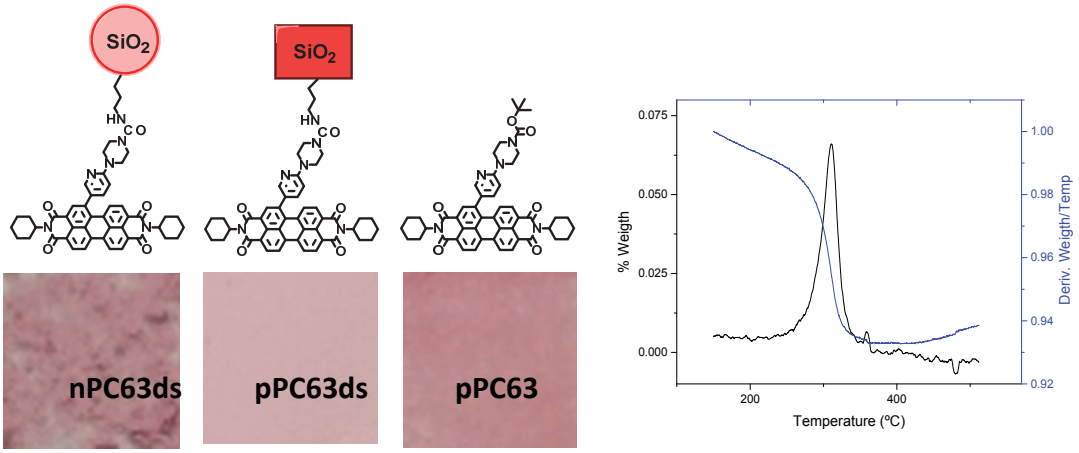

Figure 28. Left. Silica surfaces visual appearance. Right. TGA in N_2 of **nPC63ds**.

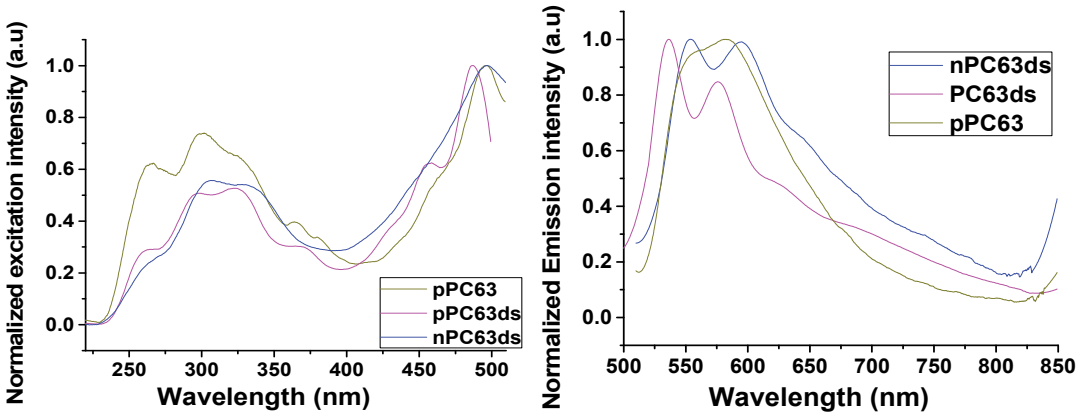

Figure 29. Emission and excitation spectra of the silica nanoparticles **nPC63ds**.

The relation probe-silica can be altered to obtain different results. The change is specially appreciated in the intensity of the colour and in the fluorescence. So, the optimum relation to show a clear increase in fluorescence was chosen. The changes in fluorescence were compared among different vapours put in the following order: Probe – TATP – HCl – H_2O_2.

The HCl sample increases the fluorescence in all cases, however, this process is different from the increase with TATP, as said before. After being under vapours of an amine, like Et_3N, the fluorescence of the HCl samples decrease again, but this process does not occur for TATP.

In order to measure the increase in fluorescence with TATP, the flux of N_2 was fixed to be 100 cm^3/min and the temperature in the TATP flask was controlled around 50 °C (Figure 30).

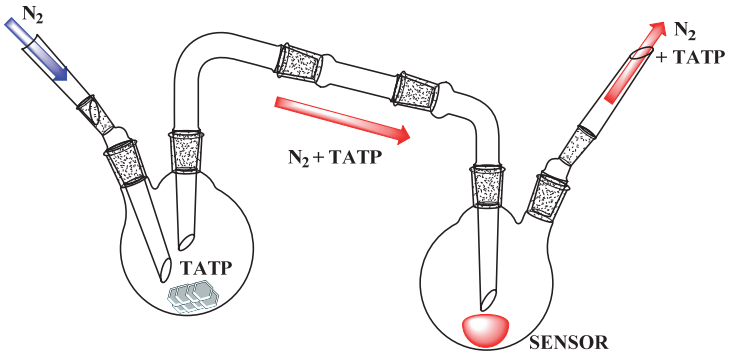

Figure 30. Schematic representation of the experimental procedure to detect TATP.

The changes were studied by three methods that give different information about the process occurred to the probe:

- C*ode of colours*. A qualitative detection of TATP presence in the environment comparing with the initial colour. It has to be taken into account that the colour and fluorescence depend on the amount of the probe that there is on the silica.
- The *excitation and fluorescence spectra* were normalized in order to obtain information from the position of the excitation and emission peaks.
- Measure of *Quantum Yield*. The fluorescence increase in solids was measured by calculation of the QY. The quantum yield depends on the quantity of the probe that is contained, however, the growth is depending on what is being measured, providing that the quantity of probe is not too high or too low.

5.7.1. Qualitative code of colours.

The colour could be distinguished better under UV light (366 nm), this allows us to differentiate among the samples and it is an example of the usefulness as fast TATP detector.

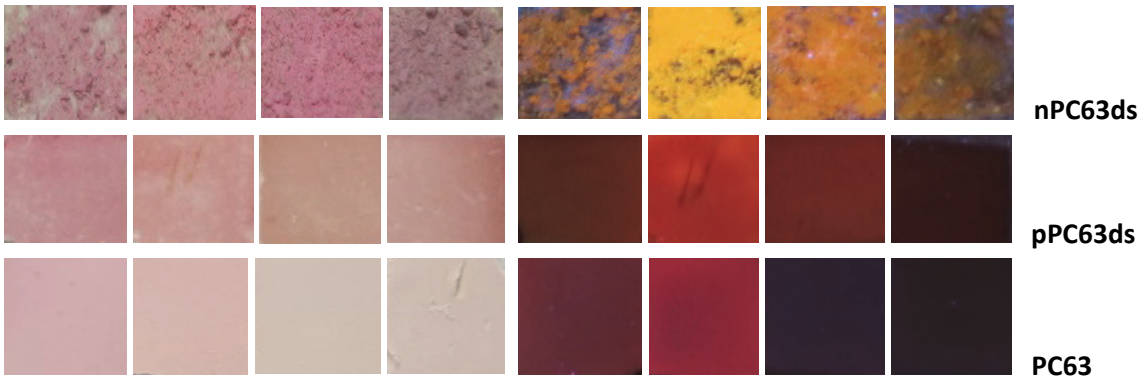

Figure 31. Photo under white light (left) and under light of 366 nm (right) of each silica-probe in the presence, from the left to the right, of **nothing**, TATP, HCl, H_2O_2. ***Upper row***: silica-probe→ **nPC63ds**. ***Medium Upper row*** silica-probe→ **pPC63ds.** ***Lower row***: silica-probe→ **PC63**.

The Figure 32 is a summary of colours of Figure 31 from RGB colour codes, in order to simplify the information. There is a change in colour for all the different samples. The colour became brighter for the TATP samples, due to an increase in fluorescence. The samples treated with HCl vapours experienced an increased fluorescence, but after being under amine vapours it is reduced until being similar to the initial. Whereas, H_2O_2 reduced the fluorescence to lower values than without anything (Figure 31). Then, this fact is very remarkable, since a major amount of detectors in the market is based on the hydrogen peroxide detection not in the TATP detection.

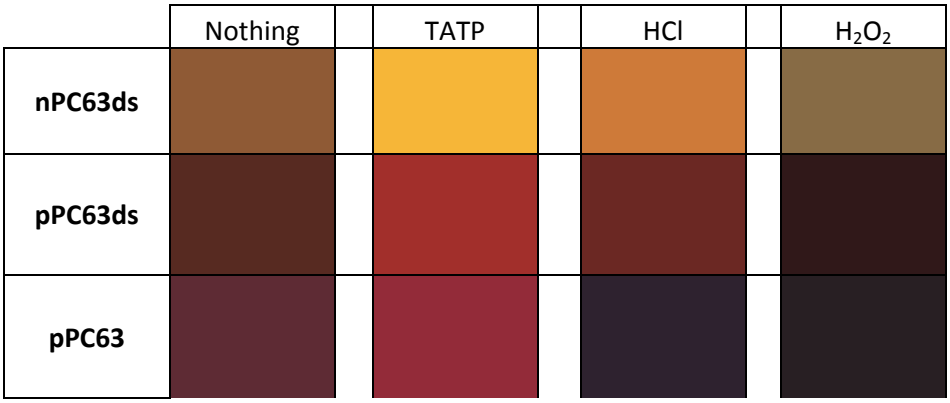

Figure 32. Colours of the different samples under light of 366 nm.

5.7.2. Qualitative study of excitation and emission spectra.

Herein, the excitation and emission spectra have been registered for each probe alone, for each probe in the presence of vapours of HCl and TATP. Moreover, the normalized excitation and emission spectra will be shown.

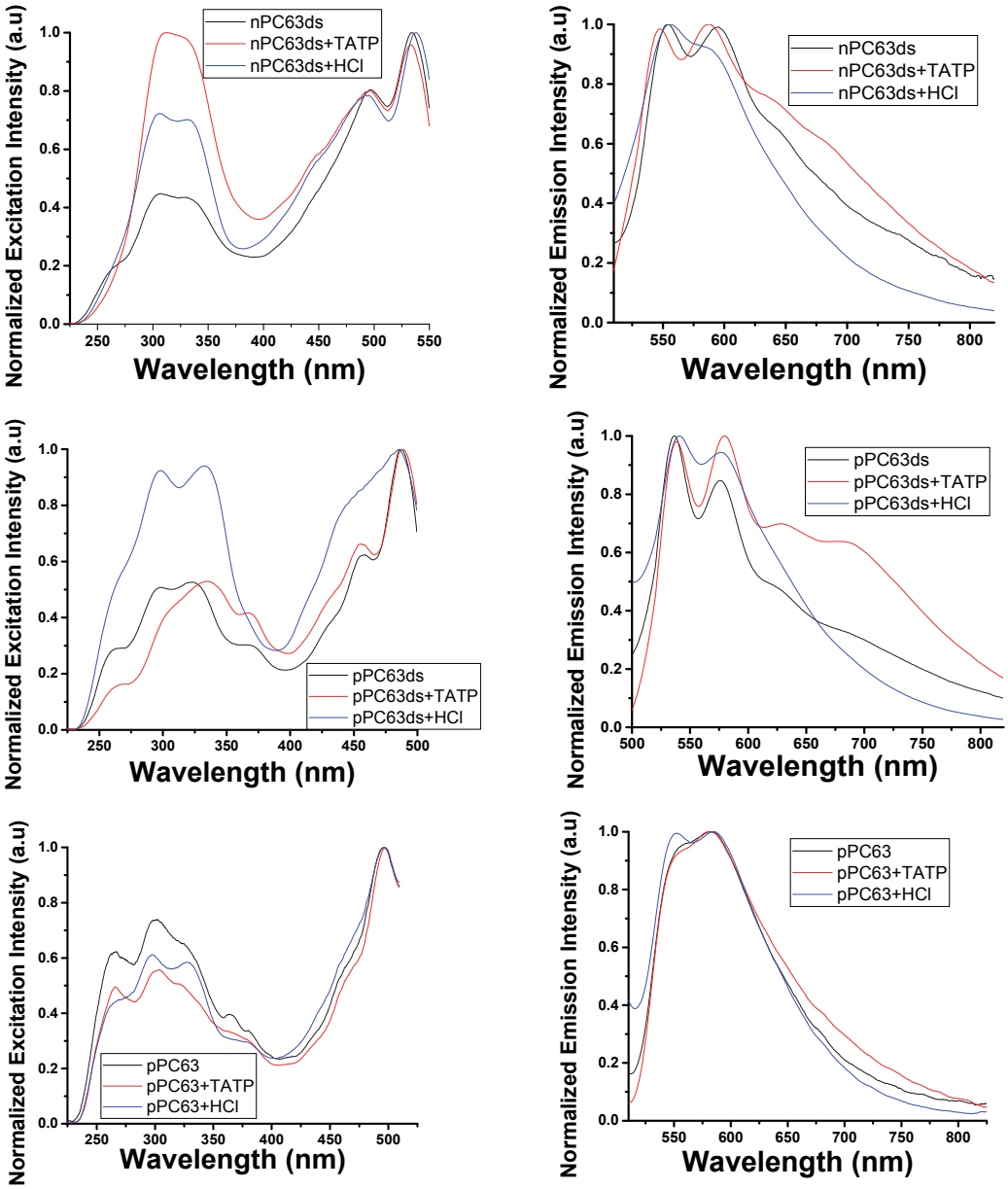

Figure 33. ***Upper graphics***. Response in excitation and fluorescence of **nPC63ds**. λexc = 495 nm, λem = 592 nm. ***Medium upper graphics***. Response in excitation and fluorescence of **pPC63ds**. λexc = 487 nm, λem = 533 nm. ***Lower graphics***. Response in excitation and fluorescence of **pPC63**. λexc = 496 nm, λem = 550 nm

These spectra allow to distinguish between hydrochloric acid and TATP in several ways. The probes **nPC63ds**, **pPC63ds** and **pPC63** increase their fluorescence at higher wavelengths only in the presence of TATP. Meanwhile, in **nPC63ds** and **pPC63ds** the excitation at lower wavelengths changes depending if it is TATP or HCl, around 320 nm whereas, **pPC63** have no significant changes.

5.7.3. Measurement of Quantum Yield.

The quantum yield was calculated by the integrated sphere methodology and the results are summarized in Table 4:

	Φ_{TATP}/Φ_0	Φ_{HCl}/Φ_0
nPC63ds	3,1	1,6
pPC63ds	3,5	1,6
pPC63	3,2	1,7

Table 4. Comparison of quantum yields of probes in the presence of TATP and HCl.

In all cases, the increase in fluorescence goes from 2 % to 4 % in the presence of TATP. The increase in fluorescence is between 3 to 3.5 times in all samples for TATP and around 1.7 times with HCl (Table 4).

6. CONCLUSIONS.

Four kinds of TATP detectors, split into two groups, have been synthetized successfully.

- A polymer group with one probe: **M5-NZ31**
- A silica group composed of three compounds: **nPC63ds**, **pPC63ds** and **pPC63**.

Therefore, some detection methods have been designed and developed to detect by fluorescence the oxidation of different probes in the presence of TATP. All of them are able to distinguish among different oxidants and acids, either by deactivation of fluorescence or by change of the fluorescent wavelength. Moreover, none of them detect hydrogen peroxide, one of the decomposition products of TATP. The detection system by both polymer and silicas is very fast, the measurements can be performed *in-situ* and a DFT calculation supports the hypothesis of TATP oxidation. The limit of detection of TATP with the polymer is around 1 mg in the air and the limit of detection with silica is lower than 4.8 mM. The Scheme 9 shows the behaviour of the probe in solution and the probe anchored to the polymer. There is a good correlation between the results obtained with the probe in solution and anchored to the polymer. Besides, **NZ29** is capable to recognize among the oxidants: MCPB acid and oxone from the TATP explosive. In the same way, **M5-NZ31** is able to distinguish between TATP and MCPB. In both states (solid and solution), the probes express a different behaviour in absorbance as well as in fluorescence.

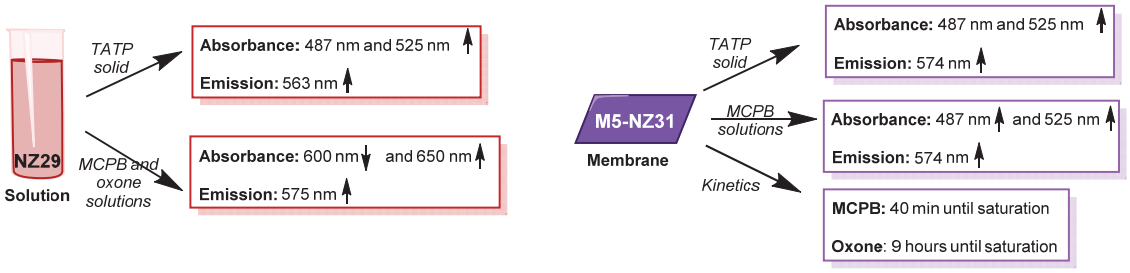

Scheme 9. UV-Vis and Fluorescence scheme of **NZ29** (in solution) and **M5-NZ31** (membrane) in the presence of TATP, MCPB, H_2O_2 and oxone.

The Scheme 10 shows the fluorescence of **nPC63ds**, **pPC63ds** and **PC63** in the presence of HCl, TATP and H_2O_2 and the behaviour of the oxidant after being in contact with amine vapours.

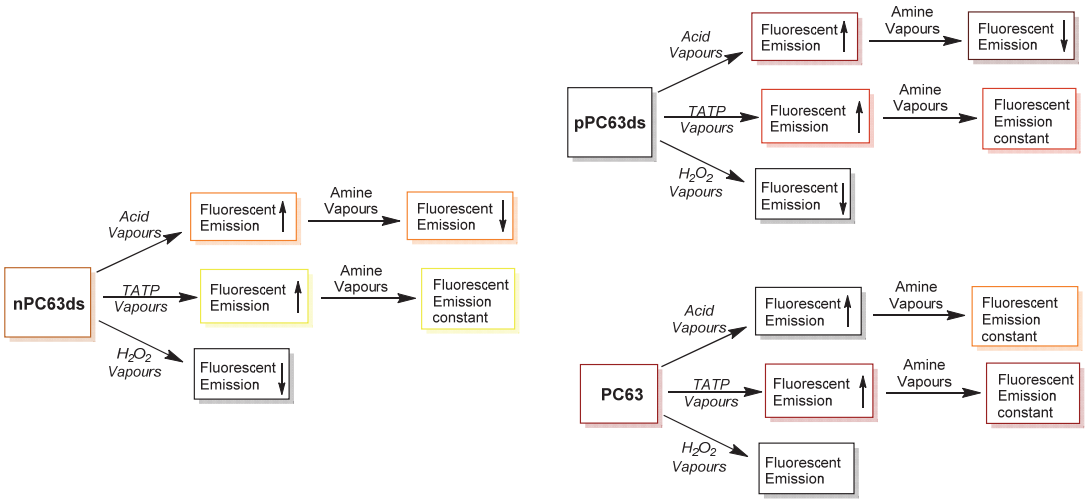

Scheme 10. Fluorescence scheme of three **silica-probes** in the presence of HCl, TATP and H_2O_2 vapours and their behaviour with amine vapours.

7. APPENDIX: FORMATION OF GOLD AND PALLADIUM NANOPARTICLES ON POLYMERS.

An unexpected application of the functionalized (with **PC117**) and non-functionalized films is the formation of gold and palladium nanoparticles; the size and the shape of nanoparticles are controlled by altering the composition of the polymer, with a possible application oriented to its use for catalysis. First of all, to consider that a particle is a nanoparticle the diameters must be between 1 to 100 nm.[47] Then, by the same process than in a previous publication of the research group,[48] the synthetized polymers for TATP detection, functionalized (**PC117**) or pristine, were studied so as to study the possibility of obtaining metal-modified polymers with new applications. Based on the many kinds of nanoparticles found in literature, numerous metal cations were tested. The salts of the different studied cations were: $HAuCl_4$, $AgClO_4$, $PdCl_2 \cdot 2NaCl$, $Co(BF_4)_2 \cdot 6H_2O$, $PtCl_2 \cdot 2NaCl$ and $Ni(ClO_4)_2 \cdot 6H_2O$ and their concentration was 5 mM in deionized water. However, only gold and palladium salts produced remarkable results. In the light of these results, six polymers were synthetized varying the co-monomers percentage, as it is indicated in Table 5. This table presents an overview of the components of each tested polymer showing the kind of nanoparticles that coat the film in the last two columns. It means that whereas gold nanoparticles were formed in all polymers, palladium nanoparticles were found as a cover in only some of them.

Films	% Co-monomers	% Cl	% PI*	% E**	$AuCl_3$	$PdCl_2$
P5	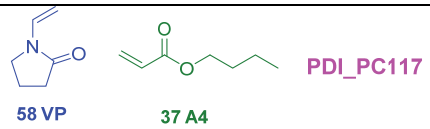		1.56 DMPA	5	Au	Pd, Cl
P10	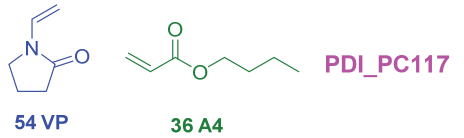		1.56 DMPA	5	Au	Pd, Cl
PB5	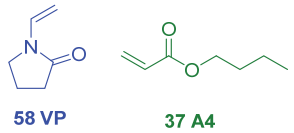		1.56 DMPA	5	Au	Pd
PB10	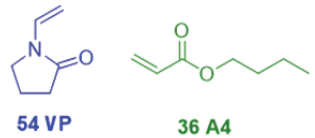		1.56 DMPA	5	Au	Pd
PB0	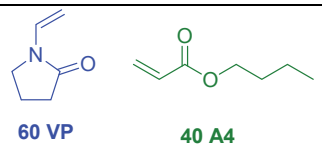	0	1.56 DMPA	0	Au	Pd
PB05	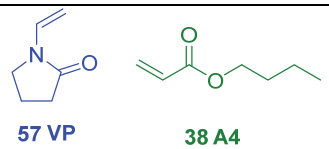	5	1.56 DMPA	0	Au	Pd

Table 5. Percentage of materials of which are composed the tested polymers and the analysis by EDS. *: Photoinitiator, **E: crosslinker.

[47] International Organization for Standardization (ISO); American Society of Testing and Materials (ASTM).

[48] J. García-Calvo, V. García-Calvo, S. Vallejos, F. C. García, M. Avella, J. M. García, T. Torroba, *ACS Appl. Mater. Interfaces*, **2016**, *8*, 24999-25004.

All these polymers share similar percentages of 1-vinyl-2-pyrrolidone (VP) and butyl acrylate (A4). Therefore, the main difference among them is the presence or absence of methacryloyl chloride (MCl) and crosslinker. All compounds were characterized by UV-Vis, included in the synthesis and characterization section, results that were in agreement with the EDS and gave information about the formed nanoparticle.

P5 in the presence of gold(III) solutions (5 mM) form gold agglomerates with a particle size from 2.3 µM to 41 nm. **P10** in the presence of gold(III) solutions (0.5 mM) form gold particles with a similar size of P5, although the concentration has been decreased 10 times (Figure 34).

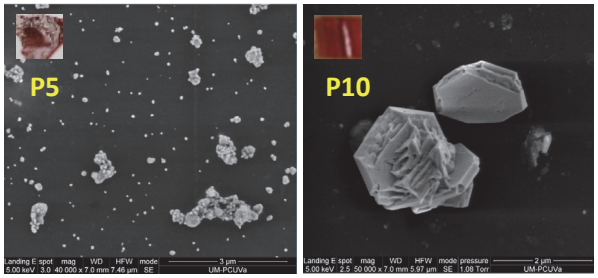

Figure 34. Gold agglomerates formed over **P5** in image SEM at 3 µm (left) and **P10** in image SEM at 2 µm (right).

P5 in the presence of palladium(II) solutions (5 mM) form agglomerates of palladium chloride with a particle size from 6 to 0.1 µM and layers of palladium chloride in size ranking from 80 to 10 µm, demonstrated by "EDS Analysis on the SEM". EDS (Energy Dispersive Spectroscopy) allows identifying what of those particular elements are and their proportions (Atomic percentage) in each sample (Figure 35).

From the images taken with SEM, **P10**, as **P5**, in the presence of palladium(II) solutions (5 mM) forms agglomerates of palladium chloride. In **P10** the layers are smaller than in **P5** and the agglomerates are more abundant than in **P5**.

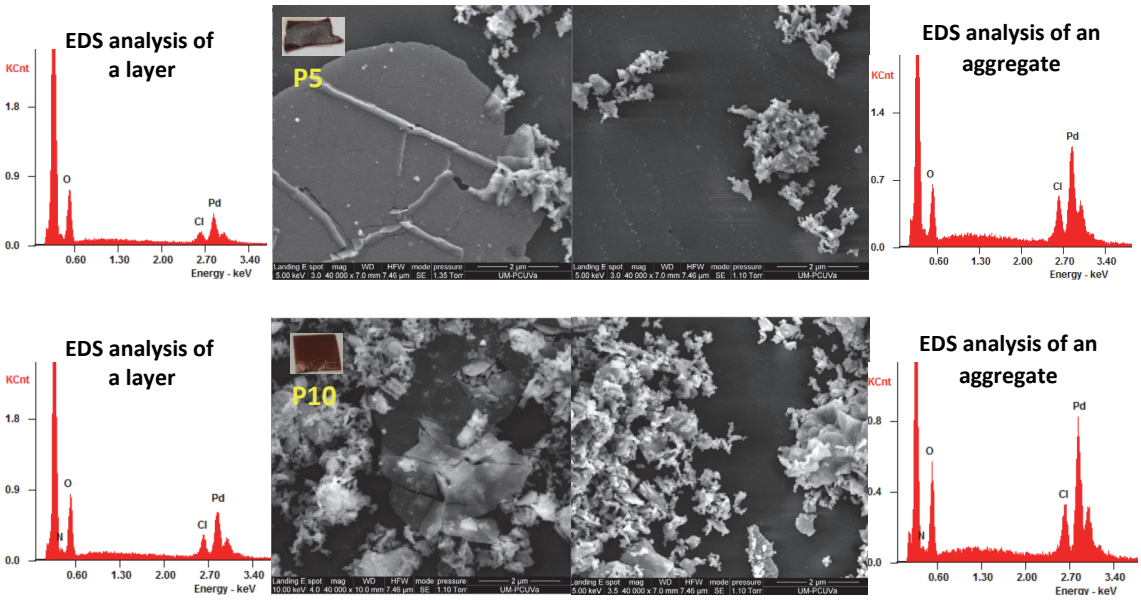

Figure 35. Palladium chloride layers and agglomerates formed over *Upper row*: **P5** and *Lower row*: **P10** in image SEM at 2 µm (left and right) and the EDS analysis for layer and aggregate.

PB5 and **PB10** in the presence of gold(III) solutions (0.5 mM) form gold particles with geometric form, such as icosahedron, desert flower, some small plates and triangles with a particle size which is oscillating between 1.6 µM to 133 nm. As occurred with **P5** and **P10**, **PB10** formed greater number of particles than **PB5** (Figure 36).

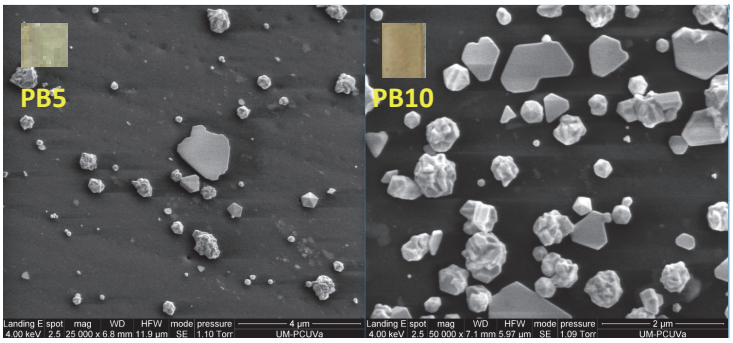

Figure 36. Gold particles formed over **PB5** in image SEM at 4 µm (left) and **PB10** in image SEM at 2 µm (right).

PB5 and **PB10** in the presence of palladium(II) solutions (0.5 mM) form agglomerates of palladium (Figure 37).

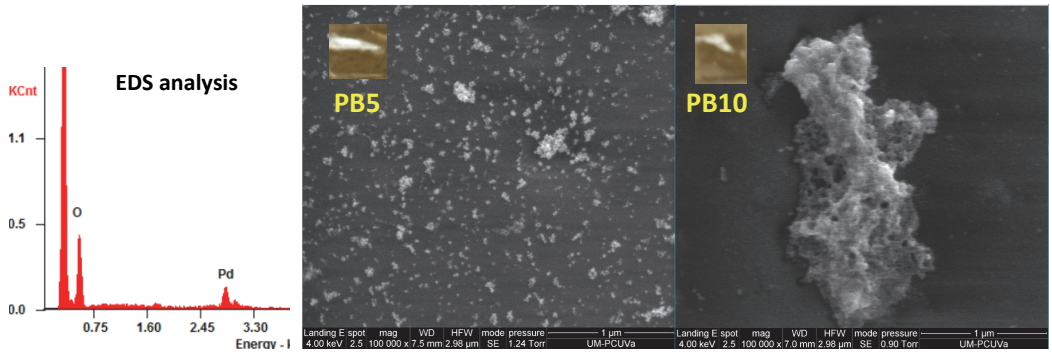

Figure 37. Palladium sponge formed over **PB5** in image SEM at 1 µm (left) and **PB10** in image SEM at 1 µm (right).

In Figure 37 , **PB5** and **PB10 the** response to palladium(II) solutions was studied, finding a dependence between the concentration of the palladium solution with the amount of formed aggregates and its homogeneity. Therefore, at higher concentration, a greater number of aggregates and smaller sizes are seen. The size of the aggregates varies from several nanometers to micrometers.

Regarding to the Figure 38, **PB0**, which is composed of 60 % of VP and 40 % of A4, takes a different colour according to the concentration of the gold NP formed in aqueous solution. It means that, when the polymer is yellow the nanoparticles are small (diameter around 220 nm) and great quantity, whereas when the polymer is grey the nanoparticles are bigger (diameter around 830 nm) and in less amount. The yellow polymer is obtained with the more concentrated solution and the purple one is found with the less concentrated solution. This polymer allows controlling the gold nanoparticles size distribution. However, the polymer **PB05**, which consists of 60 % of VP, 40 % of A4 and 5 % of methacryloyl chloride, does not have this size distribution of particles with the concentration; besides, the particles are bigger than the particles formed on **PB0**. At higher concentrations (C: 5 mM), **PB05** forms big particles (around 4.6 µm), whereas by decreasing the concentration the size of particles is smaller and with a defined shape.

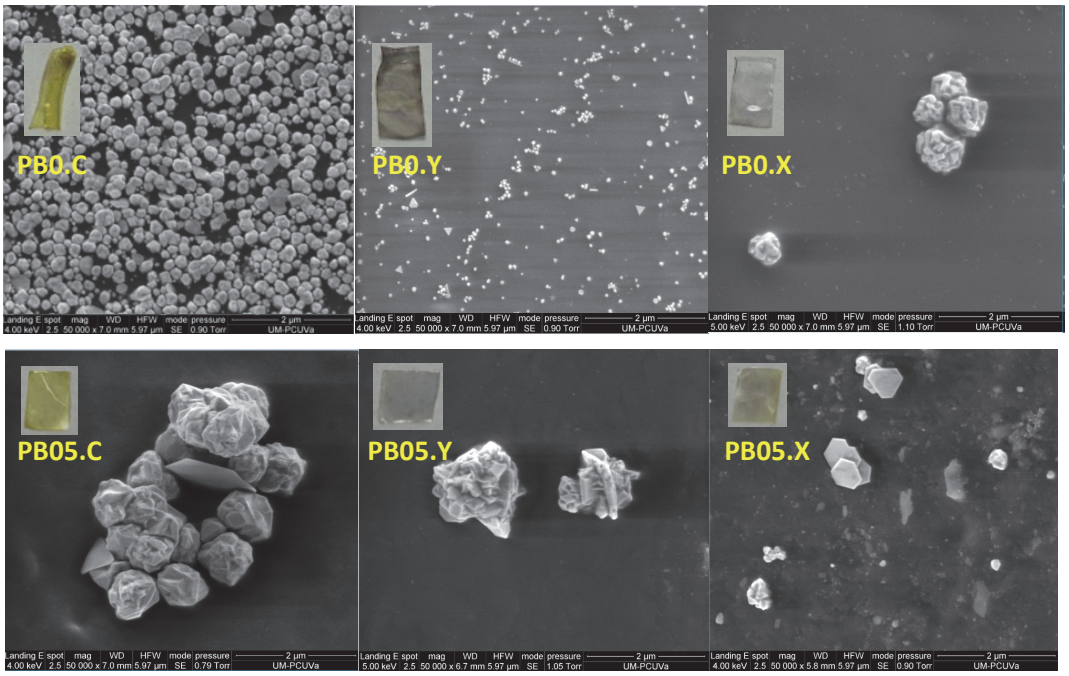

Figure 38. From left to the right at 5 mM, 0.5 mM, 0.1 mM in image SEM around 2 µm. Gold nanoparticles over ***upper row*: PB0** and ***lower row*: PB05.**

UV-Vis spectra of each formed solution of particles, as well as the polymer are measured (Figure 39). **PB0.C** shows a great absorption band at 420 nm. This broad band is attributable to gold nanospheres, which correspond to the SEM image. **PB0.X** and **PB0.Y** present two kind of bands, one at 360 nm and another one at 600 nm, it means that it is an anisotropic sample of gold particles. The band situated at 600 nm corresponds to the localized surface plasmon resonance (LSPR) of gold belonging to nanostars.[49] In contrast, the band located at 360 nm corresponds to Au(III) ions, that are measured in the Figure 39. Row graphics.

Same conclusions are derived from the UV-Vis measurements of **PB05.X** and **PB05.Y**, but the absorption band of **PB05.C** is not a clear band because it absorbs from 300 to 700 nm. For that reason, **PB05** exhibits highly anisotropic gold nanoparticles; there are shapes like desert flowers, icosahedrons, and other shapes among them.

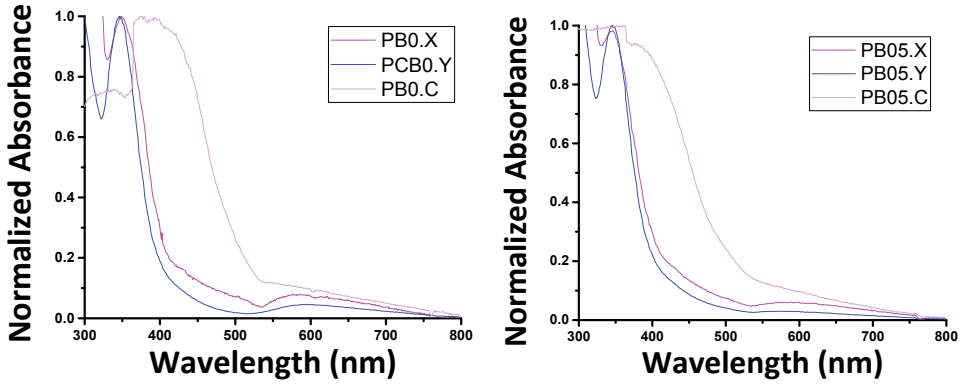

[49] M. Li, S. K. Cushing, J. Zhang, J. Lankford, Z. P. Aguilar, D. Ma, N. Wu, *Nanotechnology*, **2012**, *23*, 115501-115510.

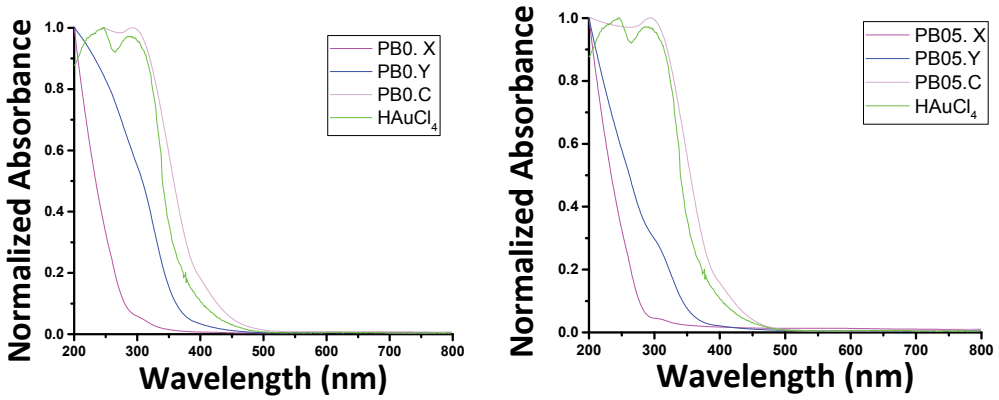

Figure 39. Upper graphics: Normalized UV-Vis spectrum of polymer covered with gold nanoparticles of **PB0** (left) and **PB05** (right). Lower graphics: Normalized UV-Vis spectrum of gold solutions of **PB0** (left) and **PB05** (right).

The former solutions of **PB0.X**, **PB0.Y**, **PB05.X** and **PB05.Y** do not present any gold nanoparticles but residual of the solution of Au(III), since both are compared with the solution of gold salt and it did not exhibit the 360 nm band (Figure 39. Row graphcis). Both **PB0.C** and **PB05.C** have the band of Au(III), this represents that the polymer is not able to reduce more quantity of gold ions and appear in the solution.

Finally, UV-Vis measurements of palladium(II) solutions and polymers were performed in order to demonstrate the reduction of Pd(II) in the presence of the films **PB0** and **PB05**. The band around 400 nm belongs to the absorption of Pd(II) ions. For reduced samples, the peak of 400 nm was absent and a broad continuous absorption was observed, indicating formation of palladium nanoparticles.[50] Figure 40 shows the presence of a mixture of Pd(II) ions and Pd(0) in the solutions that were in contact with the polymers; furthermore, it displays not only the formation of palladium nanoparticles on the polymer but the absence of Pd(II).

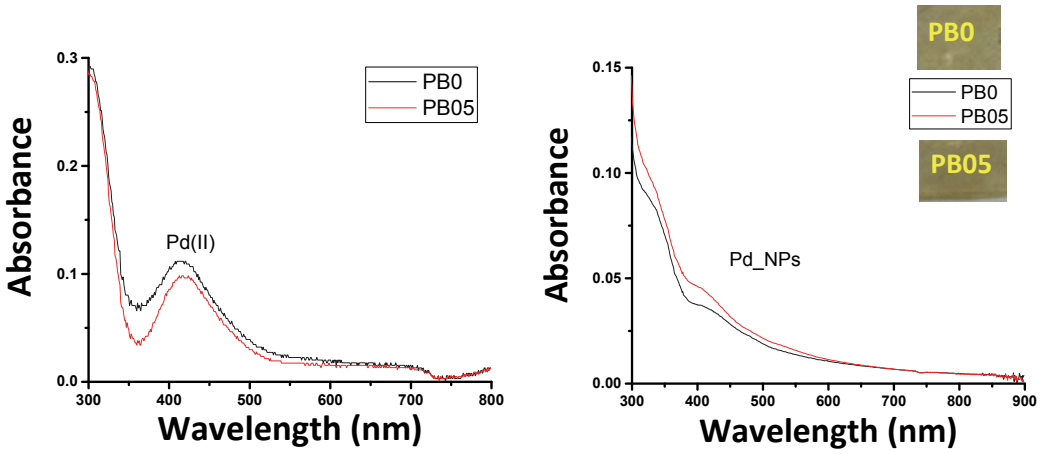

Figure 40. UV-Vis spectrum of aqueous palladium chloride solution (left) and palladium nanoparticles on the polymers (right) **PB0** and **PB05**.

In conclusion, the size and the amount of Au_NP may be controlled by removing the crosslinker, methacryloyl chloride and functionalization (**PC117**) from the polymer, since they

[50] a) S. Gurunathan, E. Kim, J. W. Han, J. H. Park, J.-H. Kim, *Molecules*, **2015**, *20*, 22476-22498.; b) G. Zhang, H. Zhou, J. Hu, M. Liu, Y. Kuang, *Green Chem.*, **2009**, *11*, 1428-1432.

prevent the growth and the homogeneity in Au_NP formation. Regarding to Pd_NP, the functionalization of the polymers leads to the absence of metal particles.

To discover what is the possible reducing agent of the gold and palladium nanoparticles it is necessary to perform a more extensive research. The synthesis of several polymers, changing the quantity and the identity of the co-monomers, the initiator (photo and thermal initiator) and the crosslinker. Therefore, the group is currently working in this topic which is part of the patent: ‘‘OBTENCIÓN DE NANO-PARTÍCULAS METÁLICAS MEDIANTE USO DE COPOLÍMEROS EN FORMA DE MEMBRANA’’. ‘‘Numero de solicitud: P201730551, fecha de recepción 31 de Marzo de 2017 y referencia: P-07535’’.

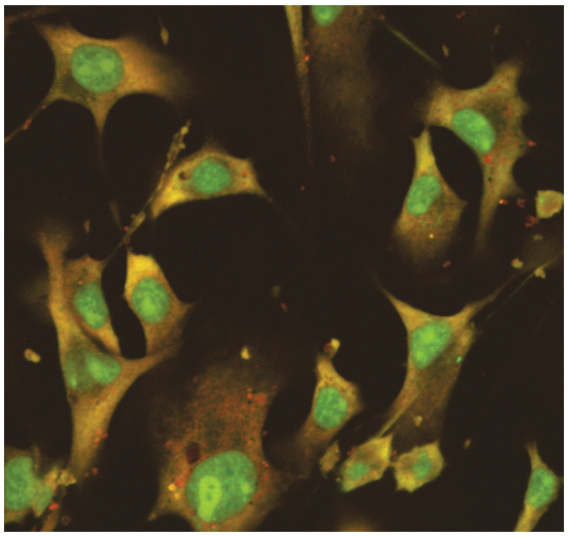

CHAPTER 2A: WATER-SOLUBLE FLUORESCENT PERYLENEDIIMIDES

PATRICIA CALVO GREDILLA Ph. D. THESIS

SUMMARY

The importance of design and synthetize several water-soluble fluorescent perylenediimides to be applied to living cells, in order to study their potential applications in detection and bioimaging, is explained.

1. INTRODUCTION.

Water is a universal biological solvent, capable of dissolving a variety of different solids and liquids and easily obtainable, so it should be aspired to create stable water-soluble dyes for biological applications and detection of harmful substances, among other applications.[1] Perylenediimides (PDIs) have attracted considerable interest and they have been employed as extremely stable fluorogenic compounds. Due to the fluorescent nature of the PDI fluorophore core, it is well suited for the tracing of cellular uptake via fluorescence microscopy, confocal imaging and other bioimaging techniques.[2] The development of water-soluble fluorogenic perylenediimides is of enormous interest in the use of tools to get information of biological processes in living cells by luminescence response. The challenge is to design simultaneously PDIs with low cytoxicity, imaging capacities and high specificity for diagnosis with high accuracy in a specific therapy with few side effects.[2] To date, a wide range of PDIs is known but only a few of them are soluble in water. As indicated in the preceding sections, PDIs display low solubility in aqueous media due to the aggregation by π-π stacking of the perylene core of perylenediimides. To increase the solubility of PDIs, ionic side groups have been introduced on the perylene core or at the imide position.[3] Recently, Proença *et al.*[4] reported symmetric and water-soluble perylenediimides substituted in peri-positions by different kinds of amino acids, obtaining good results. Gao *et al*.[5] also described water-soluble and fluorescent perylenediimides, but this time several bulky dendritic peptide groups, which suppressed the aggregation, were attached to the peri-positions and used in biological applications. Moreover, Mullen *et al*.[6] published perylenediimides substituted in the bay or imide regions by hydrophilic groups, such as sulfonic acids groups, sulfonate salts or quaternized amines (Figure 1).

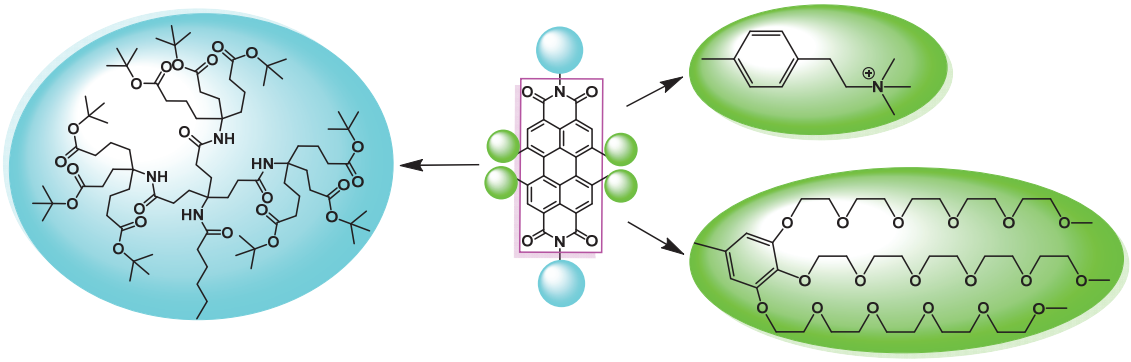

Figure 1. Current strategies to functionalize perylenediimides in bay and peri-positions to achieve their solubilization in water.

Taking into consideration the information gained, our research group has designed fluorogenic and water-soluble dyes with peri and bay-exchangeable groups. In this work, we want to prepare bay-substituted perylenediimides with phenols bearing carboxylic acid derivatives, which will allow water solubilisation and, at the same time, peri-substituted perylenediimides with an additional amine group, which will permit the attachment to

[1] C. D. Schmidt, A. Hirsch, *Ideas in Chemistry and Molecular Sciences: Advances in Synthetic Chemistry*, (ed B. Pignataro), Wiley-VCH Verlag GmbH & Co. KGaA, Weinheim, Germany, **2010**.
[2] M. Sun, K. Müllen, M. Yin, *Chem. Soc. Rev.*, **2016**, *45*, 1513-1528.
[3] Y. Ma, F. Zhang, J. Zhang, T. Jiang, *Turk. J. Chem*, **2015**, 835-842.
[4] R. F. Araújo, C. J. R. Silva, M. C. Paiva, M. M. Franco, M. F. Proença, *RSC Adv.*, **2013**, *3*, 24535-24542.
[5] B. Gao, H. Li, H. Liu, L. Zhang, Q. Bai, X. Ba, *Chem. Commun.*, **2011**, *47*, 3894-3896.
[6] a) K. Peneva, G. Mihov, F. Nolde, S. Rocha, J.-i. Hotta, K. Braeckmans, J. Hofkens, H. Uji-i, A. Herrmann, K. Müllen, *Angew. Chem. Int. Ed.*, **2008**, *47*, 3372-3375.; b) T. Tang, J. Qu, K. Müllen, S. E. Webber, *Langmuir*, **2006**, *22*, 7610-7616.; C. Kohl, T. Weil, J. Qu, K. Müllen, *Chem. Eur. J.*, **2004**, *10*, 5297-5310.

biological molecules. These compounds must exhibit features as photostability, high fluorescence, biocompatibility and absorption and emission maxima around 500 nm to minimize the autofluorescence background of cells.[7] It is expected that the fluorescent dyes will be very effective to use in bioimagen and to reach the objective planned in this chapter:

- Design of new water-soluble fluorogenic probes and their study in bioconjugation, biological detection and living cells bioimaging.

2. RESULTS AND DISCUSSION.

In order to meet the expectations of the chapter it was necessary to design water-soluble and fluorescent perylenediimides. In this sense, we designed the synthesis of PDIs with four bay-positions functionalized by groups capable of increasing solubility in water.

2.1. Synthesis of water-soluble fluorescent perylenediimides.

The PDIs will have two orthogonally functionalized peri-positions suitable for bioconjugation with biologically active groups. 1,6,7,12-Tetrachloroperylene tetracarboxylic acid dianhydride (**4Cl-PDA**) was considered the best starting material, because it exhibits high solubility in common solvents and it is sufficiently reactive to react under soft conditions.

The amidation reaction: the first reaction was performed on the peri-positions by using an amidation reaction with a *N*-boc-protected piperidine. Anhydrous DMF and 4-amino-1-(*N*''-*tert*-butoxycarbonyl)piperidine (2 equivalents) were added under nitrogen to 1,6,7,12-tetrachloroperylenetetracarboxylic acid dianhydride (1 equivalent) and DABCO (2 equivalents) and the mixture was irradiated in a microwave oven (Biotage Classic) at 110 ^{o}C for 1 hour. Then, the mixture was poured over an aqueous solution of HCl 1M and stirred for 1 hour, filtered and washed with water. Purification was carried out by silica gel flash chromatography using DCM:MeCN (80:20) as eluent to give **PC43** as an orange solid in 95 % yield. The obtained perylenediimide (**PC43**) is a green fluorescence product that showed very remarkable solvatochromic effects (Figure 2).

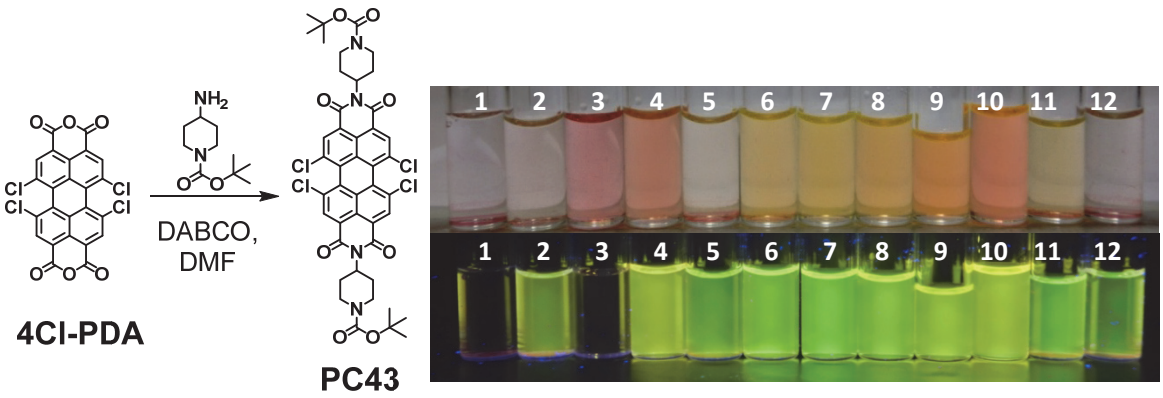

Figure 2. Synthesis and solvatochromic effects of **PC43** ($1\cdot10^{-5}$ M) in the following solvents: **1**: H_2O, **2**: MeOH, **3**: DMSO, **4**: DMF, **5**: MeCN, **6**: acetone, **7**: AcOEt, **8**: THF, **9**: DCM, **10**: toluene, **11**: ether, **12**: hexane.

[7] S. K. Yang, X. Shi, S. Park, S. Doganay, T. Ha, S. C. Zimmerman, *J. Am. Chem. Soc.*, **2011**, *133*, 9964-9967.

The Ullmann-type copper-catalysed aryl ether formation: The second reaction was an Ullmann-type copper-catalysed aryl ether formation by using suitable phenols capable to enhance the fluorescence and the solubility in water. The "Ullmann-type" reactions include copper-catalyzed nucleophilic aromatic substitution between various nucleophiles (e.g. substituted phenoxides) with aryl halides.[8,9] In this way, we have tested several phenols, from which only phenols with meta-substituted electron-withdrawing groups gave good results. One of the products, the octa(bis-trifluoromethyl)substituted derivative, isolated during this work, will be the subject of a different PhD Thesis by Daisy Carolina Romero Velásquez, which is now almost finished. The separation of the main compound from the bay-products, either with phenol A and B, was not easy due to the close proximity of the by-products in the thin layer and column chromatography (Figure 3).

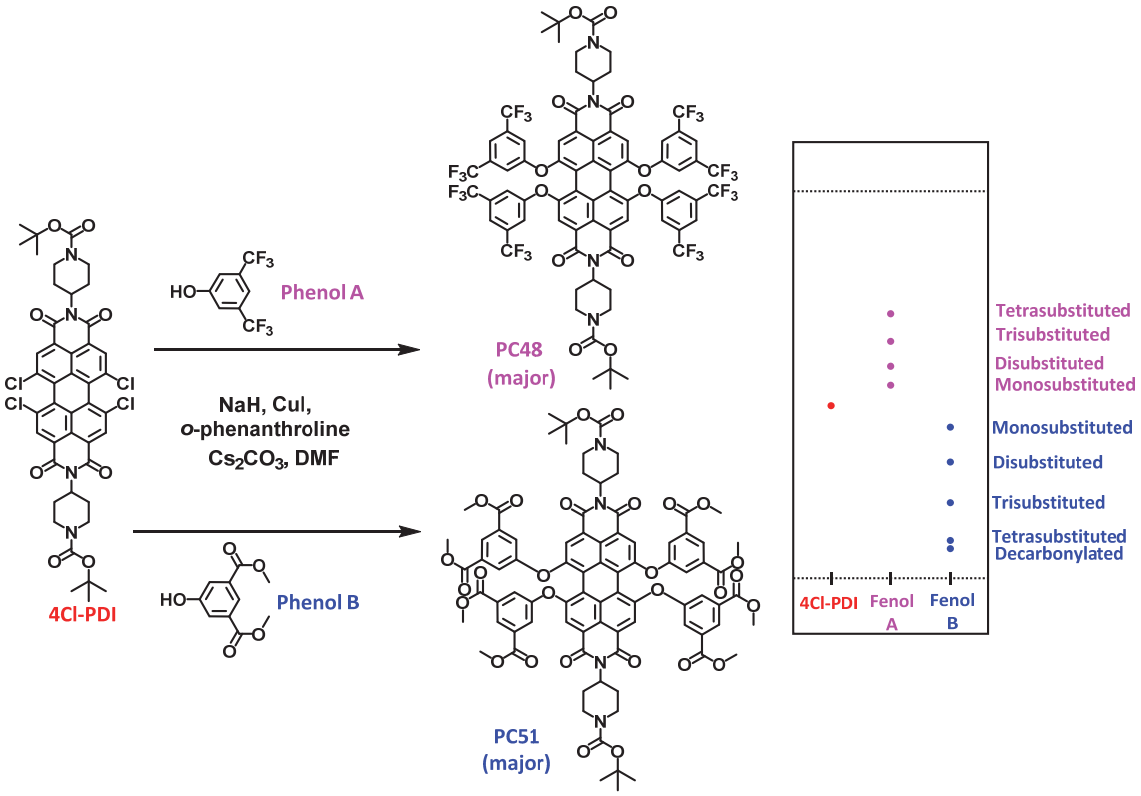

Figure 3. Preparation of substituted PDIs and the positions of the different main and by-products from both phenols in the Thin Layer Chromatography.

This reaction is subjected to two limitations:

- the number of by-products generated in the reaction and
- the conditions used in the reaction.

So, several reaction conditions were used until the best reaction conditions were achieved. As a general example, *N,N'*-bis(1-(*N''*-*tert*-butoxycarbonyl)piperidine)-1,6,7,12-tetrachloroperylene-3,4,9,10-tetracarboxylic diimide (1 equivalent), *o*-phenantroline monohydrated (60 % mol), copper(I) iodine (30 % mol) and cesium carbonate (1 equivalent)

[8] http://www.organic-chemistry.org/namedreactions/ullmann-reaction.shtm

[9] R. H. M. Carlo Sambiagio, Stephen P. Marsden, A. John Blacker, and Patrick C. McGowan, *Chem. Eur. J.*, **2014**, *20*, 17606-17615.

were added under nitrogen to a suspension of NaH (0.5 equivalents), anhydrous DMF and dimethyl-5-hydroxyisophthlate (4 equivalents). The mixture was irradiated in a microwave oven (Biotage Classic) at 110 °C for 1 hour and then the solvent was evaporated under reduced pressure. Purification was carried out by silica gel flash chromatography using DCM:MeCN (70:30) as eluent to give four substituted phenols **PC51 (**40 %), **PC51.3** (10 %), **PC51.2** (20 %), **PC51.1** (7 %) and the decarbonylated perylenediimide **PC51.d** (5 %) (Figure 4).

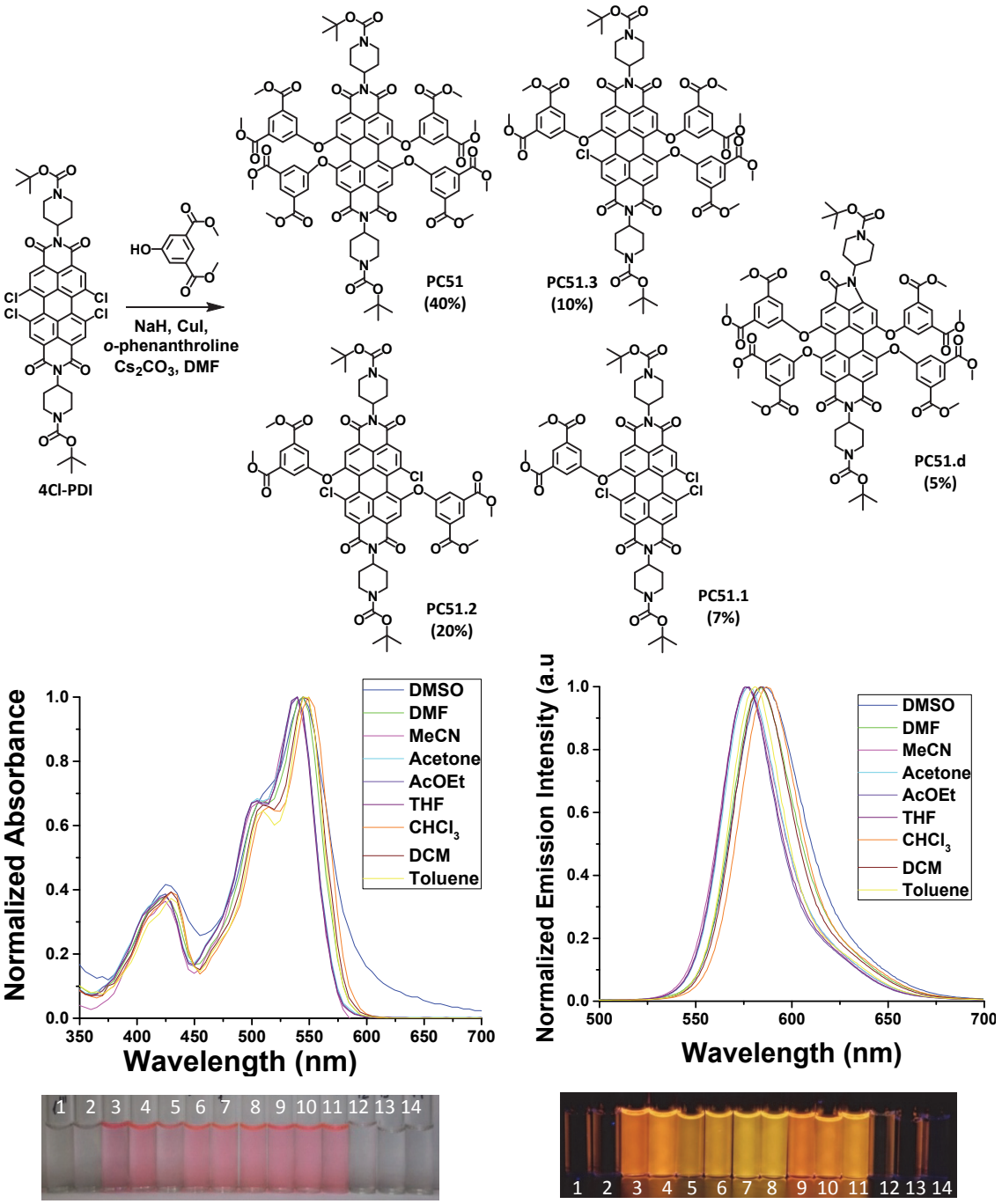

Figure 4. Synthetic route to tetrasubstituted PDIs. Inset: Normalized UV-visible and fluorescence spectra of **PC51**, and solvatochromism images. Solvents: 1: H_2O, 2: MeOH, 3: DMSO, 4: DMF, 5: MeCN, 6: acetone, 7: AcEtO, 8: THF, 9: $CHCl_3$, 10: DCM, 11: toluene, 12: diethyl ether, 13: hexane, 14: cyclohexane.

The work concentration for the solvatochromism measurements was deduced from a Lambert-Beer study. **PC51** was chosen as an example. Ten solutions of **PC51** dissolved in DCM were prepared from 2×10^{-6} M to 2×10^{-4} M. Concentrations above 2×10^{-5} M gave very high absorbance values, so the range of concentrations used is that shown in the Figure 5.

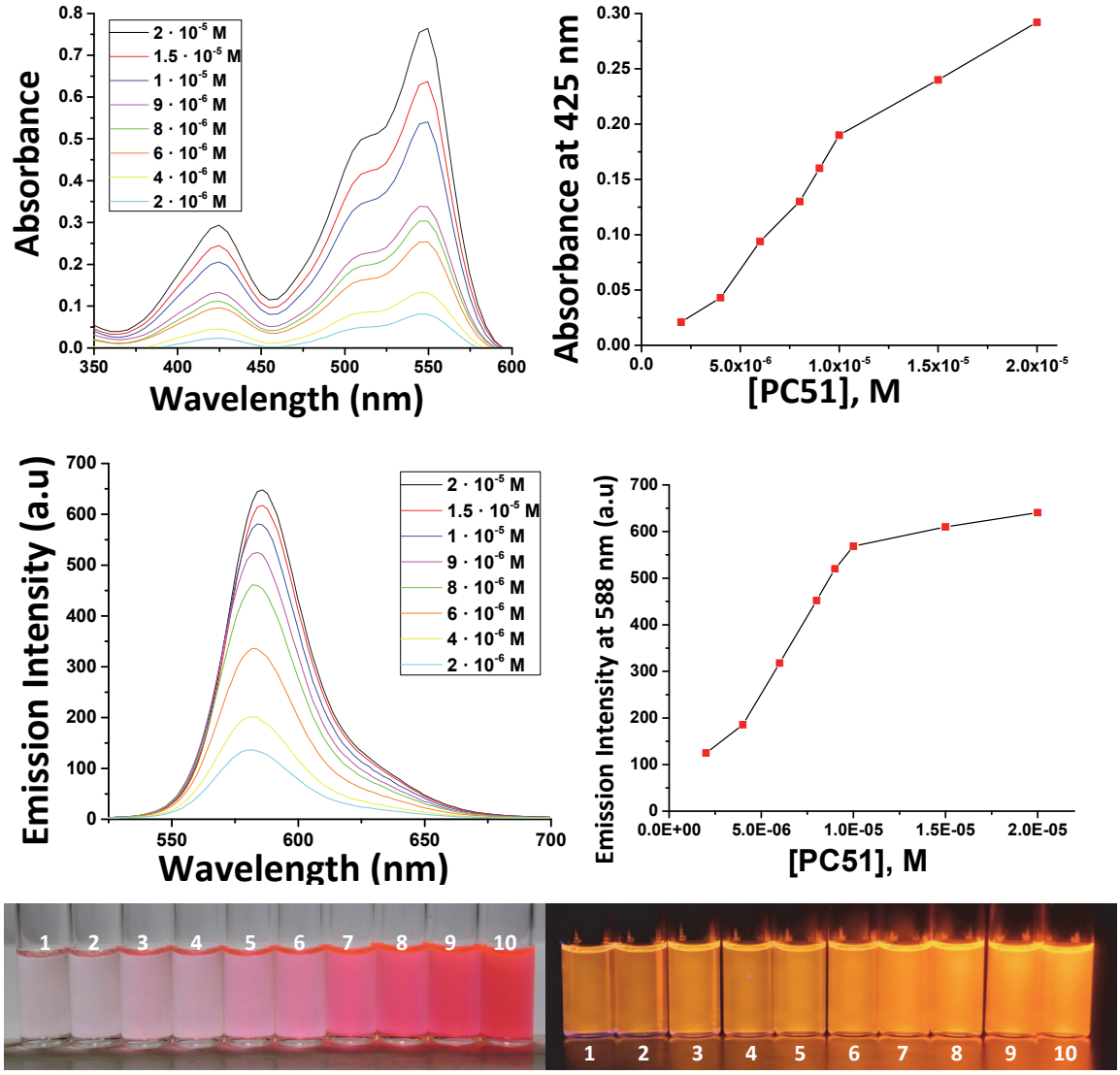

1: $2 \cdot 10^{-6}$ M, **2**: $4 \cdot 10^{-6}$ M, **3**: $6 \cdot 10^{-6}$ M, **4**: $8 \cdot 10^{-6}$ M, **5**: $9 \cdot 10^{-6}$ M, **6**: $1 \cdot 10^{-5}$ M, **7**: $1.5 \cdot 10^{-5}$ M, **8**: $2 \cdot 10^{-5}$ M, **9**: $4 \cdot 10^{-5}$ M, **10**: $8 \cdot 10^{-5}$ M.

Figure 5. **Upper**. UV-visible spectra of **PC51** and the absorbance vs concentration of **PC51** at 425 nm. **Middle**. Fluorescence spectra of **PC51** and the emission vs concentration of **PC51** at 588 nm. **Lower**. Photos of **PC51** in DCM under white light and under light of 366 nm.

With strongly absorbing chromophores such as perylenediimides, the absorbance should be low enough to prevent reabsorption processes. Moreover, the elected concentration falls into the linear range both in absorbance and fluorescence titrations. For these reasons, the chosen working concentration was 1×10^{-5} M. By similarity between structures of the perylenes it is considered that this result is extended to the rest of the synthesized compounds.

Orthogonal deprotection reactions: By a simple *N*-Boc-deprotection process in an acidic solution of **PC51** it was possible to selectively deprotect the amine groups. Trifluoroacetic acid (90 equivalentes) was added dropwise to *N,N'*-bis-(1-(*N''-tert*-butoxycarbonyl)piperidine)-1,6,7,12-tetrakis(dimethyl-5-hydroxyisophthlate)perylene-3,4,9,10-tetracarboxylic diimide (1 equivalent) dissolved in degassed DCM and the mixture was stirred at 25 °C for 2 hours, then neutralized with 10% NaOH and extracted with DCM, and the combined organic extracts were evaporated under reduced pressure to obtain **PC67** as a pink-purple product in almost quantitative yield. On the other hand, basic hydrolysis of the ester groups gave selectively the deprotected polycarboxylic acid. Lithium hydroxide (90 equivalents) dissolved in water was added to *N,N'*-bis-(1-(*N''-tert*-butoxycarbonyl)piperidine)-1,6,7,12-tetrakis(dimethyl-5-hydroxyisophthlate)perylene-3,4,9,10-tetracarboxylic diimide (1 equivalent) dissolved in THF and the mixture was stirred at 45 °C overnight, then the solvents were removed under reduced pressure to obtain **PC66** as a brown oil-solid in quantitative yield (Scheme 1.).

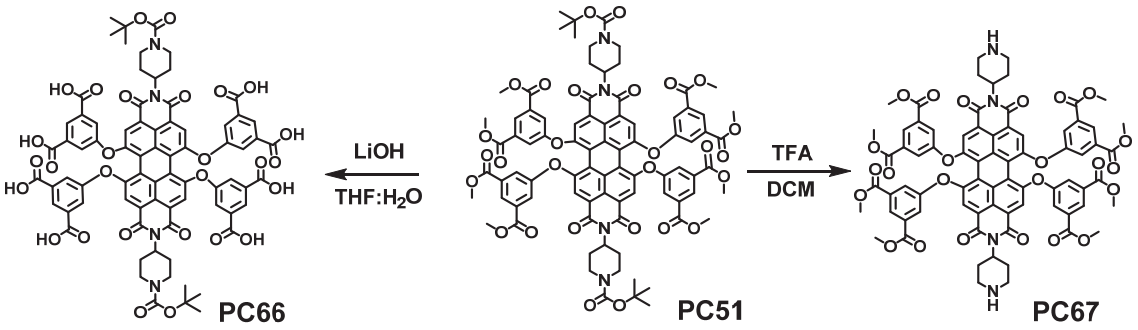

Scheme 1. Synthetic routes to deprotected PDIs.

Once we have products capable of being anchored in peri-position, **PC67**, the next step was the amide bond formation. The amide functionality is a common reaction in synthetic or natural molecules.[10] The bioconjugation will be successful if the combination of protecting groups and coupling reagents is accurate. The formation of amide bond involves two steps: the activation of the carboxyl group and the nucleophilic attack of the amino group at the active carboxylic group. The use of PyBOP, as coupling agent, and a base favour the reaction through a one-pot coupling, and by-products are less probable.[11] Although originally, the biotin derivative is activated with the *N*-succinimidyl group, the coupling agent was used to increase the yield and avoid by-products produced in this kind of reactions. Therefore, **PC73** and **PC71** were synthetized with this procedure.

Vitamin H, more commonly known as biotin, is water-soluble and is part of the B complex group of vitamins.[12] Biotin was selected to anchor to **PC67** because usually it confers water solubility and possibility to attach to avidin. Biotin is found covalently attached to histones; biotinylated histones are enriched in repeat regions in the human genome and appear to play a role in transcriptional repression of genes and genome stability.[13] Testosterone is a steroid from the androstane, which is biosynthesized in several steps from cholesterol and exerts its action through binding and activation of the androgen receptor.[14] We wanted to anchor a steroid compound to **PC67** because the steroid receptors comprise a family of ligand-activated

[10] C. A. G. N. Montalbetti, V. Falque, *Tetrahedron*, **2005**, *61*, 10827-10852.

[11] T. I. Al-Warhia, H. M. A. Al-Hazimib, A. El-Fahamb, *J. Saudi Chem. Soc.*, **2012**, *16*, 97-116.

[12] http://www.umm.edu/health/medical/altmed/supplement/vitamin-h-biotin

[13] J. Zempleni, Y. I. Hassan, S. S. Wijeratne, *Expert Rev. Endocrinol. Metab.*, **2008,** *1*, 715-724.

[14] E. Nieschlag, H. M. Behre: Testosterone, Cambridge University Press, ISBN 978-1-107-01290-5, **2012**.

transcription factors,[15] so it could be reasonable to synthetize a fluorescent molecule with a steroid attached.

In this way, *N,N'*-bis-(1-pPiperidine)-1,6,7,12-tetrakis(dimethyl-5-hydroxyisophthlate)-perylene-3,4,9,10-tetracarboxylic diimide **PC67** (1 equivalent) and PyBOP (3 equivalents) dissolved in DCM were added under nitrogen to *N*-succinimidyl-6-biotinamidohexanoate (2 equivalents) and DIPEA (6 equivalents) dissolved in DCM. The purple-pink mixture was stirred at room temperature for 2 hours until the reactant disappeared by TLC. Then the solvent was removed under reduced pressure and purification was carried out by silica gel flash chromatography using DCM:MeOH (80:20) as eluent to give compound **PC73** as a deep pink solid in 63 % yield (Scheme 2).

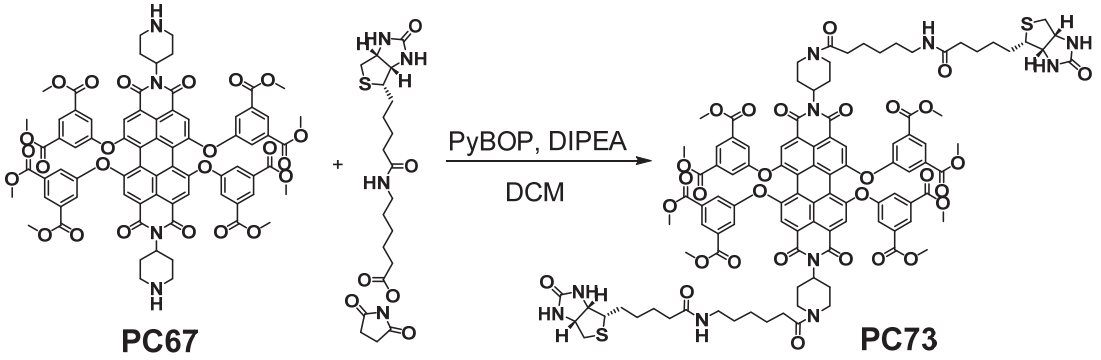

Scheme 2. Synthetic route to bioconjugation of PDIs.

Analogously, *N,N'*-bis(1-piperidine)-1,6,7,12-tetrakis(dimethyl-5-hydroxyisophthlate) perylene-3,4,9,10-tetracarboxylic diimide **PC67** (1 equivalent) and PyBOP (3 equivalents) dissolved in DCM were added under nitrogen to (4-androsten-17*β*-acetoxy-3-one-7*α*-yl)-but-2-enoic acid (2 equivalents) and DIPEA (6 equivalents) dissolved in DCM. The purple-pink mixture was stirred at room temperature for 2.5 hours until the reactant disappeared by TLC. The solvent was removed under reduced pressure. Purification was carried out by silica gel flash chromatography using DCM:MeOH (90:10) as eluent to give compound **PC71** as a deep pink solid in 68 % yield (Scheme 3).

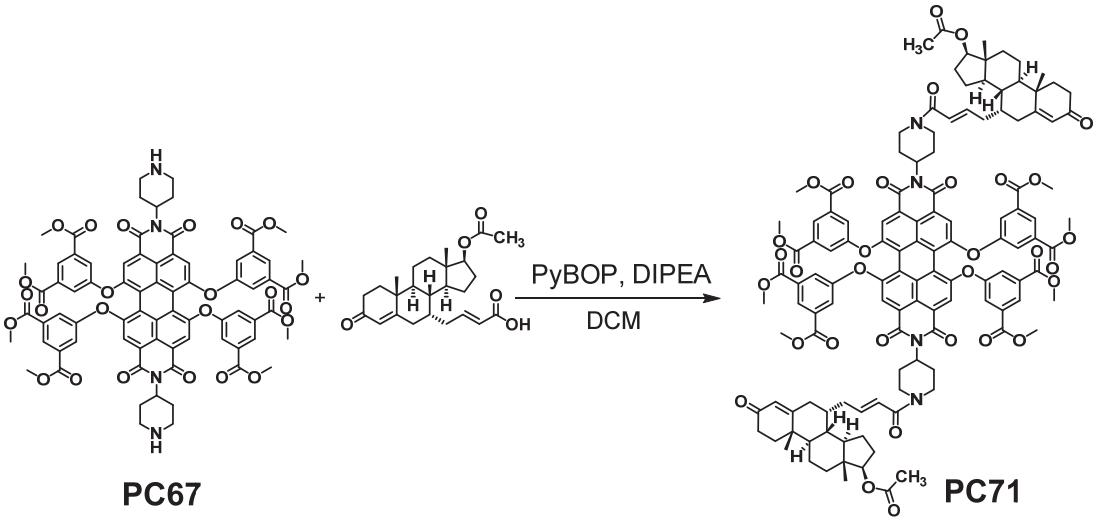

Scheme 3. Synthetic route to bioconjugation of PDIs.

[15] a) D. L. Bain, K. D. Connaghan, N. K. Maluf, Q. Yang, M. T. Miura, R. W. De Angelis, G. D. Degala, J. R. Lambert, *Nucleic Acids Res.*, **2013**, *42*, 691-700.; b) P. Chanphai, D. Agudelo, A. R. Vesper, G. Bérubé, H. A. Tajmir-Riahi, *Int. J. Biol. Macromolec.*, **2017**, *95*, 850-855.

Finally, the methyl esters of **PC73** and **PC71** were easily hydrolysed with lithium hydroxide to obtain green fluorescent and water-soluble ligands named as **PC80** and **PC79**, respectively. In the case of **PC73**, the reaction and the purification must be performed under strict conditions of nitrogen or inert gas, to avoid the oxidation of biotin (Scheme 4).

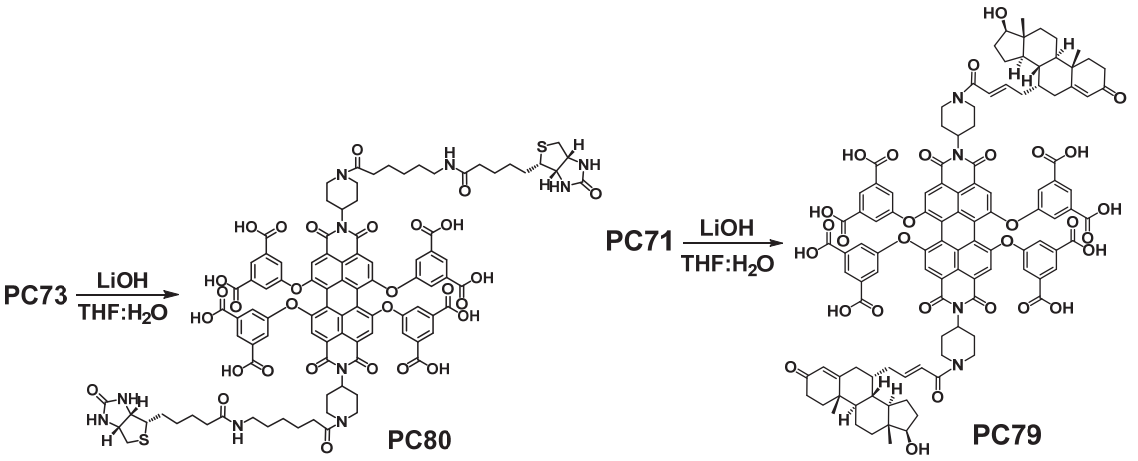

Scheme 4. Synthetic route to deprotection of bioconjugated PDIs.

To get another water soluble derivative of PDI, we synthesized **PC91** by nucleophilic substitution of the perylenediimide **PC67** with a methylated diethylenglycol halide to introduce a methylated diethylenglycol on the PDI (Scheme 5).

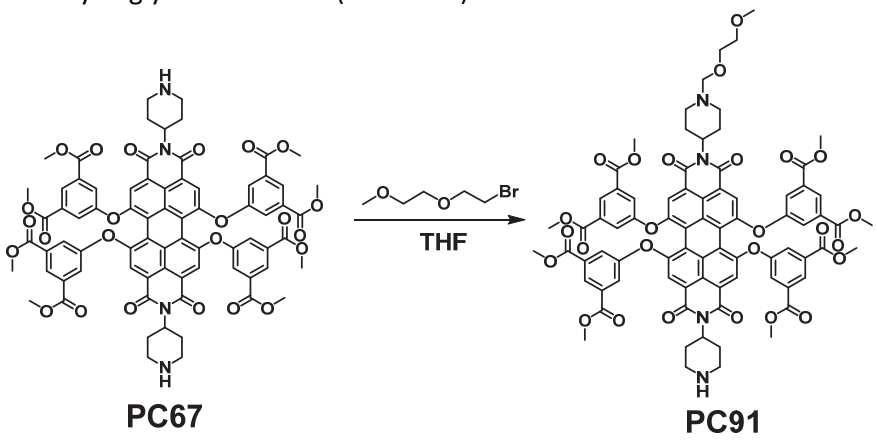

Scheme 5. Synthetic route to diethylenglycol derivatives of PDIs.

2.2. Confocal microscopy and microscopy imaging.

Cell cultures, confocal microscopy and microscopy imaging have been performed by the Dr. Mónica Lopez Fanarraga (Group of Nanomedicine-IDIVAL, University of Santander) to study the behaviour of perylenediimides inside cells. The interpretation of confocal microscopy images gives us an idea of where perylenediimides will accumulate inside the HeLa cells (immortalized human cervical cancer cells), and what organelles will be the target of PDIs.

The majority of dyes have certain affinity by cellular components. Many common dyes are positive charged molecules that are combined with cell constituents negative charged, such as nucleic acids or acid polysaccharides. This sort of dyes is able to react or concentrate in different parts of the cell or tissues and their optic properties allow us to reveal specific

regions in the cells.[16] In this sense, the perylenediimides used in this chapter express different emission behaviour depending on the cellular organelle where they are localized (depending on pH, chemical conditions), named as metachromatism.[17]

First, the perylenediimides under study were subjected to a solubility study in physiological conditions (mostly water). HeLa cells are exposed to 0.1 µM of probes in the culture medium for 72 h before fixation and processing.

The confocal microscopy images revealed that the fluorescent probes penetrated through the plasma membrane; it means that the probes were taken in the cells and cell structures were visualized (Figure 6, Figure 7 and Figure 8). Additionally, there are no obvious degenerative changes in HeLa cells at these incubation times, suggesting that perylenediimides were not toxic to these kinds of cells at this concentration (1 µM) and exposure times (72 h).

Regarding the Table 1, we can conclude that if the probes have the methyl esters in the periphery of phenols it is impossible to solubilize them in physiological conditions and for this reason **PC51**, **PC67**, **PC71** and **PC73** form aggregates.

Name of Ligands	Solubility in physiological conditions	Staining	Survival at 0,1µM
PC51	no	aggregates	72h
PC66	yes	soluble	72h
PC67	no	aggregates	72h
PC71	no	aggregates	72h
PC73	no	aggregates	72h
PC79	yes	soluble	72h
PC80	yes	soluble	72h

Table 1. Solubility study of ligands in HeLa cells cultures.

However, the probes that have been hydrolyzed in the ester groups reveal a great solubility in the preceding conditions. Therefore, **PC66**, **PC79** and **PC80** are the appropriate probes. The solubility of **PC66** in the physiological conditions indicates that it is suitable for obtaining the confocal images, although the staining of the cells is a little diffuse. The metachromatic effect of **PC66** is appreciated in the Figure 6A, since the different emission of **PC66** in each cell region has been observed.

[16] D. C. Blood, V. P. Studdert, C. C. Gay., *Saunders Comprehensive Veterinary Dictionary*, 3 ed. Elsevier Saunders, Inc., St. Louis, Missouri, USA, **2007**.
[17] M. K. Pal, M. Schubert, *J. Histochem. Cytochem.*, **1961**, *9*, 673-680.

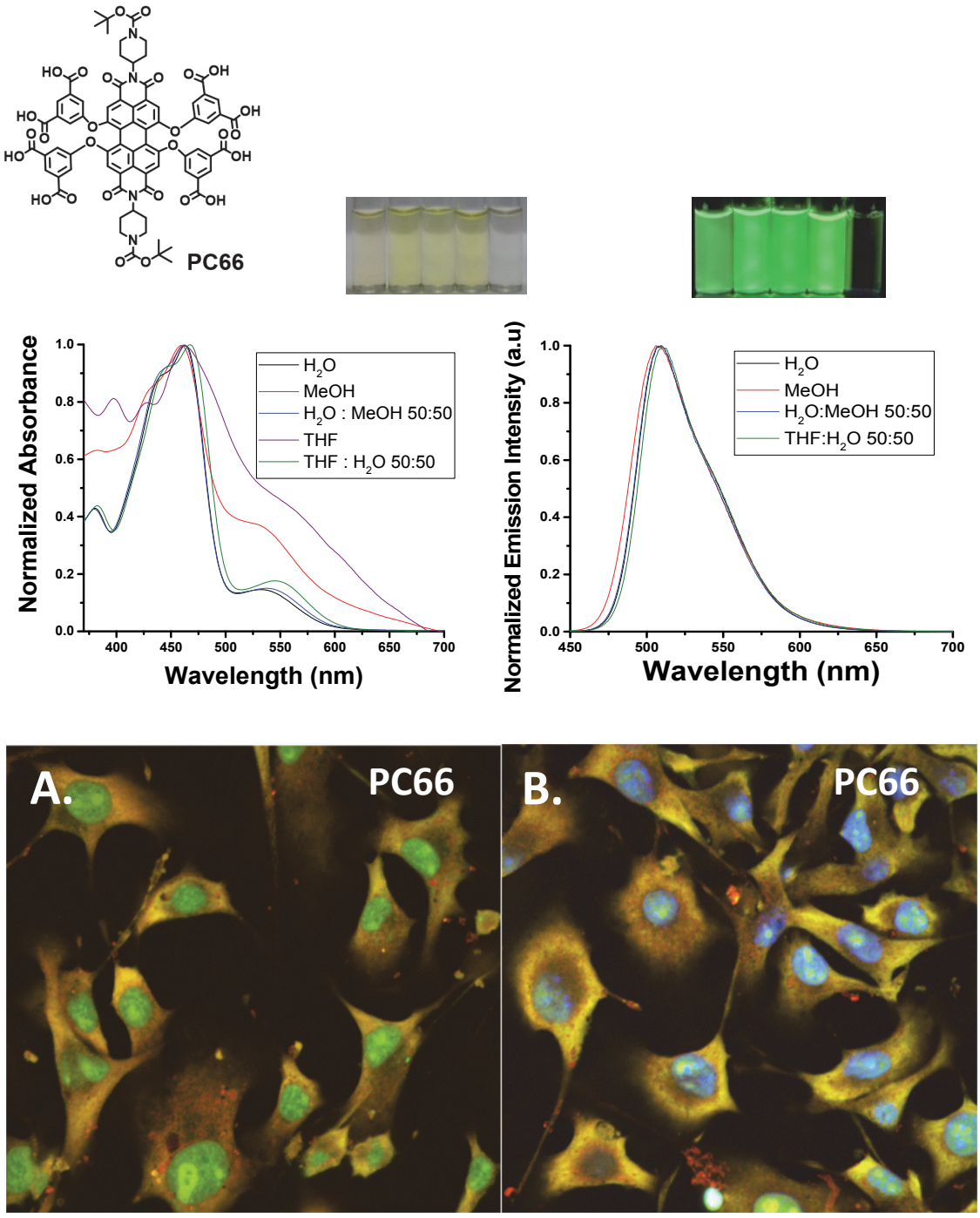

Figure 6. Confocal microscopy images of cells cultured from HeLa and treated with **PC66** for 72 h**. A)** Any region is stained (green channel) and **B)** the nucleus is stained with Hoechst 33342 (blue channel). The images are pseudocolored.

This PDI can interact differently with the cytoplasm, the nucleus and the nucleolus and for that reason each region has a different colour, orange in the case of cytoplasm, green in the case of nucleus and bright green in the case of nucleolus. The brilliance of this compound by the nucleolus indicates a great affinity for it, which is higher than for the rest of the nucleus. On the other side, the Figure 6B shows the staining of the nucleus by the dye Hoescht 33342. As stated before, **PC66** is localized in the nucleus but preferently in the nucleolus (organelles stained in orange). Therefore, **PC66** migrates to the cytoplasm and the nucleus, and more specifically to the nucleolus. Probe **PC79** dissolves scarcely in the physiological conditions. The

staining of the cells is diffuse in this case. As it could be seen in the Figure 7A and Figure 7B, **PC79** accumulates in the cytoplasm and in the nucleus; it shows vesicular distribution, perhaps in membranes (green-orange fluorescence). **PC79** does not seem as metachromatic as **PC66**, because all parts of cells have green emission (Figure 7).

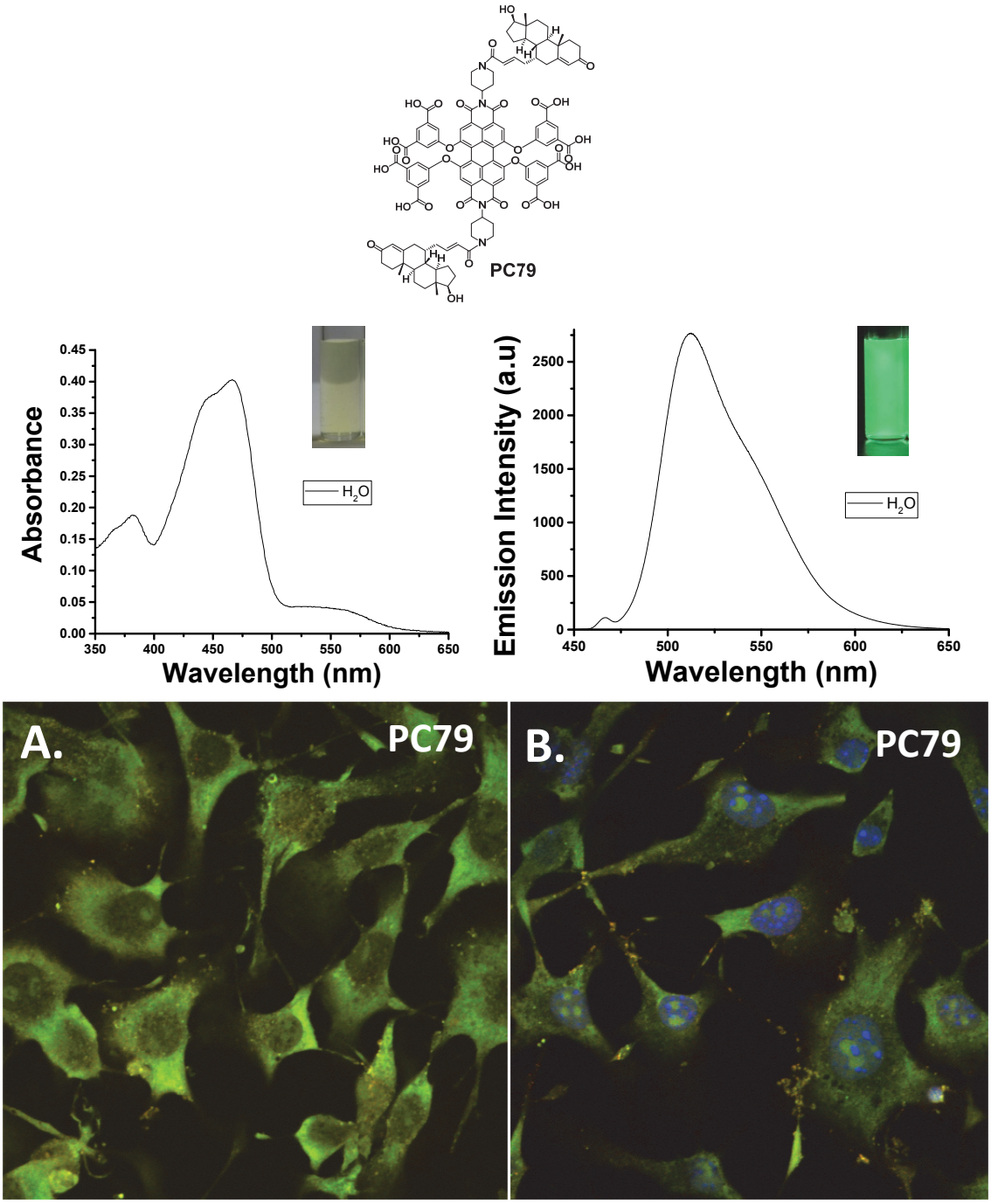

Figure 7. Confocal microscopy images of cells cultured from HeLa and treated with **PC79** for 72 h. **Left (A):** Any region is stained (green channel) and **Right (B):** The nucleus is stained with Hoechst 33342 (blue channel). The images are pseudocolored.

When **PC80** is dissolved in the physiological conditions its solubility makes it appropriate to obtain confocal images. In this case, **PC80** is mainly localized in the nucleus or the nucleolus and in a lesser extension in the cytoplasm which is not a specific region for staining with **PC80**, according to the Figure 8.

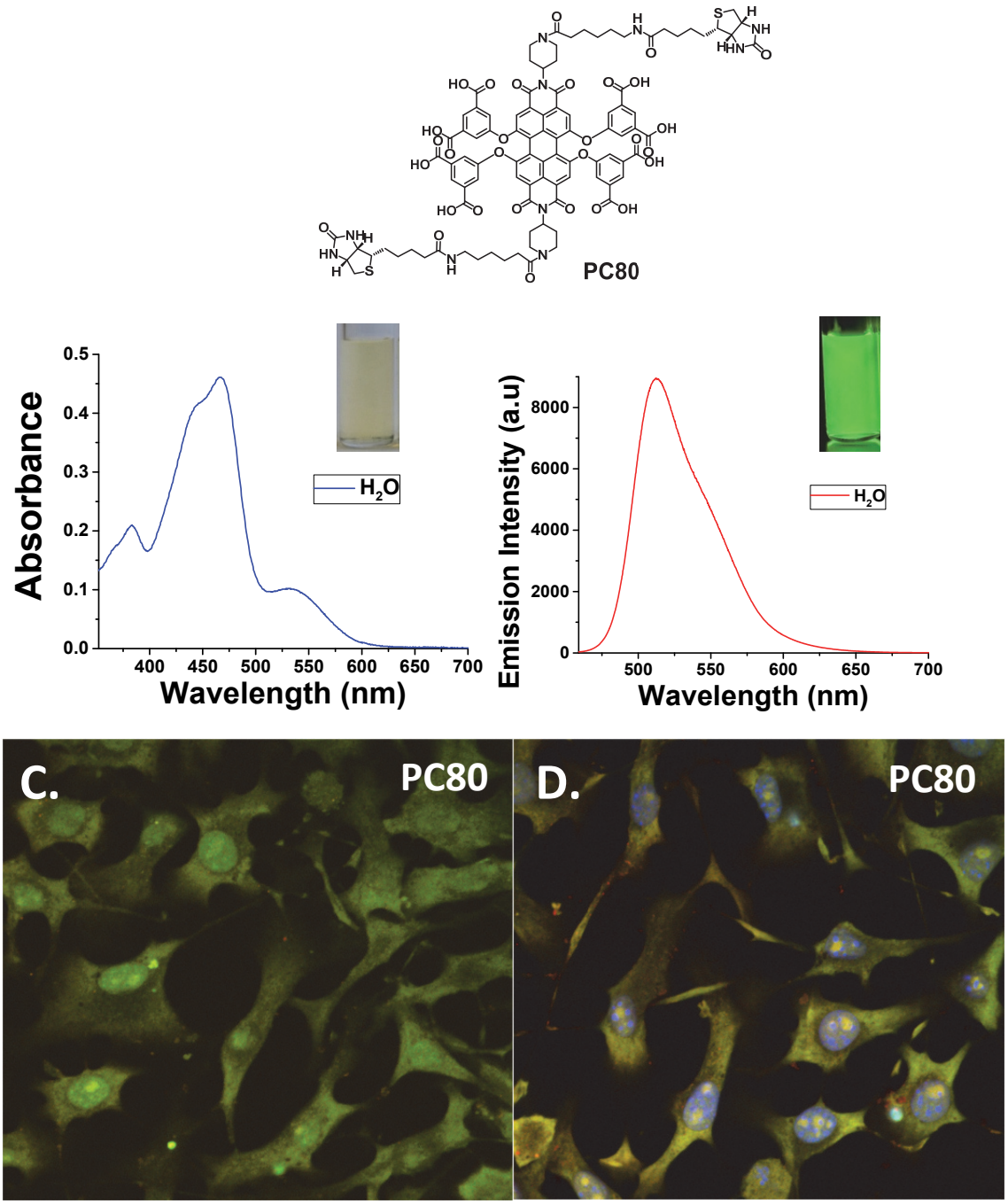

Figure 8. Confocal microscopy images of cells cultured from HeLa and treated with **PC79** (above) and **PC80** (below) for 72 h. **Left (A and C).** Any region is stained (green channel) and **Right (B and D).** The nucleus is stained with Hoechst 33342 (blue channel). The images are pseudocolored.

The probe **PC91** is also completely soluble in water. This compound was not observed in confocal microscopy because it was synthetized after the preceding studies. Therefore, the discovery of the cell regions where **PC91** migrate was performed by means bioimaging microplate reader. As observed in the Figure 9, **PC91** is successfully internalized in the cells at 10 µM within 24 h and it seems to be localized mainly in the nucleus (Figure 9.B and Figure 9.C).

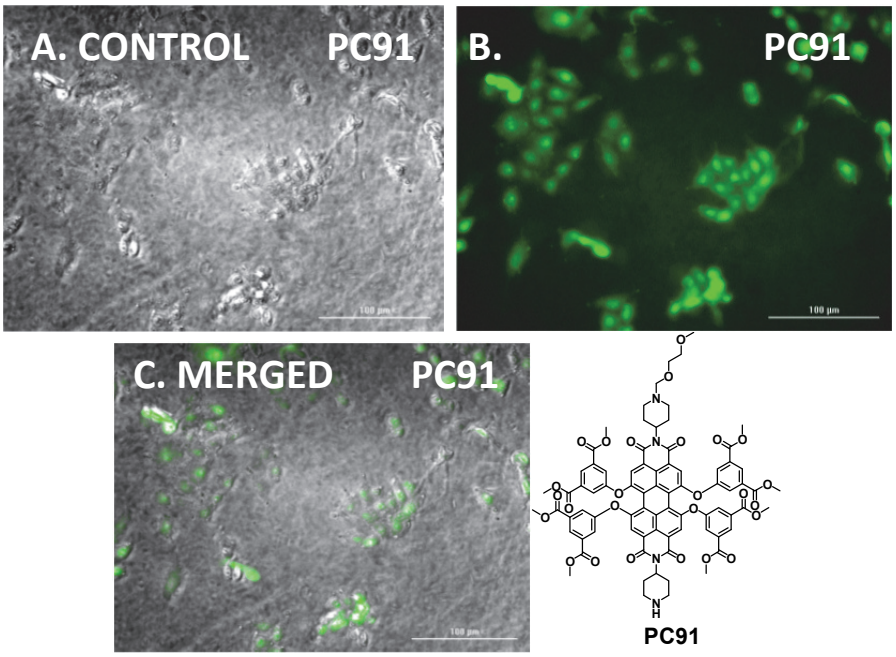

Figure 9. Images using a bioimaging microplate reader of SW480 cells (colon adenocarcinoma cells) treated with 10 µM of **PC91** after 24 h of incubation. A) Phase contrast, B) Green fluorescence emission and C) Merged.

2.3. MTT cell proliferation assay and cytoxicity.

Cytotoxicity was evaluated by means of the antiproliferative assay MTT,[18] which is a high-throughput colorimetric method widely used for the screening of new drugs that is based on the ability of the mitochondrial dehydrogenases to reduce a water soluble yellow dye, namely 3-(4,5-dimethylthiazol-2-yl)-2,5-diphenyl tetrazolium bromide, to form a water insoluble blue formazan (Figure 10). The purple colour formation is measured in a UV-Vis spectrophotometer at 590 nm and the measurement is proportional to viable cells.

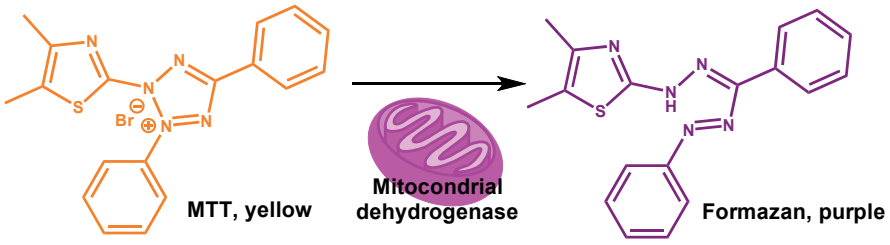

Figure 10. Reduction of MTT underwent by viable cells, which have the enzyme mitochondrial dehydrogenase.

Herein, these measures were carried out in two kind of cells: SW480 (colon adenocarcinoma cells) and in HeLa cells (cancer cells: cervical cancer) *vs*. IMR-90 (normal cells: lung fibroblasts). Cytotoxicity was expressed as IC_{50} values, that is, the concentration of the tested compound that yields 50 % of survival cells.

[18] J. van Meerloo, G. J. Kaspers, J. Cloos, *Methods Mol. Biol.*, **2011**, *731*, 237-245.

2.3.1. Cytoxicity study of ligand PC66.

The cytotoxicity of **PC66** in SW480, after 24 h of incubation time was evaluated by means of MTT proliferation assay, being the IC_{50} = 203 ± 1.5 µM, very high in comparison with the antitumor doxorubicin (IC_{50} = 65.3 ± 3.3 µM). Hence, **PC66** presents low cytoxicity. **PC66** cytotoxicity was also evaluated in HeLa and IMR-90 cells with 72 h of incubation time. As it can be deduced from Figure 10 the IC_{50} is higher than 80 µM confirming the low cytotoxic activity of **PC66** both in cancer and in healthy cells even with 72 h of exposure time (Figure 11).

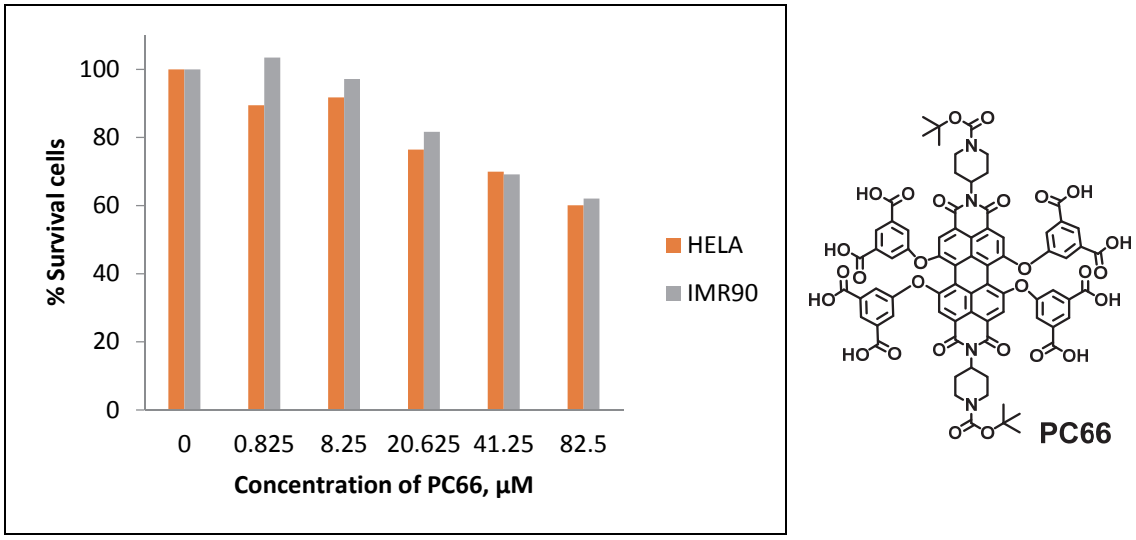

Figure 11. Cytoxicity evaluation with MTT cell proliferation assay for **PC66**.

2.3.2. Cytoxicity study of ligand PC71.

The cytotoxicity of **PC71** in SW480 after 24 h of incubation time was evaluated by means of MTT proliferation assay, being the IC_{50} = 19.8 ± 1.2 µM. In this cell line, **PC71** has higher cytotoxic activity than doxorubicin (IC_{50} = 65.3 ± 3.3 µM). This IC_{50} value is surprising due to the low or moderate cytotoxicity reported in bibliography for this kind of compounds. Its cytotoxic activity was also evaluated in HeLa and in IMR-90 cells after 72 h of exposure time, in this case, we could not evaluate cytotoxicity due to precipitation processes (Figure 12).

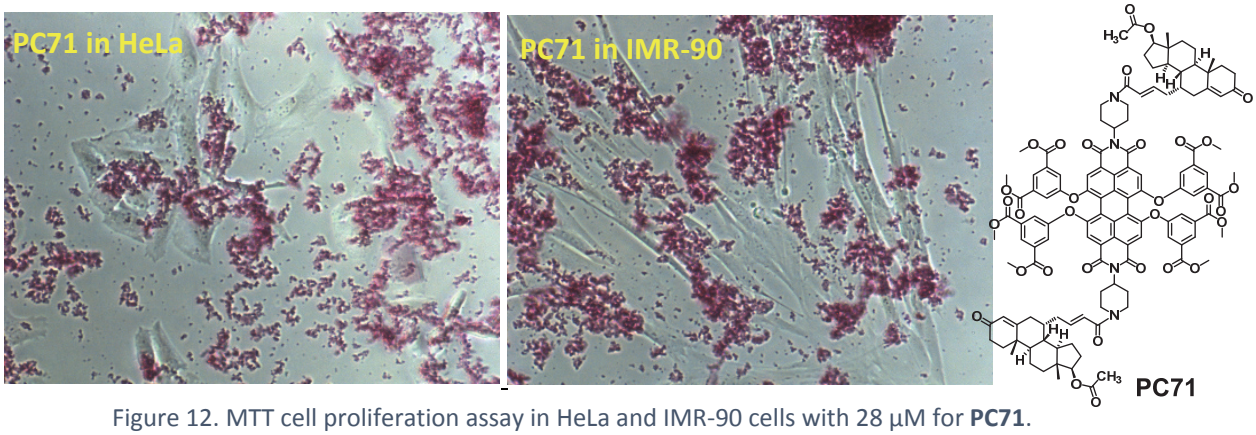

Figure 12. MTT cell proliferation assay in HeLa and IMR-90 cells with 28 µM for **PC71**.

2.3.3. Cytoxicity study of ligand PC73.

The cytotoxicity of **PC73** was not evaluated because it exhibits a very poor solubility.

2.3.4. Cytoxicity study of ligand PC79.

The cytotoxicity of **PC79** in SW480 after 24 h of incubation time is not appreciable. In fact, this ligand has a survival around 70 % after 72 h at 16 µM of **PC79** (Figure 13), where precipitation occurs (Figure 14).

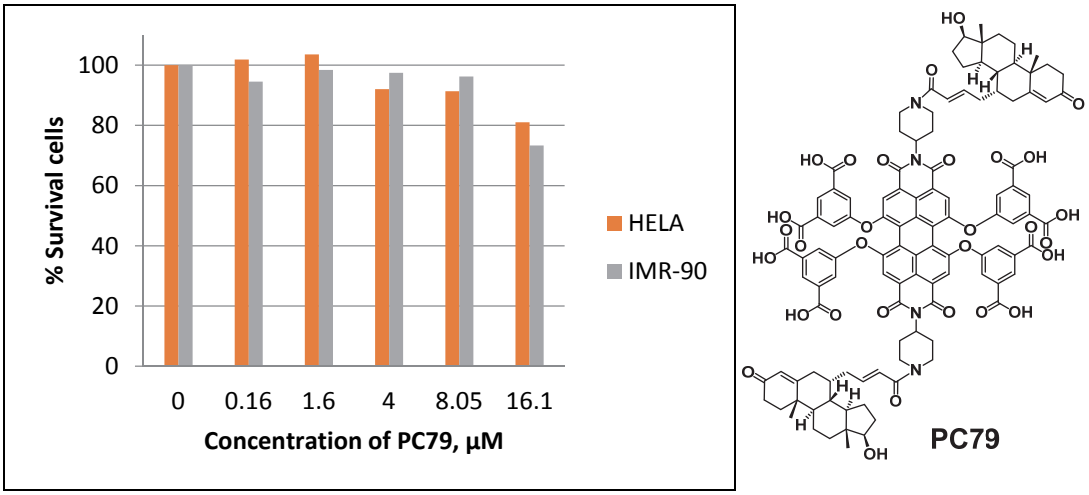

Figure 13. Cytoxicity evaluation with MTT cell proliferation assay for **PC79**.

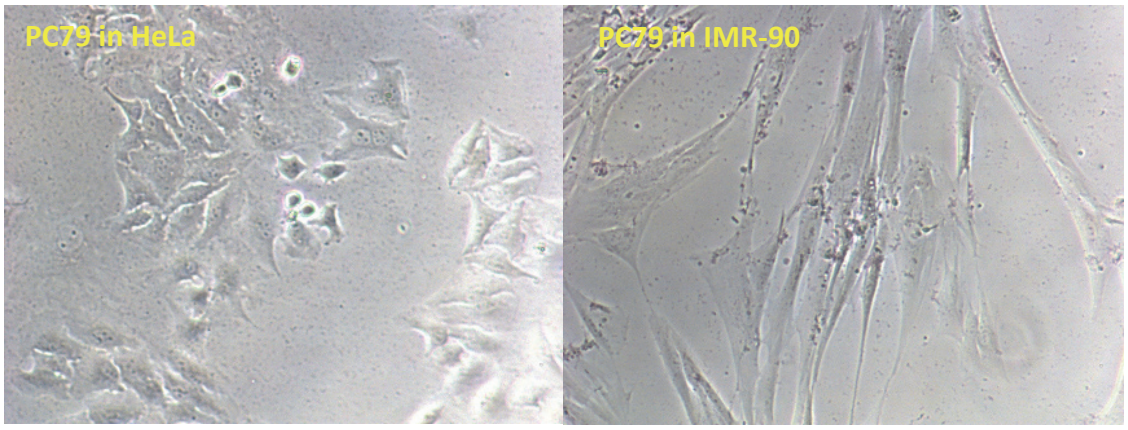

Figure 14. MTT cell proliferation assay in HeLa and IMR-90 cells with 16.1 µM of **PC79**.

2.3.5. Cytoxicity study of ligand PC91.

PC91 displays solubility problems in cell medium without FBS even at very low concentrations. It seems to be not cytotoxic at all in the concentration range tested even if cellular morphological changes are evident as a function of **PC91** concentration (Figure 16). Taken into account the MTT results, these cells finally managed to get adapted to the medium after the 72 h of incubation (Figure 15).

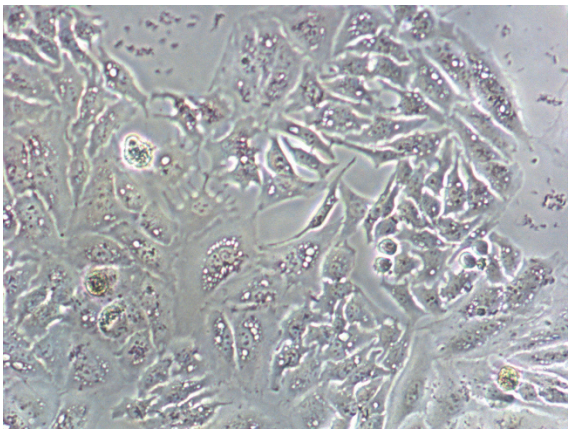

Figure 15. HeLa cells after 72 of incubation 6.25 µM of **PC91**.

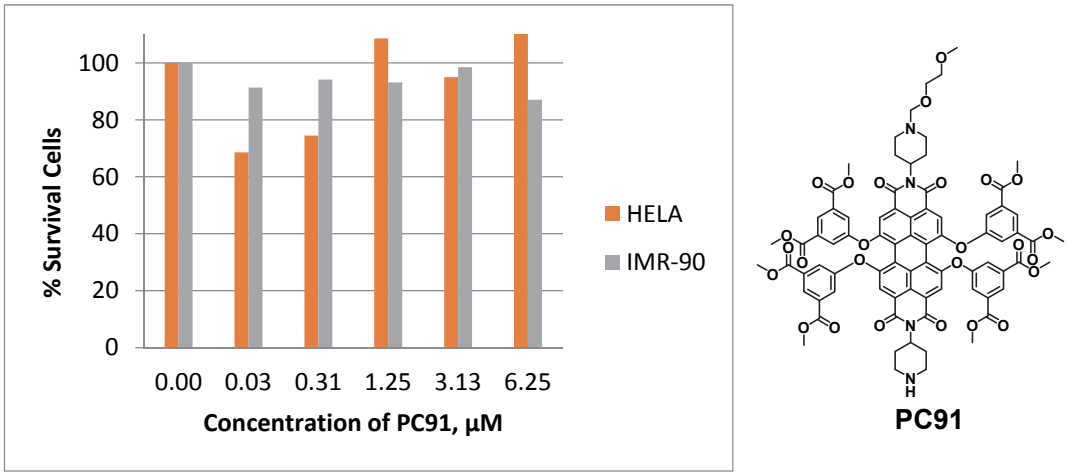

Figure 16. Cytoxicity study of **PC91** using the information of MTT cell proliferation assay.

2.3.6. Cytoxicity study of ligand PC80.

The study of the cytotoxicity of **PC80** in HeLa and IMR-90 cells after 72 h of incubation time reveals that **PC80** is more cytotoxic in healthy cells than in tumour cells (Figure 17).

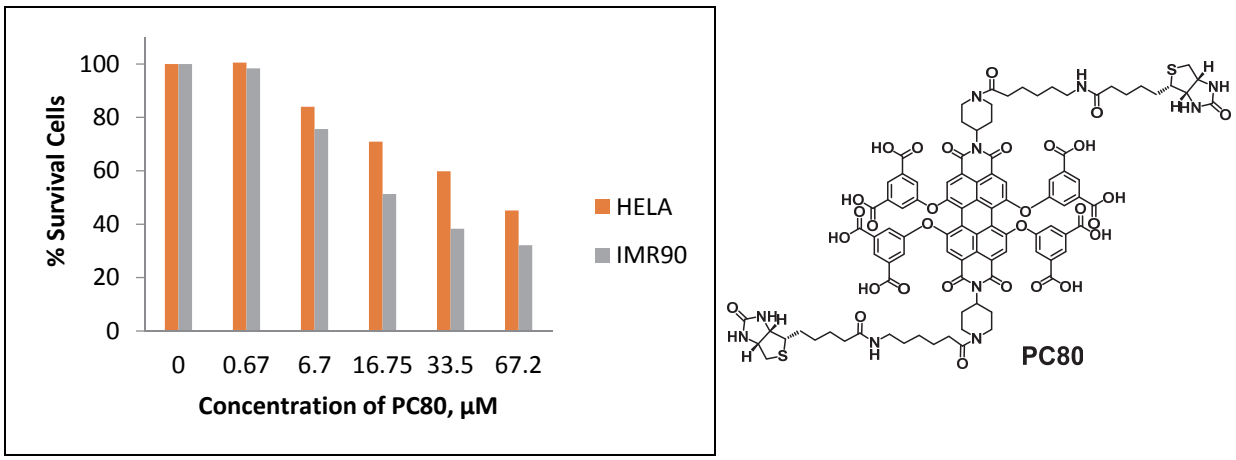

Figure 17. Cytoxicity of **PC80** in IMR-90 (normal cells) and HeLa (cancer cells).

3. CONCLUSIONS.

Potentially water-soluble and fluorescent tetra-substituted perylenediimides have been obtained. Moreover, tetra-substituted perylenediimides with biological molecules in peri positions: biotin and testosterone have been synthesized.

The water-soluble perylenediimides (**PC66**, **PC79**, **PC80** and **PC91**) are able to internalize inside the cells. As a rule, neither of these tetra-substituted perylenediimides exhibit a high cytotoxicity, consequently, their biocompatibility in cells *in-vivo* has been demonstrated.

CHAPTER 2B. TARGETING G-QUADRUPLEX STRUCTURES WITH WATER-SOLUBLE FLUORESCENT PERYLENEDIIMIDES

PATRICIA CALVO GREDILLA Ph. D. THESIS

SUMMARY

Perylenediimides with a different substitution in peri-position have been developed as water-soluble fluorescent probes to target and discriminate G-quadruplex structures from DNA duplex in solution.

1. G-QUADRUPLEX STRUCTURE.

Between the 19th and 20th centuries,[1] important discoveries led to the sequence of the human genome.[2] The knowledge of human genome provided a useful map to explore the occurrence and frequency of DNA secondary structures.[3] The best-described structure of all the possible secondary DNA or RNA assemblies (cytosine-rich regions or RNA i-motifs)[4] is G-quadruplex DNA (G4-DNA) involving the Hoogsteen bonds. The association of four guanines by a network of eight hydrogen bonds generates a planar structure called G-tetrad, which is stabilised by internal interactions between the lone pair of oxygen atoms and a cation (K^+, Na^+). The π-π stacking of several G-tetrads forms G-quadruplex (Figure 1).[5]

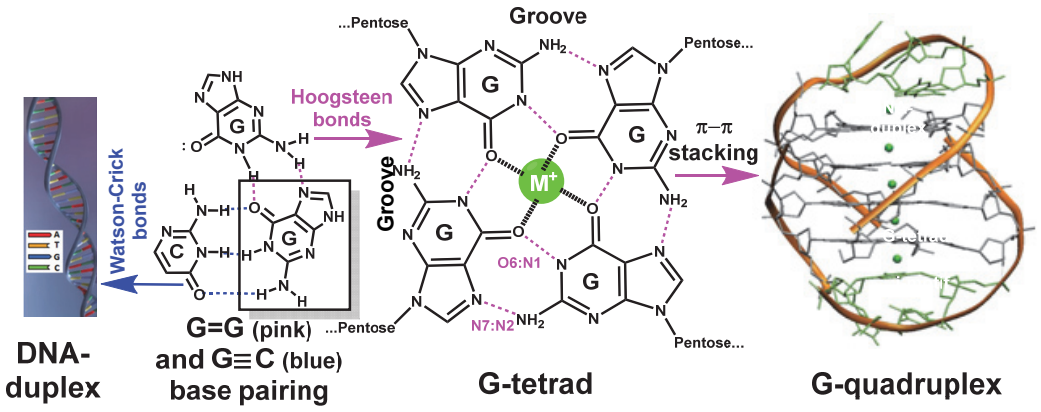

Figure 1. Schematic structure of hydrogen bonds of guanine sites involved in Watson-Crick (blue dashed lines) and Hoogsteen (pink dashed lines) base pairing. The association of C≡G generates DNA-duplex and the association of G=G generates G-tetrad. The π-π stacking of several G-tetrads forms G-quadruplex.[6]

The stacked G-tetrads linked by the pentose-phosphate backbone constitute the core of all G4 structures. So, guanosines (base-pentose) are able to form a helicoidal structure by self-assembly and π-π stacking of G-tetrads and, for this reason, they generate the structural diversity of G4. The G-quadruplex polymorphism is described by:[7]

a) Number of strands. Two categories can be described: intermolecular (formed by association of four, three or two strands) and intramolecular (ordered in a single nucleic acid strand) as it is shown in the Figure 2a.

b) Orientation of strands. It is defined by the 5'-3' directionality of the phosphate backbone. Depending on the orientation of the aromatic base towards the sugar, the guanines can adopt two different conformations within G-tetrad, syn and anti (Figure 2b).

c) Conformation of loops. Loops are the sequences located between the blocks of guanines and linked G-tetrads. The diverse conformations could be seen in the Figure 2c.

---

[1] R. Dahm, *Dev. Biol.*, **2005**, *278*, 274-288.

[2] a) I. H. G. S. Consortium, *Nature*, **2001**, *409*, 860-921; b) F. S. Collins, M. Morgan, A. Patrinos, *Science*, **2003**, *300*, 286-290.

[3] Y. Qin, L. H. Hurley, *Biochimie*, **2008**, *90*, 1149-1171.

[4] V. Brázda, L. Hároníková, J. C. C. Liao, M. Fojta, *Int. J. Mol. Sci.*, **2014**, *15*, 17493-17517.

[5] V. Casagrande, *Stabilization of G-quadruplex structures by specific ligands: towards anti-HIV aptamers and new anticancer drugs*, Ph.D. Thesis, Universita' degli studi di Roma "La sapienza", Italy, **2009**.

[6] S. Burge, G. N. Parkinson, P. Hazel, A. K. Todd, S. Neidle, *Nucleic Acids Res.*, **2006**, *34*, 5402-5415.

[7] A. Kerkour, *Study of DNA G-quadruplex structures by Nuclear Magnetic Resonance (NMR)*, Ph. D. Thesis, L'Université de Bordeaux, France, **2014**.

d) Nature of cations. Depending on the cation, two different associations can take place: interactions with the central ions inserted between G-tetrads and/or with external ions of the negative charges of the phosphate backbone.

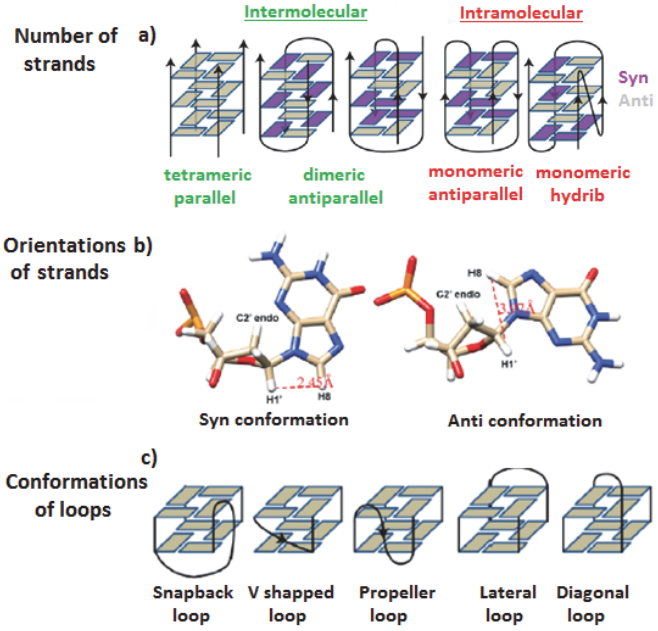

Figure 2. Overview of G-quadruplexes polymorphism.

2. BIOLOGICAL FUNCTIONS OF G-QUADRUPLEXES AND LIGANDS THAT STABILIZE THIS STRUCTURE.

Depending on the location of G4 in the genome, the biological function may be related to the following chromosome sites:

A) Promoters of genes or oncogenes,[8] which are regions of genes or oncogenes that start the transcription. The formation of G4 in different sequences of the promoters (*c-myc*, *c-kit*, *bcl2*) and their derivate processes are being studied nowadays.

B) Minisatellites, which are DNA segments mainly near the ends of the chromosomes that consist of repeating series from 5 to 100 nucleotides. These are associated with hypermutability and genomic instability.[9]

C) Genes that codified the immunoglobulin class switching regions, which are connected with meiosis and telomeres.[10]

D) RNA quadruplexes: G4 forming by RNA are presented on both coding and non-coding RNA. Such structures play a key role in regulation and translation as well as in genomic stability and disease.[11]

E) Telomeres, which are nucleoprotein complexes localized at the end of chromosomes in eukaryotic cells. Their functions are tied to the reactivation of telomere elongation

[8] L. Yuan, T. Tian, Y. Chen, S. Yan, X. Xing, Z. Zhang, Q. Zhai, L. Xu, S. Wang, X. Weng, B. Yuan, Y. Feng, X. Zhou, *Sci. Rep.*, **2013**, *3:1811*,

[9] A. J. Jeffreys, R. Barber, P. Bois, J. Buard, Y. E. Dubrova, G. Grant, C. R. H. Hollies, C. A. May, R. Neumann, M. Panayi, A. E. Ritchie, A. C. Shone, E. Signer, J. D. H. Stead, K. Tamaki, *Electrophoresis*, **1999**, *20*, 1665-1675.

[10] D. Sen, W. Gilbert, *Nature*, **1988**, *334*, 364-366.

[11] A. Bugaut, S. Balasubramanian, *Nucleic Acids Res.*, **2012**, *40*, 4727-4741.

mechanism, which usually occurs by the over-expression of telomerase and to protect the telomere function.[12]

The sequences with the potential to form quadruplexes are widely present in the genome of all organisms.[5] Therefore, the recognition and formation rules of G4 assembly is crucial to comprehend its function and theirs applications *in-vivo*. It is worth to mention that the formation of the G4-DNA occurs *in-vitro* studies, but the existence of it *in-vivo* has not absolutely been demonstrated, as well as the effect of ligands in the stabilization of G4. The stabilization often results from the π-π stacking and the electrostatic interactions.[7] The types of ligands more used for stabilizing the G4-DNA are [13,14,15] (Figure 3):

A. Protonated ligands: BRACO-19, PIPER, MMQ1, L2H2-6M(2)OTD.

B. *N*-methylated ligands: TMPyP4, 360A, Phen-DC3, RHPS4 and even metallo-organic G-quadruplex ligands with copper, manganese or nickel among them.

C. Neutral and negatively charged ligands: NMM, Telomestatin, HXDV.

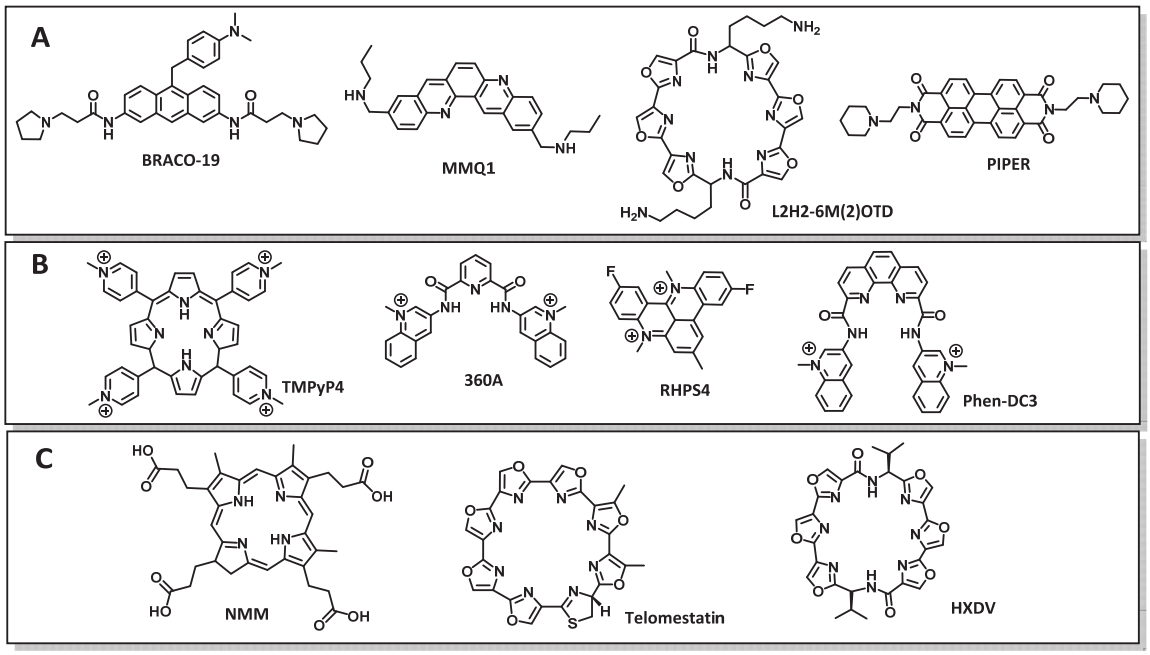

Figure 3. Three types of G4-ligands.

Hurley's *et al.* orientations pointed toward more extended aromatic molecules such as the perylenediimide PIPER. This molecule presents a broader hydrophobic core and a peculiar relationship between aggregation state and quadruplex-versus duplex-DNA selectivity.[14] More recently, according to the literature[16] high binding constants have been reported (10^5–10^7 M^{-1}) between G-quadruplex and PIPER ligand.

In this sense, cationic G-quadruplex-ligands based on perylenediimides are studied in this thesis for studying the interactions between them.

[12] A. D. Cian, L. Lacroix, C. Douarre, N. Temime-Smaali, C. Trentesaux, J.-F. Riou, J.-L. Mergny, *Biochimie*, **2008**, *90*, 131-155.

[13] A. Artese, G. Costa, F. Ortuso, L. Parrotta, S. Alcaro, *Molecules*, **2013**, *18*, 12051-12070.

[14] D. Monchaud, M.-P. Teulade-Fichou, *Org. Biomol. Chem.*, **2007**, *6*, 627-636.

[15] A. D. Rache, J.-L. Mergny, *Biochimie*, **2015**, *115*, 194-202.

[16] a) G. A. L. Bare, B. Liu, J. C. Sherman, *J. Am. Chem. Soc.*, **2013**, *135*, 11985-11989.; b) H. Yaku, T. Murashima, H. Tateishi-Karimata, S.-i. Nakano, D. Miyoshi, N. Sugimoto, *Methods*, **2013**, *64*, 19-27.

3. AIM OF THE CHAPTER.

The aim of this chapter is to improve the existing results in the important field of genomic science. Specifically, a variety of G4 ligands based on water-soluble fluorescent perylenediimides are going to be developed in order to analyse their biological effects and potential uses as biomarkers or tools on the way to inhibit telomerase action *in vitro*. The subject has been studied in collaboration to Dra. Natalia Busto Vázquez, who performed the G-quadruplex experiments, and Begoña García Ruiz, both from the Physical Chemistry research area of University of Burgos, and Dr. Jean-Louis Mergny, who directed the work and provided for the methodology (I.E.C.B, Bordeaux University, France). Our research group synthetized the perylenediimides and Dr. Gervais Beruvé (Department of Chemistry-Biochemistry and Physics, University of Québec at Trois-Rivières, Trois-Rivières, Québec, Canada) provided us the testosterone derivative. Dra. Natalia Busto performed all the biological experiments related with the G4-DNA binding, part of the G4 tests was carried out in Burgos University and another part in the IECB (Institut Européen de Chimie et Biologie) under the supervision of Dr. Jean-Louis Mergny from Bordeaux University.

4. INTERACTIONS BETWEEN PC66, PC73, PC71, PC79, PC80, PC91 AND G4-DNAs.

PC66, PC71, PC73, PC79, PC80 and **PC91** are the compounds to be tested in order to elucidate if they can distinguish G4-DNA from DNA-duplex and/or to target unambiguously G4-DNA structures. These investigations will allow us to characterise not only the different modes of binding, but also the affinity, the underlying interaction forces, the observed structural and conformational changes in the polynucleotide structure.

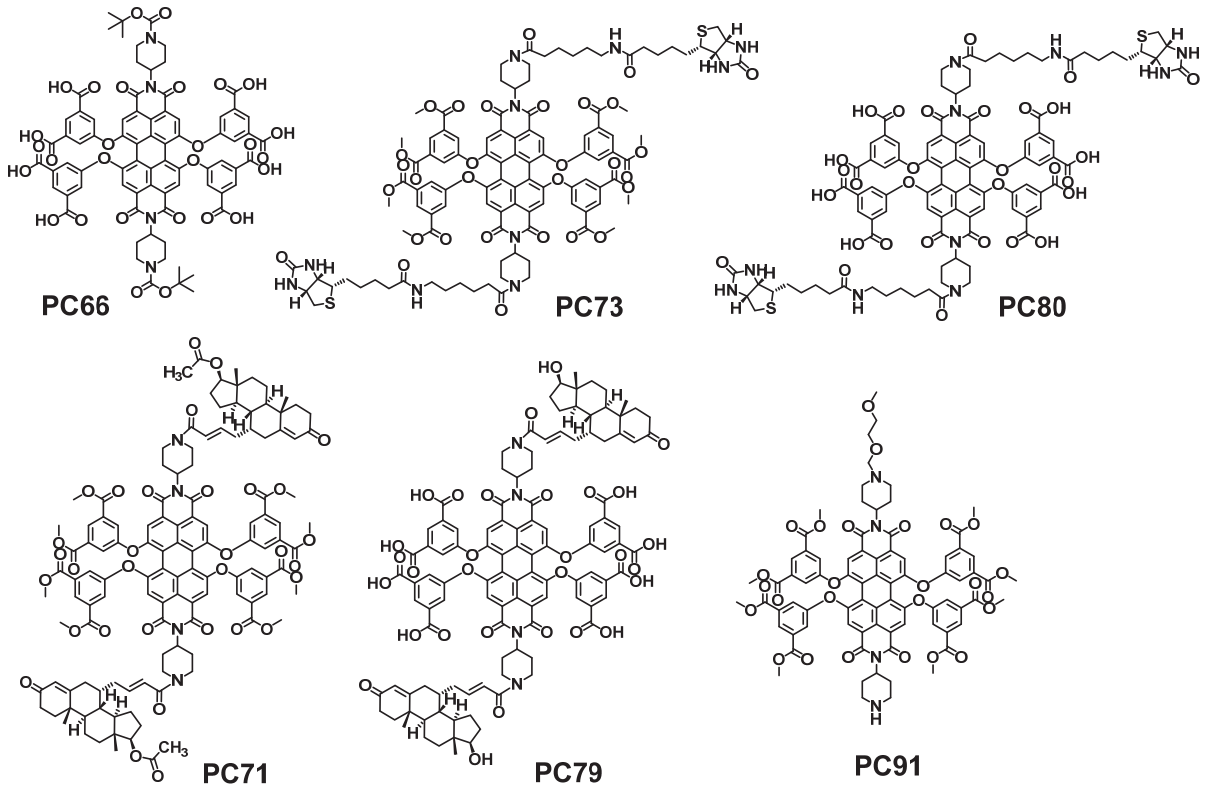

Figure 4. Structures of **PC66, PC71, PC73, PC79, PC80** and **PC91**.

Then, G4-DNA binding will be studied by including different types of telomeric G4-DNA (Tel 22) and non-telomeric structures as protooncogens (*c-myc*). In order to perform the study, the subsequent techniques were used:

- **FRET melting assay**:[15] this technique is used to measure the stabilization and selectivity of ligands towards the G-quadruplex. This consists of comparison between the thermal stabilities of G4 assembly in the presence and in the absence of ligands. As a result, the binding affinity is correlated with the increase in melting temperature (ΔT_m) of a fluorescently labelled G4. In practice, a G4-oligonucleotide is covalently labelled with a fluorophore and a quencher, FAM (6-fluorescein phosphoramidite) and TAMRA (tetramethylrhodamine) respectively,[17] to certain distance R_0 from each other (to R_0 only emits FAM) (Figure 5A). By increasing the temperature, G4 is unfolded and the distance, R, between FAM and TAMRA is higher than R_0. For that reason, the FAM emission is increased. T ½ (is the temperature value for which the normalised emission is 0.5) values, ΔT ½, is the number to indicate the stabilisation of the G-quadruplex structure due to ligand binding (Figure 5B). The higher the ΔT ½ value for a ligand, the better is its affinity with the diverse types of G4, shown in the Figure 5C.[18] The description and the sequence of used oligonucleotides in FRET Melting Assay is shown in Table 1.

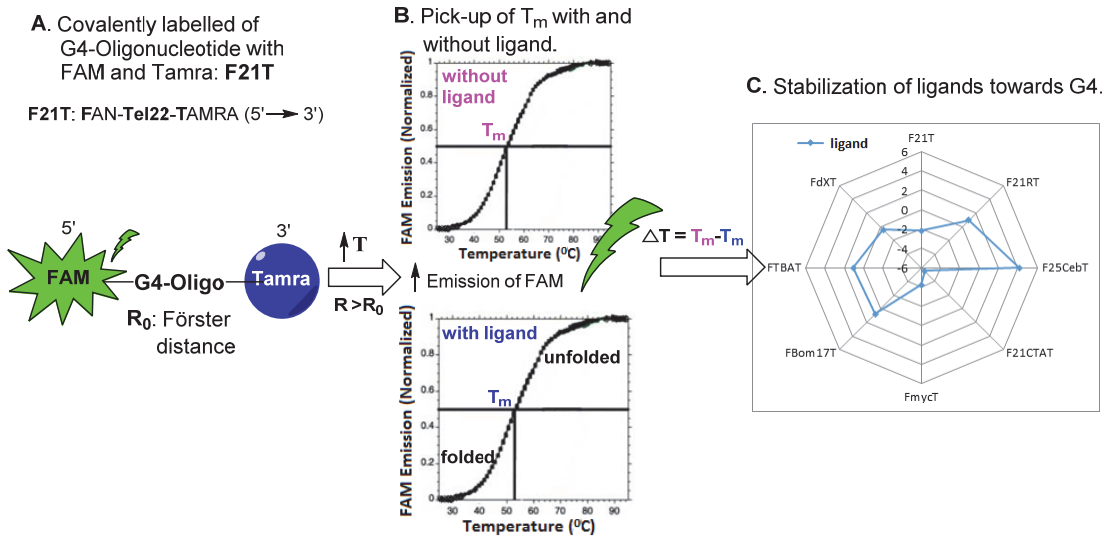

Figure 5. General steps (A→B) to obtain a radial plot, which provides an overview of the ligand selectivity (C).

Oligonucleotide	Sequence (FAM 5'-……..-3' TAMRA)
F21T–Telomeric DNA hybrid G4 (3 tetrads)	GGG TTA GGG TTA GGG TTA GGG
F21RT–Telomeric RNA hybrid G4 (3 tetrads)	GGG UUA GGG UUA GGG UUA GGG
F25CebT–Human minisatellite DNA parallel G4 (3 tetrads), long loop	A GGG T GGG TGT AAGTGT GGG T GGG T
F21CTAT–Telomeric DNA antiparallel G4 (3 tetrads)	GGG CTA GGG CTA GGG CTA GGG
FmycT–Protooncogene DNA parallel G4 (3 tetrads)	TTGA GGG T GGG TA GGG T GGG TAA
FBom17T–Telomeric DNA of *Bombyx* antiparallel G4 (2 tetrads)	GG TTA GG TTA GG TTA GG
FTBAT–Thrombin/Binding Aptamer antiparallel (2 tetrads)	GG TT GG TGT GG TT GG
FdxT–Intramolecular DNA duplex	TATAGCTAT- hexaetilenglicol-TATAGCTATA

Table 1. Used oligonucleotides in FRET Melting Assay.

[17] M. K. Johansson in: *Methods in Molecular Biology, vol. 335: Fluorescent Energy Transfer Nucleic Acid Probes: Designs and Protocols*, Edited by: V. V. Didenko, Humana Press Inc., Totowa, N.J., Chapt. 2.
[18] http://www.al-nasir.com/articles/pharmacy_chemistry/G-Quadruplex.shtml

- **Fluorescence titrations**: this technique can report molecules that become more fluorescent in the presence of quadruplex DNA. The technique used a set of G4-DNA of diverse structures and sequences to allow the screening for selectivity as to quadruplex structural type and sequence.

  Absorbance titrations: this technique determines whether there is any interaction between G4 and the ligand by shifting of the maximum position when the ligand is free or complexed with G4. The shifter the band is the more intense is the interaction strength.

  These experiments provide information such as stoichiometries and binding constants between G4-ligand.

- **CD (Circular Dicroism) experiments:**[19] this technique is able to distinguish between the orientation of strands (anti and syn) and the formed angle between the stacked tetrads in G-quadruplex. Moreover, it is also determined the number of strands and depending on whether is G-quadruplex is parallel, antiparallel and hybrid, the CD graph will display a different shape.

  The information obtained by comparison between these techniques is useful to categorize the ligand, which specifically binds to G4-DNA.

4.1. Study interactions between G-quadruplex and the ligand PC66.

- **FRET melting assay**: the ligand **PC66** does not stabilize any G4, except for **F25CebT** (Human minisatellite DNA parallel G4 (three tetrads)) that is extremely weak stabilized. Moreover, **PC66** has been excluded as ligand (Figure 6) because it does not stabilize DNA-duplex (ctDNA: calf thymus DNA) and G-quadruplex (Tel22).

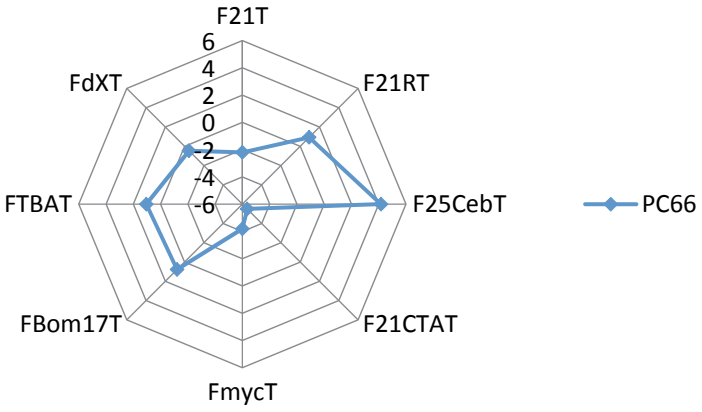

Figure 6. FRET melting selectivity profile for **PC66**.

4.2. Study interactions between G-quadruplex and the ligand PC71.

PC71 is not soluble in 100 % water, but it is soluble in a mixture of ≤ 1 % DMSO and 99 % of water. This mixture is enough to enable its study in the presence of DNA.

- **FRET melting assay**: **PC71** has been rejected as stabilizing agent, because this ligand cannot stabilize any G-quadruplex (Figure 7).

[19] L. M. Bruno Pagano, P. Zizza, J. Amato, N. Iaccarino, C. Cassiano, E. Salvati, E. Novellino, A. Biroccio, A. Casapullo, A. Randazzo, *Chem. Comm.*, **2015**, *51*, 2964-2967.

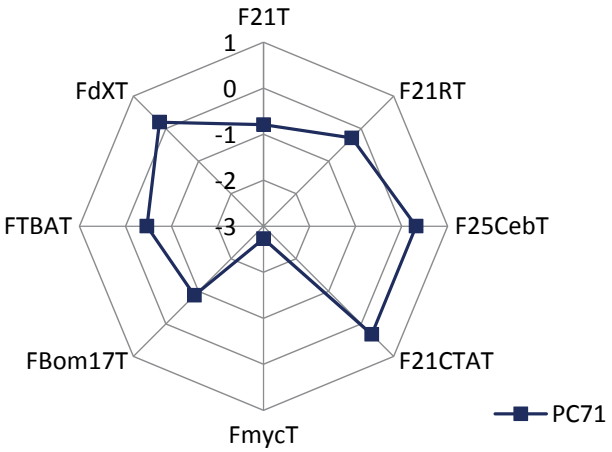

Figure 7. FRET melting selectivity profile for **PC71**.

4.3. Study interactions between G-quadruplex and the ligand PC73.

As in the case mentioned above, **PC73** is insoluble in 100 % water, but it is soluble in a mixture of ≤ 1 % DMSO and 99 % of water. This mixture is enough to be studied in the presence of DNA.

- **FRET melting assay**: the ligand **PC73** does not stabilize any G4. It is not helpful that is able to stabilize at the same time **F21RT** (telomeric RNA hybrid G4 (3 tetrads)) and **F25CebT** (Human minisatellite DNA parallel G4 (3 tetrads)). In view of the results obtained, **PC73** is not suitable as ligand of G-quadruplex (Figure 8).

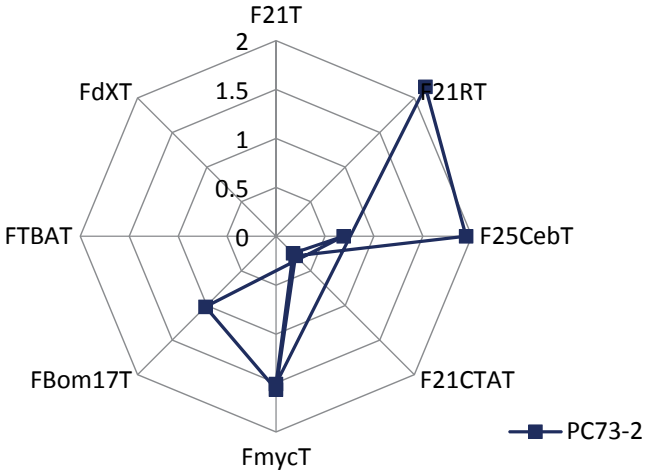

Figure 8. FRET melting selectivity profile for **PC73**.

4.4. Study interactions between G-quadruplex and the ligand PC79.

- **FRET melting assay**: the ligand **PC79** does not thermally stabilize G-quadruplex.

4.5. Study interactions between G-quadruplex and the ligand PC91.

- **FRET melting assay**: the ligand **PC91** stabilizes **FTBAT** (Thrombin-Binding Aptamer antiparallel G4 (2 tetrads)) and **FBom17T** (Telomeric DNA of Bombyx antiparallel G4 (2 tetrads)) and does not stabilize **FdxT** (intramolecular DNA duplex). As a result, the selectivity of **PC91** towards short quadruplexes was also observed in FRET since the thermal stabilization induced by **PC91** was greater for 2-tetrad than for 3-tetrad quadruplexes (Figure 9). Moreover, **PC91** becomes more stable with long G4 than with short G4.

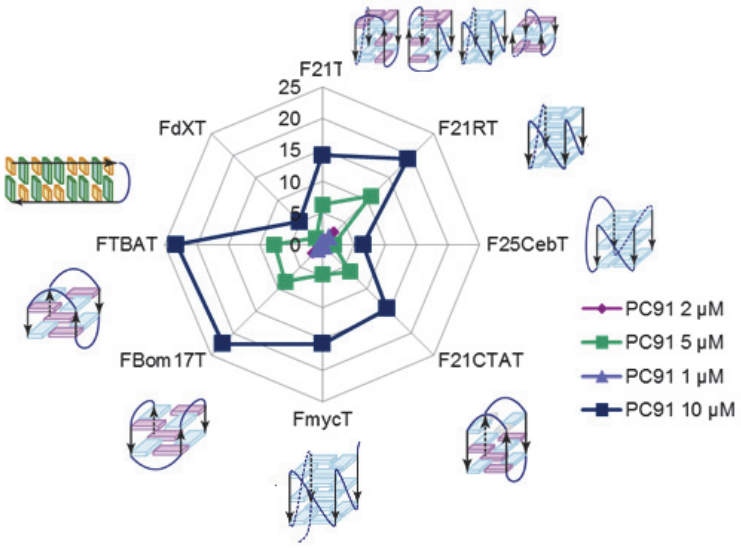

Figure 9. FRET melting selectivity profile for **PC91**.

- **Absorbance and Fluorescence titrations**:

The absorbance spectra slightly changes in the presence of increasing amounts of Tel22 (Figure 10.Top), these spectral changes are more pronounced when TBA is added instead of Tel22 (Figure 10.Bottom). The achieved binding constants are of 8.5×10^4 M^{-1} and 3.6×10^5 M^{-1} for the Tel22/**PC91** and TBA/**PC91** systems respectively. By contrast, neither binding isotherm nor analysable data were obtained when CT-DNA (duplex) is used for the titration instead of Tel22. It could be concluded that **PC91** cannot interact with double stranded DNA and that it has a higher affinity towards 2-tetrads over 3-tetrads G-quadruplexes.

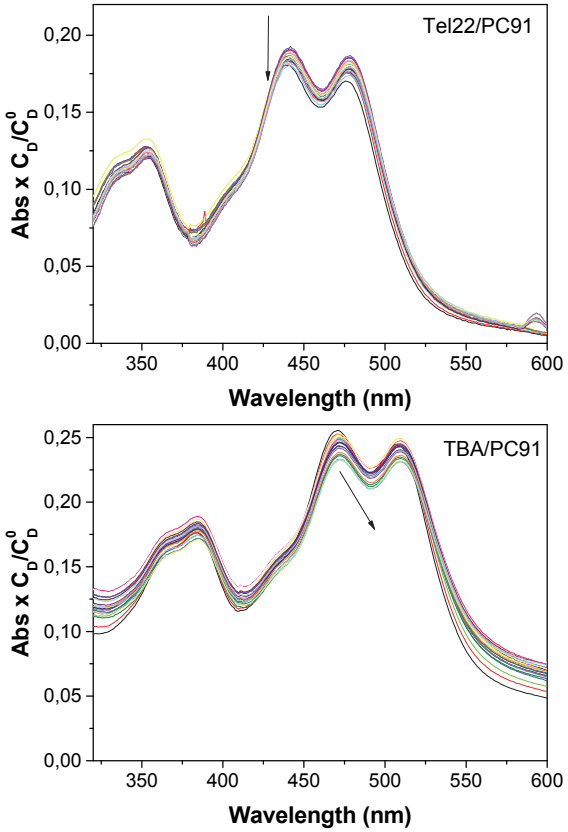

Figure 10. Absorbance spectra recorded during the titration of Tel22/**PC91** system (Top) and TBA/**PC91** system (Bottom). I = 0.11 M (10 mM LiCaC, 90 mM LiCl and 10 mM KCl, pH 7.4 and T = 25 °C. COD = 1.5×10^{-5} M.

Not significant CD change was observed by CD titrations (Figure 11).

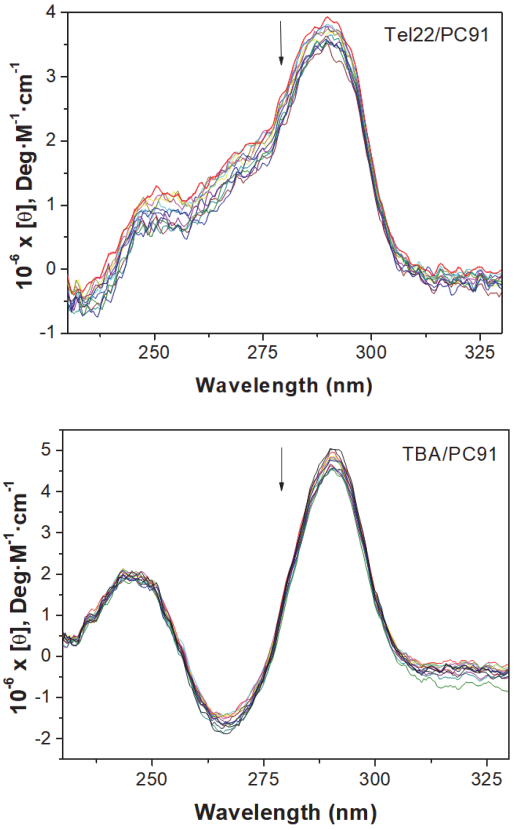

Figure 11. CD titrations of Tel22/**PC91** system (Top) and TBA/**PC91** system (Bottom). I = 0.11 M (10 mM LiCaC, 90 mM LiCl and 10 mM KCl, pH 7.4 and T = 25 °C. C0P = 20 µ M, CD/CP = 0-5.

4.6. Study of interactions between G-quadruplex and the ligand PC80.

- **FRET melting assay**: The FRET melting experiments reveal that **PC80** thermally stabilizes G-quadruplex structures. The best stabilization occurs for **FBom17T** (Telomeric DNA of Bombyx antiparallel G4 (2 tetrads)), it does not stabilize **FdxT** (intramolecular DNA duplex) and it does not distinguish between parallel and antiparallel (Figure 12).

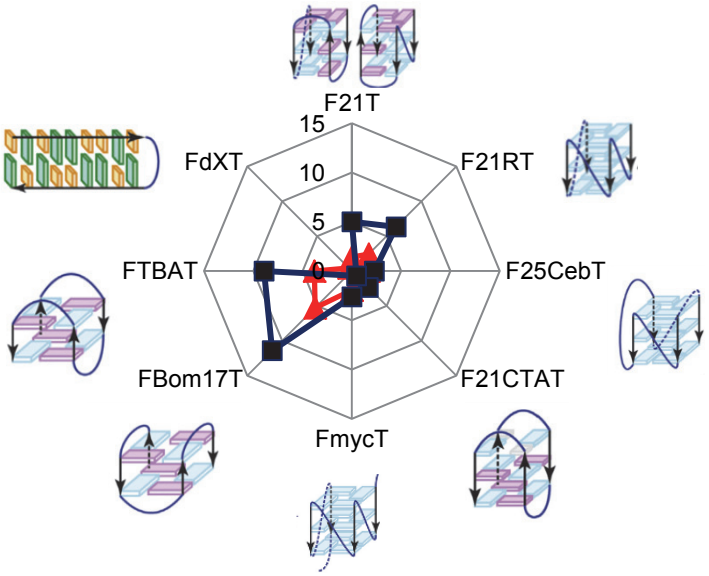

Figure 12. ΔTm Spider Plot of several oligonucleotides in the presence of (▲) 5 µM and (■) 10 µM of **PC80**. C_{Oligo} = 0.25 µM, I = 0.11 M (90 mM LiCl, 10 mM KCl, 10mM LiCaC) and pH = 7.2.

5. CONCLUSIONS.

The water-soluble perylenediimides **PC80** and **PC91** are capable to stabilize G4-DNA; even more **PC91** does not stabilize the intramolecular DNA duplex. With these findings, the work establishes an initial point to continue working in this subject.

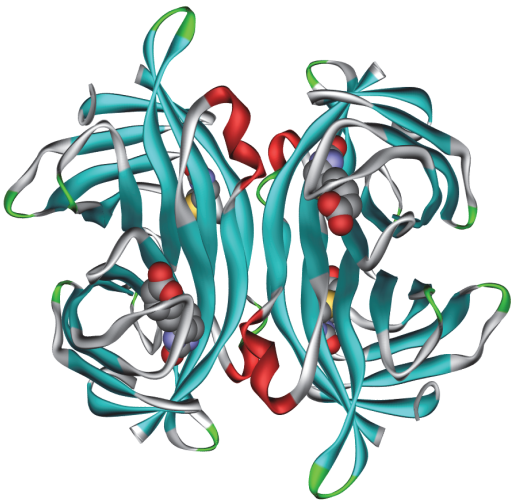

CHAPTER 2C. DETECTION OF PROTEINS THROUGH MOLECULAR RECOGNITION MEDIATED BY PERYLENEDIIMIDES

PATRICIA CALVO GREDILLA Ph. D. THESIS

SUMMARY

The detection of proteins through molecular recognition mediated by water-soluble fluorescent perylenediimides has been developed.

1. THE DETECTION OF BIOLOGICAL ANALYTES WITH FLUOROGENIC PROBES.

The detection of analytes with fluorescent probes is a useful and versatile technique not only in chemistry but also in biology because it offers the advantages of fluorescence spectroscopy, e.g. high sensitivity and straightforward detection procedure, combined with the high potential of chemical synthesis to prepare a fluorophore with the required substitution pattern. Hence, numerous probe molecules have been developed for the fluorimetric detection of biological analytes. Essentially all fluorescent probes indicate a target analyte by the change of the emission characteristics. As the steady-state emission spectra can be detected with simple and relatively cheap equipment, the majority of fluorescent probes transcribes the detection event on the molecular level into quenching or light-up effects or into significant shifts of the emission band. Fluorescent chemosensors have to fulfill several requirements to be seriously considered for the detection of biologically relevant analytes. Firstly, the probe must be sufficiently selective, i.e. it should have the ability to discriminate unambiguously between the target analyte and other components in the analyzed medium. With respect to the detection signal, emission quenching should rather be avoided, because quenching may also be induced by other external factors, such as collision with heavy atoms or paramagnetic species, electron transfer, proton transfer and energy transfer, which cannot be excluded under real conditions. In contrast, light-up probes are preferred, whose emission intensity increases strongly upon interaction with the analyte, because this effect is usually characteristic of the particular analyte. Even more desirable are probes, whose emission energy changes in the presence of an analyte, because this effect allows the determination of the ratio between the relative fluorescence intensities at two different emission wavelengths that refer to the two different emitting entities (i.e. probe with or without bound analyte) at different wavelengths, thus enabling a quantification by a ratiometric analysis with "internal" calibration. Furthermore, probes that absorb and emit at the low-energy range of the visible light or even in the near-infrared (NIR) region are especially useful for bioanalytical applications in order to minimize light-induced sample damage and to reduce autofluorescence of biological media. Last, but not least, good water-solubility or water-compatibility of the probes are a general requirements for any chemosensor that shall be applied in aqueous solutions.[1] As a new emerging area in chemical sensing, by using supramolecular aggregates, exhibits unique advantages over that using conventional small-molecule chemical sensors, in terms of high sensitivity and selectivity, and the simplicity of the sensory building blocks, inspired by specific biorecognition. Therefore, multiple noncovalent interactions operating in a cooperative manner can be used to design chemosensors with better performance than classic ones.[2] Supramolecular chemistry, dealing with a complex of molecules that are held together by noncovalent bonds, has led to the buildup of diverse supramolecular architectures in a bottom-up approach. By employing noncovalent interactions for detection of proteins or enzymes it is possible to achieve a chelating effect and the specificity in bio-recognition and sensing. Intermolecular networks of non-covalent interactions are responsible for a wide array of phenomena in fields of biology and chemistry. Biological systems use specific patterns of complementary functionality to provide exquisite control over biological recognition processes such as protein–protein and protein–nucleic acid

[1] a) J. K.-H. Wong, M. H. Todd, P. J. Rutledge, *Molecules* **2017**, 22, 200-228. b) A. Granzhan, H. Ihmels, M. Tian, *ARKIVOC,* **2015** (vi) 494-523. c) K. Chen, Q. Shu, M. Schmittel, *Chem. Soc. Rev.,* **2015**, *44*, 136-160. d) B. Daly, J. Ling, A. P. de Silva, *Chem. Soc. Rev.,* **2015**, *44*, 4203-4211. e) Z. Yang, J. Cao, Y. He, J. H. Yang, T. Kim, X. Peng, J. S. Kim, *Chem. Soc. Rev.,* **2014**, *43*, 4563-4601. f) J. Yao, M. Yang, Y. Duan, *Chem. Rev.,* **2014**, *114*, 6130-6178. g) X. Li, X. Gao, W. Shi, H. Ma, *Chem. Rev.,* **2014**, *114*, 590-659.

[2] Q. Wang, Z. Li, D.-D. Tao, Q. Zhang, P. Zhang, D.-P. Guo, Y.-B. Jiang, *Chem. Commun.*, **2016**, *52*, 12929-12939.

binding.[3] Therefore, controlled application of non-covalent interactions provides an effective tool for fabrication of new chemical sensors. One of the best methods for accurately measuring concentrations of specific proteins, even in complex mixtures, is through use of an active-site titration agent.[4] These are reagents that react stoichiometrically with the target protein and generate a defined change in absorbance or fluorescence of the solution without the need for any separation of reagents. This can be ideally achieved by using a fluorogenic probe for which the recognition is unambiguous. Perylenediimides that are soluble in water are of enormous interest for this kind of signaling systems.[5] As a proof of concept, we have selected the avidin-biotin system to test the suitability of our perylenediimide fluorescent probes for biological signaling.

2. FLUORESCENCE TITRATIONS OF A BIOTINYLATED DERIVATIVE IN THE PRESENCE OF AVIDIN.

The biotin-avidin binding has been widely exploited as a powerful tool in a variety of bioanalytical applications since the affinity between them is extremely high and the properties of various biomolecules are usually retained after biotinylation.[6] Researchers have focused on this interaction because of it is useful in many applications including immunoassays, biomolecule recognition, drug delivery, and cancer cell diagnosis.[7] Avidin, a tetrameric glycoprotein,[8] is present in the egg-white of birds, reptiles, and amphibians. A homotetramer of avidin binds up to four molecules of biotin (vitamin H or B7) through non-covalent interactions with a dissociation constant $K_d = 10^{-13}$ - 10^{-15} M (Figure 1).

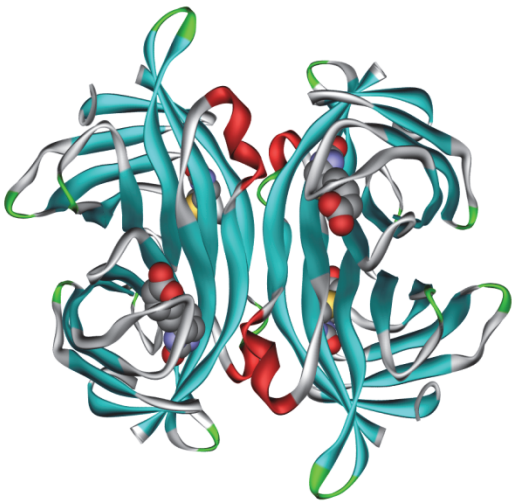

Figure 1. Representation of the tetrameric 3D-structure of avidin bonded to four biotin groups (CPK representation).

The strength of the avidin–biotin interaction is several orders of magnitude higher than the strength of typical antigen–antibody complexes, as much as that, this binding is practically

[3] V. M. Rotello, S. Thayumanavan, *Molecular Recognition and Polymers, Control of Polymer Structure and Self-Assembly*, John Wiley & Sons, Hoboken, New Jersey, **2008**.
[4] Z. Gao, M. Niikura, S. G. Withers, *Angew. Chem. Int. Ed.*, **2017**, *56*, 6112-6116.
[5] C. D. Schmidt, A. Hirsch, In: *Ideas in Chemistry and Molecular Sciences: Advances in Synthetic Chemistry.* B. Pignataro, Ed., Wiley-VCH, Weinheim, **2010**, Chapt. 13.
[6] K. K.-W. Lo, J. S.-Y. Lau, *Inorg. Chem.*, **2006**, *46*, 700-709.
[7] P. Strzelczyk, D. Pläzuk, J. Zakrzewski, G. Bujacz, *Molecules*, **2016**, *21*, 1-11.
[8] O. Livnah, E. A. Bayert, M. Wilchekt, J. L. Sussman, *Proc. Natl. Acad. Sci. USA*, **1993**, *90*, 5076-5080.

irreversible in Nature.[10] This high biotin-binding affinity is based on a large number of hydrogen bonds and hydrophobic interactions due to the architecture of the binding site. The structural motif of this protein consists of an eight-stranded antiparallel β-barrel surrounded by flexible loops. These β-strands that form the barrel are named A–H, whereas the loops surrounding the entrance to the binding pocket are designated AB, CD, EF, and GH (Figure 2).[7]

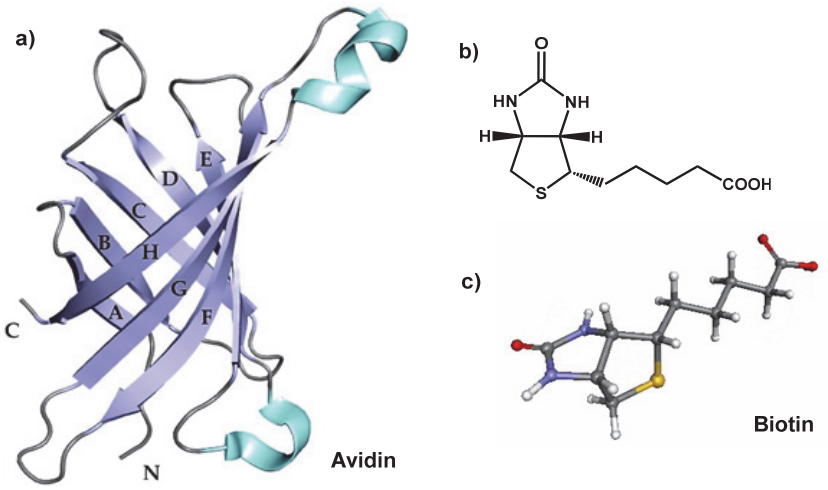

Figure 2. a) An illustrated representation of the monomeric avidin topology. b) Structure of biotin, c) 3D-structure of biotin.

Biotin is a water-soluble B-complex vitamin that is composed of an ureido (tetrahydroimidizalone) ring fused with a tetrahydrothiophene ring. One valeric acid is attached to one of the carbon atoms of the tetrahydrothiophene ring. Biotin is a coenzyme in the fatty acids and leucine metabolism and plays an important role in gluconeogenesis.[9]

Chemically synthesized biotin derivatives with ester linkage can be unstable in some in-vivo experiments. It is also possible to create derivatives possessing a C–C linkage obtained via Friedel–Crafts reaction,[10] but in general, the biotin is attached through an amide bond.

2.1. Titrations of PC73 with avidin and graphene oxide.

Biotin-avidin system is a good model for studying biomolecular interactions, such as recognition processes. It is employed in order to develop new detection paradigms. In this section the research is directed to obtain an analogous system between avidin-biotin in order to prove its behaviour, and then, to apply it to the interaction of other proteins.

The compound **PC73** (Figure 3) was prepared specifically to interact with avidin, therefore a study of the variation of the fluorescence of **PC73** in the presence of avidin and in the presence of graphene oxide was performed, then the study of the interaction between the synthetized biotinylated perylenediimide **PC73** (Figure 3) with avidin and graphene oxide was performed. Finally, a detailed fluorescent titration of **PC73** with a fixed amount of avidin was performed.

[9] A. Ghosal, H. M. Said, *Am. J. Physiol. Cell Physiol.*, **2011**, *300*, C97-C104.
[10] P. Strzelczyk, A. Bujacz, D. Plazuk, J. Zakrzewski, G. Bujacz, *Chem. Biol. Interact.*, **2013**, *204*, 6-12.

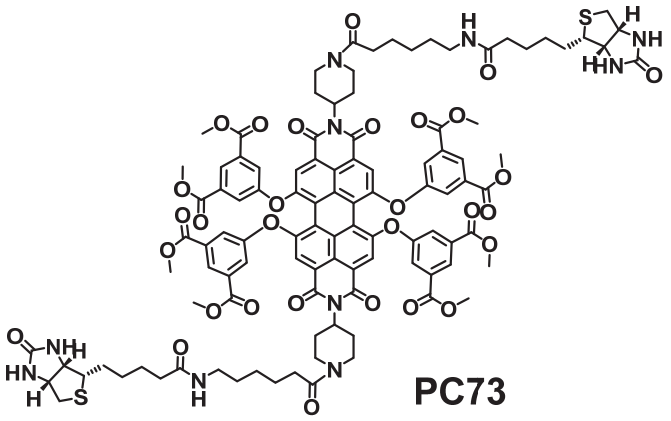

Figure 3. Structure of **PC73**.

Probe **PC73** is not soluble in water, so it is necessary to employ a co-solvent. The selected mixture of solvents was DMSO:H_2O 1:99, because this kind of perylenediimides are soluble and show fluorescence in this solvent mixture. The proportion is fixed in these parameters, owing to the future applications in cells. In this sense, DMSO is non-toxic for live cells in amounts lower than 1%. According to the strong interaction between avidin-biotin, there are four possible binding sites for biotin in the avidin moiety (Figure 4).

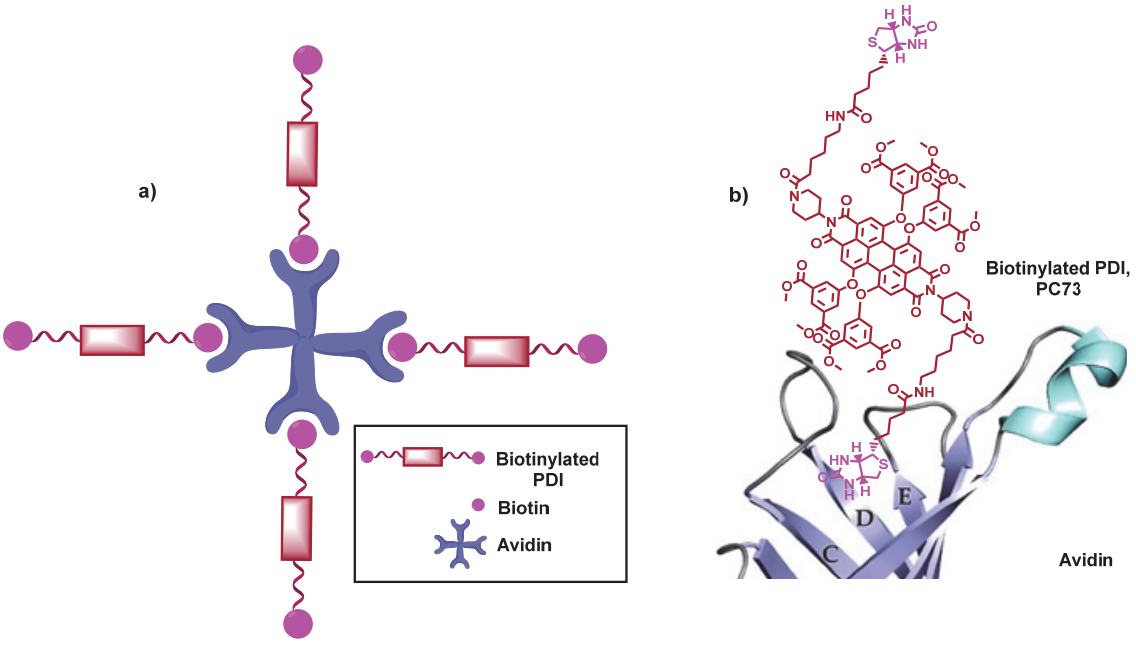

Figure 4. a) 1:4 (avidin:biotin) binding stoichiometry. b) An illustration of binding sites of avidin monomer, which could be occupied by biotin.

The next step is to study the interaction between **PC73** and avidin. The experiment is summarized in the Figure 5. In this assay the UV-Vis and Fluorescence titrations of **PC73** with avidin were carried out by adding from cero to several equivalents of avidin to the biotinylated PDI (Figure 5).

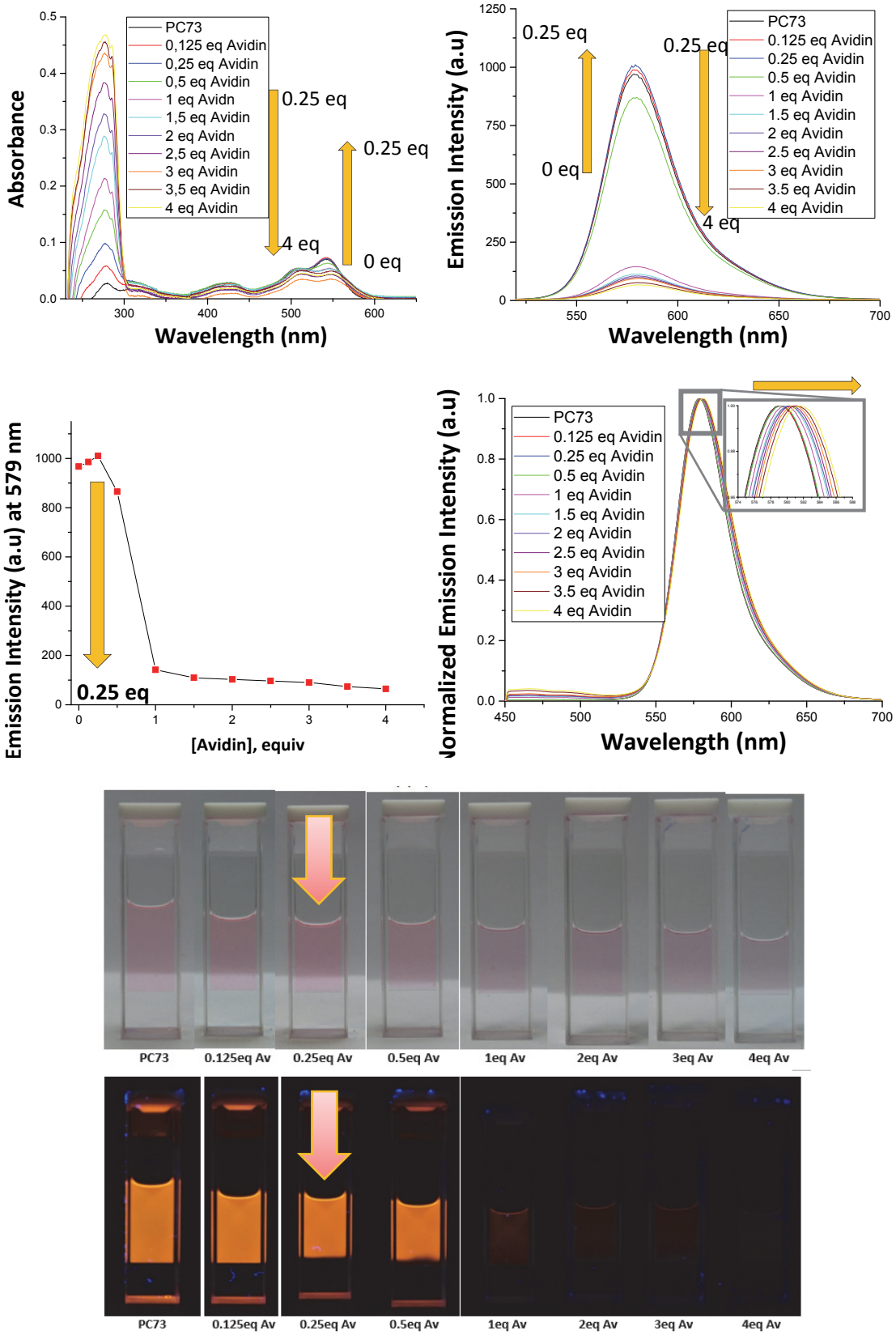

Figure 5. **Upper**: UV-Vis and Fluorescence Titration of **PC73** with Avidin at 427 nm of excitation wavelength and the concentration of **PC73** was 1×10^{-5} M. **Middle**: ***Left***: Emission Intensity at 579 nm versus concentration of avidin; ***Right***: Normalized Emission Intensity of PC73-Avidin totration. **Lower**: Photos of the UV-Vis and Fluorescence titration under white light and light of 366 nm.

The band centred at 280 nm in the absorbance titration spectra corresponds to avidin. This band increases in absorbance with increasing avidin concentration. From 0.125 to 0.25 equivalents of avidin, three bands corresponding to **PC73** slightly increase; in contrast from 0.5 to 4 equivalents the bands at 544 and 507 nm decrease in intensity; it means that the avidin present in the media is being involved in the formation of a complex **PC73**-avidin. The colour change was from pink to light purple, as it can be seen in the Figure Lower.

With respect to the fluorescence titration, the band at 579 nm increases intensity until 0.25 equivalents, in parallel to the absorbance titration, then decreases drastically until four equivalents were added. It is expected that 0.25 equivalents of avidin for each biotin should correspond to four biotins attached to one avidin, in agreement to the literature.

The graphic in the middle left of the Figure represents the emission intensity at the maximum of the fluorescence titration with respect to the concentration of avidin and gives us a clearl vision of the point at 0.25 equivalents. The graphic in the middle right of the Figure shows a small bathochromic effect in the fluorescence titration from 579 to 583 nm.

Apparently, the biotinylated PDI is able to bind to avidin, until four biotin units for avidin unit. What we can see is an effect of increasing the fluorescence of the complex BTPDI-Biotin-Avidin when there is very little concentration of avidin but decreasing the fluorescence when the concentration of avidin increases from 0.25 equivalents to some more.

In the Figure it is represented the hypothesis of the experiment in which when there is a very little amount of avidin the fluorescence of **PC73** increased, but with an excess avidin the fluorescence is deactivated by the presence of a avidin.

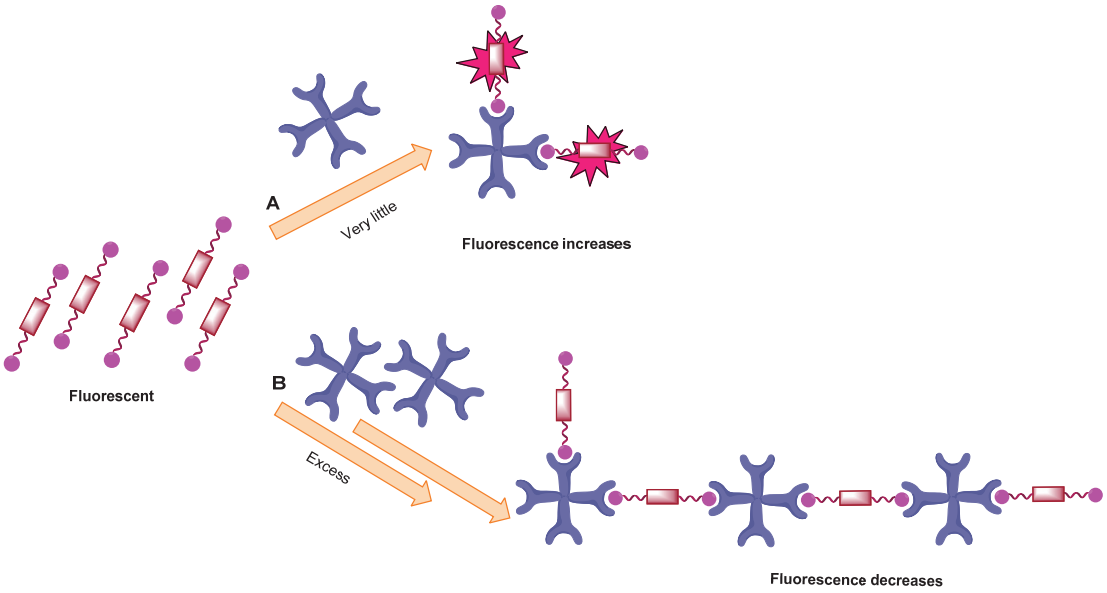

Figure 6. Illustration of **A**: increasing of **PC73** fluorescence in the presence of avidin and **B:** deactivation of **PC73** fluorescence in the presence of excess of avidin.

After that, the study of the fluorescent changes of synthetized biotinylated perylenediimide **PC73** in the presence of avidin was performed. However, this time the interaction **PC73**-avidin was studied by performing the titrations with variable amounts of **PC73** in the presence of a fixed concentration of avidin.

As mentioned before, the probe **PC73** is not soluble in 100% water, so it is necessary to employ a co-solvent. The selected mixture of solvents was DMSO:H_2O 1:99.

Previously, a titration of **PC73** with water was carried out (from 56 μM to 1 μM of probe) (Figure 7). This titration could be considered as a blank test, it was performed in order to study the variation of fluoresce with increasing amounts of water. Excitation and emission titration spectra were registered and fluorescence and excitation parameters were obtained (Figure). The excitation spectrum of **PC73** shows four bands in water. As it is diluted, the bands experiment a bathochromic shift in the case of 300 nm band and a hypsochromic shift in the case of the bands around 500-600 nm. In the fluorescence spectrum, **PC73** exhibits two bands located at 620 and 680 nm, which remained unchanged with the dilution.

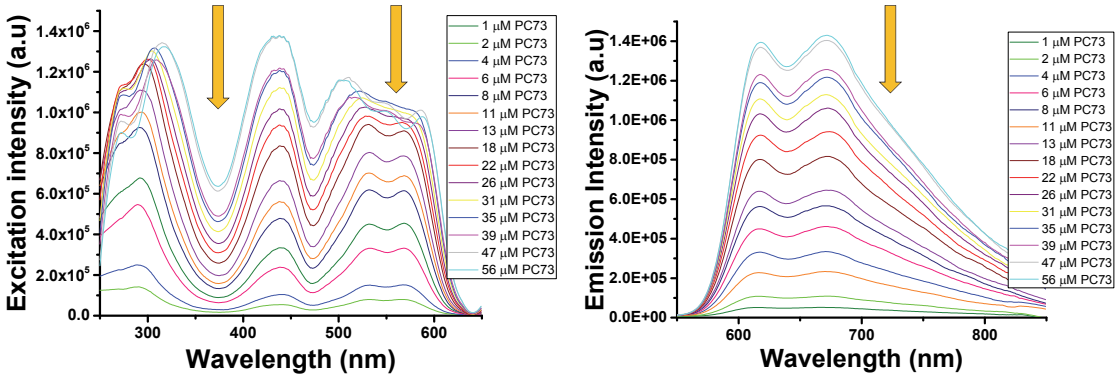

Figure 7. Excitation and Emission titration curves of **PC73** with water (56 μM **PC73**, DMSO:H_2O 0.1:9.9 v/v). λ_{excit} = 435 nm. λ_{em} = 616 and 666 nm.

Then, a titration of **PC73** in DMSO:H_2O 1:99 with avidin (15 μM in water) was performed. Twenty six points were recorded until titration curves reach saturation, being the excitation wavelength 435 nm. Figure represents excitation and emission titration spectra, respectively. Several bands appear in the excitation spectrum. In emission spectrum the 620 nm band increased in relation to the 680 nm band. This fact can be attributable to the interaction of avidin and **PC73**. Besides, the fluorescence increased until 50 μM of **PC73**, after that point, the fluorescence decreased. The Figure 9. left shows the normalized spectrum titration of **PC73** with water (blank) and the Figure 9. right shows the normalized spectrum titration of **PC73** with avidin in water. As it can be seen in the Figure 9. right, the 620 nm band experiences a bathochromic shift and the 680 nm band shows a decreasing of fluorescence, in comparison to the unaffected spectrum of the Figure 9. left. Apart from that, the job plot indicates a stoichiometry 1:1, since the molar fraction is around 0.5, even though **PC73** has two biotin units (Figure 10.). This information could be interpreted from two points of view:

- **PC73** is able to interact just with one side with avidin, although it has two anchor positions.
- **PC73** interacts from one side with an avidin and from the other side with another molecule of avidin. This explication is less probable because avidin is estimated to be between 66 – 69 kDa[11] in size, so it is thirty times bigger than biotin.

It is therefore apparent that in these conditions there is an interaction 1:1 between **PC73** and avidin that can be supported by excitation and emission spectra.

[11] J. Korpela, *Med. Biol.,* **1984**, *62 (1),* 5–26.

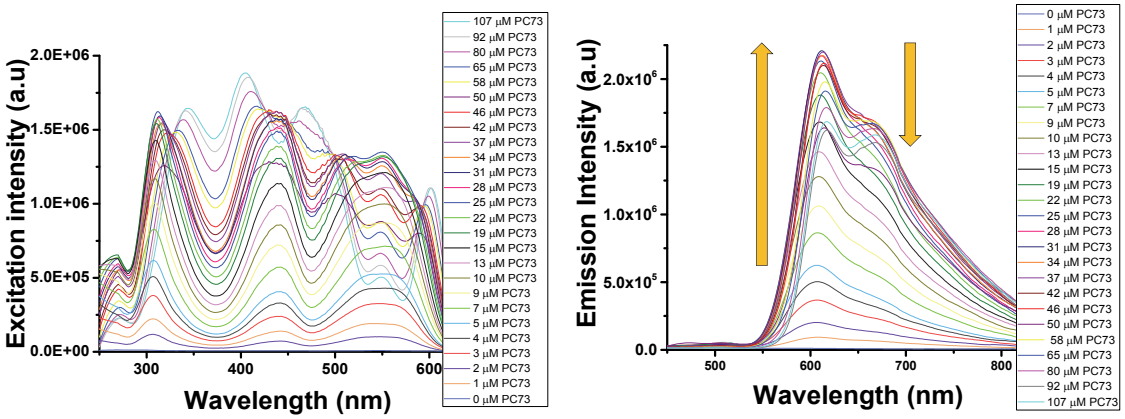

Figure 8. Excitation and Emission titration curves of avidin with **PC73** (15 µM avidin, DMSO:H_2O 0.1:9.9 v/v). λ_{excit} = 435 nm. λ_{em} = 616 and 666 nm.

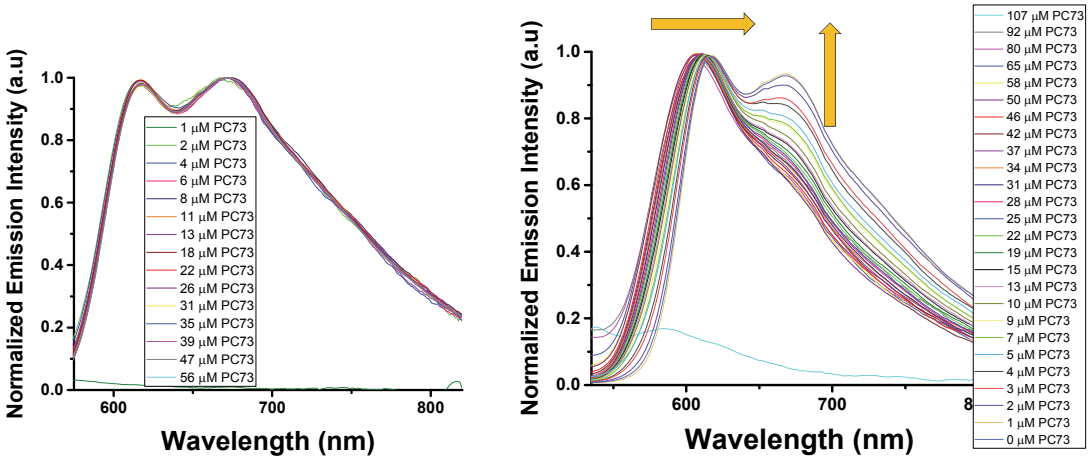

Figure 9. Left. Normalized Emission titration of **PC73** with water. Right. Normalized Emission titration of **PC73**-avidin in water. λ_{excit} = 435 nm. λ_{em} = 616 and 666 nm.

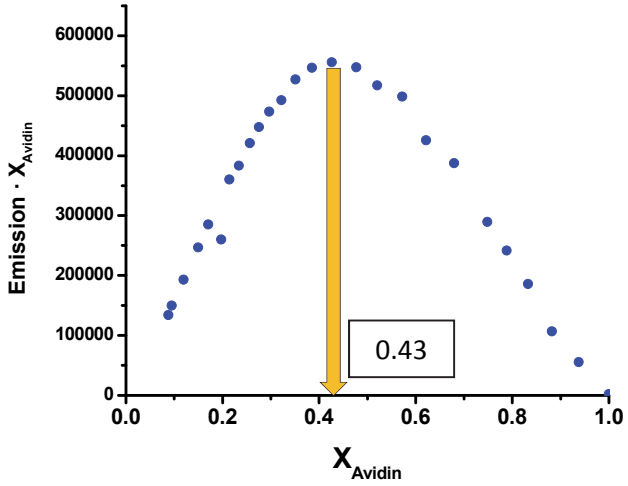

Figure 10. Job's Plot titration experiment.

3. FLUORESCENCE TITRATIONS OF THE AVIDIN-BIOTINYLATED PERYLENEDIIMIDE IN THE PRESENCE OF GRAPHENE OXIDE IN WATER.

Graphene oxide (GO), a chemically exfoliated graphene derivative, interacts with planar PBIs via non-covalent interactions with the p-surface of GO.[12] It is known that the π-surface of graphene oxide (GO) interacts with planar perylenediimides via non-covalent interactions. Some researchers try to investigate the effect of the molecular structures on the fluorescence quenching mechanism of this system. The electrons transferred from the excited state of dyes to the conductive band of graphene oxide were determined by fluorescence. The results indicated that the quenching efficiency of perylenediimides by graphene oxide was not only dependent on the difference between the lowest unoccupied molecular orbital level of dyes and the conduction band of the graphene oxide, but also mainly on the difference in the molecular structures.[13] Moreover, in order to check the fast photoinduced charge separation in well-ordered self-assemblies of perylenediimide–graphene oxide (PDI–GO) hybrid layers in aqueous environments were studied.[14] Therefore, qualitative and quantitative assays with graphene oxide were performed.

To study the interactions of GO layers with PDIs, two different bay-tetrasubstituted perylenediimides (BTPDIs) were used, **PC45** and **PC73**. These PDIs exhibit different bay and peri groups: **PC45** has chlorine atoms and amine groups (Figure 11.) and **PC73** has hydrophilic phenyl-ether groups and biotins in bay and peri-positions, respectively. Both of them were treated with graphene oxide, obtaining similar results; therefore, their deactivation of fluorescence was confirmed (Figure 11 and Figure 12). A proposed illustration for this fact is shown in the Figure 13. **PC45** experienced a gradual extinction of the fluorescence in the presence of increasing amounts of GO (Table 1) in DMSO:H_2O (0.1:9.9). The interactions BTPDIs-GO can thus be considered as suitable platforms for the design of new chemical sensors.

Vials	**Ref**	**1**	**2**	**3**	**4**	**5**	**6**	**7**	**8**	**9**	**10**	Ref diluted
µL GO (40µg/ml)	0	10	20	50	75	100	125	150	200	300	500	500µl DMSO:H_2O 0.1:9.9
µg/ml GO	0	0.2	0.4	1	1.5	2	2.5	3	4	6	10	0

Table 1. Quantity of graphene addition to each vial.

[12] Hirsch, A.; Englert, J. M.; Hauke, F. *Acc. Chem. Res*. **2013**, 46, 87-89.

[13] Y. Zhao, K. Li, Z. He, Y. Zhang, Y. Zhao, H. Zhang, Z. Miao, *Molecules*, **2016**, *30*, 1642.

[14] M. Supur, K. Ohkubo, S. Fukuzumi, *Chem. Commun.*, **2014**, *50*, 13359--13361.

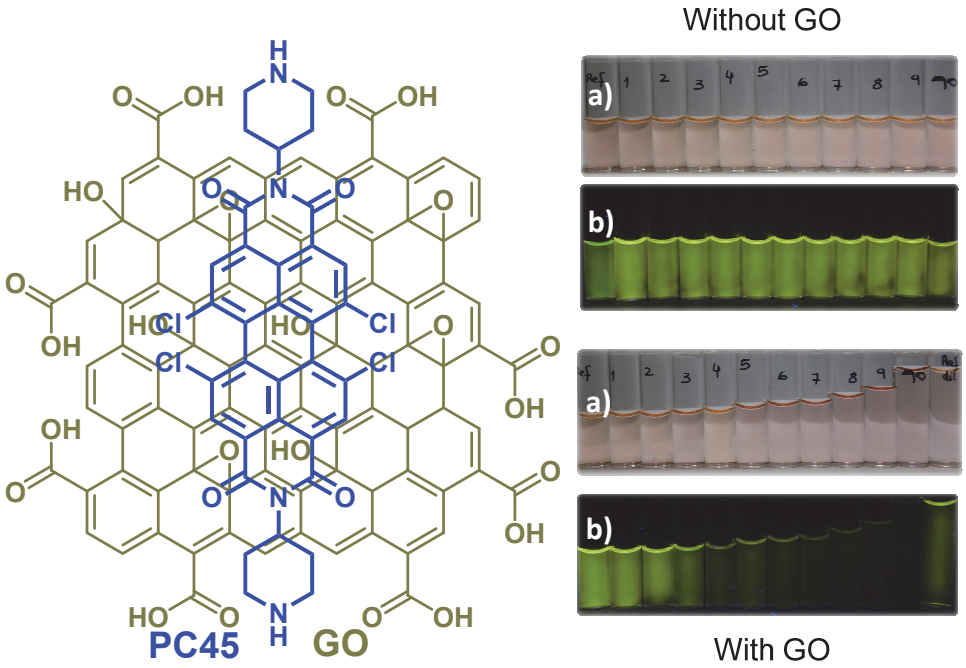

Figure 11. The concentration of **PC45** is 10^{-5} M in the presence of the quantities of GO indicated in the table 1. Top: **PC45** without GO and Bottom: **PC45** with GO. The photos were taken a) under white light and b) under 366 nm wavelength light.

In the same way, the bis-biotinylated BTPDI **PC73** showed a quenching of the fluorescence in the presence of graphene oxide (Figure 12). For **PC73** it is necessary to add a higher amount of graphene to deactivate the fluorescence than in the case of **PC45**. The behaviour of these compounds is probably related to the structure and planarity of **PC45** and **PC73**.

500 µL PC73 (8,44 µg/ml)	Ref	1	2	3	4	5	6	7	Ref dil
µL GO (de 40µg/ml)	0	10	100	200	500	200	300	500	500µl dte
µg/ml GO (500uL)	0	0.2	2	4	10	16	24	40	0

PC73 in DMSO:H_2O with different equiv of GO

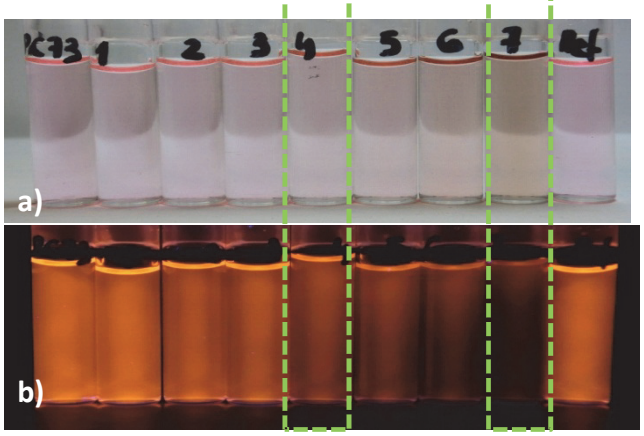

Figure 12. Quenching of the fluorescence of a biotinylated BTPDI, **PC73**, (10^{-5} M) in the presence of GO. The photos were taken a) under white light and b) under 366 nm of wavelength.

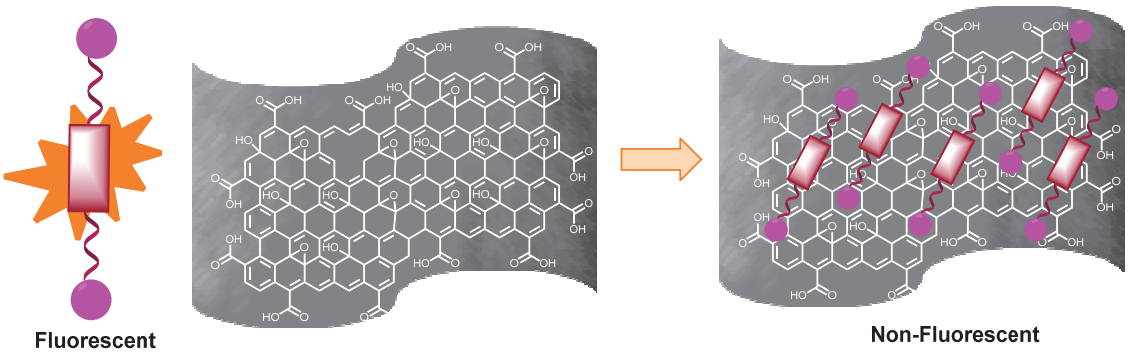

Figure 13. Illustration of deactivation of **PC73** fluorescence in the presence of graphene oxide by π-π stacking.

With the results of the interaction between the PDIs (**PC45** and **PC73**) and the graphene oxide, the next step was to study the fluorescence of **PC73** by adding avidin to **PC73**-GO. The concentration of graphene oxide in water is 40 μg/mL (500 mL), it was added to the perylenediimide whose concentration was 10^{-5} M in DMSO:H_2O 0.1:9.9. A semi-quantitative titration was performed with four additions of avidin (Figure 14.). As the images indicated, a colloid was formed when the equivalents of avidin were 0.125 and the fluorescence slightly increased. By increasing the concentration of avidin, the fluorescence of **PC73** decreased. According to the literature, avidin is partially adsorbed onto the surface of graphene oxide,[15] thus creating this colloid. Then, it was redissolved by increasing the avidin concentration.

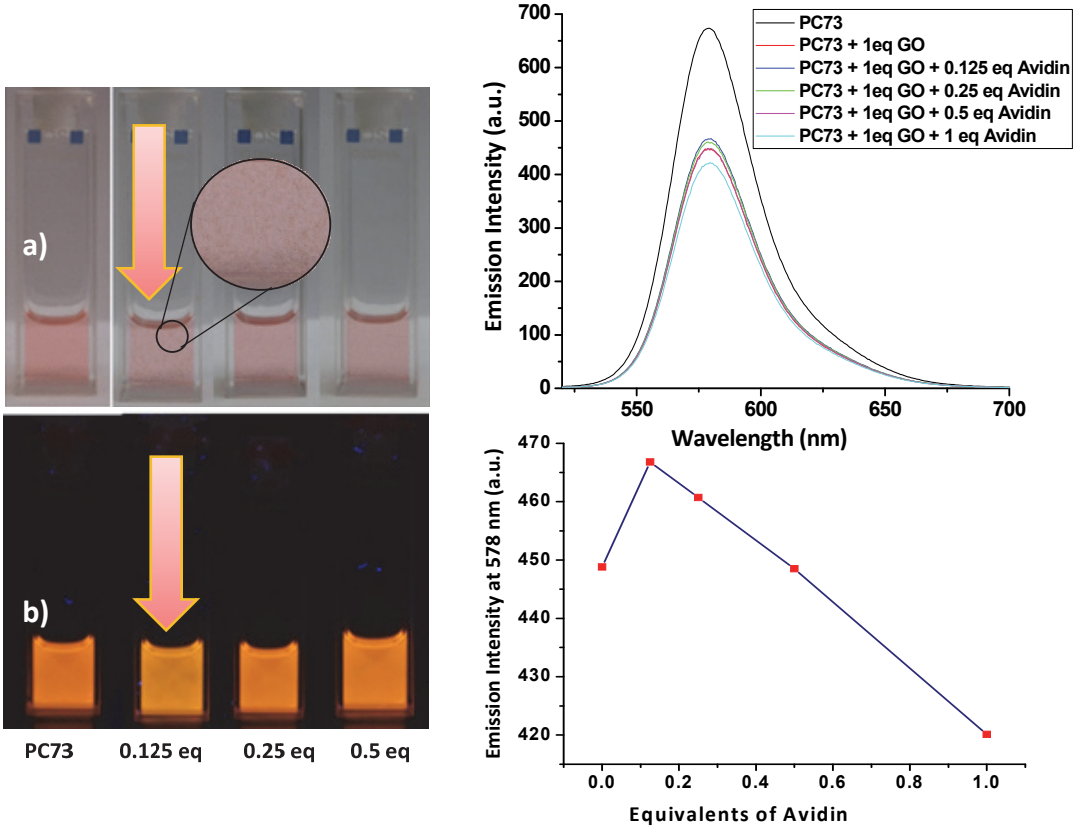

Figure 14. Fluorescence titration of the biotinylated BTPDI **PC73** (1×10^{-5} M) in the presence of avidin and GO in DMSO:H_2O/0.1:9.9. λ_{excit} = 430 nm. λ_{em} = 670 nm. The photos were taken a) under white light and b) under 366 nm wavelength light.

[15] Y. Kamiya, K. Yamazaki, T. Ogino, *J. Colloid Interface Sci.*, **2014**, *431*, 77-81.

Therefore, the interactions of GO layers and bay-tetrasubstituted perylenediimides (BTPDIs) produce quenching of the initial fluorescence of the BTPDIs (Figure 15). Then, avidin is added to PDI-GO and the fluorescence of the complex PDI-avidin is recovered, creating an OFF-ON fluorogenic system (Figure 15A). However, if the avidin concentration is higher, it conducts to the formation of colloids as indicated in the Figure 15B.

What we can see from these experiments is an effect of increasing the fluorescence of the complex BTPDI-Biotin-Avidin, when there is a very little concentration of avidin, but we see a decreasing of the fluorescence when the concentration of avidin increases to more than submicromolar concentrations. However, when there is GO in the environment, this effect is much more pronounced. When there is a very little amount of avidin, the fluorescence increases by displacing the avidin to the colorant from the GO surface, therefore, causing signal amplification of the fluorescence, because there are very few avidin molecules that displace several fluorescent molecules. When the concentration of avidin reaches some limit, the formation of micelles is observed, as well as signal amplification (Figure 15). Therefore, the system is able to sense avidin at submicromolar concentrations by signal amplification of the fluorescence.

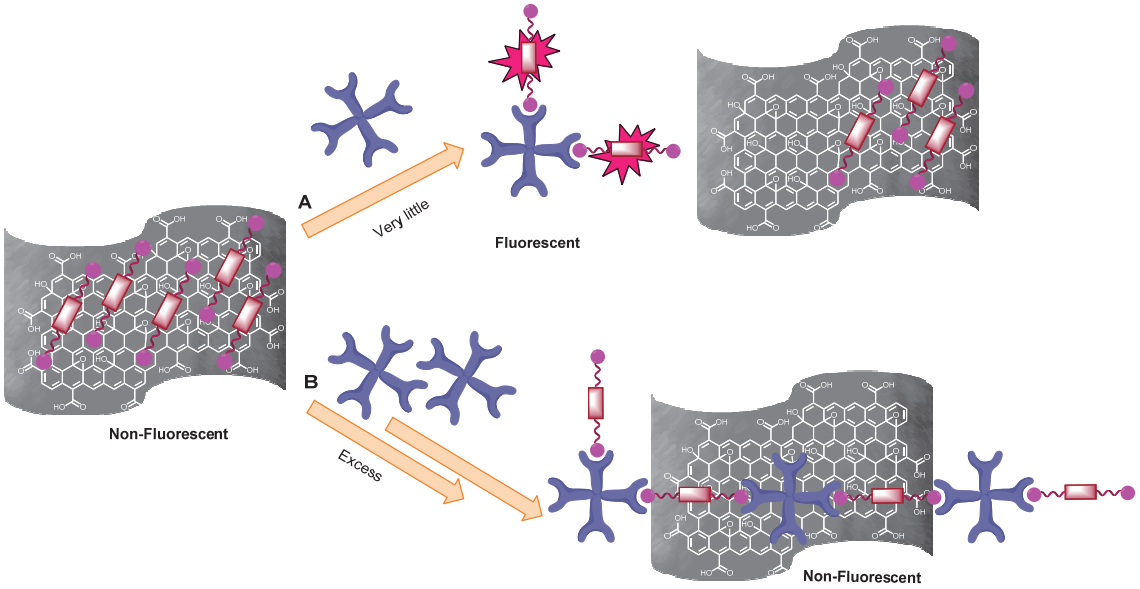

Figure 15. Illustration of **A**: increasing of **PC73** fluorescence in the presence of avidin and GO in DMSO:H_2O, and **B:** deactivation of **PC73** fluorescence in the presence of excess of avidin and GO in DMSO:H_2O.

4. APPLICATIONS OF THE SENSING SYSTEM TO PROTEIN TOXINS.

Pathogenic bacteria, such as *Listeria monocytogenes, Staphylococcus aureus*, *Salmonella* spp., *Campylobacter* spp., and pathogenic *Escherichia coli* (*E. coli*) secrete toxins, such as enterotoxins and exotoxins.[16] An exotoxin is a toxin that is produced by a bacterium and then released from the cell into the surrounding environment. An enterotoxin is a type of exotoxin that acts on the intestinal wall.[17] Enterotoxins can be classified by their basis of activity. One type of enterotoxin causes the destruction of the host cell, typically by binding with the host cell membrane where it forms a hole. A second type is known as superantigen toxins, which

[16] V. Fusco, G.-M. Quero, *Compr. Rev. Food Sci. Food Saf.*, **2014**, *13*, 493-537.

[17] R. L. Guerrant, T. S. Steiner, A. A. M. Lima, D. A. Bobak, *J. Infect. Dis.*, **1999**, *179*, S331–337.

work by overstimulation the immune response, particularly with respect to the T-cells. Finally, the third type identified as an A-B toxin. It consists of two or more toxin subunits that work together as a team to exert their destructive effect.[18] Shiga toxin (Stx) is one of the most potent biological poisons known. In humans, finding Stx is a consequence of infection with *Shigella dysenteriae* type 1 or certain serogroups of *E. coli* such as the O157:H7. There are two immunologically distinct groups of Stxs producing *E. coli* (STEC).[19] Shiga-like toxins 1 and 2 (SLT-1 and 2 or Stx-1 and 2) are proteins produced by some *E. coli* strains.[20] The toxin has two subunits, designated as A (mol. wt. 32000 D) and B (mol. wt. 7700 D. The B subunit is a pentamer that binds to specific glycolipids on the host cell, specifically globotriaosylceramide (Gb3) (in yellow, Figure 5.). Following this, the A subunit is internalized and cleaved into two parts. The A1 component then binds to the ribosome, disrupting protein synthesis. Stx-2 has been found to be about 400 times more toxic (as quantified by LD50 in mice) than Stx-1. Shiga toxin B subunit is the only suitable to be employed for tests.[21] Most strains of *E. Coli* are harmless, however, certain strains can cause infection in humans and warm-blooded animals. Human infection due to pathogenic *E. coli* may be limited to the intestinal mucosa and results in a syndrome of diarrheal disease, or can be spread throughout the body.[22] In this sense, to develop methods for the detection and identification of Shiga-like toxins to guarantee the quality of food and the health of consumers represent a challenge for the scientific community.[23]

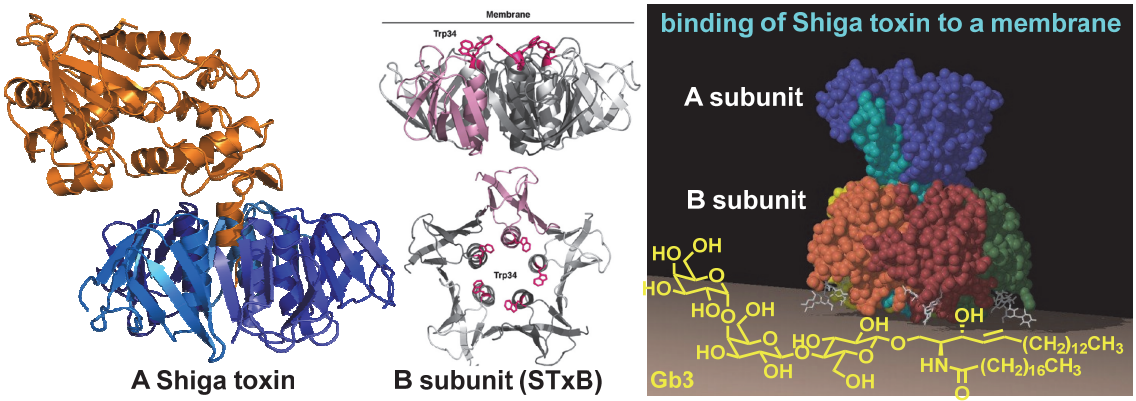

Figure 5. Left: Shiga toxin, A and B subunits. Right: model of binding of Shiga toxin the membrane of intestine cell that have a receptor of Gb3.

4.1. On the way to the design of chemical sensors for enterotoxins.

According to the literature, a chemical sensor for the detection of Shiga toxin subunit B can be synthetized on the basis of a water soluble fluorescent dye bounded to a linker with globotriaose units (Figure 6). The design of this derivate to detect the enterotoxin will need the

[18] a) S. Baron, *Medical Microbiology*., 4th edition. Galveston (TX): University of Texas Medical Branch at Galveston, **1996**. b) "Enterotoxin and Exotoxin." World of Microbiology and Immunology. Encyclopedia.com. 27 May. **2017**.

[19] A. R. Melton-Celsa, *Microbiol. Spectr.*, **2014**, *2*, 1-21.

[20] D. Philpott, F. Ebel, *E. coli Shiga Toxin Methods and Protocols, Methods in Molecular Medicine*, vol. 73, Humana Press Inc., Totowa, N.J., **2003**.

[21] P. Neri, S. I. Nagano, S.-i. Yokoyama, H. Dohi, K. Kobayashi, T. Miura, T. Inazu, T. Sugiyama, Y. Nishida, H. Mori, *Microbiol. Immunol.*, **2007**, *51*, 581-592.

[22] A. E. Heuvelink, *Verocytotoxin-producing Escherichia coli in humans and the food chain*, Ph. D. Thesis, Radboud University Nijmegen, Netherlands, **1996**.

[23] A. Martínez-Castillo, M. Muniesa, *Front. Cell Infect. Microbiol.*, **2014**, *4*, 1-8.

preparation of suitable globotriaose[24] derivatives capable of being bonded to perylenediimides that are known to have been bonded to sugar derivatives.[25]

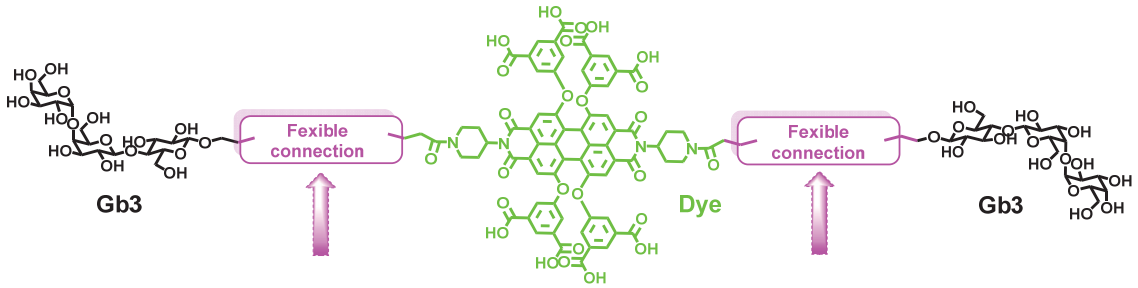

Figure 6. Two Gb3 units bonded to a PDI for Shiga toxin subunit B detection method.

4.2. Synthetic scheme of a fluorescent probe bonded to Gb3:

To prepare the required probe, the synthesis of the globotriose unit bonded to a linker suitable for attaching to derivatives of perylenediimides is described in the Scheme 1. The 4-methoxyphenyl globotriose is a commercial compound, whose anomeric carbon is a mixture between α and β phenoxy compound. This carbohydrate was per-acetylated with acetic anhydride in the presence of triethylamine and dimethylaminopyridine in dichloromethane, following the usual conditions found for this kind of polysacharide derivatives[26]. The acetylated product precipitated in the reaction mixture, obtaining **PC97** in high yield. Hydrolysis of the anomeric protecting group with cerium ammonium nitrate (CAN),[27] in a mixture of solvents to get the unprotected anomeric carbon derivative **PC98**, obtained by recrystallization from a mixture of ethyl acetate and hexane, followed by fluorination with diethylaminosulfur trifluoride (DAST),[28] afforded a mixture of α/β anomeric fluorinated compounds as demonstrated by ^{19}F-NMR spectroscopy. **PC99** was obtained within a moderate yield around 70% after purification by flash column chromatography. Once **PC99** has been synthetized, nucleophilic substitution by an azide tetraethyleneglycol was accomplished to obtain **PC100** as an inseparable mixture of α and β isomers (Scheme 1).

[24] O. M. Schütte, L. J. Patalag, L. M. C. Weber, A. Ries, W. Römer, D. B. Werz, C. Steinem, *Biophys. J.*, **2015**, *108*, 2775-2778.
[25] a). J. Hu, W. Kuang, K. Deng, W. Zou, Y. Huang, Z. Wei, C. F. J. Faul, *Adv. Funct. Mater.*, **2012**, *22*, 4149-4158.;
[26] H.-W. Hsieh, M. W. Schombs, J. Gervay-Hague, *J. Org. Chem.*, **2014**, *79*, 1736-1748.
[27] S. Shivatare, S. Chang, T. Tsai, S. Tseng, V. Shivatare, Y. Lin, Y. Cheng, C. Ren, C. Lee, S. Pawar, C. Tsai, H. Shih, Y. Zeng, C. Liang, P. Kwong, D. Burton, C. Wu, C. Wong, *Nat. Chem.*, **2016**, *8*, 338-346.
[28] G. H. Posner, S. R. Haines, *Tetrahedron Lett.*, **1985**, *26*, 5-8.

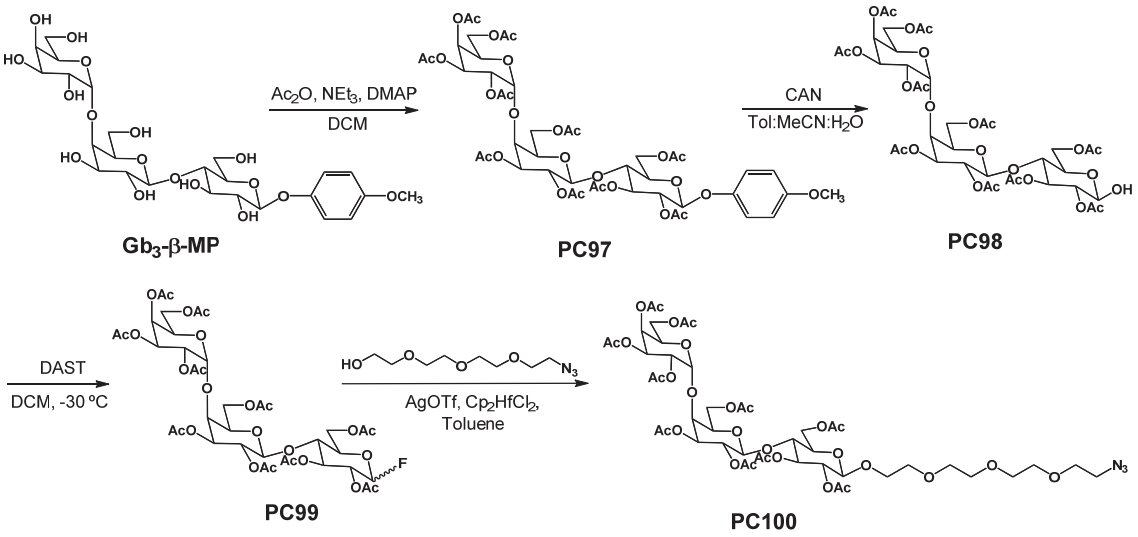

Scheme 1. Synthesis of a linkable globotriaose unit.

Then the PDI counterpart was prepared by reaction of hex-5-ynoyl chloride (2 equivalents) and *N,N'*-bis-(1-piperidine)-1,6,7,12-tetrakis(3,5-bis(methoxycarbonyl)phenoxy)perylene-3,4,9,10-tetracarboxylic diimide **PC67** (1 equivalent) dissolved in DCM under nitrogen in the presence of DIPEA (2 equivalents). The mixture was stirred at room temperature for 1.5 hours, then the solvent was evaporated under reduced pressure and purification was carried out by silica gel flash chromatography using DCM to MeOH as eluents to give compound **PC101** as a pink solid in 40% yield (Scheme 2). A similar reaction in the presence of only one equivalent of hex-5-ynoyl chloride in the same conditions afforded the monoacyl derivative **PC103** (Scheme 2). The monoacyl derivative **PC103** (1 equivalent) and PyBOP (1 equivalent) dissolved in DCM were added under nitrogen to *N*-succinimidyl 9-(biotinamido)-4,7-dioxanonanoate (1 equivalent) and DIPEA (2 equivalents) dissolved in DCM and the mixture was stirred at room temperature for 3 hours until the reactant disappeared by TLC. Then the solvent was removed under reduced pressure and the residue was purified to flash chromatography (silica, DCM:MeOH) to obtain a deep pink solid **PC104** in 54% yield, having a biotine moiety and a terminal triple bond suitable for click chemistry (Scheme 2).

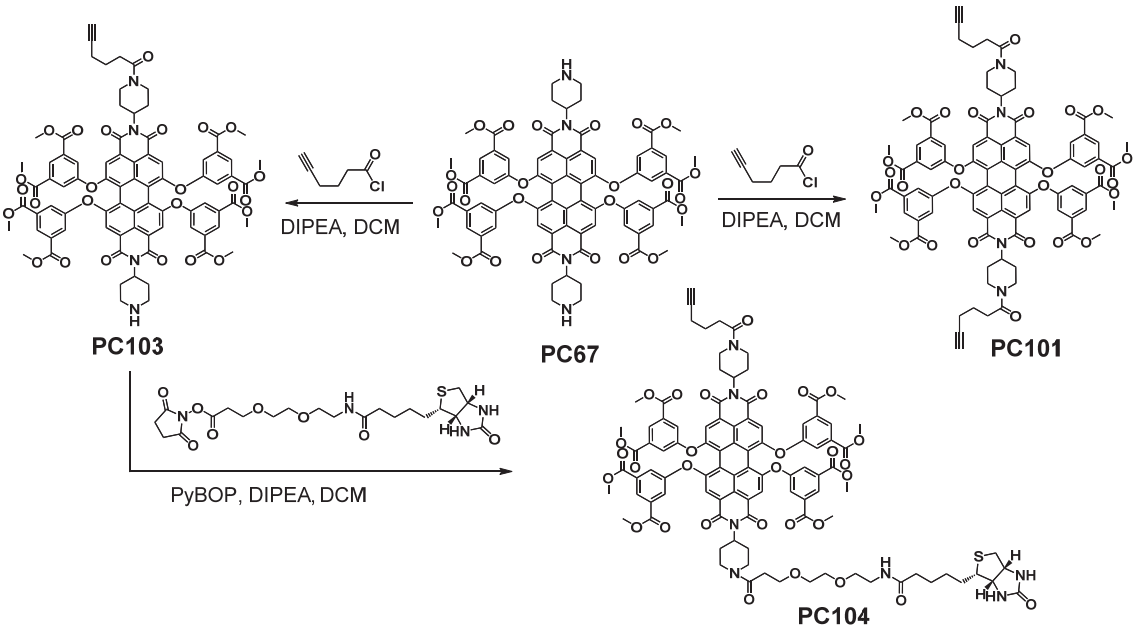

Scheme 2. Synthesis of linkable PDI units.

The Cu(I)-catalysed 1,3 dipolar cycloaddition is a common reaction that usually gives the 1,4-substituted[1,2,3]triazole regioisomer,[29] and there are some examples of substituted perylenediimides used as substrates in click chemistry.[30] The copper(I) catalysed 1,3-dipolar cycloaddition of the globotriaosyl azide **PC100** (1 equivalent) dissolved in DCM and the biotinyl-PDI **PC104** (1 equivalent) dissolved in DCM:DMF (8:0.2) under nitrogen atmosphere in the presence of the catalyst $[Cu(CH_3CN)_4]PF_6$ and tris[(1-benzyl-1H-1,2,3-triazol-4-yl)methyl]amine (TBTA), heated at 30 ^oC overnight, after work-up and flash chromatography (silica) from DCM to MeOH, afforded only starting material. Analogously, the copper(I) catalysed 1,3-dipolar cycloaddition of the globotriaosyl azide **PC100** (2 equivalents) dissolved in DCM and the biotinyl-PDI **PC101** (1 equivalent) in the presence of $[Cu(CH_3CN)_4]PF_6$ and TBTA in similar conditions did not give the expected results.

5. CONCLUSIONS.

Fluorescent titrations of the biotinylated PDI derivative in the presence of avidin have been performed as well as titrations of the biotinylated PDI derivative and avidin in the presence of graphene oxide. The interaction between the fluorescent biotin and avidin was detected by fluorescence, and the addition of graphene oxide to this system increased the sensitivity of the system, constituting an added value as an OFF-ON fluorescent sensor.

Moreover, globotriaosyl derivatives with a long chain linkable to other functional groups have been prepared, but unfortunately, globotriaosyl conjugates with tetra-substituted perylenediimides were not achieved. We have tested several attempts of the click reaction to synthesize them, but the reaction was unsuccessful in all cases studied. Another synthetic route will be proposed in a future synthesis.

[29] C. W. Tornøe, C. Christensen, M. Meldal, *J. Org. Chem.*, **2002**, *67*, 3057-3064.
[30] a) M. D. Yilmaz, O. A. Bozdemir, E. U. Akkaya, *Org. Lett.*, **2006**, *8*, 2871-2873.; b) S. Pla, L. Martín-Gomis, K. Ohkubo, S. Fukuzumi, F. Fernández-Lázaro, A. Sastre-Santos, *Asian J. Org. Chem.*, **2014**, *3*, 185-187.

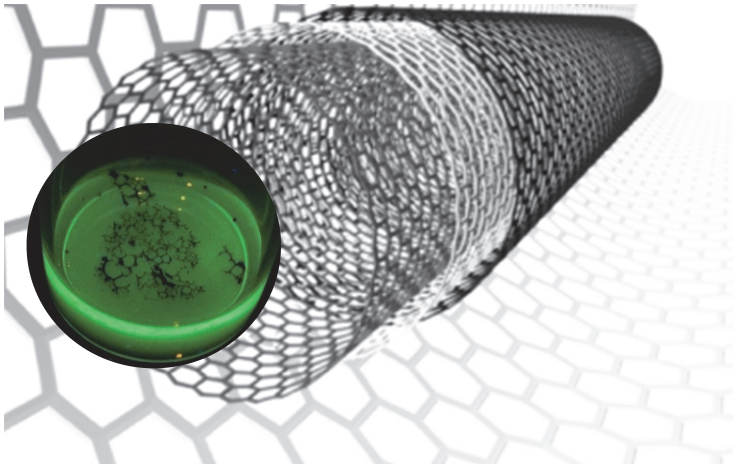

CHAPTER 3. SYNTHESIS, CHARACTERIZATION AND CELLULAR IMAGING OF FLUORESCENT CARBON NANOTUBES

PATRICIA CALVO GREDILLA Ph. D. THESIS

SUMMARY

The synthesis, characterization and cellular imaging of fluorescently functionalized multi-walled carbon nanotubes has been developed.

1. INTRODUCTION TO NANOTECHNOLOGY.

Richard Feynman (1959) introduced the notion of "nanotechnology" for the first time in his famous Caltech lecture: "There's plenty of room at the bottom: an invitation to enter a new field of physics".[1] He imagined the world of nanoscale where fundamental laws of quantum physics define the behaviour of single atoms and control the formation of different structures from the individual atoms.[2] In this way, the nanometer represents the magnitude below which materials begin to show significant deviations of their macroscopic properties.[3]

The element carbon is the "brick" of the nanotechnology due to its four valence electrons and its atomic size. It is one of the most abundant elements found around the planet and, owing to its electronic configuration ($1s^2 2s^2 2p^2$), it is capable of forming several allotropes.[4] This is because it can create different kinds of bonds with another carbon atom. Diamond and graphite have distinct optical, electrical as well as dissimilar economic value. With respect to the nanoallotropes, C_{60} buckyball was firstly discovered in spectroscopy data (Kroto *et al*, 1985),[5] followed by carbon nanotube (CNT) (Iijima *et al*, 1991)[6] and finally, graphene (single layer of graphite) (Novoselov *et al*, 2004[7] and Geim and Novoselov 2007)[8] (Figure 1).

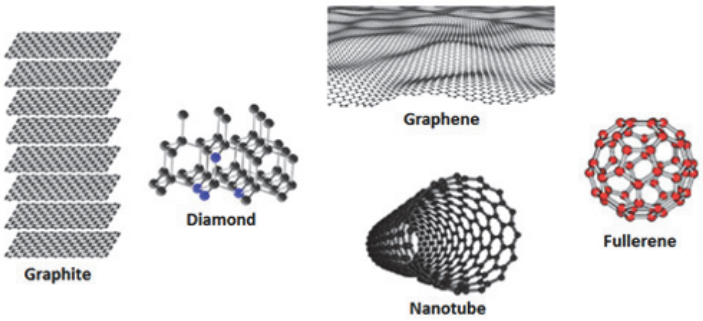

Figure 1. Allotropes of carbon.

There are two families of CNT: single-walled carbon nanotubes (SWCNTs) and multi-walled carbon nanotubes (MWCNTs). SWCNTs show cylindrical structure with diameter ranges between 0.5-5 nm and lengths in the order of μm to cm. MWCNTs are similar in structure to SWCNTs, but they present multiple concentric walls, with the spacing between walls comparable to the interlayer spacing in graphite, about 0.34 nm.[9]

---

[1] R. P. Feynman, *Eng. Sci.*, **1960**, *23*, 22-36.

[2] V. V. Mitin, D. I. Sementsov, N. Z. Vagidov, *Quantum mechanics for Nanostructures*. Cambridge University Press, Cambridge, **2010**.

[3] F. J. Martín Martínez, *Modelización molecular de nanotubos de carbono*, Ph. D. Thesis, Granada University, **2010**.

[4] N. Wachter, C. Munson, R. Jarosova, I. Berkun, T. Hogan, R. C. Rocha-Filho, G. M. Swain, *ACS Appl. Mater. Interfaces.*, **2016**, *42*, 28325–28337.

[5] H. W. Kroto, J. R. Heath, S. C. O'Brien, R. F. Curl, R. E. Smalley, *Nature*, **1985**, *318*, 162-163.

[6] S. Iijima, *Nature*, **2001**, *354*, 56-58.

[7] a) K. S. Novoselov, A. K. Geim, S. V. Morozov, D. Jiang, Y. Zhang, S. V. Dubonos, I. V. Grigorieva, A. A. Firsov, *Science*, **2004**, *306*, 666-669.; b) A. K. Geim, K. S. Novoselov, *Nat. Mater.*, **2007**, *6*, 183-191.

[8] X. Zhou, *Carbon nanotube transistors, sensors and beyond*, Ph.D. Thesis, Cornell University, EEUU, **2008**.

[9] D. Akinwande, *Carbon nanotubes: device physics, Rf circuits, surface science and nanotechnology*, Ph.D. Thesis, Standford University, EEUU, **2009**.

2. SYNTHESIS, GROWTH AND PURIFICATION OF CARBON NANOTUBES.

Nowadays, the high employment of CNTs in different kinds of applications[10] has stimulated the development of several procedures focused on their synthesis by more effective and clean routes. The most notable methods are summarized below:

- **Arc-discharge evaporation method** was the original technique used by Ijijma[6] This method is actually the most common and perhaps the simplest way to produce CNTs (Figure 2).

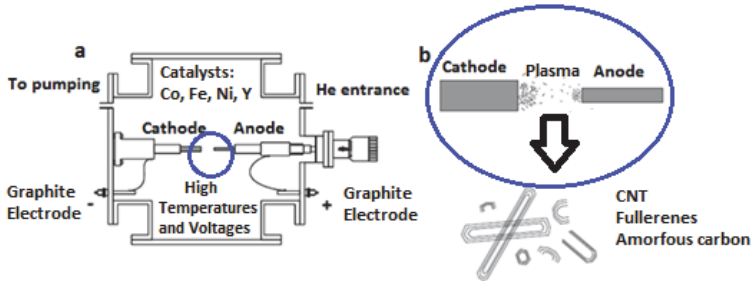

Figure 2. Schematic illustration of the arc-discharge device for carbon nanotubes synthesis.

- The **laser ablation method** was developed by Smalley and Guo *et al.* [11] The graphite is vaporized by a pulsed laser and is carried by an inert gas to a cooled Cu collector, where the CNT are formed by condensation (Figure 3).

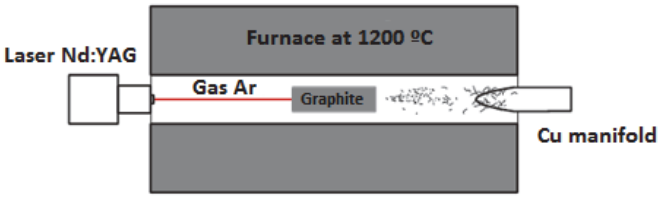

Figure 3. Schematic illustration of the laser ablation device for nanotubes synthesis.

- The **catalytic carbon vapour deposition** (CCVD) method: this method has been established as industrial scale procedure for the preparation of SWCNTs and MWCNTs from different hydrocarbons (C_nH_n)[12] (Figure 4).

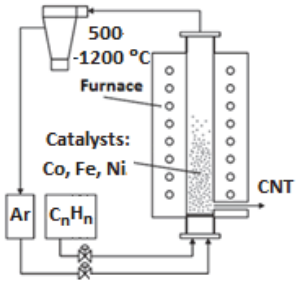

Figure 4. Schematic illustration of CCVD device for **carbon** nanotubes synthesis.

[10] S. Abdalla, F. Al-Marzouki, A. A. Al-Ghamdi, A. Abdel-Daiem, *Nanoscale Res. Lett.*, **2015**, *10:358*,
[11] T. Guo, P. Nikolaev, A. Thess, D. T. Colbert, R. E. Smalley, *Chem. Phys. Lett.*, **1995**, *243*, 49-54.
[12] J. Zhou, Y. Lan, K. Zhang, G. Xia, J. Du, Y. Zhu, Y. Qian, *Nanoscale*, **2016**, *8*, 4903-4907.

Until now, the mechanism for CNTs growth remains partially unknown, but it is dependent on their synthetic process, as Geohegan and Katuara suggest for Arc discharge and laser ablation methods. Geohegan *et al*. reveal that the growth of CNTs does not take place when carbon is in gas-phase, but when small aggregates and nanoparticles (NP) have been formed.[13] However, Katuara proposes two steps: nucleation (formation of small agglomerates) and the formation of fullerenes, which act as CNTs precursors.[14] In the case of CCVD method, two mechanisms of CNTs growing have been described: tip growth[15] and base growth.[16]

In all of these synthetic processes, different by-products and aggregations (CNTs may appear in bundles due to π–π interactions) are generated alongside with the CNTs, namely fullerenes, amorphous carbon, nanoparticles, and traces of the catalysts used in the reaction. Bearing this in mind, the development of an effective protocol for purification and sonication of CNTs constitutes a critical issue. In general terms, two procedures have been described: Dry methods consisting in removing carbon by-products through gas phase oxidation[17] and wet methods impling strongly acid treatment in order to eliminate residual metal particles.[18]

3. STRUCTURE AND PROPERTIES OF CARBON NANOTUBES.

The structure of SWCNT could be conceptualized as a wrapping of graphene layer in a cylinder.[19] SWCNT are described through the chiral vector ($C_h = na_1 + ma_2$), which assigns chirality of the nanotube, and the chiral angle (θ), which is used to define three different types of SWCNTs: zig-zag CNT ($\theta = 0^o$), armchair CNT ($\theta = 30^o$) and chiral CNT ($30^o < \theta < 0^o$) (Figure 5). [20] On the other hand, MWCNTs are defined such a stack of graphene sheets rolled up into concentric cylinders.

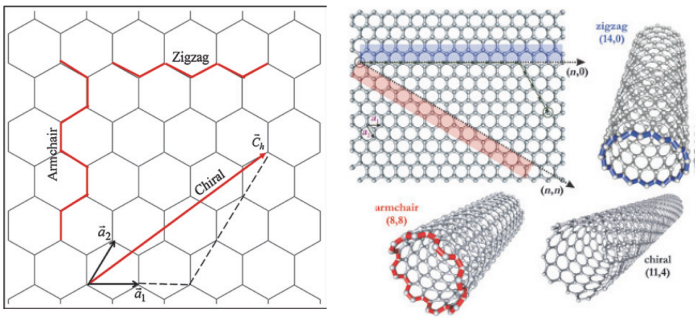

Figure 5. Diagram of a graphene sheet, which aids to the description of a number of parameters of CNTs, subsequently governing its properties. Roll-up of graphene sheet leading to the three different types of CNT.[21]

[13] D. B. Geohegan, H. Schittenhelm, X. Fan, S. J. Pennycook, A. A. Puretzky, M. A. Guillorn, D. A. Blom, D. C. Joy, *Appl. Phys. Lett.*, **2001**, *78*, 3307-3309.
[14] R. Sen, S. Suzuki, H. Kataura, Y. Achiba, *Chem. Phys. Lett.*, **2001**, *349*, 383-388.
[15] M. Chhowalla, K. B. K. Teo, C. Ducati, N. L. Rupesinghe, G. A. J. Amaratunga, A. C. Ferrari, D. Roy, J. Robertson, W. I. Milne, *J. Appl. Phys.*, **2001**, *90*, 5308-5317.
[16] J. Li, C. Papadopoulos, J. M. Xu, M. Moskovits, *Appl. Phys. Lett.*, **1999**, *75*, 367-369.
[17] T. W. Ebbesen, P. M. Ajayan, H. Hiura, K. Tanigaki, *Nature*, **1994**, *367*, 519-519.
[18] D. Chattopadhyay, I. Galeska, F. Papadimitrakopoulos, *Carbon*, **2002**, *40*, 985-988.
[19] M. Meyyappan, L. Delzeit, A. Cassell, D. Hash, *Plasma Sources Sci. Technol.*, **2003**, *12*, 205-216.
[20] J. Clark*, Microelectrode Array Fabrication for Electrochemical Detection with Carbon Nanotubes,* Ph. D. Thesis, Advanced Technology Institute University of Surrey, United Kingdom, **2016**.
[21] K. Balasubramanian, M. Burghard, *Small*, **2005**, *1*, 180–192.

The combination of size (small diameter), structure and topology confers nanotubes remarkable mechanical and electronic properties, making them raise so much expectancy, such as the highest Young's modulus (1.25 TPa)[22] or the tensile strength (150 GPa).[23] Moreover, mechanical properties can be affected by imperfections in their structure make them more versatile. The properties of CNT could be based on two structural aspects:[24]

- Topological defects: This group is composed by several defects as atom vacancies, stone-wales defects and welding CNTs.
- Substitutional doped defects: the CNT is doped with a heteroatom: B, Si, N etc. This group is divided in p-type nanoconductor, Hillocks and n-type nanoconductor.

4. FUNCTIONALIZATION AND CHARACTERIZATION OF CARBON NANOTUBES.

The functionalization of CNTs implies the addition of molecules to this nanostructures by covalent or non-covalent bonding. The sort of reactions that take place in the modification of CNTs are outlined below[25] (Figure 6):

A. Non-covalent functionalization: Mainly based on supramolecular complexation due to absorption forces, commonly Van der Waals.

B. Functionalization of defects: The irregularities in the hexagon framework can be the open caps or holes on the sidewalls, which show higher reactivity than the walls.

C. Π-staking functionalization: Special example of non-covalent union, between CNTs sidewalls and aromatic molecules such as pyrene, porphyrin, perylene, etc.

D. Covalent functionalization of sidewalls: There is a change of hybridization from sp^2 to sp^3 and various functional groups can be attached.

E. Endohedral functionalization: Filling the tubes with small atoms or molecules.

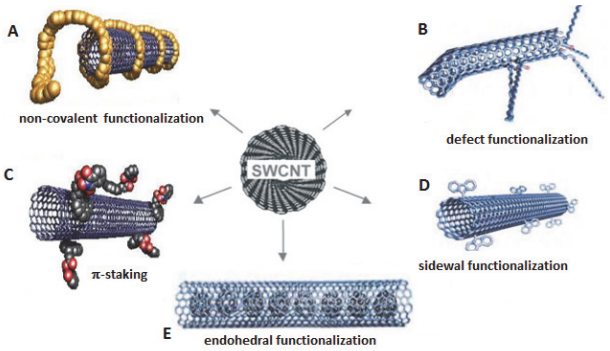

Figure 6. Different ways of functionalization of SWCNTs.

[22] A. Krishnan, E. Dujardin, T. W. Ebbesen, P. N. Yianilos, M. M. J. Treacy, *Phys. Rev. B,*, **1998**, *58(20)*, 14013-14019.

[23] B. G. Demczyk, Y. M. Wang, J. Cumings, M. Hetman, W. Han, A. Zettl, R. O. Ritchie, *Mater. Sci. Eng., A*, **2002**, *334*, 173-178.

[24] M. Rahmandoust, M.R. Ayatollahi. *Characterization of Carbon Nanotube-Based Composites Under Consideration of Defects*. Springer International Publishing Switzerland, **2016**.

[25] M. Müller, *Electronic properties of functionalized carbon nanotubes*, Ph. D. Thesis, Von der Fakultat II - Mathematik und Naturwissenschaften der Technischen Universitat Berlin, Alemany, **2010**.

As it has been shown, covalent sidewall functionalization could be carried out at the end of the CNT scaffold or on the sidewalls. Consequently, there are various reactions for direct addition to unsaturated π-electron systems that have been successfully applied.[26] Among them it can be found: 1) the [2+1]cycloaddition of nitrenes; 2) the addition of nucleophilic carbenes and 3) the addition of radicals.[27,28] This chapter focuses on covalent addition reactions on the surface of nanotubes, in particular, defect functionalization (specially CNT-carboxamides) (figure 7a), 1,3-dipolar cycloadditions (figure 7b), and oxidation of CNTs followed by 1,3-dipolar cycloadditions (figure 7c).

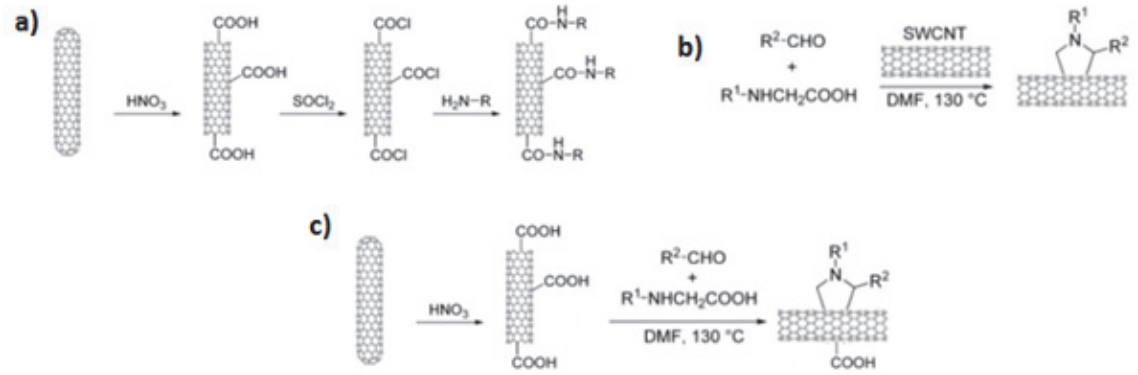

Figure 7.a) Schematic representation of oxidative etching of CNTs followed by treatment with thionyl chloride and subsequent amidation. b) Dipolar addition of azomethyne ylides to CNTs (Prato et al. addition), c) Oxidation and ulterior dipolar addition of azomethyne ylides to CNTs (combination between a and b).

The usual techniques for the CNTs characterization are Raman and IR spectroscopy, Atomic Force Microscopy (AFM), Scanning Electron Microscopy (SEM) and Transmission Electron Microscopy (TEM), Thermogravimetric Analysis (TGA) and Scanning Tunnelling Microscope (STM), among others.[29] Therefore, Raman and IR spectroscopy, SEM and TEM images will be extensively used to characterize the CNTs along the chapter.

- **Raman spectroscopy** allows elucidating many aspects, such as the nanotube diameters, the presence of disorder, as well as nanotube-nanotube interactions. MWCNTs have two main typical bands in the Raman spectra. One at 1580 cm^{-1} with a shoulder around 1604 cm^{-1}, (G-band), assigned to in-plane C-C bond vibration. Another at 1342 cm^{-1} (D-band) is activated by the existence of disorder in carbon systems (graphene, graphite or SWCNTs have not D-band).[30] Moreover, Raman spectrum also exhibits another band at 2683 cm^{-1} called G',

[26] a) P. Singh, S. Campidelli, S. Giordani, D. Bonifazi, A. Bianco, M. Prato, *Chem. Soc. Rev.*, **2009**, *38*, 2214-2230.; b) A. Hirsch, O. Vostrowsky, *Functionalization of carbon nanotubes*, Wiley-VCH, Weinheim, Germany, **2007**.

[27] M. Holzinger, O. Vostrowsky, A. Hirsch, F. Hennrich, M. Kappes, R. Weiss, F. Jellen, *Angew. Chem. Int. Ed.*, **2001**, *40*, 4002-4005

[28] T. J. J. Müller, U.H.F. Bunz, *Functional Organic Materials. Syntheses, Strategies, and Applications*, Wiley-VCH Verlag GmbH & Co. KGaA, Weinheim, Germany, **2007**.

[29] C. Ménard-Moyon, H. Ali-Boucetta, C. Fabbro, O. Chaloin, K. Kostarelos, A. Bianco, *Chem. Eur. J.*, **2015**, *21*, 1-8.

[30] C.-C. Chang, C.-C. Chen, W.-H. Hung, I.-K. Hsu, M. A. Pimenta, S. B. Cronin, *Nano Res.*, **2012**, *5*, 854-862.

attributed to the overtone of the D band.[31].The intensity ratio of Raman peaks (I_D/I_G) is reported to be an effective index to monitor the evolution of MWCNTs during functionalization stages.[32] High I_D/I_G ratios show the presence of disordered structures, such amorphous carbon, nanocrystallites, graphene stacks or functionalized areas.[33]

As regards the Raman characterization, there are two ways of interpretation spectra. On one hand, some researchers defend that if a nanotube is functionalized, the ratio I_D/I_G tend to increase, as it is showed in Figure 8. a.[34,35] On the other hand, other investigations support the idea that in Raman spectra of pristine MWCNT D-band is higher than G-band and, after functionalization, D- and G-bands equalize to the same height[36] (Figure 8. b).

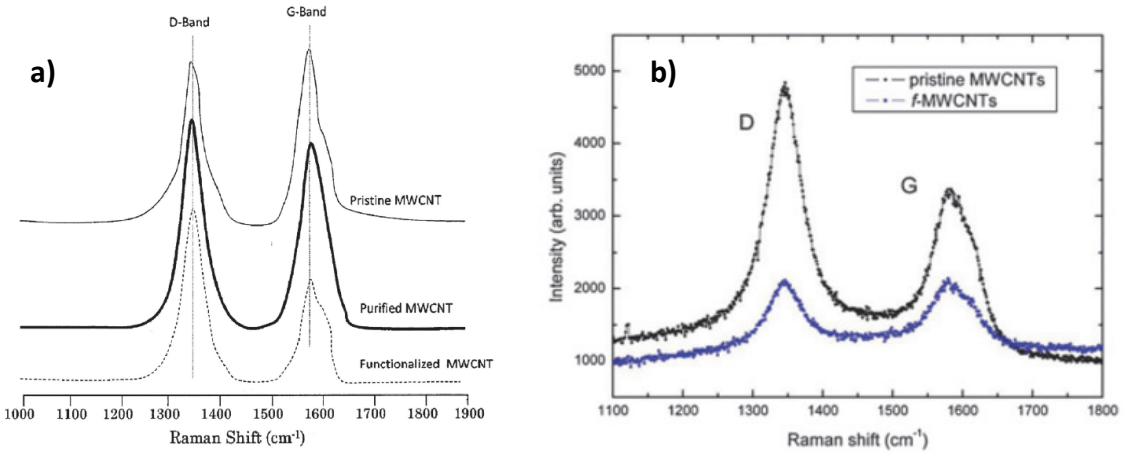

Figure 8. Two kinds of interpretation of CNTs functionalization.

➢ **FT-IR spectroscopy** shows the differences between pristine-MWCNTs (p-MWCNT) vs functionalized-MWCNTs (f-MWCNT) due to the characteristic band of the attached functional groups.[37]

➢ Finally, the **SEM** image gives an idea of the morphology and the abundance of nanotubes as well as the elemental composition of the sample (carbon and metal catalyst impurities). Additionally, the **TEM** image can give information about finest details of internal structure of CNTs.[38]

[31] L. Bokobza, J. Zhang, *Express Polym. Lett.*, **2012**, *6*, 601-608.
[32] K. S. Munir, Y. Li, D. Liang, M. Qian, W. Xu, C. Wen, *Mater. Des.*, **2015**, *88*, 138-148.
[33] K. T. Chaudharya, J. Alia, P. P. Yupapin, *Chin. Phys. B*, **2014**, *23*, 035203_035201-035203_035206.
[34] R. Yudianti, H. Onggo, S. Y. Saito, T. Iwata, J.-i. Azuma, *Open Mater. Sci. J.*, **2011**, *5*, 242-247.
[35] Y. Tsukahara, T. Yamauchi, T. Kawamoto, Y. Wada, *Bull. Chem. Soc. Jpn.*, **2008**, *81*, 387-392.
[36] G. Ghini, L. Luconi, A. Rossin, C. Bianchini, G. Giambastiani, S. Cicchi, L. Lascialfari, A. Brandi, A. Giannasi, *Chem. Commun.*, **2010**, *46*, 252-254.; G. Giambastiani, S. Cicchi, A. Giannasi, L. Luconi, A. Rossin, F. Mercuri, C. Bianchini, A. Brandi, M. Melucci, G. Ghini, P. Stagnaro, L. Conzatti, E. Passaglia, M. Zoppi, T. Montini, P. Fornasiero, *Chem. Mater.*, **2011**, *23*, 1923-1938.
[37] S. N. J. S. Z. Abidin, N. H. N. Azman, S. K. Kulandaivalu, Y. Sulaiman, *J. Nanomater.*, **2017**, Article ID 5798614, 13 pages.
[38] R. A. DiLeo, B. J. Landi, R. P. Raffaelle, *J. Appl. Phys.*, **2007**, *101*, 064307-5.

5. AIM OF THE CHAPTER.

To synthetize water-soluble fluorescent multi-walled carbon nanotubes (F-MWCNTs) functionalized with perylenediimides. These F-MWCNTs may represent a solution for advanced chemotherapy (although these cellular processes remain unknown nowadays), since certain doses of carbon nanotubes stabilized with serum produce very significant antitumor effects in melanoma resistant tumours (Figure 9).[39]

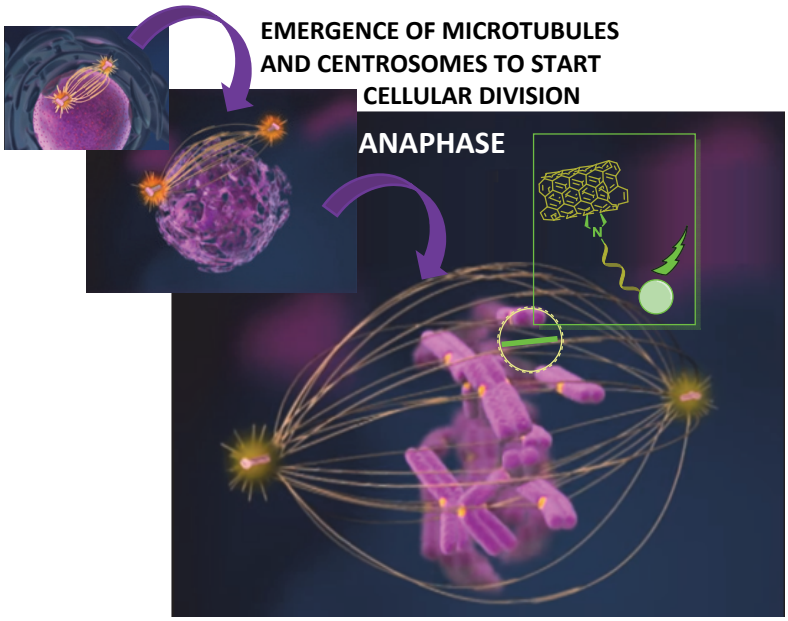

Figure 9. Picture that exemplifies the association between F-MWCNTs and microtubules in the cellular division process.

This idea is based on the fact that PDIs act as fluorophore to fluorescently label the cellular microtubules (Figure 9, green box). The importance of labelling microtubules is because they participate in the cell division cycle (Figure 9), as cellular structural support, among other crucial biological functions. According to the group of López-Fanarraga,[40,41] the multi-walled carbon nanotubes share a similar size with cellular microtubules, and this promote their intercellular association. Moreover, this group, with which we have collaborated in this chapter, is able to distinguish between of three filamentous structures of cytoskeleton (microtubules, actin and intermediate filaments).[42,43]

[39] L. García-Hevia, J. C. Villegas, F. Fernández, I. Casafont, J. González, R. Valiente, M. L. Fanarraga, *Adv. Healthc. Mater.*, **2016**, *5*, 1080-1087.
[40] F. Pampaloni, E.-L. Florin, *Trends Biotechnol.*, **2008**, *26*, 302-310.
[41] L. Rodriguez-Fernandez, R. Valiente, J. Gonzalez, J. C. Villegas, M. L. Fanarraga, *ACS Nano*, **2012**, *6*, 6614-6625.
[42] L. García-Hevia, R. Valiente, R. Martín-Rodríguez, C. Renero-Lecuna, J. González, L. Rodríguez-Fernández, F. Aguado, J. C. Villegasa, M. L. Fanarraga, *Nanoscale*, **2016**, *8*, 10963–10973.
[43] http://sunny.moorparkcollege.edu/~econnolly/CellsUnitsofLife.htm

6. RESULTS AND DISCUSSION.

As stated in the introduction, covalently functionalization of carbon nanotubes is not an easy task to develop, due to their very high insolubility in any solvent and their low reactivity. Herein, several synthetic routes have been designed to try solving these drawbacks.

The multi-walled carbon nanotubes used in this chapter were supplied by Nanocyl and Sigma-Aldrich.

6.1. Synthetic Route I.

The proposed first route was the direct anchoring of perylenediimides to multi-walled carbon nanotubes (scheme 1).

First, multi-walled carbon nanotubes (Aldrich) were sonicated with methanol, DMF and water (Figure), in order to discover which solvent was better. The used technique to study this was SEM microscopy. The pristine carbon nanotubes, p-MWCNTs were sonicated during 1 hour in the indicated solvents. Methanol is an adequate solvent to disperse the carbon nanotubes, since the image SEM presented less aggregates and bundles.

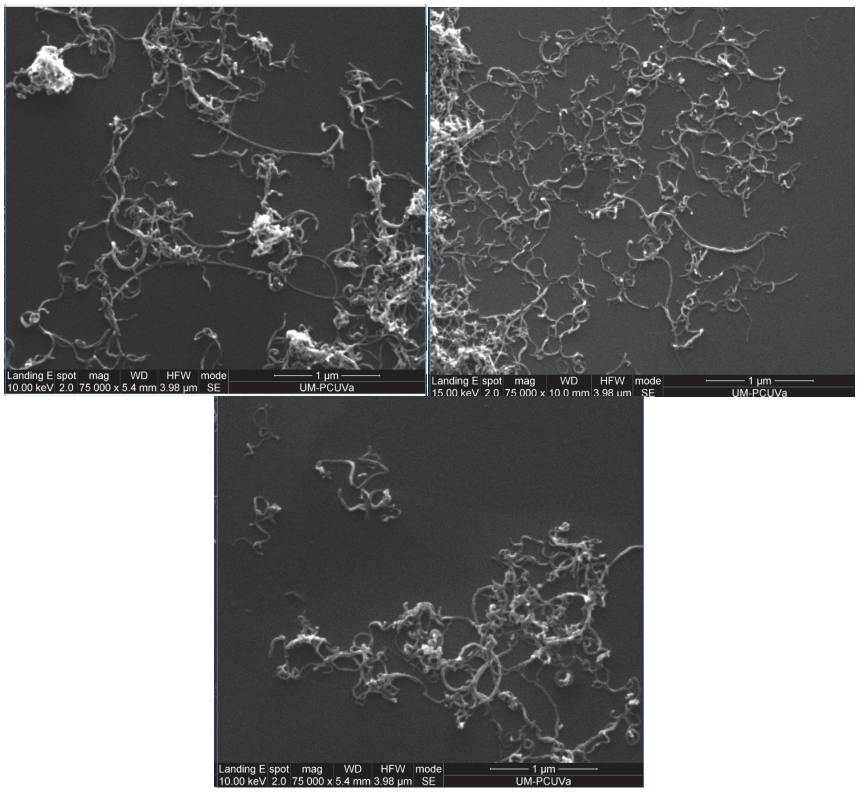

Figure 10. SEM image at 1 µm of p-MWCNTs sonicated with the tip inside a suspension in methanol, DMF and water (from the left to the right).

Once the final solvent has been chosen, the resultant black powder called **MWCNT.A.MeOH** was oxidized in a process involving extensive ultrasonic treatment in a mixture of concentrated nitric and sulfuric acid. Such drastic conditions lead to the opening of the tube caps as well as the formation holes in the sidewalls, following by an oxidative etching along the walls with the concomitant release of carbon dioxide and impurities. The obtained product consisted on nanotube fragments, whose solubility had improved, and whose ends and sidewalls were decorated with carboxylic and hydroxyl functional groups. This product was named **PC105.A**. This highly oxidized product had carboxyl groups that are useful sites for

further treatment with oxalyl chloride to form the acid chloride (**PC105.A.int**). This extremely reactive compound was covalently coupled to the amine **PC67** by forming amide **PC106.A** (Scheme 1). The amine **PC67** was previously synthetized as explained in the previous chapters. **PC106.A** was a black powder without fluorescence.

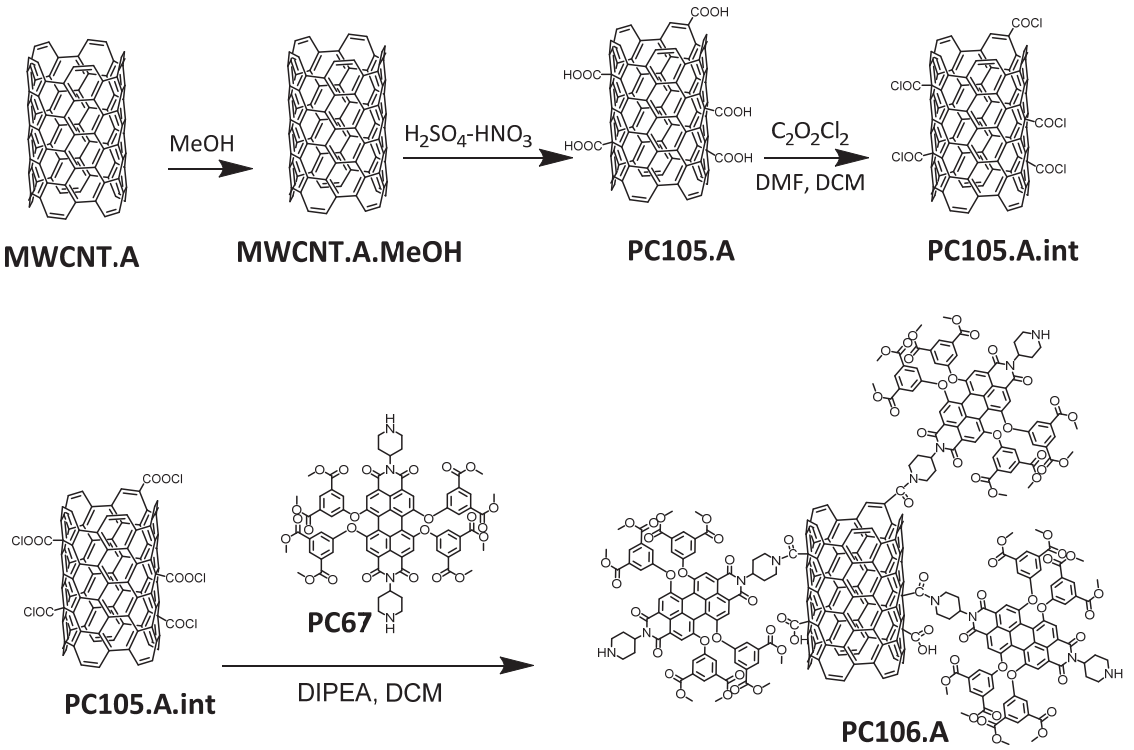

Scheme 1. Synthetic route I.

6.1.1. Characterization of compounds derived of scheme 1.

The nanotubes samples were characterized by standard analytical techniques such as Raman and IR spectroscopy.

- **Raman spectroscopy**

The Figure 1 shows the Raman spectra of three mainly compounds involved in the route I. Purified carbon nanotubes (**MWCNT.A.MeOH**) show the presence of sp^2 carbon as it was indicated by the G-band (graphitic band) at 1593 cm^{-1} and the D-band (disorder band) at 1360 cm^{-1}, in which the D band is higher than the G band. After oxidizing the purified carbon nanotubes (**PC105.A**), their D and G bands shift from 2 to 5 nm and the Raman intensity remained unchanged. However, the difference between the first two compounds and the amide functionalized carbon nanotubes (**PC106.A**) is an increase in Raman intensity, appreciable in Figure 1.

- **IR spectroscopy**

In order to ensure that the oxidation takes place, the IR band of **PC105.A** must have a broad band in 1000 and 1500 cm^{-1} belonging to C-O and C=C bonds respectively. In this case, the band of the carboxyl groups is observed in the Figure 12 rounded in green.

On the other hand, the characteristic amide bond, which it is located around 3466 cm^{-1}, is not visible. The reason why this band is not able to see is because O-H band, belong to

oxidation process, is a broad band in the same region. Apart from that, the amide-functionalization could be confirmed by the characteristic bands of **PC67** (Figure 13). The red circle in Figure 13 demonstrates the existence of C-H bonds of PDI, which are shown in figure 12. Moreover, the orange circle, seen in both IR spectra, refer to C-N and C-O bonds of PDIs.

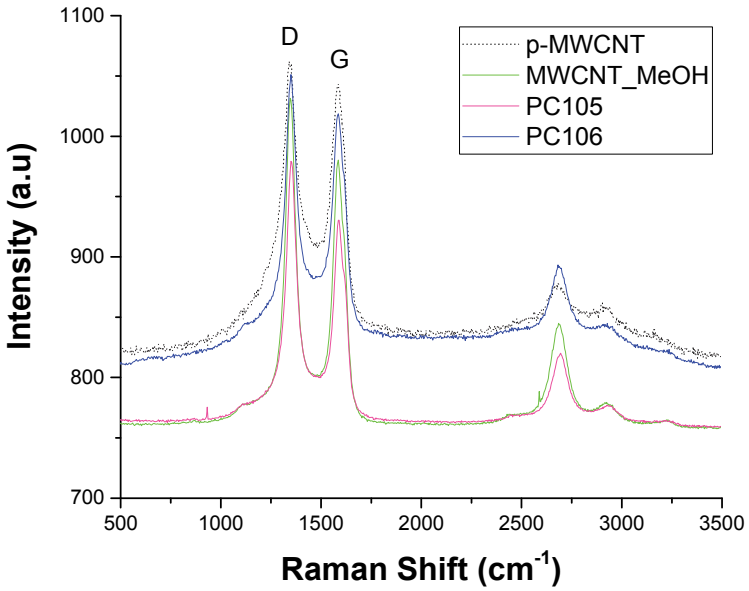

Figure 11. Raman spectra of pristine MWCNTs (dashed line), dispersed in methanol (green line), carboxyl functionalized (pink line) and amide functionalized (blue line) measured at excitation wavelength 532 nm.

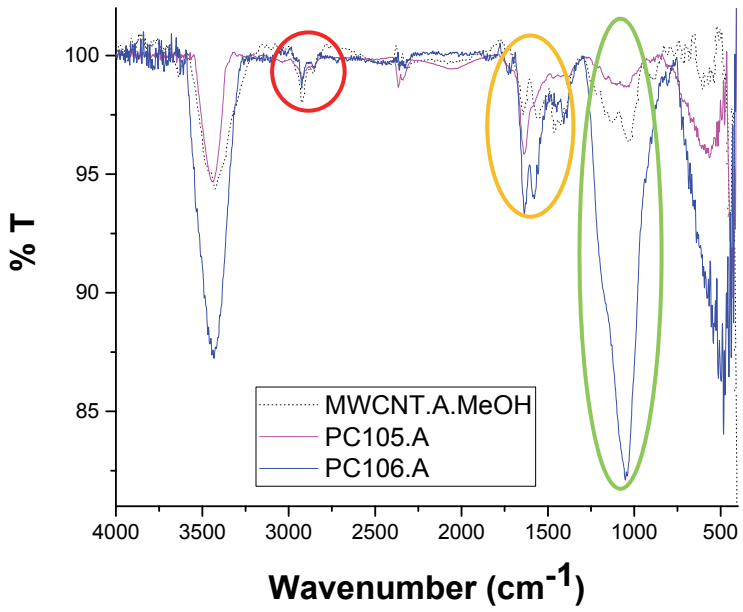

Figure 12. FT-IR spectrum of each compound from the scheme 1.

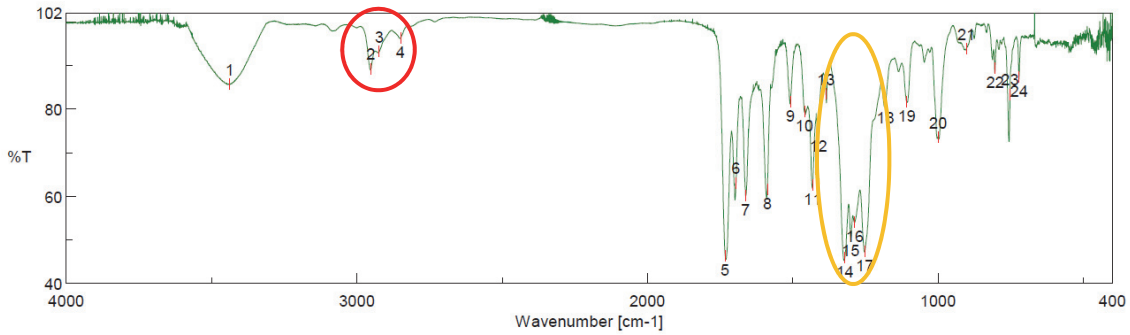

Figure 13. FT-IR spectrum of **PC67**.

6.2. Conclusions.

The functionalization of carbon nanotubes was performed but the PDI functionalized carbon nanotubes exhibit weak fluorescence that was not enough to fulfill the aim of this chapter. For this reason, the hydrolysis of **PC106.A** was not performed. Instead, the subsequent synthetic route was developed.

7. SYNTHETIC ROUTE II.

In view of the promising results, the following route will try to connect the carbon nanotubes via a chain or spacer (**PC85**) to the fluorophore (perylenediimide) to keep separated the carbon nanotubes (Figure 14) from the PDIs and therefore to increase the luminescence of CNTs in water solution. The proposed mechanism is shown in the Scheme 2. Although this mechanism is longer than the first one, it is expected to have better results.

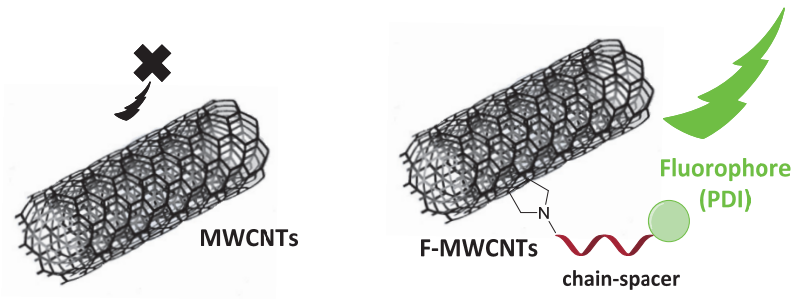

Figure 14. Scheme of the formation of the fluorescent functionalized-MWCNTs (F-MWCNTs).

First, the intermediate was synthetized in three steps (Scheme 2). The spacer (**PC85**) was previously reported in the literature[44] and it was a good option due to its long length. It consisted of a functionalized polyethylenglycol that is suitable to be bonded to the PDI. The initial diamine 2,2´-(ethylenedioxy)bis(ethylamine) was selectively protected as a carbamate just in one side. Then, the free amine of **PC83** was able to react with benzyl bromoacetate to give the mono-benzylated product **PC84**. After that, the benzyl group of **PC84** was removed by hydrogenation catalyzed by Pd/C, generating the free acid **PC85** (Scheme 2). The carbon

[44] a) V. Georgakilas, N. Tagmatarchis, D. Pantarotto, A. Bianco, J.-P. Briand, M. Prato, *Chem. Commun.*, **2002**, 3050-3051.; b) F. Orozco, K. Setyowati, M. Piao, *Synthesis of 2-[2-(2-tertButoxy carbonylamino-ethoxy)-ethoxy]-ethylamino}-acetic acid*, McNair Research Project.

nanotubes employed in this route were provided by IDIVAL (Nanocyl, partially oxidized and dispersed in water, homogeneous suspension by repeated sonication and centrifugation).

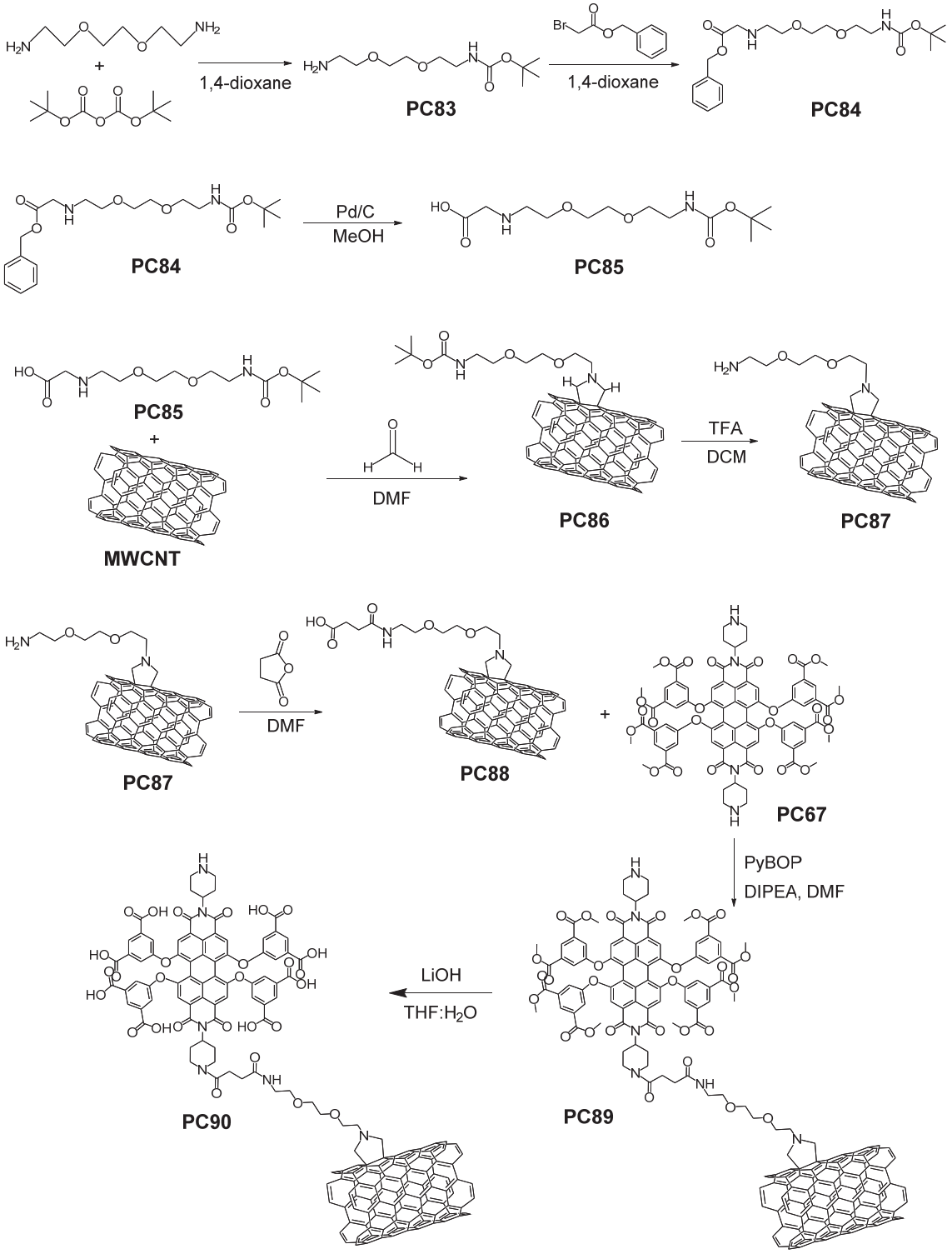

Scheme 2. Synthetic Route II to reach the fluorescent water-soluble MWCNTs (F-MWCNTs): **PC90.**

The 1,3-dipolar cycloaddition illustrated in Scheme 2 occurs by condensation of the amine of the aminoacid (**PC85**) and the carbonyl group of formaldehyde to form a 1,3-dipole intermediate, which is able to react with several double bonds present in the multi-walled

carbon nanotubes, both on their sidewalls and on their tips[45] obtaining **PC86**. Subsequently, the Boc group of **PC86** was removed in acidic medium leaving a free amine. After that, reaction of succinic anhydride with the obtained primary amine **PC87** gave a carboxylic acid derivative **PC88**. Then, **PC88** was reacted with the amine **PC67** giving an amide **PC89** and then the esters of the PDI were hydrolysed to be transformed in a water soluble PDI, **PC90**. It is worth to mention that **PC90** was fluorescent and completely soluble in water. **PC90** was a black solid without any emission as a solid under the light of 366 nm, but it was perfectly suspended in water and the emission was green.

7.1. Characterization of compounds.

As mentioned before, samples were characterized by standard analytical techniques such as Raman and IR spectroscopy.

- **Raman spectroscopy**

The Raman spectrum of Figure 15 includes each intermediate of the scheme 2. The D- and G-bands of the p-MWCNTs (**MWCNT**) almost have the same heigh; it means that the nanotubes do not have many defects in their structure. The difference between **PC86** and **MWCNT** is not very remarkable, except that the G band decreases. However, when the amine was deprotected (**PC87**) the D-band increases considerably with respect to **PC86** and p-MWCNTs, so according to the literature a defect has been introduced in the MWCNT structure. **PC88** does not provide relevant information. **PC89** reveals a background emission in solid state due to the attached fluorophore that has an elevated quantum yield and the optic characteristics confirm that the emission is due to attachment of the perylenediimide. Moreover, the G-band of **PC89** is split in two bands and it exhibits a blue shift. According to the literature,[46] the splitting of G-band (1556 and 1606 cm^{-1}) can indicate that there is an interaction between different shells of the MWCNTs, perhaps the bonding between the carbon nanotubes and the perylenediimide causes this interaction. The appearance of D''-band at 1451 cm^{-1} is clearly seen. Reviewing the existing references at this respect, this band could be attributed to CH_2 band;[47] in another publication the band at 1462 cm^{-1} suggests the existence of sp^3 C–H structures in aromatic rings;[48] in another publication the band at 1451 cm^{-1} is related to CH_2 scissoring[49] and also the band at 1451 cm^{-1} can be interpreted as a second-order scattering processes of lower modes of 1613 cm^{-1} in the Raman mode that corresponds to one of the strongest B3g-symmetric modes of the perylene core,[50] in this case the perylenediimide, which contains this kind of bonds in its structure, is attached onto the surface of carbon nanotubes.

---

[45] F. M. Toma, *Covalently functionalized carbon nanotubes and their biological applications*, Ph. D. Thesis, International School for Advanced studies, SISSA, Italy, **2006**.

[46] J. H. Lehman, M. Terrones, E. Mansfield, K. E. Hurst, V. Meunier, *Carbon*, **2011**, *49*, 2581-2601.

[47] E. E. Rossi, A. L. Pinheiro, O. C. Baltatu, M. T. T. Pacheco, L. S. Jr., *J. Photochem. Photobiol. B*, **2012**, *107*, 73-78.;

[48] E. He, J. Wang, H. Xu, Z. He, H. Wang, H. Zhao, Y. Zhang, R. Zhang, H. Zhang, *J. Mater. Sci.*, **2016**, *51*, 6583-6589.

[49] P. Knief, C. Clarke, E. Herzog, M. Davoren, F. M. Lyng, A. D. Meade, H. J. Byrne, *Analyst*, **2009**, *134*, 1182-1191.

[50] R. Scholz, A. Y. Kobitski, T. U. Kampen, M. Schreiber, D. R. T. Zahn, *Phys. Rev. B,*, **2000**, *61*, 13659-13669.

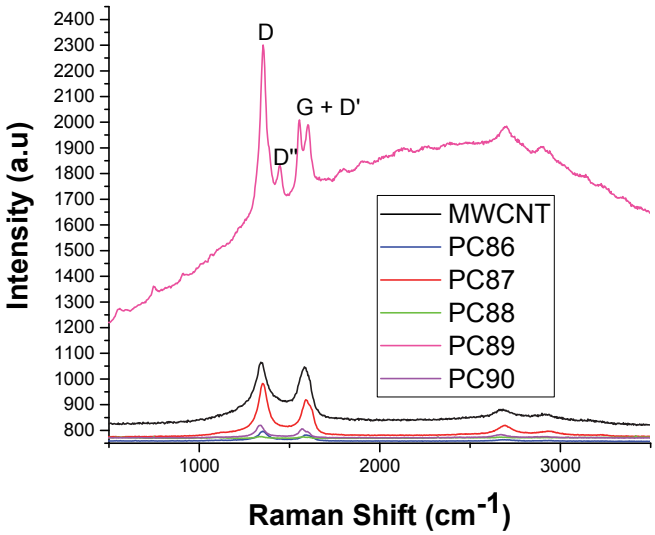

Compounds	I_D/I_G
MWCNT	1,537
PC86	1,534
PC87	1,543
PC88	1,541
PC89	0,889
PC89_Backg	2,274
PC90	1,543

Figure 15. Raman spectrum of all intermediates until to obtain **PC90** and **MWCNT.**

In conclusion, the emission of **PC90** has decreased but the ratio D- and G bands remained stable in comparison with **PC89**. Additionally, the splitting of the G-band seems to be maintained. All results are consistent with the bonding of the carbon nanotubes to the fluorescent dye. More details are given in the Figure 16.

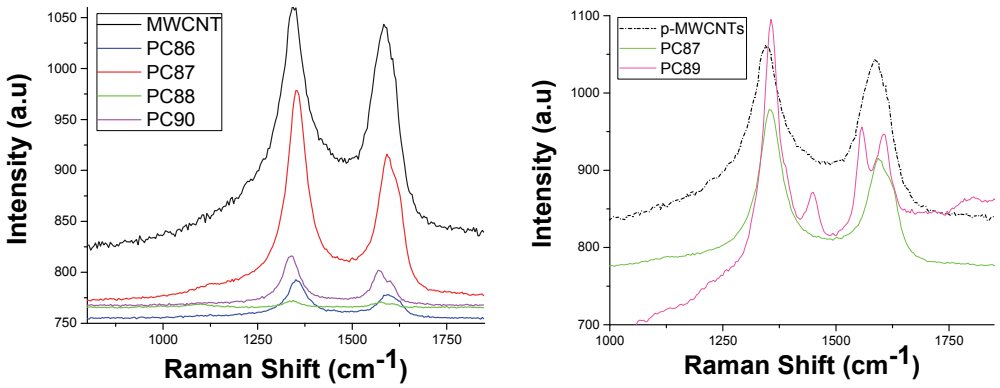

Figure 16. Enlargement of First-order Scattering zone.

➢ **Infrared spectroscopy**

The FT-IR spectra of **MWCNT** of every compound from the Scheme 2 are summarized in Figure 17. It can be observed clear changes between the spectra of all compounds. In contrast to Raman results, there is a pronounced difference between IR of **MWCNT** and the corresponding to **PC86**. The bands around 3000 cm^{-1} belong to C-H bonds, that can be related to the spacer introduced in the Prato reaction. Moreover, the infrared spectra of **PC89** and **PC90** have several small bands from 1500 to 1550 cm^{-1} that may be due to C-H aryl bonds of PDIs. These bands are less sharp than in the rest of cases because the amount of perylenediimide with respect to carbon nanotube is lower.

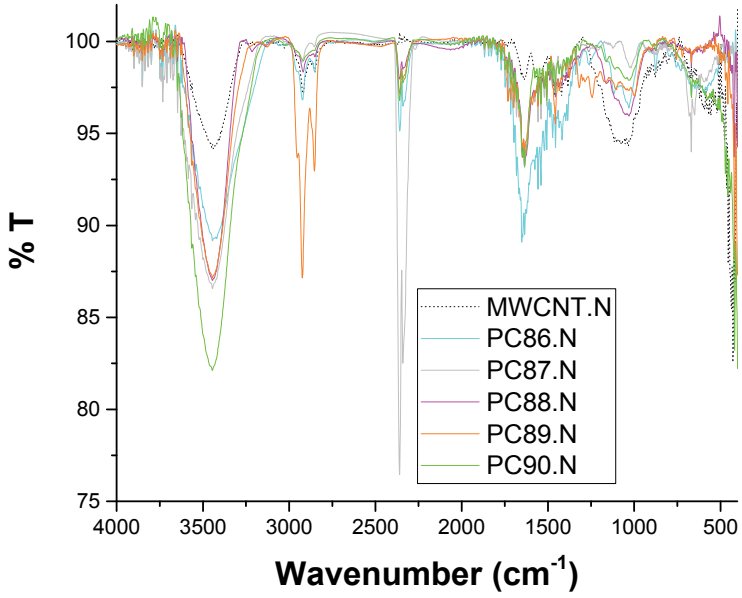

Figure 17. FT-IR spectrum of each compound of Scheme 2.

- **UV-Visible and Fluorescence Spectroscopy**

The behaviour of **PC90** in different solvents was studied to identify what is the appropriate solvent. **PC90** was dispersed in solvents such as: water, tetrahydrofuran, methanol, MeOH:H_2O 1:1. **PC90** exhibited a green emission in water (Figure 18).

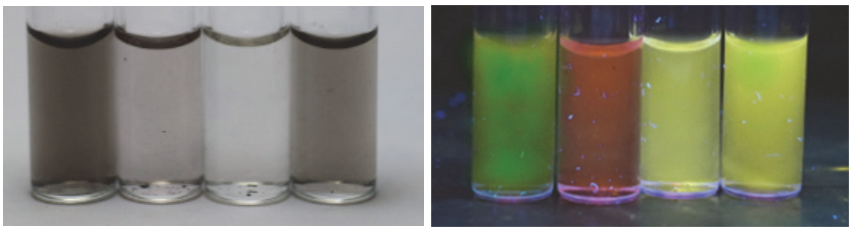

Figure 18. **PC89** dissolved in water, methanol, tetrahydrofuran, THF:H_2O 1:1 from the left to the right. The photos were taken left: under white light and right: under light of 366 nm of wavelength.

The excitation and emission spectra of the fluorophores **PC66** and **PC67** as well as the F-MWCNTs **PC89** and **PC90** were registered for comparison between them. The Figure 19 shows the excitation and emission spectra of **PC66**.

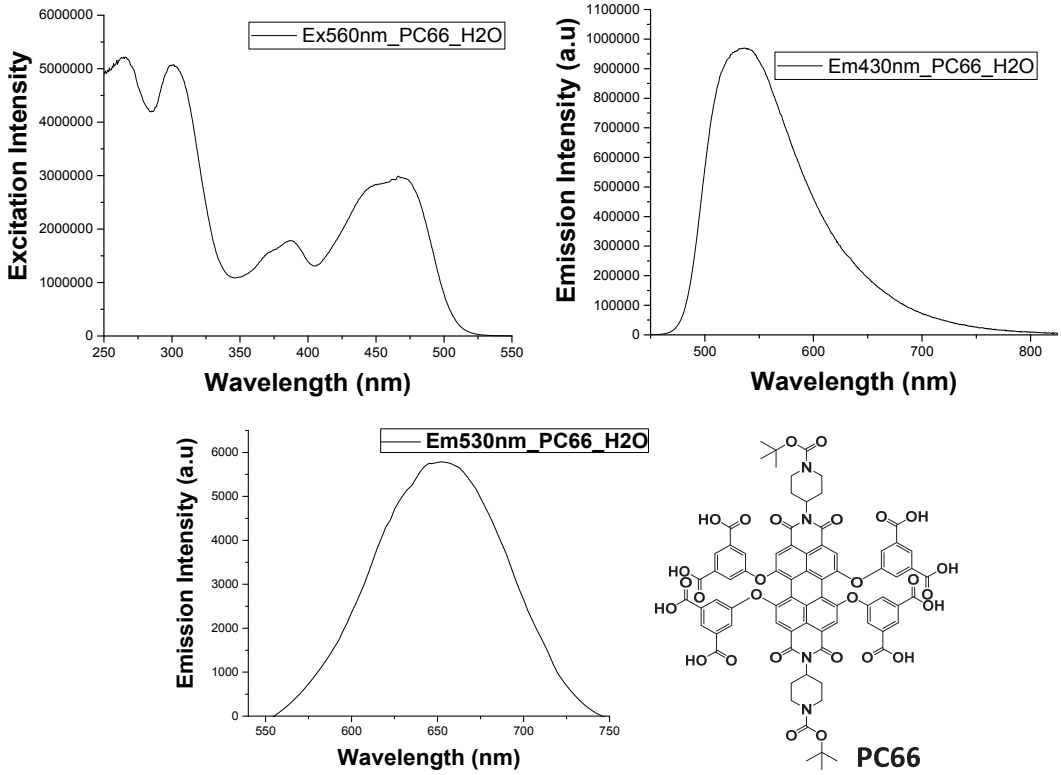

Figure 19. Excitation and emission spectra of **PC66** in water.

The excitation spectrum was registered fixing the emission wavelength in 560 nm and the emission spectrum fixing the excitation wavelength in 430 nm and in 530 nm to obtain two bands separately. In this sense, **PC66** presents two emission bands centred on 516 nm (green) and on 657 nm (red). As it can be seen in the Figure 19 the red band is less intense than the green one. The Figure 20 shows the excitation and emission spectra of **PC67**.

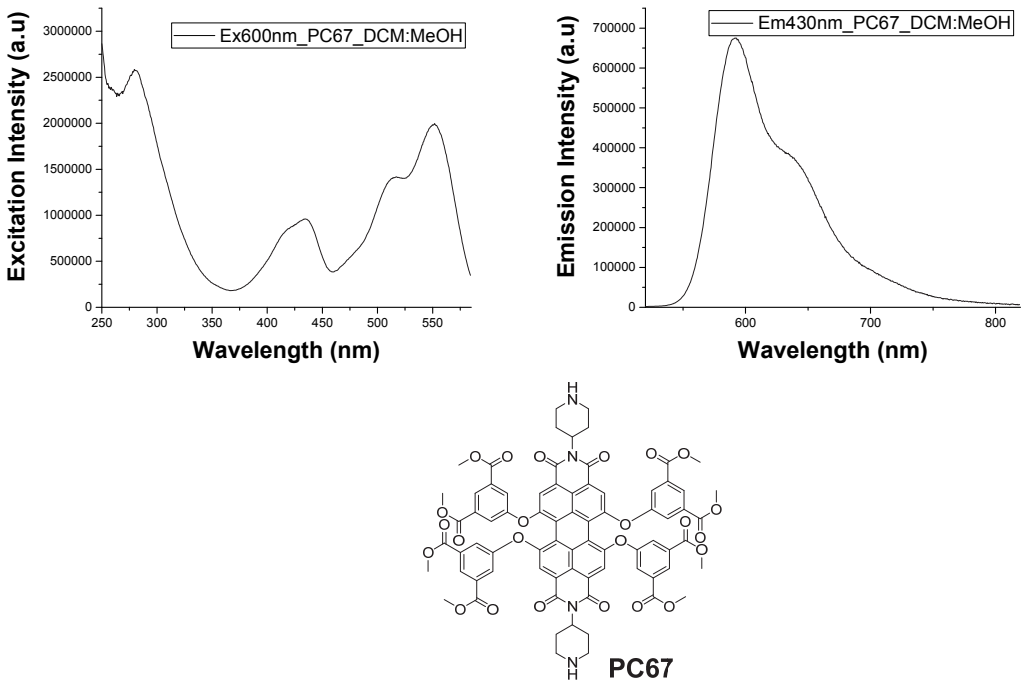

Figure 20. Excitation and emission spectra of **PC67** in DCM:MeOH 1:1.

The excitation spectrum was registered fixing the emission wavelength in 600 nm and the emission spectrum fixing the excitation wavelength in 430 nm. Consequently, **PC67** presents one emission band centred on 593 nm (orange) and a shoulder centred in 643 (red) as it can be observed in Figure 20. Then, **PC67** and **PC89** were analysed by excitation and emission spectra in DCM:MeOH solution and in solid state. A mixture of **PC67** and p-MWCNTs was also registered. The spectrum of **PC89** in solid state was also recorded. All spectra were normalized to compare the shape of bands. Figure shows that the spectra of **PC67**, the mixture of **PC67** and p-MWCNTs and **PC89** are quite similar. Instead, the emission spectrum of **PC89** in solid state (**PC89 solid**) is very different (Figure 21).

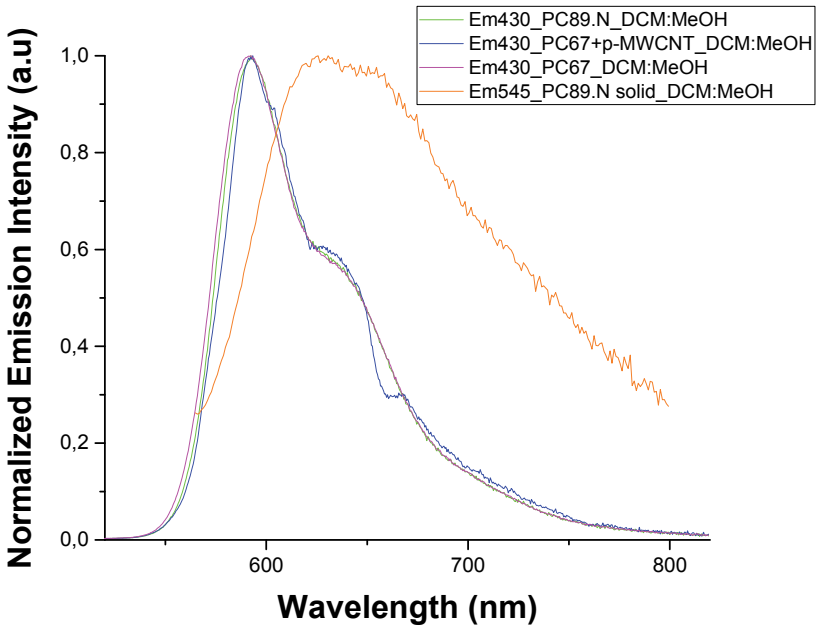

Figure 21. Emission spectra of **PC67** and **PC89** in DCM:MeOH 1:1.

Then **PC90** was suspended in water and was centrifuged until separation of the smallest carbon nanotubes from the largest carbon nanotubes. The carbon nanotubes in solution were called **liqPC90** and the solid residual carbon nanotubes **solPC90**. All spectra are shown in the Figure 22. **liqPC90** exhibits two emission bands centred on 512 nm (green) and 654 nm (red). The solution of **PC90** in water and **PC90** in solid show the same bands but with different intensity.

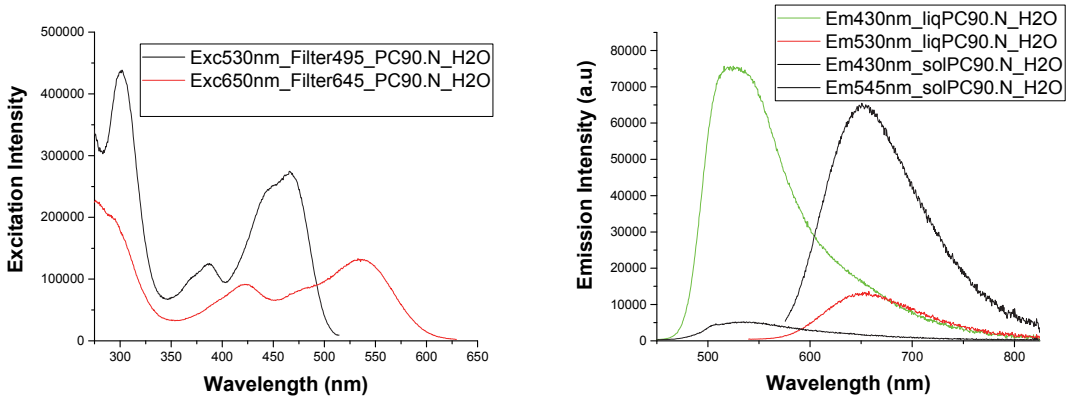

Figure 22. Excitation and emission spectra of **PC90** in water.

Then, the behaviour of **PC90** in water and buffer solutions is observed. This experiment is carried out with the aim of the future behaviour in cells cultures where the pH is controlled within a narrow range (Figure 23).

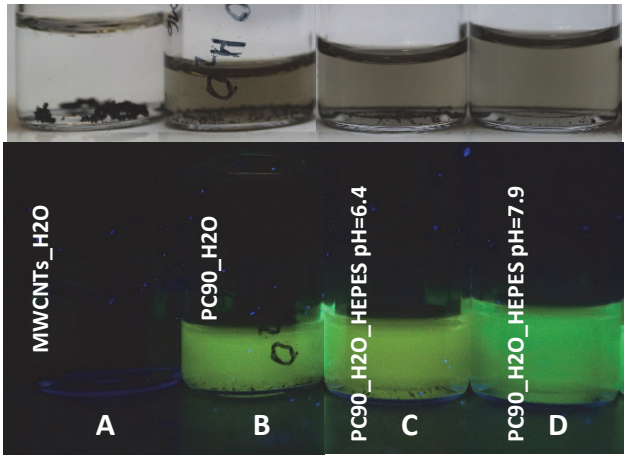

Figure 23. **PC90** in water and buffer media.

The pH has been controlled with HCl 0.1 M and NaOH 5% and the used buffer was HEPES (5 mM) at pH 6.4 and 7.9. The references were MWCNTs in water and **PC90** in water (Figure 23.A and B and Figure 24). **PC90** decreases the emission intensity in buffer media pH = 6.4 (Figure .C) and slightly increases at pH = 7.9 (Figure 23.D and Figure 24); but **PC90** appreciably increases the emission after 3 hours in buffered basic solution with decrease of the red band that could be due to degradation of the material by hydrolysis of amide bonds (Figure 24).

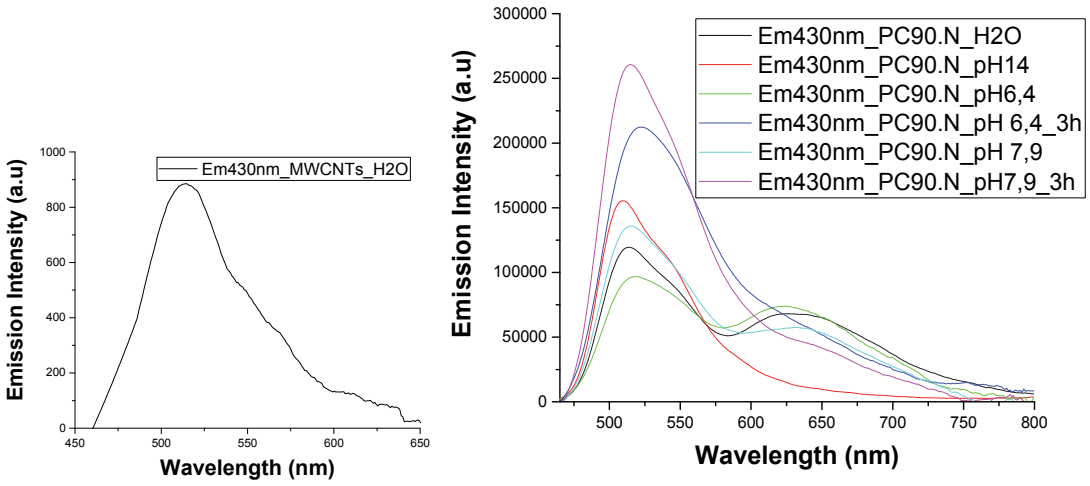

Figure 24. Emission spectra of MWCNTs and **PC90** in water and buffer solutions.

➢ **Transmission electron microscopy (TEM) images**

The morphology of pristine-MWCNTs was observed using (TEM). Pristine-MWCNTs were measured in two different TEM apparatus, at the IDIVAL institute in the University of Cantabria (Figure 25) and at the University of Valladolid (Figure 26). The Figure represents the characterization by TEM images of the p-MWCNTs. It can be observed that the carbon nanotubes form aggregates with a number of walls from 3 to 12, with the outer diameter ranging from 5 to 15 nm and the inner diameter between 3 and 10 nm. The circles seen below the carbon nanotubes correspond to the support to perform the TEM images.

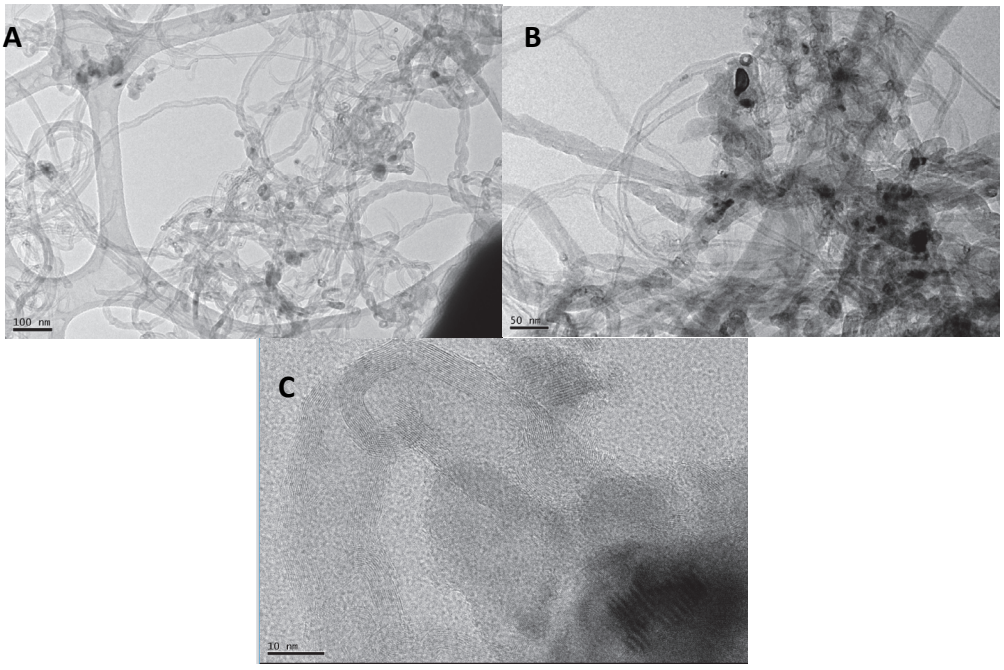

Figure 25. TEM images (JEOL- model JEM 1011 equipped with Gatan digital camera of high resolution) of pristine-MWCNTs supplied by IDIVAL institute magnified at 100 nm (A), 50 nm (B) and 10 nm (C).

The Figure 27 shows the existence of a sponge layer around the MWCNT surface. The TEM image displays that carbon nanotubes form aggregates and these exhibit a very long length in micrometres.

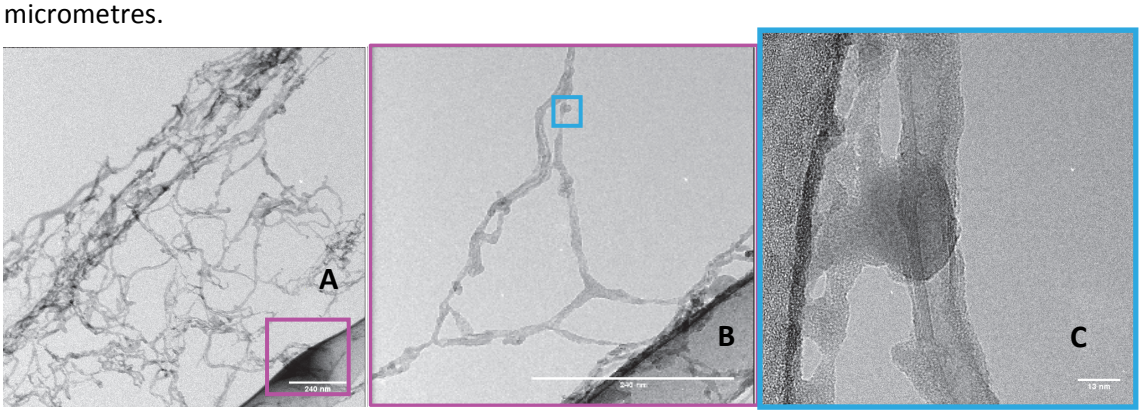

Figure 26. TEM images (TEM; JEOL JEM-FS2200 HRP) with a range of accelerating voltage from 80 to 200 kV) showing pristine-MWCNTs at different magnification 15000X (**A**), 50000X (**B**, pink box) and 200000X (**C**, blue box).

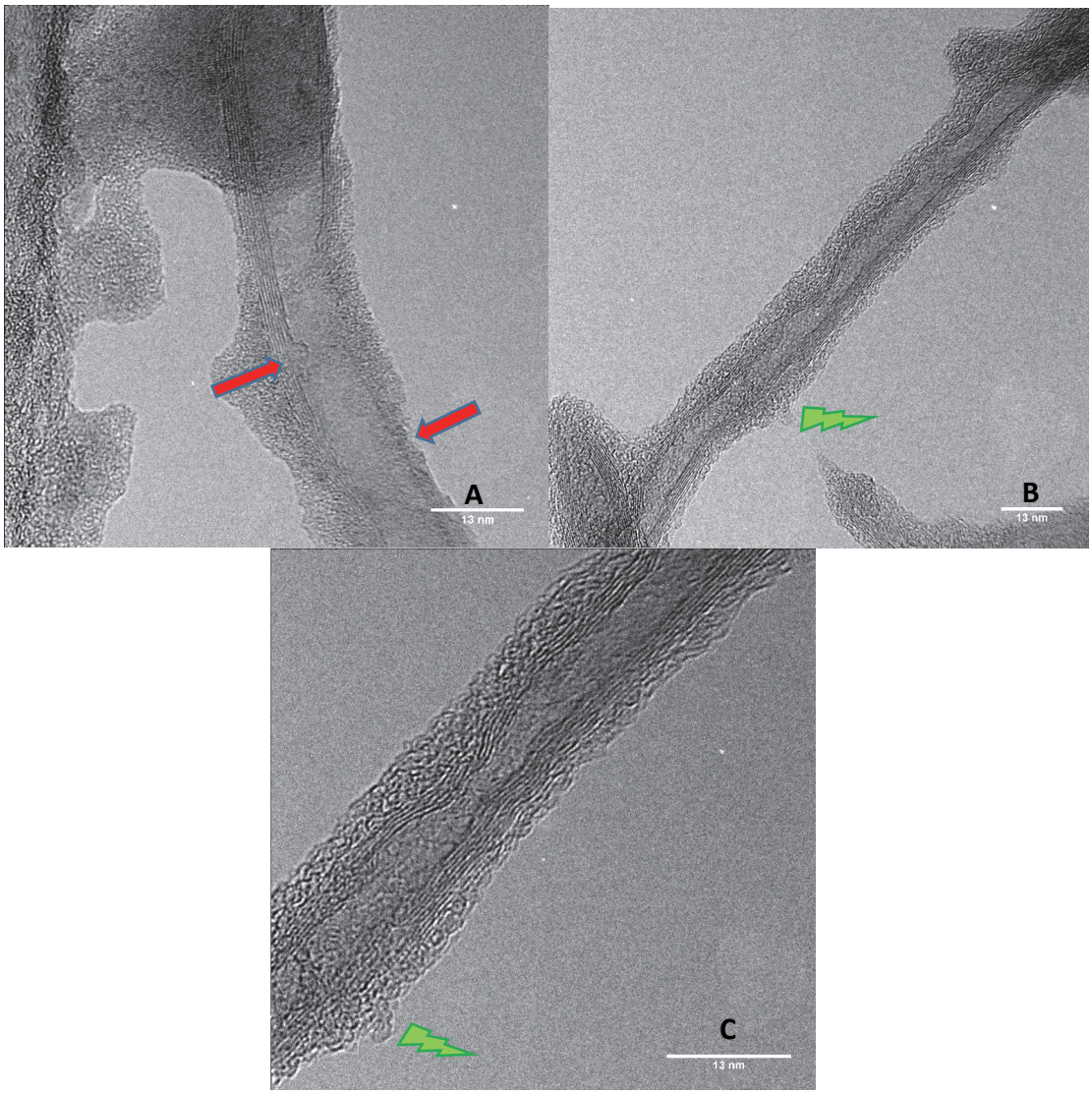

Figure 27. TEM images (TEM; JEOL JEM-FS2200 HRP) with a range of accelerating voltage from 80 to 200 kV) and the magnification is 300000X of pristine-MWCNTs (**A**), 200000X of **PC90** (**B**), and 400000 of **PC90** (**C**).

From TEM images (Figure 27) it can be seen that the number of walls of the pristine carbon nanotubes varies from 7 to 9, the inner diameter between 7 and 9 nm and the outer diameter ranging from 17 to 20 nm. The thickness of the sponge is from 6 to 2 nm. The pristine carbon nanotubes have several defects (highlighted with red arrows) along the wall that could generate secondary reactions or that places accumulated more impurities than in the rest increasing the thick of nanotube.

The difference between the Figure 27A with the Figure 27B is the homogeneous and defined sponge along the nanotube whereas the sidewall of the pristine MWCNT shows that the sponge is much less homogeneous. There are protuberances in different images marked in green at the surface of the nanotube. From the literature[51,52] we can confirm that these

[51] K. A. Wepasnick, B. A. Smith, K. E. Schrote, H. K. Wilson, S. R. Diegelmann, D. H. Fairbrother, *Carbon*, **2011**, *49*, 24-36.
[52] V. Mittal, *Surface Modification of Nanotube Fillers*, Wiley-VCH, Weinheim, Germany, **2011**.

differences in the homogeneity sponge and the protuberances could be related with a covalent functionalization if the Figure 27 B and C in comparison to A.

7.2. Results in HeLa cells.

HeLa cells are used to observe if the functionalized carbon nanotubes (**PC90**) are internalized by them. In preliminary studies performed by IDIVAL Institute, the fluorophore **PC66** was preferably accumulated in the nucleus and in the nucleolus of these cells (see images of confocal microscopy in Chapter 2), moreover **PC66** was also accumulated in the cytoplasm.

After the incubation of **PC90** with HeLa cells, the confocal microscopy demonstrate that **PC90** was internalized in the cells (Figure 28).

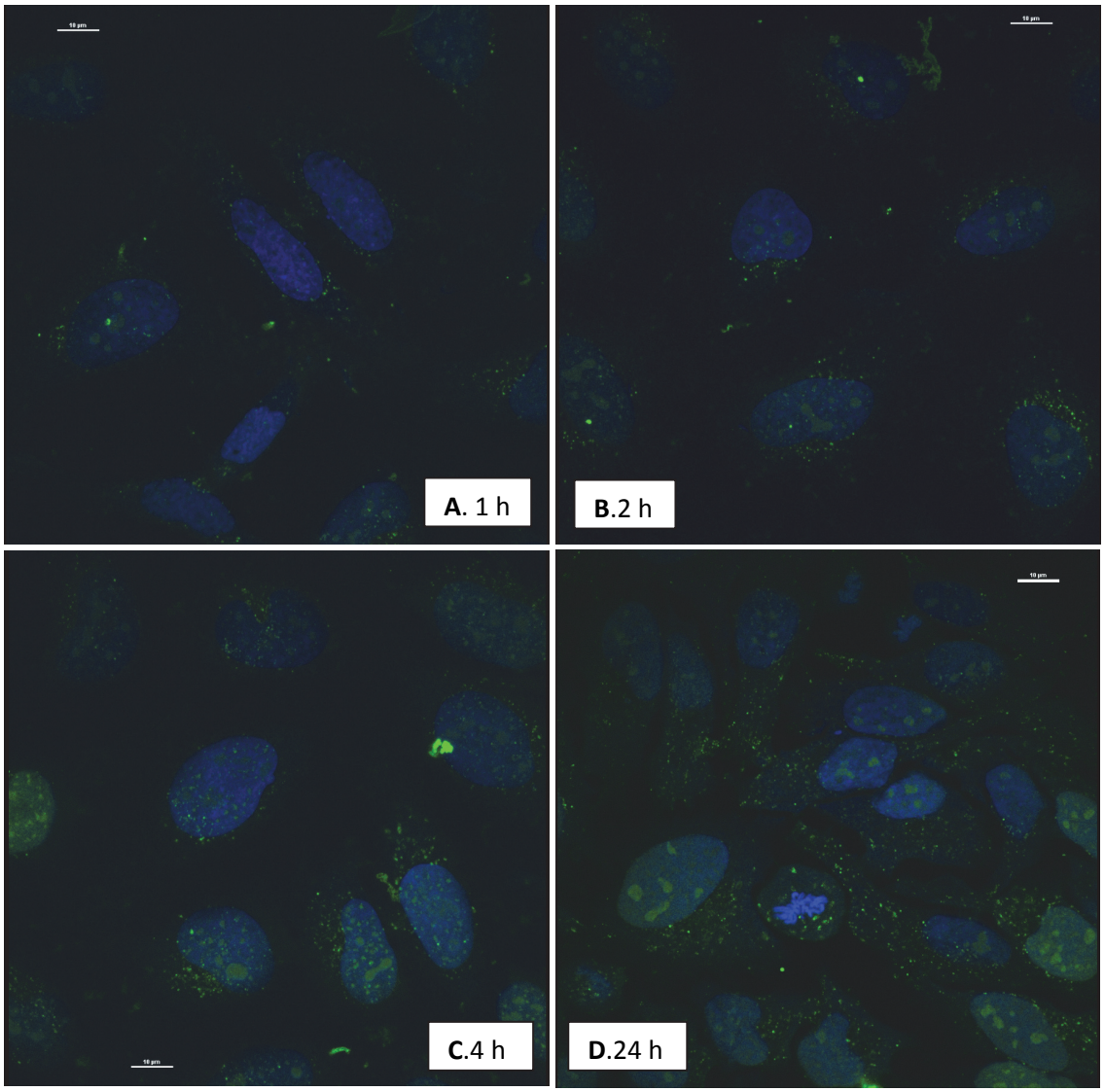

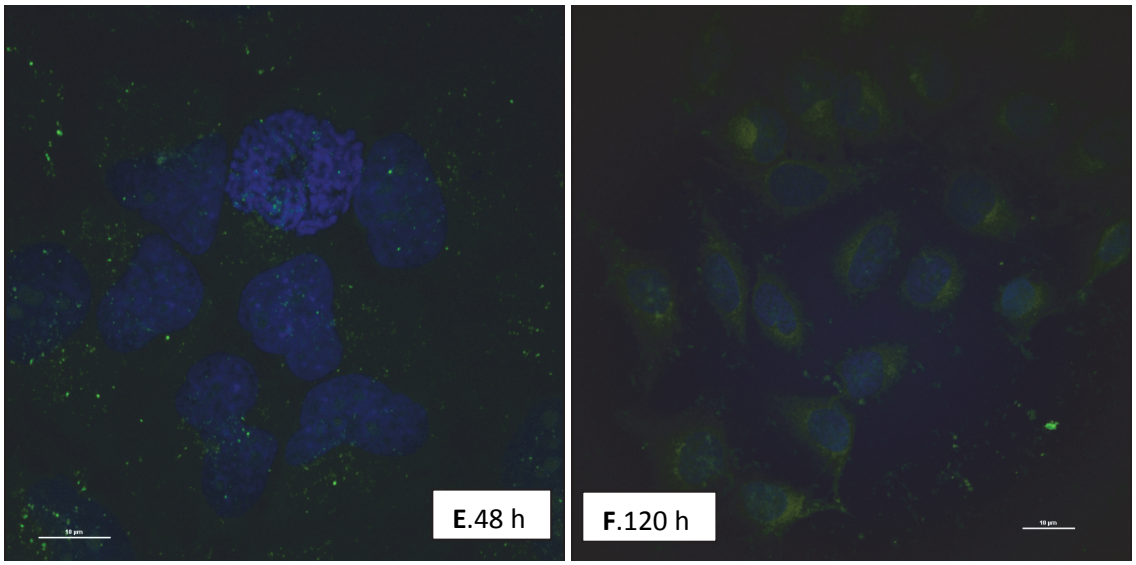

Figure 28. Images of confocal microscopy of HeLa cells incubated with **CNT.N.F1** stained with Hoechst. A. for 1 hour. B. for 2 hours. C. for 4 hours D. for 24 hours. E. for 48 hours, F. for 120 hours.

The Figure shows the cellular timeline from 1h to 120 h. At the beginning (1 hour), the carbon nanotubes are localized in the cytoplasm, but after 4 hours the carbon nanotubes accumulated in the nucleus even the nucleolus and finally the amide bond is hydrolized by the protease activity and after 120 hours the fluorophore is localized in all the cytoplasm.

7.3. Conclusions.

The water-soluble covalently functionalized carbon nanotubes with fluorescent perylenediimides are internalized by HeLa cells as shown by the confocal imaging, albeit after several days the probe **PC66** was released from the carbon nanotubes. As a result, another alternative synthetic route, which is summarized in the next section, was designed.

8. SYNTHETIC ROUTE III.

The route in the Scheme and Scheme 4 was developed. The difference with the synthetic route II is the binding between the carbon nanotube to the perylenediimide; in the previous sequence the bonding reaction was an amidation, in this case it will be a click reaction. The synthetic route is similar to the previous one but this time the amidation sequence was performed with an azido polyethylenglycol carboxylic acid to give **CNT.oPN$_3$** (Scheme 3).

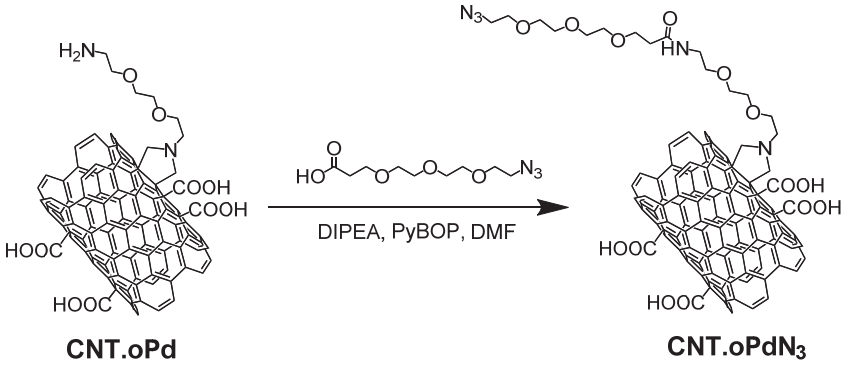

Scheme 3. First step of the synthesis of fluorescent water-soluble MWCNTs.

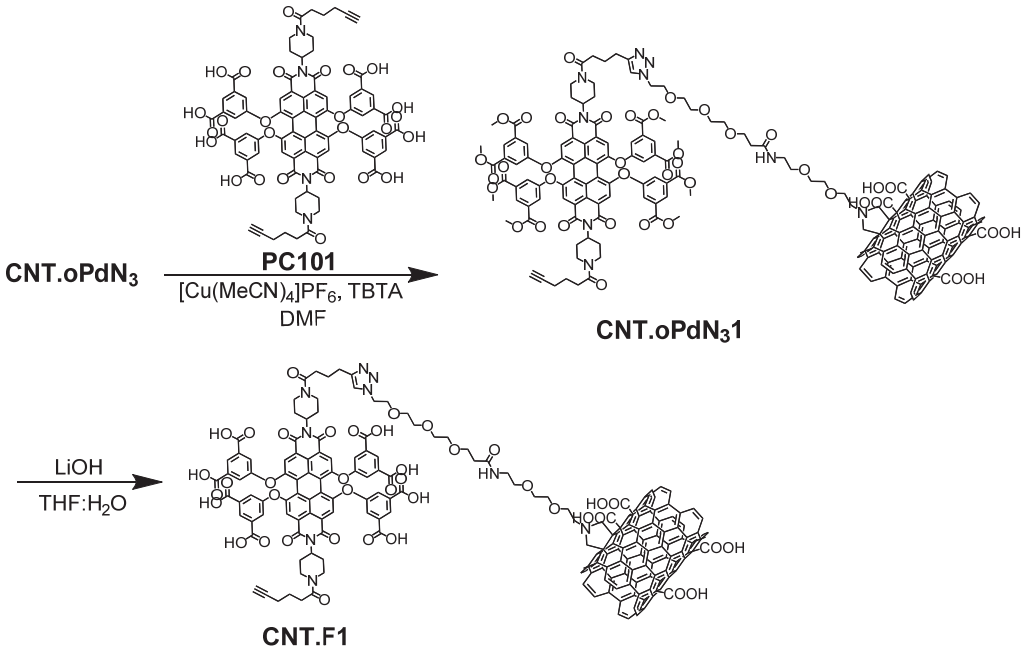

Scheme 4. Synthetic Route III to reach the fluorescent water-soluble MWCNTs **CNT.F1**.

CNT.oPN$_3$ from Scheme 3 was then subjected to react with the perylenediimide **PC101** (from chapter 2) through a click reaction.[53] Two click conditions were tested to try obtaining best results. The first click consisted in treating **CNT.oPdN$_3$** with Cu(MeCN)4]PF6 and TBTA[54] and **PC101** dissolved in DMF (Scheme 4). In the second click reaction, the source of copper was copper(II), and the copper(I) species was generated by sodium ascorbate.[55] **CNT.oPN$_3$1** and **CNT.oPN$_3$2** were obtained from the first and the second click reactions, respectively. Finally, the products were hydrolyzed with lithium hydroxide in THF/water to generate the functionalized carbon nanotubes susceptible to be internalizez by HeLa cells.

- **SEM and TEM images of oxidised and functionalized carbon nanotubes**

After the initial oxidation, the obtained products formed aggregates (Figure 29. left), whereas after the cycloaddition the carbon nanotubes gave dispersed suspensions (Figure 29. right).

[53] a) D. D. Díaz, M. G. Fin, K. B. Sharpless, V. V. Fokin, C. J. Hawker, *An. Quim.*, **2008**, *104(3)*, 173-180; b) A. Suárez, *An. Quím.* **2012**, *108(4)*, 306-313.
[54] T. Kwon, W-J. Kim, H-S. Kim, *Method of separating carbon nanotubes,* U.S. Patent 20140066631 A1, Ago 22, **2013**.
[55] S. Rana, J. W. Cho, *Nanoscale*, **2010**, *2*, 2550-2556.

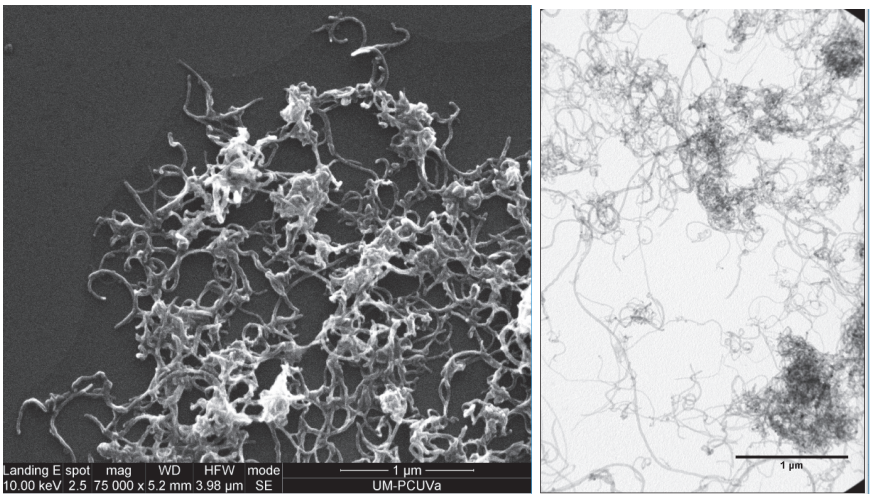

Figure 29. SEM image at 1 µm of **CNT.o** (left). TEM image at 1 µm of **CNT.oP** (right). It is noticeable a better dispersion than for the pristine carbon nanotubes (DMF), the length of the nanotubes has not been much affected.

8.1. Characterization of compounds.

As in previous sections, samples were characterized by standard analytical techniques such as Raman and SEM and TEM spectroscopy.

- **Raman spectroscopy**

The Figure 30, Figure 31 and Figure 32 show the Raman spectra of all intermediates on the way to obtain **CNT.F1** and **CNT.F2**. The intermediate **CNT.oPdN$_3$1** exhibit the same Raman spectrum than **PC89**. For the same reasons than in the previous section, **CNT.F1** is the selected probe to perform tests in HeLa cells.

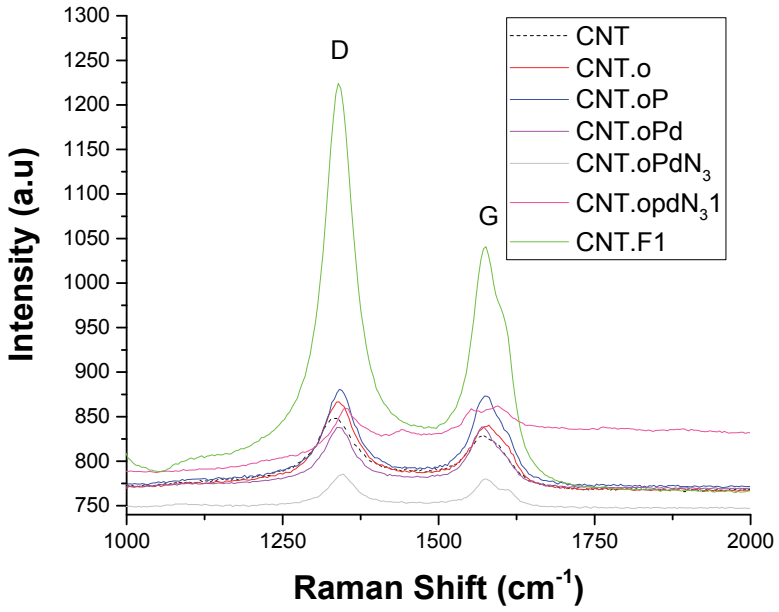

Figure 30. Raman spectra of all intermediates on the way to obtain **CNT.F1.**

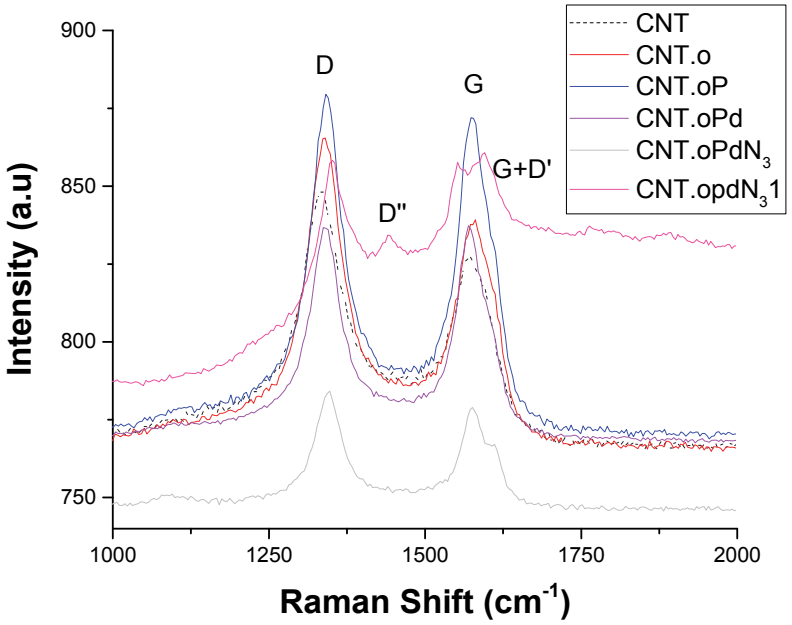

Figure 31. Raman spectra of all intermediates on the way to obtain **CNT.F1** (**CNT.F1** was not represented)**.**

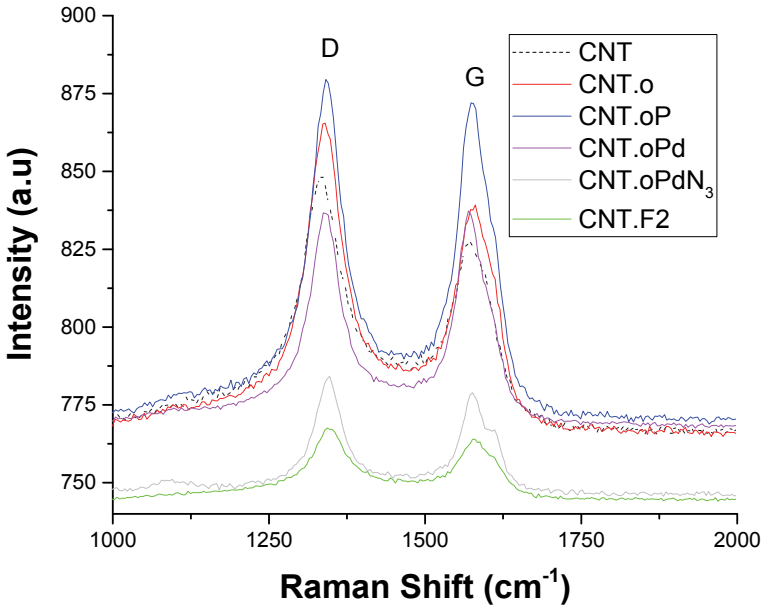

Figure 32. Raman spectrum of all intermediates on the way to obtain **CNT.F2.**

8.2. Results in HeLa cells.

The Figure 33 shows the confocal images of cells at a timeline: 1 hour, 24 hours and 120 hours. After 1 hour (Figure 33.A), the blue stained chromosomes (in blue) are visible due to the

cell is in the metaphase, the functionalized carbon nanotubes are green fluorescent (yellow arrows). **CNT.F1** appears as agglomerates of carbon nanotubes (red channel) in the second image (Figure 33.B). An elongated filament is observed in the cytoplasm (Figure 33.C). Red arrows define this filament, that could be **CNT.F1**. The nucleolus is dyed, which may indicate degradation of the dye from the carbon nanotubes (yellow arrow).

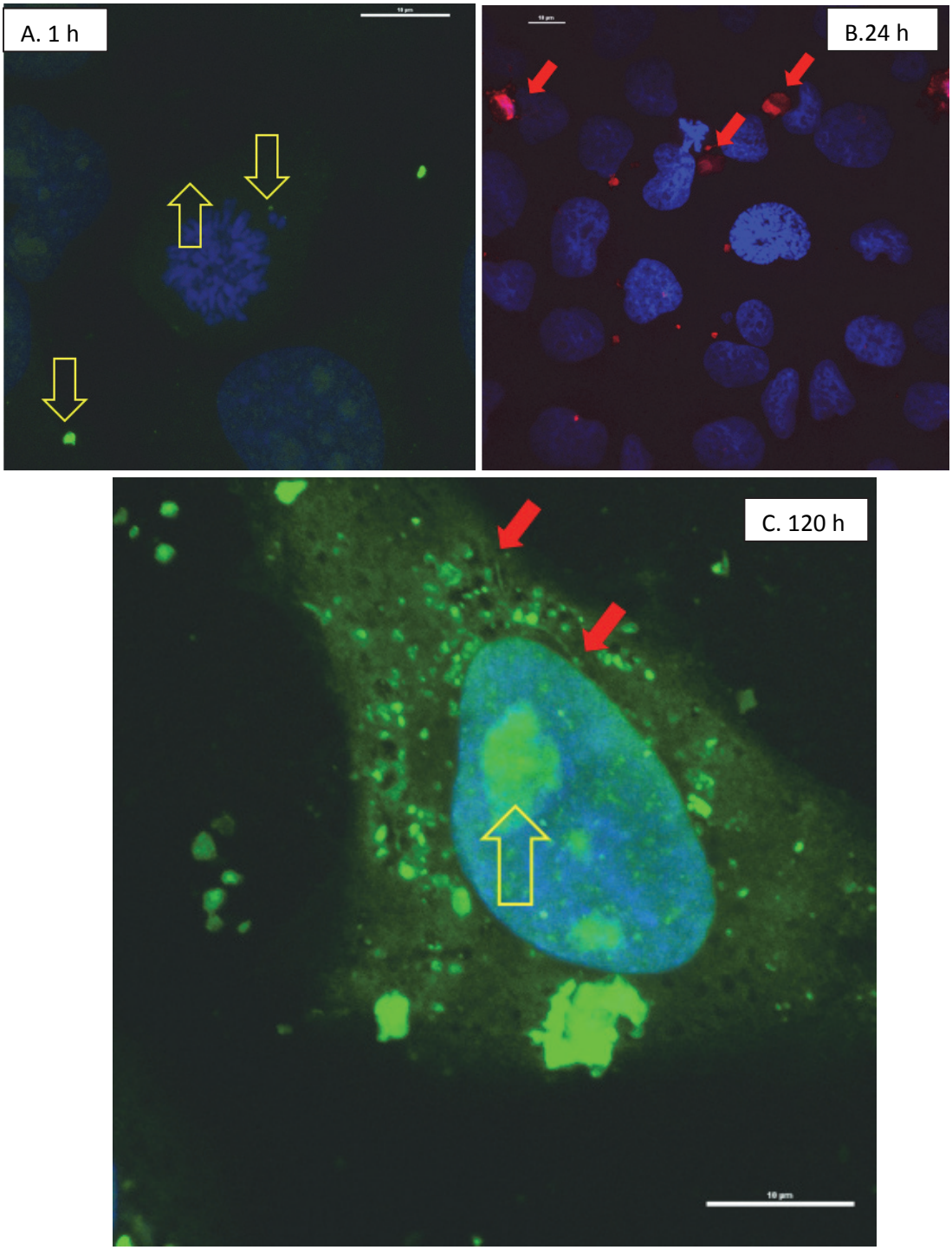

Figure 33. Image of confocal microscopy of HeLa cells incubated with **CNT.F1** and the nucleus stained with Hoechst. **A**. for 1 hour (green channel). **B**. for 24 hours. **C**. for 120 hours.

8.3. Conclusions.

The results of this section confirmed the results obtained in the previous section. The water-soluble covalently functionalized carbon nanotubes with fluorescent perylenediimides are internalized by HeLa cells as shown by the confocal imaging, albeit after several days the fluorescent perylenediimide dye was released from the carbon nanotubes.

CONCLUSIONS

In this Ph. D. Thesis, two new families of perylenediimides have been successful synthesized to be useful for in-situ TATP detection and biomagen.

- **Family I**: The amine cyclohexylamine was introduced in peri-positions of perylenedianhydride and the resulting perylenediimides were mono- and bis-functionalized in bay positions by Suzuki coupling with three different boronic esters.
- **Family II**: A functionalizable amine was introduced in peri-positions and water-solubilizing phenols in bay positions of perylenediimides were introduced by copper(I) catalysed nucleophilic substitution of chlorines in aromatic carbon positions.

The first chapter achieved the preparation of new easy and portable devices for the rapid and in-situ fluorescent detection of TATP. Different solid materials to detect and discriminate among home-made explosives and classic oxidants have been developed.

- Perylenediimides bearing donor groups have been synthetized.
- Absorbance and fluorescence titrations have been carried out in order to discriminate among TATP explosive and classical oxidizing reagents.
- Perylenediimides bearing donor groups have been anchored on different silica supports.
- The solid supported fluorogenic probes have been able to detect and discriminate gaseous traces of TATP explosives from other oxidants with a LOD = 3.3 mM.
- A polymer anchored to perylenediimides bearing donor groups has been prepared.
- The polymer is able to detect and discriminate in air flow traces of TATP from their precursors (acetone and hydrogen peroxide) wit a LOD = 4.8 mM.
- In addition, this polymer has a second application in the preparation of solid supported gold and palladium nanoparticles useful for catalysis.

The second chapter achieved the development of water-soluble fluorogenic probes for their study in cellular imaging and for the fluorogenic detection of proteins and potential toxins.

- In the chapter 2A:
  - Potentially water-soluble fluorescent tetra-substituted perylenediimides have been obtained.
  - Tetra-substituted perylenediimides bioconjugated to biological molecules in peri positions, biotin and testosterone, have been synthesized.
  - Systematical internalization, biocompatibility and cytotoxicity of tetra-substituted perylenediimides in cells *in-vivo* have been studied.
  - The activity of the synthesized materials against DNA strands of quadruple helix have been analysed.
- In the chapter 2B:
  - Fluorescent titrations of the biotinylated derivatives in the presence of avidin have been performed as well as the study of the behaviour of avidin and

biotinylated perylenediimide derivatives in the presence of graphene oxide. The interaction between biotin and avidin was quantitatively detected by fluorescence, the addition of graphene oxide to this system was an added value as an OFF-ON sensor.

- In the chapter 2C:

  - Globotriaosyl derivatives with a long chain linkable to other functional groups have been prepared and tetra-substituted perylenediimides, ready for the bioconjugation to globotriaosyl derivatives, have been synthetized.

The third chapter achieved the development of an application of the **family B** to be anchored on carbon nanotubes that were subsequently solubilized in water.

- The design and accomplishment of different ways for CNT-functionalization have been performed.

- The confocal imaging of differently functionalized CNT in HeLa cells has been accomplished.

SYNTHESIS AND CHARACTERIZATION: CHAPTER 1

1. Synthesis of perylenediimides: cyclohexylamine.

1.1. Synthesis of *N,N'*-bis(cyclohexyl)-perylene-3,4,9,10-tetracarboxylic diimide (PC36).

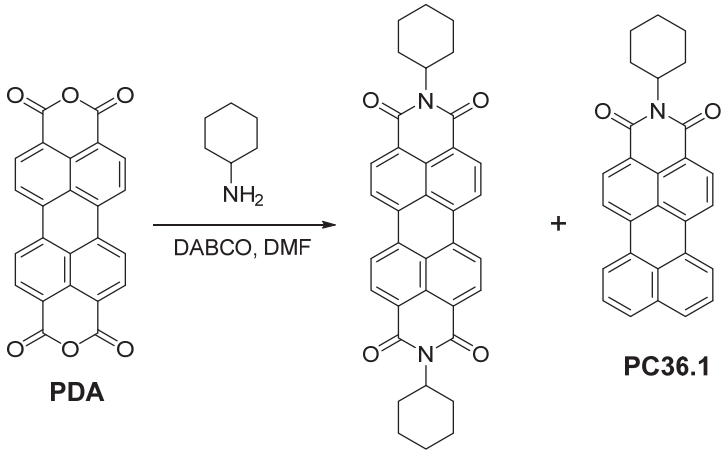

Anhydrous DMF (20 mL) and cyclohexylamine (0.65 g, 6.55 mmol) were added under nitrogen to perylene-3,4,9,10-tetracarboxylic dianhydride (0.54 g, 1.27 mmol) and DABCO (0.90 g, 8.02 mmol). The mixture was irradiated in a microwave device at 200 °C for one hour. Then it was poured over an aqueous solution of HCl 1M (15 mL), stirred for one hour, filtered and washed with water (30 mL). Purification was carried out by silica gel flash chromatography using DCM:MeOH (70:30) as eluent to give compound **PC36** and **PC36.1**.

***N,N'*-bis(Cyclohexyl)-perylene-3,4,9,10-tetracarboxylic diimide (PC36).**

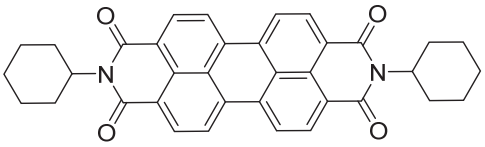

PC36

Red solid 66 % yield (0.46 g, 0.83 mmol). **R_f (DCM:MeOH 50:1):** 0.6. **Mp (°C):** > 350 °C. **FT-IR (KBr, cm^{-1}):** 2924 (C-H), 2852 (C-H), 1691 (C=O), 1651 (C=O), 1594 (C=C), 1407 (CH_2), 1338 (C-N), 1260, 1178, 1119, 1031, 972, 809, 743, 650 (fingerprint region). **^{1}H NMR (300 MHz, $CDCl_3$) *δ*:** 8.66 – 8.57 (m, 8H, H_{Ar}), 5.09 – 5.01 (m, 2H, N-CH), 2.63 – 2.51 (m, 5H, CH_2), 1.92 (d, *J* = 13.3 Hz, 4H, CH_2), 1.79 (d, *J* = 10.0 Hz, 5H, CH_2), 1.53 – 1.36 (m, 6H, CH_2). **^{13}C NMR (101 MHz, $CDCl_3$) *δ*:** 164.1 (C=O), 134.7 (C_{Ar}), 131.6 (C_{Ar}), 126.7 (C_{Ar}), 124.4 (C_{Ar}), 124.1 (C_{Ar}), 123.3 (C_{Ar}), 54.3 (N-CH), 33.5 (CH_2), 32.2 (CH_2), 29.9 (CH_2), 29.4 (CH_2), 26.8 (CH_2), 25.8 (CH_2), 25.7 (CH_2), 25.2 (CH_2), 23.9 (CH_2), 22.9 (CH_2). **HRMS (MALDI+, DCTB):** m/z calcd. for $C_{36}H_{30}N_2O_4$ ($[M]^+$): 554.2200; found: 554.2426.

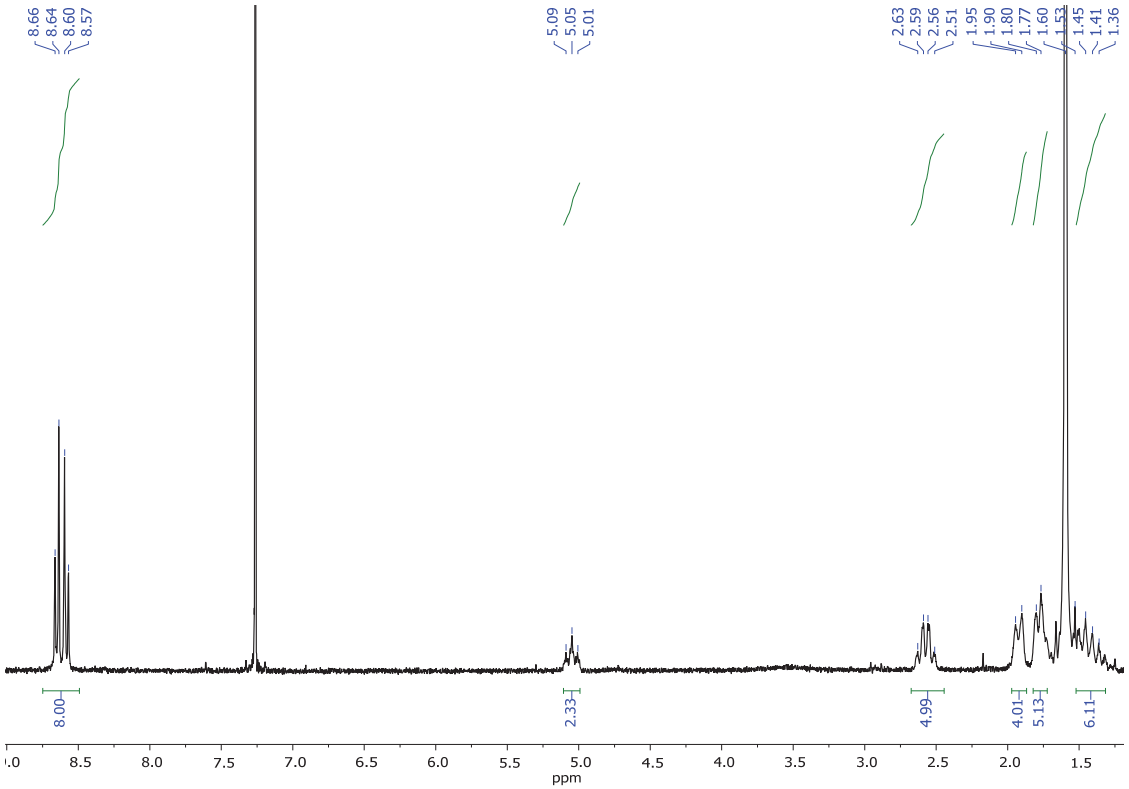

Figure 1. ^{1}H NMR (300 MHz, $CDCl_3$) of PC36

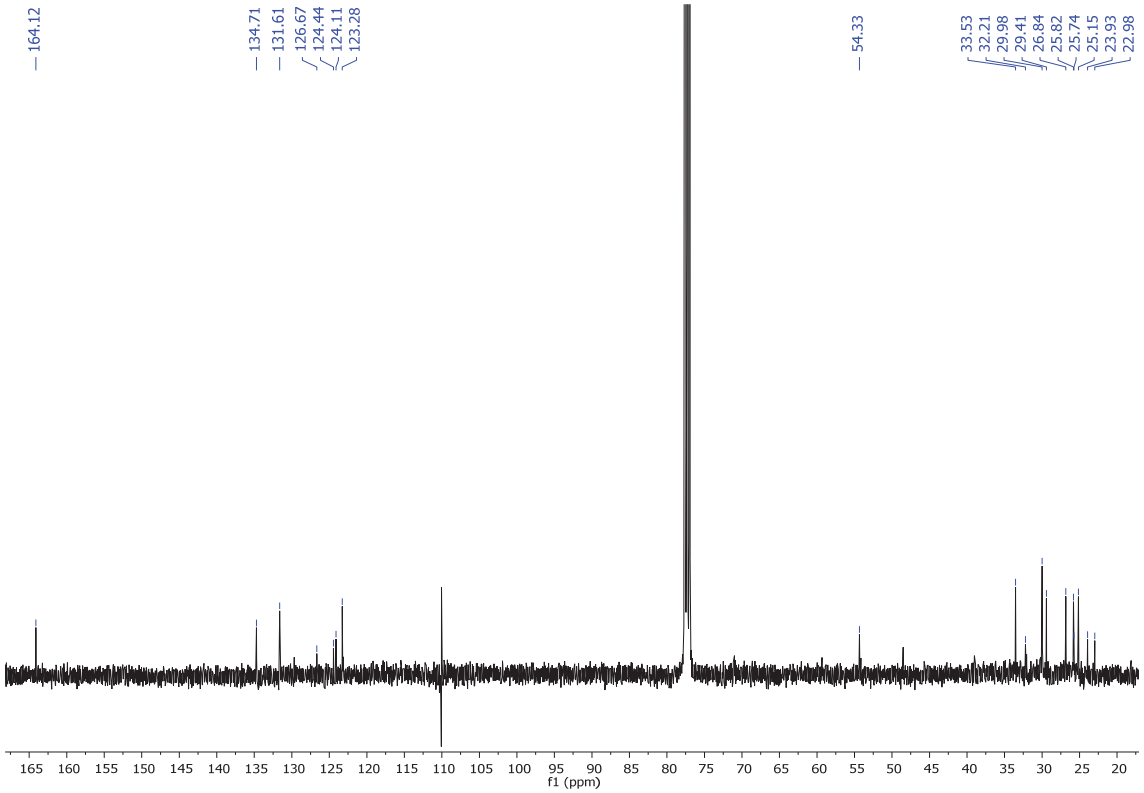

Figure 2. ^{13}C NMR (101 MHz, $CDCl_3$) of PC36

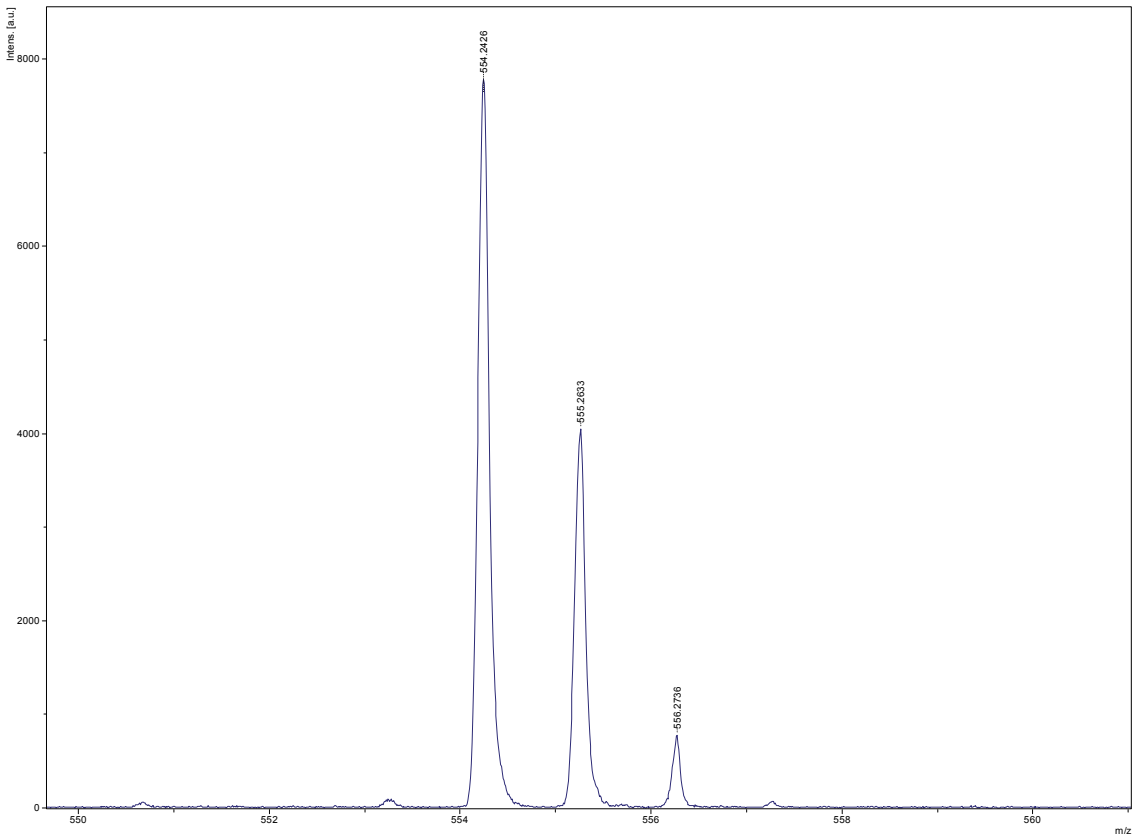

Figure 3. Mass spectrum (MALDI+, DCTB) of PC36

***N*-(Cyclohexyl)-perylene-3,4-dicarboxylic monoimide (PC36.1).**

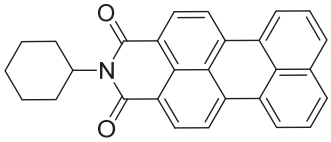

PC36.1

Orange solid 4% yield (2 mg, 0.05 mmol). **R_f (DCM:MeOH, 50:1):** 0.9. **Mp (^oC):** 315 – 317 ^oC. **FT-IR (KBr, cm^{-1}):** 2921 (C-H), 2851 (C-H), 1727 (C=O), 1696 (C=O), 1644 (C=O), 1596 (C_{Ar}-C_{Ar}), 1461 (C_{Ar}-C_{Ar}), 1357 (C-N), 1261, 1178, 1053, 811 (fingerprint region). **^{1}H NMR (300 MHz, $CDCl_3$) δ:** 8.55 (d, *J* = 8.0 Hz, 2H, H_{Ar}), 8.40 (t, *J* = 8.0 Hz, 4H, H_{Ar}), 7.88 (d, *J* = 8.2 Hz, 2H, H_{Ar}), 7.64 – 7.59 (t, *J* = 7.9 Hz, 2H, H_{Ar}), 5.13 – 5.01 (m, 2H, N-CH), 2.62 – 2.53 (m, 5H, CH_2), 1.91 (d, *J* = 12.1 Hz, 4H, CH_2), 1.73 (d, *J* = 17.6 Hz, 5H, CH_2), 1.45 – 1.41 (m, 6H, CH_2). **^{13}C NMR (75 MHz, $CDCl_3$) δ:** 164.7 (C=O), 137.0 (C_{Ar}), 134.5 (C_{Ar}), 131.53 (C_{Ar}), 130.9 (C_{Ar}), 127.2 (C_{Ar}), 123.7 (C_{Ar}), 120.3 (C_{Ar}), 53.8 (N-CH), 32.1 (CH_2), 29.8 (CH_2), 29.5 (CH_2), 29.3 (CH_2), 26.7 (CH_2), 25.7 (CH_2), 22.9 (CH_2). **HRMS (MALDI+, DCTB):** m/z calcd. for $C_{28}H_{21}N_1O_2$ ($[M]^+$): 403.1567; found: 403.1602.

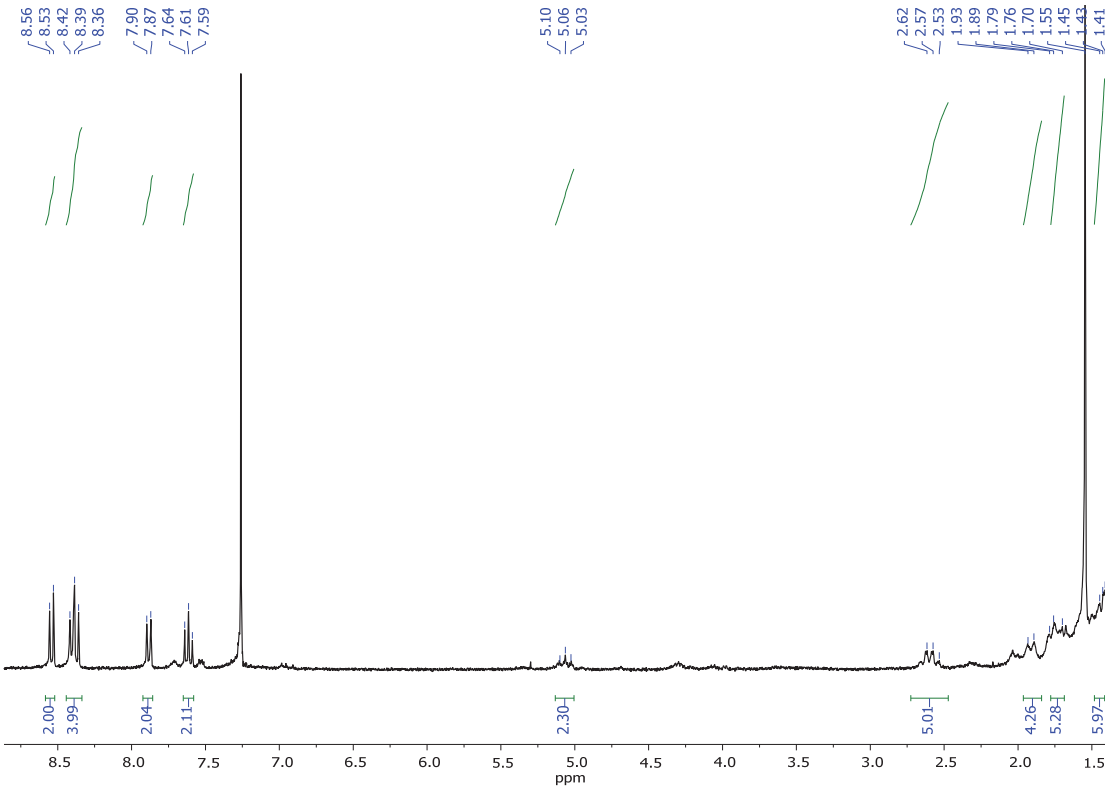

Figure 4. ^{1}H NMR (300 MHz, $CDCl_3$) of PC36.1

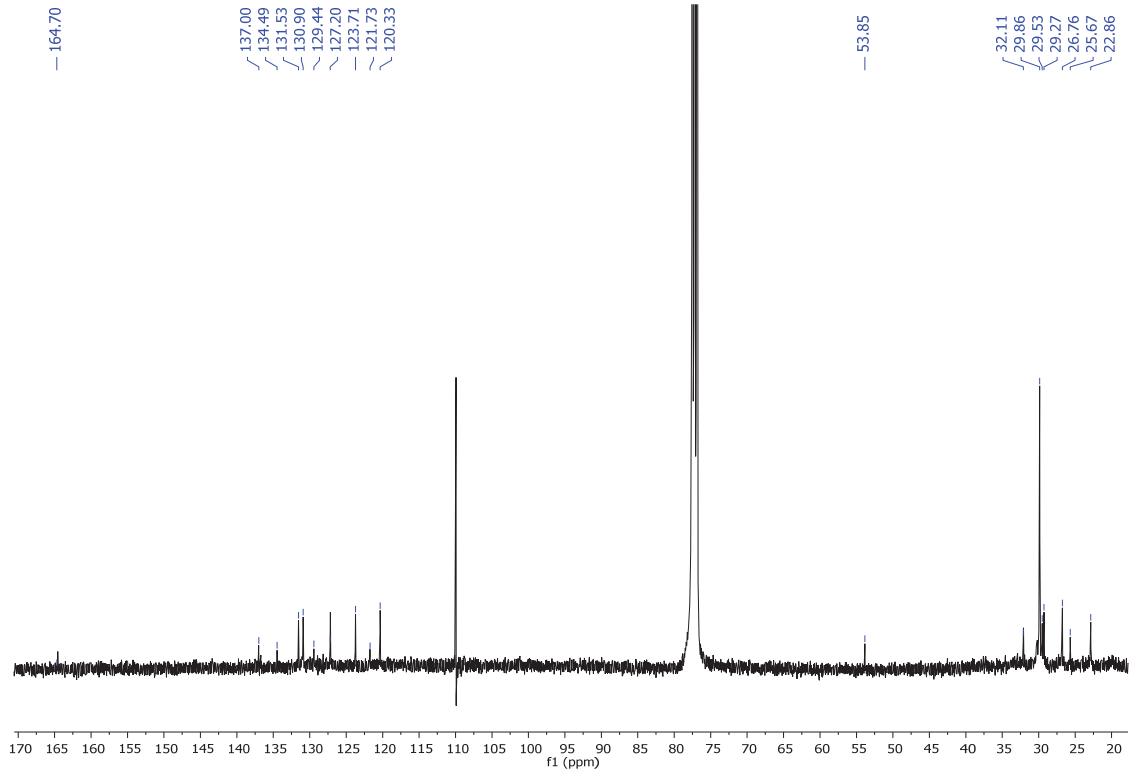

Figure 5. ^{13}C NMR (75 MHz, $CDCl_3$) of PC36.1

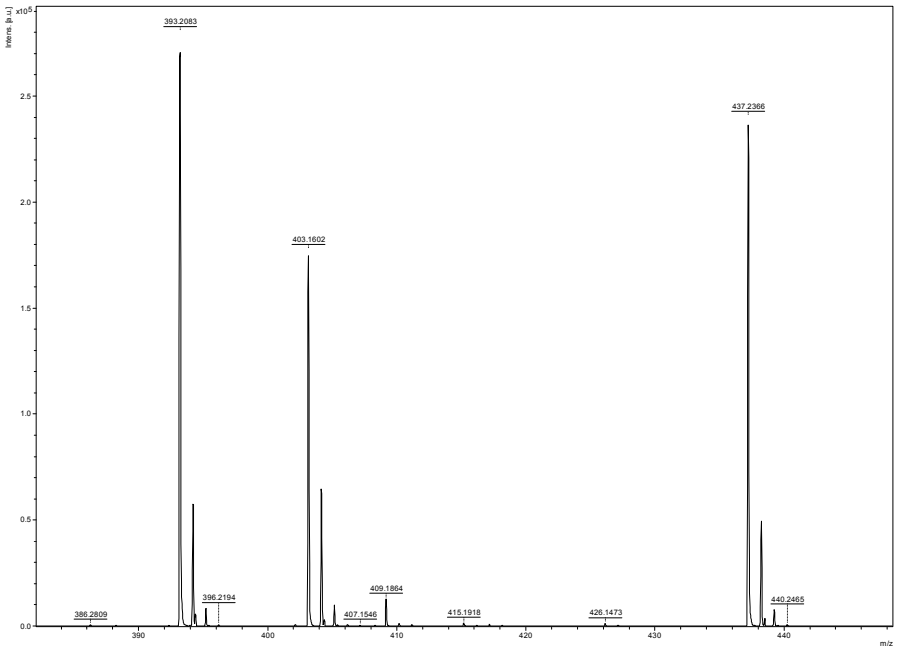

Figure 6. Mass spectrum (MALDI+, DCTB) of PC36.1

1.2. Synthesis of brominated-perylene-3,4,9,10-tetracarboxylic diimides (PC39, 1,6- and 1,7-PC37, PC38).

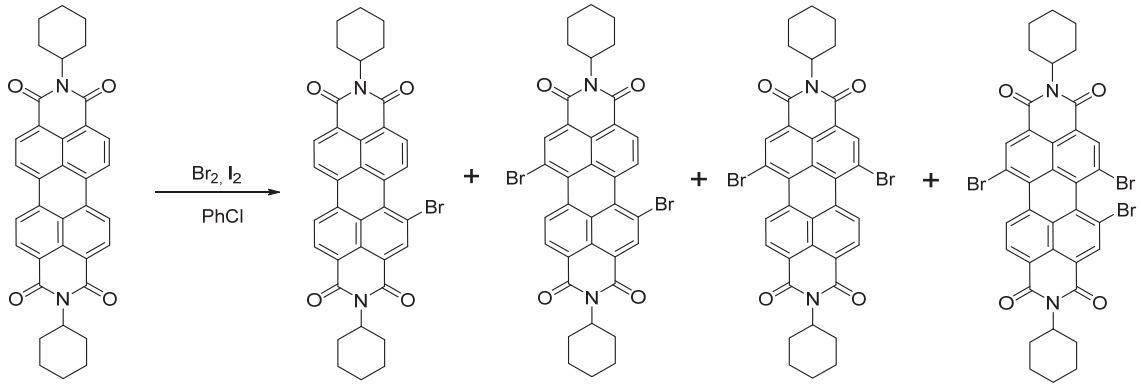

A catalytic amount of iodine and bromine (0.4 mL, 7.82 mmol) were added to *N,N'*-bis(cyclohexyl)-perylene-3,4,9,10-tetracarboxylic diimide (136mg, 0.24 mmol) dissolved in chlorobenzene (5 mL). The mixture was irradiated in a microwave device at 135 °C for one hour. Then, the mixture was poured into saturated Na_2SO_3 aqueous solution and extracted with DCM (20 mL). The combined organic extracts were evaporated under reduced pressure. Purification was carried out by silica gel flash chromatography using DCM:hexane (50:50) to DCM:MeCN (80:20) as eluents to give brominated-perylenes **PC39**, mixture of **1,6-** and **1,7-PC37** and **PC38**.

***N,N'*-bis(Cyclohexyl)-1-bromoperylene-3,4,9,10-tetracarboxylic diimide (PC39).**

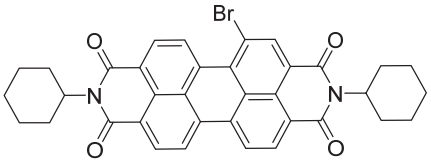

PC39

Red solid, 10 % yield (15 mg, 0.02 mmol). **R_f (DCM):** 0.4. **Mp (°C):** > 350 °C. **FT-IR (KBr, cm^{-1}):** 2917 (C-H), 2851 (C-H), 1700 (C=O), 1648 (C=O), 1589 (C_{Ar}-C_{Ar}), 1454, 1392, 1333 (C-N), 1240, 1192, 1150, 1119, 1029 (C-Br), 977, 849, 804, 742 (fingerprint region). **^{1}H NMR (300 MHz, $CDCl_3$) *δ*:** 9.72 (d, *J* = 8.2 Hz, 1H, H_{Ar}), 8.83 (s, 1H, H_{Ar}), 8.63 (d, *J* = 8.2 Hz, 3H, H_{Ar}), 8.52 (d, *J* = 8.2 Hz, 2H, H_{Ar}), 5.06 – 4.97 (m, 2H, N-CH), 2.85 – 2.52 (m, 5H, CH_2), 1.93 (d, *J* = 12.8 Hz, 4H, CH_2), 1.79 (d, *J* = 9.8 Hz, 5H, CH_2), 1.41 – 1.32 (m, 6H, CH_2). **^{13}C NMR (101 MHz, $CDCl_3$) *δ*:** 164.1 (C=O), 163.8 (C=O), 163.7 (C=O), 162.8 (C=O), 139.2 (C_{Ar}), 133.9 (C_{Ar}), 133.6 (C_{Ar}), 133.6 (C_{Ar}), 133.5 (C_{Ar}), 131.1 (C_{Ar}), 130.6 (C_{Ar}), 128.9 (C_{Ar}), 128.8 (C_{Ar}), 128.2 (C_{Ar}), 128.1 (C_{Ar}), 127.1 (C_{Ar}), 127.0 (C_{Ar}), 124.2 (C_{Ar}), 124.0 (C_{Ar}), 123.9 (C_{Ar}), 123.8 (C_{Ar}), 123.4 (C_{Ar}), 123.1 (C_{Ar}), 121.0 (C-Br), 54.4 (N-CH), 54.2 (N-CH), 29.9 (CH_2), 29.3 (CH_2), 29.2 (CH_2), 26.7 (CH_2), 25.6 (CH_2). **HRMS (MALDI-, DIT):** m/z calcd. for $C_{36}H_{29}BrN_2O_4$ ($[M]^+$): 632.1305; found: 632.1246.

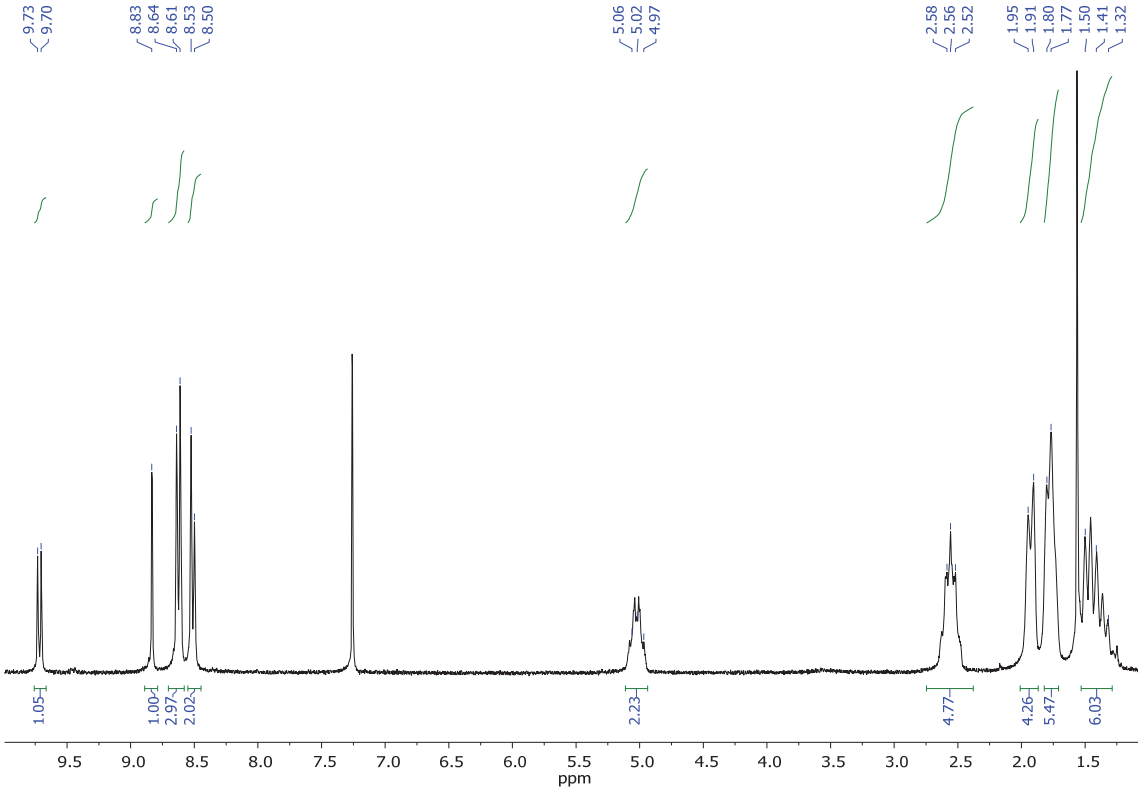

Figure 7. ^{1}H NMR (300 MHz, $CDCl_3$) of PC39

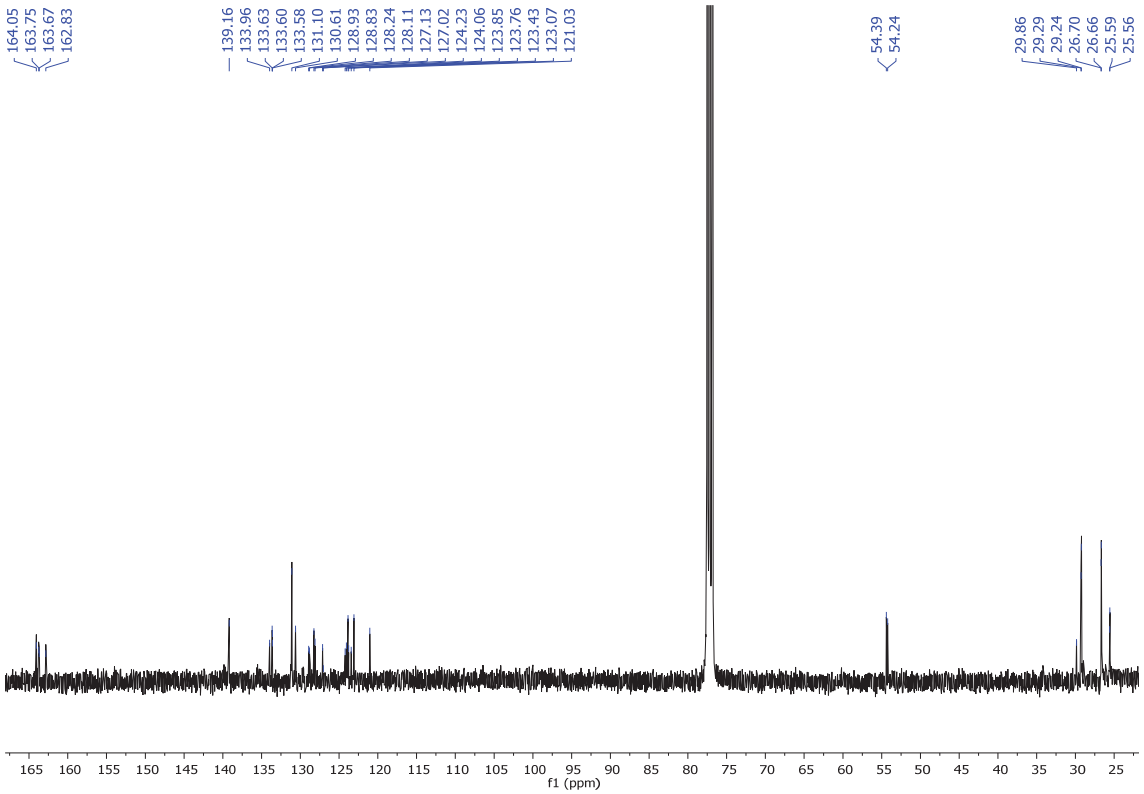

Figure 8. ^{13}C NMR (101 MHz, $CDCl_3$) of PC39

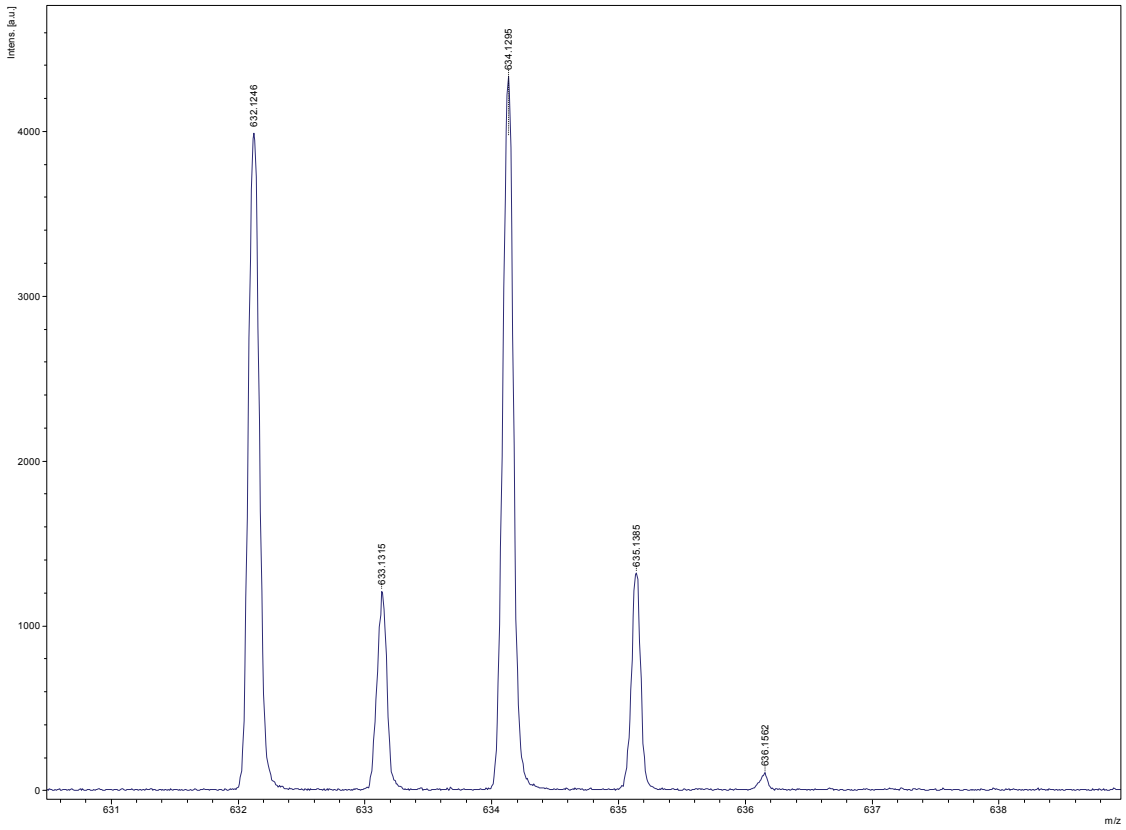

Figure 9. Mass spectrum (MALDI-, DIT) of PC39

1,7 and 1,6-Dibromo-*N,N'*-bis(cyclohexyl)-perylene-3,4,9,10-tetracarboxylic diimide (1,6- and 1,7-PC37).

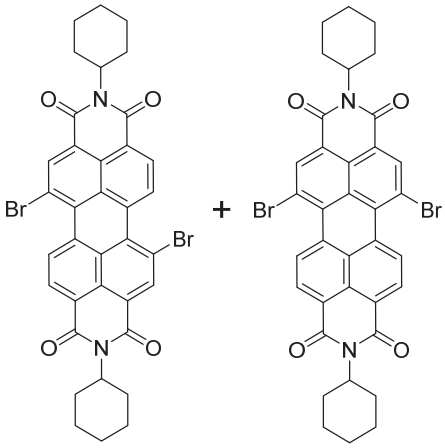

1,7-PC37 **1,6-PC37**

Red solid, 62 % yield (105.6 mg, 0.15 mmol). **R_f (DCM):** 0.6. **Mp (°C):** > 350 °C. **FT-IR (KBr, cm^{-1}):** 2921 (C-H), 2848 (C-H), 1700 (C=O), 1651 (C=O), 1589 (C_{Ar}-C_{Ar}), 1385, 1326 (C-N), 1233, 1188, 1139, 1029 (C-Br), 977, 853, 811, 742 (fingerprint region). **^{1}H NMR (300 MHz, $CDCl_3$) *δ*:** 9.33 (d, *J* = 8.2 Hz, 2H, H_{Ar}), 8.74 (s, 2H, H_{Ar}), 8.56 (d, *J* = 8.2 Hz, 2H, H_{Ar}), 5.01 – 4.94 (m, 2H, N-CH), 2.56 – 2.49 (m, 5H, CH_2), 1.91 (d, *J* = 12.1 Hz, 4H, CH_2), 1.73 (d, *J* = 11.0 Hz, 5H, CH_2), 1.48 – 1.39 (m, 6H, CH_2). **^{13}C NMR (101 MHz, $CDCl_3$) *δ*:** 163.8 (C=O), 163.4 (C=O), 162.9 (C=O), 162.5 (C=O), 138.2 (C_{Ar}), 138.1 (C_{Ar}), 133.1 (C_{Ar}), 132.9 (C_{Ar}), 132.8 (C_{Ar}), 132.4 (C_{Ar}), 130.4 (C_{Ar}), 130.1 (C_{Ar}), 129.9 (C_{Ar}), 129.3 (C_{Ar}), 128.6 (C_{Ar}), 128.2 (C_{Ar}), 128.1 (C_{Ar}), 127.1 (C_{Ar}), 124.0 (C_{Ar}), 123.8 (C_{Ar}), 123.4 (C_{Ar}), 123.1 (C_{Ar}), 121.7 (C-Br), 120.8 (C-Br), 54.4 (N-CH), 29.3 (CH_2), 29.2 (CH_2), 29.2 (CH_2), 26.7 (CH_2), 26.6 (CH_2), 25.5 (CH_2). **HRMS (MALDI+, DCTB):** m/z calcd. for $C_{36}H_{28}Br_2N_2O_4$ ($[M]^+$): 710.0410; found: 710.0403.

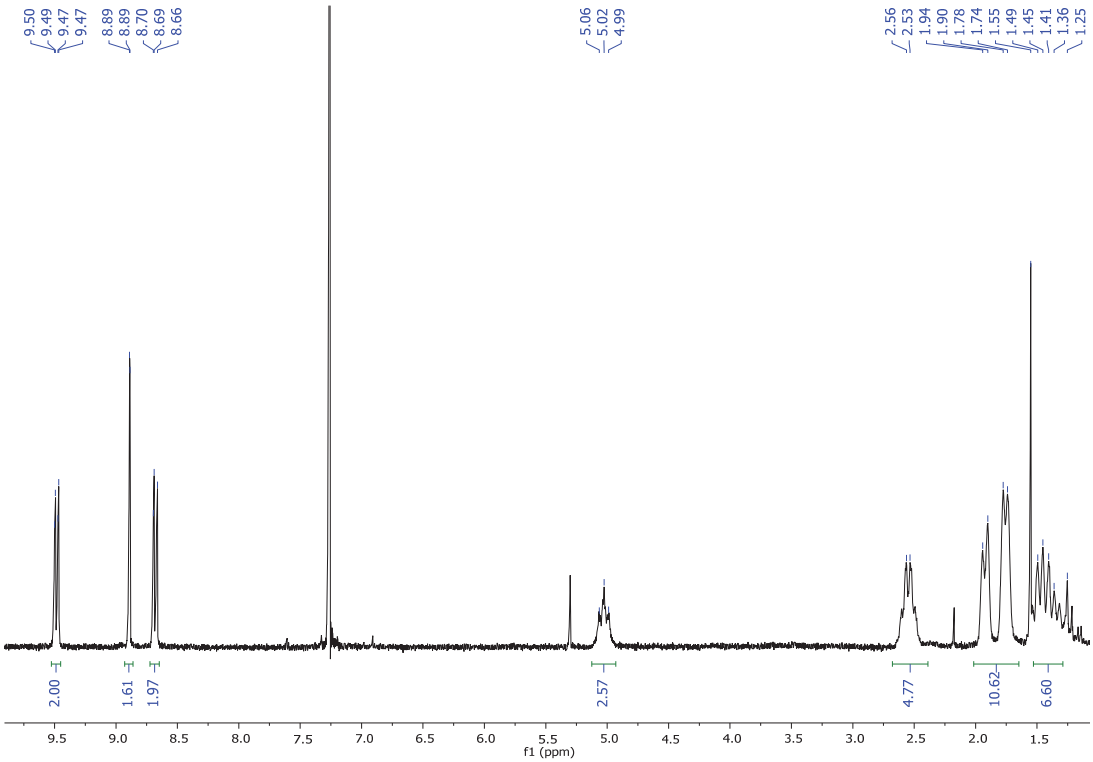

Figure 10. ^{1}H NMR (300 MHz, $CDCl_3$) of 1,6- and 1,7-PC37

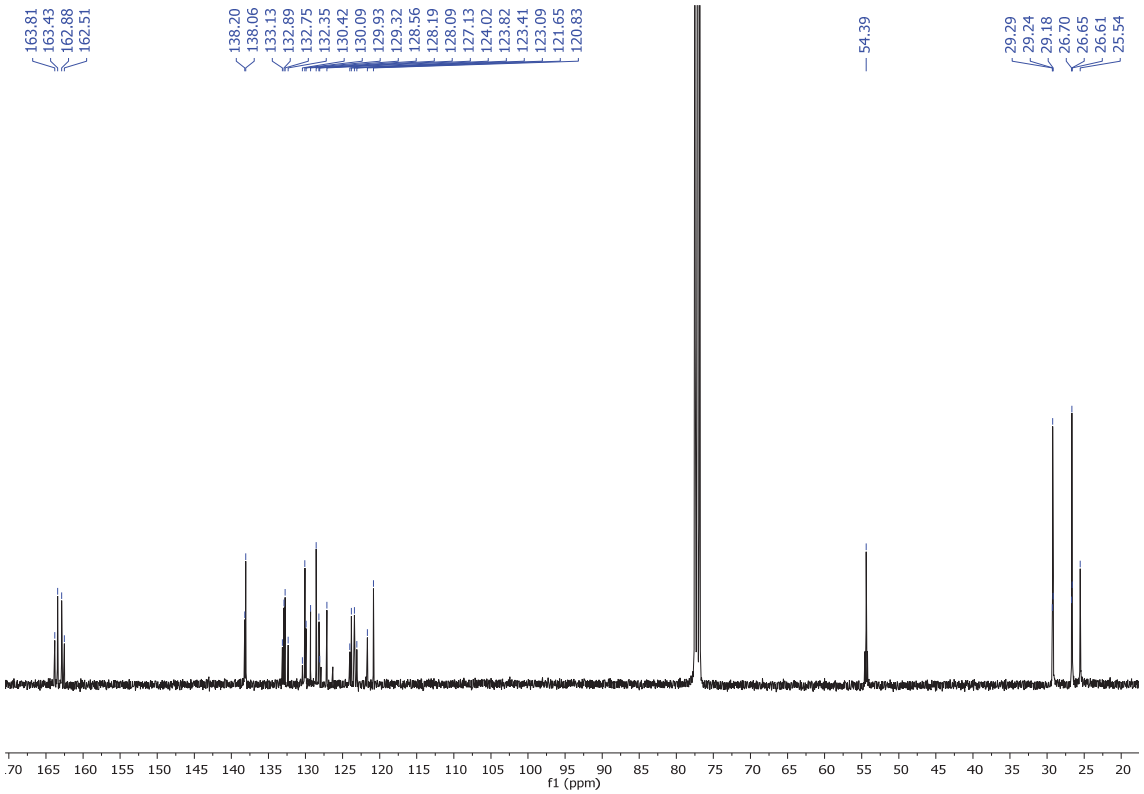

Figure 11. ^{13}C NMR (101 MHz, $CDCl_3$) of 1,6- and 1,7-PC37

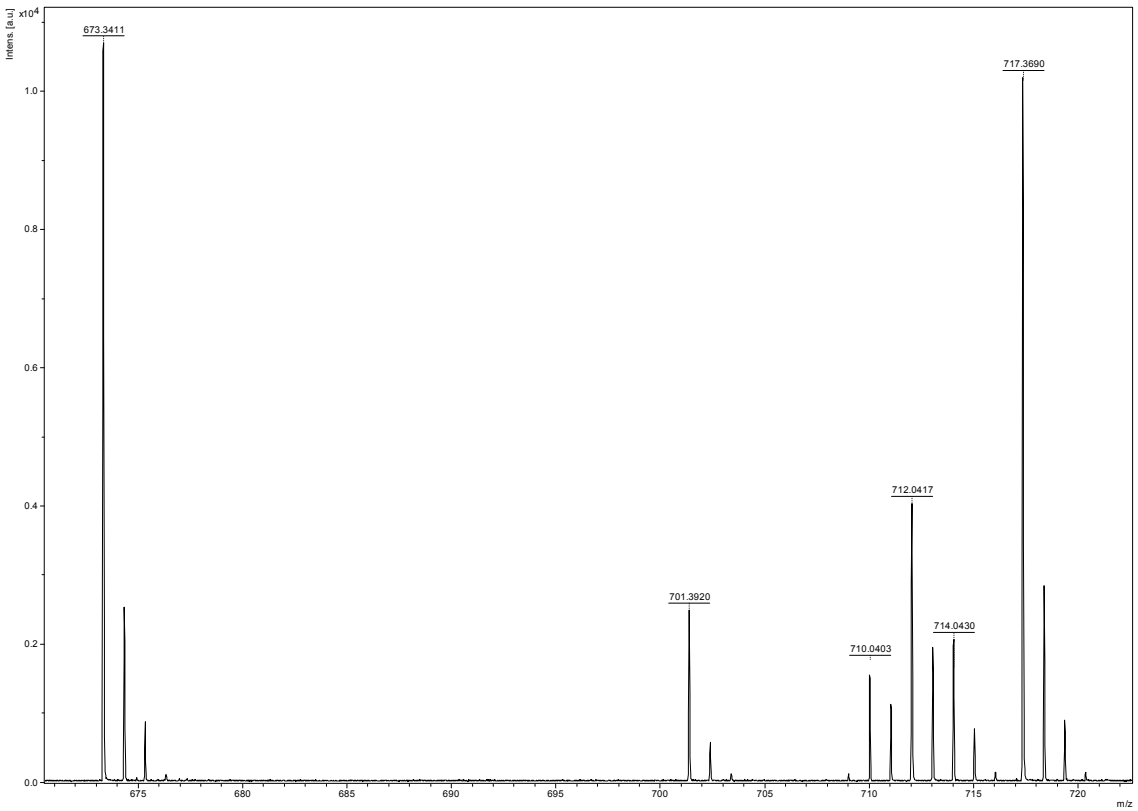

Figure 12. Mass spectrum (MALDI+, DCTB) of 1,6- and 1,7-PC37

1,6,7-Tribromo-*N,N'*-bis(cyclohexyl)-perylene-3,4,9,10-tetracarboxylic diimide (PC38).

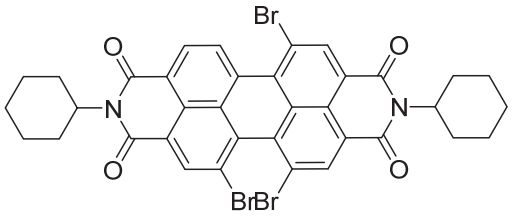

PC38

Red solid, 5 % yield (9.5 mg, 0.01 mmol). **R_f (DCM):** 0.9. **Mp (°C):** > 350 °C. **FT-IR (KBr, cm^{-1}):** 2955 (C-H), 2921 (C-H), 2851 (C-H), 1727 (C=O), 1693 (C=O), 1655 (C=O), 1589 (C_{Ar}-C_{Ar}), 1451 (CH_2), 1368 (C-N), 1295, 1233, 1188, 1150, 1074, 1043 (C-Br), 980, 808, 745, 690, 648 (fingerprint region). **^{1}H NMR (400 MHz, $CDCl_3$) *δ*:** 9.42 (d, *J* = 8.2 Hz, 1H, H_{Ar}), 8.88 (s, 1H, H_{Ar}), 8.79 (d, *J* = 1.4 Hz, 2H, H_{Ar}), 8.68 (d, *J* = 7.3 Hz, 1H, H_{Ar}), 5.04 – 5.01 (t, *J* = 12.0 Hz, 2H, N-CH), 2.57 – 2.51 (m, 5H, CH_2), 1.92 (d, *J* = 11.0 Hz, 5H, CH_2), 1.74 (d, *J* = 10.4 Hz, 6H, CH_2), 1.49 – 1.32 (m, 6H, CH_2). **^{13}C NMR (101 MHz, $CDCl_3$) *δ*:** 163.5 (C=O), 163.1 (C=O), 162.7 (C=O), 162.6 (C=O), 137.5 (C_{Ar}), 136.7 (C_{Ar}), 136.5 (C_{Ar}), 133.4 (C_{Ar}), 133.2 (C_{Ar}), 131.5 (C_{Ar}), 131.3 (C_{Ar}), 130.9 (C_{Ar}), 130.2 (C_{Ar}), 129.9 (C_{Ar}), 129.7 (C_{Ar}), 128.9 (C_{Ar}), 128.1 (C_{Ar}), 126.1 (C_{Ar}), 125.3 (C_{Ar}), 124.4 (C_{Ar}), 123.9 (C_{Ar}), 123.5 (C_{Ar}), 123.1 (C_{Ar}), 121.4 (C-Br), 54.6 (N-CH), 54.4 (N-CH), 32.1 (CH_2), 29.9 (CH_2), 29.5 (CH_2), 29.3 (CH_2), 26.5 (CH_2), 25.4 (CH_2), 22.9 (CH_2). **HRMS (MALDI+, DCTB):** m/z calcd. for $C_{36}H_{27}Br_3N_2O_4$ ([M]$^+$): 789.9497; found: 789.9507.

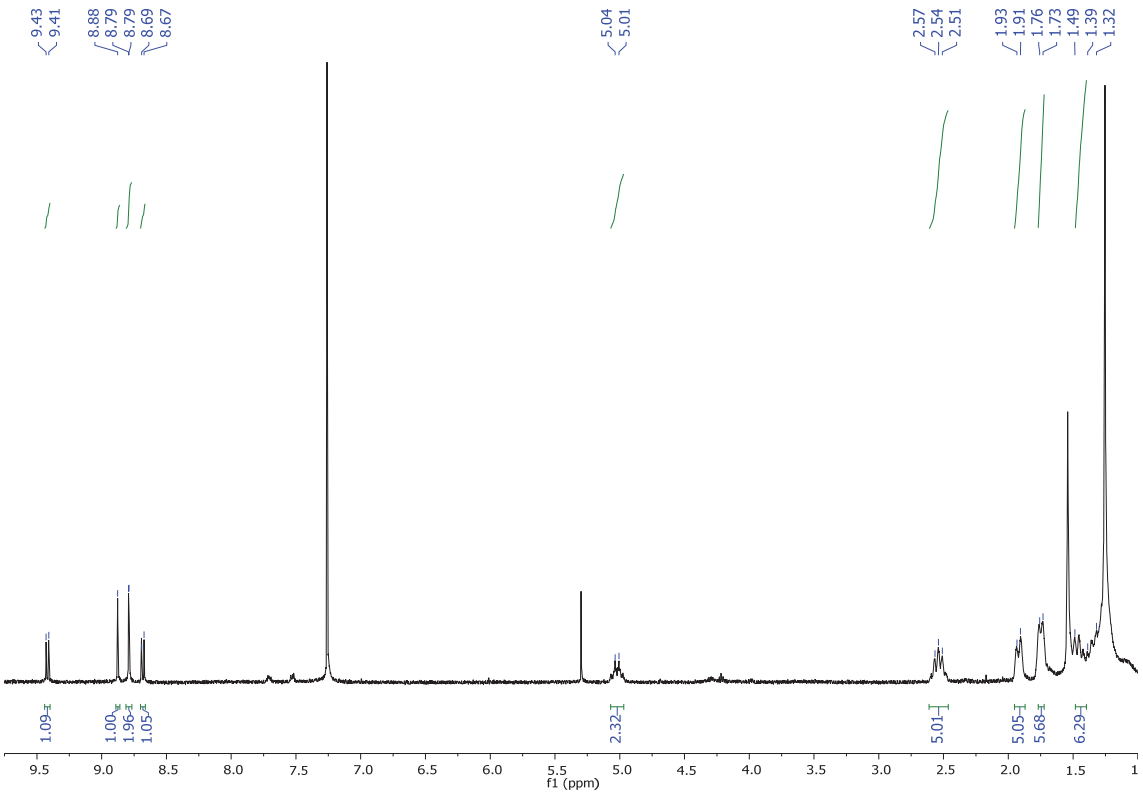

Figure 13. ^{1}H NMR (400 MHz, $CDCl_3$) of PC38

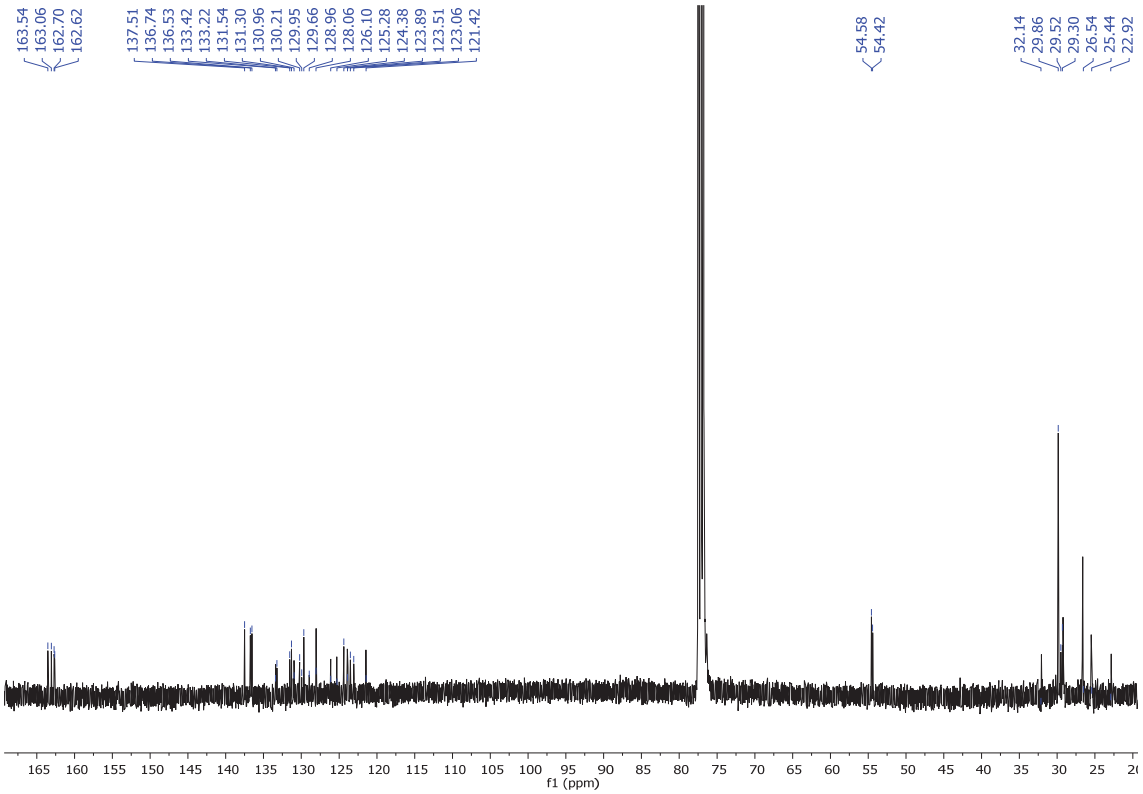

Figure 14. ^{13}C NMR (101 MHz, $CDCl_3$) of PC38

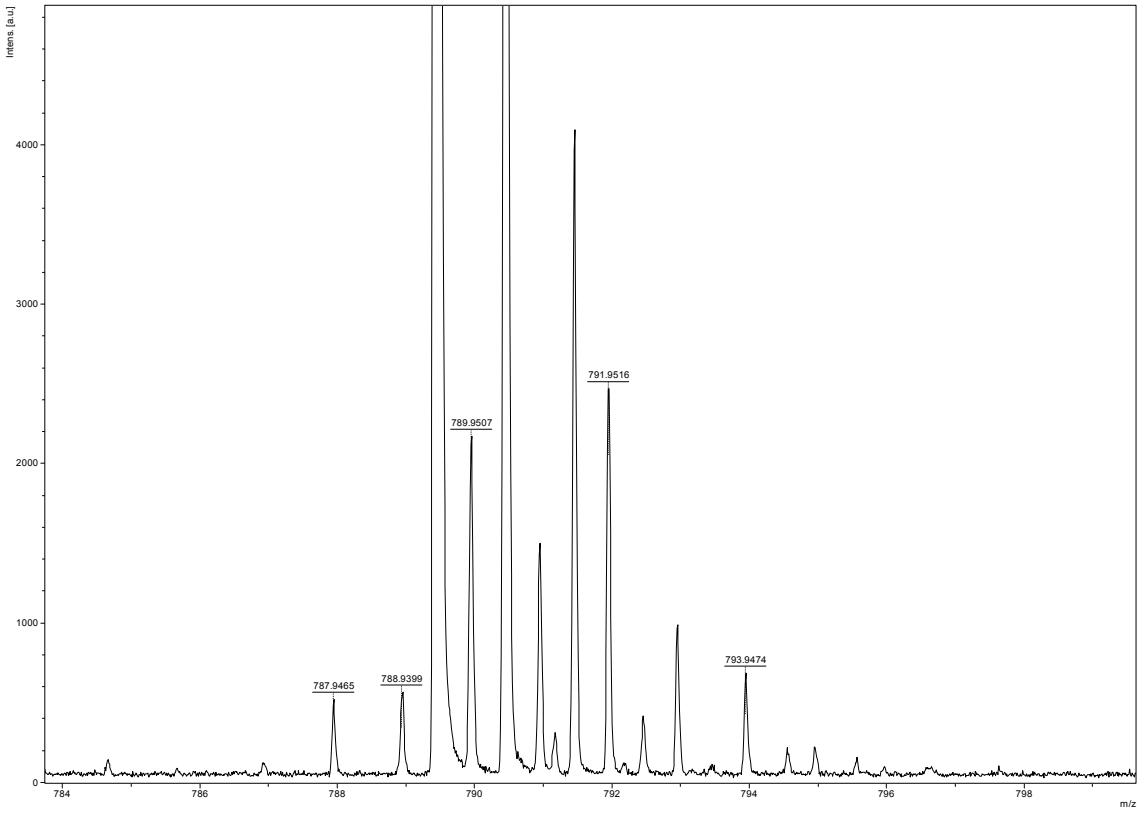

Figure 15. Mass spectrum (MALDI+, DCTB) of PC38

1.3. Synthesis of *N,N'*-bis(cyclohexyl)-1-(4-[4-(*N''*-*tert*-butoxycarbonyl)piperazin-1-yl]phenyl)perylene-3,4,9,10-tetracarboxylic diimide (PC53).

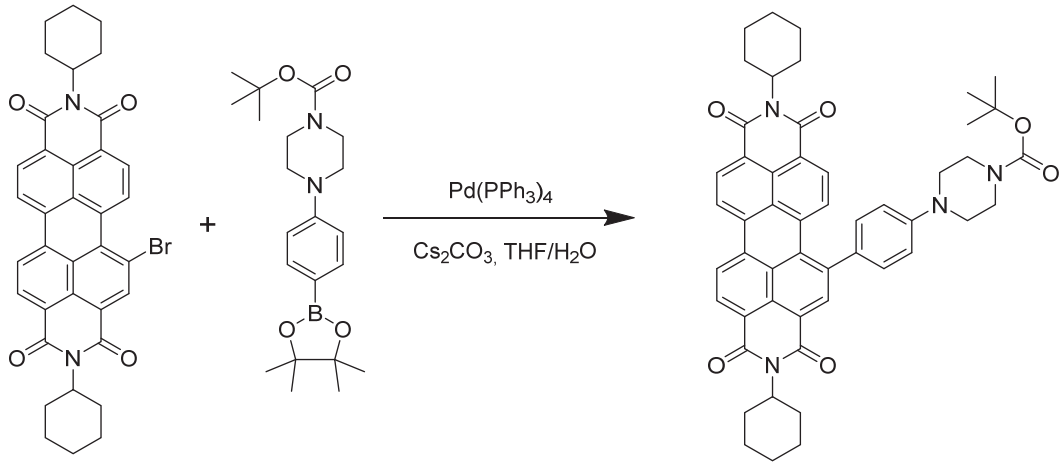

PC39 **PC53**

4-[4-(*N''*-*tert*-Butoxycarbonyl)piperazin-1-yl]phenylboronic acid pinacol ester (68 mg, 0.17 mmol), cesium carbonate (156 mg, 0.48 mmol) and a catalytic amount of tetrakis (triphenylphosphine) palladium (0) were added under nitrogen to *N,N'*-dicyclohexyl-1-bromoperylene-3,4,9,10-tetracarboxylic diimide (100 mg, 0.16 mmol) dissolved in THF:H_2O (20:2 mL). The mixture was heated at reflux for 24 hours and extracted with DCM (3 x 20 mL). The combined organic extracts were dried over anhydrous sodium sulphate, filtered and evaporated under reduced pressure. Purification was carried out by silica gel flash chromatography using DCM:MeCN (90:10) as eluent to give compound **PC53** as a deep purple solid in 65% yield (84 mg, 0.11 mmol). **R_f (DCM:MeOH, 50:1):** 0.45. **Mp (°C):** 263 – 265 °C. **FT-IR (KBr, cm^{-1}):** 2971, 2925 (C-H), 2852 (C-H), 1695 (C=O), 1655 (C=O), 1590 (C_{Ar}-C_{Ar}), 1522 (C_{Ar}-C_{Ar}), 1505, 1454, 1405 (CH_2), 1334 (C-N), 1235, 1167, 1118, 979, 908, 865, 809, 755, 698, 644, 570 (fingerprint region). **^{1}H NMR (300 MHz, $CDCl_3$) *δ*:** 8.60 (d, *J* = 8.0 Hz, 1H, H_{Ar}), 8.56 (d, *J* = 8.0 Hz, 1H, H_{Ar}), 8.49 (s, 1H, H_{Ar}), 8.44 (d, *J* = 8.2 Hz, 1H, H_{Ar}), 8.09 (d, *J* = 8.3 Hz, 1H, H_{Ar}), 7.88 (d, *J* = 8.2 Hz, 1H, H_{Ar}), 7.30 (d, *J* = 8.7 Hz, 2H, H_{Ar}), 6.99 (d, *J* = 8.7 Hz, 2H, H_{Ar}), 5.08 – 4.96 (m, 2H, N-CH), 3.65 (t, *J* = 11.5 Hz, 4H, CH_2), 3.27 (t, *J* = 11.1 Hz 4H, CH_2), 2.60 – 2.52 (m, 4H, CH_2), 1.91 (d, *J* = 11.1 Hz, 4H, CH_2), 1.76 (d, *J* = 11.7 Hz, 5H, CH_2), 1.52 (s, 9H, CH_3), 1.47 – 1.30 (m, 6H, CH_2). **^{13}C NMR (101 MHz, $CDCl_3$) *δ*:** 164.1 (C=O), 164.1 (C=O), 163.9 (C=O), 154.8 (**C**OOC$(CH_3)_3$), 151.3 (C_{quat}-N), 141.8 (C_{quat}-PDI), 136.3 (C_{Ar}), 135.1 (C_{Ar}), 134.6 (C_{Ar}), 134.5 (C_{Ar}), 133.4 (C_{Ar}), 132.1 (C_{Ar}), 131.0 (C_{Ar}), 130.6 (C_{Ar}), 130.2 (C_{Ar}), 129.7 (C_{Ar}), 129.5 (C_{Ar}), 129.0 (C_{Ar}), 128.2 (C_{Ar}), 127.6 (C_{Ar}) 123.7 (C_{Ar}), 123.5 (C_{Ar}), 122.8 (C_{Ar}), 122.5 (C_{Ar}), 122.5 (C_{Ar}), 117.4 (C_{Ar}), 80.2 (**C**$(CH_3)_3$), 54.2 (NCOCO-**C**H), 54.1 (NCOCO-**C**H), 48.7 (N-CH_2-CH_2-N), 29.3 (CH_2), 28.6 (CH_3), 26.7 (CH_2), 25.6 (CH_2). **HRMS (MALDI+, DCTB):** m/z calcd. for $C_{51}H_{50}N_4O_6$ ($[M]^+$): 814.3725; found: 814.3798.

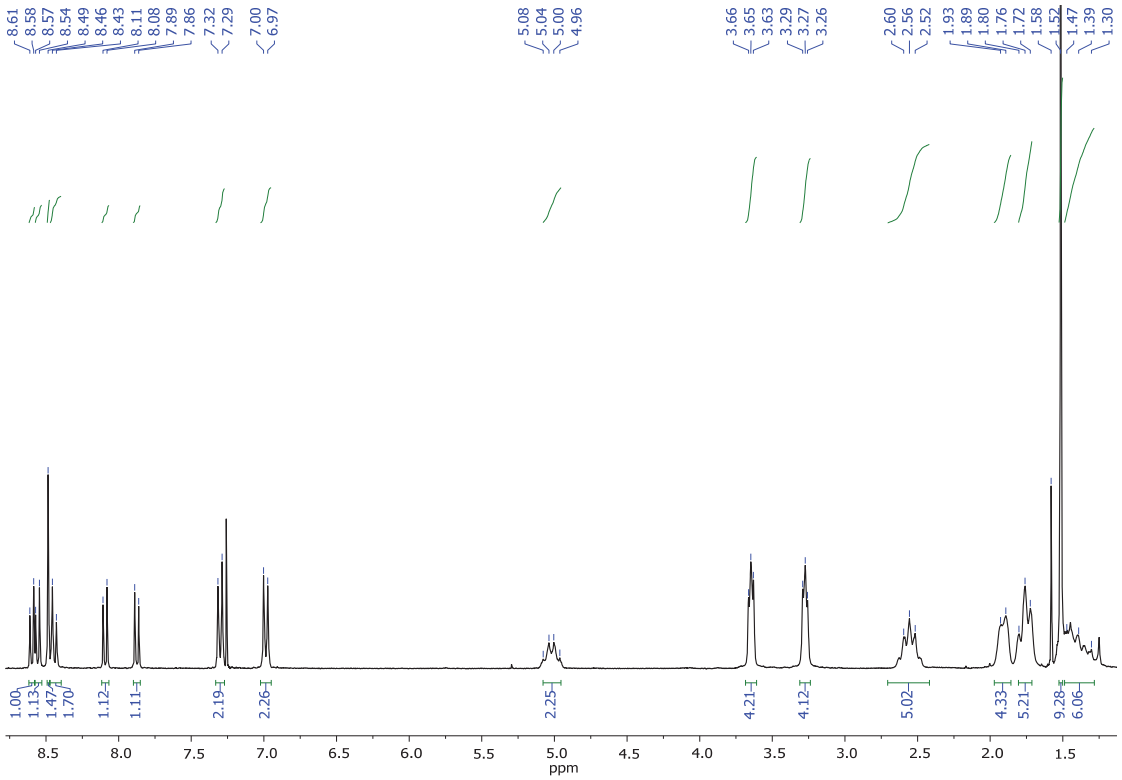

Figure 16. ^{1}H NMR (300 MHz, $CDCl_3$) of PC53

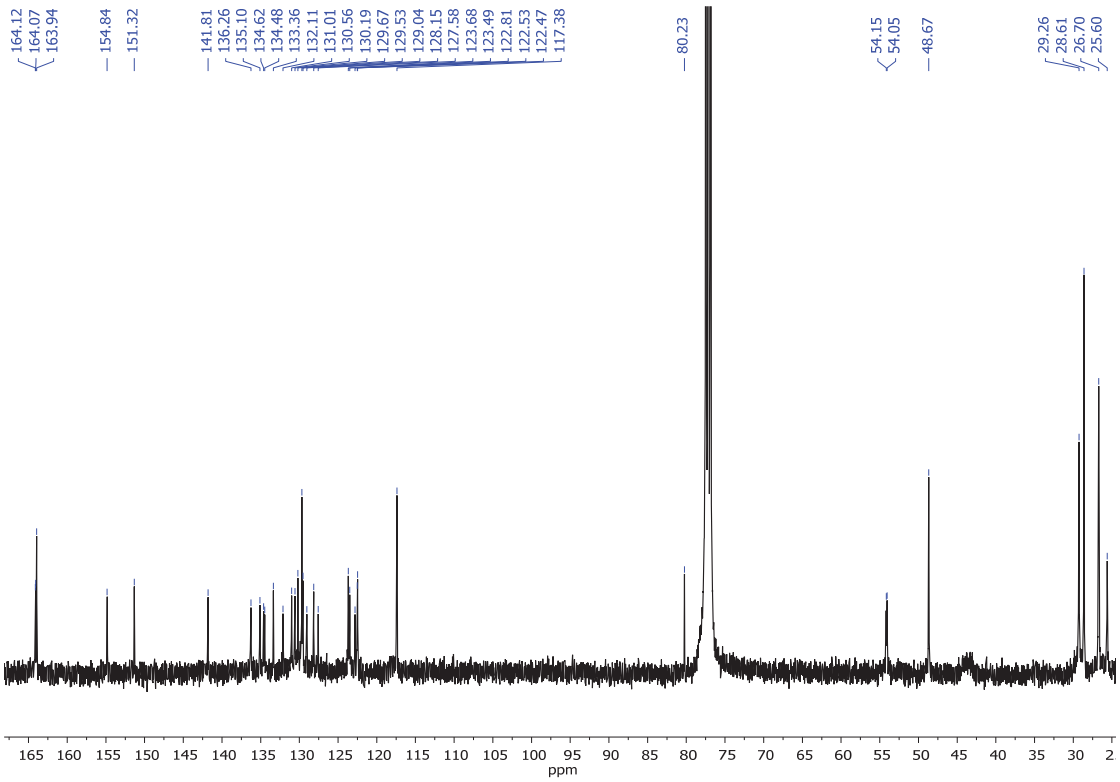

Figure 17. ^{13}C NMR (101 MHz, $CDCl_3$) of PC53

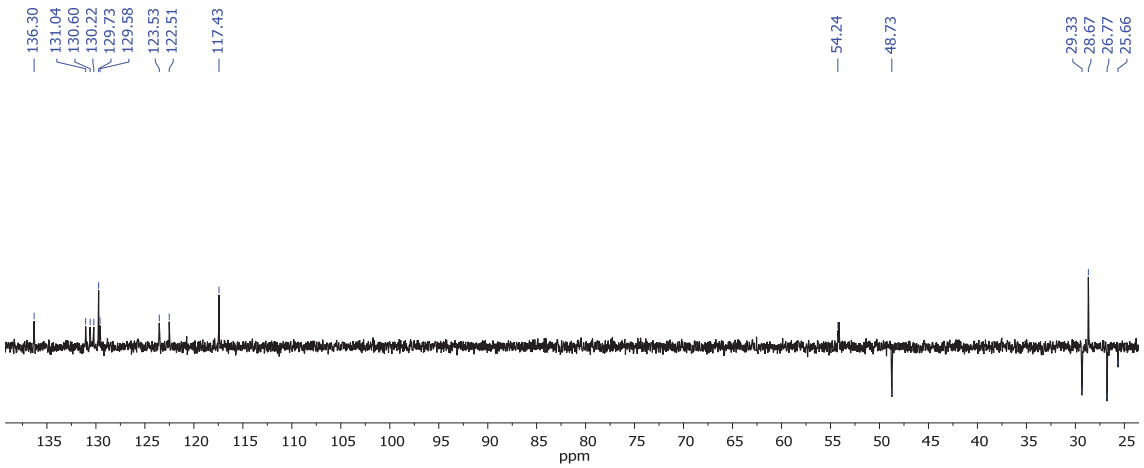

Figure 18. ^{13}C NMR-DEPT-135 (101 MHz, $CDCl_3$) of PC53

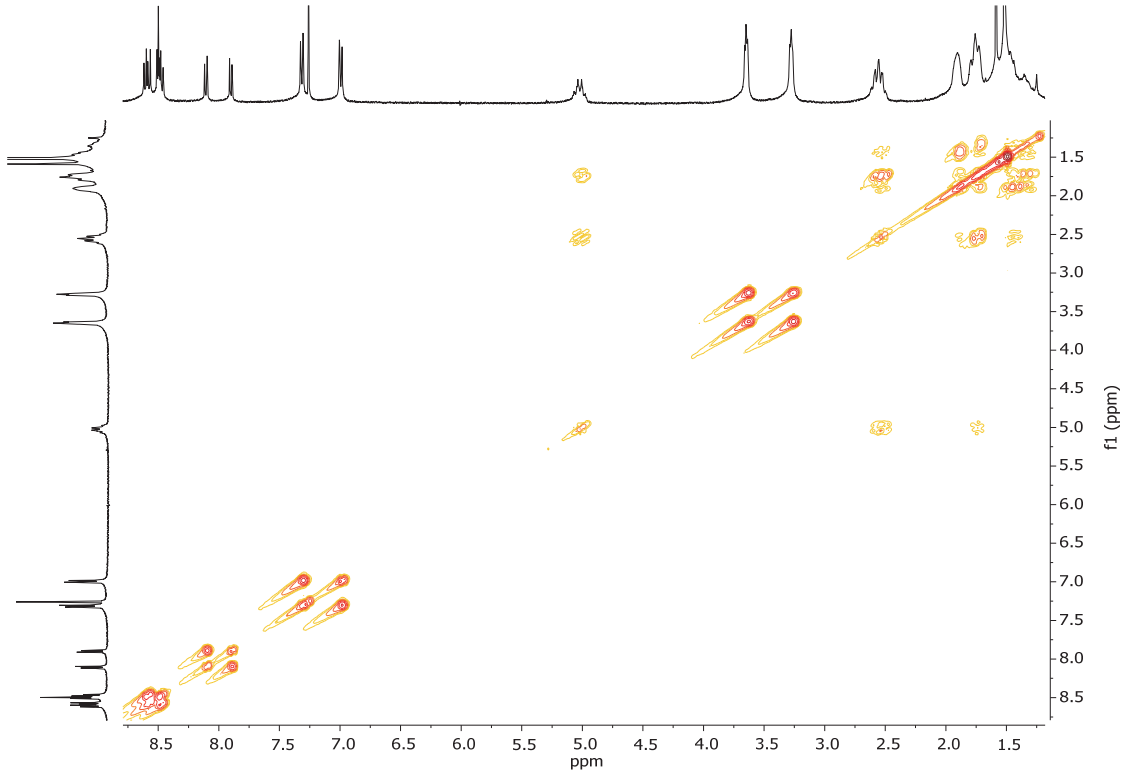

Figure 19. ^{1}H-^{1}H-COSY spectrum of PC53

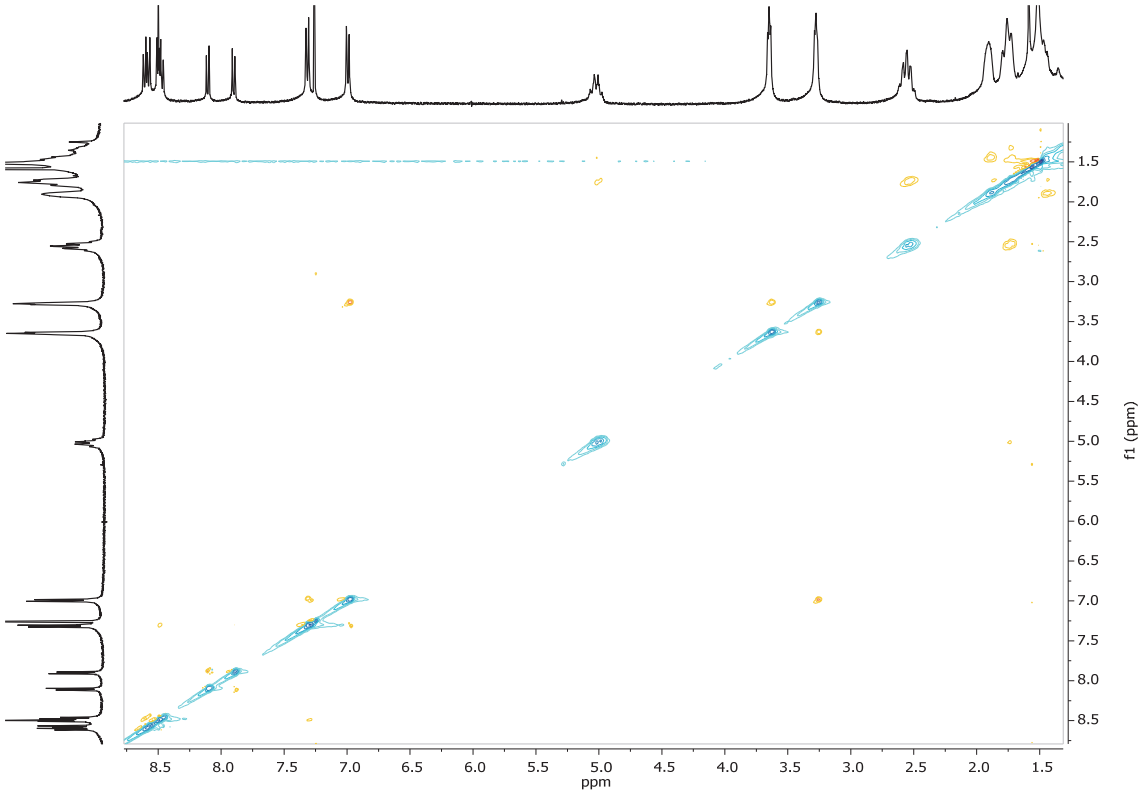

Figure 20. ^{1}H-^{1}H-NOESY spectrum of PC53

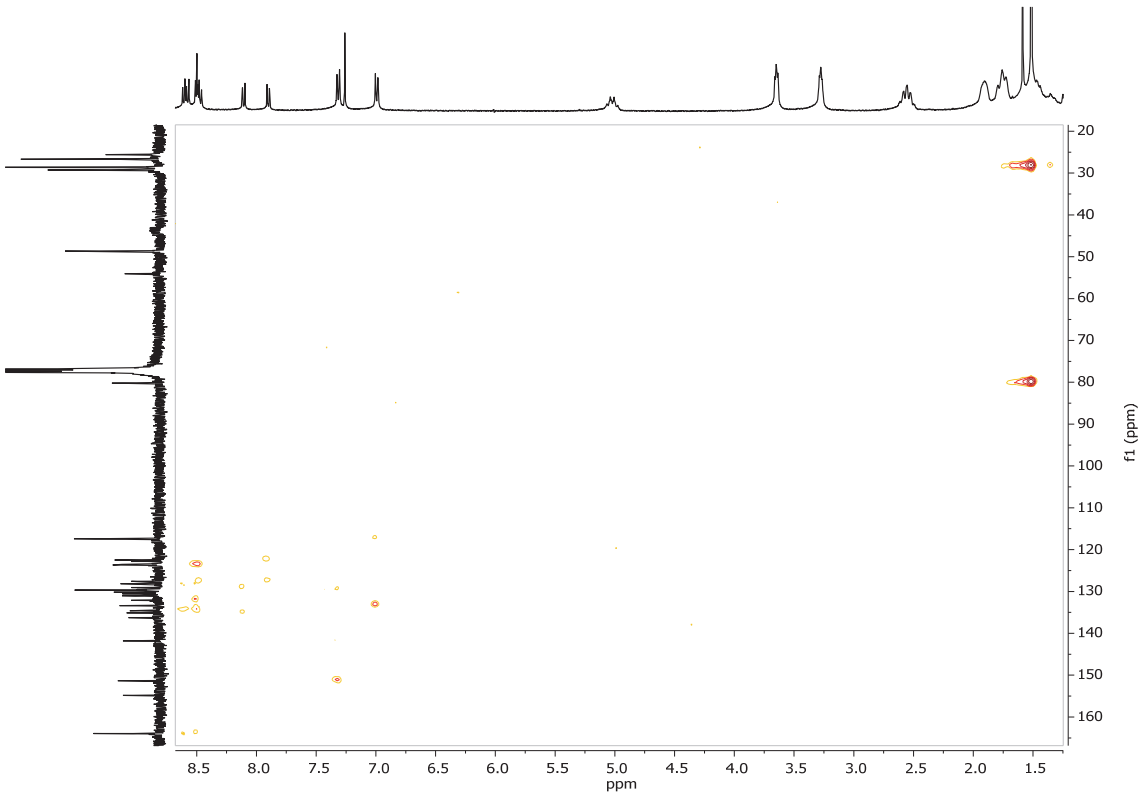

Figure 21. ^{1}H-^{13}C-HMBC spectrum of PC53

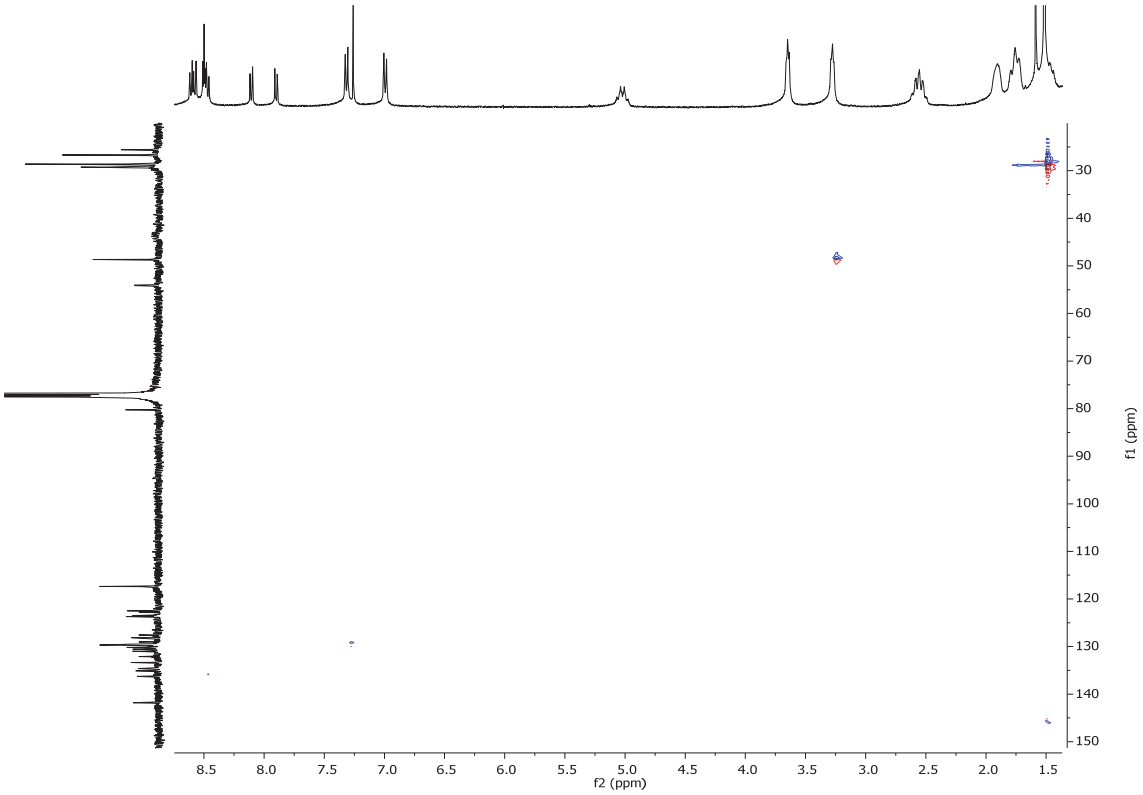

Figure 22. ^{1}H-^{13}C-HMQC spectrum of PC53

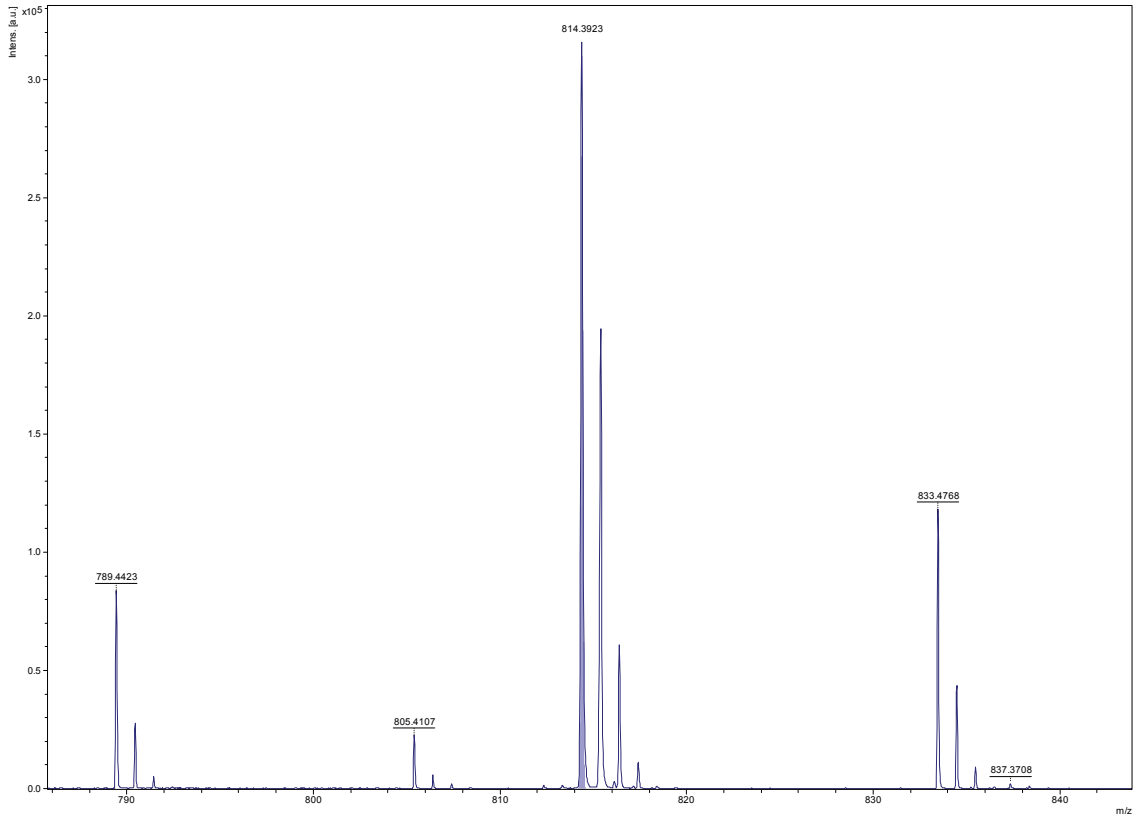

Figure 23. Mass spectrum (MALDI+, DCTB) of PC53

Solvatochromism:

The concentration of **PC53** is $1 \cdot 10^{-5}$ M. The excitation wavelength is 480 nm. The absorption and emission spectra have been measured in the listed solvents below in the range between 200 to 900 nm. The used solvents are: MeOH, DMSO, DMF, MeCN, acetone, AcOEt, THF, $CHCl_3$, DCM, toluene, diethyl ether, hexane and cyclohexane.

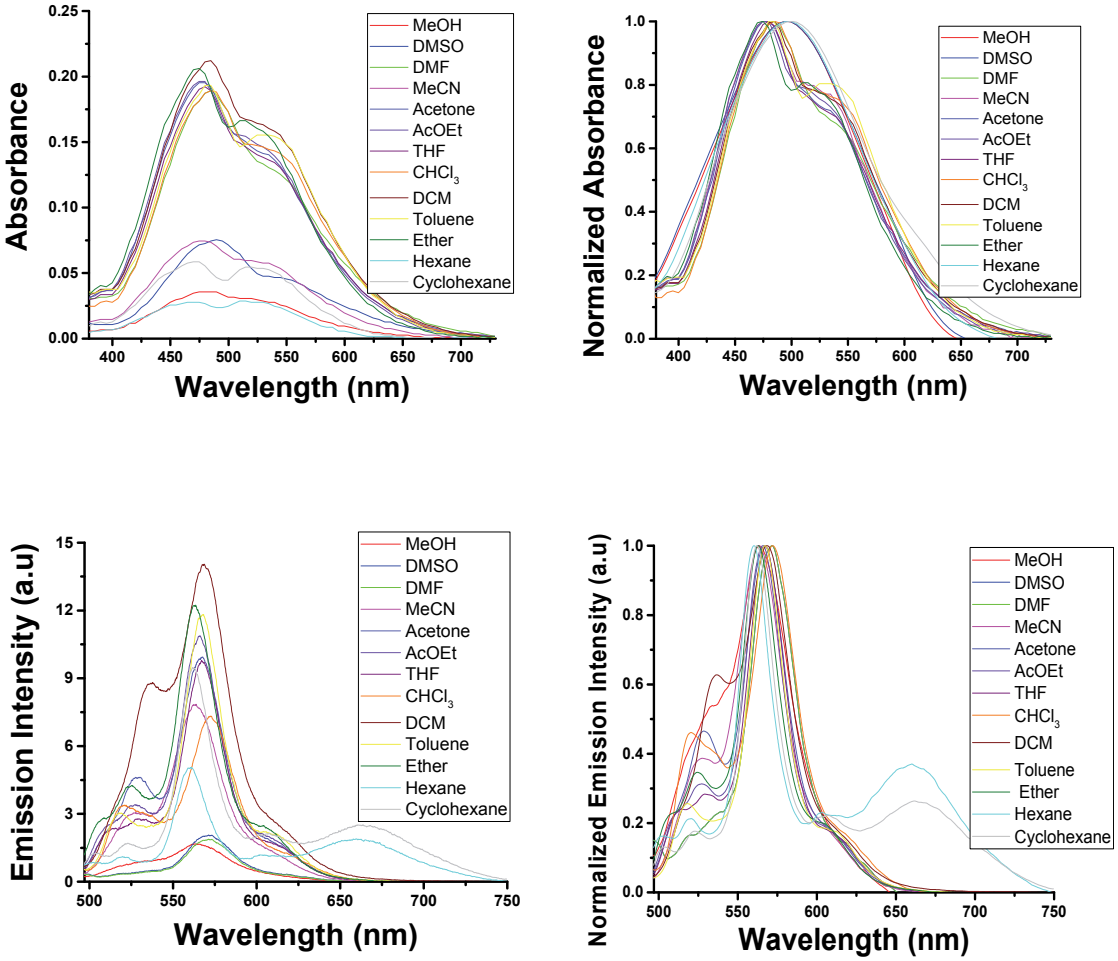

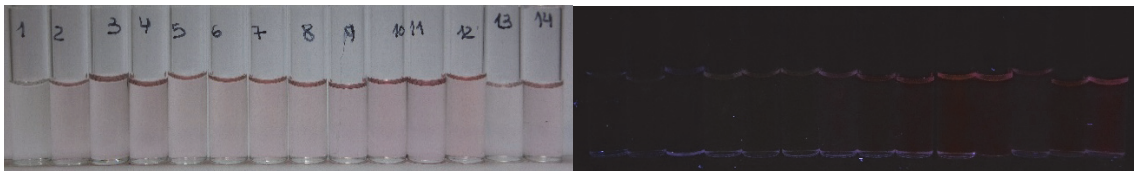

Solvents: 1: Water, 2: MeOH, 3: DMSO, 4: DMF, 5: MeCN, 6: acetone, 7: AcOEt, 8: THF, 9: $CHCl_3$, 10: DCM, 11: toluene, 12: diethyl ether, 13: hexane, 14: cyclohexane.

Figure 24. Upper. Absorbance and Normalized absorbance spectra of PC53. Middle: Fluorescence and Normalized fluorescence spectra of PC53. Lower. Solvatochromic effect of PC53 under white light and light of 366 nm.

1.4. Synthesis of N,N'-bis(cyclohexyl)-1-(4-[4-piperazin-1-yl]phenyl)perylene-3,4,9,10-tetracarboxylic diimide (PC117).

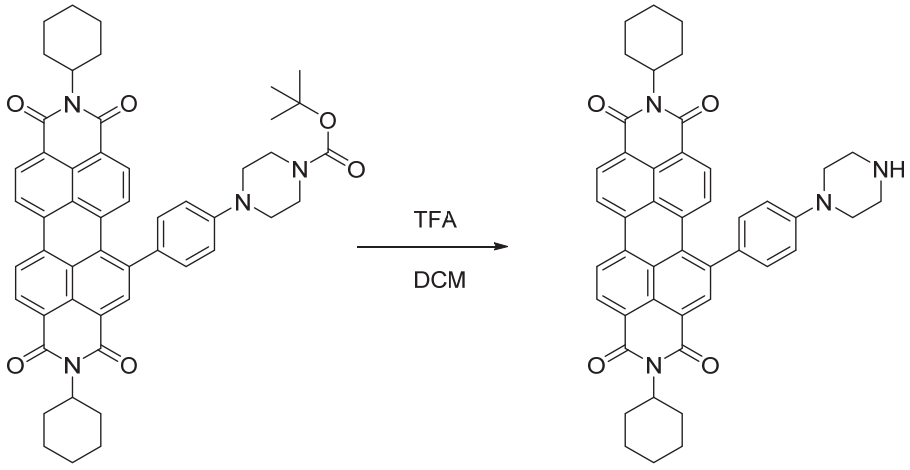

PC53 **PC117**

Trifluoroacetic acid (368 µL, 0.01 mmol) was added dropwise to *N,N'*-bis(cyclohexyl)-1-(4-[4-(*N''-tert*-butoxycarbonyl)piperazin-1-yl]phenyl)perylene-3,4,9,10-tetracarboxylic diimide (30 mg, 0.04 mmol) dissolved in DCM (5 mL). The mixture was stirred at room temperature for 2 hours, then NaOH was added to neutralize the reaction until pH = 6-8 and it was extracted with DCM (3 x 20 mL). The combined organic extracts were dried over anhydrous sodium sulphate, filtered and evaporated under reduced pressure to obtain a black solid with a yield 95 % (30 mg, 0.04 mmol). **R_f (DCM:MeOH, 50:4):** 0. **Mp (°C):** > 350 °C. **FT-IR (KBr, cm^{-1}):** 2928 (C-H), 2852 (C-H), 1696 (C=O), 1652 (C=O), 1590 (C_{Ar}-C_{Ar}), 1502, 1454 (CH_2), 1402 (C-N), 1328, 1240, 1195, 1127, 982, 919, 811, 749, 721, 644 (fingerprint region). **^{1}H NMR (300 MHz, $CDCl_3$) *δ*:** 8.63 (d, *J* = 8.1 Hz, 1H, H_{Ar}), 8.57 (d, *J* = 10.9 Hz, 1H, H_{Ar}), 8.51 (t, *J* = 4.3 Hz, 2H, H_{Ar}), 8.14 (d, *J* = 8.2 Hz, 1H, H_{Ar}), 7.91 (d, *J* = 8.3 Hz, 1H, H_{Ar}), 7.37 (d, *J* = 8.4 Hz, 2H, H_{Ar}), 7.03 (d, *J* = 8.6 Hz, 2H, H_{Ar}), 5.07 – 4.97 (m, 2H, N-CH), 3.52 (t, *J* = 11.5 Hz, 4H, CH_2), 3.36 (t, *J* = 12.1 Hz, 4H, CH_2), 2.63 – 2.51 (m, 5H, CH_2), 1.90 (s, 4H, CH_2), 1.79 – 1.72 (m, 5H, CH_2), 1.49 – 1.32 (m, 6H, CH_2). **^{13}C NMR (75 MHz, $CDCl_3$) *δ*:** 163.9 (C=O), 163.9 (C=O), 163.8 (C=O), 163.7 (C=O), 150.5 (C_{quat}-N), 141.3 (C_{Ar}), 136.0 (C_{Ar}), 134.7 (C_{Ar}), 134.4 (C_{Ar}), 134.1 (C_{Ar}), 131.9 (C_{Ar}), 130.8 (C_{Ar}), 130.5 (C_{Ar}), 129.9 (C_{Ar}), 129.8 (C_{Ar}), 129.5 (C_{Ar}), 128.8 (C_{Ar}), 128.0 (C_{Ar}), 127.9 (C_{Ar}), 127.3 (C_{Ar}), 123.6 (C_{Ar}), 123.6 (C_{Ar}), 123.4 (C_{Ar}), 122.7 (C_{Ar}), 122.5 (C_{Ar}), 122.4 (C_{Ar}), 117.9 (C_{Ar}), 47.2 (NCOCO**C**H), 44.1 (N-CH_2-CH_2-N), 29.2 (CH_2), 26.7 (CH_2), 25.6 (CH_2). **HRMS (MALDI+, DCTB):** m/z calcd. for $C_{46}H_{42}N_4O_4$ ($[M+H]^+$): 715.3279; found: 715.3261.

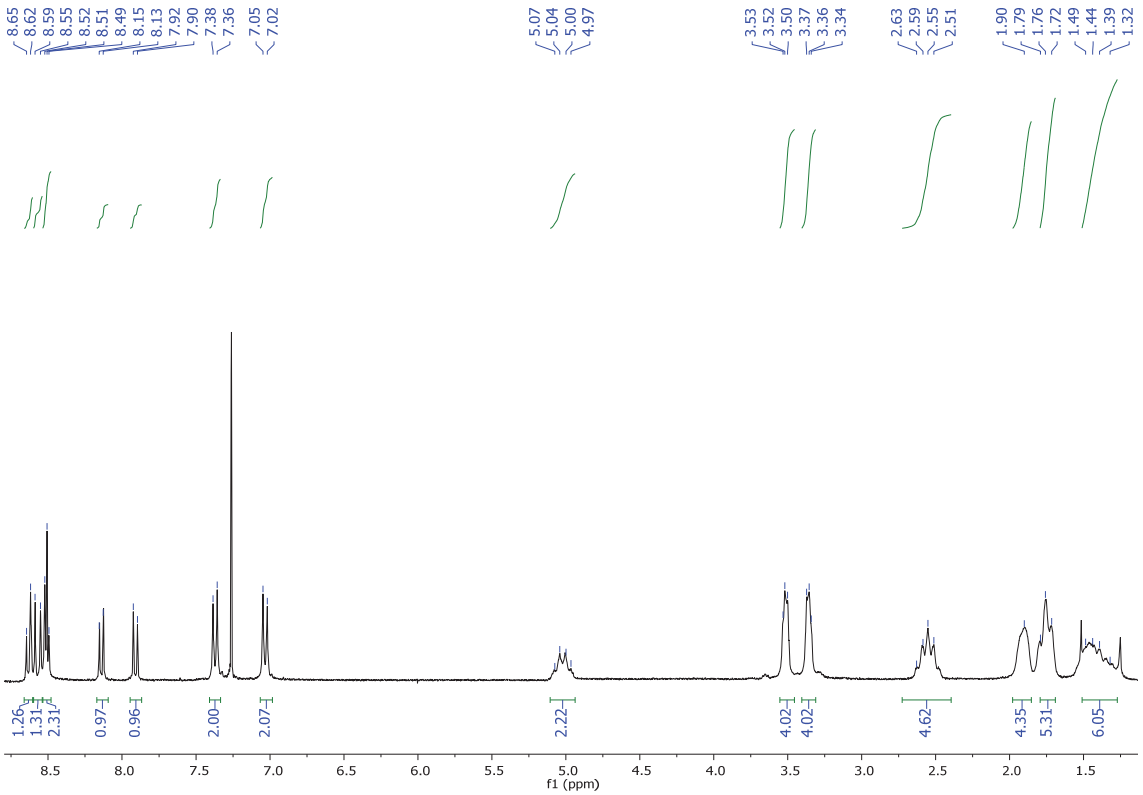

Figure 25. ^{1}H NMR (300 MHz, $CDCl_3$) of PC117

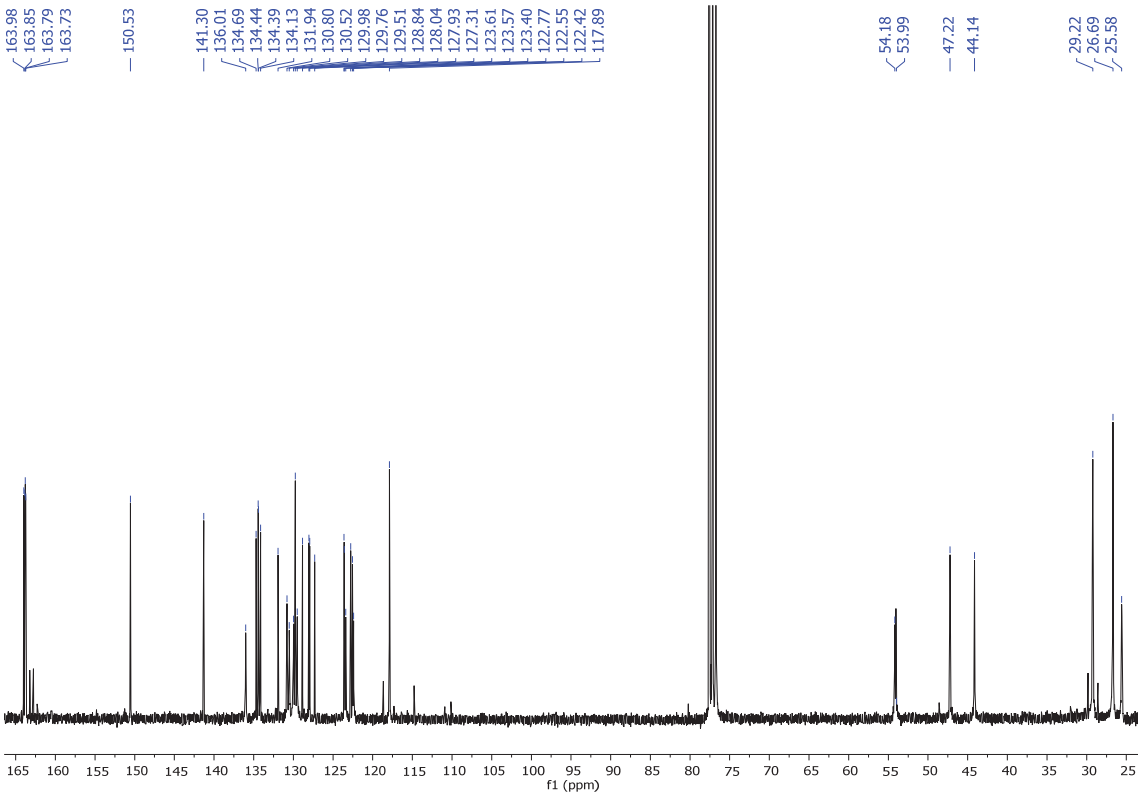

Figure 26. ^{13}C NMR (75 MHz, $CDCl_3$) of PC117

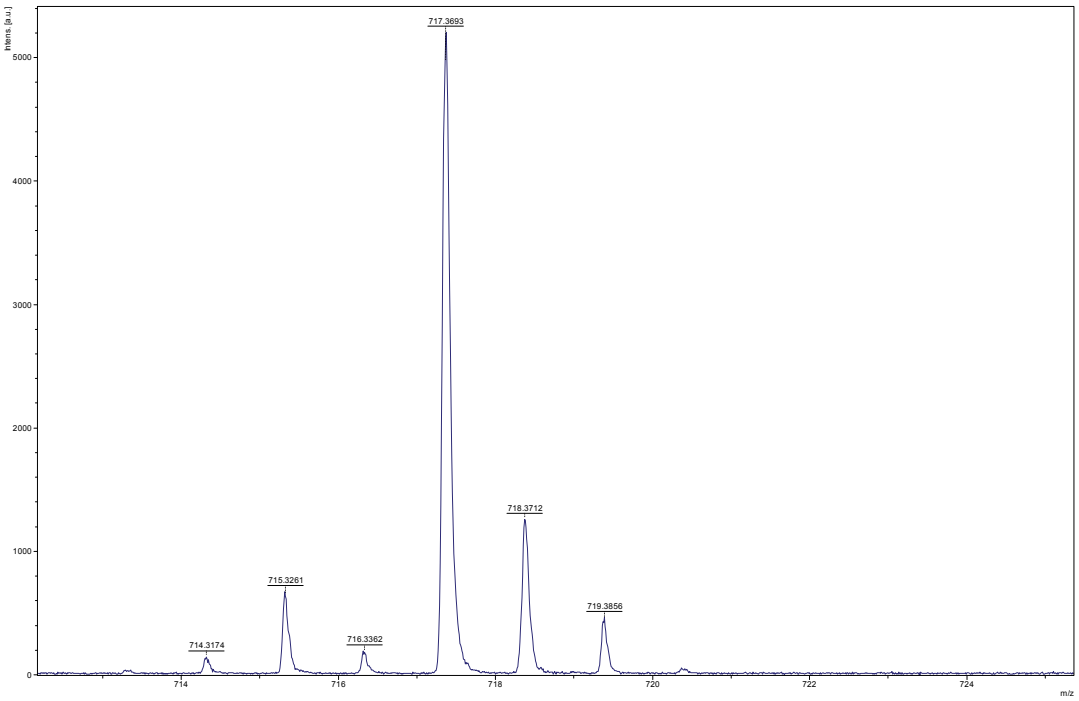

Figure 27. Mass spectrum (MALDI+, DCTB) of PC117

1.5. Synthesis of *N,N'*-bis(cyclohexyl)-1-(4-[4-(*N''*-*tert*-butoxycarbonyl)piperazin-1-yl]pyridine)perylene-3,4,9,10-tetracarboxylic diimide (PC63).

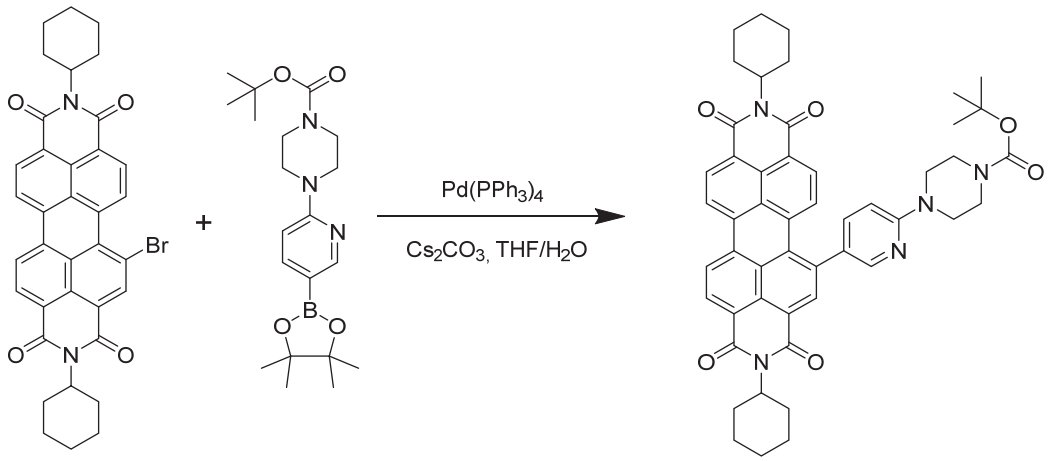

PC39 **PC63**

4-[4-(*N''*-*tert*-Butoxycarbonyl)piperazin-1-yl]pyridine-5-boronic acid pinacol ester (67 mg, 0.17 mmol) and cesium carbonate (168 mg, 0.47 mmol) and a catalytic amount of tetrakis (triphenylphosphine) palladium (0) were added under nitrogen to *N,N'*-dicyclohexyl-1-bromoperylene-3,4,9,10-tetracarboxilyc diimide (100 mg, 0.16 mmol) dissolved in THF:H_2O (20:2 mL). The mixture was heated at reflux for 24 hours and extracted with DCM (3 x 20 mL). The combined organic extracts were dried over anhydrous sodium sulphate, filtered and evaporated under reduced pressure. Purification was carried out by silica gel flash chromatography using DCM:MeCN (90:10) as eluent to give compound **PC63** as a deep purple solid in 14% yield (18 mg, 0.022 mmol). **R_f (DCM:MeOH, 50:1):** 0.43. **Mp (^{o}C):** 214 – 216 ^{o}C. **FT-IR (KBr, cm^{-1}):** 2926 (C-H), 2855 (C-H), 1698 (C=O), 1658 (C=O), 1590 (C_{Ar}-C_{Ar}), 1493, 1454 (CH_2),

1405 (C-N), 1331, 1235, 1164, 1118, 1022, 860, 811, 749 (fingerprint region). **^{1}H NMR (300 MHz, $CDCl_3$) δ:** 8.65 – 8.50 (m, 5H, H_{Ar}), 8.49 (s, 1H, H_{Ar}), 8.31 (d, *J* = 2.5 Hz, 1H, H_{Ar}), 8.20 (d, *J* = 8.2 Hz, 1H, H_{Ar}), 8.06 (d, *J* = 8.2 Hz, 1H, H_{Ar}), 7.52 (dd, *J* = 8.8, 2.5 Hz, 1H, H_{Ar}), 6.72 (d, *J* = 8.9 Hz, 1H, H_{Ar}), 5.08 – 4.96 (m, 2H, N-CH), 3.66 – 3.63 (m, 8H, CH_2), 2.59 – 2.51 (m, 5H, CH_2), 1.91 (d, *J* = 12.1 Hz, 4H, CH_2), 1.74 (d, *J* = 11.6 Hz, 5H, CH_2), 1.52 (s, 9H, CH_3), 1.48 – 1.30 (m, 6H, CH_2). **^{13}C NMR (101 MHz, $CDCl_3$) δ:** 163.9 (C=O), 163.9 (C=O), 163.8 (C=O), 163.74 (C=O), 158.6 (C_{quat}-N), 154.9 (**C**OOC$(CH_3)_3$), 147.8 (CH), 138.6 (C_{Ar}), 138.1 (CH), 136.0 (CH), 134.8 (C_{Ar}), 134.5 (C_{Ar}), 134.3 (C_{Ar}), 132.2 (C_{Ar}), 131.2 (CH), 131.0 (CH), 130.6 (CH), 130.2 (CH), 129.3 (CH), 129.0 (C_{Ar}), 128.2 (C_{Ar}), 128.1 (C_{Ar}), 127.6 (C_{Ar}), 127.5 (C_{Ar}), 123.7 (CH), 123.6 (C_{Ar}), 123.1 (C_{Ar}), 122.9 (C_{Ar}), 122.7 (CH), 122.5 (C_{Ar}), 107.7 (CH), 80.3 (**C**$(CH_3)_3$), 54.2 (NCOCO**C**H), 54.1 (NCOCO**C**H), 44.9 (N-CH_2-N-CH_2), 29.3 (CH_2), 29.2 (CH_2), 28.6 (CH_3), 26.7 (CH_2), 26.7 (CH_2), 25.6 (CH_2). **HRMS (MALDI-, DIT):** m/z calcd. for $C_{50}H_{49}N_5O_6$ ($[M]^-$): 815.3677; found: 815.3680. **UV-Vis (DCM), λ_{max} nm (log ε):** 484 (4.4), 521 (4.4).

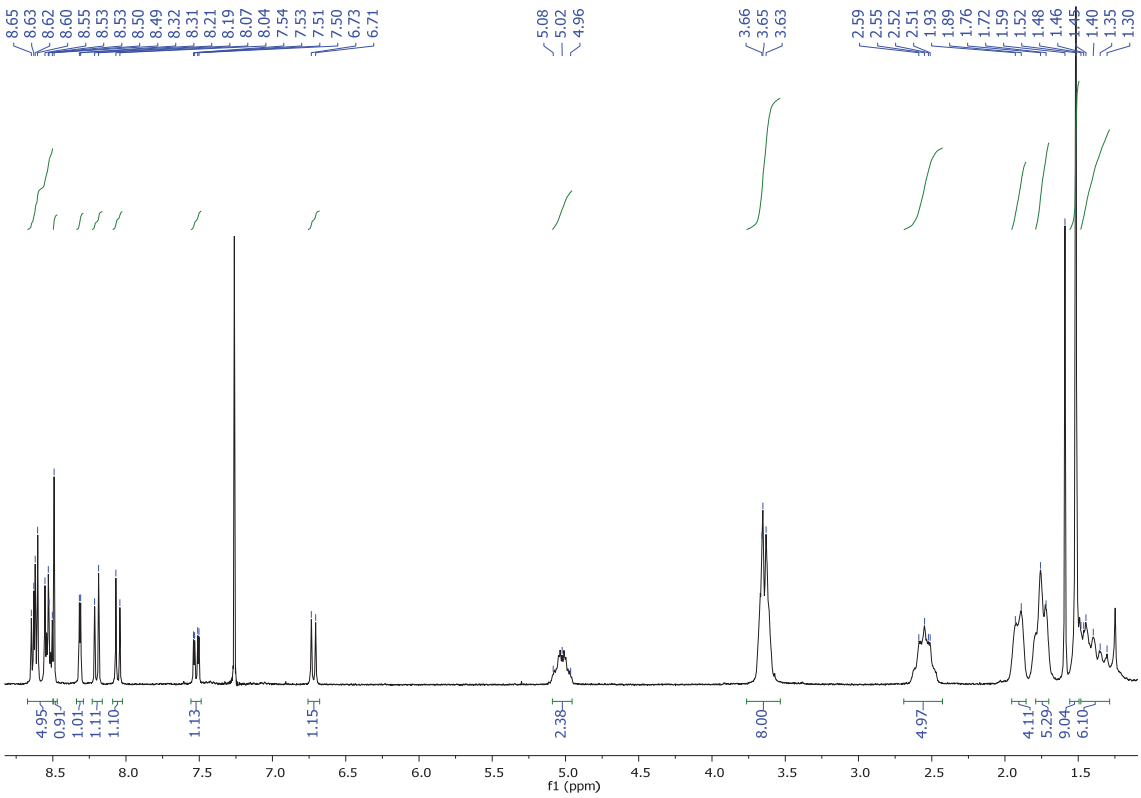

Figure 28. ^{1}H NMR (300 MHz, $CDCl_3$) of PC63

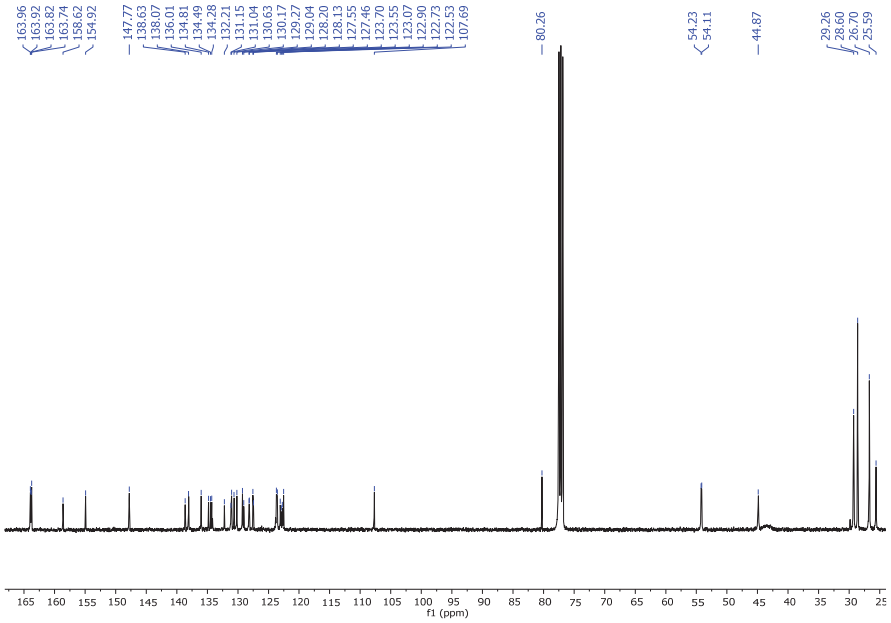

Figure 29. ^{13}C NMR (101 MHz, $CDCl_3$) of PC63

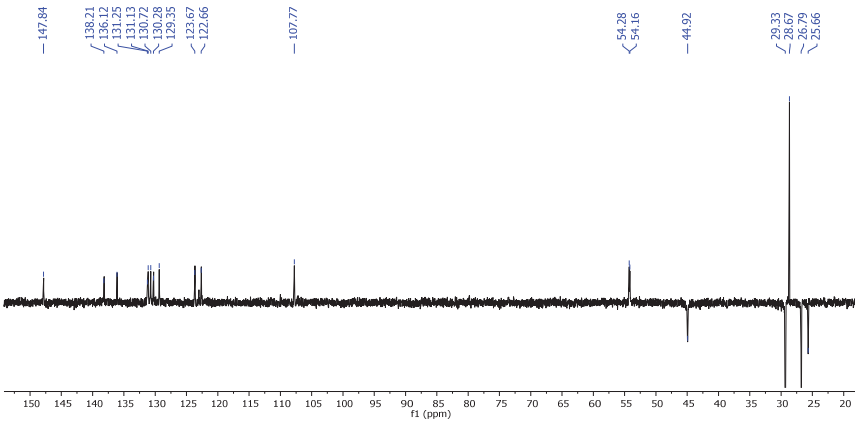

Figure 30. ^{13}C NMR-DEPT-135 (101 MHz, $CDCl_3$) of PC63

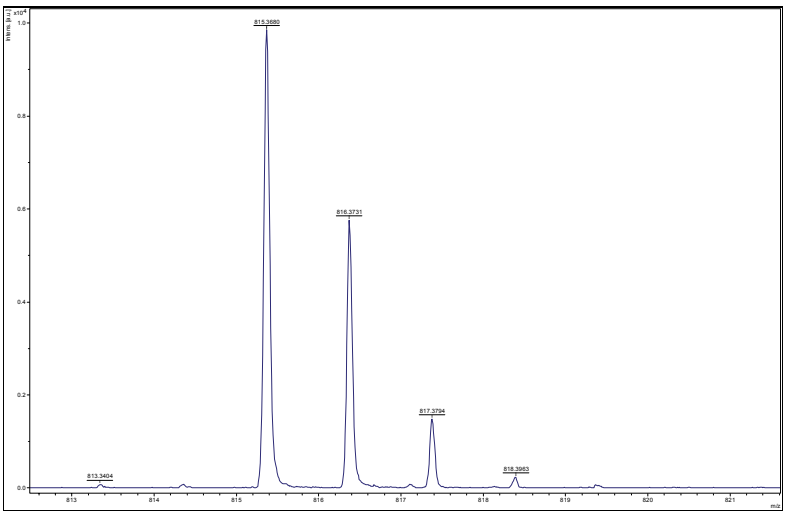

Figure 31. Mass spectrum (MALDI-, DIT) of PC63

Solvatochromism:

The concentration of **PC63** is $1 \cdot 10^{-5}$ M. The excitation wavelength is 483 nm. The absorption and emission spectra have been measured in the listed solvents below in the range between 200 to 900 nm. The used solvents are: MeOH, DMSO, DMF, MeCN, acetone, AcOEt, THF, $CHCl_3$, DCM, toluene, diethyl ether, hexane and cyclohexane.

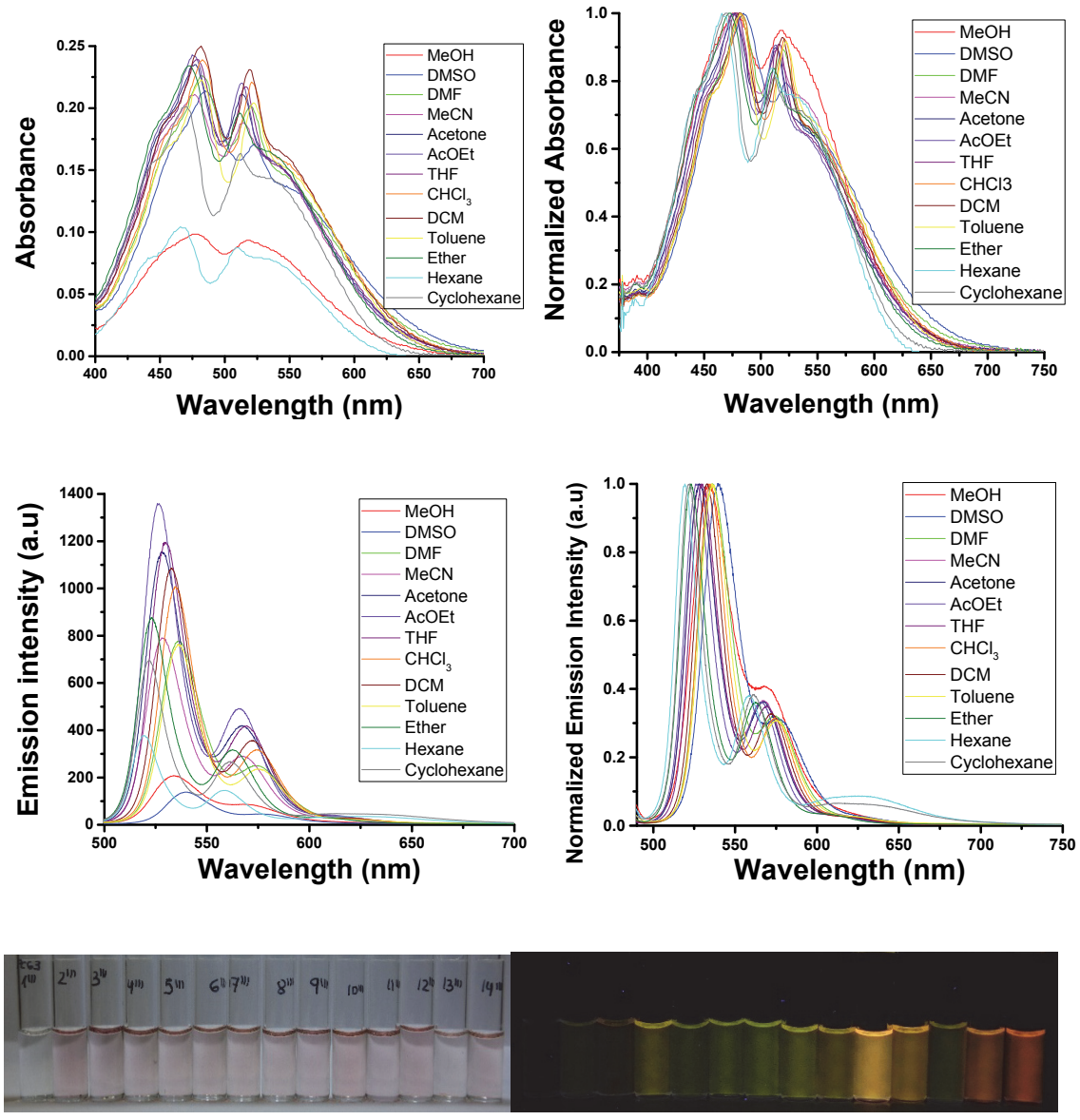

Solvents: 1: Water, 2: MeOH, 3: DMSO, 4: DMF, 5: MeCN, 6: acetone, 7: AcOEt, 8: THF, 9: $CHCl_3$, 10: DCM, 11: toluene, 12: diethyl ether, 13: hexane, 14: cyclohexane.

Figure 32. Upper. Absorbance and Normalized absorbance spectra of PC63. Middle: Fluorescence and Normalized fluorescence spectra of PC63. Lower. Solvatochromic effect of PC63 under white light and light of 366 nm.

1.6. Synthesis of *N,N'*-bis(cyclohexyl)-1-(4-[piperazin-1-yl]pyridine)perylene-3,4,9,10-tetracarboxylic diimide (PC63d).

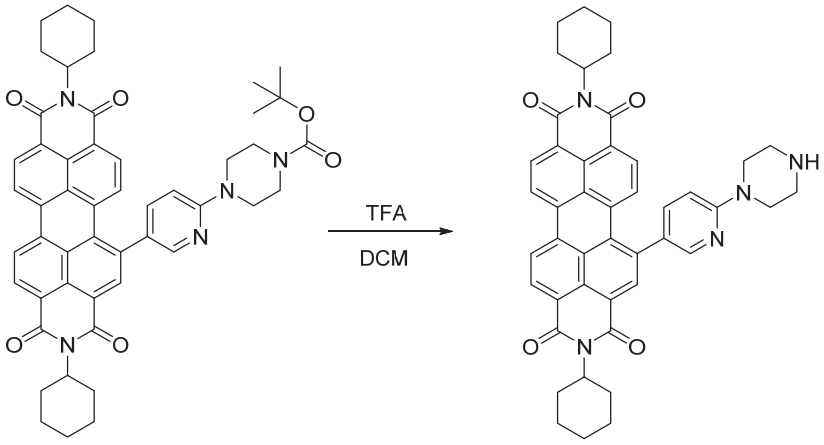

PC63 **PC63d**

Trifluoroacetic acid (368 µL, 0.01 mmol) was added dropwise to *N,N'*-bis(cyclohexyl)-1-(4-[4-(*N''*-*tert*-butoxycarbonyl)piperazin-1-yl]pyridine)perylene-3,4,9,10-tetracarboxylic diimide (20 mg, 0.03 mmol) dissolved in DCM (5 mL). The mixture was stirred at room temperature for 2 hours, then NaOH was added to neutralize the reaction until pH = 6-8 and it was extracted with DCM (3 x 20 mL). The combined organic extracts were dried over anhydrous sodium sulphate, filtered and evaporated under reduced pressure to obtain a purple-red solid with a yield 93 % (16.7 mg, 0.02 mmol). **R_f (DCM:MeOH 50:4):** 0. **Mp (°C):** 220 – 222 °C. **FT-IR (KBr, cm^{-1}):** 2926 (C_{Ar}-H), 2852 (C-H), 1696 (C=O), 1658 (C=O), 1592 (C_{Ar}-C_{Ar}), 1493 (C-O), 1451, 1405, 1331 (C-N), 1238, 1166, 1112, 1019, 928, 862, 808, 749 (fingerprint region). **^{1}H NMR (300 MHz, $CDCl_3$) *δ*:** 8.63 – 8.57 (m, 2H, H_{Ar}), 8.52 – 8.46 (m, 3H, H_{Ar}), 8.31 (d, *J* = 2.6 Hz, 1H, H_{Ar}), 8.20 (d, *J* = 8.2 Hz, 1H, H_{Ar}), 8.05 (d, *J* = 8.4 Hz, 1H, H_{Ar}), 7.49 (dd, *J* = 8.8, *J* = 2.5 Hz, 1H, H_{Ar}), 6.71 (d, *J* = 9.0 Hz, 1H, H_{Ar}), 5.05 – 5.01 (m, 2H, N-CH), 3.66 (t, *J* = 5.0 Hz, 4H, CH_2), 3.06 (t, *J* = 5.0 Hz, 4H, CH_2), 2.59 – 2.52 (m, 5H, CH_2), 1.89 (d, *J* = 12.3 Hz, 4H, CH_2), 1.76 (d, *J* = 11.9 Hz, 5H, CH_2), 1.49 – 1.37 (m, 4H, CH_2). **^{13}C NMR (75 MHz, $CDCl_3$) *δ*:** 164.1 (C=O), 163.9 (C=O), 163.9 (C=O), 163.9 (C=O), 159.0 (C_{quat}-N), 147.8 (C_{quat}-N), 138.9 (C_{Ar}), 138.0 (C_{Ar}), 136.2 (C_{Ar}), 135.0 (C_{Ar}), 134.6 (C_{Ar}), 134.5 (C_{Ar}), 132.3 (C_{Ar}), 131.2 (C_{Ar}), 130.7 (C_{Ar}), 130.3 (C_{Ar}), 129.9 (C_{Ar}), 129.3 (C_{Ar}), 128.3 (C_{Ar}), 127.6 (C_{Ar}), 127.3 (C_{Ar}), 123.9 (C_{Ar}), 123.8 (C_{Ar}), 123.7 (C_{Ar}), 123.1 (C_{Ar}), 122.8 (C_{Ar}), 122.6 (C_{Ar}), 107.6 (C_{Ar}), 54.2 (NCOCO-**C**H), 46.0 (N-**C**H_2-N-CH_2), 45.9 (N-CH_2-N-**C**H_2), 32.1 (CH_2), 29.9 (CH_2), 29.3 (CH_2), 26.7 (CH_2), 25.6 (CH_2). **HRMS (MALDI+, DCTB):** m/z calcd. for $C_{45}H_{41}N_5O_4$ ($[M+H]^+$): 716.3231; found: 716.3255.

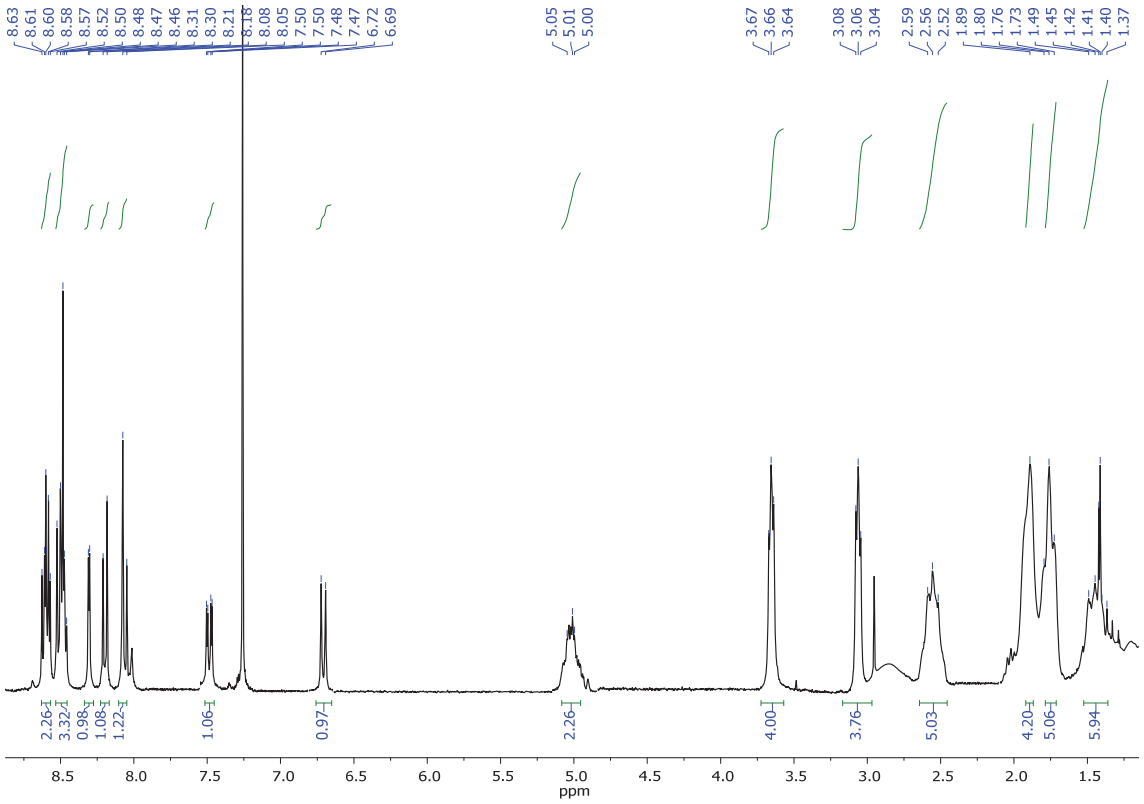

Figure 33. ^{1}H NMR (300 MHz, $CDCl_3$) of PC63d

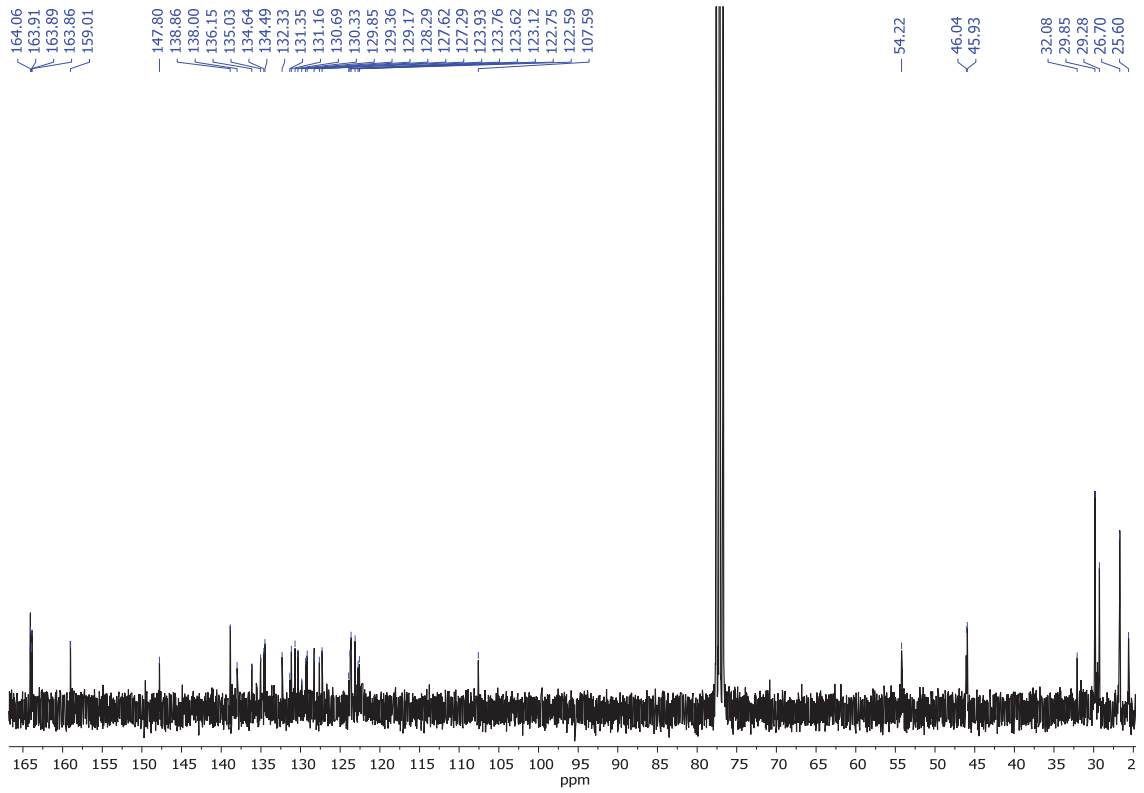

Figure 34. ^{13}C NMR (75 MHz, $CDCl_3$) of PC63d

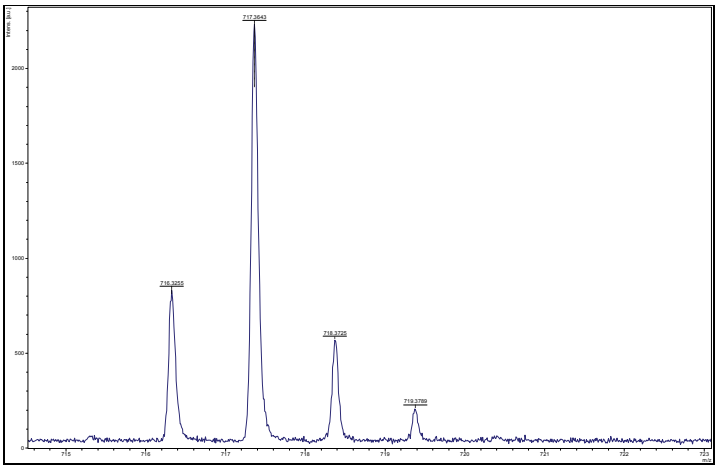

Figure 35. Mass spectrum (MALDI+, DCTB) of PC63d

Solvatochromism: The concentration of **PC63d** is $1 \cdot 10^{-5}$ M. The excitation wavelength is 483 nm. The absorption and emission spectra have been measured in the listed solvents below in the range between 200 to 900 nm. The used solvents are: MeOH, DMSO, DMF, MeCN, acetone, AcOEt, THF, $CHCl_3$, DCM, toluene, diethyl ether, hexane and cyclohexane.

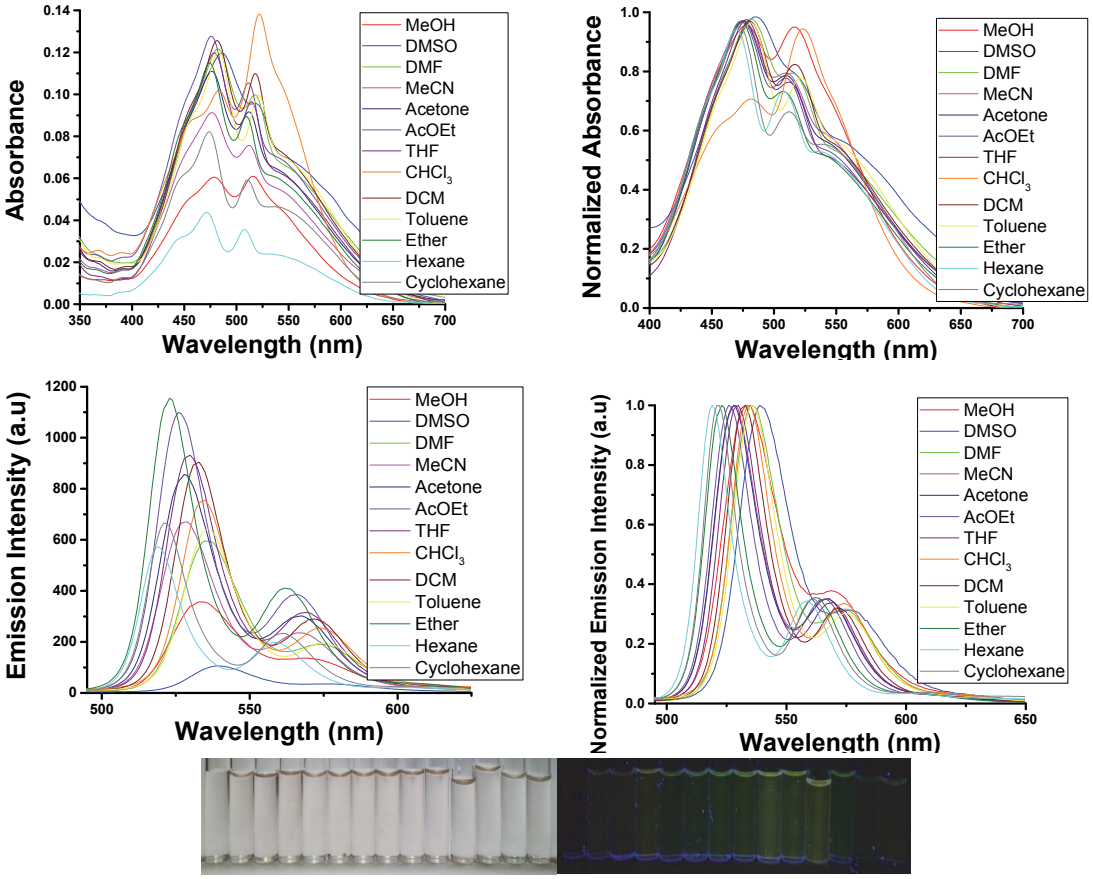

Solvents: 1: Water, 2: MeOH, 3: DMSO, 4: DMF, 5: MeCN, 6: acetone, 7: AcOEt, 8: THF, 9: $CHCl_3$, 10: DCM, 11: toluene, 12: diethyl ether, 13: hexane, 14: cyclohexane.

Figure 36. Upper. Absorbance and Normalized absorbance spectra of PC63d. Middle: Fluorescence and Normalized fluorescence spectra of PC63d. Lower. Solvatochromic effect of PC63d under white light and light of 366 nm.

1.7. Synthesis of *N,N'*-bis(cyclohexyl)-1-(4-[4-(*N''*-*tert*-butoxycarbonyl)piperazin-1-yl]pyrimidine)perylene-3,4,9,10-tetracarboxylic diimide (PC64).

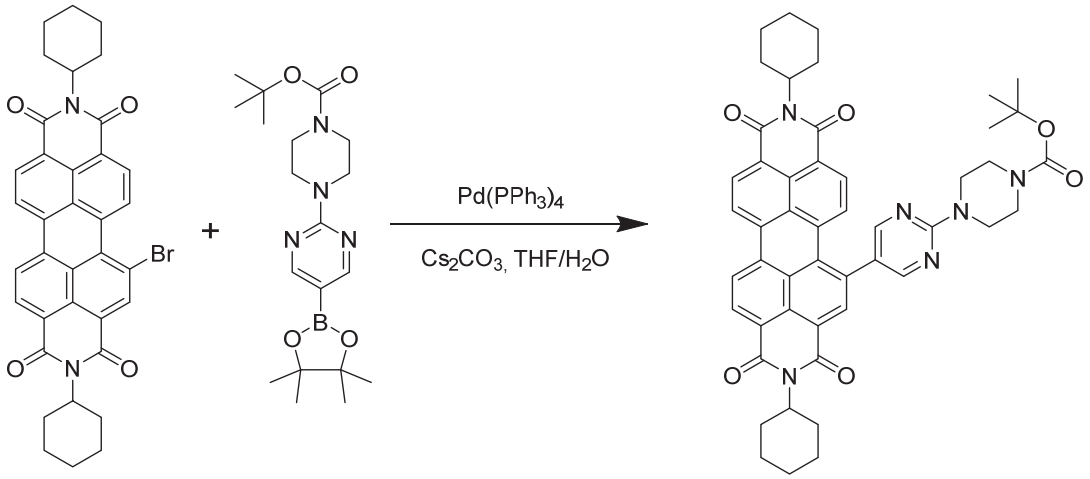

PC39 **PC64**

4-[4-(*N''*-*tert*-Butoxycarbonyl)piperazin-1-yl]pyrimidine-5-boronic acid pinacol ester (68 mg, 0.17 mmol), cesium carbonate (169 mg, 0.47 mmol) and a catalytic amount of tetrakis (triphenylphosphine) palladium (0) were added under nitrogen to *N,N'*-dicyclohexyl-1-bromoperylene-3,4,9,10-tetracarboxilyc diimide (100 mg, 0.16 mmol) dissolved in THF:H_2O (20:2 mL). The mixture was heated at reflux for 24 hours and extracted with DCM (3 x 20 mL). The combined organic extracts were dried over anhydrous sodium sulphate, filtered and evaporated under reduced pressure. Purification was carried out by silica gel flash chromatography using DCM:MeCN (90:10) as eluent to give compound **PC64** as a deep purple solid in 60 % yield (78 mg, 0.10 mmol). **R_f (DCM:MeOH, 50:4):** 0. **Mp (°C):** 234 – 236 °C. **FT-IR (KBr, cm^{-1}):** 2928 (CAr-H), 2852 (C-H), 1696 (C=O Imide), 1658 (C=O), 1590 (CAr-CAr), 1513, 1451, 1417, 1400, 1331 (C-N), 1240, 1166, 1130, 997, 860, 814, 749 (fingerprint region). **^{1}H NMR (300 MHz, $CDCl_3$) *δ*:** 8.64 – 8.57 (m, 2H, H_{Ar}), 8.52 – 8.46 (m, 2H, H_{Ar}), 8.40 (d, *J* = 8.2 Hz, 1H, H_{Ar}), 8.08 (d, *J* = 8.2 Hz, 1H, H_{Ar}), 5.07 – 4.97 (m, 2H, N-CH), 3.91 (t, *J* = 11.5 Hz, 4H, CH_2), 3.57 (t, *J* = 11.0 Hz, 4H, CH_2), 2.57 – 2.52 (m, 5H, CH_2), 1.92 (d, *J* = 10.2 Hz, 4H, CH_2), 1.76 (d, *J* = 11.3 Hz, 4H, CH_2), 1.52 (s, 9H, CH_3) 1.45 – 1.30 (m, 6H, CH_2). **^{13}C NMR (101 MHz, $CDCl_3$) *δ*:** 163.9 (C=O), 163.9 (C=O), 163.8 (C=O), 163.7 (C=O), 160.8 (C_{quat}-N), 157.8 (**C**OOC(CH_3)$_3$), 154.9 (C_{quat}-N), 135.7 (CH), 135.5 (C_{Ar}), 134.8 (C_{Ar}), 134.4 (C_{Ar}), 132.6 (C_{Ar}), 131.4 (CH), 131.0 (CH), 130.4 (CH), 129.3 (C_{Ar}), 129.2 (CH), 128.3 (CH), 127.6 (CH), 125.0 (C_{Ar}), 123.9 (C_{Ar}), 123.8 (C_{Ar}), 123.5 (C_{Ar}), 123.1 (C_{Ar}), 122.9 (C_{Ar}), 54.3 (NCOCO-**C**H), 54.2 (NCOCO-**C**H), 43.89 (N-CH_2-N-CH_2), 29.27 (CH_2), 28.62 (CH_3), 26.69 (CH_2), 25.58 (CH_2). **HRMS (MALDI-, DIT):** m/z calcd. for $C_{49}H_{48}N_6O_6$ ($[M]^-$): 816.3630; found: 816.3665. **UV-Vis (DCM), λ_{max} nm (log ε):** 459 (4.6), 537 (4.7).

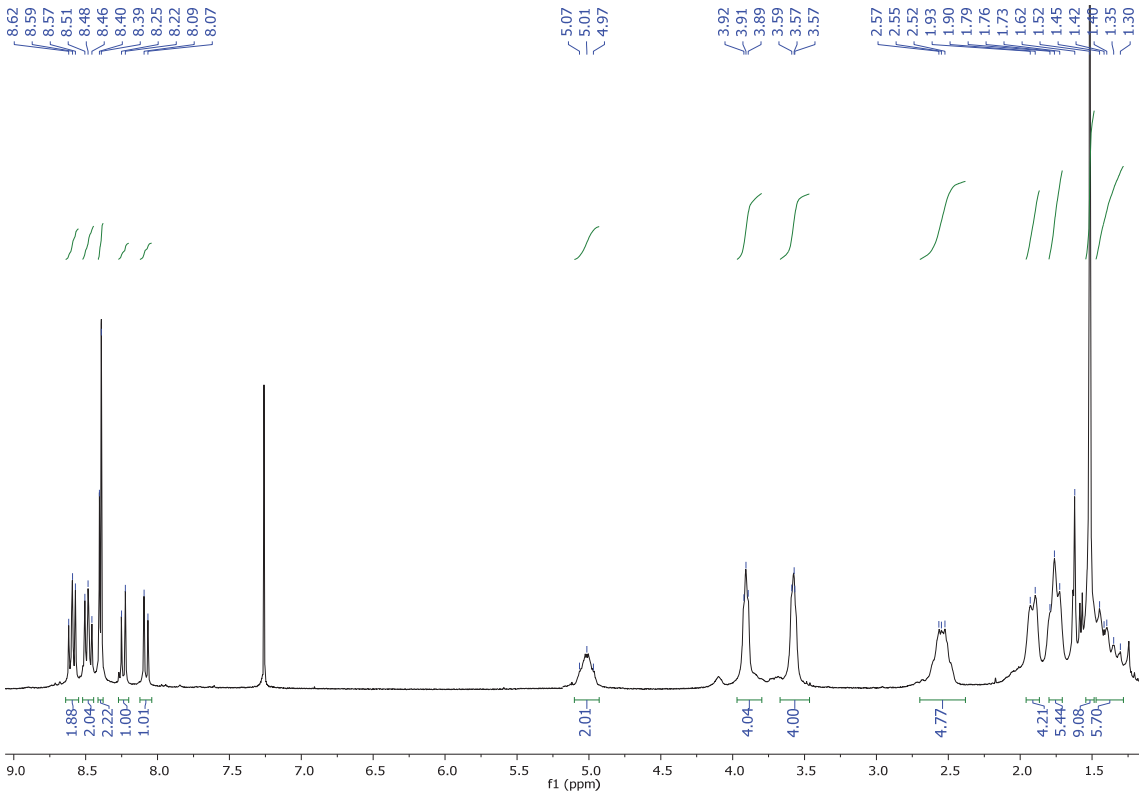

Figure 37. ^{1}H NMR (300 MHz, $CDCl_3$) of PC64

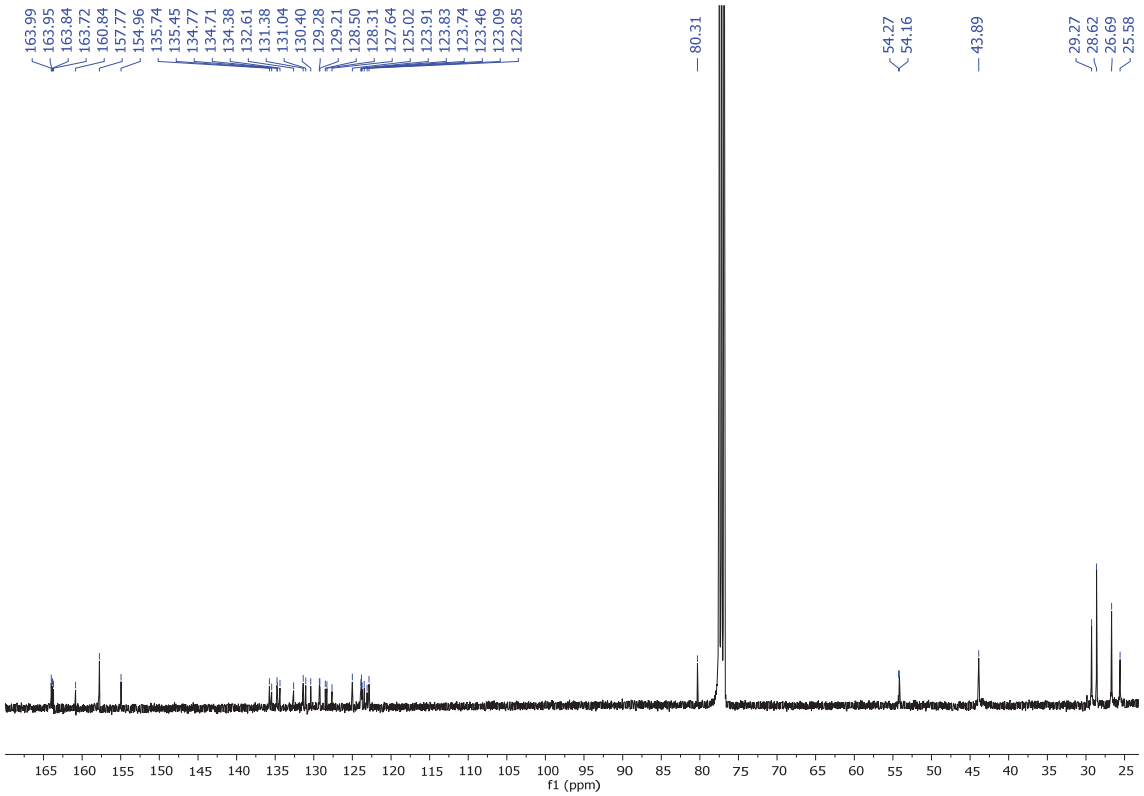

Figure 38. ^{13}C NMR (101 MHz, $CDCl_3$) of PC64

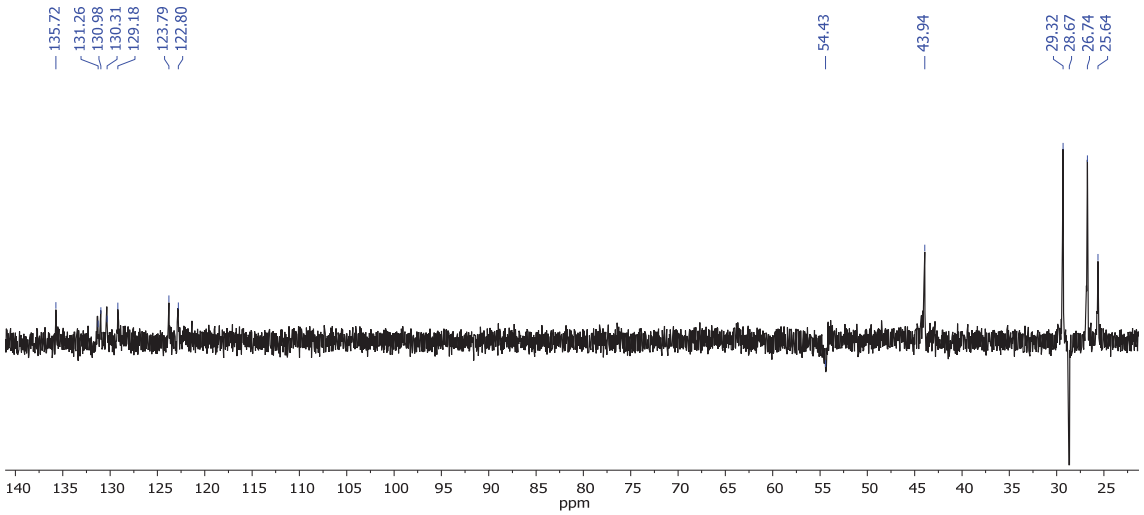

Figure 39. ^{13}C NMR-DEPT-135 (101 MHz, $CDCl_3$) of PC64

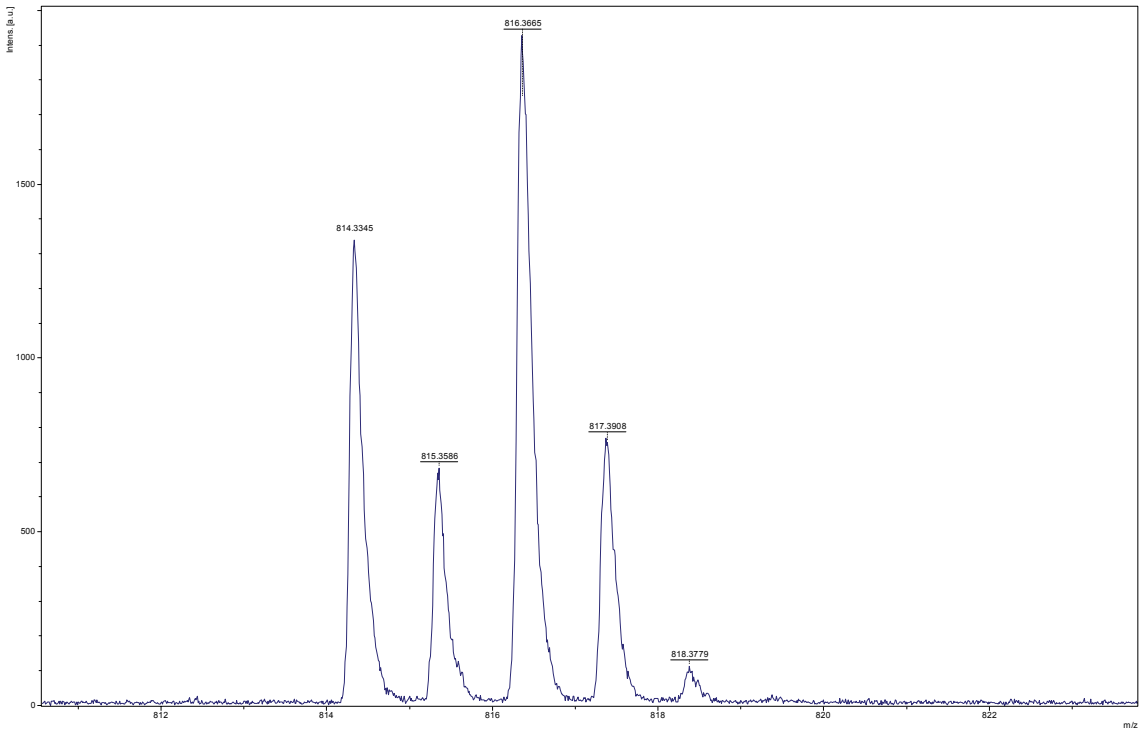

Figure 40. Mass spectrum (MALDI-, DIT) of PC64

Solvatochromism:

The concentration of **PC64** is $1 \cdot 10^{-5}$ M. The excitation wavelength is 460 nm. The absorption and emission spectra have been measured in the listed solvents below in the range between 200 to 900 nm. The used solvents are: MeOH, DMSO, DMF, MeCN, acetone, AcOEt, THF, $CHCl_3$, DCM, toluene, diethyl ether, hexane and cyclohexane.

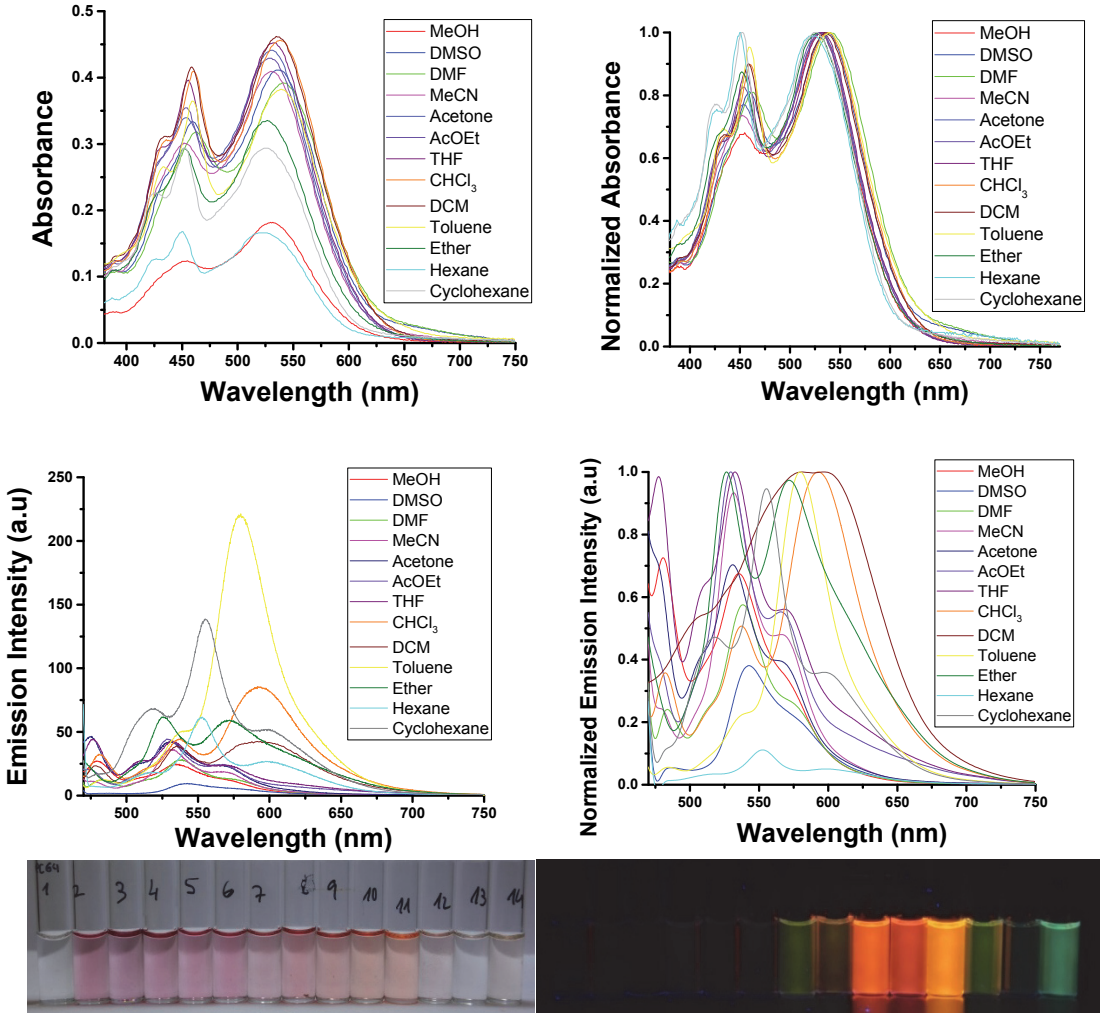

Solvents: 1: Water, 2: MeOH, 3: DMSO, 4: DMF, 5: MeCN, 6: acetone, 7: AcOEt, 8: THF, 9: $CHCl_3$, 10: DCM, 11: toluene, 12: diethyl ether, 13: hexane, 14: cyclohexane.

Figure 41. Upper. Absorbance and Normalized absorbance spectra of PC64. Middle: Fluorescence and Normalized fluorescence spectra of PC64. Lower. Solvatochromic effect of PC64 under white light and light of 366 nm.

1.8. Synthesis of *N,N'*-bis(cyclohexyl)-1-(4-[piperazin-1-yl]pyrimidine)perylene-3,4,9,10-tetracarboxylic diimide (PC119).

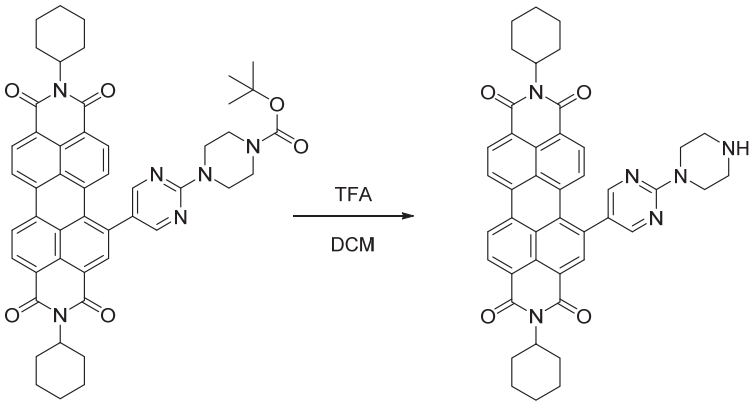

PC64 **PC119**

Trifluoroacetic acid (368 µL, 0.01 mmol) was added dropwise to *N,N'*-bis(cyclohexyl)-1-(4-[4-(*N''-tert*-butoxycarbonyl)piperazin-1-yl]pyrimidine)perylene-3,4,9,10-tetracarboxylic diimide (20 mg, 0.03 mmol) dissolved in DCM (5 mL). The mixture was stirred at room temperature for 2 hours, then NaOH was added to neutralize the reaction until pH = 6-8 and it was extracted with DCM (3 x 20 mL). The combined organic extracts were dried over anhydrous sodium sulphate, filtered and evaporated under reduced pressure to obtain a purple-red solid in 96 % yield (17.3 mg, 0.02 mmol). **R_f (DCM:MeOH, 50:4):** 0. **Mp (°C):** > 350 °C. **FT-IR (KBr, cm^{-1}):** 2923 (C_{Ar}-H), 2855 (C-H), 1766, 1709 (C=O), 1655 (C=O), 1595 (C_{Ar}-C_{Ar}), 1534, 1388, 1354 (C-N), 1323, 1261, 1213, 1127, 1027, 905, 865, 806, 724, 681, 649 (fingerprint region).

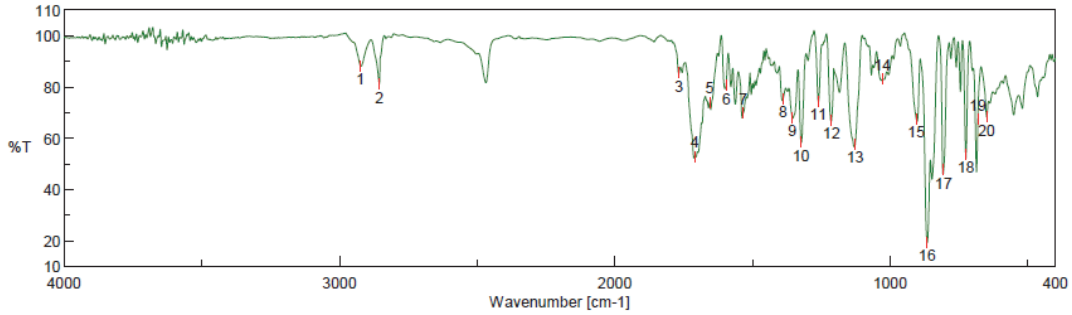

Figure 42. FT-IR (KBr) spectrum of PC119

1.9. Synthesis of *N,N'*-bis(cyclohexyl)-1,7-bis-((4-[4-(*N''-tert*-butoxycarbonyl)piperazin-1-yl]phenyl))perylene-3,4,9,10-tetracarboxylic diimide (1,7-PC54).

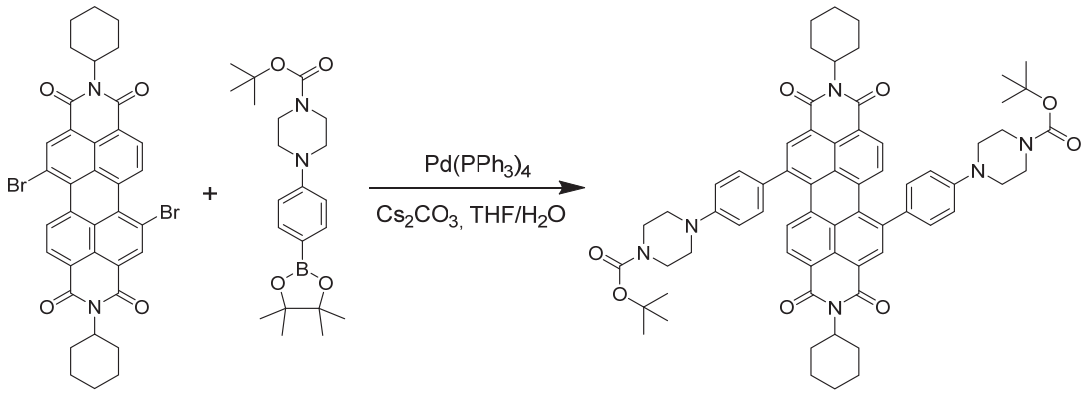

PC37 **1,7-PC54**

4-[4-(*N''-tert*-butoxycarbonyl)piperazin-1-yl]phenylboronic acid pinacol ester (250 mg, 0.65 mmol), cesium carbonate (300 mg, 0.93 mmol) and a catalytic amount of tetrakis (triphenylphosphine) palladium (0) were added under nitrogen to *N,N'*-bis(cyclohexyl)-1,6- and 1,7-dibromoperylene-3,4,9,10-tetracarboxylic diimide (220 mg, 0.31 mmol) dissolved in THF:H_2O (40:4 mL). The mixture was heated at reflux for 24 hours and extracted with DCM (3 x 40 mL). The combined organic extracts were dried over anhydrous sodium sulphate, filtered and evaporated under reduced pressure. Purification was carried out by silica gel flash chromatography using DCM:MeCN (80:20) as a mixture of 1,6- and 1,7-PC54 with a yield 60 % (200 mg, 0.186 mmol). Further silica gel flash chromatography using DCM:MeCN (80:20) gave 1,7-PC54 with a 10% yield (33.3 mg, 0.03 mmol). **R_f (DCM:MeOH, 50:1):** 0.63. **Mp (°C):** > 350 °C. **FT-IR (KBr, cm^{-1}):** 2976 (C-H), 2931 (C-H), 2851 (C-H), 1700 (C=O), 1658 (C=O), 1589 (C_{Ar}-C_{Ar}), 1503 (C_{Ar}-C_{Ar}), 1454 (CH_2), 1409 (CH_2), 1323 (C-N), 1233, 1167, 1129, 994, 915, 863, 808, 756 (fingerprint region). **^{1}H NMR (400 MHz, $CDCl_3$) δ:** 8.58 (s, 2H, H_{Ar}), 8.12 (d, *J* = 8.1 Hz, 1H, H_{Ar}), 7.91 (d, *J* = 9.0 Hz, 2H, H_{Ar}), 7.43 (d, *J* = 8.5 Hz, 4H, H_{Ar}), 6.98 (d, *J* = 8.6 Hz, 4H, H_{Ar}), 5.05 – 4.97 (m, 2H, N-CH), 3.64 (t, *J* = 5.1 Hz, 8H, CH_2), 3.27 (t, *J* = 5.3 Hz, 8H, CH_2), 2.55 – 2.51 (m, 5H, CH_2),

1.89 (d, *J* = 11.1 Hz, 4H, CH_2), 1.72 (d, *J* = 11.9 Hz, 6H, CH_2), 1.51 (s, 18H, CH_3), 1.42 – 1.30 (m, 6H, CH_2). **^{13}C NMR (101 MHz, $CDCl_3$) *δ*:** 164.2 (C=O), 164.1 (C=O), 164.1 (C=O), 164.0 (C=O), 154.8 (**C**$OOC(CH_3)_3$), 151.2 (C_{quat}-N), 142.1 (C_{quat}-PDI), 140.8 (C_{quat}-PDI), 135.3 (C_{Ar}), 135.2 (C_{Ar}), 135.1 (C_{Ar}), 134.8 (C_{Ar}), 133.7 (C_{Ar}), 133.1 (C_{Ar}), 132.5 (C_{Ar}), 132.1 (C_{Ar}), 130.2 (C_{Ar}), 130.0 (C_{Ar}), 129.7 (C_{Ar}), 129.5 (C_{Ar}), 129.4 (C_{Ar}), 129.2 (C_{Ar}), 128.9 (C_{Ar}), 127.5 (C_{Ar}), 122.9 (C_{Ar}), 122.7 (C_{Ar}), 122.1 (C_{Ar}), 117.2 (C_{Ar}), 117.1 (C_{Ar}), 80.2 (**C**$(CH_3)_3$), 54.0 (NCOCO-**C**H), 48.7 (N-**C**H_2-CH_2-N), 48.6 (N-CH_2-**C**H_2-N), 29.3 (CH_2), 28.6 (CH_3), 26.7 (CH_2), 25.6 (CH_2). **HRMS (MALDI+, DCTB):** m/z calcd. for $C_{66}H_{70}N_6O_8$ ($[M]^+$): 1074.5250; found: 1074.6237.

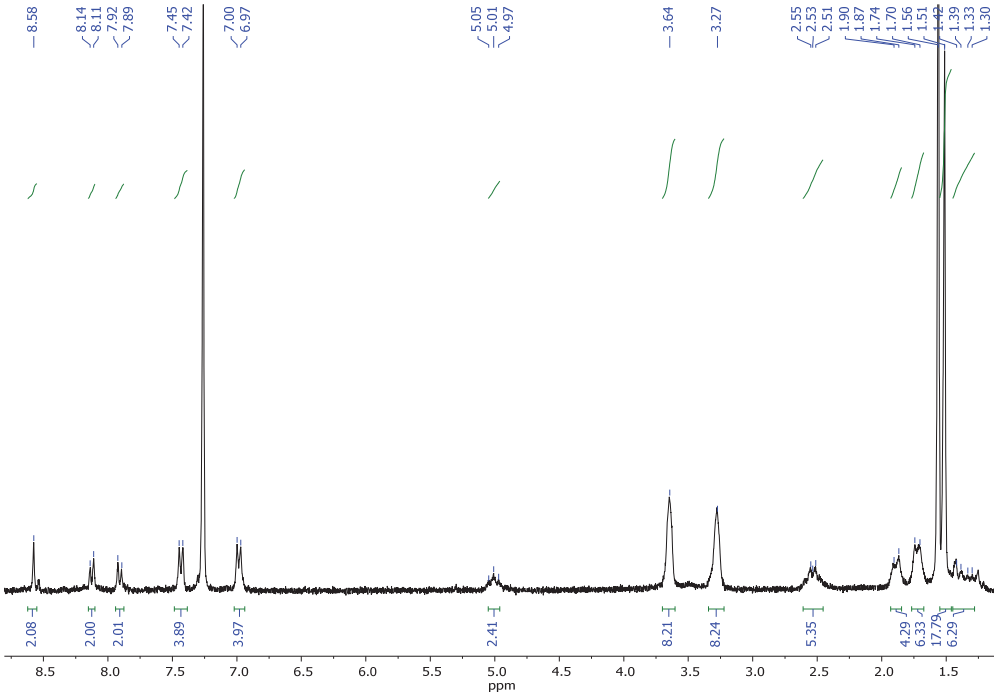

Figure 43. ^{1}H NMR (400 MHz, $CDCl_3$) of PC54

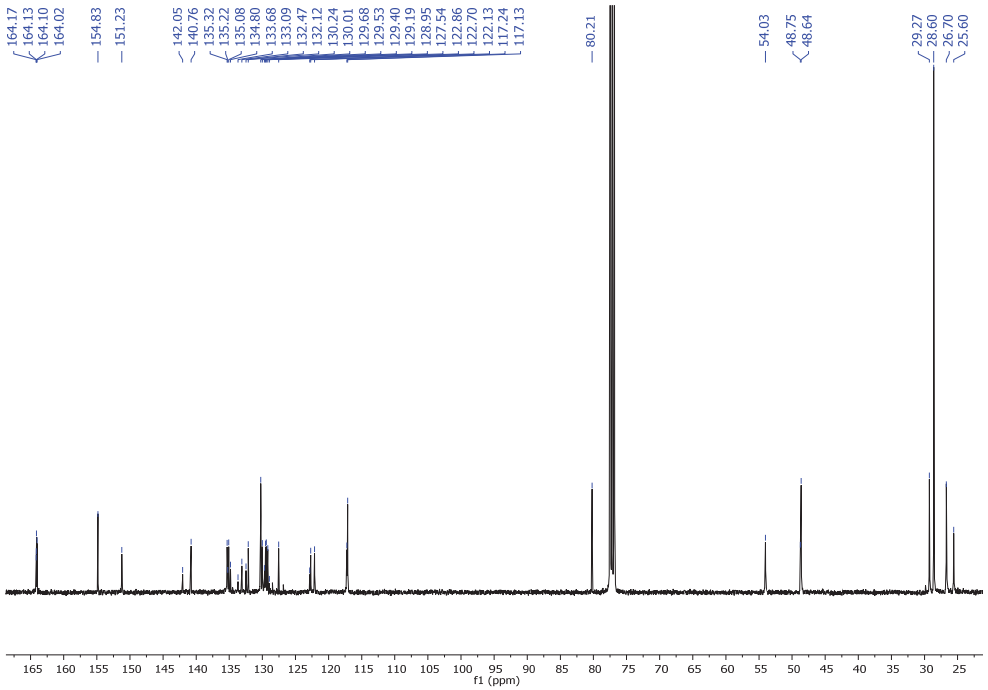

Figure 44. ^{13}C NMR (101 MHz, $CDCl_3$) of PC54

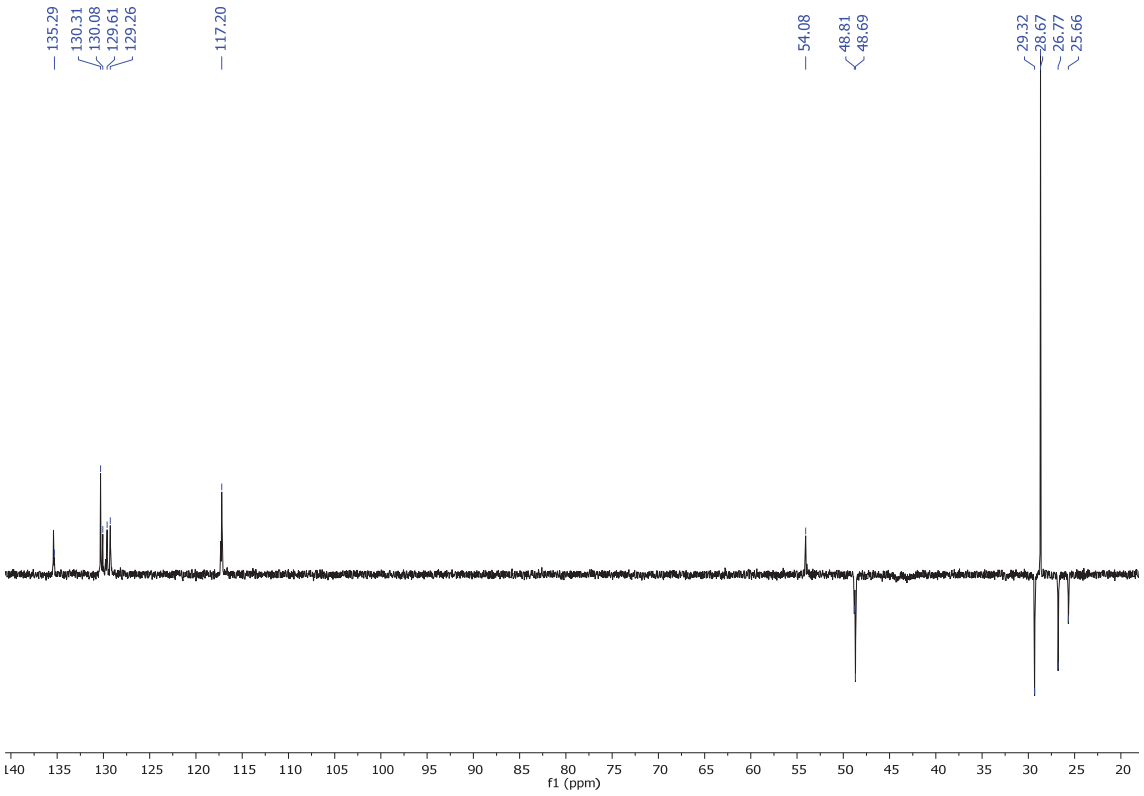

Figure 45. ^{13}C NMR-DEPT-135 (101 MHz, $CDCl_3$) of PC54

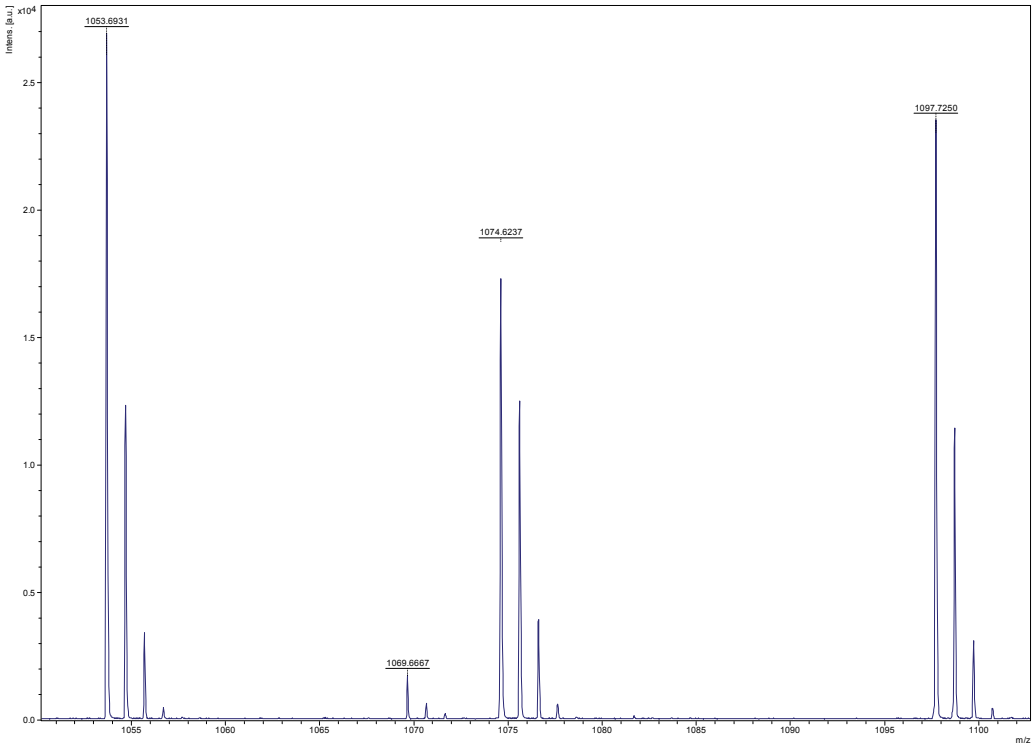

Figure 46. Mass spectrum (MALDI+, DCTB) of PC54

Solvatochromism:

The concentration of **PC54** is $1 \cdot 10^{-5}$ M. The excitation wavelength is 452 nm. The absorption and emission spectra have been measured in the listed solvents below in the range between 200 to 900 nm. The used solvents are: DMSO, DMF, MeCN, acetone, AcOEt, THF, $CHCl_3$, DCM, toluene, diethyl ether, hexane and cyclohexane.

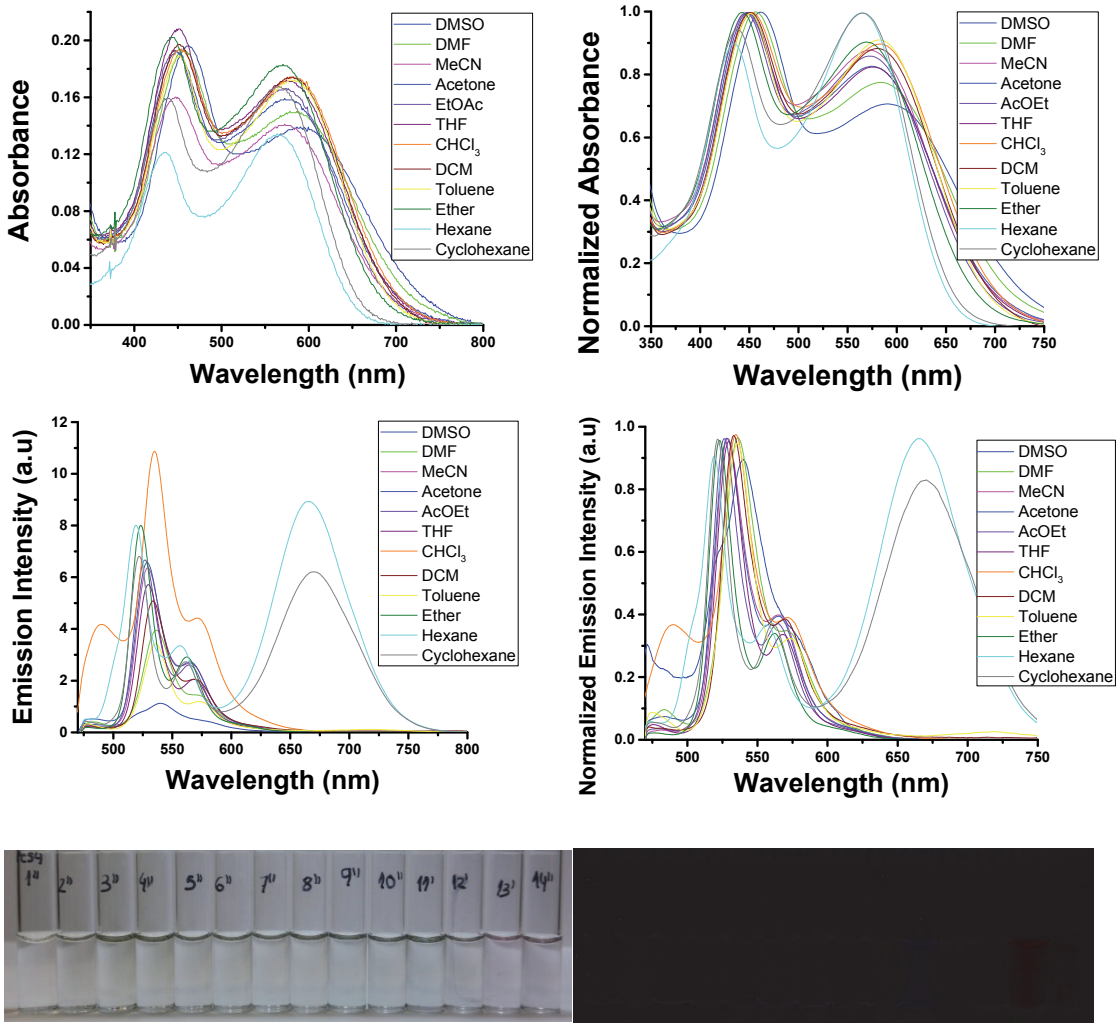

Solvents: 1: Water, 2: MeOH, 3: DMSO, 4: DMF, 5: MeCN, 6: acetone, 7: AcOEt, 8: THF, 9: $CHCl_3$, 10: DCM, 11: toluene, 12: diethyl ether, 13: hexane, 14: cyclohexane.

Figure 47. Upper. Absorbance and Normalized absorbance spectra of PC54. Middle: Fluorescence and Normalized fluorescence spectra of PC54. Lower. Solvatochromic effect of PC54 under white light and light of 366 nm.

1.10. Synthesis of *N,N'*-bis(cyclohexyl)-1,7-bis-((4-[4-piperazin-1-yl]phenyl))perylene-3,4,9,10-tetracarboxylic diimide (1,7-PC114).

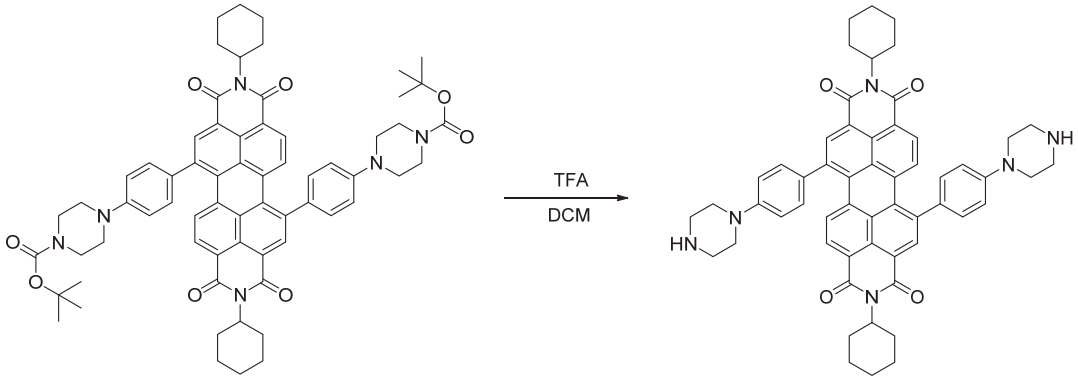

1,7-PC54 **1,7-PC114**

Trifluoroacetic acid (557 µL, 4.86 mmol) was added dropwise to *N,N'*-bis(cyclohexyl)-1,7-di-(4-[4-(*N''-tert*-butoxycarbonyl)piperazin-1-yl]phenyl)perylene-3,4,9,10-tetracarboxylic diimide (40 mg, 0.04 mmol) dissolved in DCM (3 mL). The mixture was stirred at room temperature for 2 hours, then NaOH was added to neutralize the reaction until pH = 6-8 and it was extracted with DCM (3 x 20 mL). The combined organic extracts were dried over anhydrous sodium sulphate, filtered and evaporated under reduced pressure to obtain a black solid with a yield 95 % (30 mg, 0.04 mmol). **R_f (DCM:MeOH, 50:4):** 0. **Mp (°C):** > 350 °C. **FT-IR (KBr, cm^{-1}):** 2928 (C-H), 2852 (C-H), 1682 (C=O), 1651 (C=O), 1603 (C_{Ar}-C_{Ar}), 1496 (C_{Ar}-C_{Ar}), 1433 (CH_2), 1406 (CH_2), 1322 (C-N), 1205, 1132, 838, 801, 725 (fingerprint region). **^{1}H NMR (300 MHz, $CDCl_3$) δ:** 8.54 (d, *J* = 5.1 Hz, 2H, H_{Ar}), 8.11 (d, *J* = 5.3 Hz, 2H, H_{Ar}), 7.89 (d, *J* = 8.2, 1.2 Hz, 2H, H_{Ar}), 7.41 (d, *J* = 8.7 Hz, 4H, H_{Ar}), 6.97 (d, *J* = 8.7, 3.6 Hz, 4H, H_{Ar}), 5.00 (m, 2H, N-CH), 3.29 (t, *J* = 5.2 Hz, 8H, CH_2), 3.11 (t, *J* = 5.3 Hz, 8H, CH_2), 2.60 – 2.49 (m, 5H, CH_2), 1.90 (d, *J* = 10.0 Hz, 4H, CH_2), 1.73 (d, *J* = 9.7 Hz, 5H, CH_2), 1.47 – 1.34 (m, 6H, CH_2). **^{13}C NMR (101 MHz, $CDCl_3$) δ:** 164.1 (C=O), 164.0 (C=O), 164.0 (C=O), 164.0 (C=O), 151.4 (C_{quat}-N), 142.7 (C_{quat}-PDI), 135.2 (C_{Ar}), 135.1 (C_{Ar}), 135.1 (C_{Ar}), 134.9 (C_{Ar}), 134.7 (C_{Ar}), 134.7 (C_{Ar}), 132.3 (C_{Ar}), 130.0 (C_{Ar}), 129.9 (C_{Ar}), 129.6 (C_{Ar}), 129.0 (C_{Ar}), 127.5 (C_{Ar}), 127.2 (C_{Ar}), 125.7 (C_{Ar}), 122.6 (C_{Ar}), 122.6 (C_{Ar}), 121.9 (C_{Ar}), 121.8 (C_{Ar}), 116.7 (C_{Ar}), 116.3 (C_{Ar}), 54.1 (NCOCO-**C**H), 49.1 (N-**C**H_2-CH_2-N), 45.8 (N-CH_2-**C**H_2-N), 29.7 (CH_2), 29.1 (CH_2), 26.7 (CH_2), 25.4 (CH_2). **HRMS (MALDI+, DIT):** m/z calcd. for $C_{56}H_{54}N_6O_4$ ([M+H]$^+$): 875.4279; found: 875.4387.

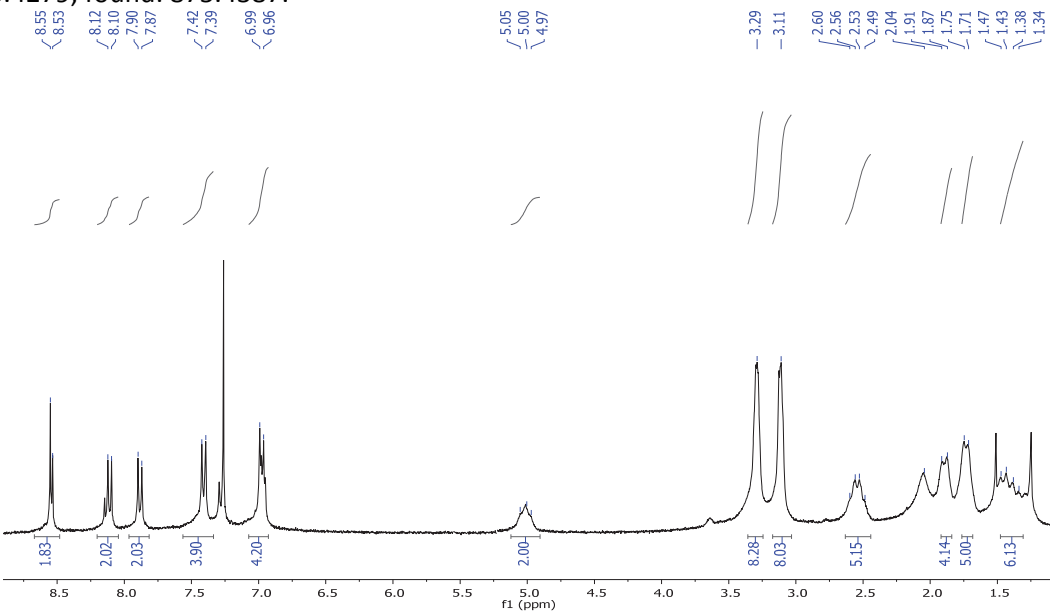

Figure 48. ^{1}H NMR (300 MHz, $CDCl_3$) of PC114

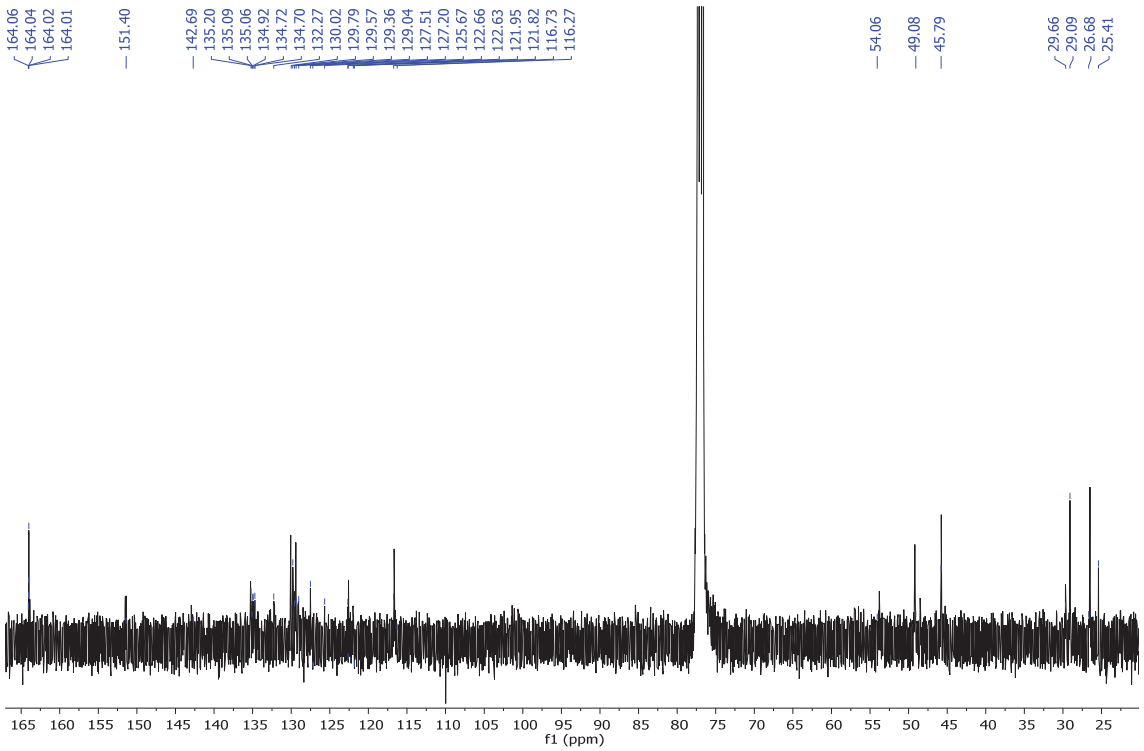

Figure 49. ^{13}C NMR (101 MHz, $CDCl_3$) of PC114

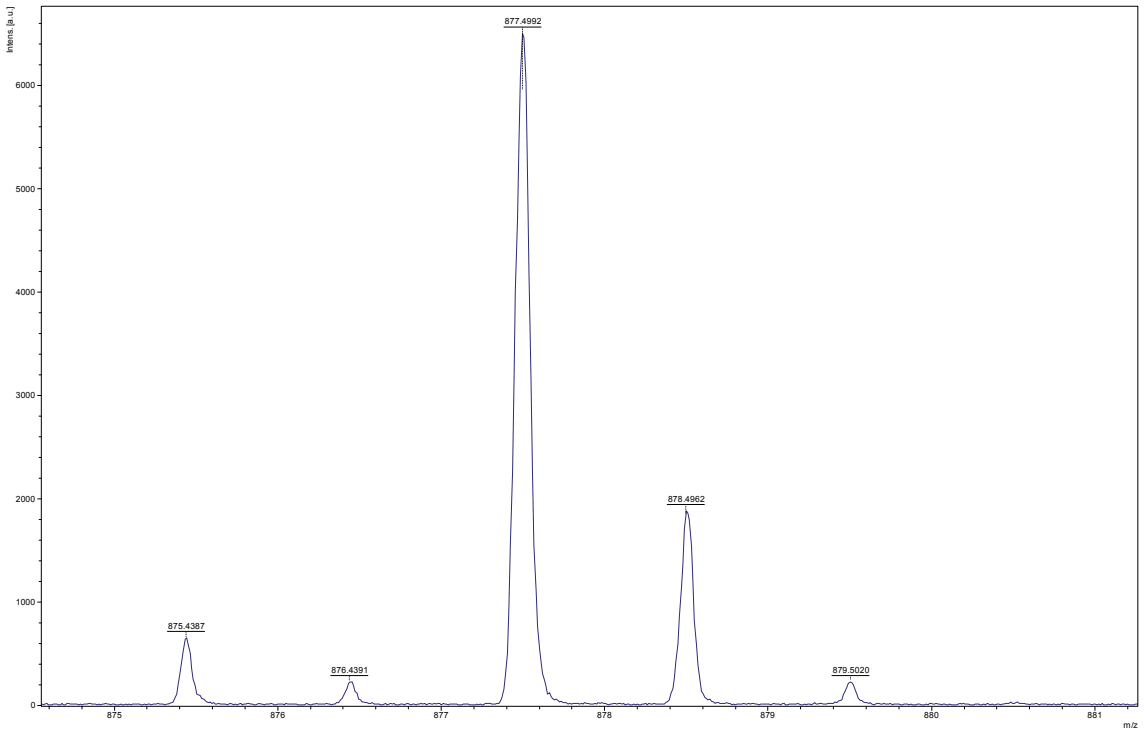

Figure 50. Mass spectrum (MALDI+, DIT) of PC114

1.11. Synthesis of *N,N'*-bis(cyclohexyl)-1,7-bis-(4-[4-(*N''*-*tert*-butoxycarbonyl)piperazin-1-yl]pyridil)perylene-3,4,9, 10-tetracarboxylic diimide (1,7-PC57).

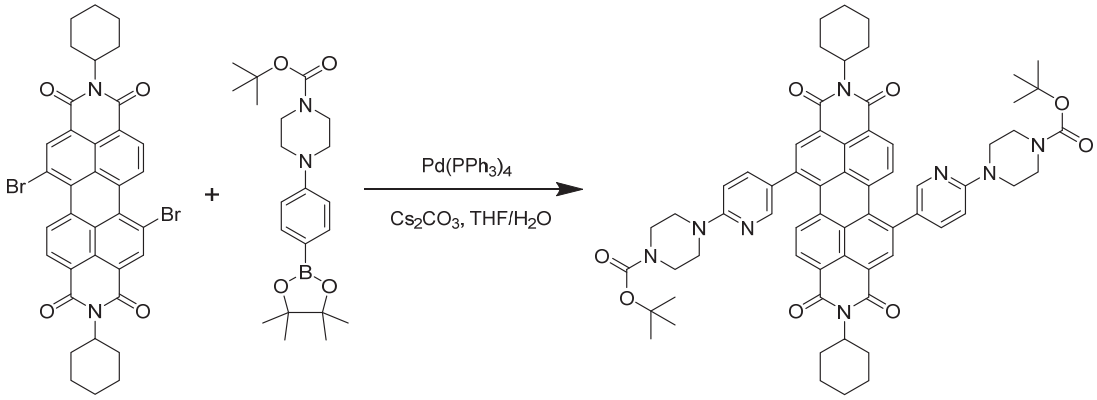

PC37 **1,7-PC57**

4-[4-(*N''*-*tert*-butoxycarbonyl)piperazin-1-yl]pyridine-5-boronic acid pinacol ester (89.5 mg, 0.23 mmol), cesium carbonate (0.11 mg, 0.34 mmol) and a catalytic amount of tetrakis (triphenylphosphine) palladium (0) were added under nitrogen to *N,N'*-bis(cyclohexyl)-1,6- and 1,7-dibromoperylene-3,4,9,10-tetracarboxylic diimide (89 mg, 0.11 mmol) dissolved in THF:H_2O (12:1.2 mL). The mixture was heated at reflux for 24 hours and extracted with DCM (3 x 20 mL). The combined organic extracts were dried over anhydrous sodium sulphate, filtered and evaporated under reduced pressure. Purification was carried out by silica gel flash chromatography using DCM:MeCN (80:20) a mixture of 1,6- and 1,7-PC57 with a yield 60 % (71 mg, 0.06 mmol). Further silica gel flash chromatography using DCM:MeCN (80:20) gave 1,7-PC57 with a 10% yield (12 mg, 0.01 mmol). **R_f (DCM:MeOH, 50:2):** 0.29. **Mp (°C):** > 350 °C. **FT-IR (KBr, cm^{-1}):** 2927 (C-H), 2858 (C-H), 1700 (C=O), 1658 (C=O), 1589 (C_{Ar}-C_{Ar}), 1544 (C_{Ar}-C_{Ar}), 1496 (C_{Ar}-C_{Ar}), 1447 (CH_2), 1406 (CH_2), 1368, 1323 (C-N), 1240, 1164, 1129, 998, 925, 859, 811, 763, 718 (fingerprint region). **^{1}H NMR (400 MHz, $CDCl_3$) *δ*:** 8.53 (s, 2H, H_{Ar}), 8.39 (s, 2H, H_{Ar}), 8.18 (d, *J* = 8.1 Hz, 2H, H_{Ar}), 7.98 (d, *J* = 8.1 Hz, 2H, H_{Ar}), 6.69 (d, *J* = 8.8 Hz, 2H, H_{Ar}), 5.04 – 4.98 (m, 2H, N-CH), 3.67 – 3.62 (m, 16H, CH_2), 2.58 – 2.50 (m, 5H, CH_2), 1.90 (d, *J* = 12.4 Hz, 4H, CH_2), 1.74 (d, *J* = 11.3 Hz, 5H, CH_2), 1.51 (s, 14H, C-(CH_3)$_3$), 1.48 – 1.35 (m, 6H, CH_2). **^{13}C NMR (101 MHz, $CDCl_3$) *δ*:** 164.0 (C=O), 163.9 (C=O), 158.6 (C_{quat}-N), 154.9 (**C**OOC(CH_3)$_3$), 148.3 (C_{quat}-N), 138.6 (C_{quat}-PDI), 137.9 (C_{quat}-PDI), 135.2 (C_{Ar}), 135.0 (C_{quat}), 132.3 (C_{quat}), 129.6 (C_{Ar}), 129.4 (C_{Ar}), 127.9 (C_{quat}), 127.3 (C_{quat}), 123.1 (C_{quat}), 122.4 (C_{quat}), 107.5 (C_{Ar}), 80.3 (**C**(CH_3)$_3$), 54.1 (NCOCO-**C**H), 44.9 (N-**C**H_2-CH_2-N), 29.9 (CH_2), 29.3 (CH_2), 28.6 (CH_3), 26.7(CH_2), 25.6 (CH_2). **HRMS (MALDI+, DCTB):** m/z calcd for $C_{64}H_{68}N_8O_8$ ([M]$^+$): 1076.5156; found: 1076.5155.

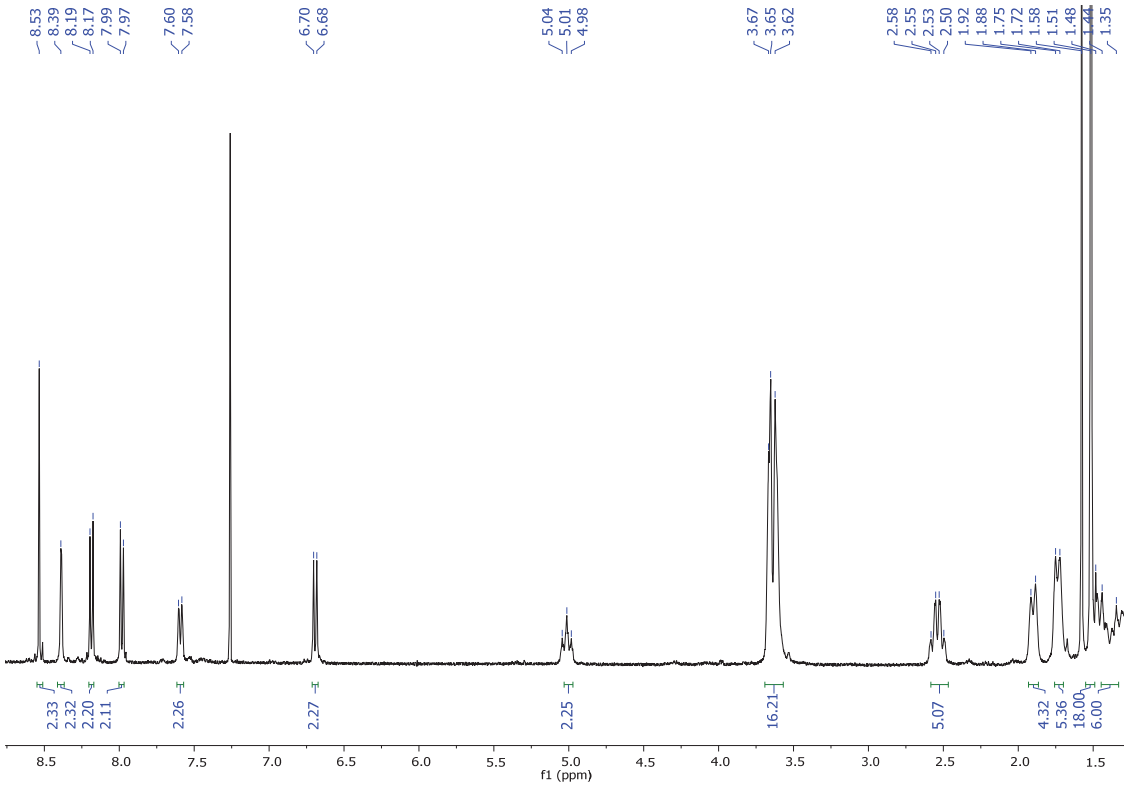

Figure 51. ^{1}H NMR (400 MHz, $CDCl_3$) of 1,7-PC57

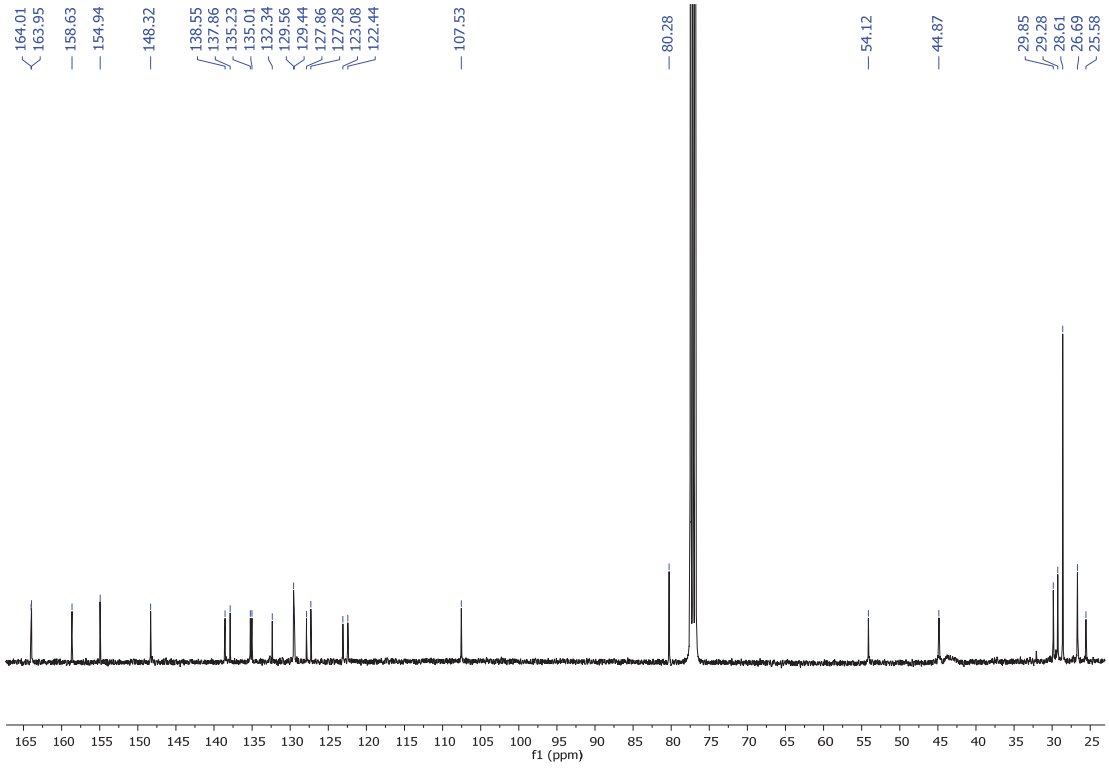

Figure 52. ^{13}C NMR (101 MHz, $CDCl_3$) of 1,7-PC57

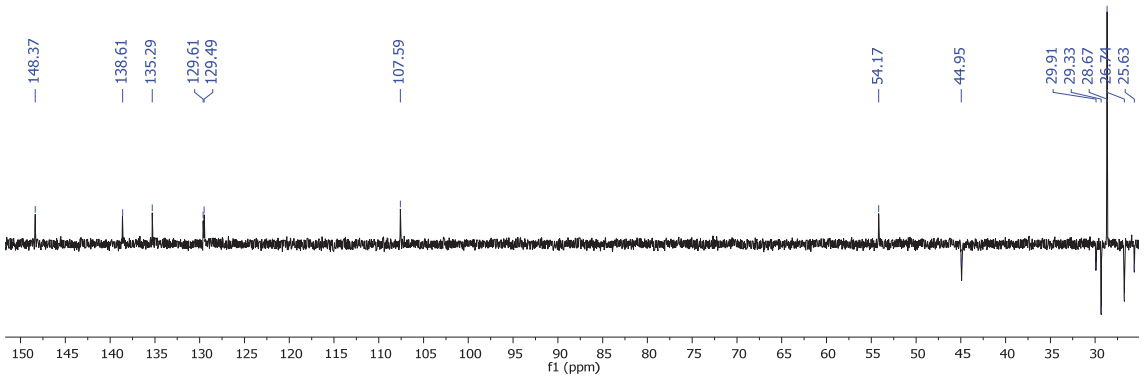

Figure 53. ^{13}C NMR-DEPT-135 (101 MHz, $CDCl_3$) of 1,7-PC57

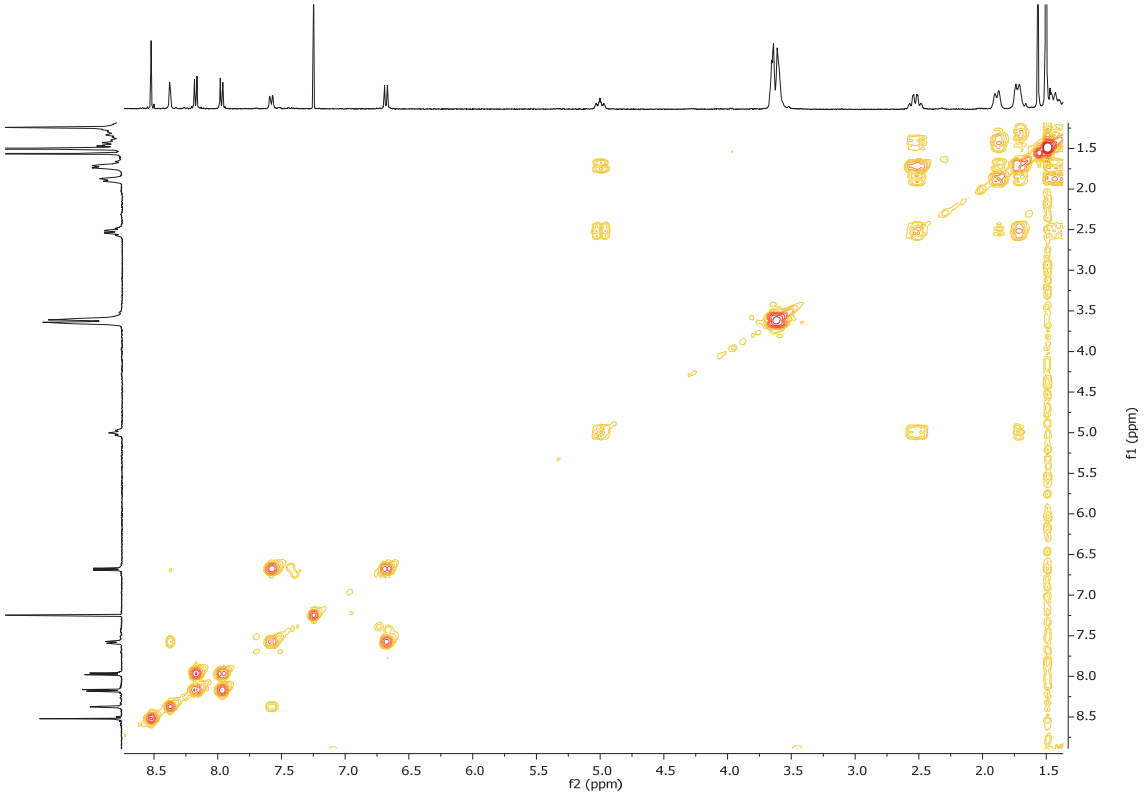

Figure 54. ^{1}H-^{1}H-COSY spectrum of 1,7-PC57

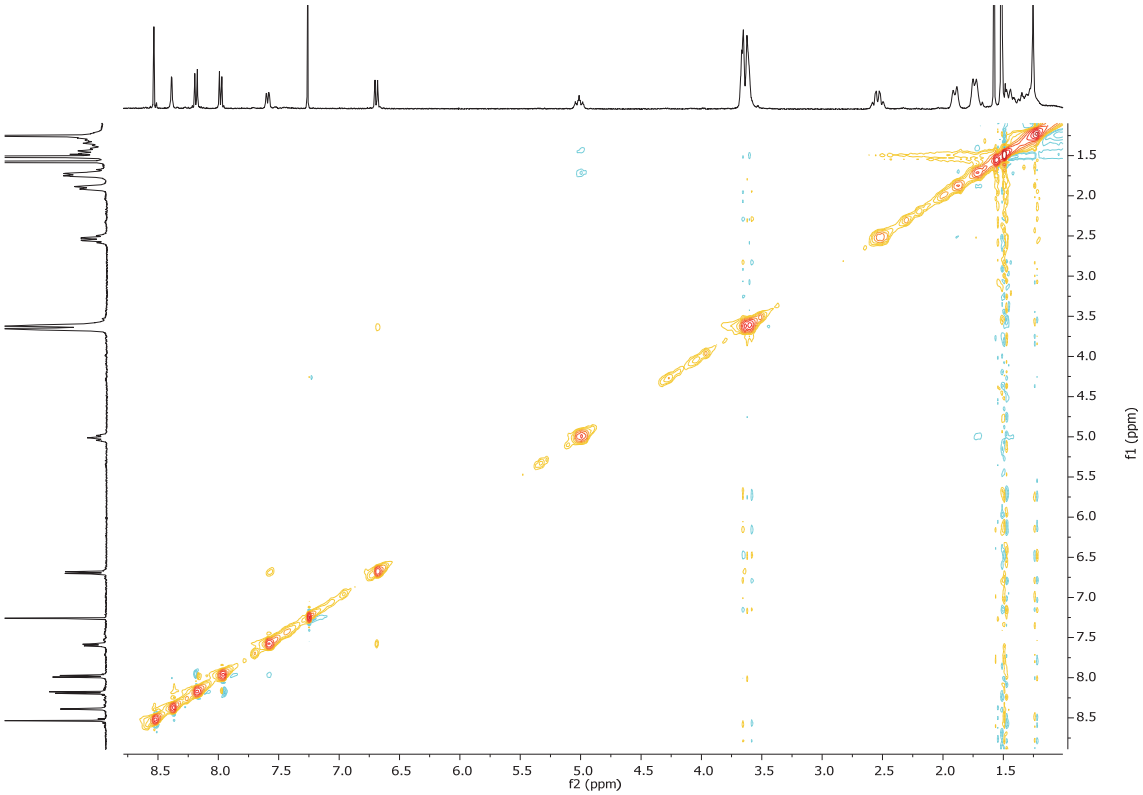

Figure 55. ^{1}H-^{1}H-NOESY spectrum of 1,7-PC57

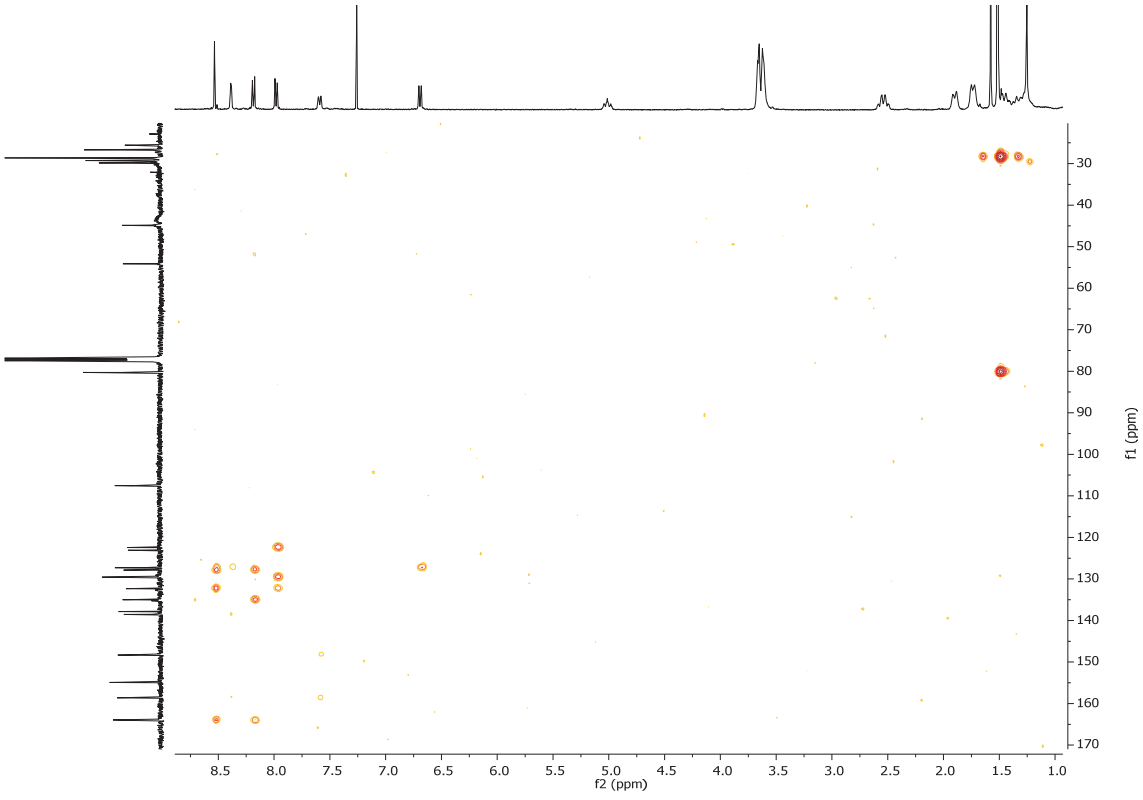

Figure 56. ^{1}H-^{13}C-HMBC spectrum of 1,7-PC57

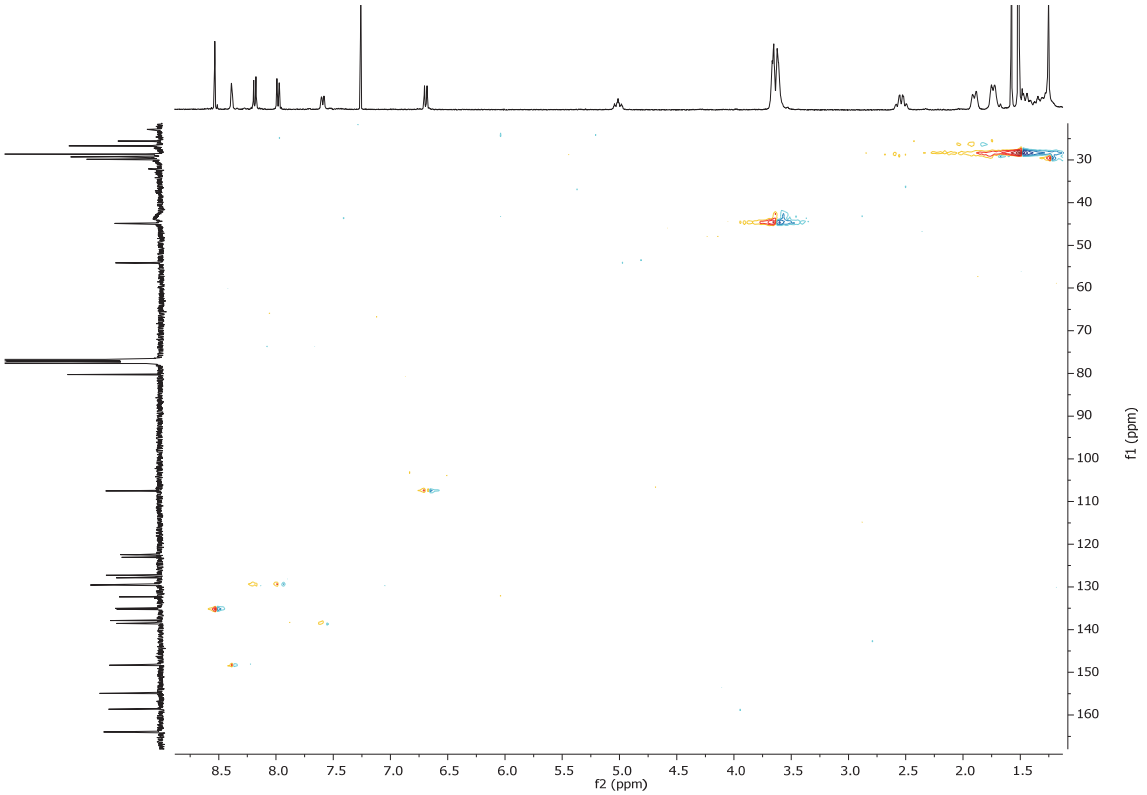

Figure 57. ^{1}H-^{13}C-HMQC spectrum of 1,7-PC57

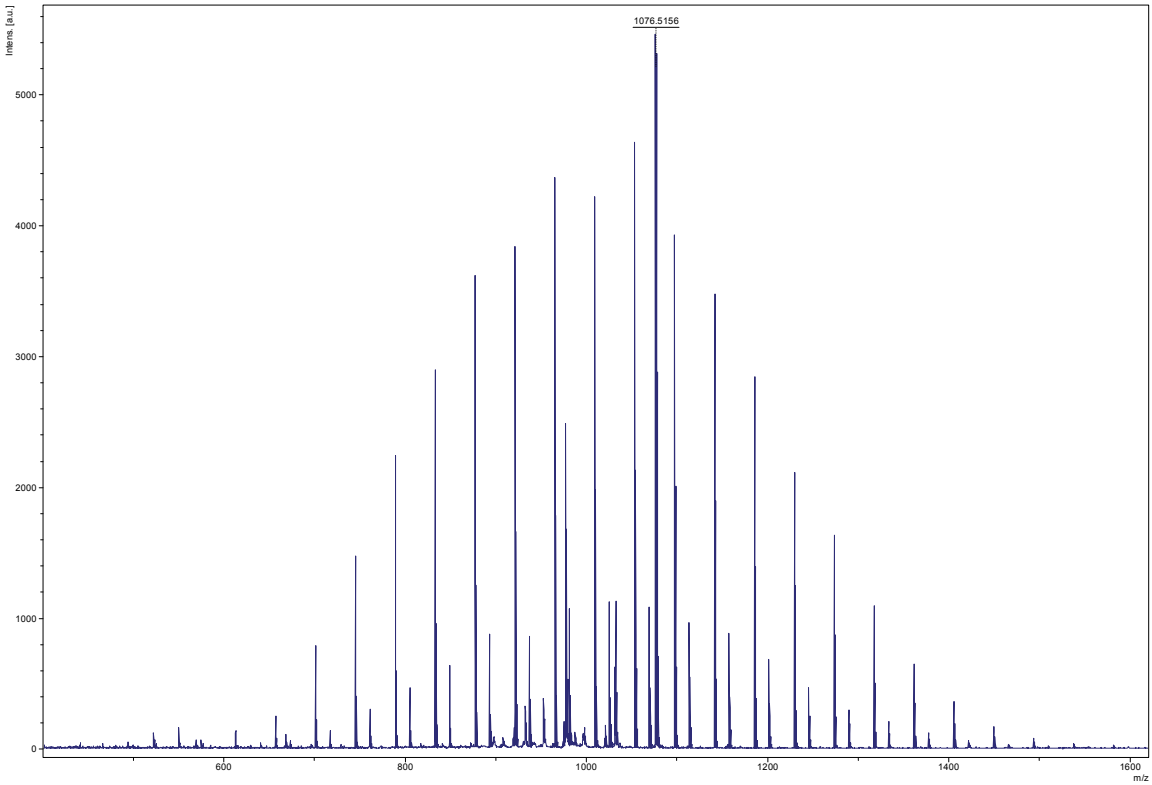

Figure 58. Mass spectrum (MALDI+, DCTB) of 1,7-PC57

Solvatochromism:

The concentration of **PC57** is $1 \cdot 10^{-5}$ M. The excitation wavelength is 450 nm. The absorption and emission spectra have been measured in the listed solvents below in the range between 200 to 900 nm. The used solvents are: MeOH, DMSO, DMF, MeCN, acetone, AcOEt, THF, $CHCl_3$, DCM, toluene, diethyl ether, hexane and cyclohexane.

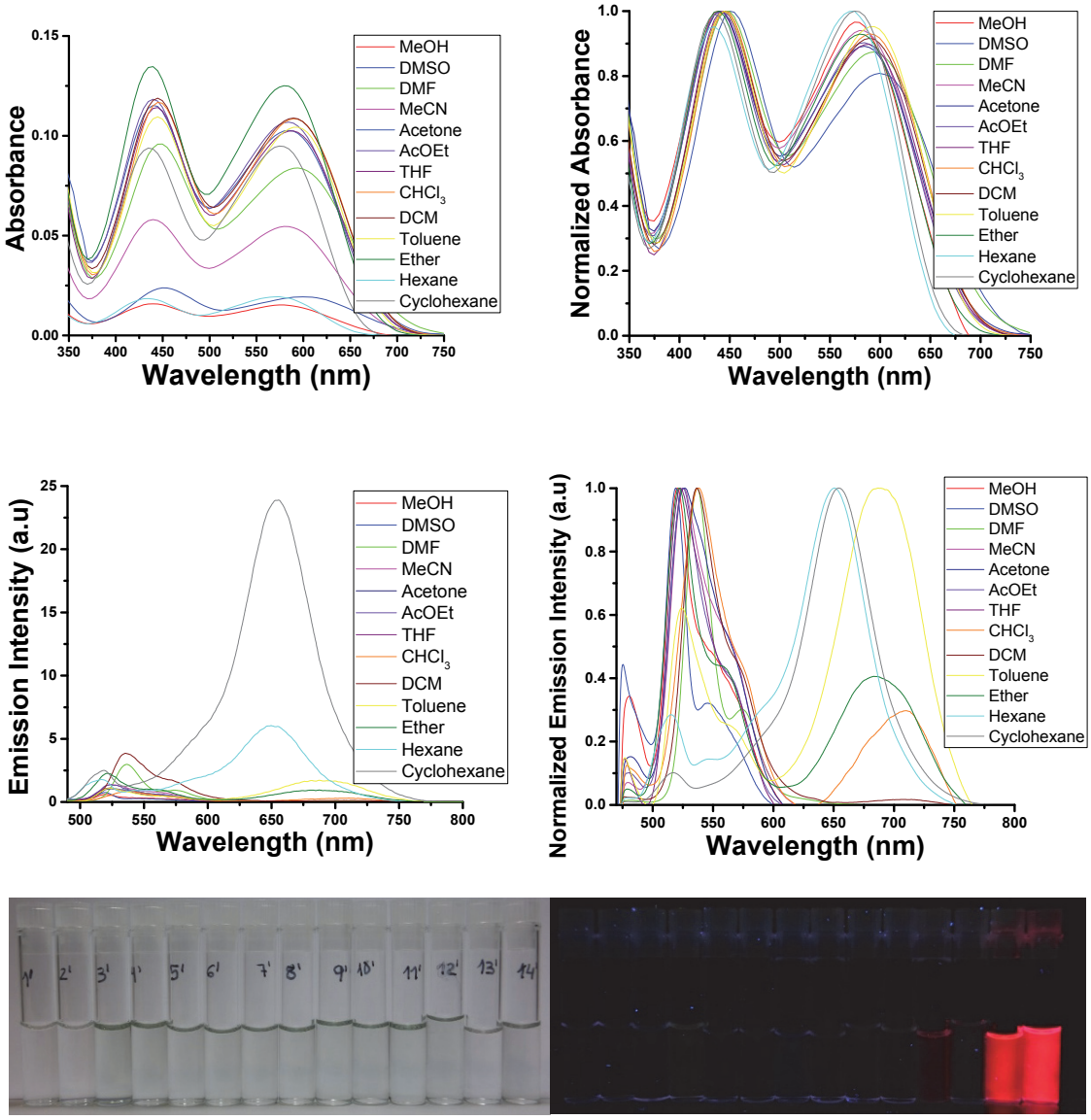

Solvents: 1: Water, 2: MeOH, 3: DMSO, 4: DMF, 5: MeCN, 6: acetone, 7: AcOEt, 8: THF, 9: $CHCl_3$, 10: DCM, 11: toluene, 12: diethyl ether, 13: hexane, 14: cyclohexane.

Figure 59. Upper. Absorbance and Normalized absorbance spectra of PC57. Middle: Fluorescence and Normalized fluorescence spectra of PC57. Lower. Solvatochromic effect of PC57 under white light and light of 366 nm.

1.12. Synthesis of *N,N'*-bis(cyclohexyl)-1,7-bis-((4-[4-piperazin-1-yl]pyridil))perylene-3,4,9,10-tetracarboxylic diimide (1,7-PC115).

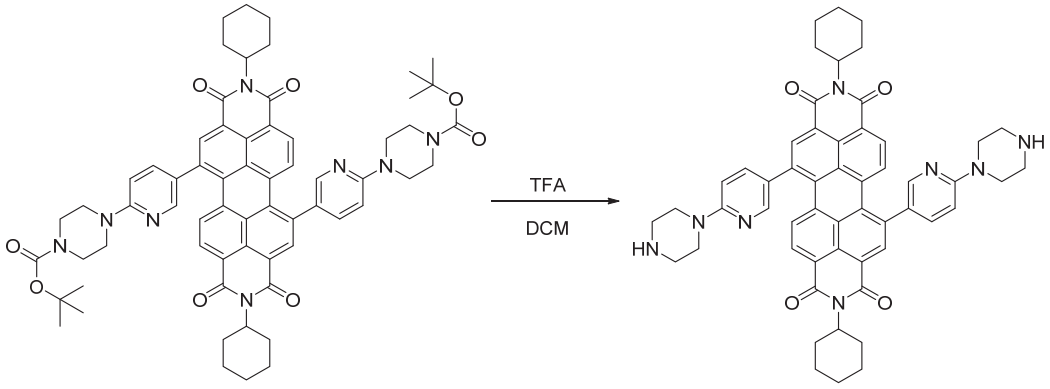

1,7-PC57 **1,7-PC115**

Trifluoroacetic acid (557 µL, 4.86 mmol) was added dropwise to *N,N'*-bis(cyclohexyl)-1,7-di-(4-[4-(*N''-tert*-butoxycarbonyl)piperazin-1-yl]pyridil)perylene-3,4,9,10-tetracarboxylic diimide (40 mg, 0.04 mmol) dissolved in DCM (4 mL). The mixture was stirred at room temperature for 2 hours, then NaOH was added to neutralize the reaction until pH = 6-8 and it was extracted with DCM (3 x 20 mL). The combined organic extracts were dried over anhydrous sodium sulphate, filtered and evaporated under reduced pressure to obtain a black solid with a yield 95 % (30 mg, 0.04 mmol). **R_f (DCM:MeOH, 50:4):** 0. **Mp (°C):** > 350 °C. **FT-IR (KBr, cm^{-1}):** 2955 (C-H), 2924 (C-H), 2855 (C-H), 1738, 1697 (C=O), 1655 (C=O), 1590 (C_{Ar}-C_{Ar}), 1492 (C_{Ar}-C_{Ar}), 1455 (CH_2), 1416 (CH_2), 1378 (C-N), 1243, 1130, 811, 728, 618 (fingerprint region). **^{1}H NMR (300 MHz, $CDCl_3$) δ:** 8.56 – 8.55 (d, *J* = 12.8 Hz, 2H, H_{Ar}), 8.52 (s, 1H, H_{Ar}), 8.41 (s, 1H, H_{Ar}), 8.29 – 8.19 (m, 2H, H_{Ar}), 8.04 – 7.97 (m, 2H, H_{Ar}), 7.60 (d, *J* = 6.7 Hz, 1H, H_{Ar}), 7.43 (s, 1H, H_{Ar}), 6.72 – 6.67 (m, 2H, H_{Ar}), 5.04 – 4.98 (m, 2H, N-CH), 3.67 (d, *J* = 23.5 Hz, 9H, CH_2), 3.13 (s, 7H, CH_2), 2.57 – 2.51 (m, 5H, CH_2), 1.88 (s, 5H, CH_2), 1.74 (s, 4H, CH_2), 1.46 – 1.34 (m, 6H, CH_2). **HRMS (MALDI+, DIT):** m/z calcd. for $C_{54}H_{52}N_8O_4$ [$(M+H)^+$]: 877.4184; found: 877.4149.

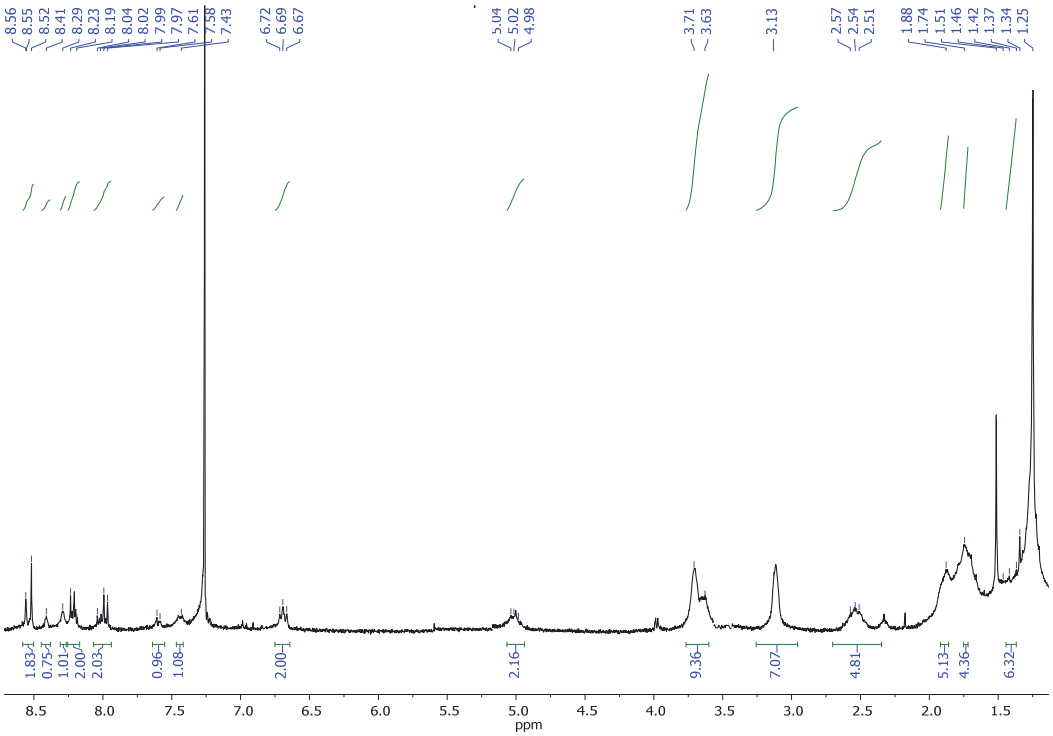

Figure 60. ^{1}H NMR (300 MHz, $CDCl_3$) of 1,7-PC115

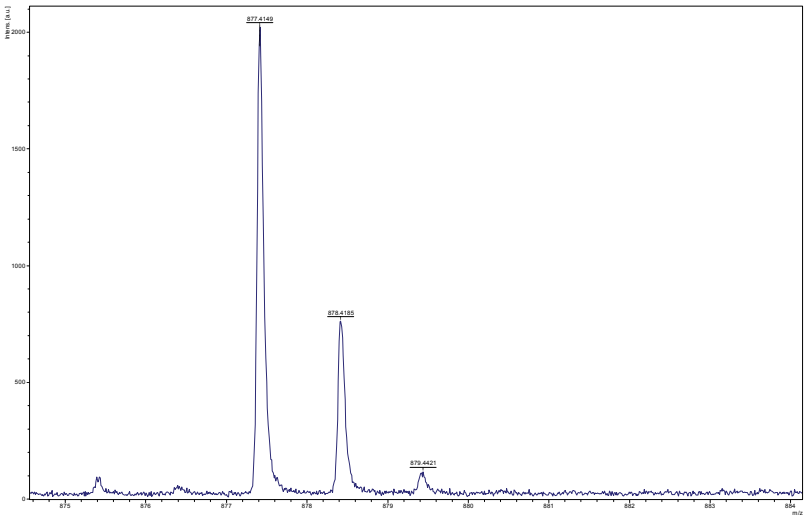

Figure 61. Mass spectrum (MALDI+, DIT) of PC115

1.13. Synthesis of *N,N'*-bis(cyclohexyl)-1,7-bis-(4-[4-(*N''*-*tert*-butoxycarbonyl)piperazin-1-yl]pyrimidine)perylene-3,4,9,10-tetracarboxylic diimide (1,7-PC60).

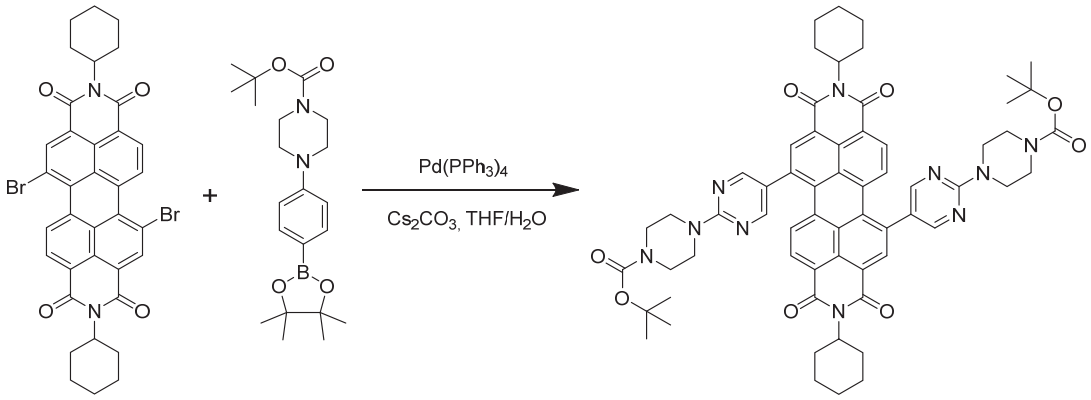

PC37 **1,7-PC60**

4-[4-(*N''*-*tert*-butoxycarbonyl)piperazin-1-yl]pyrimidine-5-boronic acid pinacol ester (289 mg, 0.74 mmol), cesium carbonate (342 mg, 1.05 mmol) and a catalytic amount of tetrakis (triphenylphosphine) palladium (0) were added under nitrogen to *N,N'*-bis(cyclohexyl)-1,6- and 1,7-dibromoperylene-3,4,9,10-tetracarboxylic diimide (250 mg, 0.35 mmol) dissolved in THF:H_2O (50:5 mL). The mixture was heated at reflux for 24 hours and extracted with DCM (3 x 20 mL). The combined organic extracts were dried over anhydrous sodium sulphate, filtered and evaporated under reduced pressure. Purification was carried out by silica gel flash chromatography using DCM:MeCN (80:20) as eluent to give compound as eluent to give a mixture of 1,6- and 1,7-PC60 with a yield 60 % (226 mg, 0.21 mmol). Further silica gel flash chromatography using DCM:MeCN (80:20) gave 1,7-PC60 with a 10% yield (37 mg, 0.03 mmol). **R_f (DCM:MeOH, 50:2):** 0.7. **Mp (°C):** > 350 °C. **FT-IR (KBr, cm^{-1}):** 2972 (C-H), 2927 (C-H), 2855 (C-H), 1696 (C=O), 1658 (C=O), 1589 (C_{Ar}-C_{Ar}), 1513, 1454 (CH_2), 1413 (CH_2), 1392 (C-N), 1361, 1347, 1323, 1240, 1164, 1129, 998, 859, 756, 714 (fingerprint region). **^{1}H NMR (300 MHz, $CDCl_3$) δ:** 8.49 (s, 6H, H_{Ar}), 8.27 (d, *J* = 8.2 Hz, 2H, H_{Ar}), 8.06 (d, *J* = 8.1 Hz, 2H, H_{Ar}), 5.05 – 4.96 (m, 2H, N-CH), 3.89 (t, *J* = 3.5 Hz, 8H, CH_2), 3.57 (t, *J* = 3.4 Hz, 8H, CH_2), 2.58 – 2.47 (m, 5H, CH_2), 1.90 (d, *J* = 11.1 Hz, 4H, CH_2), 1.74 (d, *J* = 10.6 Hz, 5H, CH_2), 1.51 (s, 18H, CH_3), 1.44 – 1.35 (m, 6H, CH_2). **^{13}C NMR (101 MHz, $CDCl_3$) δ:** 164.3 (C=O), 163.8 (C=O), 163.7 (C=O), 160.8 (C_{quat}-N), 158.1 (C_{quat}-N), 154.9 (**C**OOC$(CH_3)_3$), 134.9 (C_{Ar}), 134.9 (C_{Ar}), 134.8 (C_{quat}), 132.3 (C_{quat}), 129.9 (C_{Ar}), 129.3 (C_{Ar}), 128.1 (C_{quat}), 124.5 (C_{quat}), 123.5 (C_{quat}), 122.8 (C_{quat}), 80.3 (**C**$(CH_3)_3$), 54.2

(NCOCO-**C**H), 43.9 (N-**C**H_2-CH_2-N), 43.6 (N-CH_2-**C**H_2-N), 29.3 (CH_2), 28.6 (CH_3), 26.8 (CH_2), 25.6 (CH_2), 24.9 (CH_2). **HRMS (MALDI+, DCTB):** m/z calcd. for $C_{62}H_{66}N_{10}O_8$ ($[M]^+$): 1078.5060; found: 1078.5146.

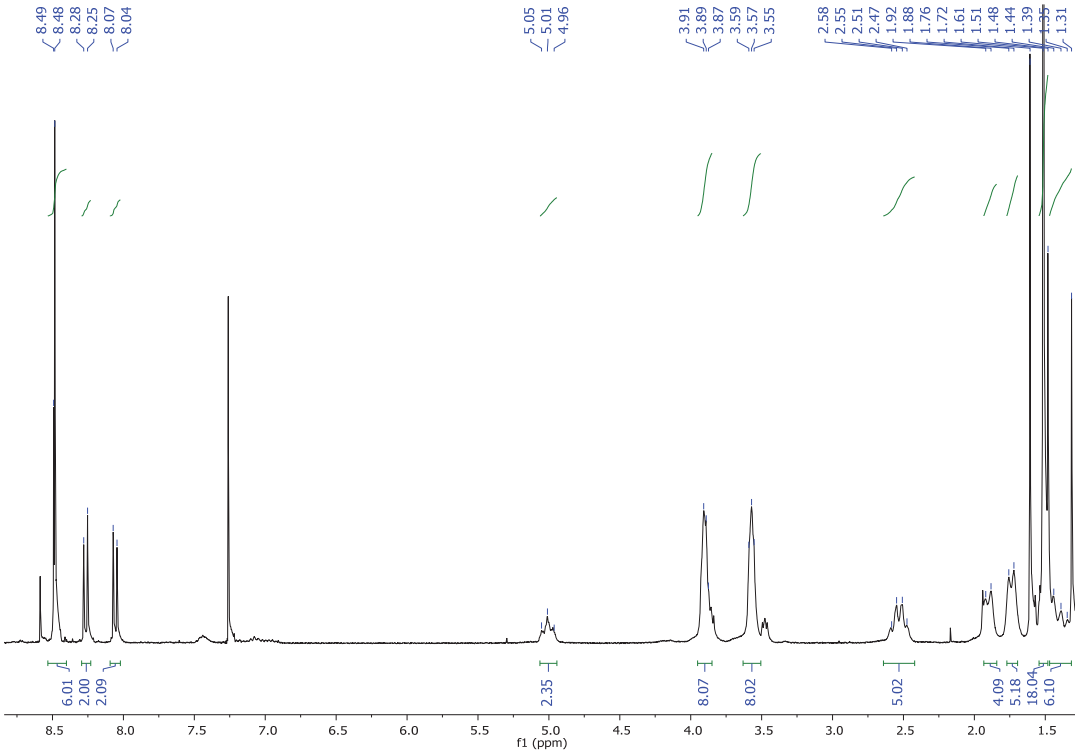

Figure 62. ^{1}H NMR (300 MHz, $CDCl_3$) of 1,7-PC60

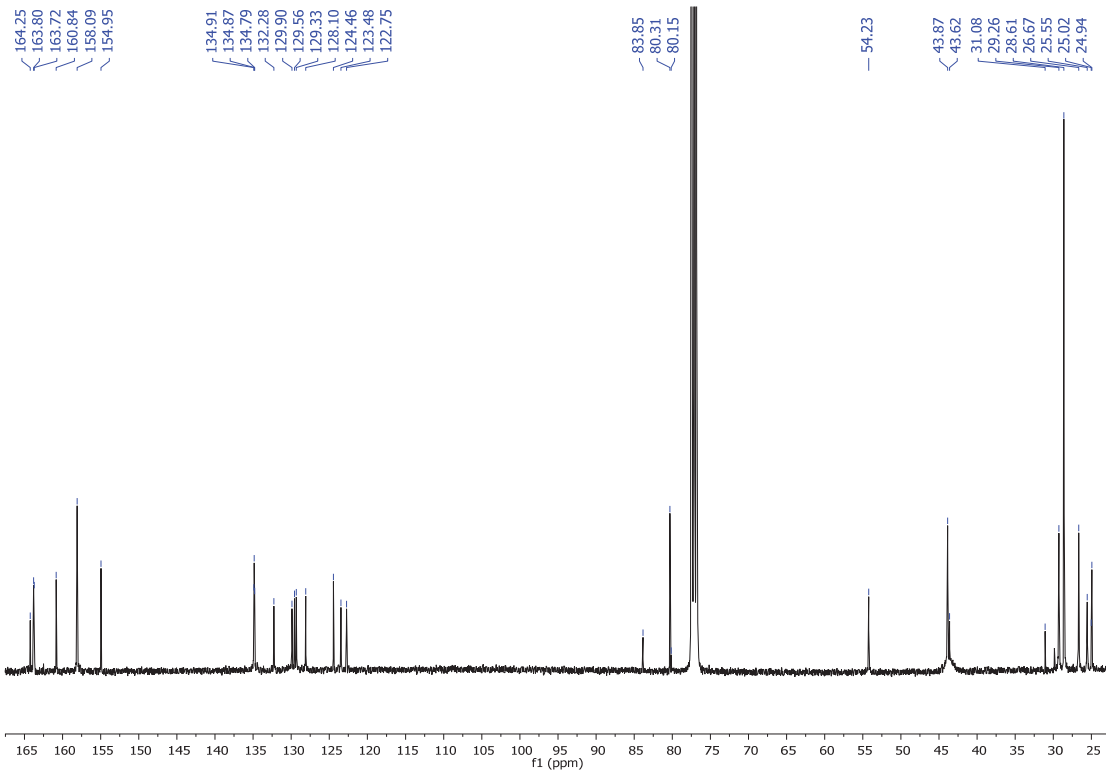

Figure 63. ^{13}C NMR (101 MHz, $CDCl_3$) of 1,7-PC60

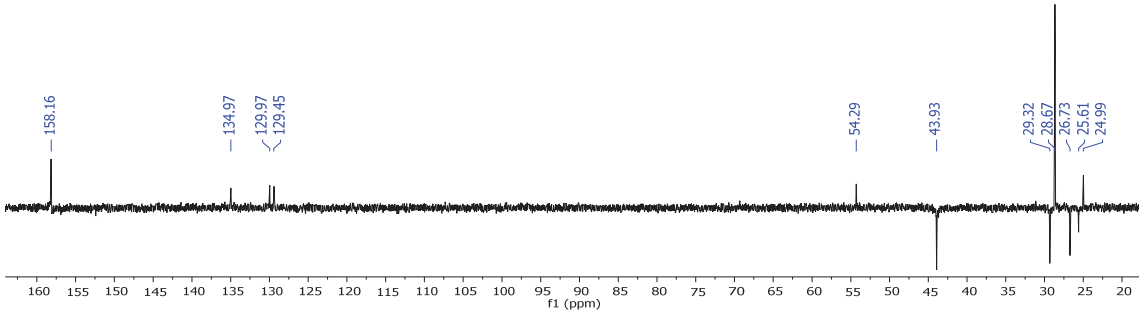

Figure 64. ^{13}C NMR-DEPT-135 (101 MHz, $CDCl_3$) of 1,7-PC60

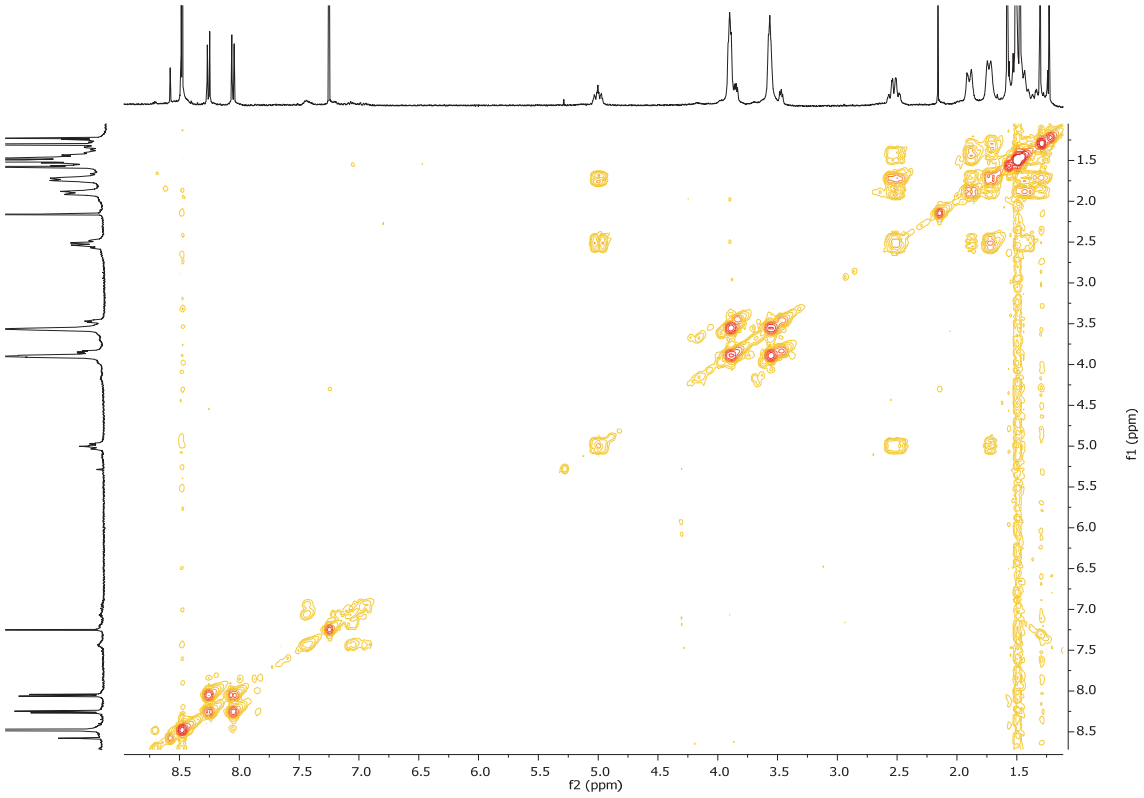

Figure 65. ^{1}H-^{1}H-COSY spectrum of 1,7-PC60

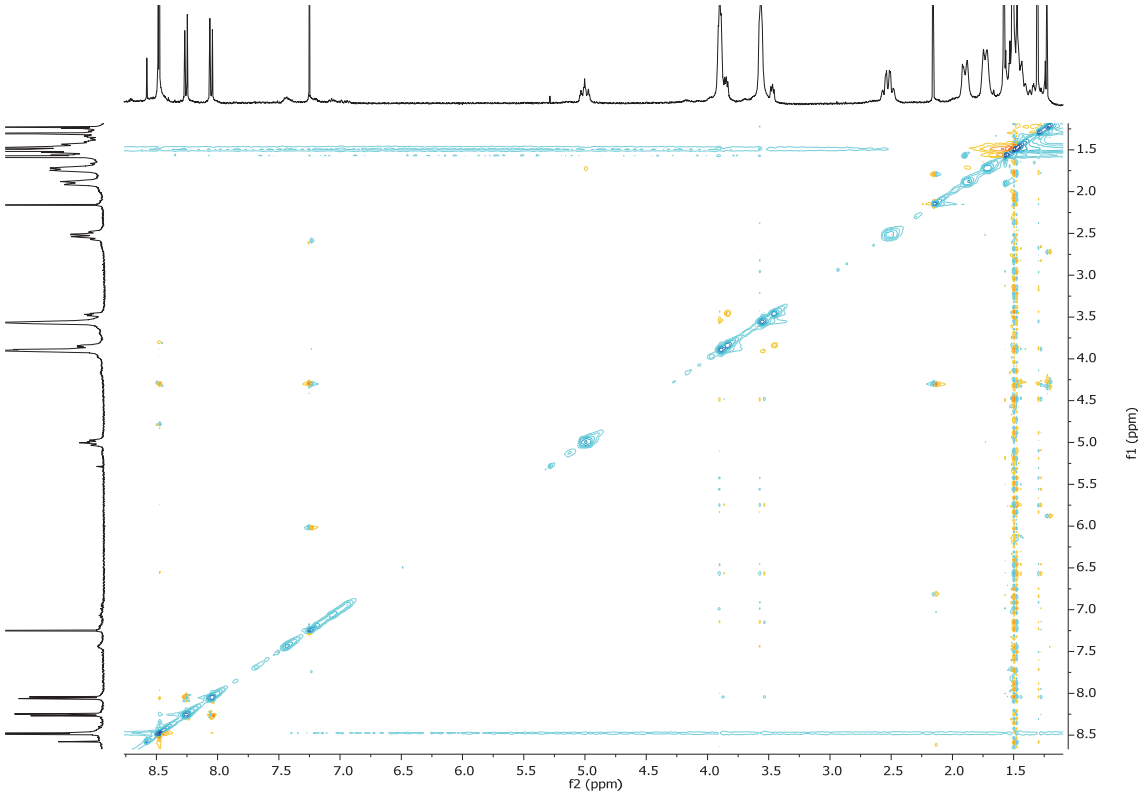

Figure 66. ^{1}H-^{1}H-NOESY spectrum of 1,7-PC60

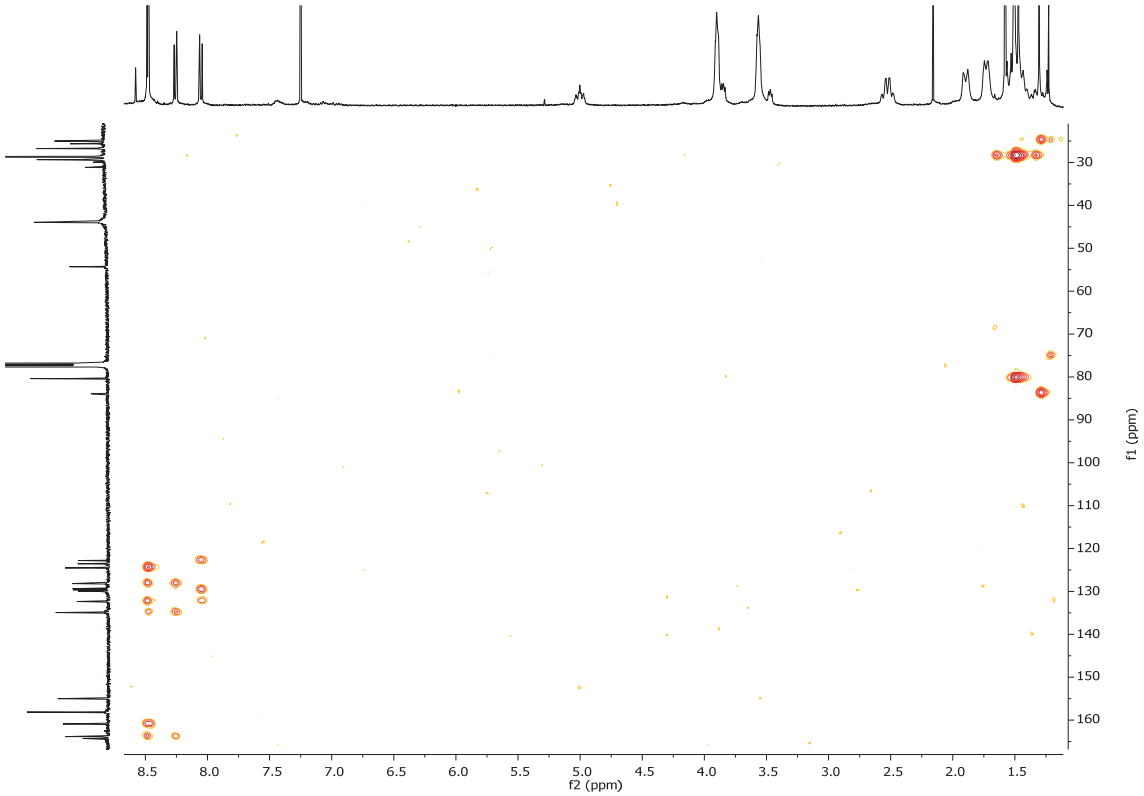

Figure 67. ^{1}H-^{13}C-HMBC spectrum of 1,7-PC60

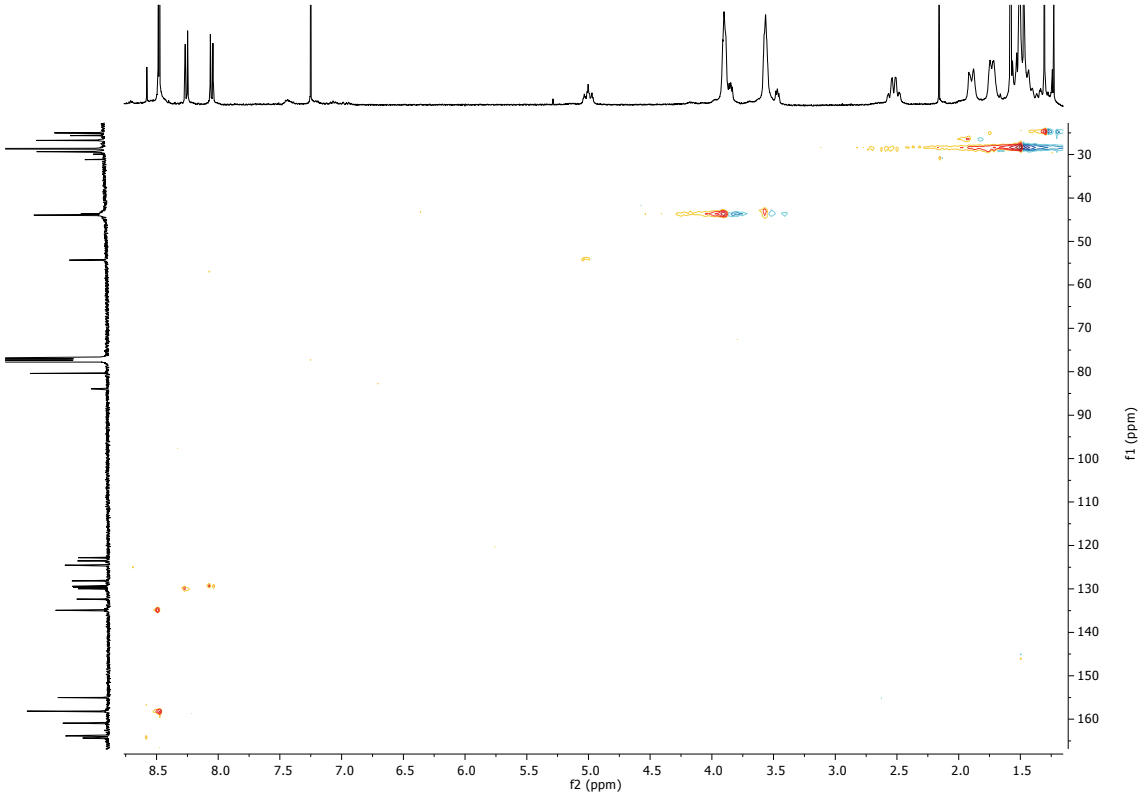

Figure 68. ^{1}H-^{13}C-HMQC spectrum of 1,7-PC60

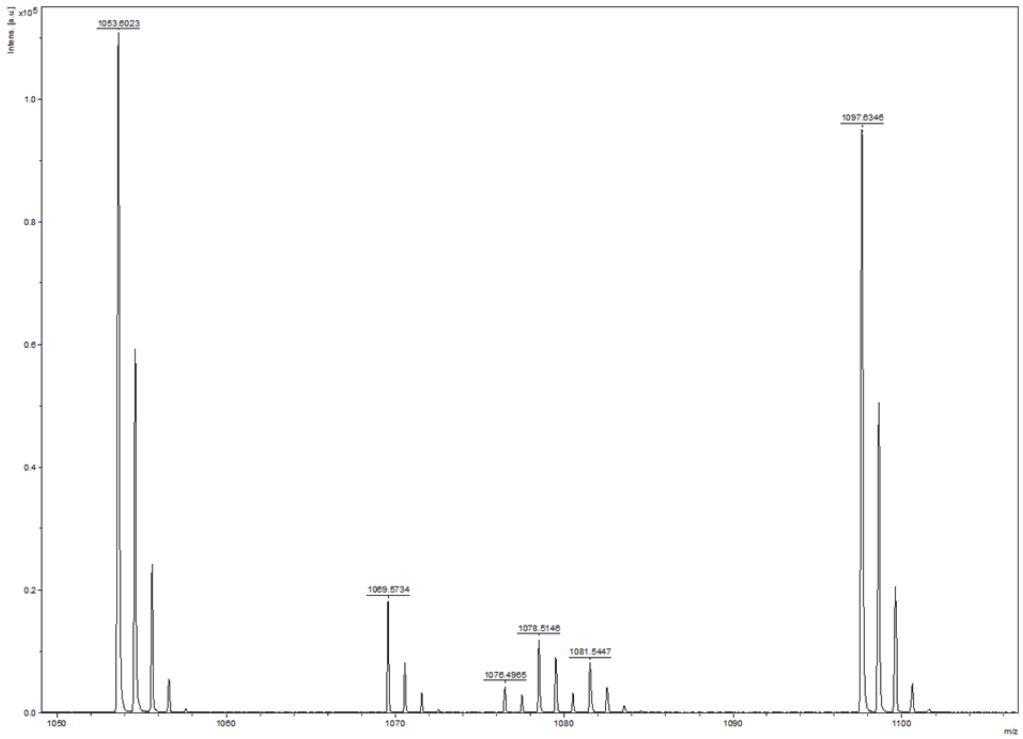

Figure 69. Mass spectrum (MALDI+, DCTB) of 1,7-PC60

Solvatochromism:

The concentration of **PC60** is $1 \cdot 10^{-5}$ M. The excitation wavelength is 430 nm. The absorption and emission spectra have been measured in the listed solvents below in the range between 200 to 900 nm. The used solvents are: MeOH, DMSO, DMF, MeCN, acetone, AcOEt, THF, $CHCl_3$, DCM, toluene, diethyl ether, hexane and cyclohexane.

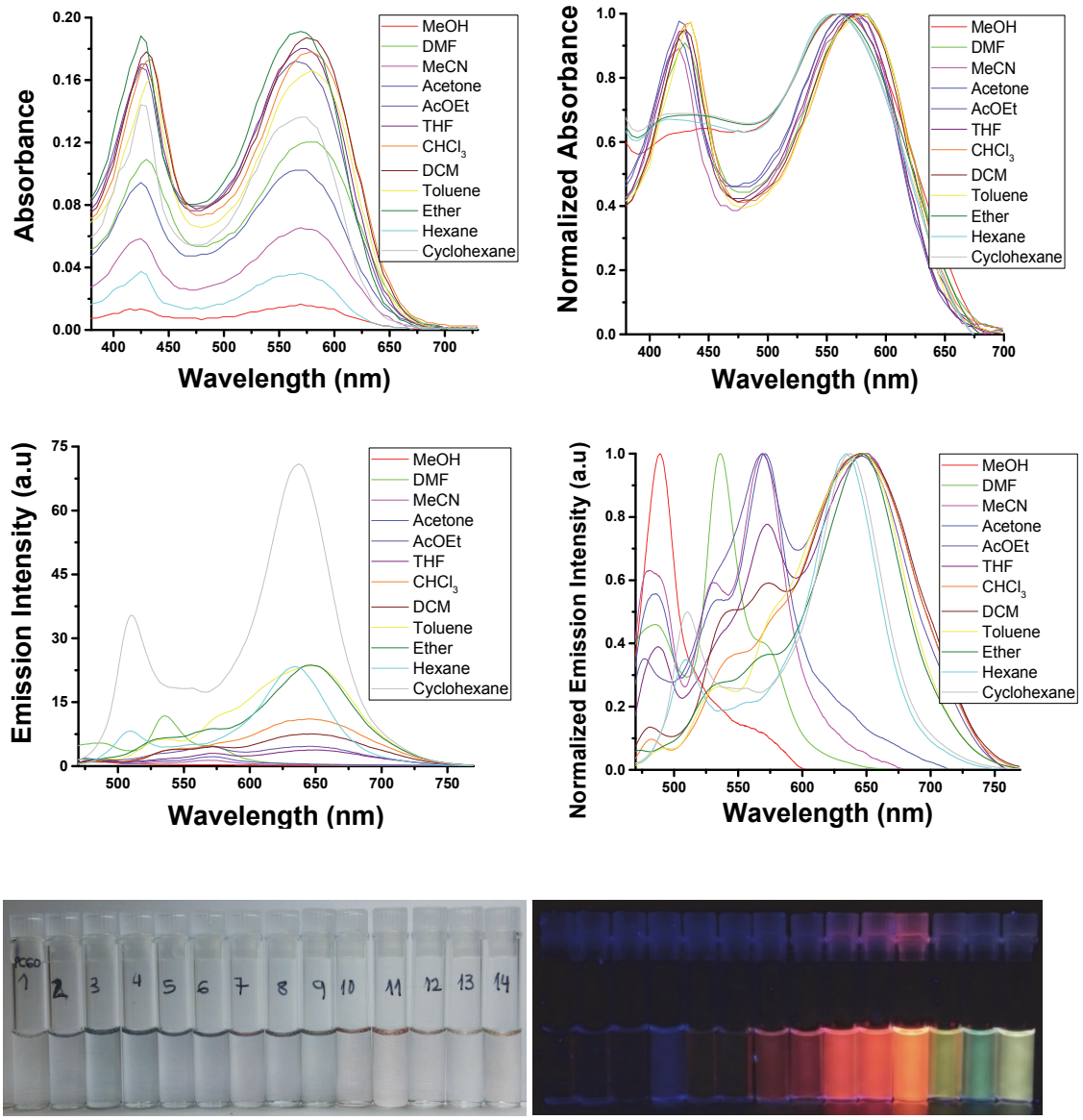

Solvents: 1: Water, 2: MeOH, 3: DMSO, 4: DMF, 5: MeCN, 6: acetone, 7: AcOEt, 8: THF, 9: $CHCl_3$, 10: DCM, 11: toluene, 12: diethyl ether, 13: hexane, 14: cyclohexane.

Figure 70. Upper. Absorbance and Normalized absorbance spectra of PC60. Middle: Fluorescence and Normalized fluorescence spectra of PC60. Lower. Solvatochromic effect of PC60 under white light and light of 366 nm.

1.14. Synthesis of *N,N'*-bis(cyclohexyl)-1,7-bis-(2-[piperazin-1-yl]pyrimidin)perylene-3,4,9,10-tetracarboxylic diimide (1,7-PC116).

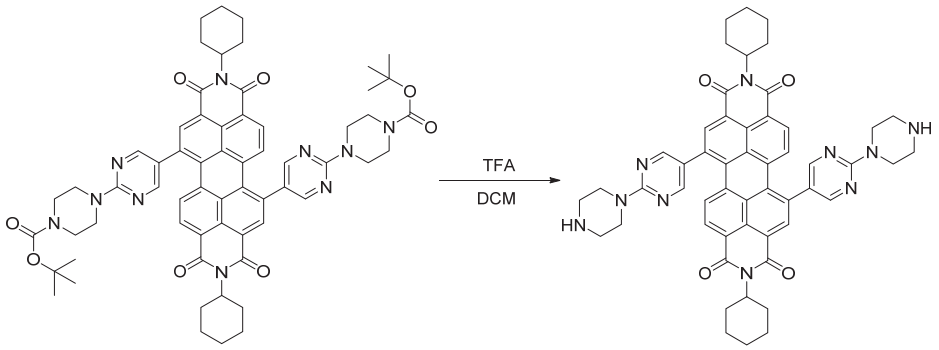

1,7-PC60 **1,7-PC116**

Trifluoroacetic acid (557 µL, 4.86 mmol) was added dropwise to *N,N'*-bis(cyclohexyl)-1,7-di-(4-[4-(*N''-tert*-butoxycarbonyl)piperazin-1-yl]pyridimidin)perylene-3,4,9,10-tetracarboxylic diimide (40 mg, 0.037 mmol) dissolved in DCM (4 mL). The mixture was stirred at room temperature for 2 hours, then NaOH was added to neutralize the reaction until pH = 6-8 and it was extracted with DCM (3 x 20 mL). The combined organic extracts were dried over anhydrous sodium sulphate, filtered and evaporated under reduced pressure to obtain a black solid with a yield 95 % (30 mg, 0.04 mmol). **R_f (DCM:MeOH, 50:4):** 0. **Mp (°C):** > 350 °C. **FT-IR (KBr, cm^{-1}):** 2926 (C-H), 2852 (C-H), 1696 (C=O), 1655 (C=O), 1588 (C_{Ar}-C_{Ar}), 1448 (CH_2), 1394 (C-N), 1343, 1318, 1255, 1198, 1132, 1042, 951, 916, 862, 814, 797, 721 (fingerprint region). **^{1}H NMR (400 MHz, $CDCl_3$) δ:** 8.48 (d, *J* = 5.1 Hz, 3H, H_{Ar}), 8.35 (s, 3H, H_{Ar}), 8.30 (d, *J* = 7.9 Hz, 2H, H_{Ar}), 8.07 (d, *J* = 8.1 Hz, 2H, H_{Ar}), 5.03 – 5.00 (m, 2H, N-CH), 3.96 – 3.93 (t, *J* = 11.5 Hz, 8H, CH_2), 3.07 – 3.03 (t, *J* = 12.1 Hz, 8H, CH_2), 2.56 – 2.51 (m, 5H, CH_2), 1.89 (d, *J* = 11.1 Hz, 4H, CH_2), 1.74 (d, *J* = 8.6 Hz, 5H, CH_2), 1.48 – 1.43 (m, 6H, CH_2). **^{13}C NMR (101 MHz, $CDCl_3$) δ:** 163.7 (C=O), 163.5, (C=O) 160.6 (C_{quat}-N), 157.7 (C_{quat}-N), 135.9 (C_{Ar}), 134.8 (C_{Ar}), 134.1 (C_{Ar}), 132.5 (C_{Ar}), 130.0 (C_{Ar}), 124.4 (C_{Ar}), 123.3 (C_{Ar}), 122.6 (C_{Ar}), 54.1 (NCOCO-**C**H), 53.9 (NCOCO-**C**H), 45.6 (N-**C**H_2-CH_2-N), 44.5 (N-CH_2-**C**H_2-N), 29.7 (CH_2), 29.1 (CH_2), 26.5 (CH_2). **HRMS (MALDI+, DIT):** m/z calcd. for $C_{52}H_{50}N_{10}O_4$ ($[M+H]^+$): 879.4089; found: 879.4314.

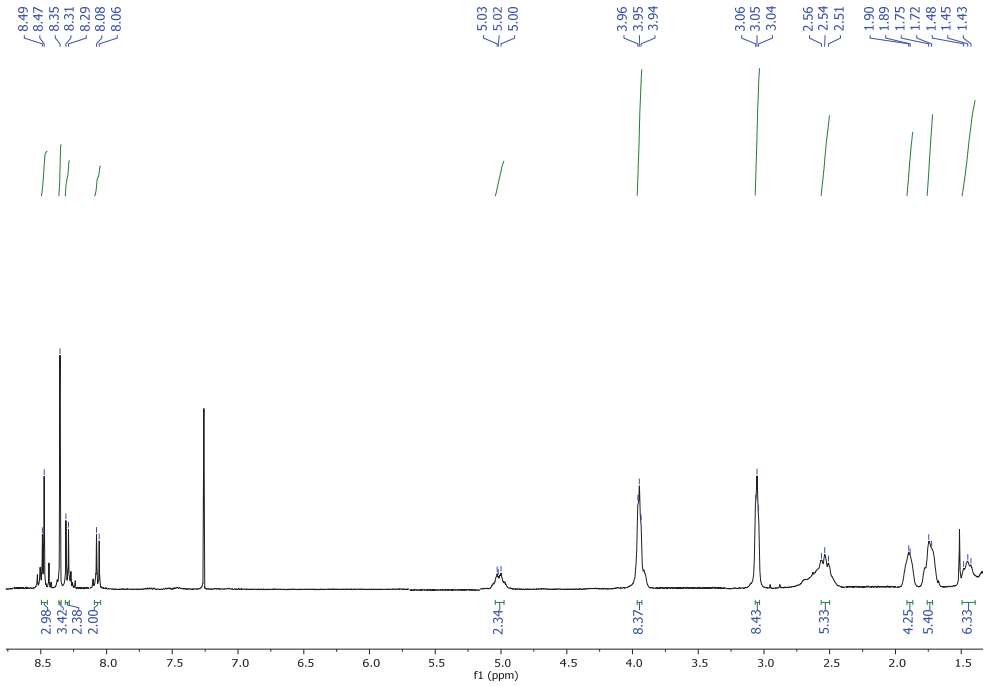

Figure 71. ^{1}H NMR (400 MHz, $CDCl_3$) of 1,7-PC116

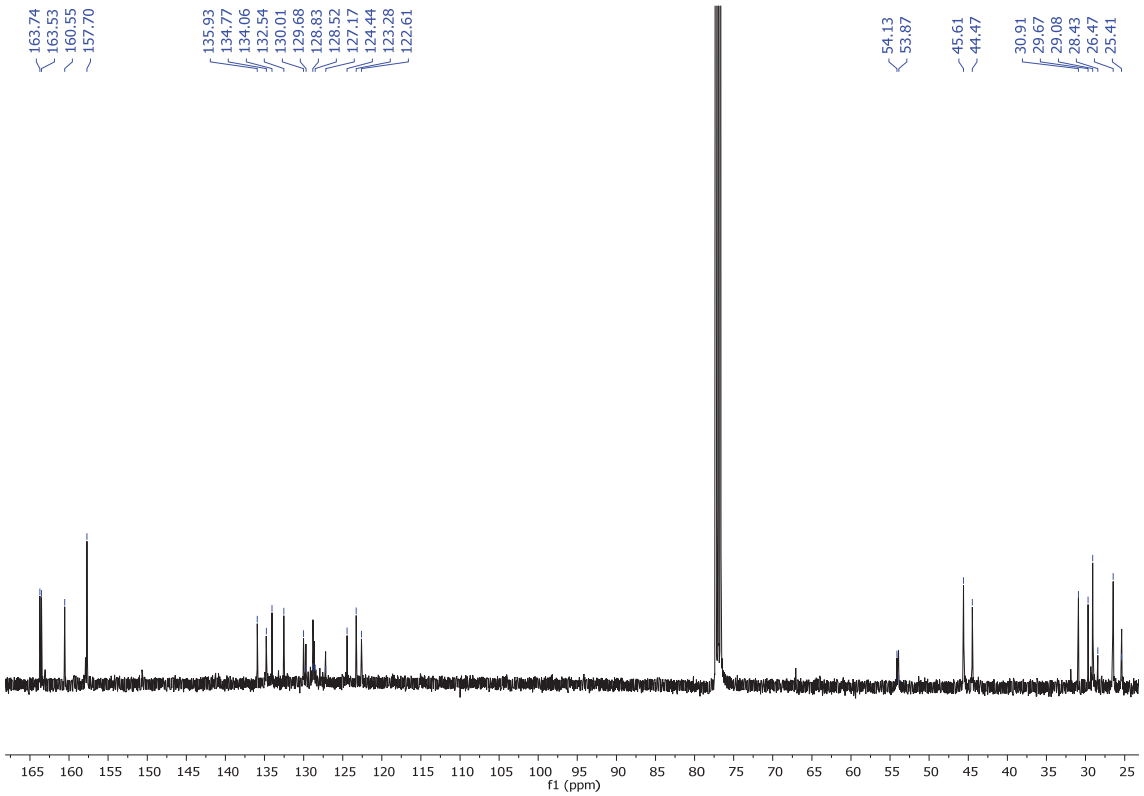

Figure 72. ^{13}C NMR (101 MHz, $CDCl_3$) of 1,7-PC116

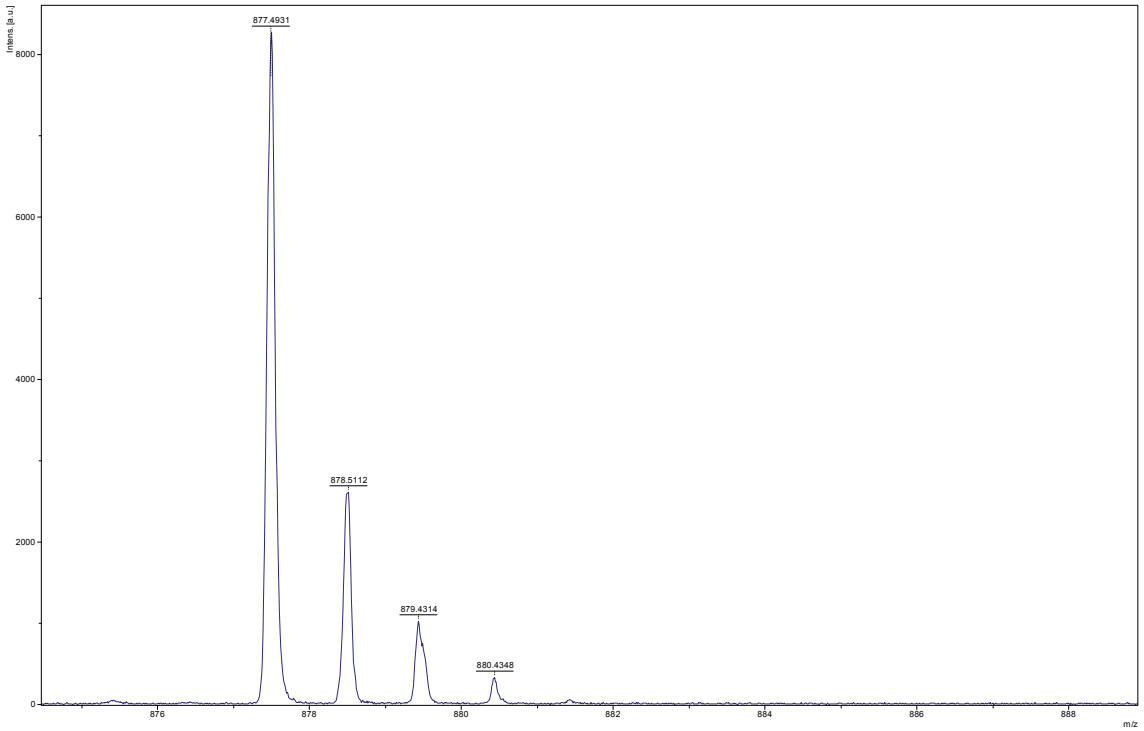

Figure 73. Mass spectrum (MALDI+, DIT) of PC116

2. Synthesis of perylenediimides: hexylheptyl.

2.1. Synthesis of *N,N'*-di-(1'-hexylheptyl)-1-[*p*-(*N'''*-*tert*-butoxycarbonylpiperazin-*N''*-yl)phenyl]-3,4,9,10-perylenetetracarboxylic diimide (NZ29).

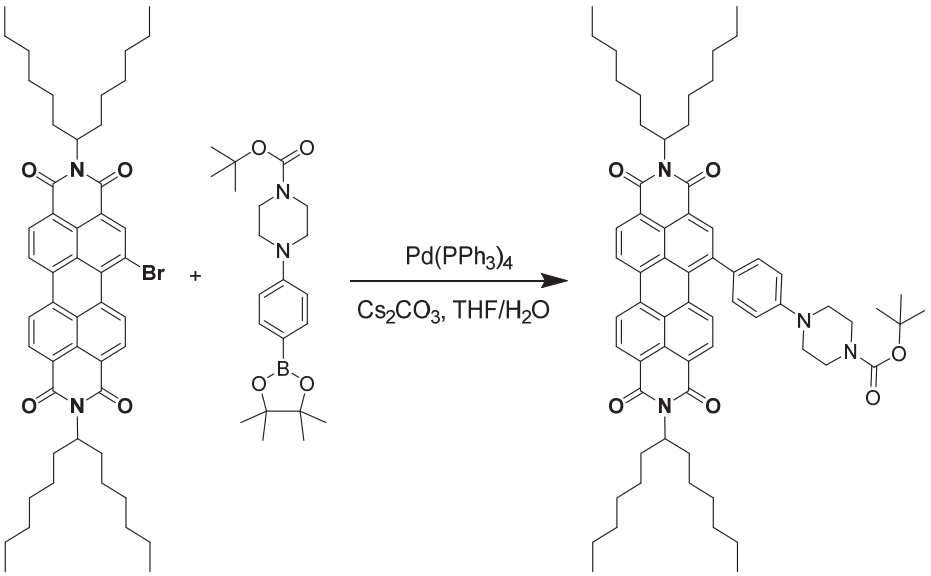

NZ20 **NZ29**

$Pd(PPh_3)_4$ (27 mg, 0.024 mmol) was added, under argon atmosphere, to a solution of *N,N'*-di-(1'-hexylheptyl)-1-bromo-3,4,9,10-perylenetetracarboxy diimide (200 mg, 0.24 mmol), *p*-(*N'-tert*-butoxycarbonylpiperazin-*N*-yl)phenylboronic acid pinacol ester (110 mg, 0.28 mmol) and sodium carbonate (73 mg, 0.7 mmol) in THF (20 mL) and water (2.5 mL). The reaction was heated at reflux overnight and, after cooling, it was extracted with DCM (30 mL x 3). The combined organic extracts were dried over anhydrous sodium sulphate, filtered and evaporated under reduced pressure. Purification was carried out by silica gel flash chromatography using DCM:MeOH (97:3) as eluent to give compound **NZ29** as a red powder in 78 % yield (0.19 g, 0.18 mmol). **R_f (50:1, DCM:MeOH):** 0.4. **Mp (°C):** 160-161 °C. **FT-IR (KBr, cm^{-1}):** 2920 (C-H), 2856 (C-H), 1695 (C=O), 1660 (C=O), 1590 (C_{Ar}-C_{Ar}), 1403 (C_{Ar}-C_{Ar}), 1333 (C-N), 1228, 1170, 808 (fingerprint region). **^{1}H NMR (300 MHz, $CDCl_3$) δ:** 0.75 (t, 12H, CH_2), 1.15 (m, 32H, CH_2), 1.44 (s, 9H, CH_3), 1.76 (m, 4H, CH_2), 2.15 (m, 4H, CH_2), 3.22 (t, *J* = 4.9 Hz, 4H, CH_2), 3.57 (t, *J* = 5.1 Hz, 4H, CH_2), 5.09 (m, 2H, N-CH), 6.98 (d, *J* = 8.6 Hz, 2H, H_{Ar}), 7.34 (d, *J* = 8.7 Hz, 2H, H_{Ar}), 7.96 (d, *J* = 8.2 Hz, 1H, H_{Ar}), 8.08 (m, 1H, H_{Ar}), 8.52 (m, 5H, H_{Ar}). **^{13}C NMR (75 MHz, $CDCl_3$) δ:** 14.0 (CH_2), 22.6 (CH_2), 26.9 (CH_2), 28.4 (CH_3), 29.2 (CH_2), 31.7 (CH_2), 32.4 (CH_2), 48.7(N-**C**H_2-CH_2-N), 54.6 (NCOCO-**C**H), 54.7 (NCOCO-**C**H), 80.1 (**C**$(CH_3)_3$),, 117.4 (C_{Ar}), 122.4 (C_{Ar}), 123.4 (C_{Ar}), 127.6 (C_{Ar}), 128.2 (C_{Ar}), 128.3 (C_{Ar}), 129.2 (C_{Ar}), 129.4 (C_{Ar}), 129.6 (C_{Ar}), 130.6 (C_{Ar}), 131.5 (C_{Ar}), 132.2 (C_{Ar}), 133.5 (C_{Ar}), 134.6 (C_{Ar}), 134.7 (C_{Ar}), 135.1 (C_{Ar}), 136.1 (C_{Ar}), 136.7 (C_{Ar}), 141.7 (C_{quat}-PDI), 151.0 (C_{quat}-N), 154.7 (**C**OOC$(CH_3)_3$), 163.8 (C=O), 164.7 (C=O). **HRMS (MALDI+, DCTB):** m/z calcd. for $C_{65}H_{82}N_4O_6$ ($[M]^+$): 1014.6234; found: 1014.6241.

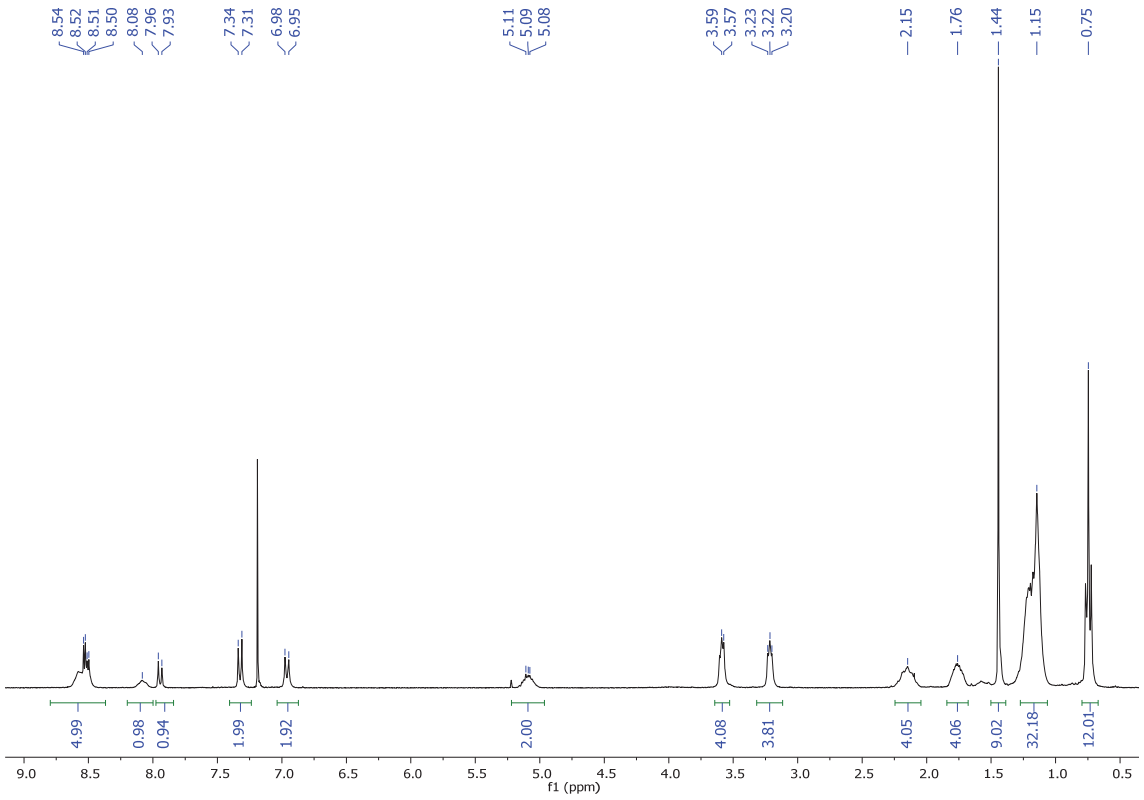

Figure 74. ^{1}H NMR (300 MHz, $CDCl_3$) of NZ29

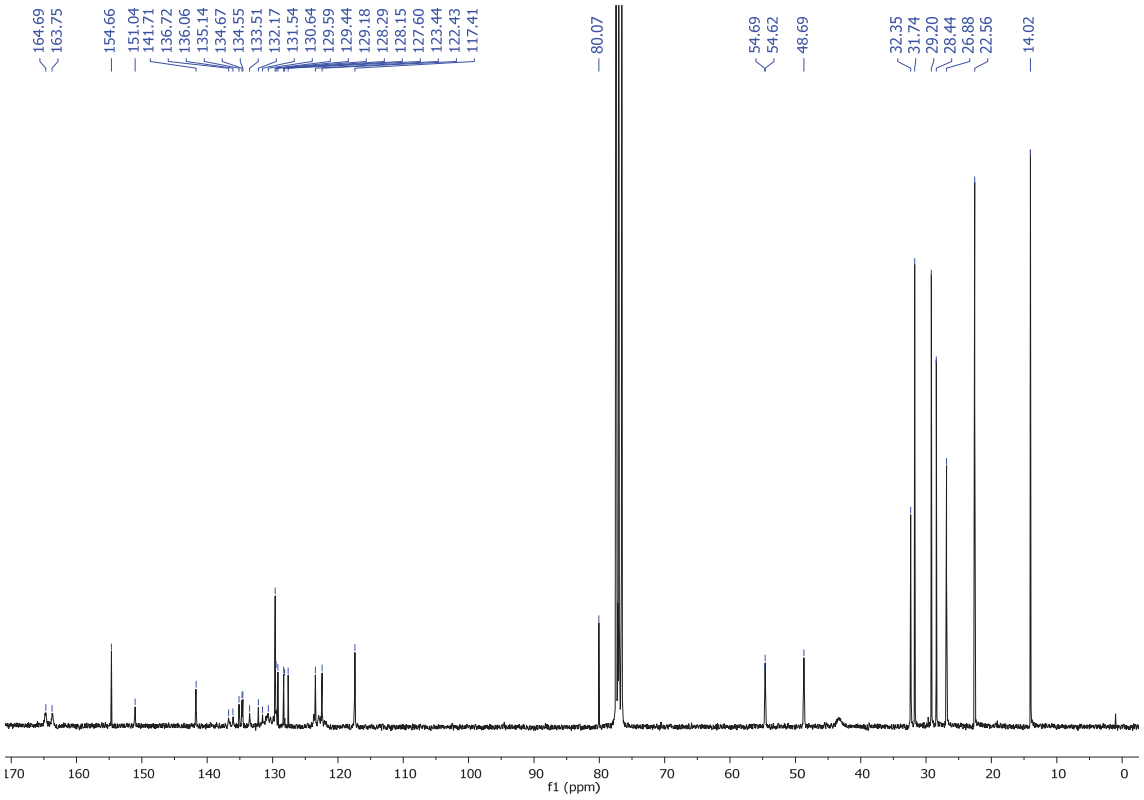

Figure 75. ^{13}C NMR (75 MHz, $CDCl_3$) of NZ29

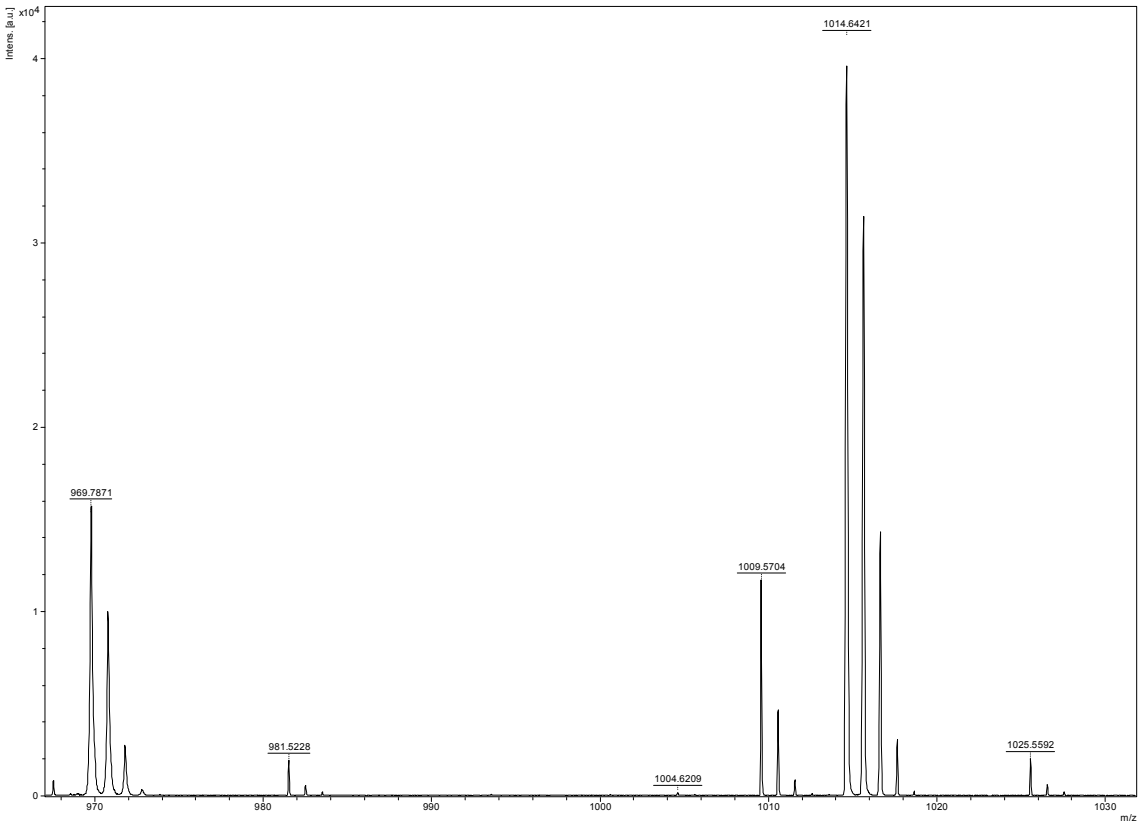

Figure 76. Mass spectrum (MALDI+, DCTB) of NZ29

Test of oxidants:

A. NZ29 ($5 \cdot 10^{-5}$ M) dissolved in $CHCl_3$:MeOH 9:1 v/v. **B. NZ29** with 40 eq of each compound (dissolved in water or $CHCl_3$, $5 \cdot 10^{-2}$ M). **C.** NZ29 with 40 eq of each compound and added a buffer HEPES pH = 8 (30 µL). **From the left to right. Ref: NZ29** dissolved in $CHCl_3$:MeOH 9:1 v/v, **H_2O:** Addictions of water, **Solv: NZ29** dissolved in $CHCl_3$:MeOH, **1: NZ29** with pTsOH, **2: NZ29** with CH_3HSO_3, **3: NZ29** with H_2SO_4, **4: NZ29** with HCl, **5: NZ29** with HNO_3, **6: NZ29** with oxone, **7: NZ29** with benzoyl peroxide, **8: NZ29** with H_2O_2, **9: NZ29** with MCPB.

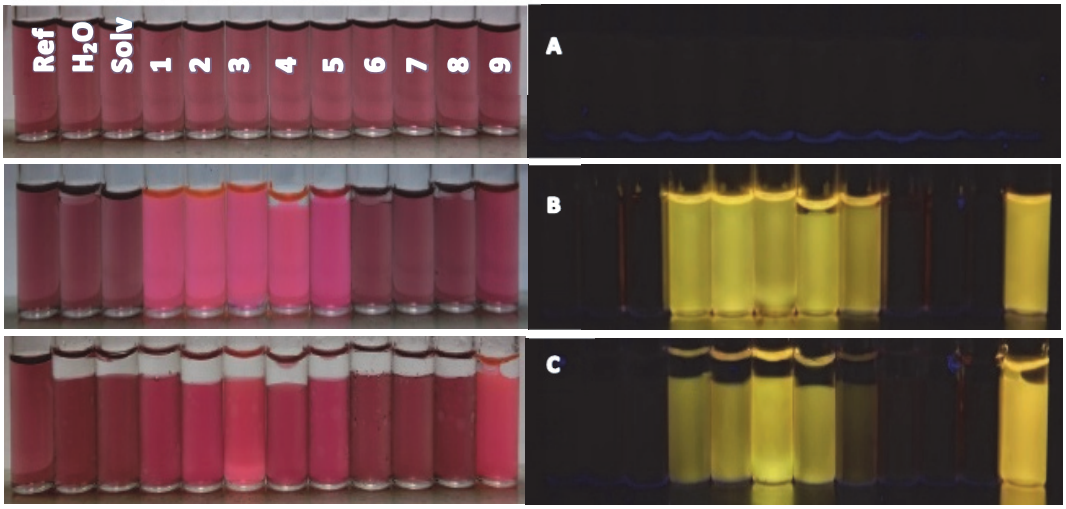

Figure 77. Photos of NZ29 under white light and light of 366 nm in the presence of different kind of oxidants and acids.

2.2. Synthesis of *N,N'*-di-(1'-hexylheptyl)-1-(*p*-piperazin-*N''*-ylphenyl)-3,4,9,10-perylenetetracarboxylic diimide (NZ31).

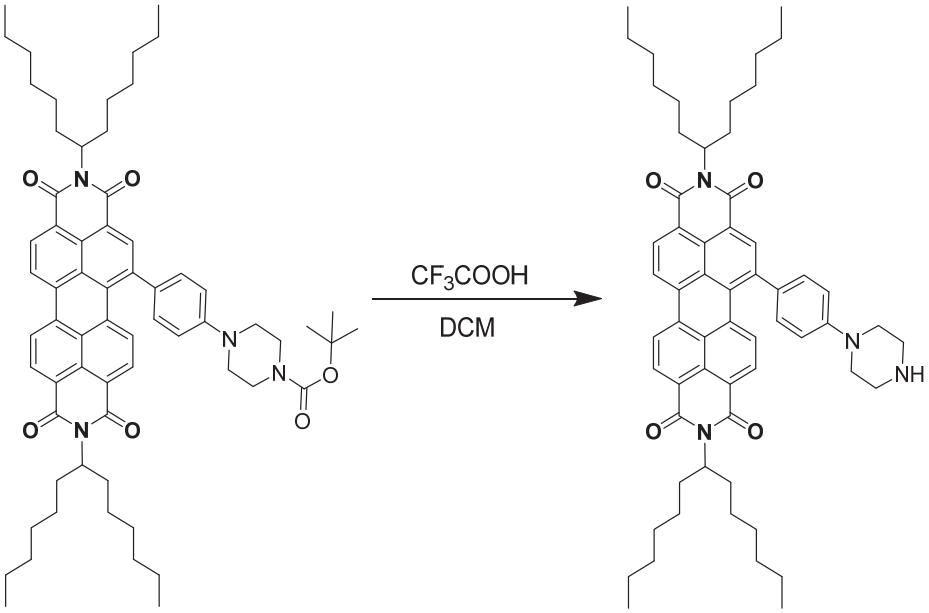

NZ29 **NZ31**

Trifluoroacetic acid (0.33 mL, 4.6 mmol) was added to a solution of **NZ29** (80 mg, 0.078 mmol) in DCM (0.5 mL). After 15 minutes stirring at room temperature, the reaction was stopped with water and extracted with DCM (30 mL x 3). The combined organic extracts were dried over anhydrous sodium sulphate, filtered and evaporated under reduced pressure. Purification was carried out by silica gel flash chromatography using DCM:MeOH (6:0.5) as eluent to give compound **NZ31** as a red powder in 90 % yield (65 mg, 0.07 mmol). **R_f (DCM:MeOH, 50:4):** 0. **Mp (°C):** 169-170 °C. **FT-IR (KBr, cm^{-1}):** 3416 (N-H), 2926 (C-H), 2844 (C-H), 1695 (C=O), 1648 (C=O), 1590 (C_{Ar}-C_{Ar}), 1461(CH_2), 1327 (C-N), 1246, 1100, 1018, 814 (fingerprint region). **^{1}H NMR (300 MHz, $CDCl_3$) δ:** 0.82 (m, 12H, CH_2), 1.22 (m, 32H, CH_2), 1.85 (m, 4H, CH_2), 2.22 (m, 4H, CH_2), 3.33 (t, *J* = 3.9 Hz, 4H, CH_2), 3.50 (t, *J* = 4.8 Hz, 4H, CH_2), 5.18 (m, 2H, N-CH), 7.06 (d, *J* = 8.7 Hz, 2H, H_{Ar}), 7.44 (d, *J* = 8.7 Hz, 2H, H_{Ar}), 8.02 (d, *J* = 8.2, Hz 1H, H_{Ar}), 8.17 (m, 1H, H_{Ar}), 8.60 (m, 5H, H_{Ar}). **^{13}C NMR (101 MHz, $CDCl_3$) δ:** 13.9 (CH_2), 22.4 (CH_2), 26.8 (CH_2), 29.1 (CH_2), 31.6 (CH_2), 32.2 (CH_2), 44.6 (N-CH_2-**C**H_2-N), 47.7 (N-**C**H_2-CH_2-N), 54.5 (NCOCO-**C**H), 117.5 (C_{Ar}), 122.4 (C_{Ar}), 123.4 (C_{Ar}), 127.5 (C_{Ar}), 128.0 (C_{Ar}), 128.2 (C_{Ar}), 129.1 (C_{Ar}), 129.6 (C_{Ar}), 134.0 (C_{Ar}), 134.6 (C_{Ar}), 141.4 (C_{quat}-PDI), 150.7 (C_{quat}-N), 150.7 (C_{quat}-N), 163.6 (C=O), 164.6 (C=O). **HRMS (MALDI+, DCTB):** m/z calcd. for $C_{60}H_{74}N_4O_4$ ($[M]^+$): 914.5710; found: 914.5690.

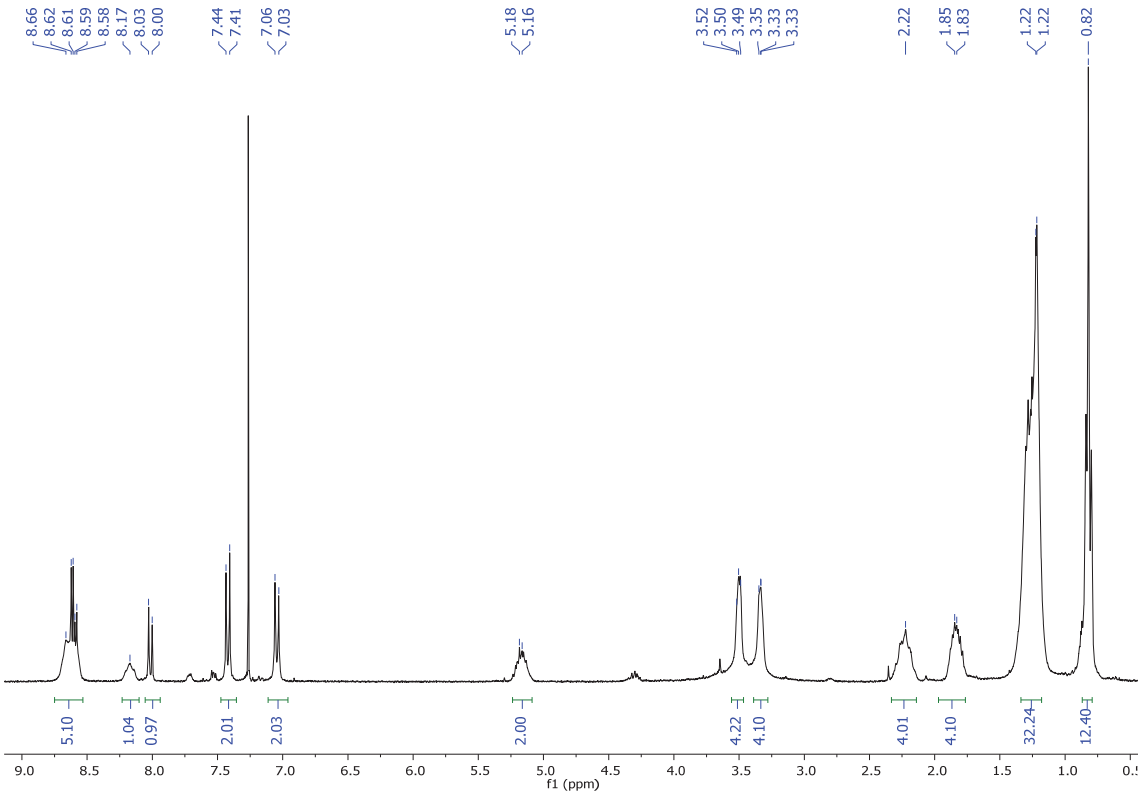

Figure 78. ^{1}H NMR (300 MHz, $CDCl_3$) of NZ31

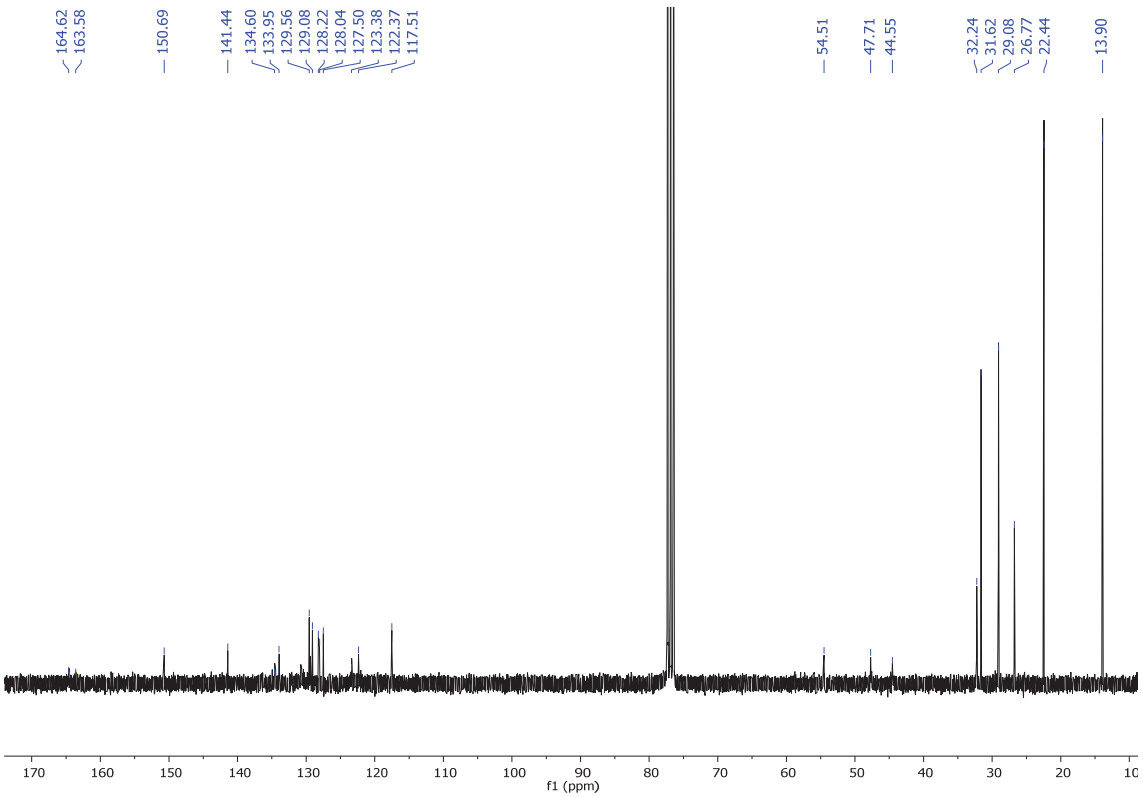

Figure 79. ^{13}C NMR (75 MHz, $CDCl_3$) of NZ31

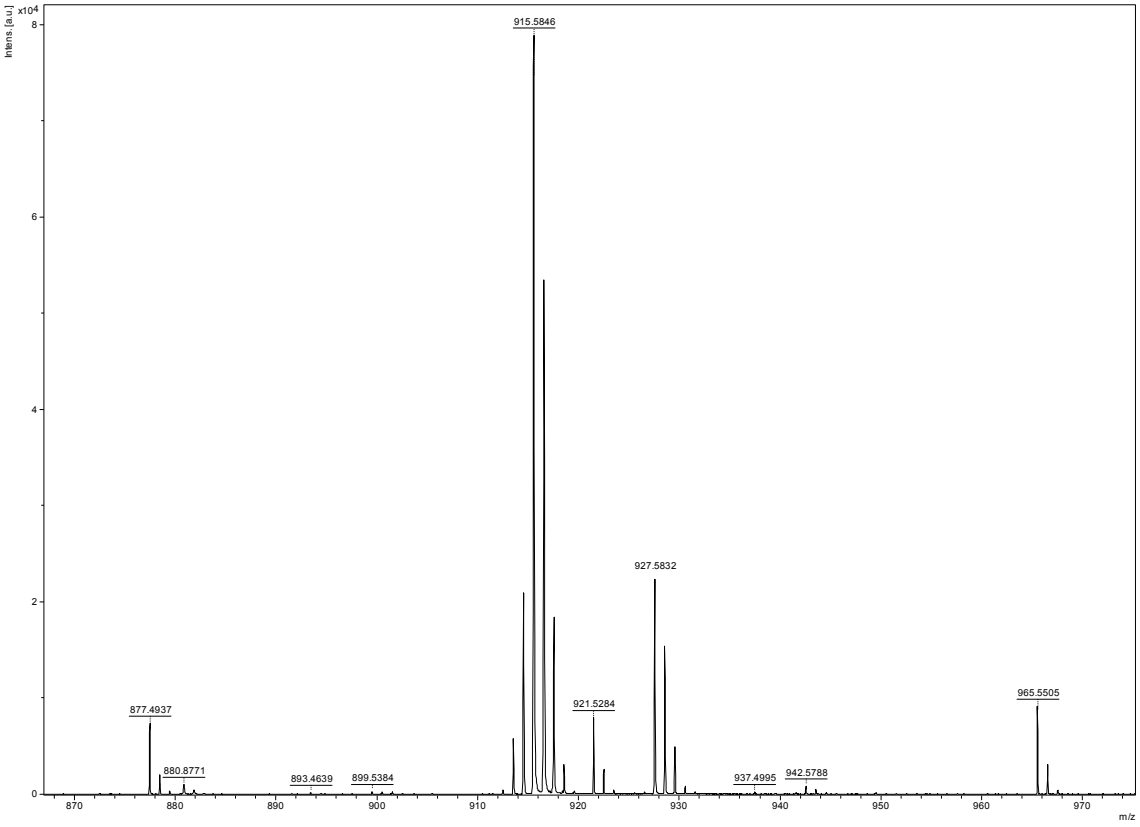

Figure 80. Mass spectrum (MALDI+, DCTB) of NZ31

Test of oxidants:

A. NZ31 ($5 \cdot 10^{-5}$ M) dissolved in $CHCl_3$:MeOH 9:1 v/v. **B. NZ31** with 40 eq of each compound (dissolved in water or $CHCl_3$, $5 \cdot 10^{-2}$ M). **C. NZ31** with 40 eq of each compound and added a buffer HEPES pH = 8 (30 µL). **From the left to right. Ref: NZ31** dissolved in $CHCl_3$:MeOH 9:1 v/v, **H_2O:** Addictions of water, **Solv: NZ31** dissolved in $CHCl_3$:MeOH, **3: NZ31** with H_2SO_4, **6: NZ31** with oxone, **7: NZ31** with benzoyl peroxide, **8: NZ31** with H_2O_2, **9: NZ31** with MCPB.

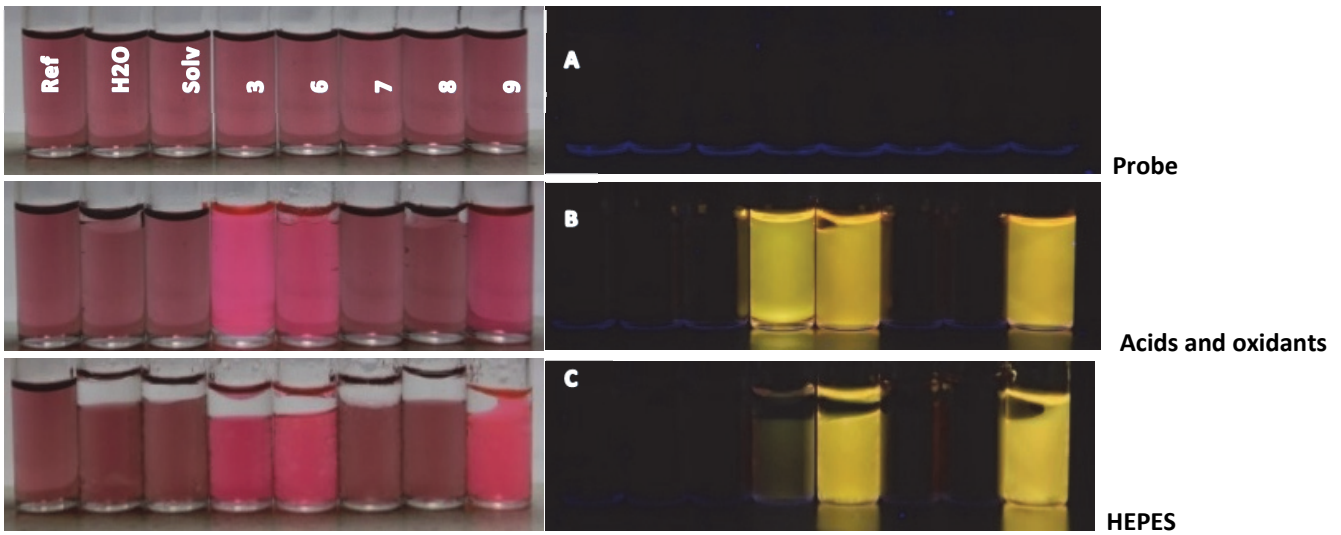

Figure 81. Photos of NZ31 under white light and light of 366 nm in the presence of different kind of oxidants and acids.

2.3. Synthesis of *N,N'*-di-(1'-hexylheptyl)-1,7-di[*p*-(*N'''*-*tert*-butoxycarbonylpiperazin-*N''*-yl)phenyl]-3,4,9,10-perylenetetracarboxylic diimide (NZ26).

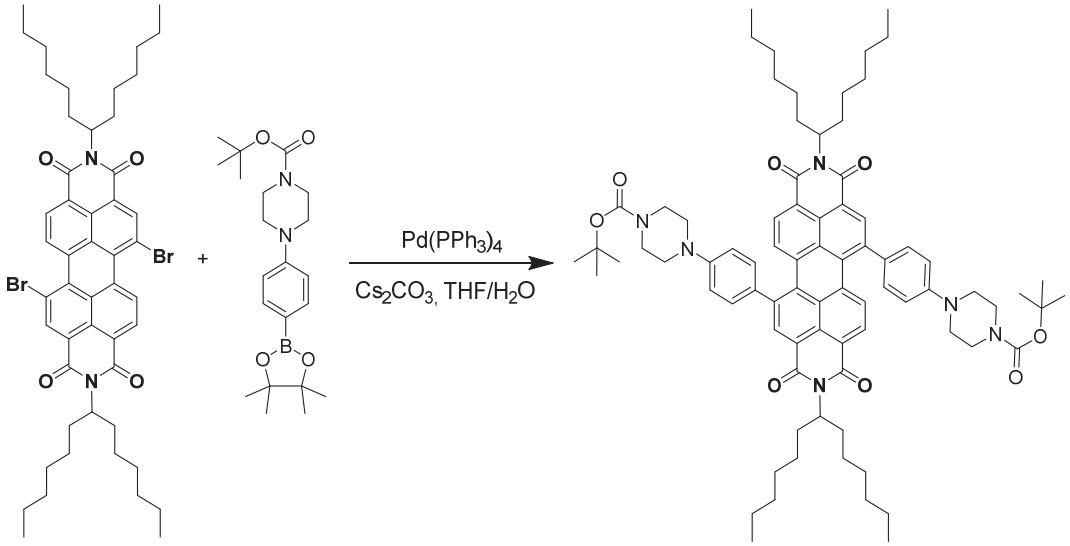

NZ21 **NZ26**

$Pd(PPh_3)_4$ (25 mg, 0.022 mmol) was added, under argon atmosphere, to a solution of *N,N'*-di-(1'-hexylheptyl)-1,7-dibromo-3,4,9,10-perylenetetracarboxylic diimide (200 mg, 0.22 mmol, regioisomeric mixture, 0.22 mmol), *p*-(*N'-tert*-butoxycarbonylpiperazin-*N*-yl)phenylboronic acid pinacol ester (170 mg, 0.44 mmol) and sodium carbonate (73 mg, 0.7 mmol) in THF (20 mL) and water (2.5 mL). The reaction was heated at reflux overnight and, after cooling, it was extracted with DCM (30 mL x 3). The combined organic extracts were dried over anhydrous sodium sulphate, filtered and evaporated under reduced pressure. Purification was carried out by silica gel flash chromatography using DCM:MeOH (100:1) as eluent to give compound **NZ26** (pure 1,7 isomer) as a black powder in 60 % yield (0.163 g, 0.132 mmol). **R_f (DCM:MeOH, 50:1):** 0.5. **Mp (°C):** 263-264 °C. **FT-IR (KBr, cm^{-1}):** 2932 (C-H), 2850 (C-H), 1699 (C=O), 1654 (C=O), 1596 (C_{Ar}-C_{Ar}), 1409 (CH_2), 1327 (C-N), 1228, 1158, 815 (fingerprint region). **^{1}H NMR (300 MHz, $CDCl_3$) *δ*:** 0.82 (t, *J* = 6.6 Hz, 12H, CH_2), 1.25 (m, 32H, CH_2), 1.51 (s, 18H, CH_3), 1.82 (m, 4H, CH_2), 2.22 (m, 4H, CH_2), 3.30 (t, *J* = 5.2 Hz, 8H, CH_2), 3.68 (t, *J* = 5.4 Hz, 8H, CH_2), 5.15 (m, 2H, N-CH), 7.05 (m, 4H, H_{Ar}), 7.48 (d, 4H, H_{Ar}), 7.93 (d, 2H, H_{Ar}), 8.13 (m, 2H, H_{Ar}), 8.60 (s, 2H, H_{Ar}). **^{13}C NMR (75 MHz, $CDCl_3$) *δ*:** 14.0 (CH_2), 22.6 (CH_2), 26.9 (CH_2), 28.4 (CH_3), 29.2 (CH_2), 31.7 (CH_2), 32.4 (CH_2), 48.5 (N-CH_2-**C**H_2-N), 54.6 (NCOCO-**C**H), 80.0(**C**$(CH_3)_3$), 117.1 (C_{Ar}), 127.7 (C_{Ar}), 128.8 (C_{Ar}), 129.5 (C_{Ar}), 129.6 (C_{Ar}), 129.8 (C_{Ar}), 130.1 (C_{Ar}), 133.0 (C_{Ar}), 133.5 (C_{Ar}), 135.3 (C_{Ar}), 140.8 (C_{quat}-PDI)142.0 (C_{quat}-PDI), 151.1 (C_{quat}-N), 154.7 (**C**OOC$(CH_3)_3$),, 163.8 (C=O), 164.8 (C=O). **HRMS (MALDI+, DCTB):** m/z calcd. for $C_{80}H_{102}N_6O_8$ ($[M]^+$): 1274.7754; found: 1274.7788.

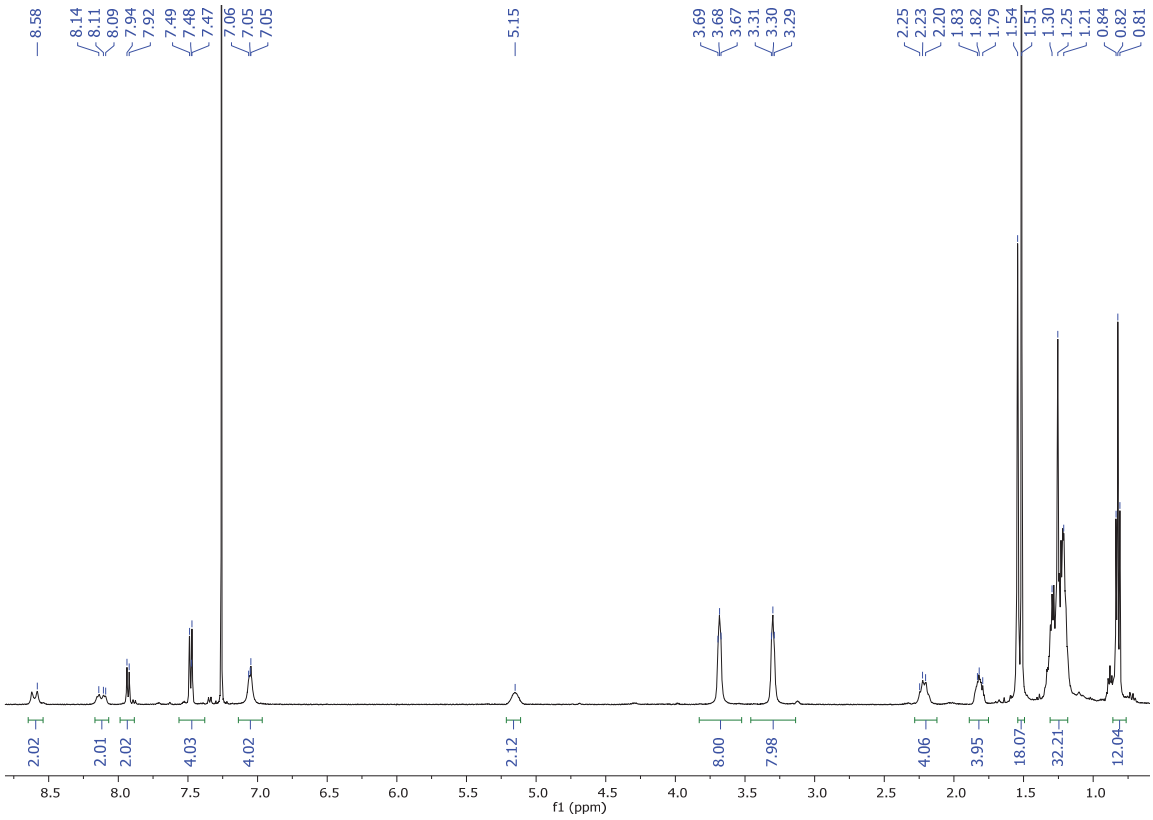

Figure 82. ^{1}H NMR (300 MHz, $CDCl_3$) of NZ26

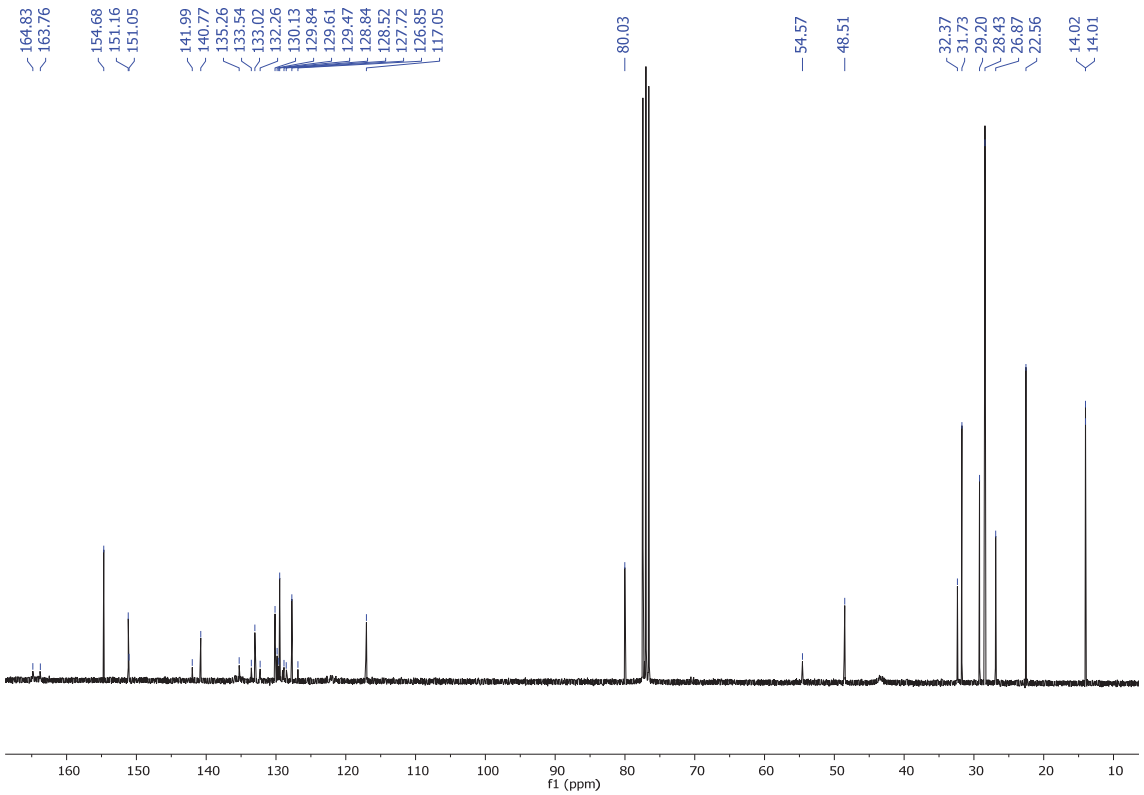

Figure 83. ^{13}C NMR (75 MHz, $CDCl_3$) of NZ26

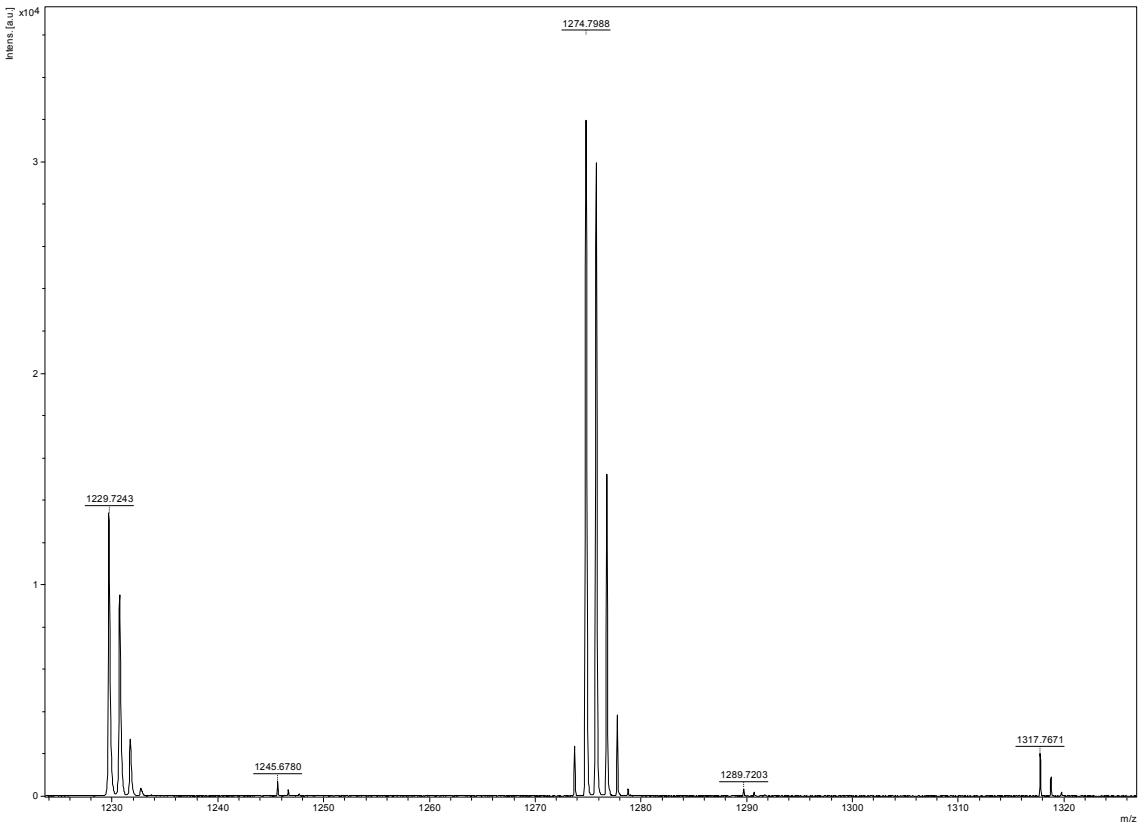

Figure 84. Mass spectrum (MALDI+, DCTB) of NZ26

Test of oxidants:

A. NZ26 ($5 \cdot 10^{-5}$ M) dissolved in $CHCl_3$:MeOH 9:1 v/v. **B. NZ26** with 40 eq of each compound (dissolved in water or $CHCl_3$, $5 \cdot 10^{-2}$ M). **C. NZ26** with 40 eq of each compound and added a buffer HEPES pH = 8 (30 µL). **From the left to right. Ref: NZ26** dissolved in $CHCl_3$:MeOH 9:1 v/v, **H_2O:** Addictions of water, **Solv: NZ26** dissolved in $CHCl_3$:MeOH, **1: NZ26** with pTsOH, **2: NZ26** with CH_3HSO_3, **3: NZ26** with H_2SO_4, **4: NZ26** with HCl, **5: NZ26** with HNO_3, **6: NZ26** with oxone, **7: NZ26** with benzoyl peroxide, **8: NZ26** with H_2O_2, **9: NZ26** with MCPB.

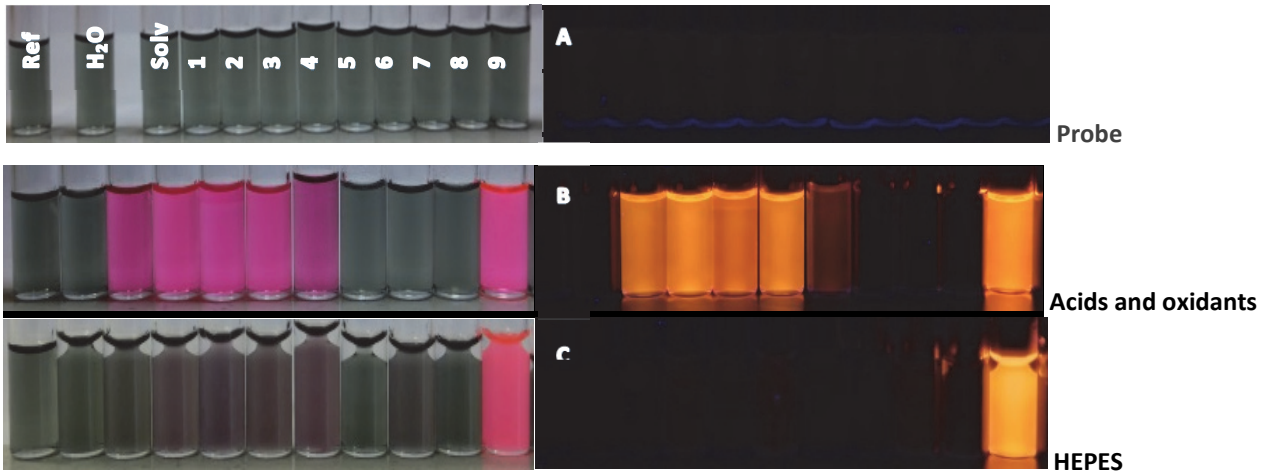

Figure 85. Photos of NZ26 under white light and light of 366 nm in the presence of different kind of oxidants and acids.

2.4. Synthesis of *N,N'*-di-(1'-hexylheptyl)-1,7-di(*p*-piperazin-*N''*-ylphenyl)-3,4,9,10-perylenetetracarboxylic diimide (NZ33).

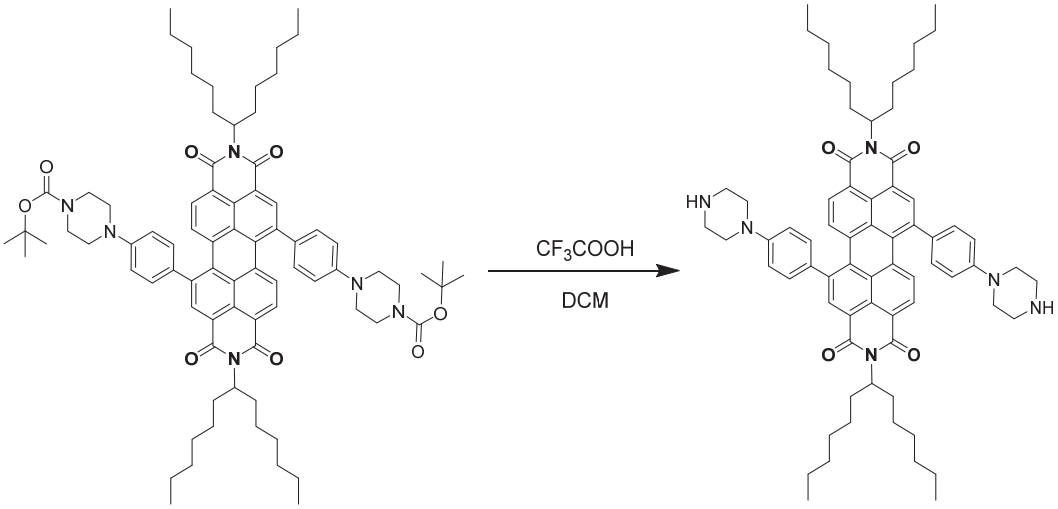

NZ26 **NZ33**

Trifluoroacetic acid (0.1 mL, 1.3 mmol) was added to a solution of **NZ26** (30 mg, 0.02 mmol) in DCM (0.5 mL). After 20 minutes stirring at room temperature, the reaction was stopped with water and extracted with DCM (10 mL x 3). The combined organic extracts were dried over anhydrous sodium sulphate, filtered and evaporated under reduced pressure. Purification was carried out by silica gel flash chromatography using DCM:MeOH (5:0.5) as eluent to give compound **NZ33** as a black powder in 90 % yield (23 mg, 0.018 mmol). **R_f (DCM):** 0. **Mp (°C):** 248-249 °C. **FT-IR (KBr, cm^{-1}):** 3427 (N-H), 2929 (C-H), 2843 (C-H), 1695 (C=O), 1653 (C-O), 1576 (C_{Ar}-C_{Ar}), 1519 (C_{Ar}-C_{Ar}), 1446 (CH_2), 1409 (CH_2), 1327 (C-N), 1254, 1196, 1139, 927, 808, 718 (fingerprint region). **^{1}H NMR (300 MHz, $CDCl_3$) *δ*:** 0.81 (t, *J* = 6.5 Hz, 12H, CH_2), 1.21 (m, 32H , CH_2), 1.82 (m, 4H, CH_2), 2.22 (m, 4H, CH_2), 2.40 (m, 2H, CH_2), 3.48 (m, *J* = 9.1 Hz, 8H, CH_2), 3.65 (m, *J* = 9.1 Hz, 8H, CH_2), 5.15 (m, 2H, N-CH), 7.02 (d, *J* = 4.2 Hz, 4H, H_{Ar}), 7.50 (d, *J* = 4.6 Hz, 4H, H_{Ar}), 7.90 (d, *J* = 4.2 Hz, 2H, H_{Ar}), 8.15 (m, 2H, H_{Ar}), 8.58 (s, 2H, H_{Ar}). **^{13}C NMR (75 MHz, $CDCl_3$) *δ*:** 14.0 (CH_2), 22.6 (CH_2), 26.9 (CH_2), 29.2 (CH_2), 31.7 (CH_2), 32.4 (CH_2), 43.4 (N-CH_2-**C**H_2-N), 46.3 (N-**C**H_2-CH_2-N), 54.7 (NCOCO-**C**H), 117.9 (C_{Ar}), 121.6 (C_{Ar}), 122.3 (C_{Ar}), 122.8 (C_{Ar}), 127.8 (C_{Ar}), 129.4 (C_{Ar}), 130.3 (C_{Ar}), 132.4 (C_{Ar}), 134.8 (C_{Ar}), 140.4 (C_{quat}-PDI), 149.9 (C_{quat}-N), 163.7 (C=O), 164.7 (C=O). **HRMS (MALDI+, DCTB):** m/z calcd. for $C_{70}H_{86}N_6O_6$ ($[M]^+$): 1074.6711; found: 1074.6750.

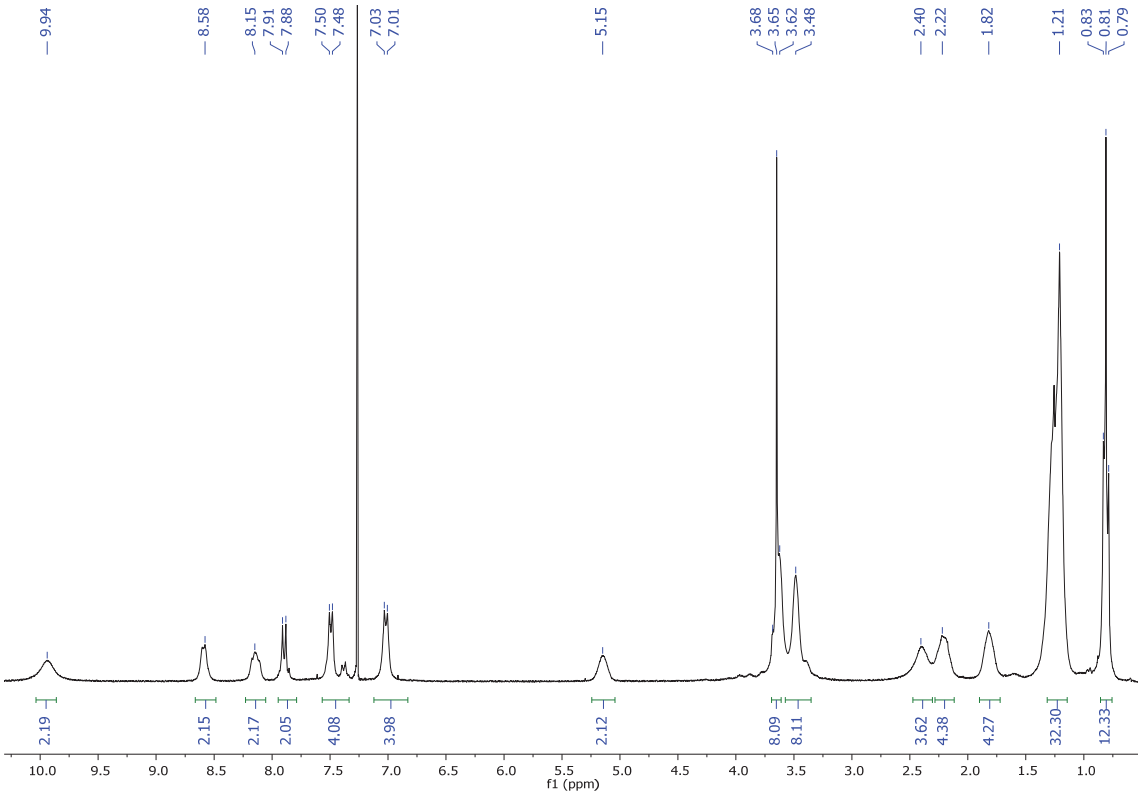

Figure 86. ^{1}H NMR (300 MHz, $CDCl_3$) of NZ33

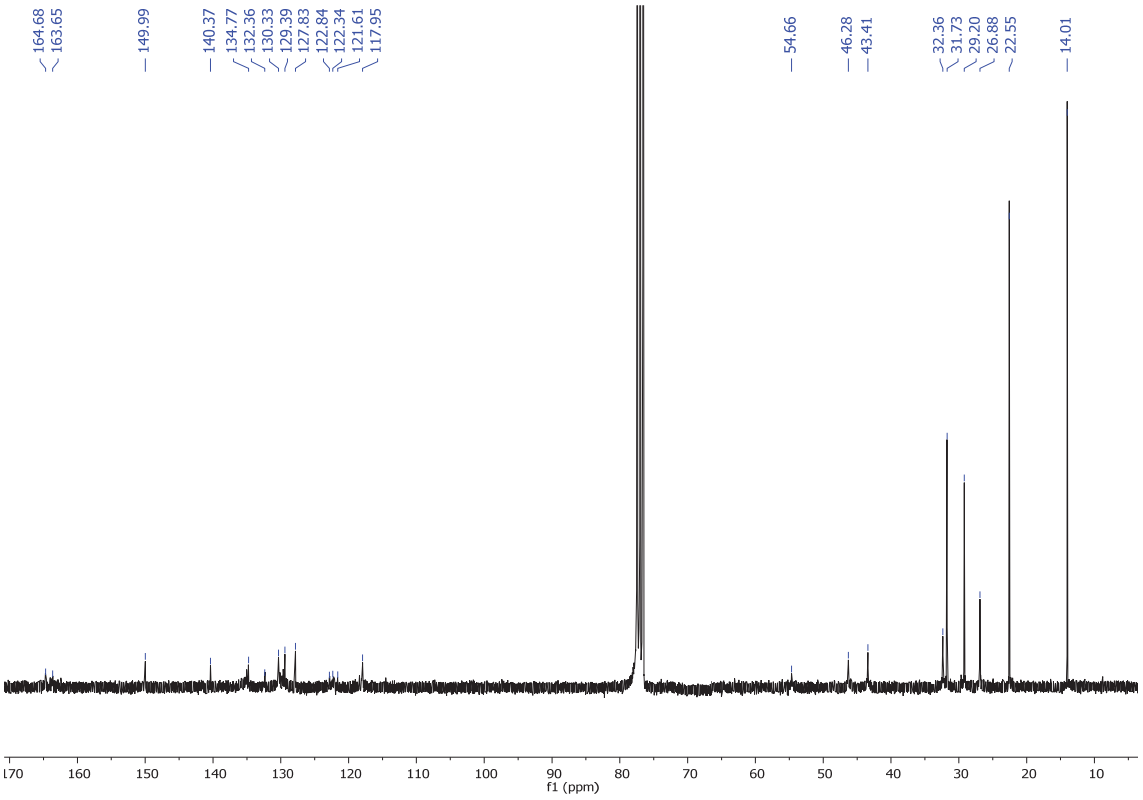

Figure 87. ^{13}C NMR (75 MHz, $CDCl_3$) of NZ33

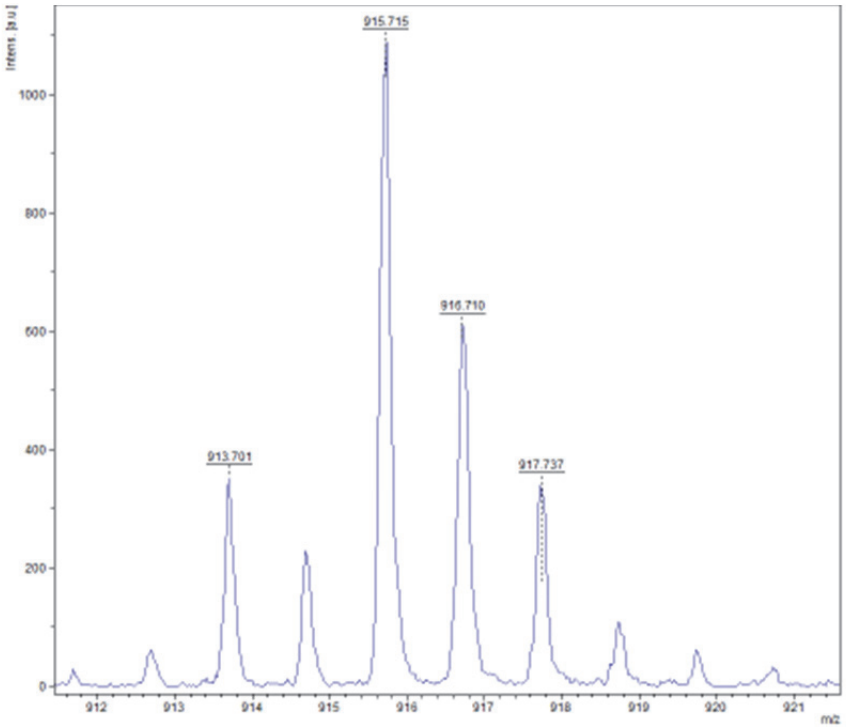

Figure 88. Mass spectrum (MALDI+, DCTB) of NZ33

Test of oxidants:

NZ33 ($5 \cdot 10^{-5}$ M) dissolved in $CHCl_3$:MeOH 9:1 v/v. **B. NZ33** with 40 eq of each compound (dissolved in water or $CHCl_3$, $5 \cdot 10^{-2}$ M). **C. NZ33** with 40 eq of each compound and added a buffer HEPES pH = 8 (30 µL). **From the left to right. Ref: NZ33** dissolved in $CHCl_3$:MeOH 9:1 v/v, H_2O: Addictions of water, **Solv: NZ33** dissolved in $CHCl_3$:MeOH, **1: NZ33** with pTsOH, **2: NZ33** with CH_3HSO_3, **3: NZ33** with H_2SO_4, **4: NZ33** with HCl, **5: NZ33** with HNO_3, **6: NZ33** with oxone, **7: NZ33** with benzoyl peroxide, **8: NZ33** with H_2O_2, **9: NZ33** with MCPB.

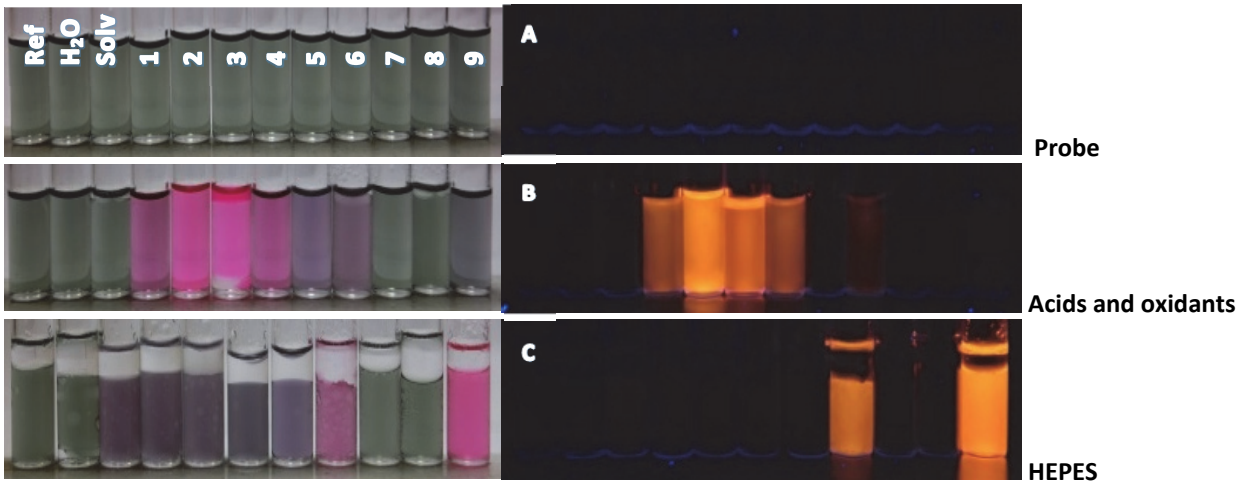

Figure 89. Photos of NZ33 under white light and light of 366 nm in the presence of different kind of oxidants and acids.

3. Preparation of membranes.

The sensory dense membranes (**M2** and **M5**) were prepared with film shapes by radical polymerisation of VP, A4 and MCl using EGDMA as cross-linking agent and DMPA as radical photoinitiator. The co-monomer molar ratios VP/A4/MCl/EGDMA were 57.5/37.5/5.0/2 for **M2**, and 57.5/37.5/5.0/5 for **M5**, using in both synthesis 1.5 % of DMPA. The homogenous comprised solutions of VP, A4, MCl, EGDMA and DMPA were transferred to an ampoule, degassed by nitrogen bubbling for 15 minutes and injected into an oxygen-free atmosphere in a 100-µm-thick salinized glass hermetic mould. In this mould, the photoinitiated bulk polymerisation was performed for two hours. Then, the membranes were demoulded and conditioned by standing in nitrogen atmosphere at room temperature overnight. The structure of the co-monomers and the constitution of the membranes are depicted in Scheme 1.

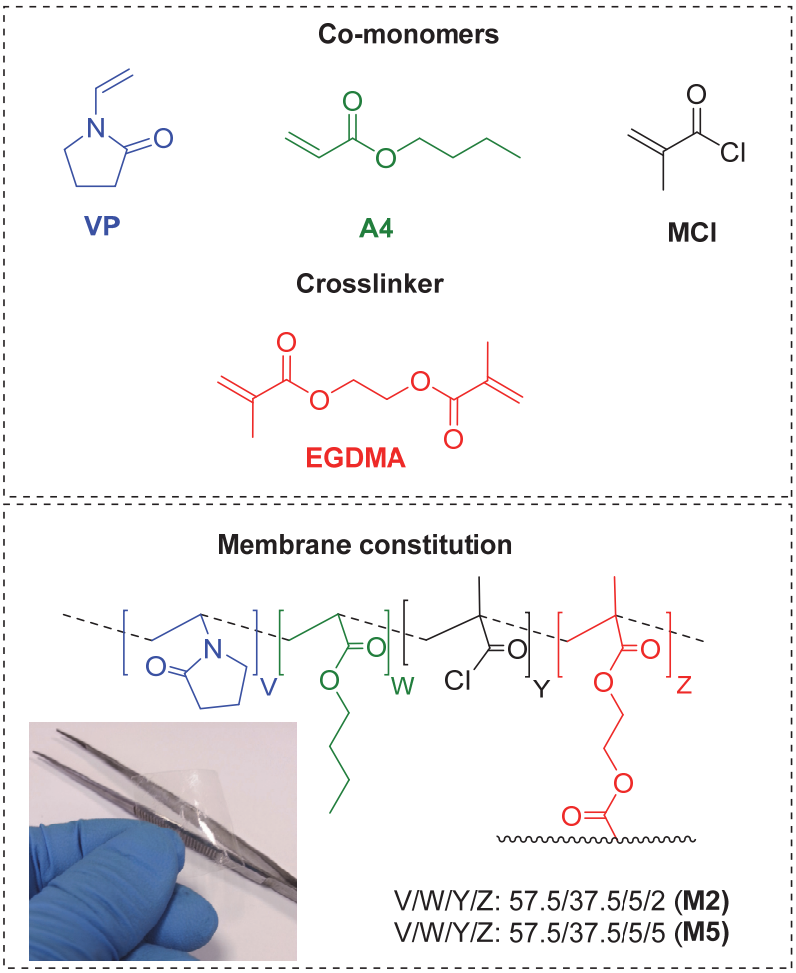

Scheme 1. Chemical structure of sensory dense membranes.

3.1. Preparation of the functional materials.

The functional membranes **M2** and **M5** containing the highly reactive acid chloride groups were straightforward prepared from commercial monomers using conventional bulk photochemically initiated free-radical polymerization. The molar content of the reactive chloride groups was 5 %. This content was relatively low for not altering both the mechanical performance, *i.e.*, tractability, in dry and the swelled state of the materials and the amphiphilic nature of the functional materials and the derived materials after further functionalization.

These parameters were tuned with the crosslinking molar content, 2 and 5 % for membranes **M2** and **M5** respectively. The thickness of both membranes was of 131 µm.

3.2. Synthesis of the films M5-NZ31 and M2-NZ31.

The membranes **M2** and **M5** were modified with the synthesized perylenediimides by the next procedure.

Synthesis of *N,N'*-bis(ciclohexyl)-1-(4-[4-(*N*-[M5])piperazin-1-yl]phenyl)perylene-3,4,9,10-tetracarboxylic diimide (M5-NZ31).

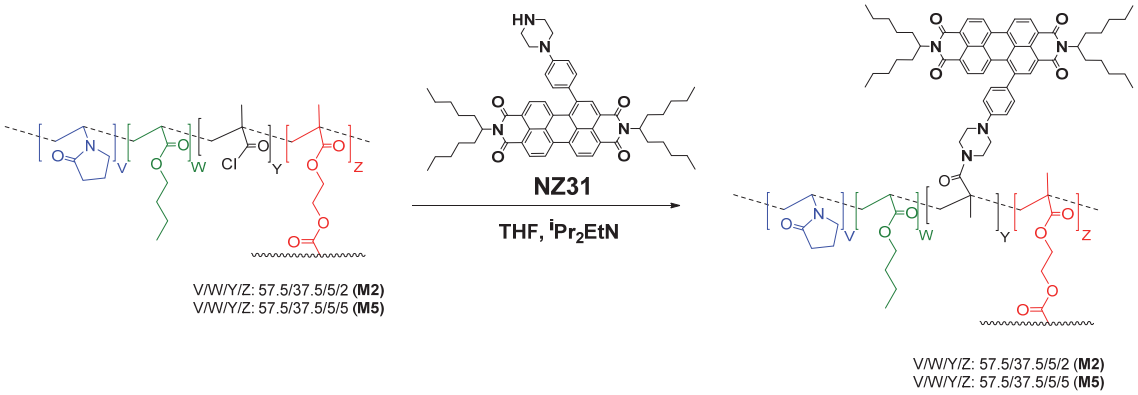

Scheme 2. Synthesis of M5-NZ31 and M2-NZ31.

The polymer (0.16 g, 0.013 mmol), consisting of vinylpyrrolidone (57.5 %), butyl acrylate (37.5 %), methacryloyl chloride (5 %), crosslinking (5 %) and photoinitiator (1.56 %), was dried in a 500 mL Kitasato flask by three vacuum-nitrogen cycles; then, 60 mL of anhydrous THF were added for 30 minutes. Subsequently, *N,N'*-bis(ciclohexyl)-1-(4-[4-piperazin-1-yl]phenyl)perylene-3,4,9,10-tetracarboxylic acid bisimide (0.6 mg, 6.6·10-4 mmol) and three drops of *N,N*-diisopropylethylamine were added. The mixture was stirred for 24 hours in an orbital shaker. After removing the solvent, the obtained film was washed with THF, then acetone and finally water.

3.3. Synthesis of N,N'-bis(ciclohexyl)-1-(4-[4-(N-[M2])piperazin-1-yl]phenyl)perylene-3,4,9,10-tetracarboxylic diimide (M2-NZ31).

The polymer (0.17 g, 0.011 mmol), consisting of vinylpyrrolidone (57.5 %), butyl acrylate (37.5 %), methacryloyl chloride (5 %), crosslinking (2 %) and photoinitiator (1.56 %), was dried in a 500 ml Kitasato flask by three vacuum-nitrogen cycles; then, 60 mL of anhydrous THF were added for 30 minutes. Subsequently *N,N'*-bis(cyclohexyl)-1-(4-[4-piperazin-1-yl]phenyl)perylene-3,4,9,10-tetracarboxylic acid bisimide (0.55 mg, 6.6·10-4 mmol) and three drops of *N,N*-diisopropylethylamine were added. The mixture was stirred for 24 hours in an orbital shaker. After removing of the solvent, the obtained film was washed with THF, then acetone and finally water.

3.4. Design of the functional materials.

The main composition of the membranes, comprised of **VP**, **A4** and **EGDMMA,** was chosen to provide the polymer membranes with: a) good mechanical and thermal properties in dry and in water and organic-solvent swelled state; b) amphiphilic nature.[1,2] The crosslinker content, **EGDMMA**, permitted the tuning of these properties. The former was needed for good tractability and the later for the subsequent performance as sensory materials both in water and organic solvents. Regarding this point, a swelling higher than 40 % is usually needed for the target species to enter into the membrane by diffusion where the interaction with the sensory motifs occur in solid state, and more precisely, in gel or organogel state. Moreover, the affinity between membrane and target species is also a prerequisite for vapour sensing because the target also have to permeate into the membrane by the double diving force, diffusion and solubility. The compared aspect of the pristine and functionalized membranes can be seen in Figure 90.

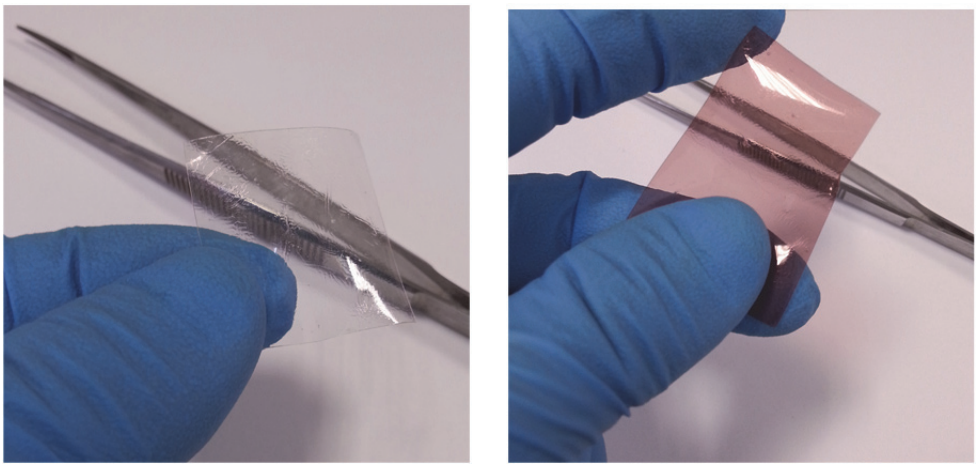

Figure 90. Picture of membranes M5 (left) and M5-NZ31 (right).

3.5. Characterization of the functional materials.

The excellent thermal and mechanical performance of the **VP** and **A4** copolymers are described elsewhere.[1,2] From our viewpoint, the materials have been characterized by TGA, FTIR, SEM and UV/Vis in order to address the presence of acid chloride moieties and their transformation upon reaction with the sensory motif containing an amine group to render pendant amide groups with these sensory motifs chemically anchored to the structure of the membrane.

The TGA data and patterns (Table 1 and Figure 91) clearly shows the influence of thermally labile acid chloride group, that causes a weight loss between 5 and 8 % observed as a TGA step with onset around 170 °C for **M2** and **M5**. This step is not observed after reaction of the acid chloride groups with **NZ31** to give the sensory motif chemically anchored to the polymer structure through the highly thermally stable amide group, and accordingly, **M2-NZ31** and **M5-NZ31** shows the conventional patters of the **VP** and **A4** copolymers with Tonset at about 380 °C.

[1] B. Redondo-Foj, M. Carsi, P. Ortiz-Serna, M. J. Sanchis, S. Vallejos, F. Garcia, J. M. Garcia, *Macromolecules*, **2014**, *47*, 5334–5346.
[2] B. Redondo-Foj, M. Carsi, P. Ortiz-Serna, M. J. Sanchis, F. Garcia, J. M. Garcia, *J. Phys. D: Appl. Phys.*, **2013**, *56*, 295304.

Table 1. TGA data.

Membrane	Weight loss below 275 °C (%)	T_5 (°C)	T_{10} (°C)	Char yield (%)
M2	5.5	281	368	5
M2-NZ31	<1	366	380	7
M5	7.6	199	366	5
M5-NZ31	<1	370	384	5

T_5 and T_{10}: temperature at which a weight loss of 5 % and 10 % is observed. Char yield residue at 800 °C under nitrogen atmosphere.

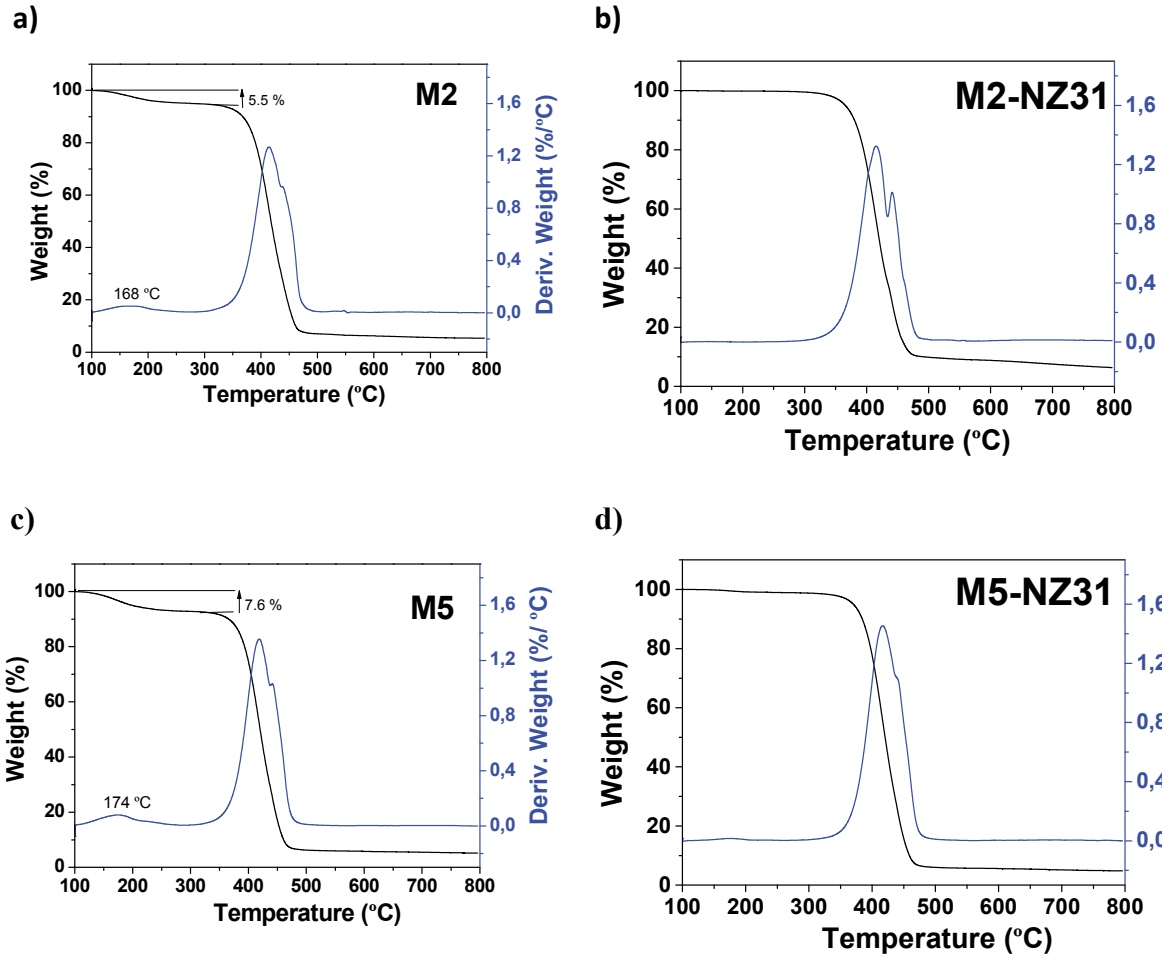

Figure 91. TGA of sensory functional membranes, a) and c), and modified functional membranes containing the sensory motifs, b) and d).

As it has been previously pointed out, the membrane compositions were designed to provide high hydrophilicity and a reasonable swelling percentage in organic solvents to allow

reactive amine groups to enter into the membrane by diffusion and to reach and interact with the sensory motifs, chloride groups, evenly distributed all along the swelled membrane. The amphiphilic character of the membrane was related to the solvent-swelling percentage (SSP), i.e., it was related to the weight percentage of solvent uptake by the film upon soaking until equilibrium in pure water, THF, and acetone at rt (see Table 2). The membranes prepared have a SSP higher than 40 and lower than 120 % is good for both the rapid diffusion of chemicals into the membrane and for maintaining the tractability in terms of the mechanical properties of the solvent-swelled materials. Moreover, to prove the presence and the potential of the functional material, the hydrolysis of the acid chloride groups with NaOH rendered the highly hydrophilic sodium carboxylate groups, increasing the water uptake.

Table 2. Solvent swelling percentage (%) of membranes.

Membrane	water	THF	acetone	water (after NaOHaq treatment)
M2	53	120	114	101
M2-NZ31	45	--	--	--
M5	40	89	68	54
M5-NZ31	52	--	--	--

The FT-IR spectra of modified and unmodified functional materials were fairly similar, as expected (see Figure 92). However, the reaction of acid chloride groups with secondary amine of the sensory molecule **NZ31** rendered amide groups that can be noticed in the evolution of the band centred at 3430 cm^{-1}.

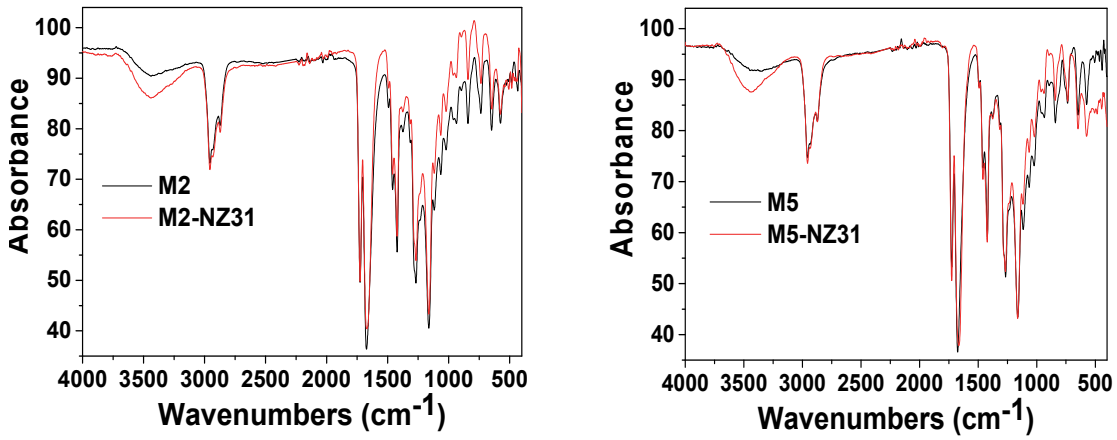

Figure 92. FT-IR spectra of functional membranes before (M2 and M5) and after functionalization (M2-NZ31 and M5-NZ31).

SEM images of functional membranes before and after functionalization showed the conventional structure of dense membrane without any appreciable changes. As an example,

Figure 93 depicts the cross section of membranes **M5** and **M5-NZ31** obtained by cryogenic fracture of the materials. On the other hand, EDS analysis showed the clear presence of Cl in good agreement with the theoretical content in **M2** and **M5**, and its absence in **M2-NZ31** and **M5-NZ31**, which confirms the reactivity of chloride motifs in the initial membranes and the effectiveness of the modification reaction.

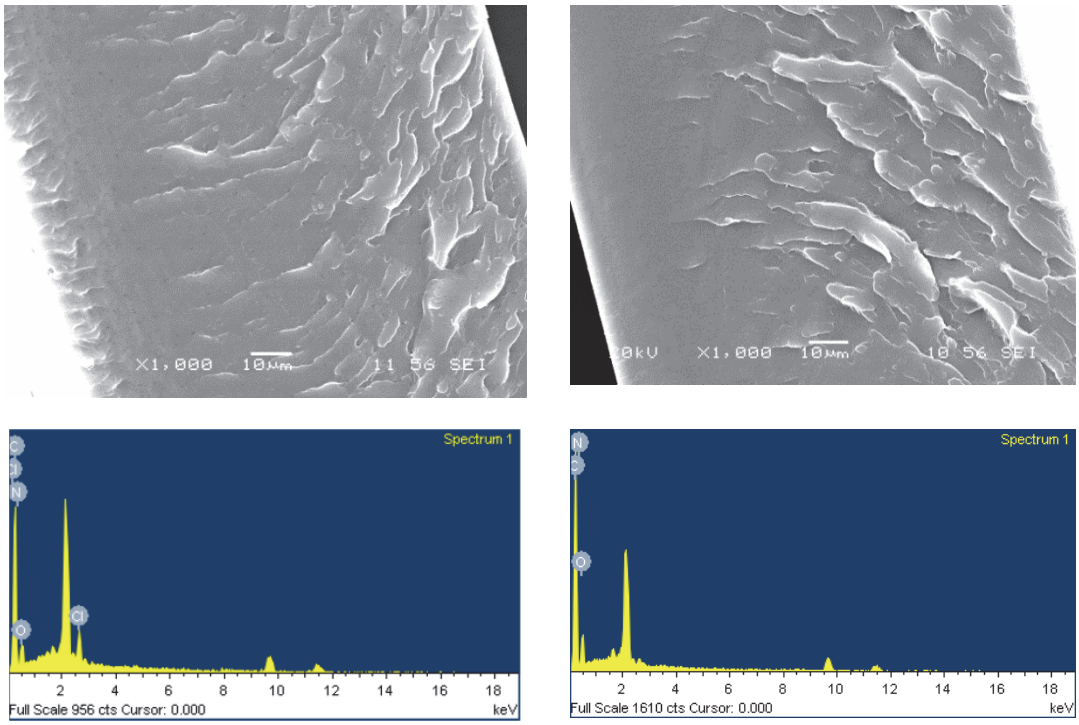

Figure 93. Cross-section and EDS analysis of membranes M5 and M5-NZ31, left and right, respectively.

The anchoring of the sensory probe **NZ31** to the membrane by means of its reaction with acid chloride moieties of membranes **M2** and **M5** was also confirmed by UV/Vis, as shown in Figure 94. The colourless membranes **M2** and **M5** turned purplish upon reaction with **NZ31** to render **M2-NZ31** and **M5- NZ31**, which was followed by the development of an absorption peak at 485 nm. Regarding the fluorescence behaviour on the membranes, none of them were fluorescent.

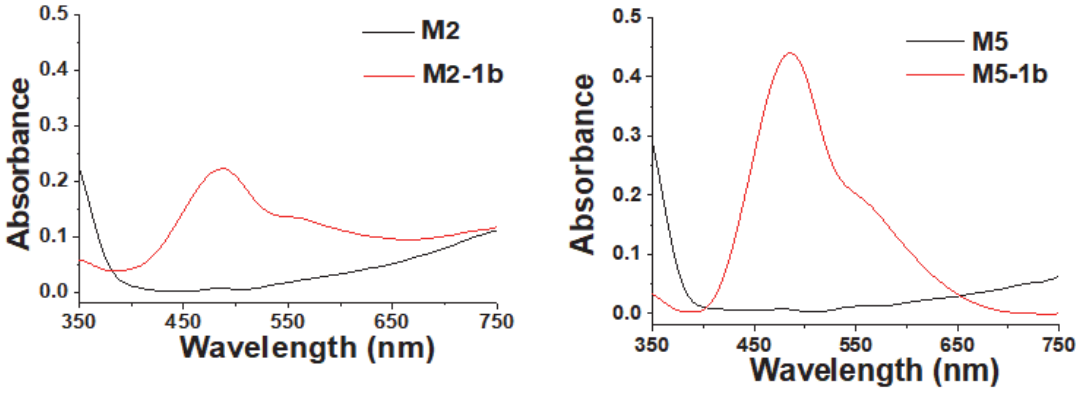

Figure 94. UV/Vis spectra obtained from membranes before and after heterogeneous reaction with the secondary amine of the sensory molecule NZ31.

4. Synthesis of silica substituted nanoparticles.

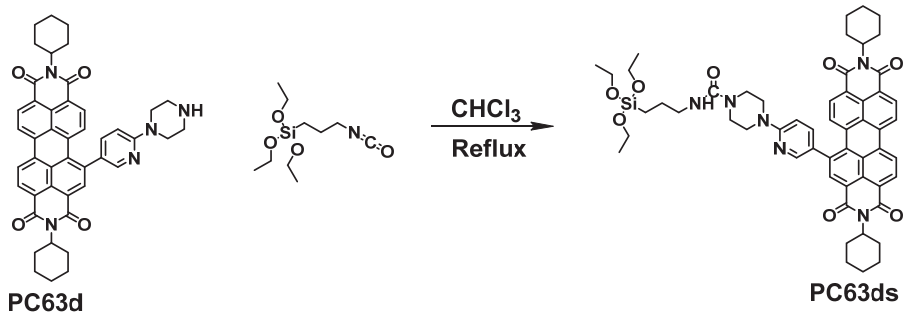

Scheme 3. Synthesis of PC63ds.

4.1. Synthesis of the triethoxysilyl derivative of PC63d (PC63ds).

The perylenediimide **PC63d** (20 mg) was dissolved in 5 mL of $CHCl_3$, then triethoxy-(3-isocyanatopropyl)silane (8 mg, 0.32 mmol) was added to the solution and stirred under reflux for 24 hours. The resultant product was checked by NMR and used in the next reaction without further purification.

Scheme 4. Synthesis of pPC63ds.

4.2. Synthesis of anchored silica derivatives of PC63ds, on silica nanoparticles (n) and on a TLC (p).

Substituted silica nanoparticles were prepared by reaction between 500 mg of silicon dioxide 10-20 nm nanoparticles and 4 mg of the triethoxysilyl perylene derivative (**PC63ds**). The mixture was refluxed at 112 ºC in a mixture of toluene:water 500:10 µL for 24 hours. Finally, nanoparticles were washed with toluene (2 x 2 mL), DCM (2 x 2 mL) and Et_2O (2 x 2 mL). The obtained product was called **nPC63ds**. **FT-IR (KBr, cm^{-1}):** 3429 (O-H), 1634, 1091, 956, 797, 544, 469 (fingerprint region). **Pure silica (10-20 mm). FT-IR (KBr, cm^{-1}):** 3429 (O-H), 1627, 1088, 960, 801, 555, 465.

By the same way, silane derivatives were bound to a thin layer silica supported plate, 0.1 mg of **PC63d** for 1 cm^2 plate. Instead of refluxed, it was heated at 60 ºC for 48 hours until solutions have neither colour nor fluorescence. Then, the plate was cleaned with toluene (2 x 2 mL), DCM (2 x 2 mL) and Et_2O (2 x 2 mL). The obtained product was called **pPC63ds**.

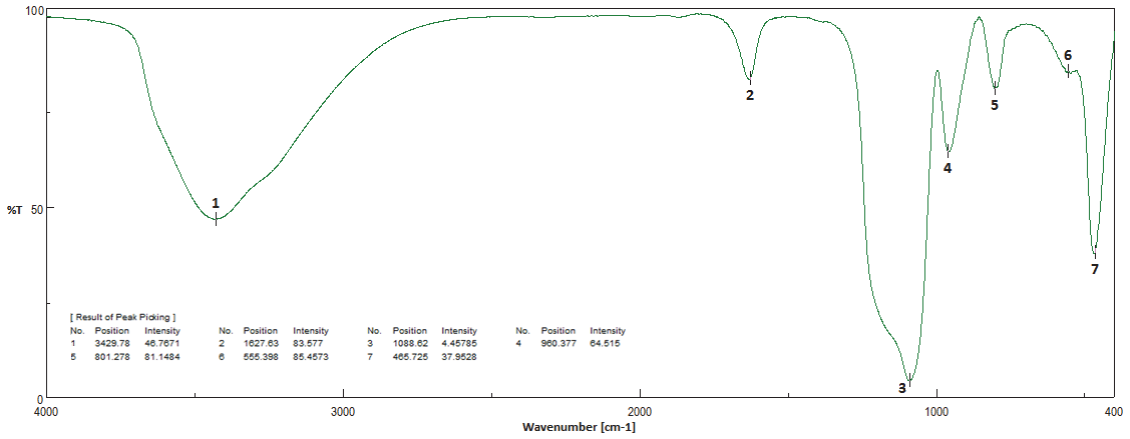

Figure 95. FT-IR (KBr) spectrum of Pure silica (10-20 mm).

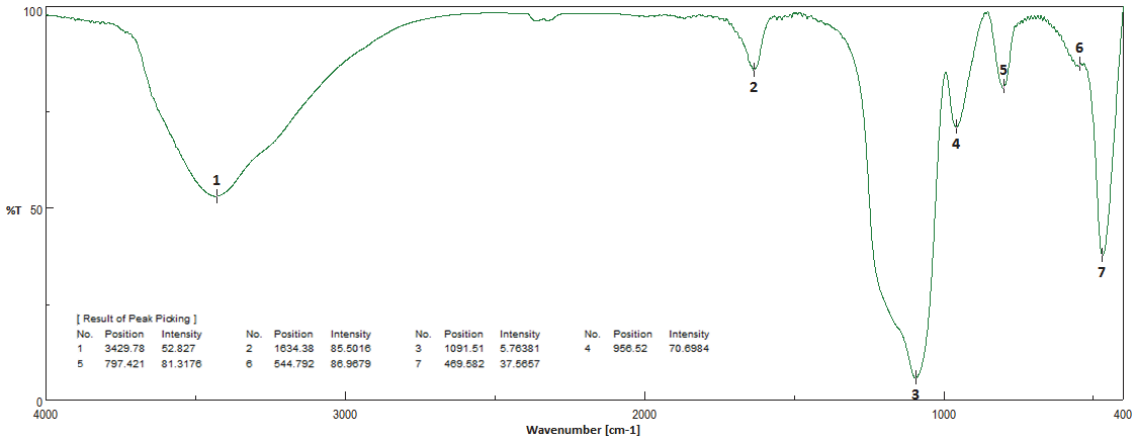

Figure 96. FT-IR (KBr) spectrum of nPC63ds.

SYNTHESIS AND CHARACTERIZATION: CHAPTER 2

1. Synthesis and characterization of water soluble perylenediimides.

1.1. Synthesis of *N,N'*-bis((*N''*-*tert*-butoxycarbonyl)piperidine)-1,6,7,12-tetrachloroperylene-3,4,9,10-tetracarboxylic diimide (PC43).

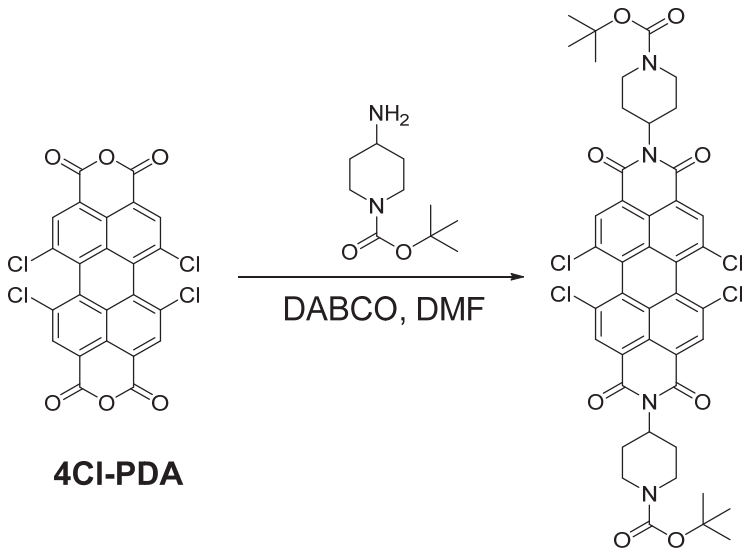

Anhydrous DMF (20 mL) and 4-amino-1-(*N''*-*tert*-butoxycarbonyl)piperidine (0.47 g, 2.30 mmol) were added under nitrogen to 1,6,7,12-tetrachloroperylenetetracarboxylic acid dianhydride (0.50 g, 0.94 mmol) and DABCO (0.26 g, 2.30 mmol). The mixture was irradiated in a microwave device at 110 ^{o}C for 1 hour. Then, it was poured over an aqueous solution of HCl 1M (15 mL), stirred for 1 hour, filtered and washed with water (30 mL). Purification was carried out by silica gel flash chromatography using DCM:MeCN (80:20) as eluent to give **PC43** as an orange solid in 95% yield (0.79 g, 0.89 mmol). **R_f (DCM:MeOH 50:2):** 0.6. **Mp (^{o}C):** > 350 ^{o}C. **FT-IR (KBr, cm^{-1}):** 2977 (C-H), 2931 (C-H), 2852 (C-H), 1701 (C=O), 1661 (CONH), 1590 (C_{Ar}-C_{Ar}), 1420 (CH_2), 1366 (C-N), 1337 (C-O), 1275, 1243, 1150, 1005, 951, 908, 749, 684, 547 (fingerprint region). **^{1}H NMR (300 MHz, $CDCl_3$) *δ*:** 8.65 (s, 4H, H_{Ar}), 5.24 – 5.15 (m, 2H, N-CH), 4.32 (s, 4H, CH_2), 2.88 – 2.72 (m, 9H, CH_2), 1.70 (d, *J* = 12.8 Hz, 3H, CH_2), 1.51 (s, 18H, $COOC(CH_3)_3$). **^{13}C NMR (75 MHz, $CDCl_3$) *δ*:** 162.7 (**C**ON**C**O$_{Imide}$), 154.8 (**C**OOC$(CH_3)_3$), 135.5 (C_{Ar}), 133.2 (CH), 131.5 (C_{Ar}), 128.6 (C_{Ar}), 123.6 (C_{Ar}), 123.4 (C_{Ar}), 79.9 (COO**C**$(CH_3)_3$), 52.6 (**C**HN$_{imide}$), 44.2 (**C**H$_2$), 43.9 (**C**H$_2$), 29.8 (**C**H$_2$), 28.6 (COOC(**C**H$_3$)$_3$), 28.4 (**C**H$_2$). **HRMS (MALDI+, DCTB):** m/z calcd. for $C_{39}H_{33}Cl_4N_4O_6$ ($[M+H-(COOC(CH_3)_3)]^+$): 793.1149; found: 793.1142.

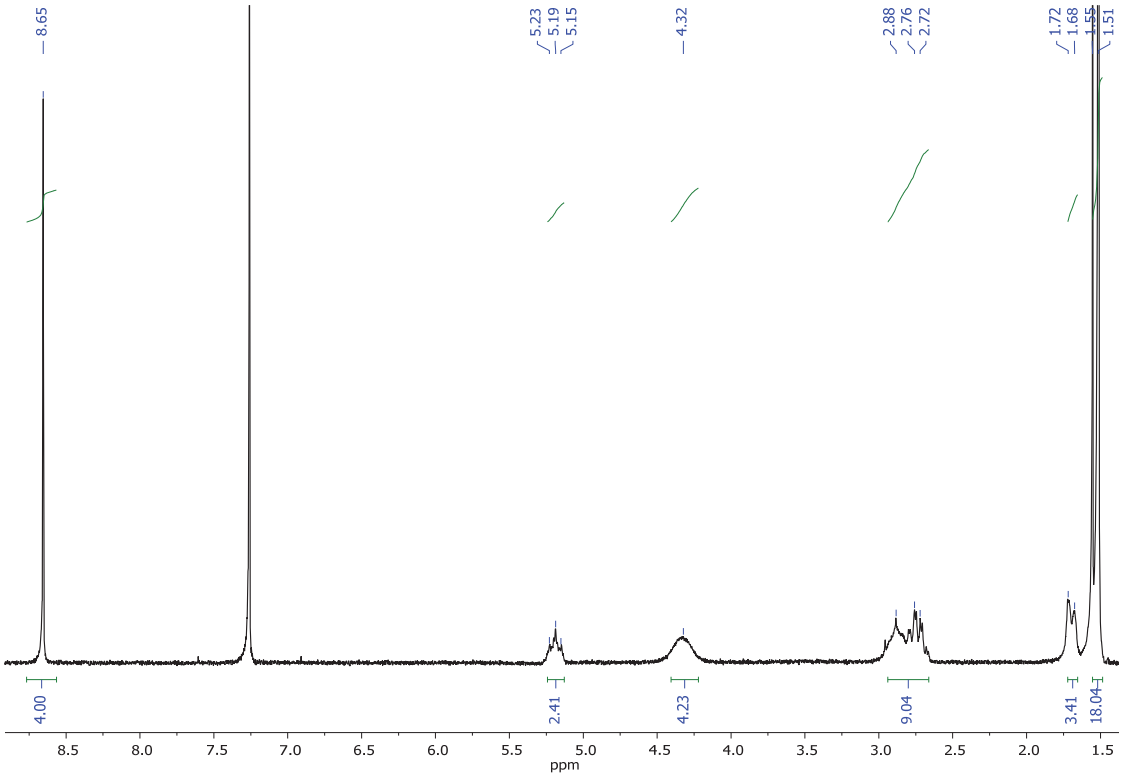

Figure 1. ^{1}H NMR (300 MHz, $CDCl_3$) of PC43

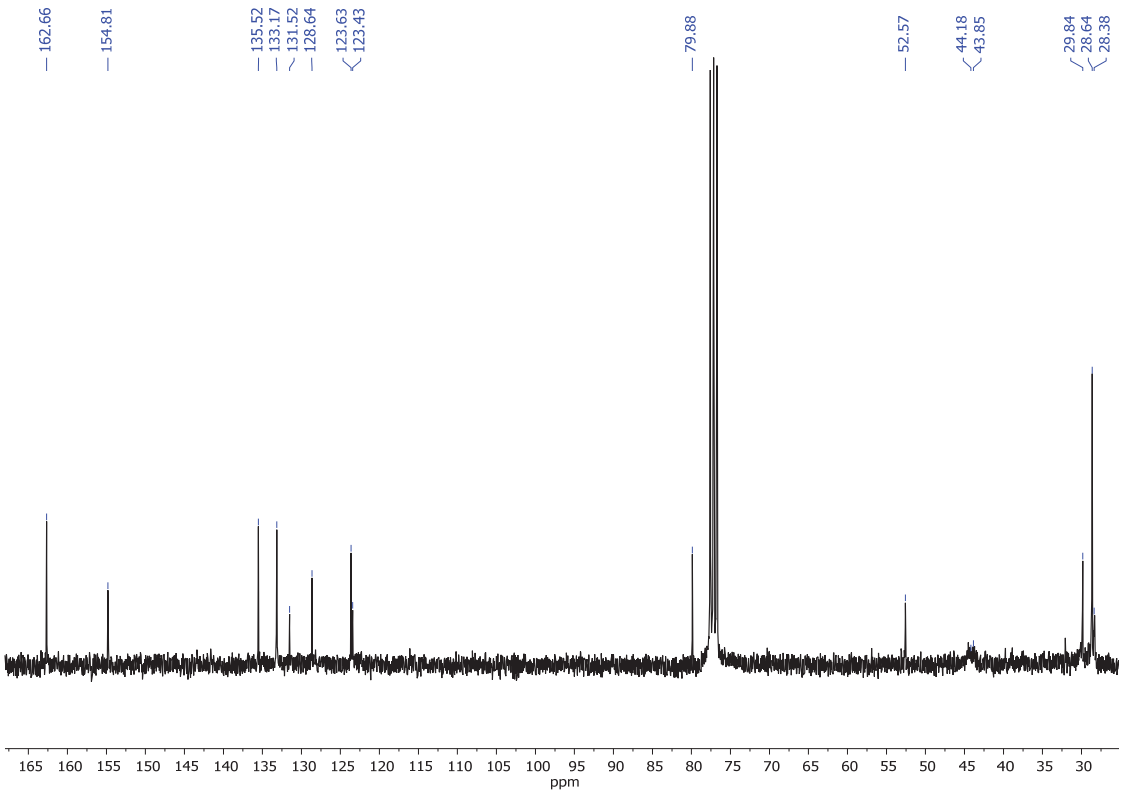

Figure 2. ^{13}C NMR (75 MHz, $CDCl_3$) of PC43

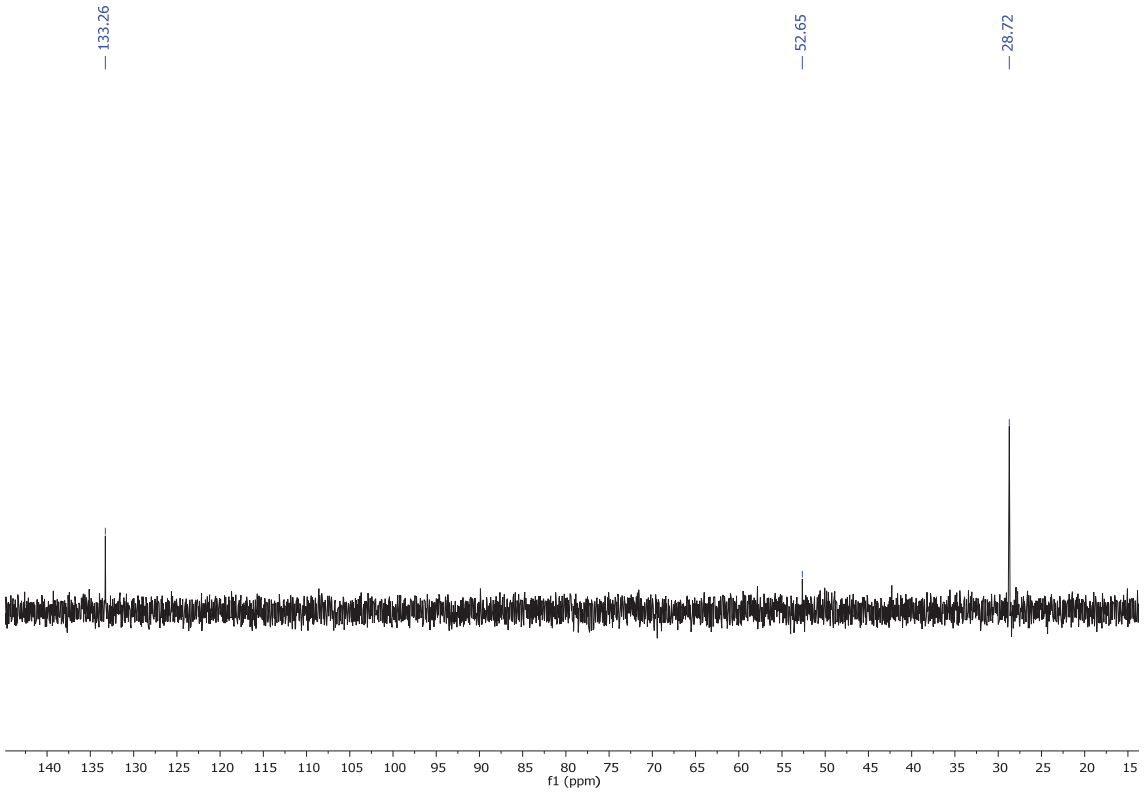

Figure 3. ^{13}C NMR-DEPT-135 (101 MHz, $CDCl_3$) of PC43

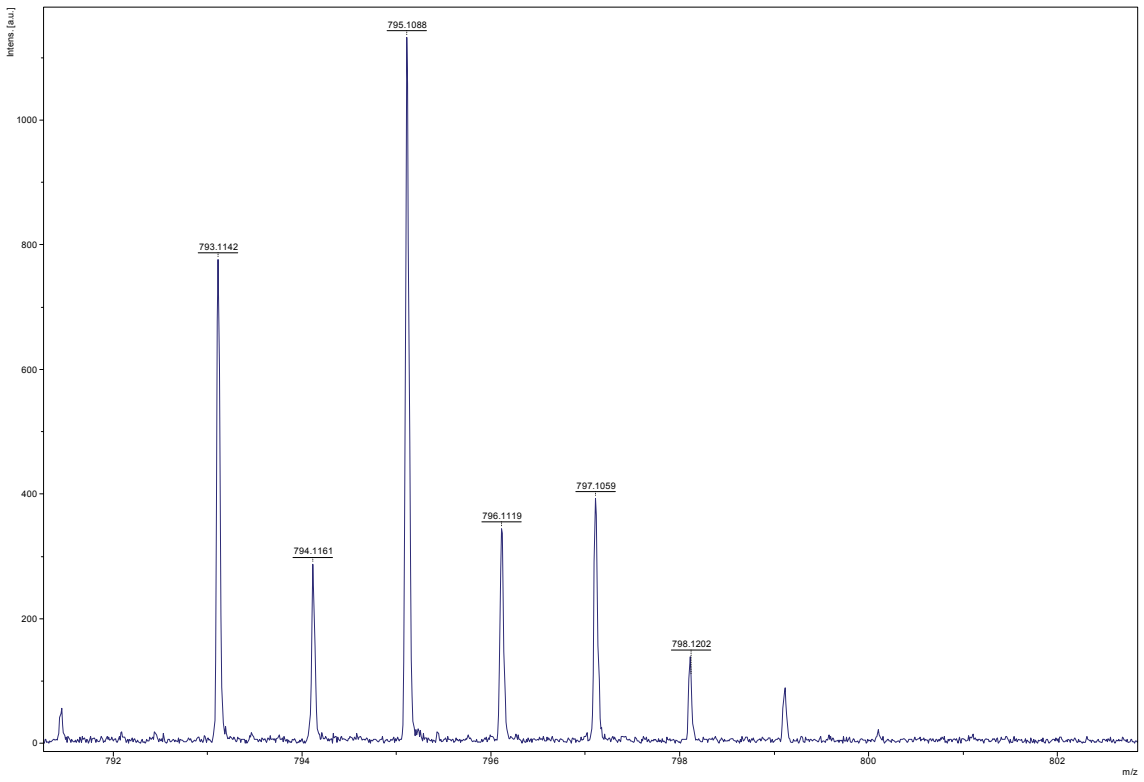

Figure 4. Mass spectrum (MALDI+, DCTB) of PC43

Solvatochromism:

The concentration of **PC43** is $1 \cdot 10^{-5}$ M. The excitation wavelength is 366 nm. The absorption and emission spectra have been measured in the listed solvents below in the range between 200 to 900 nm. The used solvents are: MeOH, DMSO, DMF, MeCN, acetone, AcOEt, THF, $CHCl_3$, DCM, toluene, diethyl ether, hexane and cyclohexane.

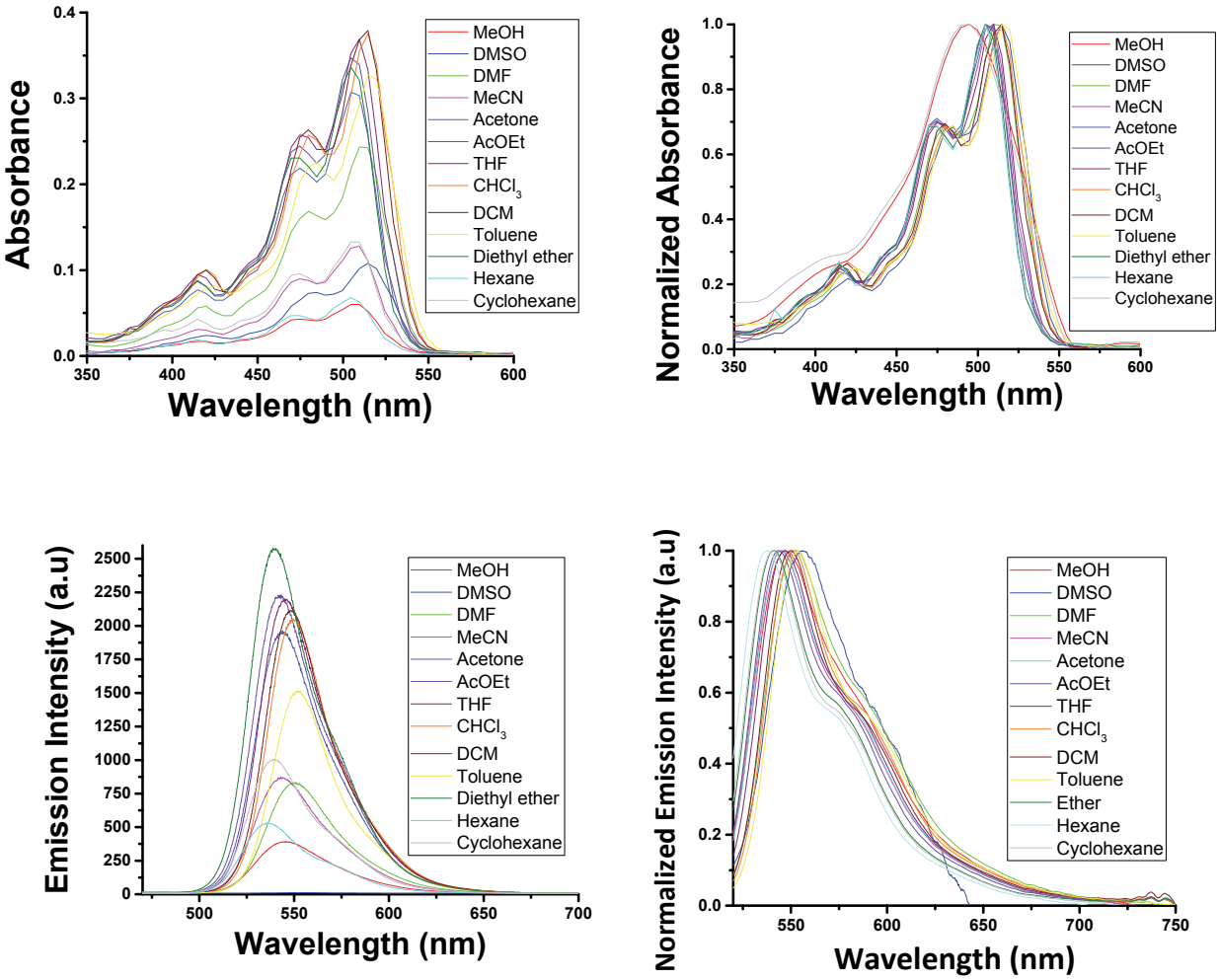

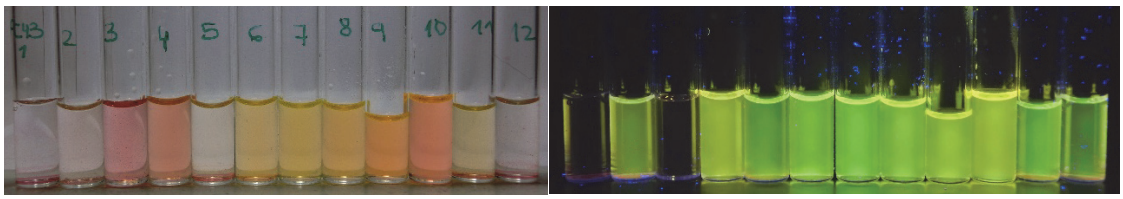

Solvents: 1: Water, 2: MeOH, 3: DMSO, 4: DMF, 5: MeCN, 6: acetone, 7: AcOEt, 8: THF, 9: $CHCl_3$, 10: DCM, 11: toluene, 12: diethyl ether, 13: hexane, 14: cyclohexane.

Figure 5. Upper. Absorbance spectra and Normalized absorbance spectra of PC43. Middle: Fluorescence spectra and Normalized and corrected fluorescence spectra of PC43. Lower. Solvatochromic effect of PC43 under white light and light of 366 nm.

1.2. *N,N'*-bis-Piperidine-1,6,7,12-tetrachloroperylene-3,4,9,10-tetracarboxylic diimide (PC45).

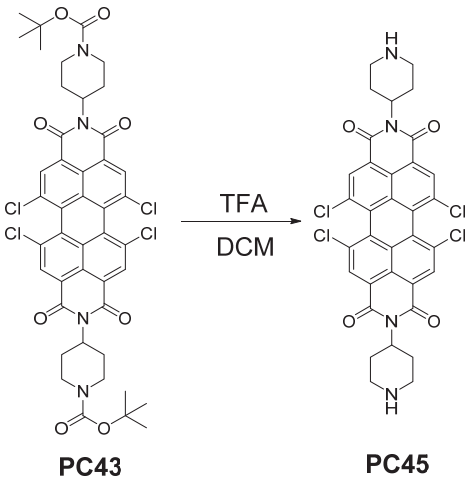

N,N'-bis-(1-(*N''-tert*-butoxycarbonyl)-piperidine)-1,6,7,12-tetrachloroperylene-3,4,9,10-tetracarboxylic diimide (100 mg, 0.11 mmol) was dissolved in 15 ml of DCM and trifluoroacetic acid (3.7 g, 32.4 mmol) was added. The solution was stirred at room temperature for 30 minutes. The reaction was neutralized with 5% NaOH solution. The crude was extracted with DCM and dried over anhydrous sodium sulphate. **PC45** was obtained as a red solid in 90 % yield (70 mg, 0.09 mmol). **R_f (DCM:MeOH 50:4):** 0. **Mp:** > 350 °C. **FT-IR (KBr, cm^{-1}):** 2921 (C-H), 2851 (C-H), 1700 (C=O), 1651 (CONH), 1586 (C_{Ar}-C_{Ar}), 1366 (C-N), 1316 (C-O), 1261, 1236, 1001, 804, 745 (fingerprint region). **^{1}H NMR (300 MHz, $CDCl_3$) δ:** 8.65 (s, 4H, HAr), 5.24 – 5.15 (m, 2H, N-CH), 4.32 (s, 4H, CH_2), 2.88 – 2.72 (m, 9H, CH_2), 1.70 (d, J = 12.8 Hz, 3H, CH_2). **MS (ESI+)**: m/z: calcd. for ($[M+H]^+$): 693.0624; found: 693.0618.

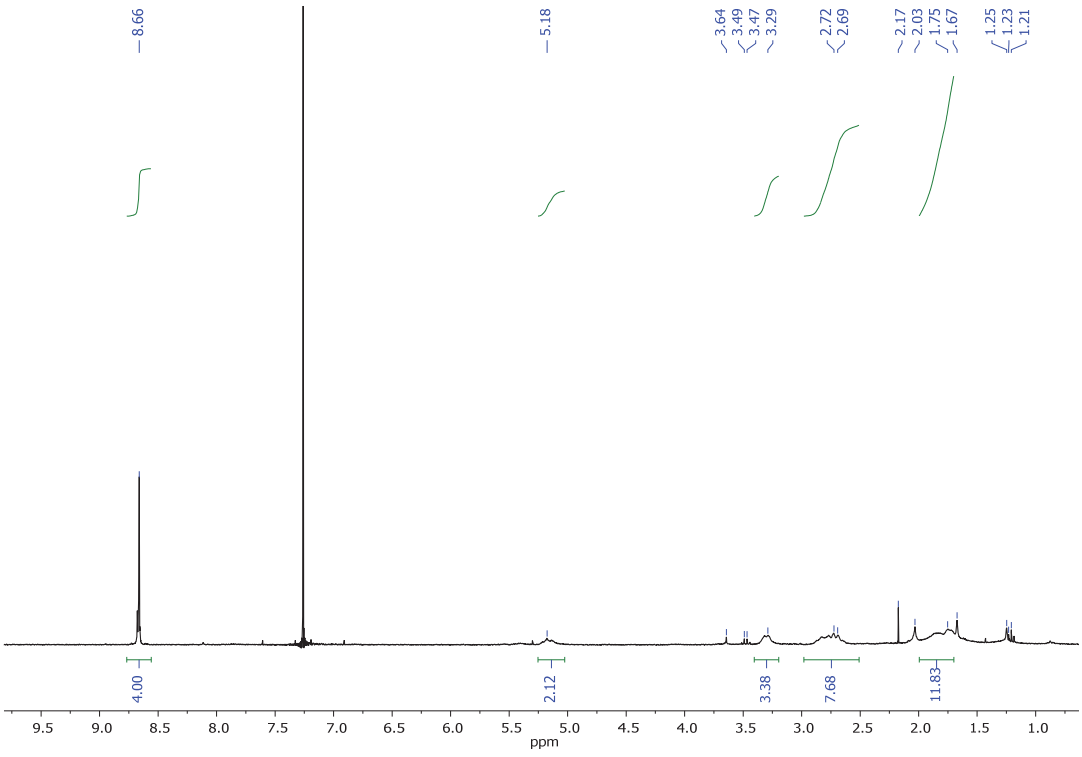

Figure 6. ^{1}H NMR (300 MHz, $CDCl_3$) of PC45

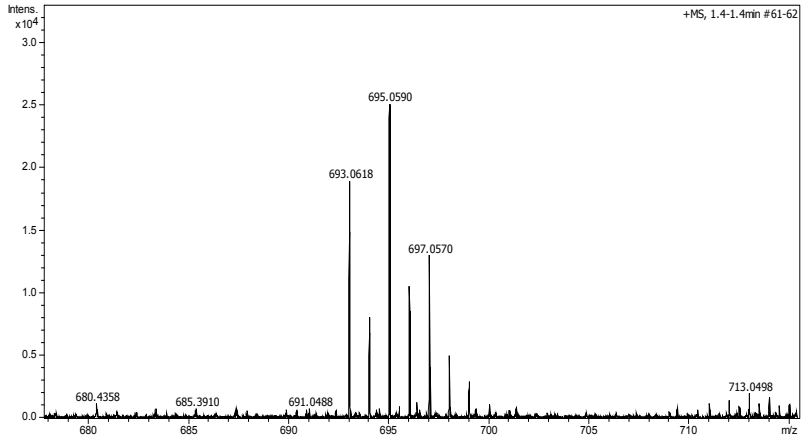

Figure 7. Mass spectrum (MALDI+, DCTB) of PC45

Solvatochromism:

The concentration of **PC43** is $1 \cdot 10^{-5}$ M. The excitation wavelength is 479 nm. The absorption and emission spectra have been measured in the listed solvents below in the range between 200 to 900 nm. The used solvents are: MeOH, DMSO, DMF, MeCN, acetone, AcOEt, THF, $CHCl_3$, DCM, toluene and diethyl ether.

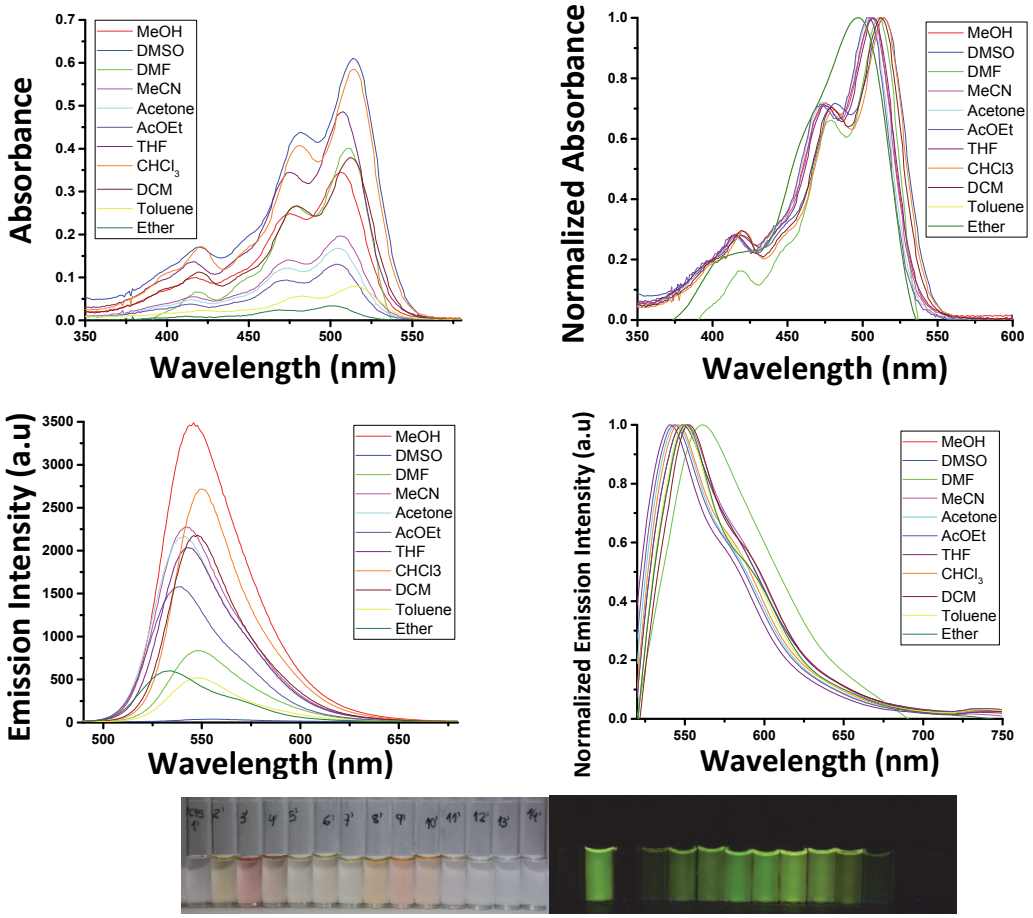

Solvents: 1: Water, 2: MeOH, 3: DMSO, 4: DMF, 5: MeCN, 6: acetone, 7: AcOEt, 8: THF, 9: $CHCl_3$, 10: DCM, 11: toluene, 12: diethyl ether, 13: hexane, 14: cyclohexane.

Figure 8. Upper. Absorbance spectra and Normalized absorbance spectra of PC45. Middle: Fluorescence spectra and Normalized and corrected fluorescence spectra of PC45. Lower. Solvatochromic effect of PC45 under white light and light of 366 nm.

1.3. Synthesis of *N,N'*-bis(1-(*N''*-*tert*-butoxycarbonyl)piperidine)-1,6,7,12-tetrakis(3,5-bis(trifluoromethyl)phenoxy)perylene-3,4,9,10-tetracarboxylic diimide (PC48).

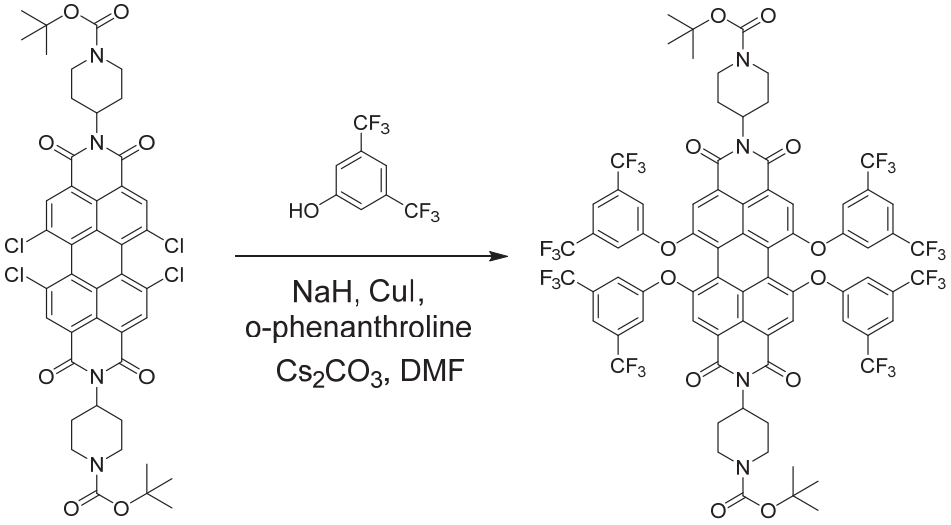

PC43 **PC48**

N,N'-bis-(1-(*N''*-*tert*-butoxycarbonyl)piperidine)-1,6,7,12-tetrachloroperylene-3,4,9,10-tetracarboxylic diimide (20 mg, 0.02 mmol), *o*-phenantroline monohydrated (3.15 mg, 0.02 mmol), copper (I) iodine (3 mg, 0.01 mmol) and cesium carbonate (86.1 mg, 0.26 mmol) were added under nitrogen to a suspension of NaH (5 mg, 0.11 mmol), anhydrous DMF (5 mL) and 3,5-bis(trifluoromethyl)phenol (96 mg, 0.20 mmol). The mixture was irradiated in a microwave device at 110 ^{o}C for 1 hour. The solvent was evaporated under reduced pressure. Purification was carried out by silica gel flash chromatography using DCM:MeCN (97:3) as eluent to give **PC48** as deep red solid in 51 % yield (18.7 mg, 0.01 mmol). **R_f (DCM:MeOH 50:1):** 0.6. **Mp (^{o}C):** > 350 ^{o}C. **FT-IR (KBr, cm^{-1}):** 3067 (C-H), 2977 (C-H), 2928 (C-H), 2863 (C-H), 1701 (C=O), 1661 (CONH), 1593 (C_{Ar}-C_{Ar}), 1510 (C_{Ar}-C_{Ar}), 1459 (CH_2), 1411 (CH_2), 1371 (CH_2), 1334 (C-N), 1303 (C-O), 1280, 1178, 1138, 1033, 988, 951, 885, 806, 729, 704, 678, 664 (fingerprint region). **^{1}H NMR (300 MHz, $CDCl_3$) δ:** 8.19 (s, 4H, H_{Ar}), 7.61 (t, *J* = 1.4 Hz, 4H, H_{Ar}), 7.29 (d, *J* = 1.4 Hz, 8H, H_{Ar}), 5.13 – 5.05 (m, 2H, N-CH), 4.28 – 4.25 (s, 4H, CH_2), 2.81 – 2.61 (m, 10H, CH_2), 1.64 (d, *J* = 9.1 Hz, 3H, CH_2), 1.40 (s, 18H, $COOC(CH_3)_3$). **^{13}C NMR (101 MHz, $CDCl_3$) δ:** 162.7 (**C**ON**C**O$_{Imide}$), 156.5 (-C_q-O-**C**$_{qPhenol}$), 154.7 (-**C**$_q$-O-$C_{qPhenol}$), 154.6 (**C**OOC$(CH_3)_3$), 134.6 (C_{Ar}), 134.3 (C_{Ar}), 133.9 (C_{Ar}), 133.6 (C_{Ar}), 133.1 (C_{Ar}), 126.5 (C_{Ar}), 124.7 (CF_3), 123.8 (C_{Ar}), 121.5 (C_{Ar}), 121.3 (C_{Ar}), 121.1, 119.6 (C_{Ar}), 118.6 (C_{Ar}), 109.9 (C_{quat}), 79.8 (**C**$(CH_3)_3$), 52.6 (**C**HN$_{imide}$), 44.3 (CH_2), 43.4 (CH_2), 31.1 (CH_2), 29.9 (CH_2), 28.6 ($COOC(\mathbf{C}H_3)_3$), 28.3 (CH_2). **HRMS (MALDI-, DCTB):** m/z calcd. for $C_{76}H_{52}F_{24}N_4O_{12}$ ($[M]^+$): 1668.3198; found: 1668.3254.

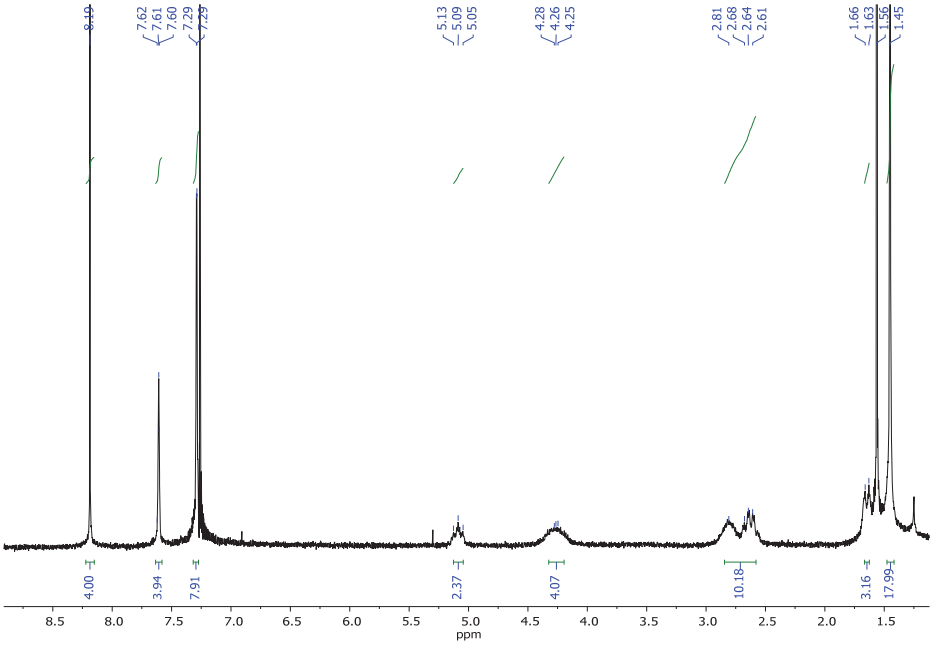

Figure 9. ^{1}H NMR (300 MHz, $CDCl_3$) of PC48

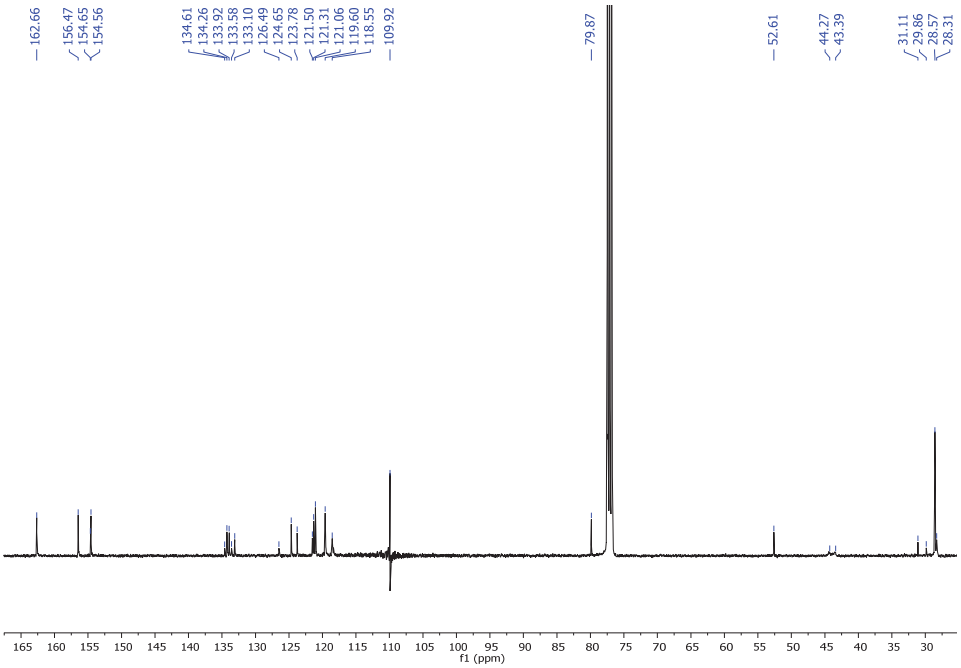

Figure 10. ^{13}C NMR (101 MHz, $CDCl_3$) of PC48

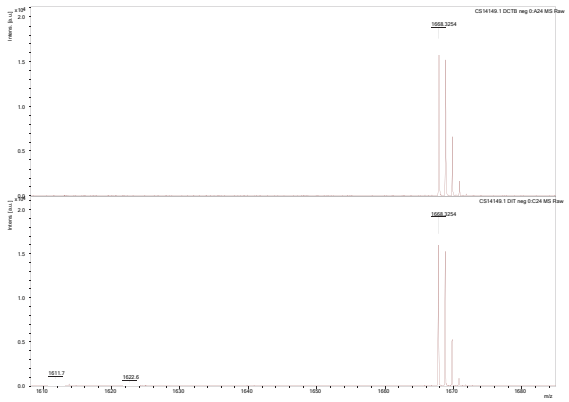

Figure 11. Mass spectrum (MALDI-, DCTB) of PC48

Solvatochromism: The concentration of **PC48** is $1 \cdot 10^{-5}$ M. The excitation wavelength is 479 nm. The absorption and emission spectra have been measured in the listed solvents below in the range between 200 to 900 nm. The used solvents are: DMF, MeCN, acetone, AcOEt, THF, $CHCl_3$, DCM, toluene and diethyl ether.

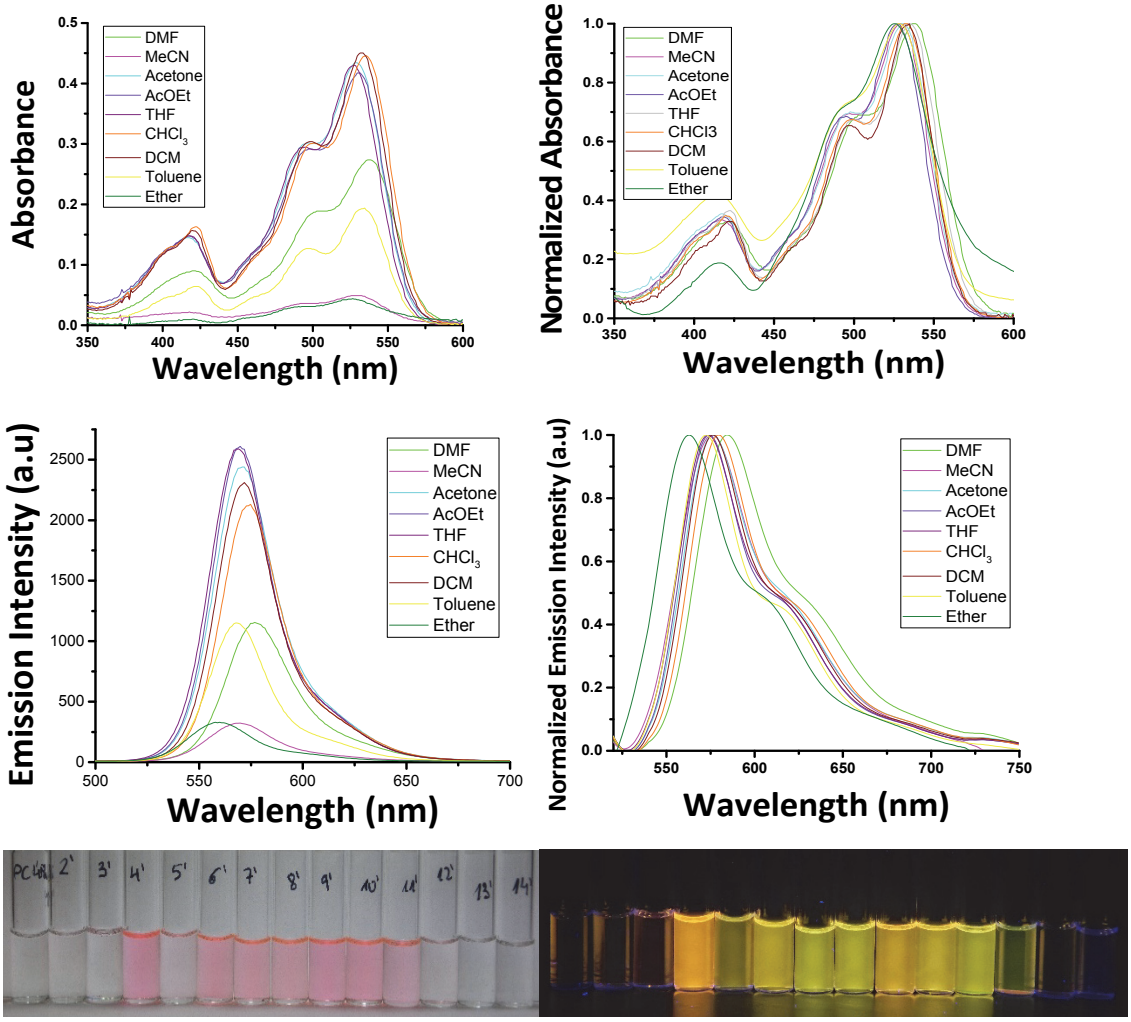

Solvents: 1: Water, 2: MeOH, 3: DMSO, 4: DMF, 5: MeCN, 6: acetone, 7: AcOEt, 8: THF, 9: $CHCl_3$, 10: DCM, 11: toluene, 12: diethyl ether, 13: hexane, 14: cyclohexane.

Figure 12. Upper. Absorbance spectra and Normalized absorbance spectra of PC48. Middle: Fluorescence spectra and Normalized and corrected fluorescence spectra of PC48. Lower. Solvatochromic effect of PC48 under white light and light of 366 nm.

1.4. Synthesis of *N,N'*-bis(1-(*N''*-*tert*-butoxycarbonyl)piperidine)-1,6,7,12-tetrakis(3,5-bis(methoxycarbonyl)phenoxy)perylene-3,4,9,10-tetracarboxylic diimide (PC51).

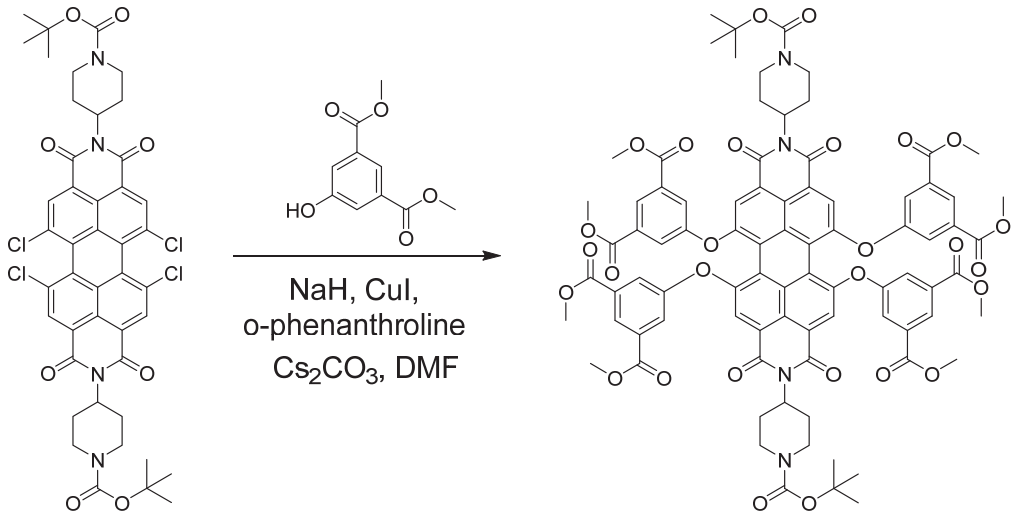

PC43 **PC51**

N,N'-bis(1-(*N''*-*tert*-Butoxycarbonyl)piperidine)-1,6,7,12-tetrachloroperylene-3,4,9,10-tetracarboxylic diimide (100 mg, 0.1 mmol), *o*-phenantroline monohydrated (12.60 mg, 0.06 mmol), copper (I) iodine (6 mg, 0.03 mmol) and cesium carbonate (430 mg, 1.32 mmol) were added under nitrogen to a suspension of NaH (17.6 mg, 0.44 mmol), anhydrous DMF (20 mL) and dimethyl-5-hydroxyisophthlate (104.2 mg, 0.49 mmol). The mixture was irradiated in a microwave device at 110 ^{o}C for 1 hour. The solvent was evaporated under reduced pressure. Purification was carried out by silica gel flash chromatography using DCM:MeCN (70:30) as eluent to give four substituted phenols (**PC51**, **PC51.3**, **PC51.2**, **PC51.1**) and the decarbonylated perylenediimide **PC51.d**.

PC51 was obtained as deep pink solid in 40 % yield (69.70 mg, 0.04 mmol). **R_f (DCM:MeOH 50:2):** 0.2. **Mp (^{o}C):** > 350 ^{o}C. **FT-IR (KBr, cm^{-1}):** 2951 (C-H), 2925 (C-H), 2849 (C-H), 1735 (C=O), 1698 (C=O), 1664 (CONH), 1587 (C_{Ar}-C_{Ar}), 1505 (C_{Ar}-C_{Ar}), 1454 (CH_2), 1431 (CH_2), 1414 (CH_2), 1320 (C-N), 1297 (C-O), 1280, 1249, 1175, 1004, 999, 792, 758, 721, 669 (fingerprint region). **^{1}H NMR (300 MHz, $CDCl_3$) δ:** 8.31 (t, *J* = 1.4 Hz, 4H, H_{Ar}), 8.13 (s, 4H, H_{Ar}), 7.67 (d, *J* = 1.4 Hz, 8H, H_{Ar}), 5.08 – 5.00 (m, 2H, N-CH), 4.21 (s, 4H, CH_2), 3.86 (s, 24H, $COOCH_3$), 2.75 – 2.52 (m, 9H, CH_2), 1.60 (d, *J* = 11.6 Hz, 3H, CH_2), 1.40 (s, 18H, $COOC(CH_3)_3$). **^{13}C NMR (101 MHz, $CDCl_3$) δ:** 165.1 (**C**$OOCH_3$), 163.1 (**C**O**C**O_{Imide}), 155.9 (-C_q-O-**C_q**$_{Phenol}$), 154.9 (-**C_q**-O-$C_{qPhenol}$), 154.7 (**C**$OOC(CH_3)_3$), 133.1 (C_{Ar}), 132.7 (C_{Ar}), 132.0 (C_{Ar}), 126.5 (CH), 124.5 (CH), 124.0 (C_{Ar}), 121.2 (CH), 121.1 (C_{Ar}), 120.9 (CH), 120.9 (C_{Ar}), 79.8 (COO**C**$(CH_3)_3$), 52.7 (COO**C**H_3), 52.6 (**C**HN_{imide}), 52.4 (**C**HN_{imide}), 44.1 (CH_2), 43.6 (CH_2), 29.9 (CH_2), 28.6 ($COOC(CH_3)_3$), 28.4 (CH_2). **HRMS (MALDI-, DCTB):** m/z calcd. for $C_{84}H_{76}N_4O_{28}$ ([M$^-$]): 1588.4641; found: 1588.0849.

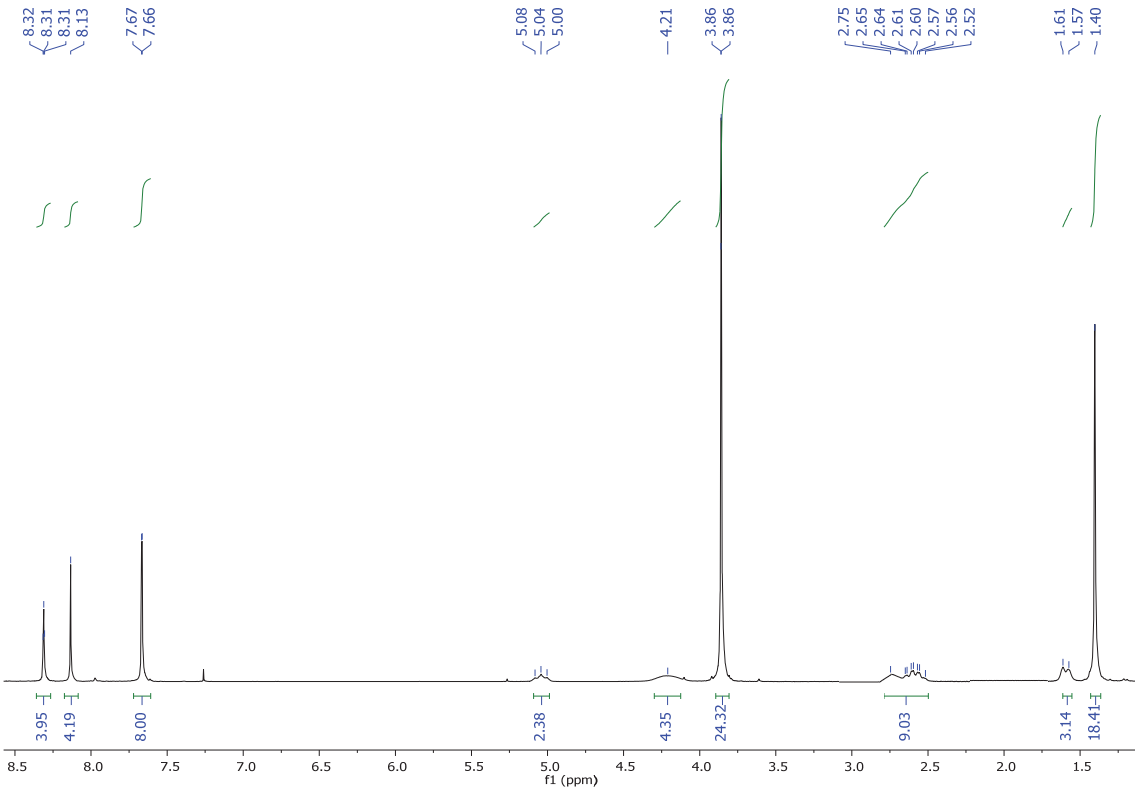

Figure 13. ^{1}H NMR (300 MHz, $CDCl_3$) of PC51

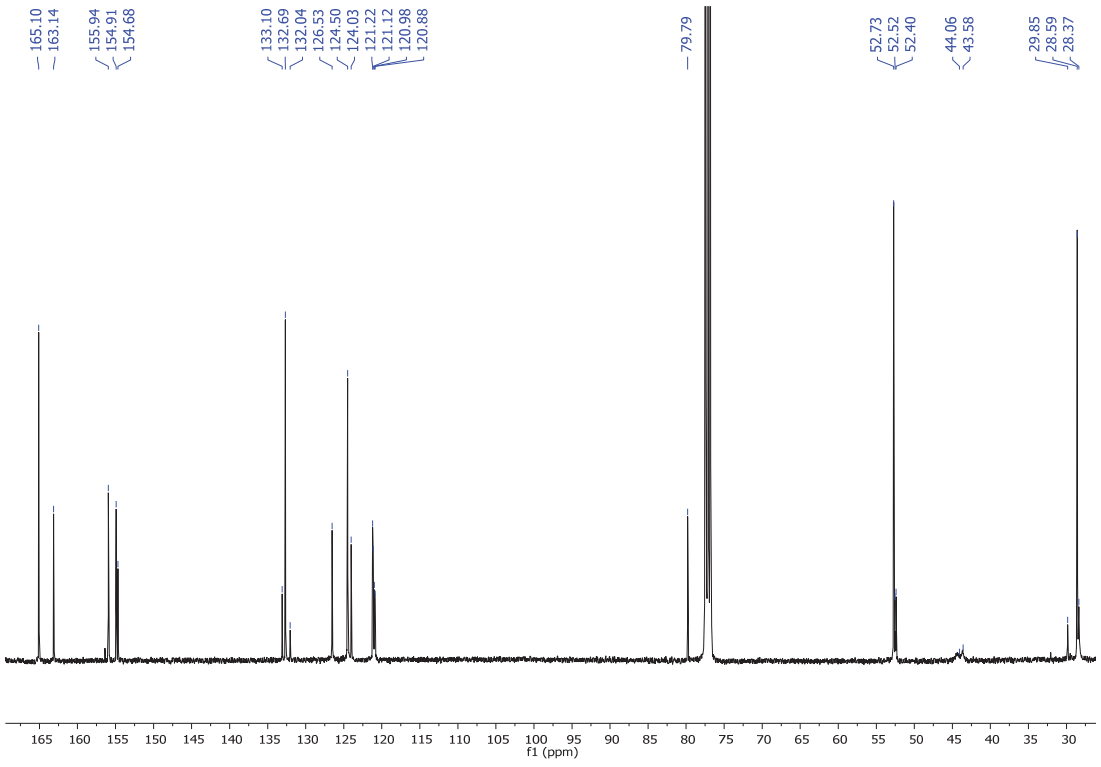

Figure 14. ^{13}C NMR (101 MHz, $CDCl_3$) of PC51

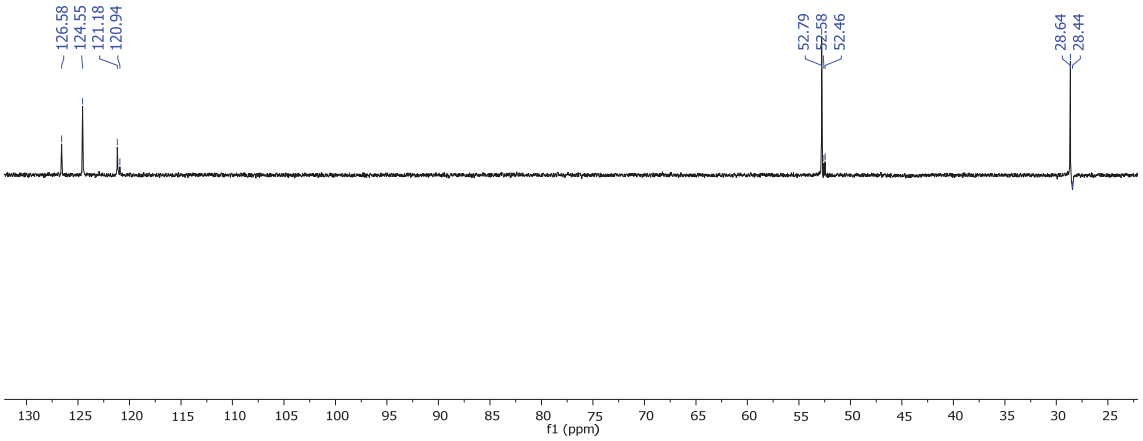

Figure 15. ^{13}C NMR-DEPT-135 (101 MHz, $CDCl_3$) of PC51

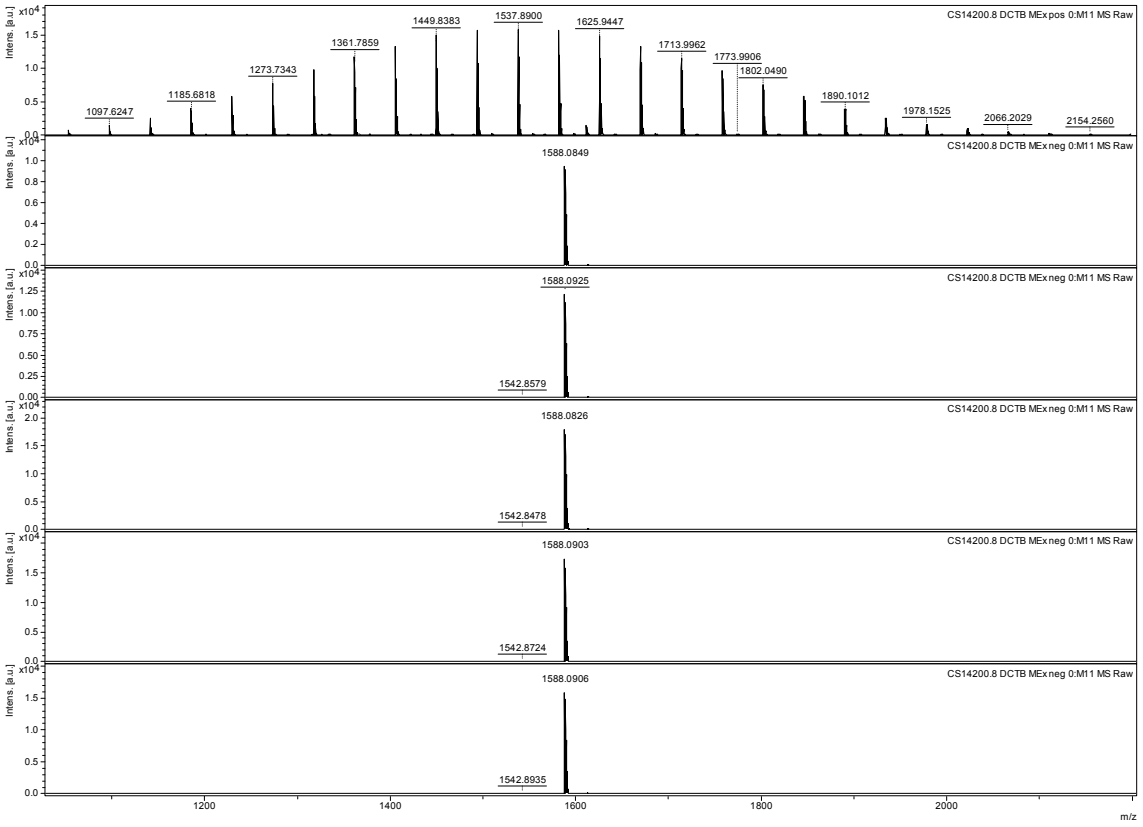

Figure 16. Mass spectrum (MALDI-, DCTB) of PC51

Solvatochromism:

The concentration of **PC51** is $1 \cdot 10^{-5}$ M. The excitation wavelength is 366 nm. The absorption and emission spectra have been measured in the listed solvents below in the range between 200 to 900 nm. The used solvents are: DMSO, DMF, MeCN, acetone, AcOEt, THF, $CHCl_3$, DCM, and toluene.

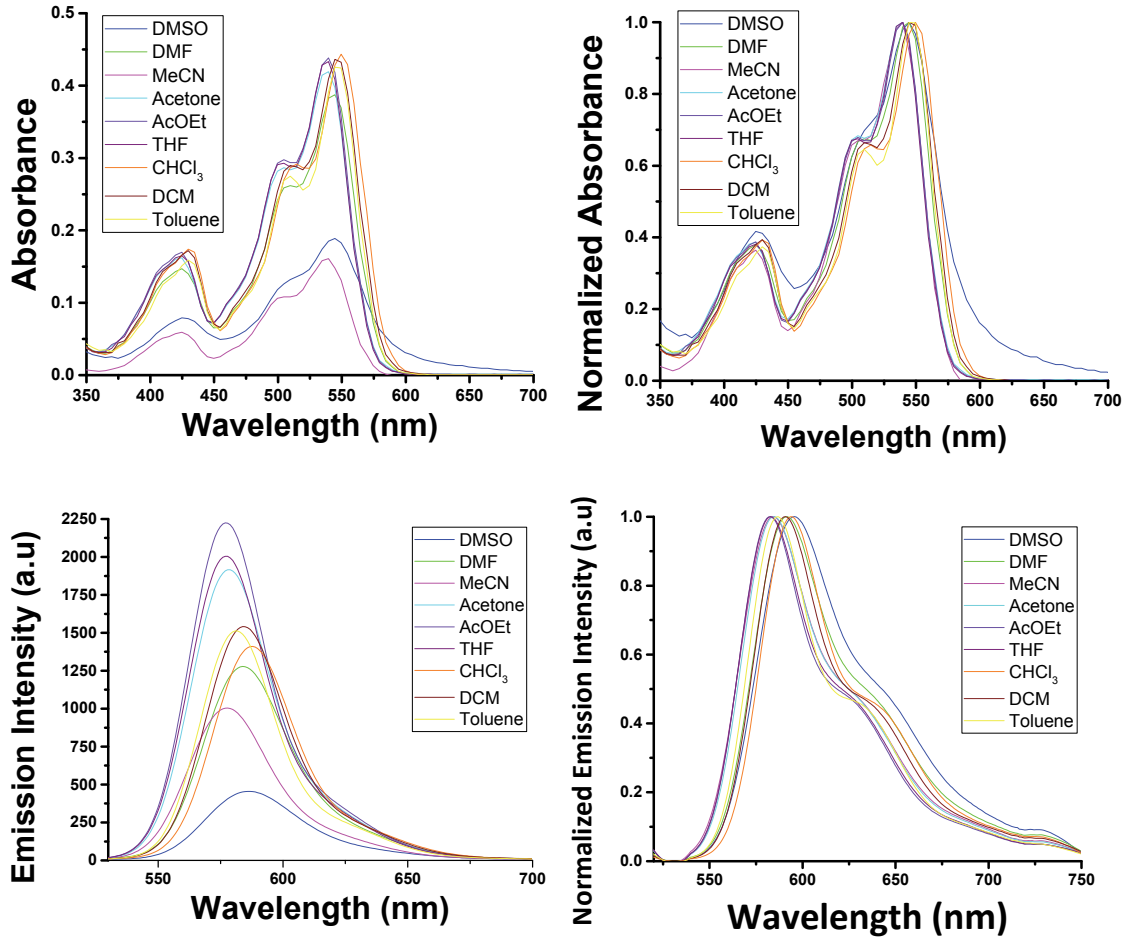

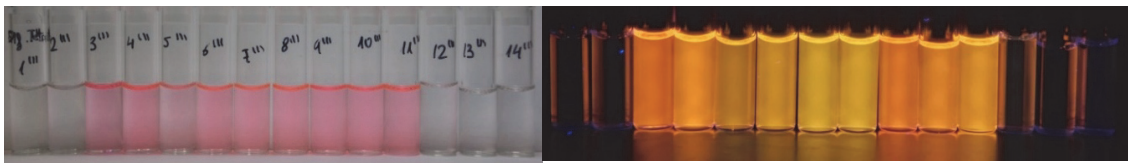

Solvents: 1: Water, 2: MeOH, 3: DMSO, 4: DMF, 5: MeCN, 6: acetone, 7: AcOEt, 8: THF, 9: $CHCl_3$, 10: DCM, 11: toluene, 12: diethyl ether, 13: hexane, 14: cyclohexane.

Figure 17. Upper. Absorbance spectra and Normalized absorbance spectra of PC51. Middle: Fluorescence spectra and Normalized and corrected fluorescence spectra of PC51. Lower. Solvatochromic effect of PC51 under white light and light of 366 nm.

1.5. *N,N'*-bis(1-(*N''*-tert-butoxycarbonyl)piperidine)-1-chloro-6,7,12-tris(3,5-bis(methoxy-carbonyl)phenoxy)perylene-3,4,9,10-tetracarboxylic diimide (PC51.3).

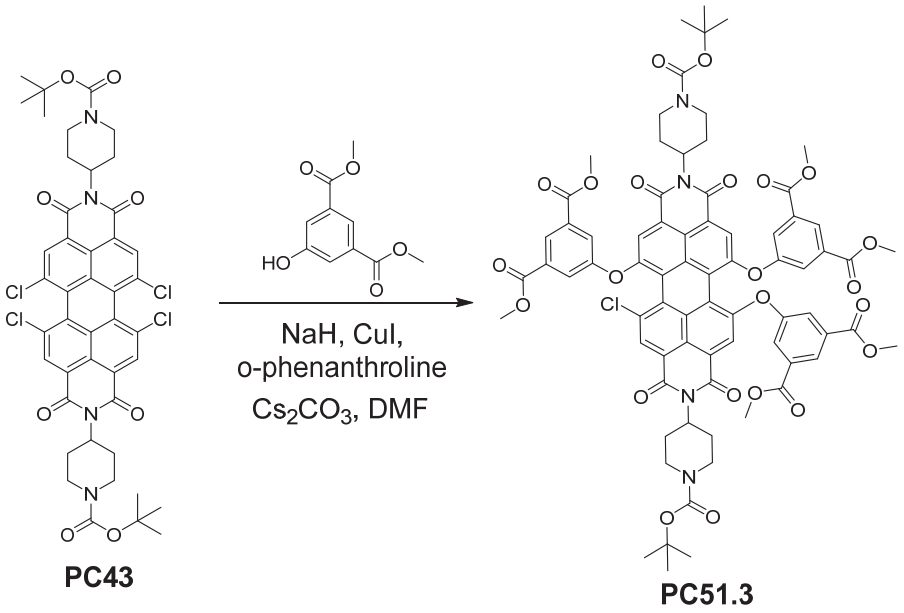

PC51.3 was obtained as pink solid in 10 % yield (15.5 mg, 0.01 mmol). **R_f (DCM:MeOH 50:2):** 0.4. **Mp (°C):** > 350 °C. **^{1}H NMR (300 MHz, $CDCl_3$) *δ*:** 8.57 (d, *J* = 1.5 Hz, 2H, H_{Ar}), 8.32 (d, *J* = 1.4 Hz, 2H, H_{Ar}), 8.16 (d, *J* = 2.4 Hz, 2H, H_{Ar}), 8.13 (s, 1H, H_{Ar}), 8.02 (d, *J* = 1.4 Hz, 2H, H_{Ar}), 7.69 – 7.62 (m, 4H, H_{Ar}), 5.11 – 5.03 (m, 2H, N-CH), 4.26 (s, 6H, CH_2), 3.90 (d, *J* = 22.4 Hz, 18H, $COOCH_3$), 2.86 – 2.53 (m, 10H, CH_2), 1.66 – 1.61 (m, 7H, CH_2), 1.42 (d, , *J* = 1.4 Hz, 18H, $COOC(CH_3)_3$). **HRMS (MALDI-, DCTB):** m/z calcd. for $C_{74}H_{67}ClN_4O_{23}$ ($[M]^-$): 1414.3879; found: 1414.4285.

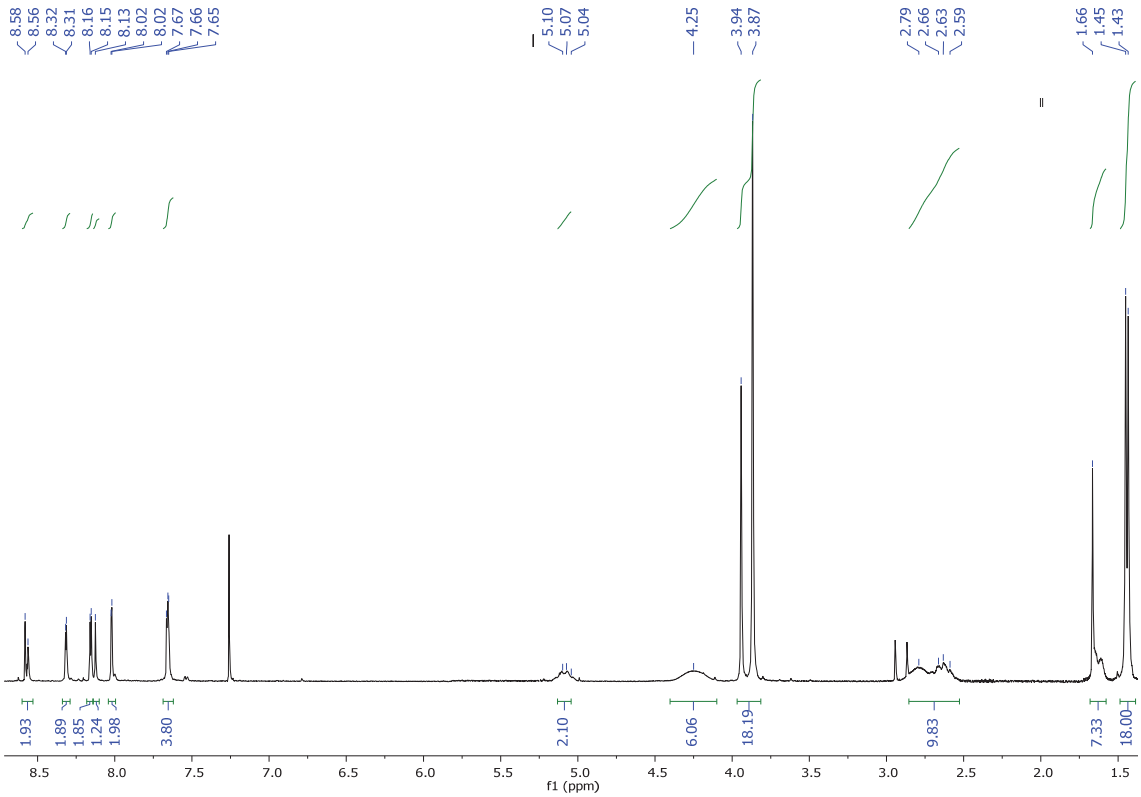

Figure 18. ^{1}H NMR (300 MHz, $CDCl_3$) of PC51.3

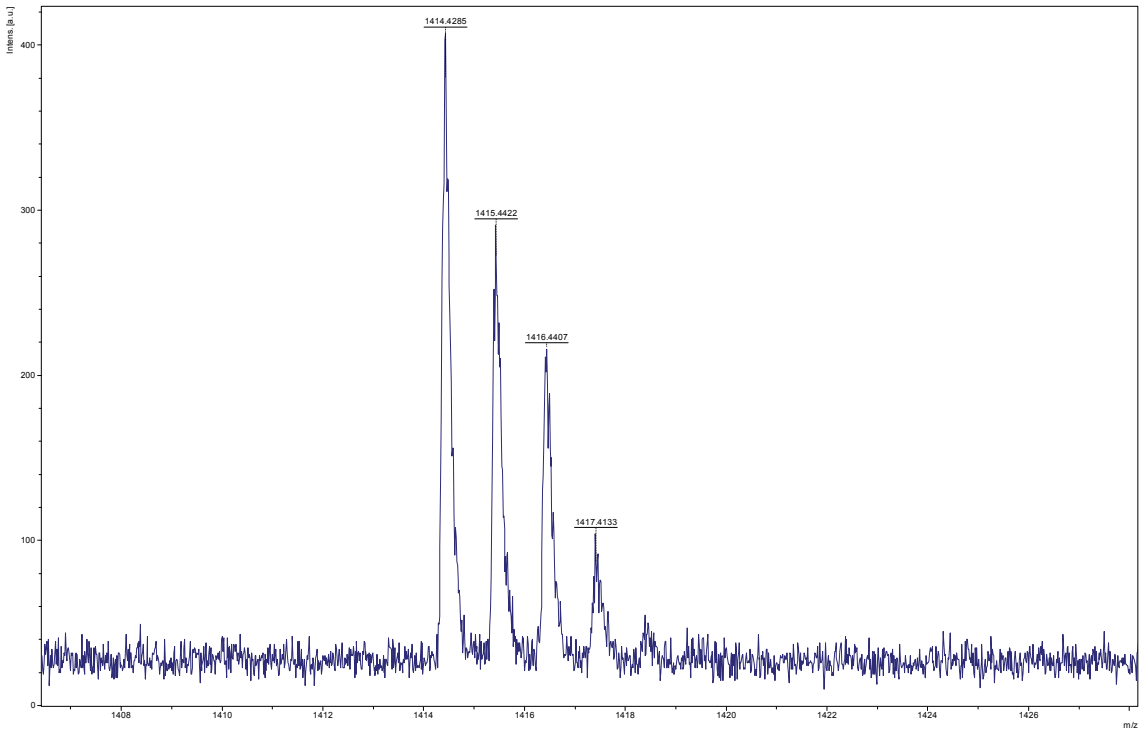

Figure 19. Mass spectrum (MALDI-, DCTB) of PC51.3

1.6. Synthesis of *N,N'*-bis(1-(*N''*-*tert*-butoxycarbonyl)piperidine)-1,7-dichloro-6,12-bis(3,5-bis(methoxycarbonyl)phenoxy)perylene-3,4,9,10-tetracarboxylic diimide (PC51.2).

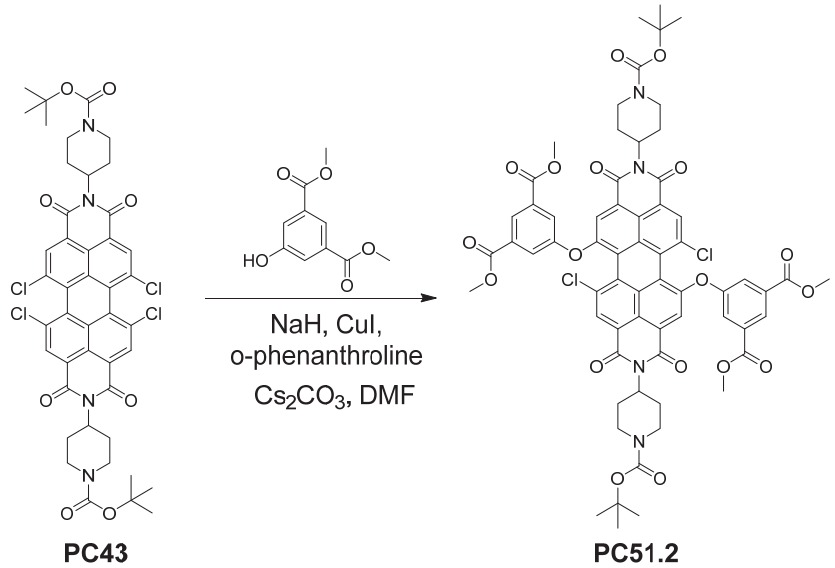

PC43 **PC51.2**

PC51.2 was obtained as pink solid in 20 % yield (27.3 mg, 0.02 mmol). **R_f (DCM:MeOH 50:2):** 0.3. **Mp (°C):** > 350 °C. **FT-IR (KBr, cm^{-1}):** 2951 (C-H), 2928 (C-H), 2854 (C-H), 1732 (C=O), 1701 (C=O), 1667 (CONH), 1587 (C_{Ar}-C_{Ar}), 1502 (C_{Ar}-C_{Ar}), 1459 (CH_2), 1431 (CH_2), 1408 (CH_2), 1402 (CH_2), 1366 (CH_3), 1323 (C-N), 1292 (C-O), 1249, 1170, 1135, 1107, 1032, 1002, 905, 755, 721, 669 (fingerprint region). **^{1}H NMR (400 MHz, $CDCl_3$) δ:** 8.65 (d, *J* = 1.2 Hz, 2H, H_{Ar}), 8.33 (t, *J* = 1.3 Hz, 2H, H_{Ar}), 8.23 (t, *J* = 1.3 Hz, 1H, H_{Ar}), 8.17 (s, 2H, H_{Ar}), 7.70 (d, *J* = 1.2 Hz, 1H, H_{Ar}), 7.65 (d, *J* = 1.3 Hz, 3H, H_{Ar}), 5.17 – 5.09 (m, 2H, N-CH), 4.29 (s, 4H, CH_2), 3.88 (s, 12H, $COOCH_3$), 2.90 – 2.60 (m, 9H, CH_2), 1.66 (d, *J* = 12.7 Hz, 3H, CH_2), 1.53 (s, 18H, $COOC(CH_3)_3$). **^{13}C NMR (101 MHz,**

$CDCl_3$) *δ*: 166.2 (**C**$OOCH_3$), 165.0 (**C**$OOCH_3$), 162.9 (**C**ON**C**O_{Imide}), 162.9 (**C**ON**C**O_{Imide}), 156.2 (-C_q-O-**C_q**$_{Phenol}$), 155.8 (-**C_q**-O-$C_{qPhenol}$), 154.9 (**C**$OOC(CH_3)_3$), 154.8 (**C**$OOC(CH_3)_3$), 135.4 (C_{Ar}), 132.7 (CH), 132.5 (C_{Ar}), 132.4 (C_{Ar}), 132.1 (C_{Ar}), 129.7 (C_{Ar}), 126.6 (CH), 124.4 (CH), 124.2 (C_{Ar}), 123.5 (C_{Ar}), 123.1 (CH), 122.2 (C_{Ar}), 121.7 (CH), 120.9 (CH), 120.2 (C_{Ar}), 79.9 (COO**C**$(CH_3)_3$), 52.8 (COO**C**H_3), 52.6 (**C**HN_{imide}), 52.5 (**C**HN_{imide}), 44.3 (CH_2), 43.9 (CH_2), 29.9 (CH_2), 28.6 (COOC(**C**$H_3)_3$), 28.4 (CH_2). **HRMS (MALDI-, DCTB):** m/z: calcd. for ($[M]^+$) 1240.3123 found, 1239.9412.

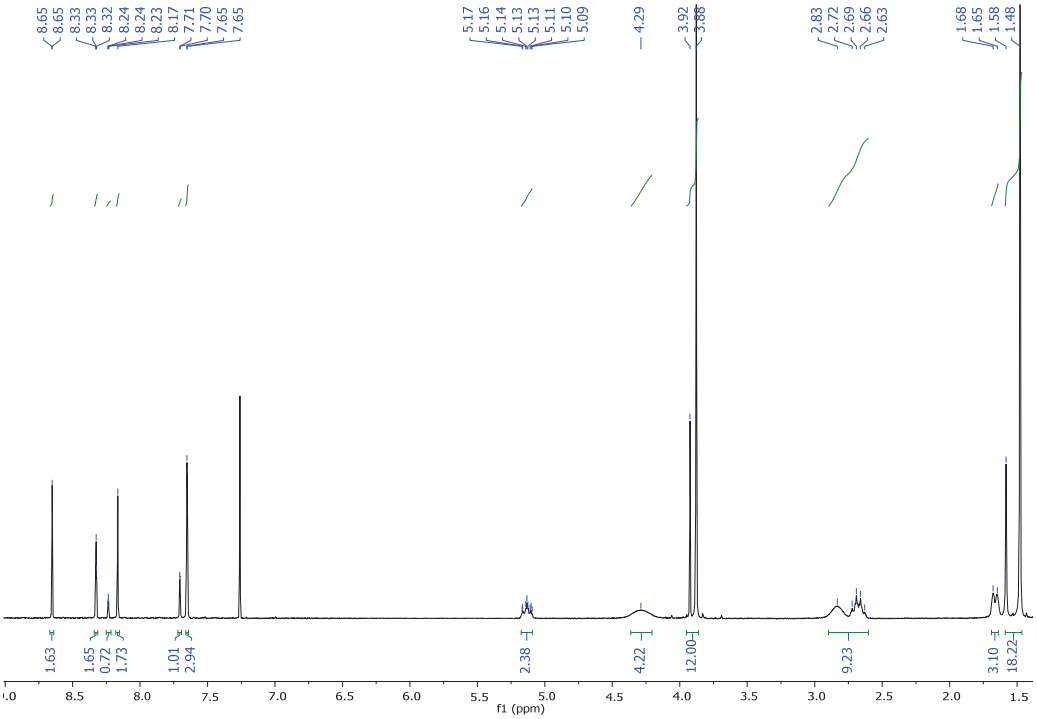

Figure 20. ^{1}H NMR (400 MHz, $CDCl_3$) of PC51.2

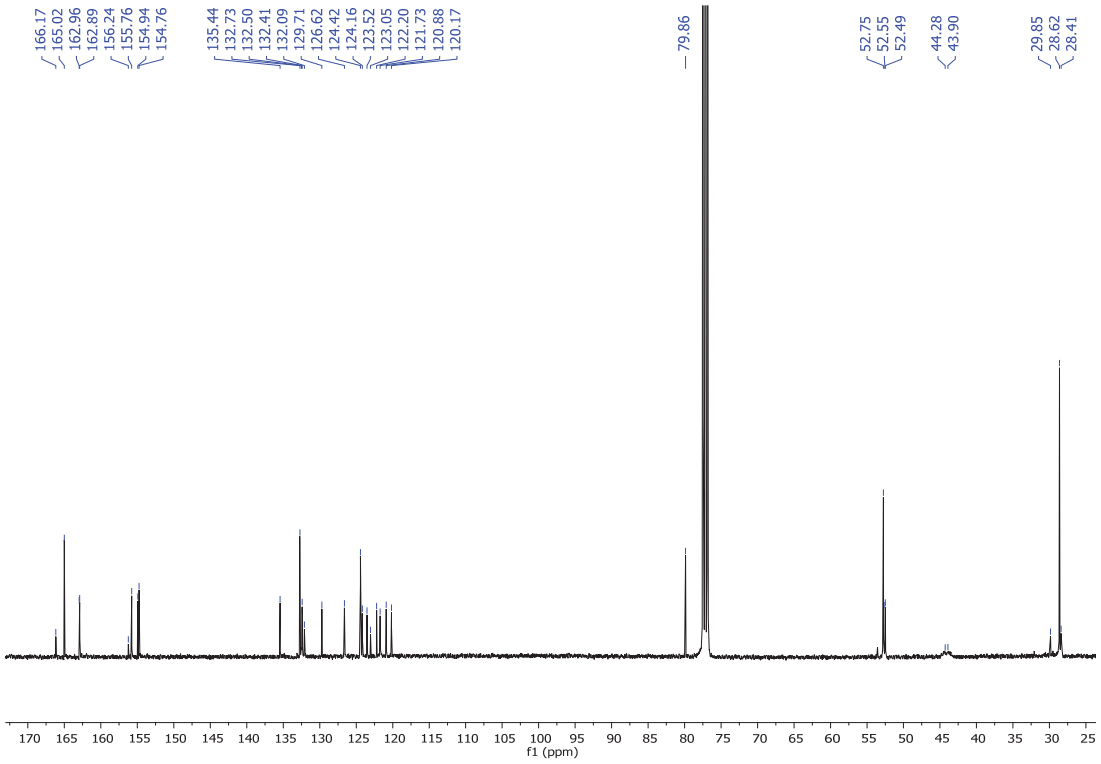

Figure 21. ^{13}C NMR (101 MHz, $CDCl_3$) of PC51.2

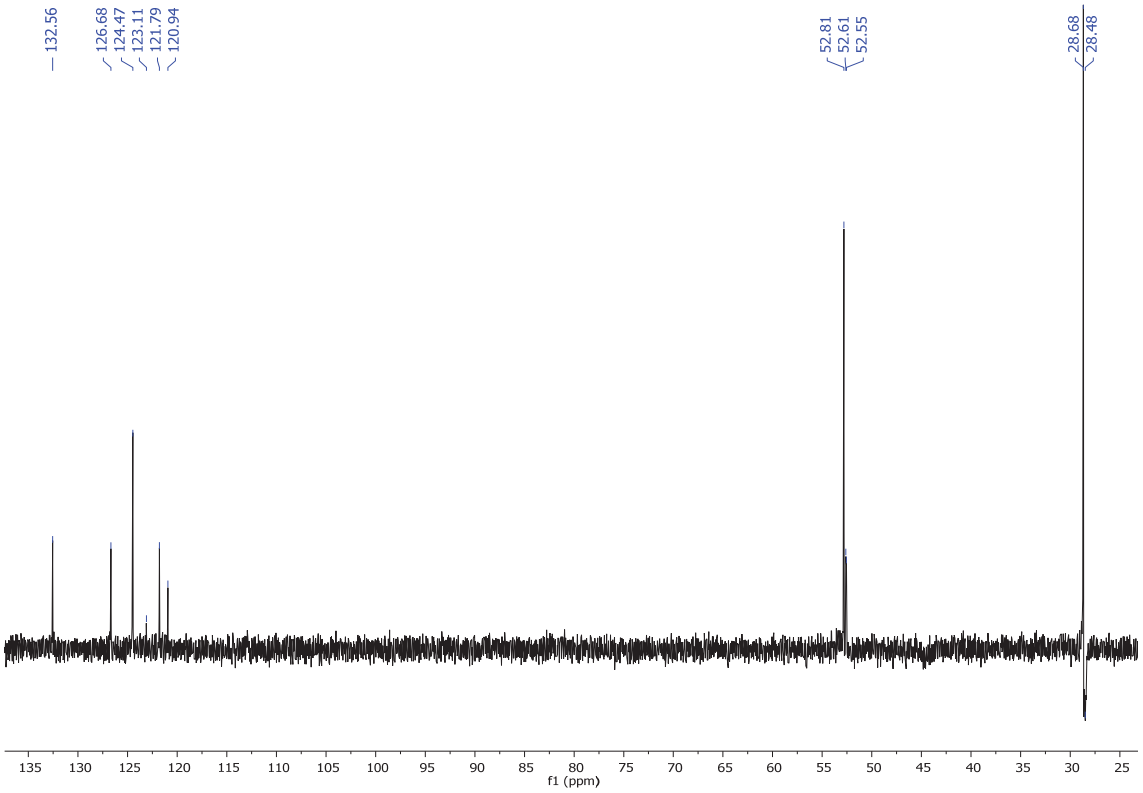

Figure 22. ^{13}C NMR-DEPT-135 (101 MHz, $CDCl_3$) of PC51.2

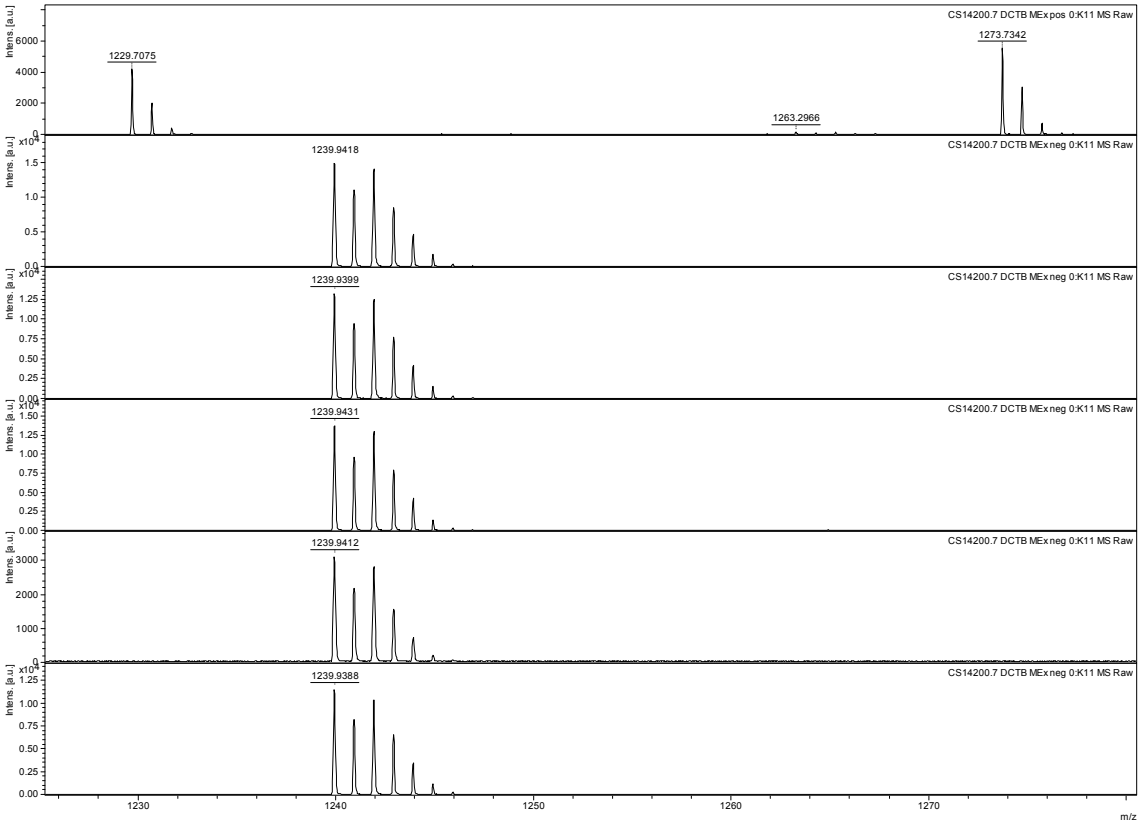

Figure 23. Mass spectrum (MALDI-, DCTB) of PC51.2

Solvatochromism:

The concentration of **PC51.2** is $1 \cdot 10^{-5}$ M. The excitation wavelength is 366 nm. The absorption and emission spectra have been measured in the listed solvents below in the range between 200 to 900 nm. The used solvents are: MeOH, DMSO, DMF, MeCN, acetone, AcOEt, THF, $CHCl_3$, DCM, toluene, ether, hexane and cyclohexane.

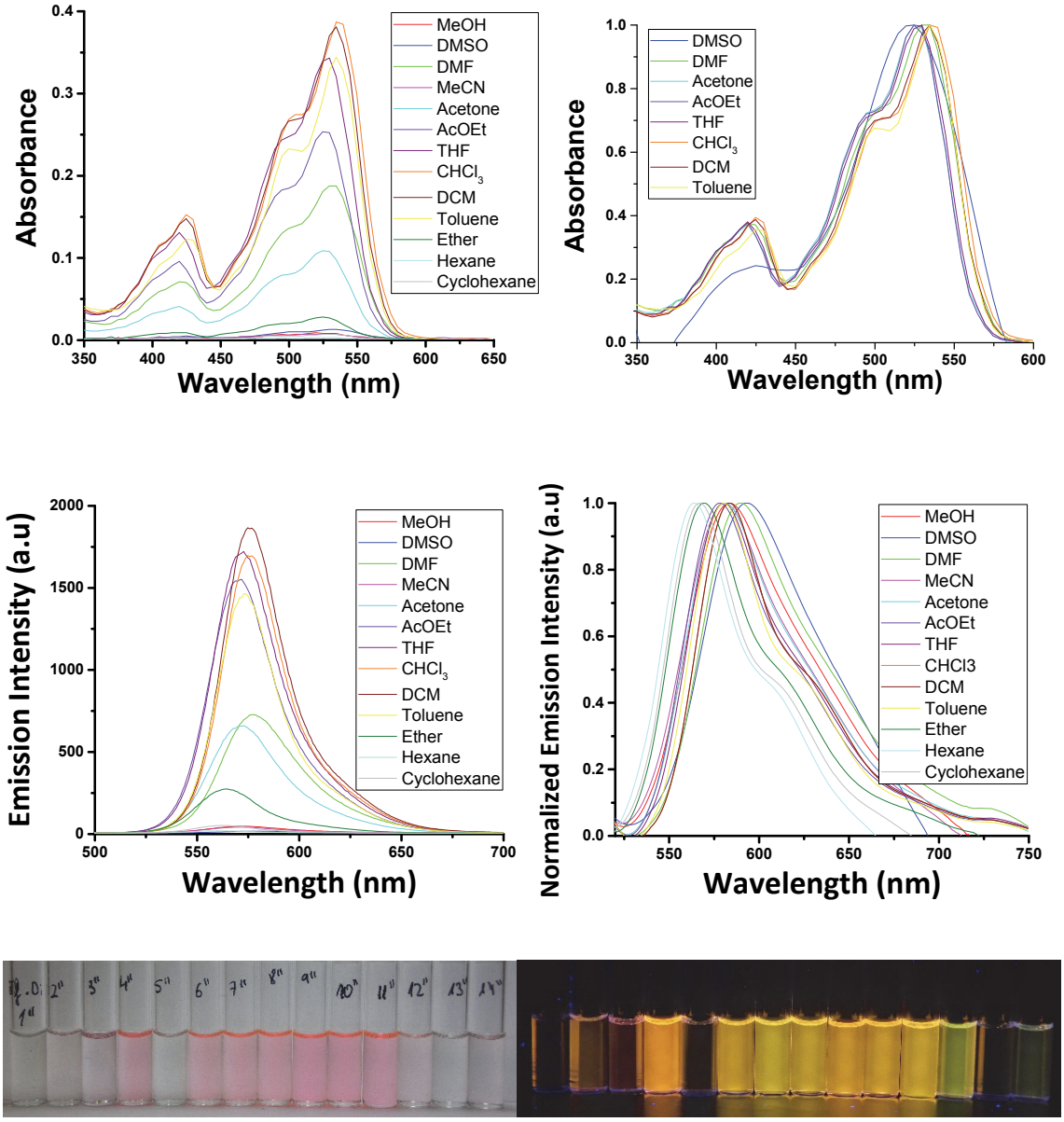

Solvents: 1: Water, 2: MeOH, 3: DMSO, 4: DMF, 5: MeCN, 6: acetone, 7: AcOEt, 8: THF, 9: $CHCl_3$, 10: DCM, 11: toluene, 12: diethyl ether, 13: hexane, 14: cyclohexane.

Figure 24. Upper. Absorbance spectra and Normalized absorbance spectra of PC51.2. Middle: Fluorescence spectra and Normalized and corrected fluorescence spectra of PC51.2. Lower. Solvatochromic effect of PC51.2 under white light and light of 366 nm.

1.7. Synthesis of *N,N'*-bis(1-(*N''*-*tert*-butoxycarbonyl)piperidine)-1,7,12-trichloro-6-(3,5-bis(methoxycarbonyl)phenoxy)perylene-3,4,9,10-tetracarboxylic diimide (PC51.1).

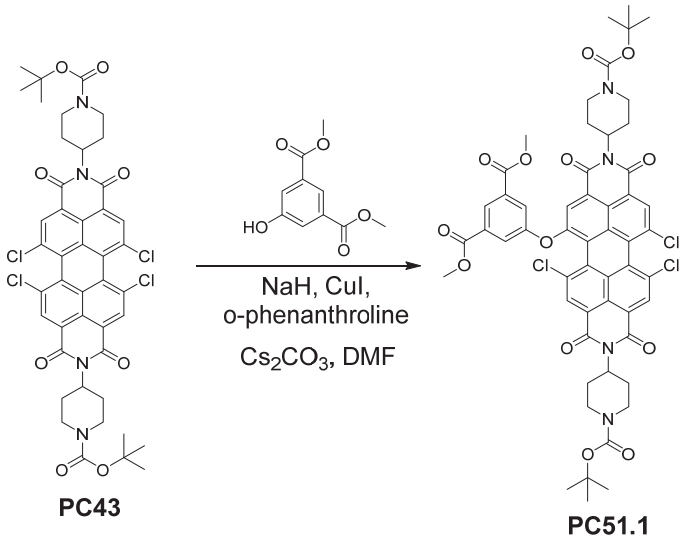

PC43 **PC51.1**

PC51.1 was obtained as soft pink solid in 7 % yield (8.2 mg, 0.01 mmol). **R_f (DCM:MeOH 50:2):** 0.5. **Mp (°C):** > 350 °C. **^{1}H NMR (300 MHz, $CDCl_3$) δ:** 8.72 – 8.52 (m, 4H, H_{Ar}), 8.35 (dt, *J* = 11.2 Hz and 1.4 Hz, 1H, H_{Ar}), 8.17 (s, 1H, H_{Ar}), 7.76 (d, *J* = 1.4 Hz, 1H, H_{Ar}), 5.16 – 5.08 (m, 2H, N-CH), 4.31 (s, 4H, CH_2), 3.94 – 3.95 (d, *J* = 14.4 Hz, 6H, $COOCH_3$), 2.86 – 2.65 (m, 9H, CH_2), 1.69 – 1.63 (m, 6H, CH_2), 1.48 (s, 18H, $COOC(CH_3)_3$). **HRMS (MALDI-, DCTB):** m/z: calcd. for ($[M]^-$) 1066.2362; found: 1066.2439.

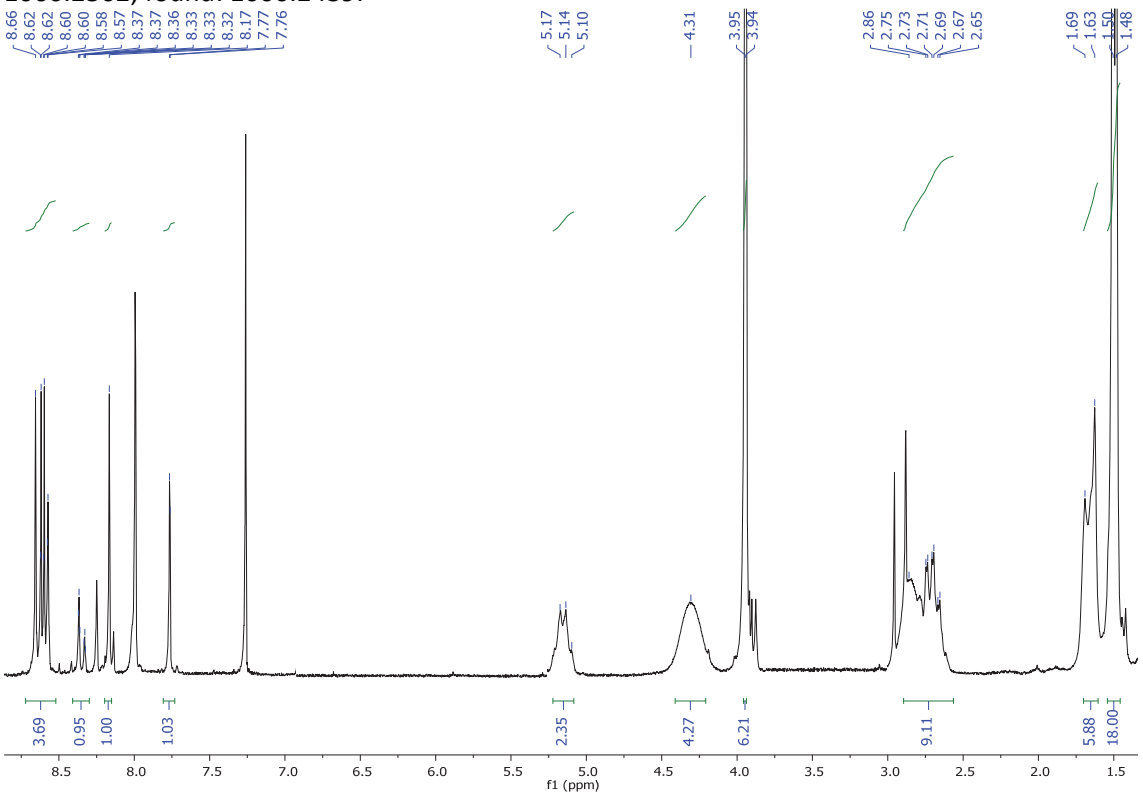

Figure 25. ^{1}H NMR (300 MHz, $CDCl_3$) of PC51.1

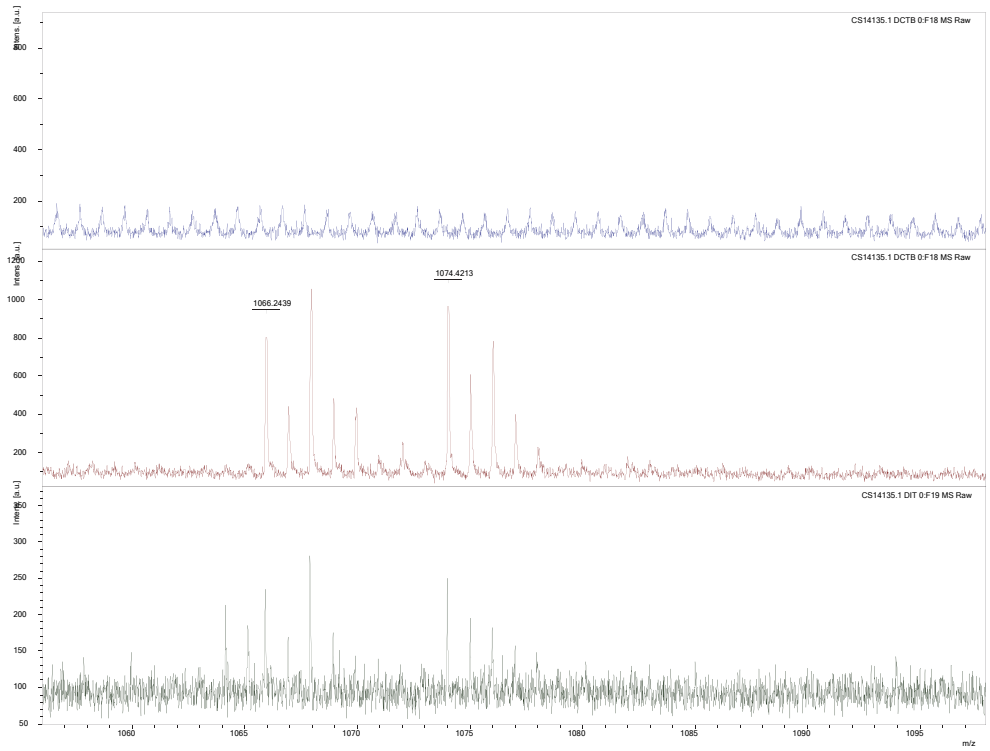

Figure 26. Mass spectrum (MALDI-, DCTB) of PC51.1

1.8. Synthesis of *N,N'*-bis(1-(*N''*-*tert*-butoxycarbonyl)piperidine)-1,6,7,12-tetrakis(3,5-bis(methoxycarbonyl)phenoxy)perylene-3,9,10-tricarboxylic diimide (PC51.d).

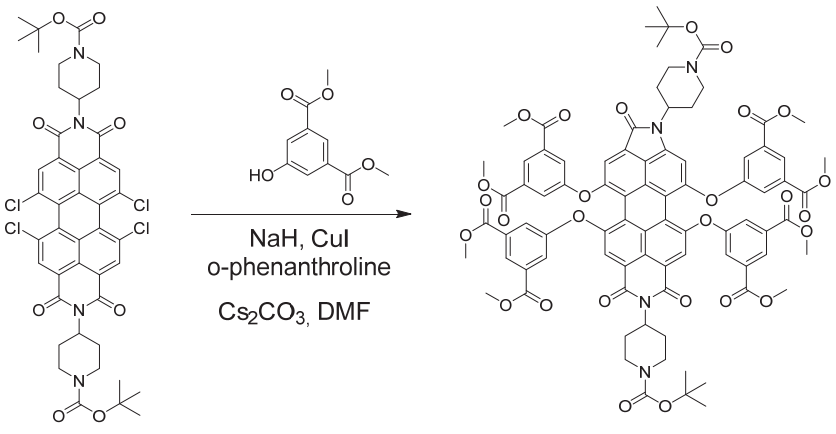

PC43 **PC51.d**

PC51.d was obtained as purple solid in 5 % yield (8.6 mg, 0.02 mmol). **R_f (DCM:MeOH 50:2):** 0.2. **Mp (°C):** > 350 °C. **FT-IR (KBr, cm^{-1}):** 2954 (C-H), 2926 (C-H), 2852 (C-H), 1735 (C=O), 1698 (C=O), 1665 (CONH), 1590 (C_{Ar}-C_{Ar}), 1496 (C_{Ar}-C_{Ar}), 1454 (CH_2), 1428 (CH_2), 1391 (CH_2), 1363 (C-N), 1323 (C-N), 1243 (C-O), 1175, 1005, 1002, 914, 803, 757, 721 (fingerprint region). **^{1}H NMR (400 MHz, $CDCl_3$) δ:** 8.33 (t, *J* = 1.4 Hz, 1H, H_{Ar}), 8.31 (t, *J* = 1.4 Hz, 1H, H_{Ar}), 8.30 (t, *J* = 1.4 Hz, 1H, H_{Ar}), 8.27 (t, *J* = 1.4 Hz, 1H, H_{Ar}), 8.16 (d, *J* = 3.4 Hz, 2H, H_{Ar}), 7.75 (s, 1H, H_{Ar}), 7.67 (d, *J* = 5.1 Hz, *J* = 1.4 Hz, 4H, H_{Ar}), 7.61 (t, *J* = 1.5 Hz, 4H, H_{Ar}), 6.81 (s, 1H, H_{Ar}), 5.07 (tt, *J* = 12.0 Hz and 3.7 Hz, 1H, N-CH), 4.47 (tt, *J* = 12.1 Hz and 3.7 Hz, 1H, N-CH), 4.21 (s, 4H, CH_2), 3.90 (dd, *J* = 3.8 Hz and 1.1 Hz, 24H, $COOCH_3$), 2.80 – 2.57 (m, 7H, CH_2), 1.82 (d, *J* = 11.1 Hz, 2H, CH_2), 1.43 (s, 9H, CH_3), 1.34 (s, 9H, CH_3). **^{13}C NMR (101 MHz, $CDCl_3$) δ:** 166.6 (N-**C**O), 165.2 (**C**$OOCH_3$), 165.2 (**C**$OOCH_3$), 165.2 (**C**$OOCH_3$), 165.1 (**C**$OOCH_3$), 163.3 (**C**ON**C**O_{Imide}), 156.9 (-C_q-O-**C_q**$_{Phenol}$), 156.8 (-

C_q-O-**C_q**$_{Phenol}$), 156.7 (-C_q-O-**C_q**$_{Phenol}$), 156.6 (-C_q-O-**C_q**$_{Phenol}$), 156.3 (-**C_q**-O-$C_{qPhenol}$), 155.8 (-**C_q**-O-$C_{qPhenol}$), 154.7 (-**C_q**-O-$C_{qPhenol}$), 154.6 (-**C_q**-O-$C_{qPhenol}$), 154.2 (**C**OOC$(CH_3)_3$), 152.6 (**C**OOC$(CH_3)_3$), 139.9 (**C_q**-N-CO), 132.6 (C_{Ar}), 132.6 (C_{Ar}), 132.5 (C_{Ar}), 132.4 (C_{Ar}), 132.2 (C_{Ar}), 129.6 (C_{Ar}), 126.3 (C_{Ar}), 126.2 (C_{Ar}), 126.2 (CH), 125.9 (CH), 125.6 (CH), 124.5 (CH), 124.3 (CH), 123.9 (CH), 123.9 (C_{Ar}), 123.3 (C_{Ar}), 123.1 (CH), 122.3 (C_{Ar}), 122.2 (C_{Ar}), 122.1 (C_{Ar}), 122.0 (C_{Ar}), 121.5 (C_{Ar}), 121.4 (CH), 118.5 (C_{Ar}), 116.5 (CH), 111.2 (CH), 102.5 (CH), 80.0 (COO**C**$(CH_3)_3$), 79.7 (COO**C**$(CH_3)_3$), 52.7 (**C**HN_{imide}), 52.3 (**C**HN_{imide}), 50.5 (COO**C**H_3), 44.5 (**C**H_2), 44.4 (**C**H_2), 29.9 (**C**H_2), 28.6 (COOC(**C**$H_3)_3$), 28.4 (COOC(**C**$H_3)_3$). **HRMS (MALDI-, DCTB):** m/z calcd. for $C_{83}H_{76}N_4O_{27}$ ([M]$^+$): 1560.4691; found: 1560.4898.

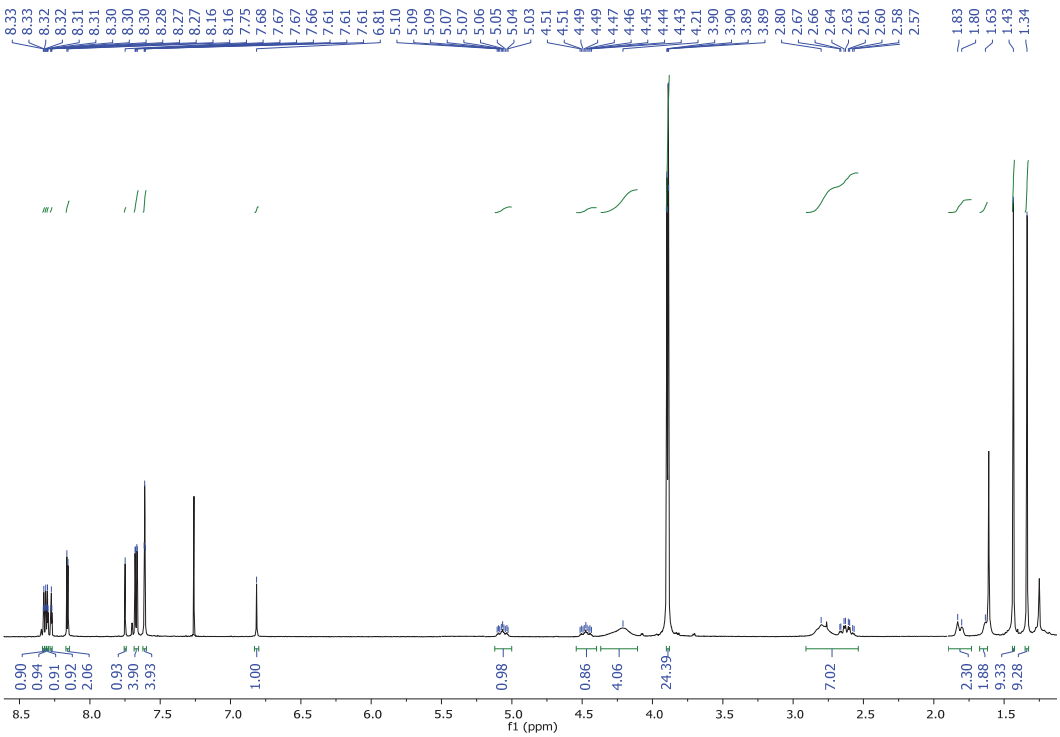

Figure 27. ^{1}H NMR (400 MHz, $CDCl_3$) of PC51.d

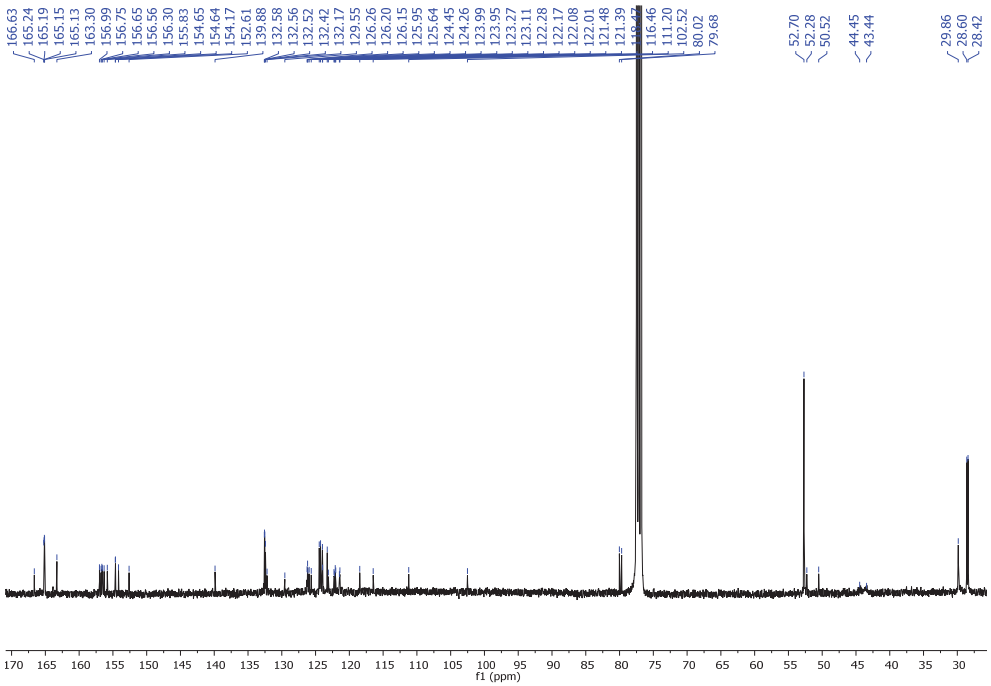

Figure 28. ^{13}C NMR (101 MHz, $CDCl_3$) of PC51.d

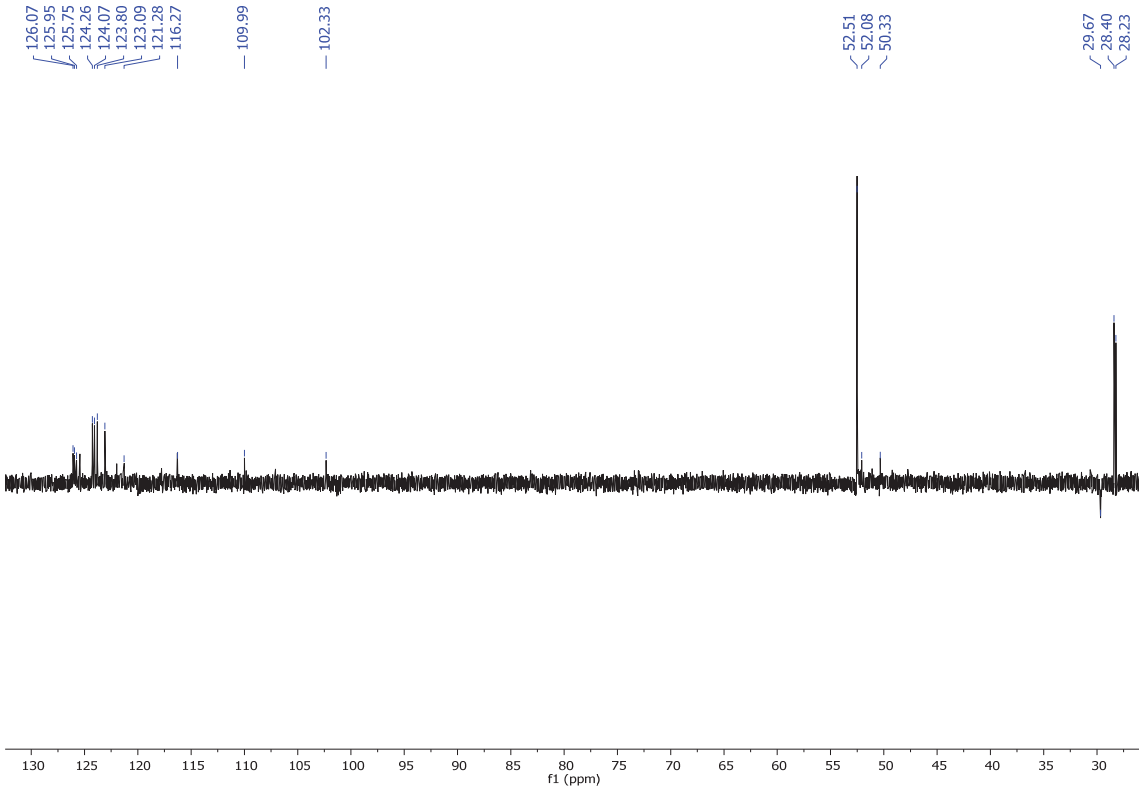

Figure 29. ^{13}C NMR-DEPT-135 (101 MHz, $CDCl_3$) of PC51.d

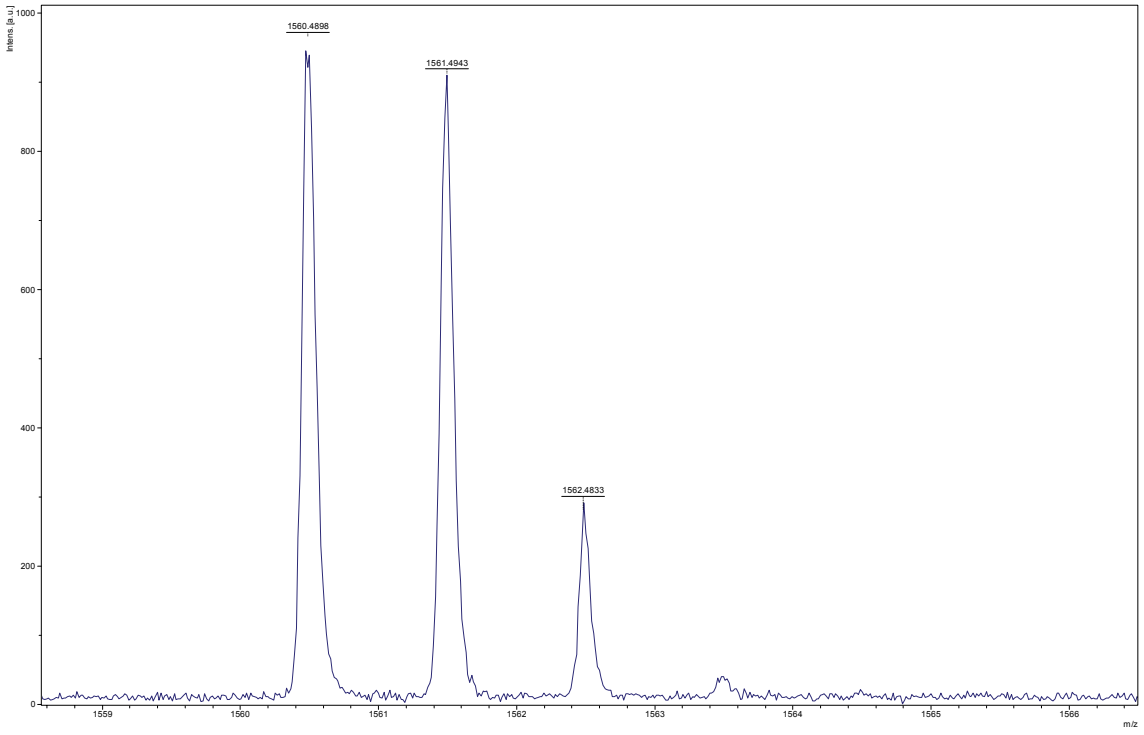

Figure 30. Mass spectrum (MALDI-, DCTB) of PC51.d

1.9. Synthesis of *N,N'*-bis(1-piperidine)-1,6,7,12-tetrakis(3,5-bis(methoxycarbonyl)phenoxy)perylene-3,4,9,10-tetracarboxylic diimide (PC67).

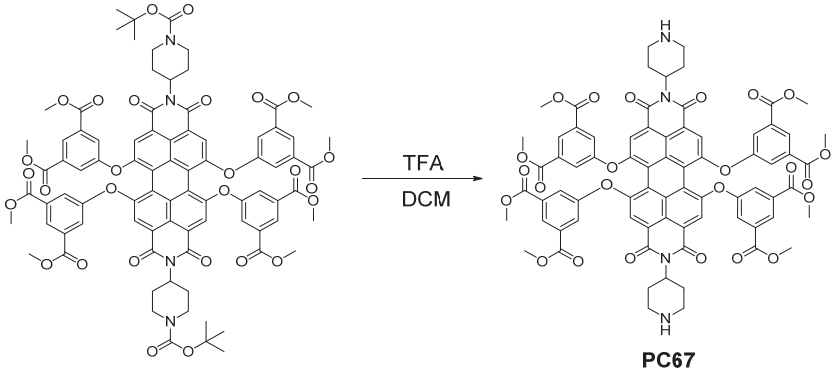

PC51 **PC67**

Trifluoroacetic acid (4.36 mL, 56.97 mmol) was added dropwise to *N,N'*-bis-(1-(*N''-tert*-butoxycarbonyl)piperidine)-1,6,7,12-tetrakis(3,5-bis(methoxycarbonyl)phenoxy)perylene-3,4,9,10-tetracarboxylic diimide (170 mg, 0.097 mmol) dissolved in degassed DCM (6.5 mL). The mixture was stirred at 25 °C for 2 hours, neutralized with 10 % NaOH (15 mL) and extracted with DCM (3 x 20 mL). The combined organic extracts were evaporated under reduced pressure to obtain **PC67** as a pink-purple product in 97 % yield (144 mg, 0.11 mmol). **R_f (DCM:MeOH 50:4):** 0. **Mp (°C):** > 350 °C. **FT-IR (KBr, cm^{-1}):** 3437 (NH), 2951 (C-H), 2923 (C-H), 2849 (C-H), 1732 (C=O), 1695 (C=O), 1661 (CONH), 1587 (C_{Ar}-C_{Ar}), 1508 (C_{Ar}-C_{Ar}), 1459 (CH_2), 1431 (CH_2), 1411 (CH_2), 1385 (CH_3), 1320 (C-N), 1300 (C-O), 1286 (C-O), 1252, 1181, 1007, 999, 903, 803, 752, 721 (fingerprint region). **^{1}H NMR (400 MHz, $CDCl_3$) *δ*:** 8.34 (t, *J* = 1.4 Hz, 4H, H_{Ar}), 8.17 (s, 4H, H_{Ar}), 7.70 (d, *J* = 2.1 Hz, 8H, H_{Ar}), 5.08 – 5.02 (m, 2H, N-CH), 3.89 (s, 24H, $COOCH_3$), 3.20 (d, *J* = 12.5 Hz, 4H, CH_2), 2.74 – 2.55 (m, 9H, CH_2), 1.64 (s, 3H, CH_2). **^{13}C NMR (101 MHz, $CDCl_3$) *δ*:** 165.1 (**C**$OOCH_3$), 163.1 (**C**O**N**C**O**$_{Imide}$), 155.9 (-C_q-O-**C**$_{qPhenol}$), 154.9 (-**C**$_q$-O-$C_{qPhenol}$), 133.1 (C_{Ar}), 132.7 (C_{Ar}), 126.5 (CH), 124.5 (CH), 124.2 (C_{Ar}), 121.2 (CH), 121.1 (C_{Ar}), 120.9 (C_{Ar}), 120.9 (C_{Ar}), 52.7 (COO**C**H_3), 52.6 (**C**HN_{imide}), 46.9 (CH_2), 30.1 (CH_2), 29.9 (CH_2). **HRMS (MALDI+, DCTB):** m/z calcd for $C_{74}H_{60}N_4O_{24}$ ($[M+H]^+$): 1389.3703; found: 1389.3803.

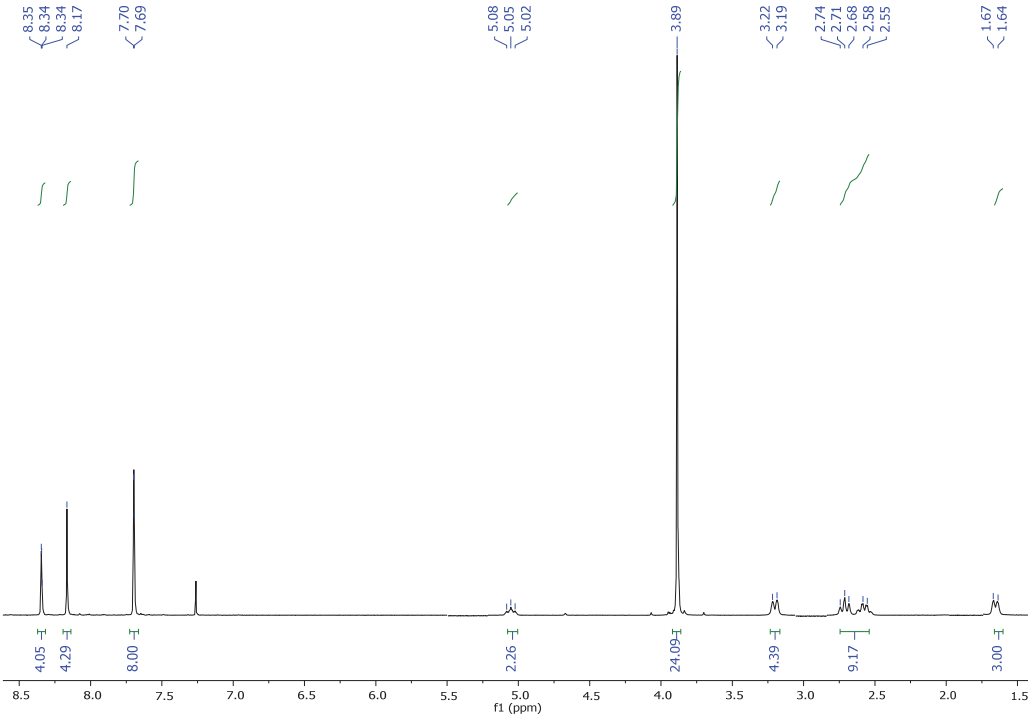

Figure 31. ^{1}H NMR (400 MHz, $CDCl_3$) of PC67

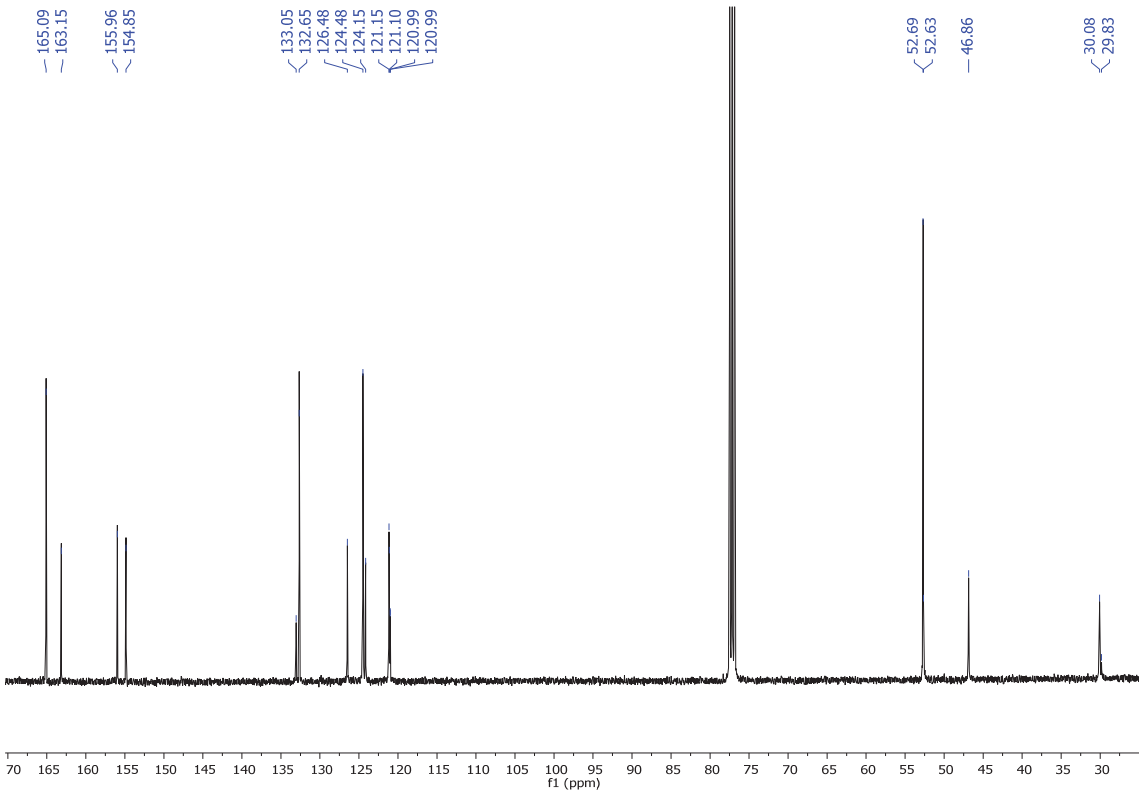

Figure 32. ^{13}C NMR (101 MHz, $CDCl_3$) of PC67

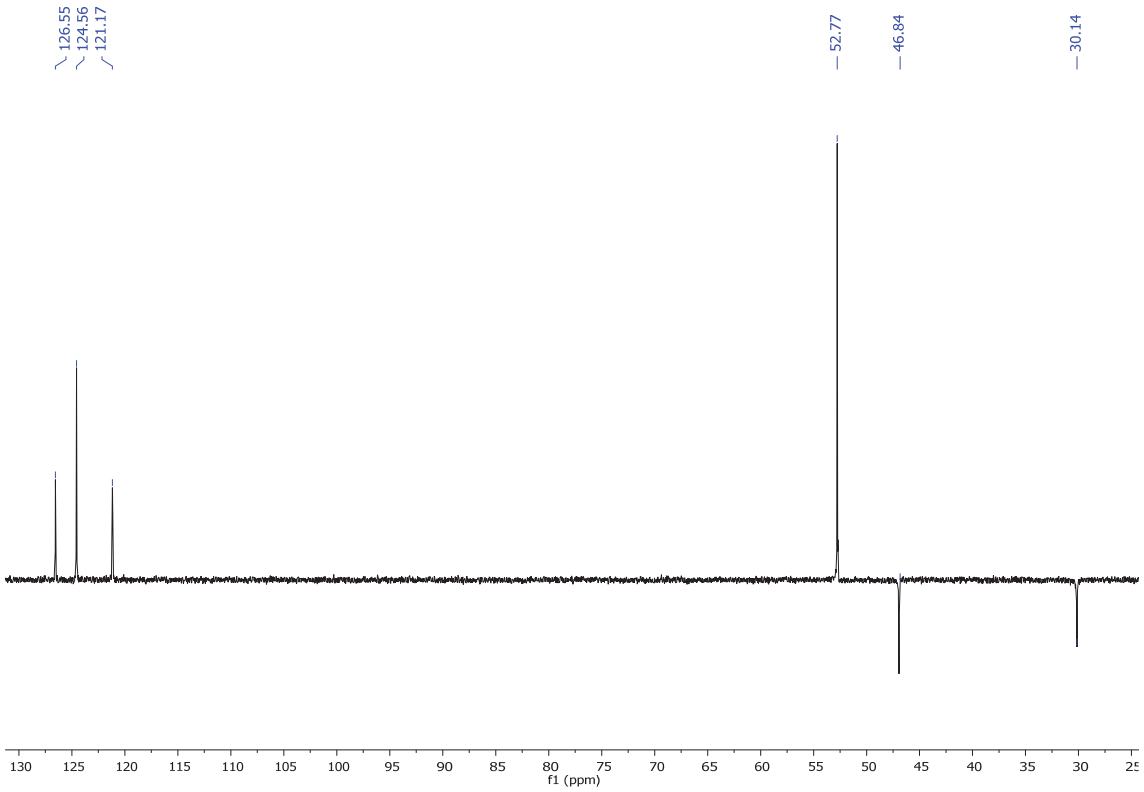

Figure 33. ^{13}C NMR-DEPT-135 (101 MHz, $CDCl_3$) of PC67

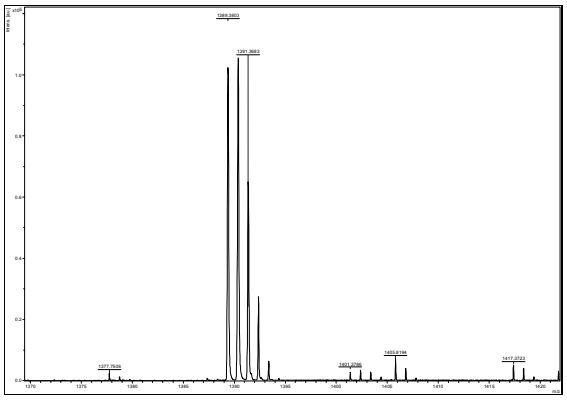

Figure 342. Mass spectrum (MALDI+, DCTB) of PC67

Solvatochromism: The concentration of **PC67** is $1 \cdot 10^{-5}$ M. The excitation wavelength is 430 nm. The absorption and emission spectra have been measured in the listed solvents below in the range between 200 to 900 nm. The used solvents are: MeOH, DMSO, DMF, MeCN, acetone, ethyl acetate, THF, $CHCl_3$, DCM and toluene.

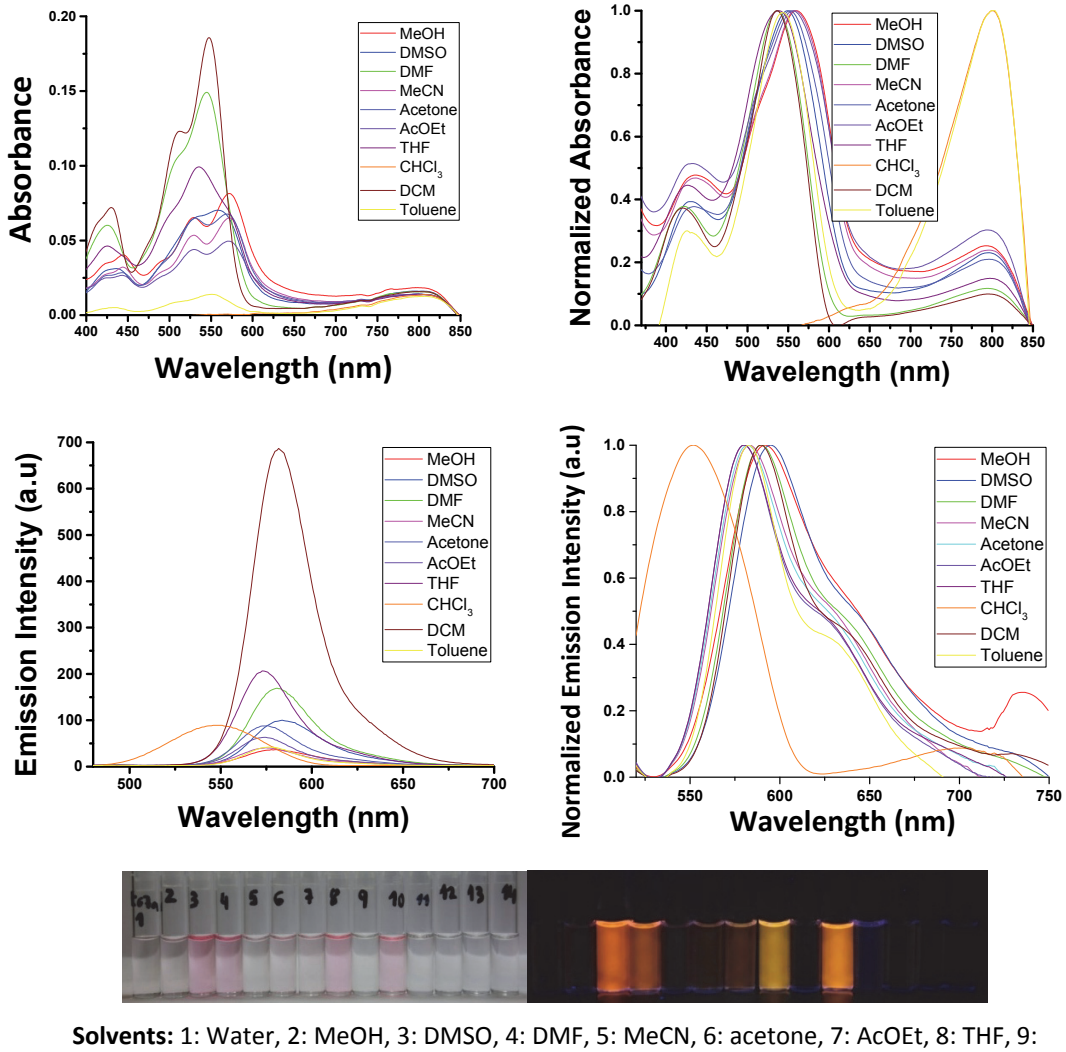

Solvents: 1: Water, 2: MeOH, 3: DMSO, 4: DMF, 5: MeCN, 6: acetone, 7: AcOEt, 8: THF, 9: $CHCl_3$, 10: DCM, 11: toluene, 12: diethyl ether, 13: hexane, 14: cyclohexane.

Figure 35. Upper. Absorbance spectra and Normalized absorbance spectra of PC67. Middle: Fluorescence spectra and Normalized and corrected fluorescence spectra of PC67. Lower. Solvatochromic effect of PC67 under white light and light of 366 nm.

1.10. Synthesis of *N,N'*-bis(1-(*N''*-*tert*-butoxycarbonyl)piperidine)-1,6,7,12-tetrakis(3,5-bis(hydroxycarbonyl)phenoxy)perylene-3,4,9,10-tetracarboxylic diimide (PC66).

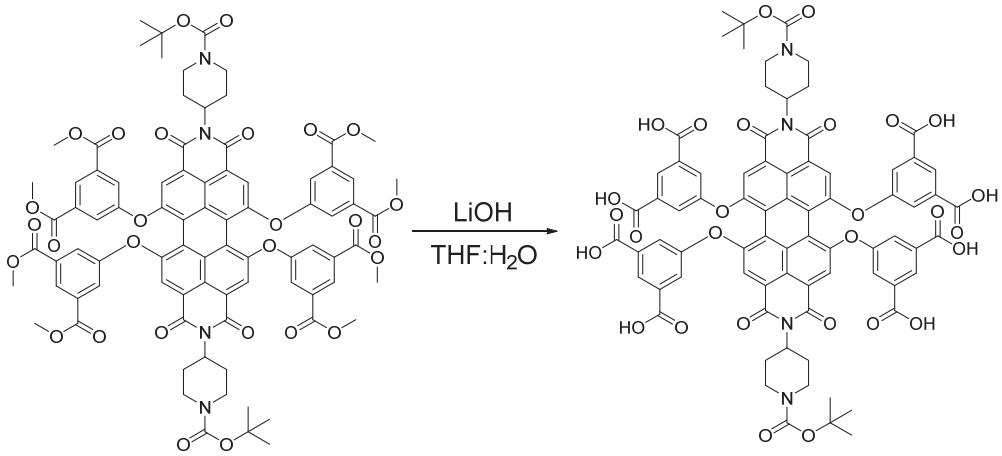

PC51 **PC66**

Lithium hydroxide (38 mg, 0.96 mmol) dissolved in H_2O (2 mL) were added to *N,N'*-bis-(1-(*N''*-*tert*-butoxycarbonyl)piperidine)-1,6,7,12-tetrakis(3,5-bis(methoxycarbonyl)phenoxy)-perylene-3,4,9,10-tetracarboxylic diimide (20 mg, 0.01 mmol) dissolved in THF (8 mL). The mixture was stirred at 45 °C overnight. The solvents were removed under reduced pressure to obtain **PC66** as a brown oil-solid in 99 % yield (17.6 mg, 0.01 mmol). **R_f (MeOH):** 0. **Mp**: > 350 °C. **FT-IR (KBr, cm^{-1}):** 3445 (O-H), 2067 (C-H), 1638 (CONH), 1380 (O-H), 1252 (C-O), 993, 624 (fingerprint region). **^{1}H NMR (300 MHz, D_2O) δ:** 8.42 (s, 2H, H_{Ar}), 7.87 – 7.82 (m, 5H, H_{Ar}), 7.51 – 7.47 (m, 11H, H_{Ar}), 7.27 (d, *J* = 7.2 Hz, 2H, H_{Ar}), 7.16 (s, 1H, H_{Ar}), 3.93 – 3.87 (m, 7H, CH_2), 2.99 – 2.90 (m, 6H, CH_2), 1.98 – 1.88 (m, 5H, CH_2), 1.39 (s, 18H, CH_3).

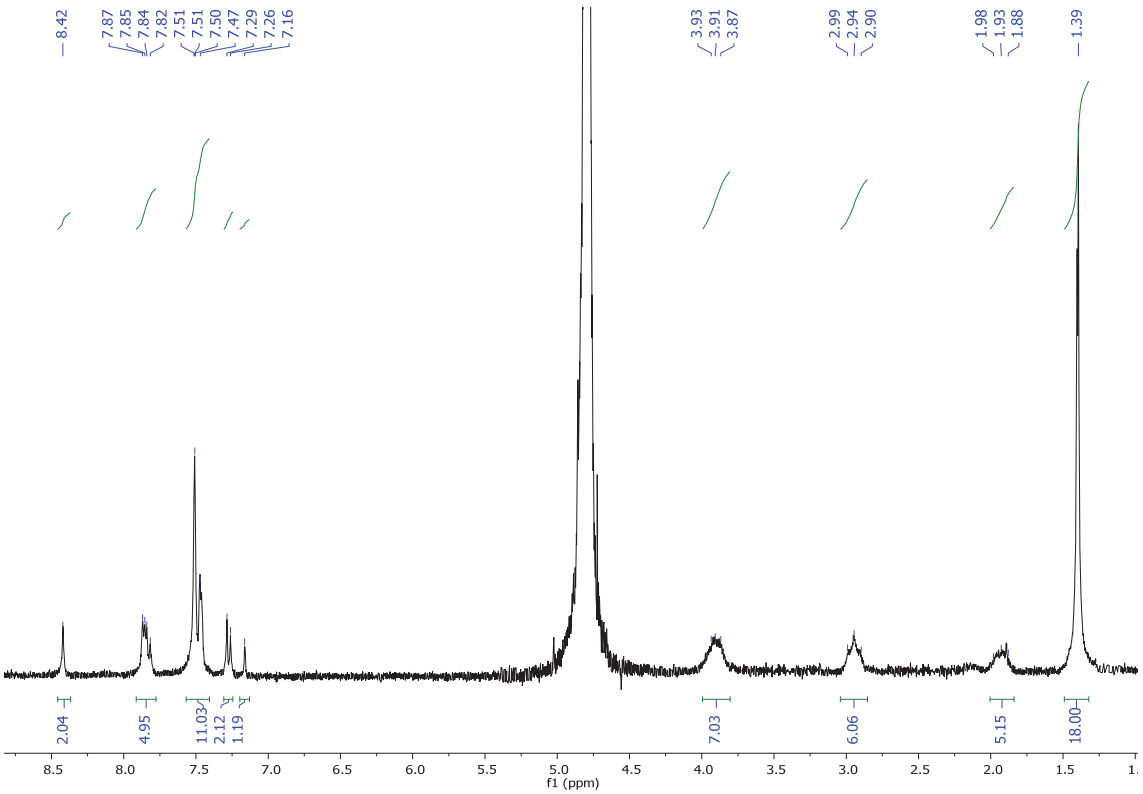

Figure 36. ^{1}H NMR (300 MHz, $CDCl_3$) of PC66

Solvatochromism:

The concentration of **PC66** is $1 \cdot 10^{-5}$ M. The excitation wavelength is 438 nm. The absorption and emission spectra have been measured in the listed solvents below in the range between 200 to 900 nm. The used solvents are: H_2O, MeOH, MeOH:H_2O 50:50, THF, THF:H_2O 50:50.

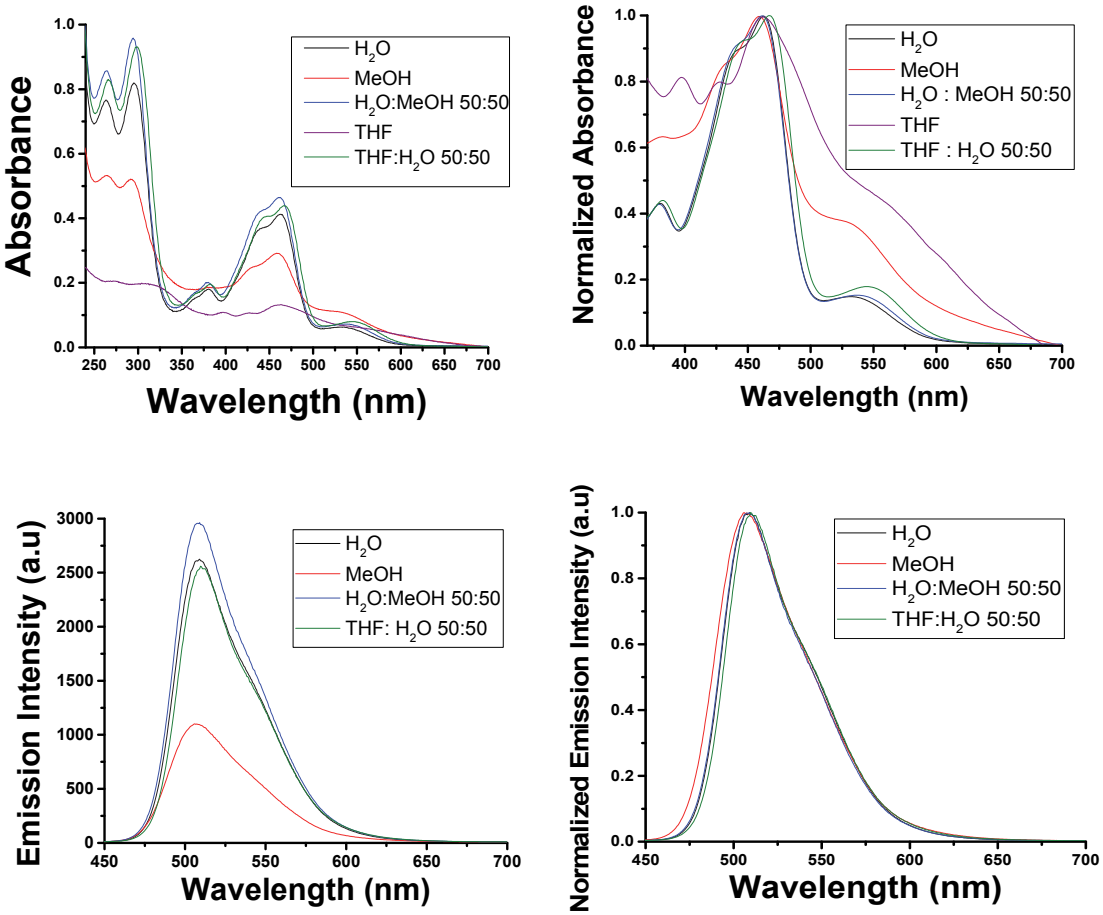

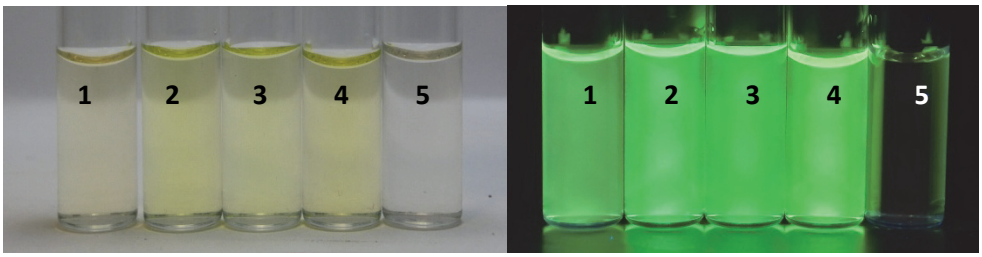

Solvents: 1: H_2O, 2: MeOH, 3: MeOH:H_2O 50:50, 4: THF, 5: THF:H_2O 50:50.

Figure 37. Upper. Absorbance and Normalized absorbance spectra of PC66. Middle: Fluorescence and Normalized fluorescence spectra of PC66. Lower. Solvatochromic effect of PC66 under white light and light of 366 nm.

1.11. Synthesis of *N,N'*-bis(1-(piperidin-1-yl)-6-biotinamidohexan-1-one)-1,6,7,12-tetrakis(3,5-bis(methoxycarbonyl)phenoxy)perylene-3,4,9,10-tetracarboxylic diimide (PC73).

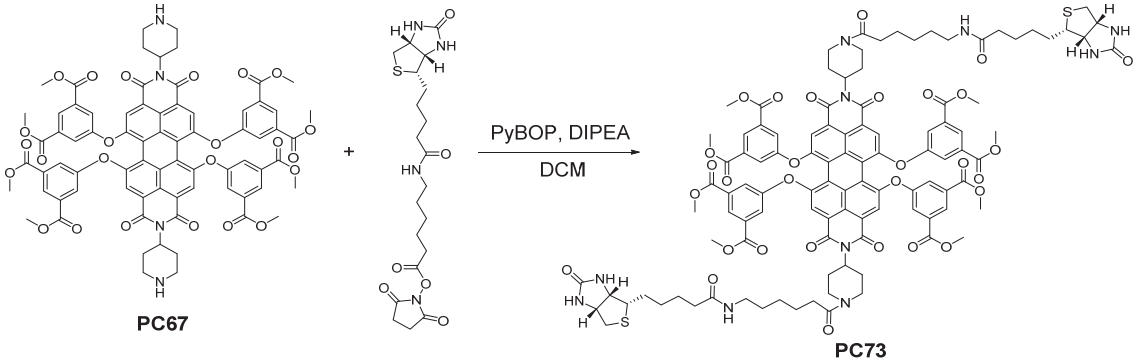

N,N'-bis-(1-Piperidine)-1,6,7,12-tetrakis(3,5-bis(methoxycarbonyl)phenoxy)perylene-3,4,9,10-tetracarboxylic diimide **PC67** (20 mg, 0.01 mmol) and PyBOP (14.6 mg 0.03 mmol) dissolved in DCM (1.1 mL) were added under nitrogen to *N*-succinimidyl-6-biotinamidohexanoate (12.7 mg, 0.03 mmol) and DIPEA (10 µL, 0.06 mmol) dissolved in DCM (0.7 mL). The purple-pink mixture was stirred at room temperature for 2 hours until the reactant disappears in TLC. The solvent was removed under reduced pressure. Purification was carried out by silica gel flash chromatography using DCM:MeOH (80:20) as eluent to give compound **PC73** as a deep pink solid in 63 % yield (18.1 mg, 0.009 mmol). **R_f (DCM:MeOH 50:4):** 0.41. **Mp (°C):** > 350 °C. **FT-IR (KBr, cm^{-1}):** 2957 (C-H), 2925 (C-H), 2854 (C-H), 1732 (C=O), 1701 (C=O), 1647 (CONH), 1590 (C_{Ar}-C_{Ar}), 1462 (CH_2), 1428 (CH_2), 1326 (C-N), 1300 (C-O), 1286 (C-O), 1258, 1107, 996, 758 (fingerprint region). **^{1}H NMR (300 MHz, $CDCl_3$) δ:** 8.31 (t, *J* = 1.5 Hz, 4H, **H**$_{Ar}$), 8.13 (s, 4H, **H**$_{Ar}$), 7.67 (d, *J* = 1.5 Hz, 8H, **H**$_{Ar}$), 6.66 (s, 1H, N**H**CO), 6.07 (d, *J* = 6.0 Hz, 1H, N**H**CO), 5.18 – 5.10 (m, 2H, N-C**H**), 4.72 (d, *J* = 9.6 Hz, 3H, C**H**$_2$), 4.47 – 4.43 (m, 2H, C**H**NHCO), 4.32 – 4.22 (m, 2H, C**H**NHCO), 3.86 (s, 24H, COOC**H**$_3$), 3.70 – 3.61 (m, 2H, SC**H**CH_2), 3.17 – 3.04 (m, 2H+4H, CH_2+CONHC**H**$_2$), 2.85 (dd, *J* = 12.9 Hz and 4.9 Hz, 2H, C**H**$_2$S), 2.68 (d, *J* = 12.9 Hz, 2H, C**H**$_2$S), 2.63 – 2.55 (m, 7H, C**H**$_2$), 2.37 – 2.30 (m, 4H, C**H**$_2$NHCOCH_2), 2.13 (t, *J* = 7.3 Hz, 4H, C**H**$_2$CON$_{piperidine}$), 1.79 – 1.51 (m, 15H, C**H**$_2$), 1.48 – 1.34 (m, 8H, C**H**$_2$). **^{13}C NMR (101 MHz, $CDCl_3$:MeOD) δ:** 174.1 (**C**ONH), 171.9 (**C**ON$_{piperidine}$), 165.1 (**C**OOCH_3), 163.1 (**C**ON**C**O$_{Imide}$), 162.9 (-NH**C**ONH-), 155.8 (-C_q-O-**C$_q$**$_{Phenol}$), 154.7 (-**C$_q$**-O-$C_{qPhenol}$), 132.9 (C_{Ar}), 132.5 (C_{Ar}), 126.3 (CH), 124.3 (CH), 123.8 (C_{Ar}), 123.7 (C_{Ar}), 123.6 (C_{Ar}), 120.9 (CH), 120.8 (CH), 61.9 (CONH**C**HCH_2), 60.1 (CONH**C**HCH), 55.3 (CH**C**HS), 54.2 (**C**HN$_{imide}$), 52.5 (COO**C**H_3), 43.8 (CH_2), 43.7 (CH_2), 40.3 (CH**C**H_2S), 38.9 (CH_2), 36.3 (CH_2), 35.6 (CH_2), 30.7 (CH_2), 29.6 (CH_2), 28.5 (CH_2), 28.1 (CH_2), 27.8 (CH_2), 26.4 (CH_2), 25.4 (CH_2), 25.1 (CH_2). **HRMS (MALDI+, DCTB):** m/z calcd for $C_{106}H_{110}N_{10}O_30S_2$ ($[M+H]^+$): 2067.6904; found: 2067.6920.

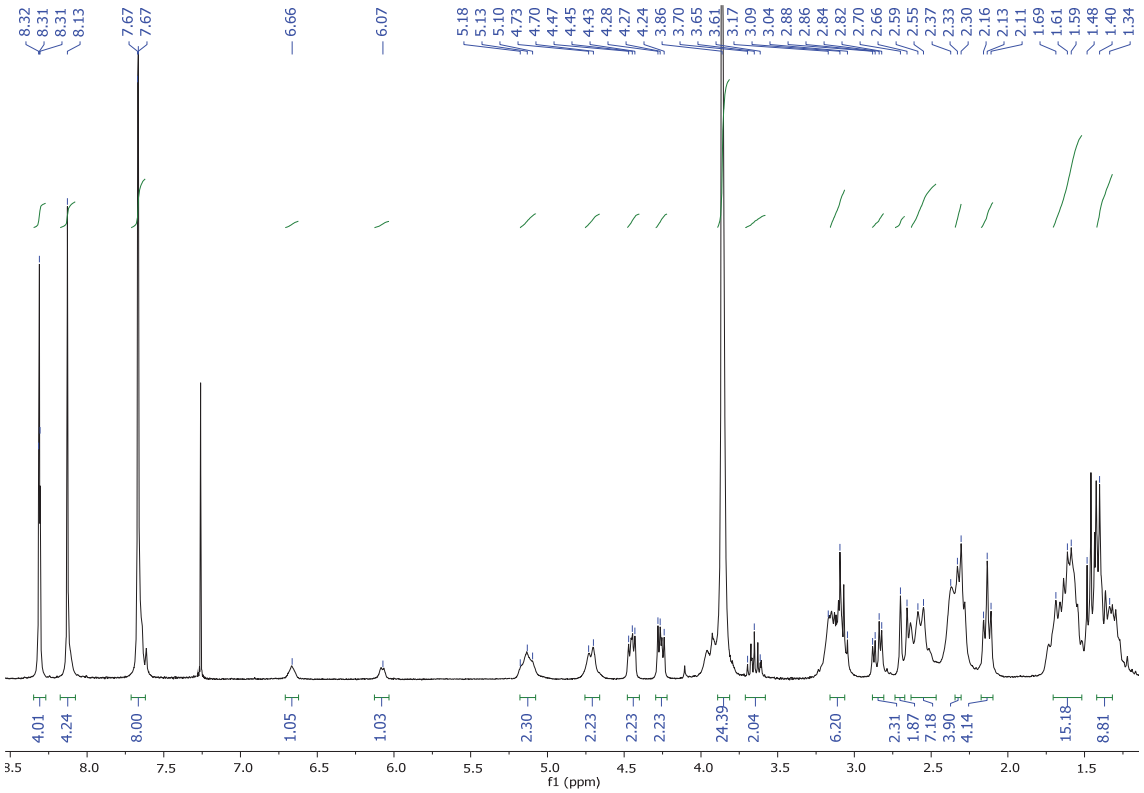

Figure 38. ^{1}H NMR (300 MHz, $CDCl_3$) of PC73

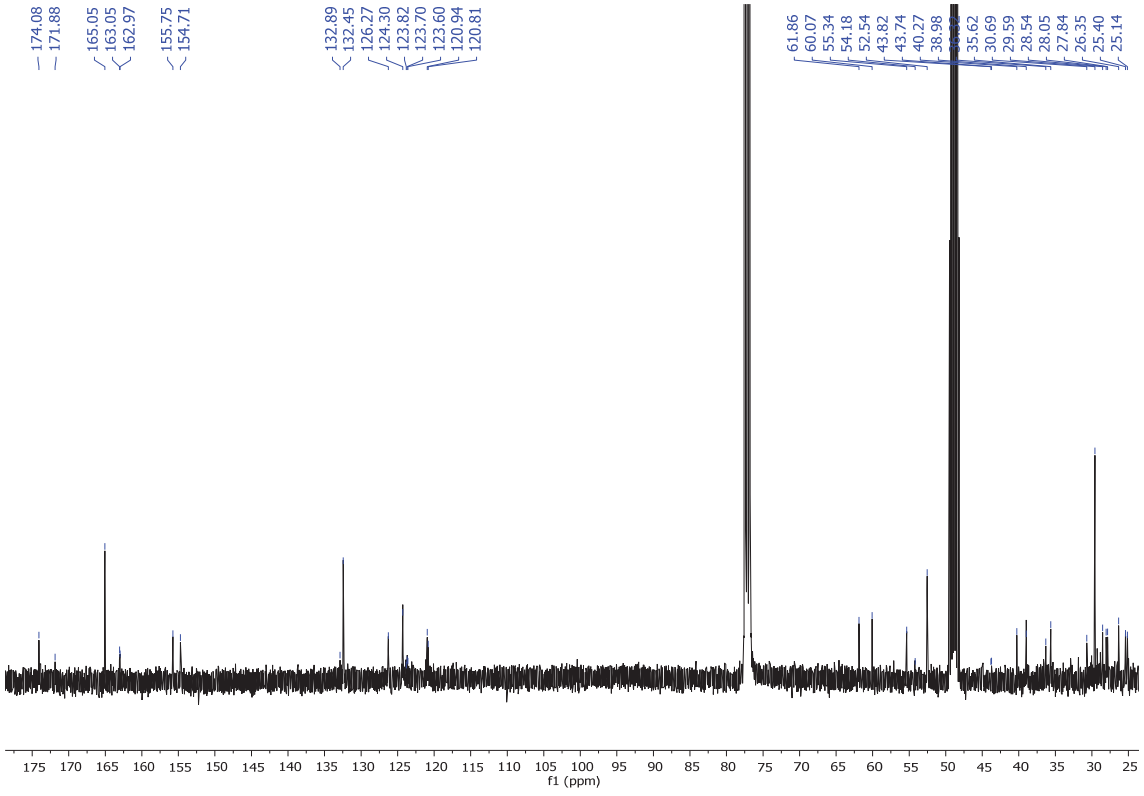

Figure 39. ^{13}C NMR (101 MHz, $CDCl_3$:MeOD) of PC73

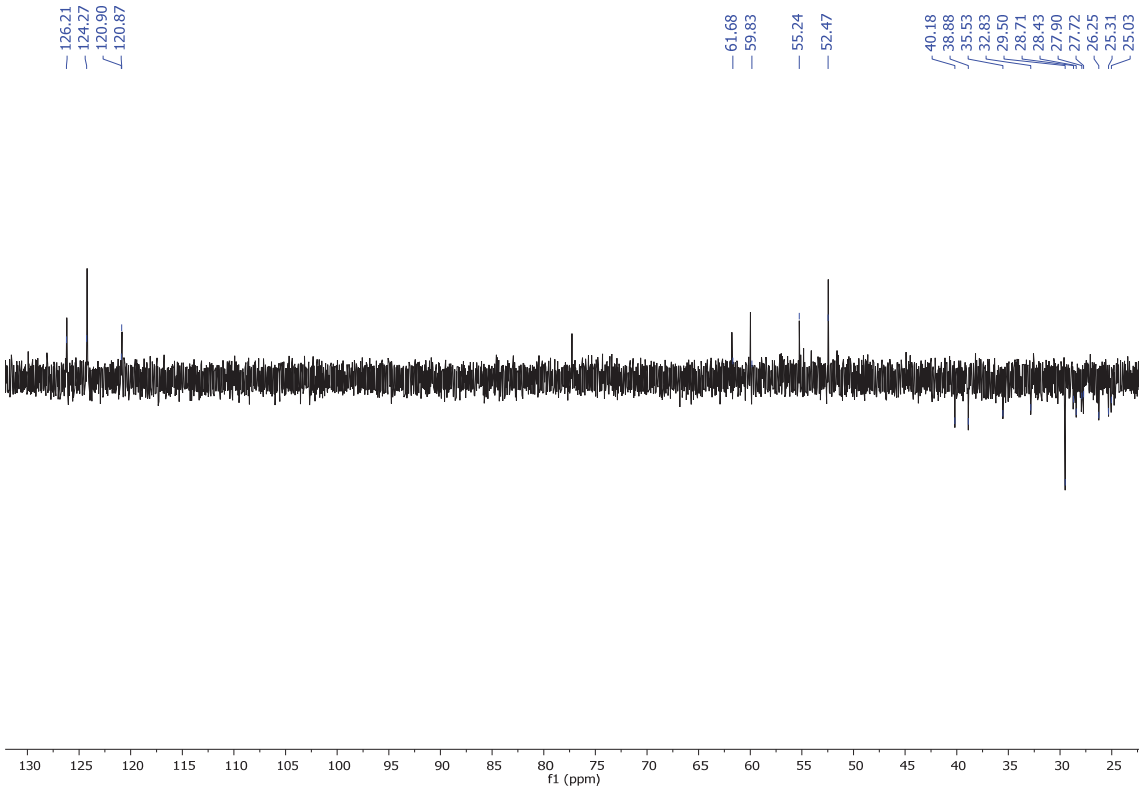

Figure 40. ^{13}C NMR-DEPT-135 (101 MHz, $CDCl_3$:MeOD) of PC73

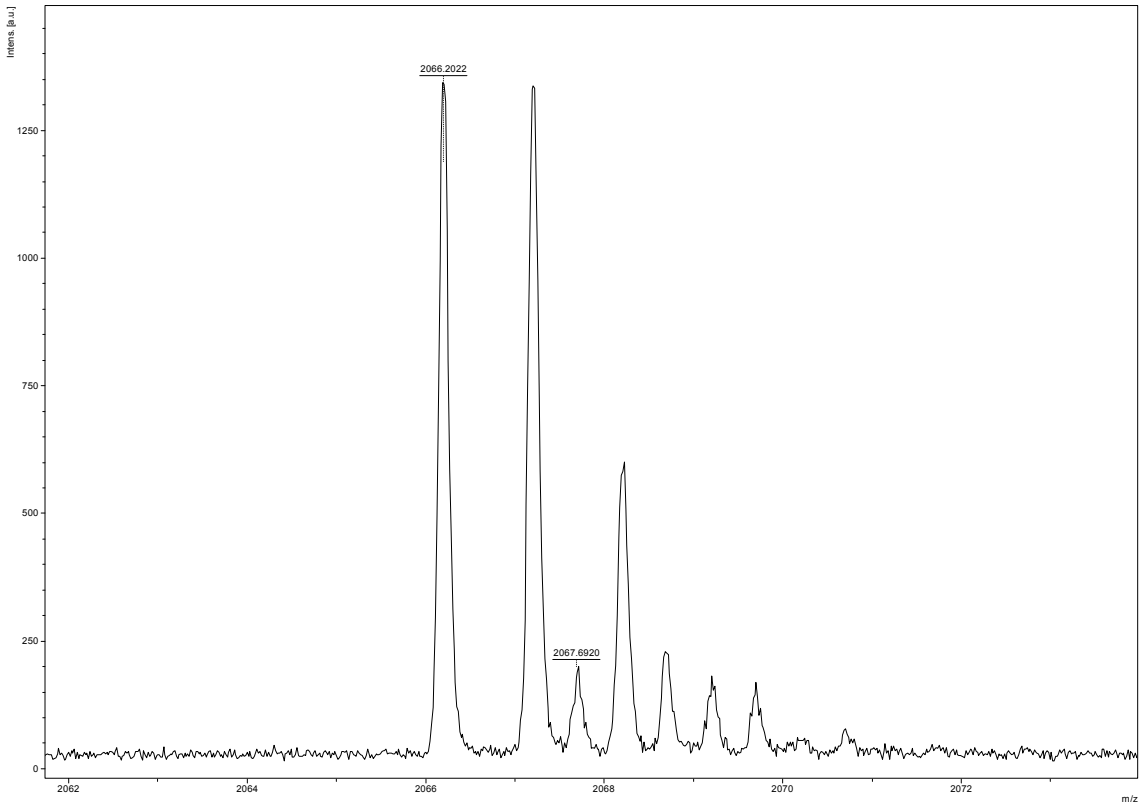

Figure 41. Mass spectrum (MALDI+, DCTB) of PC73

Solvatochromism:

The concentration of **PC73** is $1 \cdot 10^{-5}$ M. The excitation wavelength is 434 nm. The absorption and emission spectra have been measured in the listed solvents below in the range between 200 to 900 nm. The used solvents are: MeOH, DMSO, DMF, MeCN, acetone, ethyl acetate, THF, $CHCl_3$ and DCM.

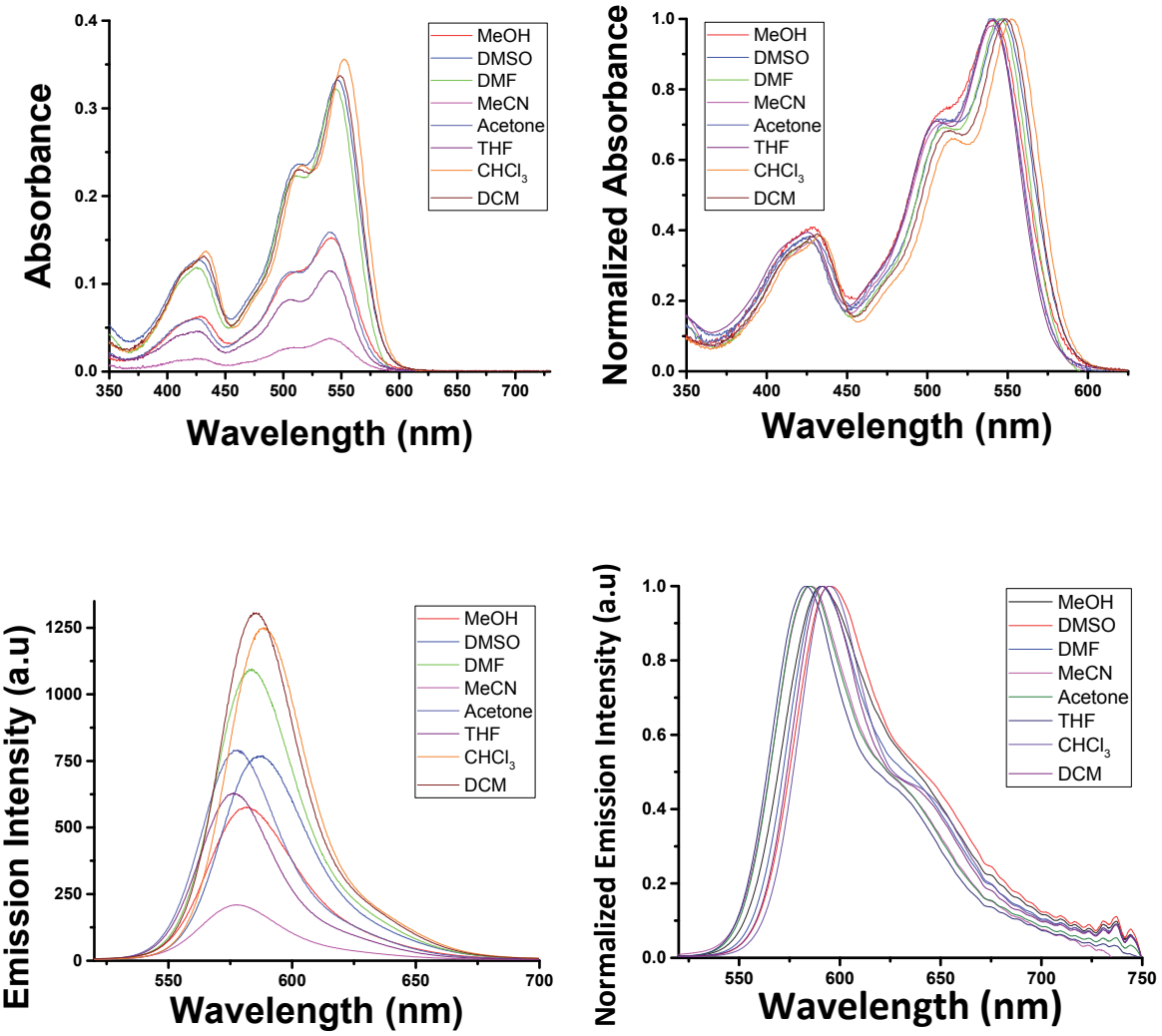

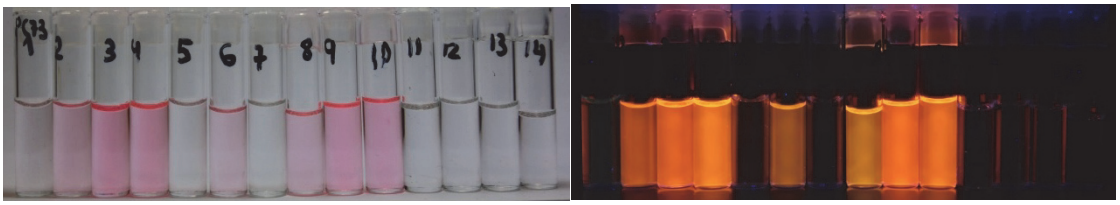

Solvents: 1: Water, 2: MeOH, 3: DMSO, 4: DMF, 5: MeCN, 6: acetone, 7: AcOEt, 8: THF, 9: $CHCl_3$, 10: DCM, 11: toluene, 12: diethyl ether, 13: hexane, 14: cyclohexane.

Figure 42. Upper. Absorbance spectra and Normalized absorbance spectra of PC73. Middle: Fluorescence spectra and Normalized and corrected fluorescence spectra of PC73. Lower. Solvatochromic effect of PC73 under white light and light of 366 nm.

1.12. Synthesis of *N,N'*-bis-(1-(piperidin-1-yl)-6-biotinamidohexan-1-one)-1,6,7,12-tetrakis(3,5-bis(hydroxycarbonyl)phenoxy)perylene-3,4,9,10-tetracarboxylic diimide (PC80).

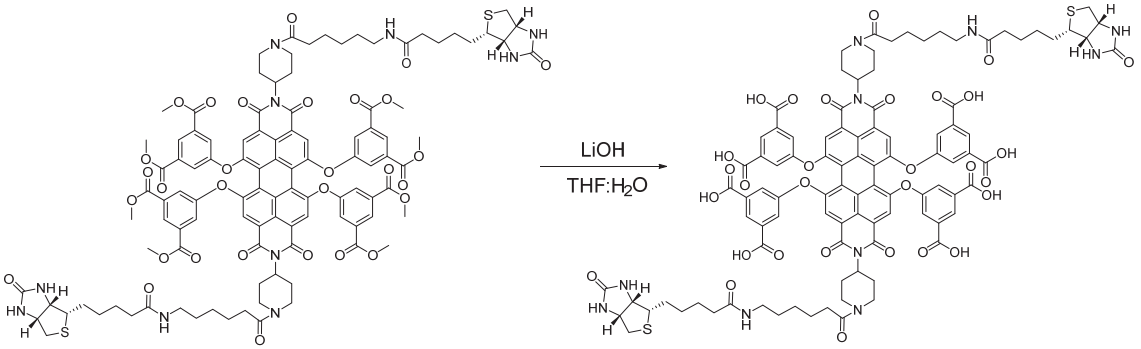

PC73 **PC80**

Lithium hydroxide (21 mg, 0.92 mmol) dissolved in H_2O (2 mL) were added to *N,N'*-bis(1-(piperidin-1-yl)-6-biotinamidohexan-1-one)-1,6,7,12-tetrakis(3,5-bis(methoxycarbonyl)-phenoxy)perylene-3,4,9,10-tetracarboxylic diimide **PC73** (24 mg, 0.01 mmol) dissolved in THF (8 mL). The mixture was stirred at 45 °C overnight. The solvents were removed under reduced pressure to obtain a brown oil-solid in 99 % yield (23.5 mg, 0.01 mmol). **R_f (MeOH):** 0. **Mp**: > 350 °C. **FT-IR (KBr, cm^{-1}):** 3431 (O-H), 2940 (C-H), 2857 (C-H), 2781 (C-H), 1976 (C-H), 1635 (CONH), 1567 (C_{Ar}-C_{Ar}), 1454 (CH_2), 1408 (CH_2), 1385 (O-H), 1320 (C-N), 1260 (C-O), 1206, 1152, 1124, 1104, 1022, 968, 871, 596 (fingerprint region). **^{1}H NMR (300 MHz, D_2O) *δ*:** 7.88 (s, 2H, H_{Ar}), 7.77 (d, *J* = 8.7 Hz, 2H, H_{Ar}), 7.64 (d, *J* = 6.8 Hz, 2H, H_{Ar}), 7.53 (s, 4H, H_{Ar}), 7.43 – 7.32 (m, 6H, H_{Ar}), 4.56 – 4.53 (m, 2H, CH), 4.36 – 4.32 (d, 2H, CH), 3.62 – 3.50 (m, 2H, CH_2), 3.32 – 3.22 (m, 4H, CH_2), 3.13 (t, *J* = 6.8 Hz, 3H, CH_2), 2.93 (dd, *J* = 18.1 Hz *J* = 5.3 Hz, 4H, CH_2), 2.73 (d, *J* = 13.1 Hz, 2H, CH_2), 2.59 (m, 3H, CH_2), 2.42 – 2.28 (m, 4H, CH_2), 2.14 (m, 5H, CH_2), 2.01 (s, 5H, CH_2), 1.57 – 1.45 (m, 15H, CH_2), 1.35 – 1.29 (m, 10H, CH_2). **^{13}C NMR (101 MHz, D_2O) *δ*:** 176.8 (**C**ONH), 165.5 (**C**OOH), 143.4 (C_{Ar}), 127.4 (C_{Ar}), 125.3 (CH), 125.3 (CH), 117.9 (C_{Ar}), 111.5 (CH), 62.2 (NH-**C**H-CH_2), 60.4 (NH-**C**H-CH), 55.5 (CH**C**HS), 39.9 (CH_2), 39.4 (CH**C**H_2S), 37.7 (CH_2), 35.7 (CH_2), 28.3 (CH_2), 28.0 (CH_2), 27.8 (CH_2), 27.3 (CH_2), 26.3 (CH_2), 25.7 (CH_2), 25.4 (CH_2).

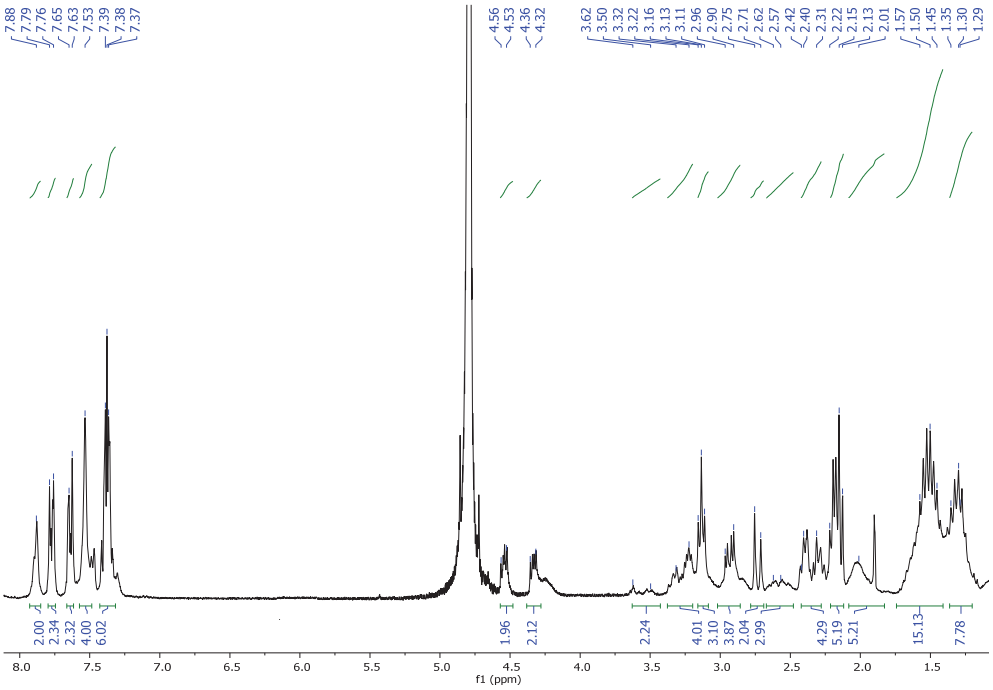

Figure 43. ^{1}H NMR (300 MHz, D_2O) of PC80

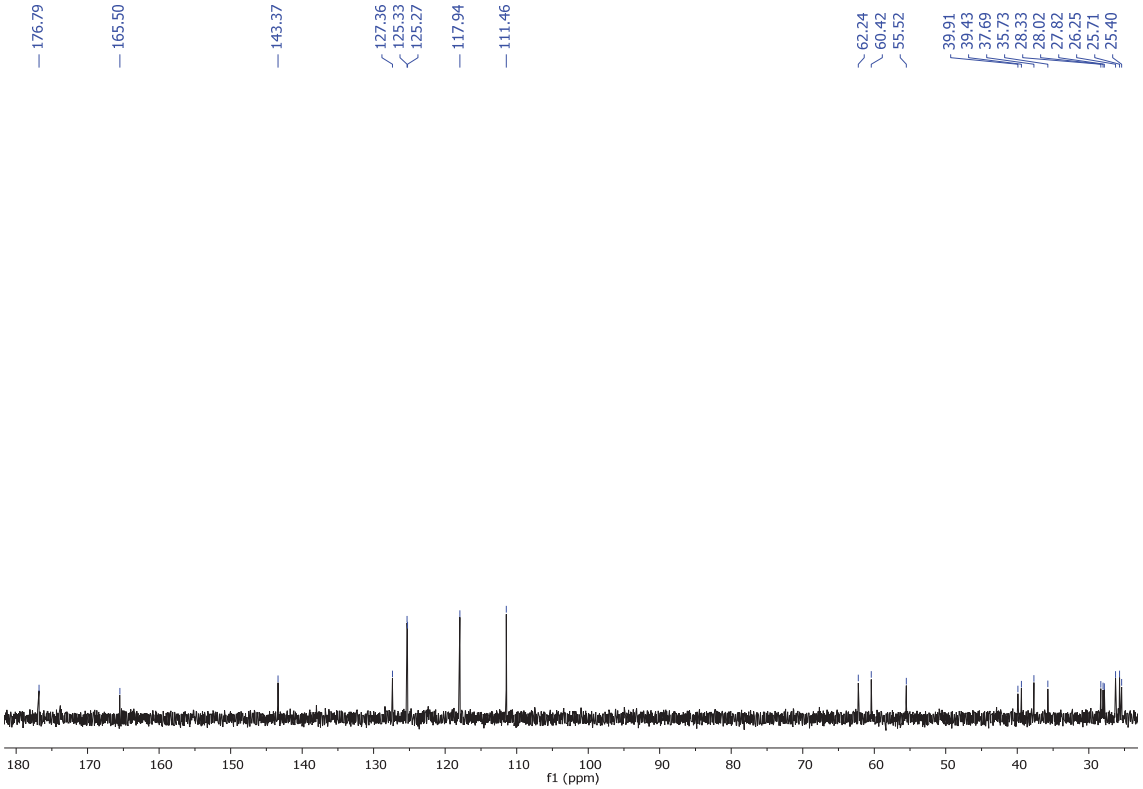

Figure 44. ^{13}C NMR (101 MHz, D_2O) of PC80

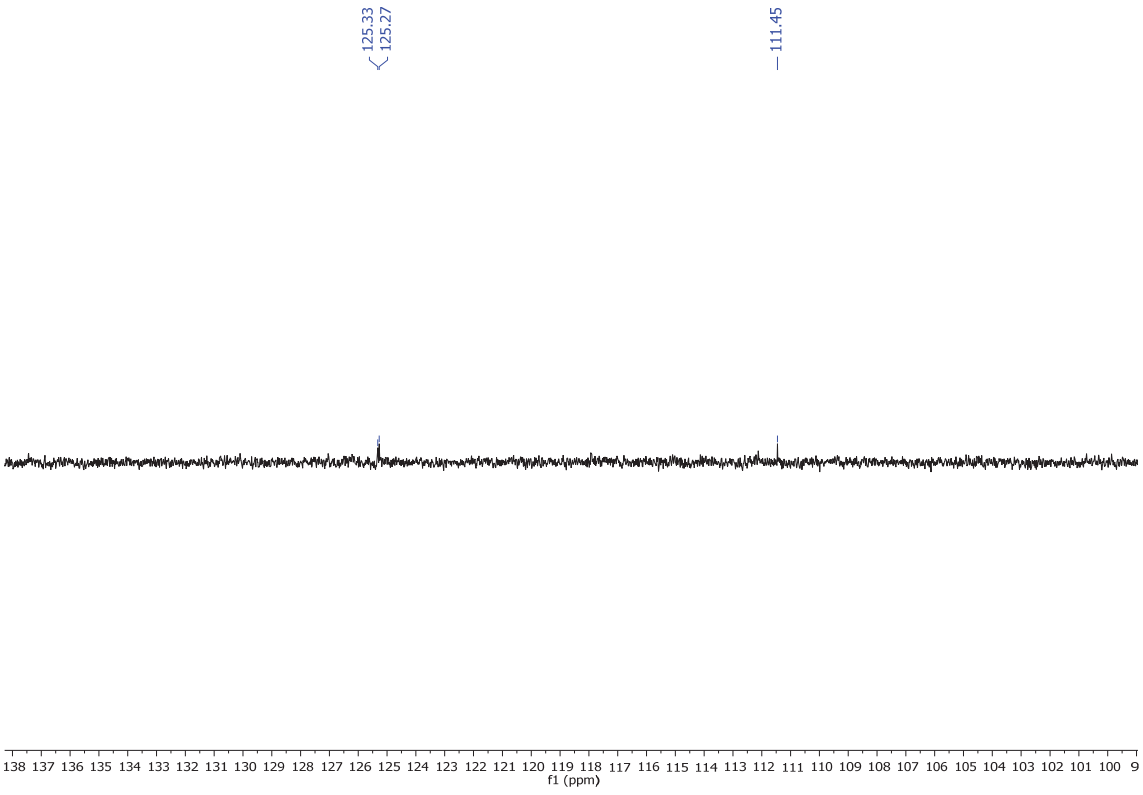

Figure 45. ^{13}C NMR-DEPT-135 (101 MHz, D_2O) of PC80

Solvatochromism:

The concentration of **PC80** is $1 \cdot 10^{-5}$ M. The excitation wavelength is 440 nm. The absorption and emission spectra have been measured in the listed solvents below in the range between 200 to 900 nm. The used solvents are: H_2O.

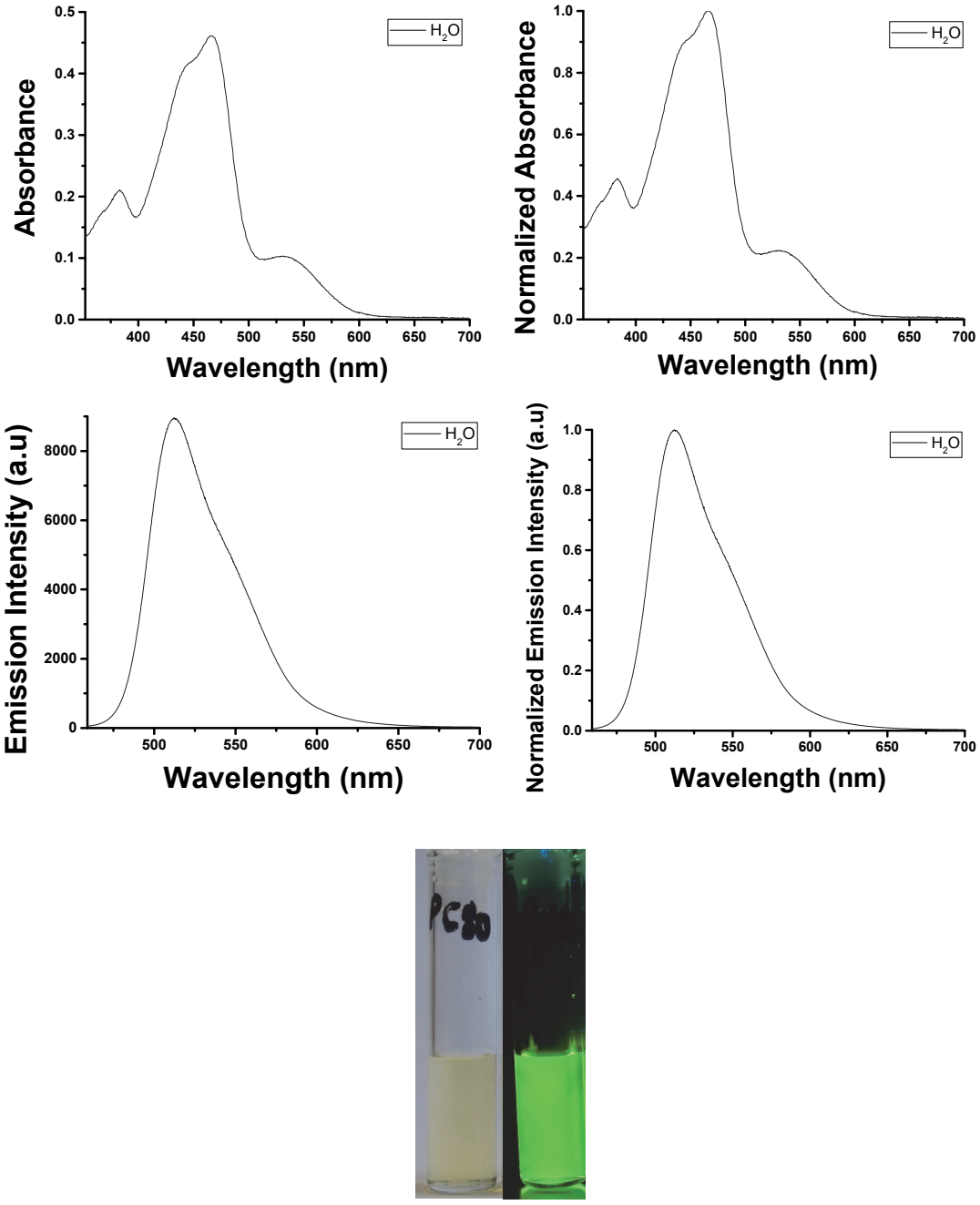

Solvents: 1: Water.

Figure 46. Upper. Absorbance and Normalized absorbance spectra of PC80. Middle: Fluorescence and Normalized fluorescence spectra of PC80. Lower. Solvatochromic effect of PC80 under white light and light of 366 nm.

1.13. Synthesis of *N,N'*-bis-(((1-(piperidin-1-yl)-4-androsten-17*β*-acetoxy-3-one-7*α*-yl)but-2-en-1-one))-1,6,7,12-tetrakis(3,5-bis(methoxycarbonyl)phenoxy)perylene-3,4,9,10-tetracarboxylic diimide (PC71).

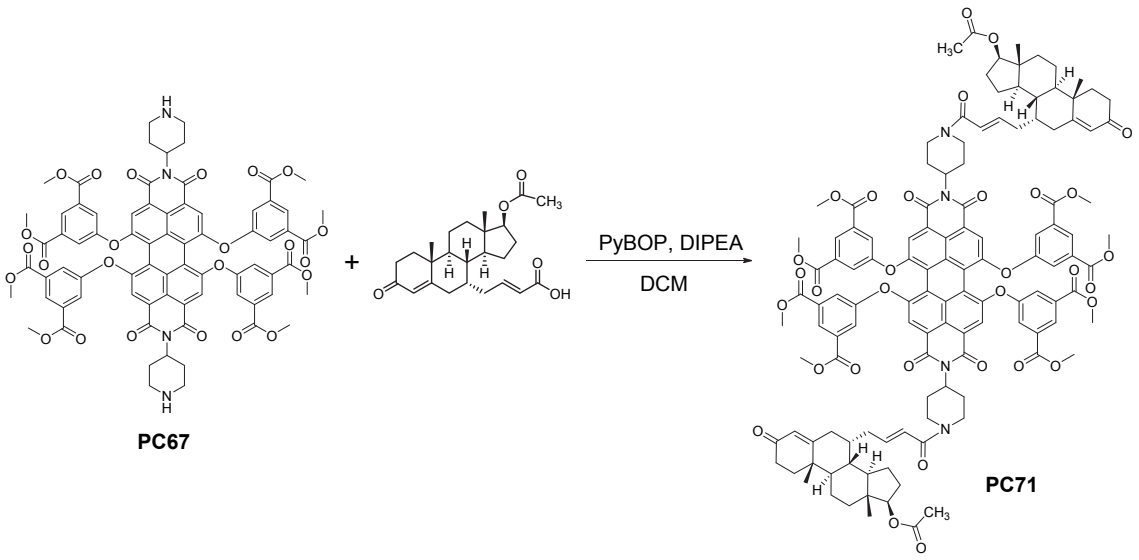

PC67 **PC71**

N,N'-bis(1-Piperidine)-1,6,7,12-tetrakis(3,5-bis(methoxycarbonyl)phenoxy)perylene-3,4,9,10-tetracarboxylic diimide **PC67** (20 mg, 0.01 mmol) and PyBOP (14.6 mg 0.03 mmol) dissolved in DCM (1.1 mL) were added under nitrogen to (4-androsten-17*β*-acetoxy-3-one-7*α*-yl)-but-2-enoic acid (12 mg, 0.03 mmol) and DIPEA (10 µL, 0.06 mmol) dissolved in DCM (0.7 mL). The purple-pink mixture was stirred at room temperature for 2.5 hours until the reactant disappears in TLC. The solvent was removed under reduced pressure. Purification was carried out by silica gel flash chromatography using DCM:MeOH (90:10) as eluent to give compound PC71 as a deep pink solid in 68 % yield (21 mg, 0.01 mmol). **R_f (DCM:MeOH 50:4):** 0.41. **Mp (°C):** > 350 °C. **FT-IR (KBr, cm^{-1}):** 2951 (C-H), 2923 (C-H), 2852 (C-H), 1729 (C=O), 1701 (C=O), 1664 (CONH), 1587 (C_{Ar}-C_{Ar}), 1505 (C_{Ar}-C_{Ar}), 1451 (CH_2), 1434 (CH_2), 1411 (CH_2), 1320 (C-N), 1303 (C-O), 1283 (C-O), 1249, 1184, 1104, 1039, 999, 905, 803, 755, 721 (fingerprint region). **^{1}H NMR (300 MHz, $CDCl_3$) *δ*:** 8.35 (t, *J* = 1.5 Hz, 4H, H_{Ar}), 8.16 (s, 4H, H_{Ar}), 7.70 (d, *J* = 1.5 Hz, 8H, H_{Ar}), 6.73 – 6.65 (m, 2H, C**H**=CHCON$_{piperidine}$), 6.23 (d, *J* = 14.8 Hz, 2H, CH=C**H**CON$_{piperidine}$), 5.65 (s, 2H, C=CH-CO), 5.22 – 5.14 (m, 2H, N-CH), 4.82 (d, *J* = 8.3 Hz, 2H, CH_2), 4.61 (t, *J* = 8.4 Hz, 2H, C**H**OCOCH$_3$), 4.32 – 4.22 (m, 2H, C**H**NHCO), 3.89 (s, 24H, COOCH$_3$), 3.20 – 3.11 (m, 4H, CH_2), 2.70 – 2.63 (m, 8H, CH_2), 2.42 – 2.35 (m, 8H, C**H$_2$**CC**H$_2$**CH=CH-CON$_{piperidine}$), 2.27 – 2.14 (m, 6H, CH$_2$C**H$_2$**CO+C**H**), 2.04 (s, 6H, CHOCOC**H**$_3$), 1.91 – 1.87 (m, 4H, CH_2), 1.79 – 1.69 (m, 10H, CH_2), 1.66 – 1.55 (m, 4H, CH_2), 1.41 – 1.34 (m, 6H, CH+CH_2), 1.25 (s, 6H, CH_3), 1.19 (m, 4H, CH+CH_2), 1.19 – 1.14 (m, 6H, CH), 0.84 (s, 6H, CH_3). **^{13}C NMR (101 MHz, $CDCl_3$) *δ*:** 198.9 (**C**=OCH=C), 171.3 (C=OCH=**C**;2xCO**C**OCH$_3$), 168.9 (CON$_{piperidine}$), 165.1 (**C**OOCH$_3$), 163.1 (**C**ON**C**O$_{Imide}$), 155.9 (-C_q-O-**C$_q$**$_{Phenol}$), 154.9 (-**C$_q$**-O-$C_{qPhenol}$), 145.0 (CH_2**C**H=CHCON$_{piperidine}$), 133.1 (C_{Ar}), 132.7 (C_{Ar}), 126.6 (C_{Ar}), 126.4 (C_{Ar}), 124.5 (CH), 123.9 (C_{Ar}), 122.2 (C_{Ar}), 122.1 (C_{Ar}), 121.3 (C_{Ar}), 121.2 (C_{Ar}), 120.9 (CH_2CH=**C**HCON$_{piperidine}$), 82.6 (**C**OCOCH$_3$), 52.8 (COO**C**H$_3$+**C**HN$_{imide}$), 52.0 (**C**HCH$_2$CH$_2$COCOCH$_3$), 47.2 (CH), 46.3 (CH), 42.7 (CH_2), 42.4 (CH_2), 38.8 (CH; 2xC_{quat}), 38.3 (CH_2), 36.6 (CH_2), 36.1 (CH_2), 34.2 (CH_2), 29.9 (CH_2), 28.2 (CH_2), 27.4 (CH_2), 23.0 (CH_2), 21.3 (CH_2), 20.9 (CH_3), 18.1 (CH_3), 12.1 (CH_3). **HRMS (MALDI+, DCTB):** m/z calcd. for $C_{124}H_{124}N_4O_{32}$ ([M+H]$^+$): 2181.8271; found: 2181.8421.

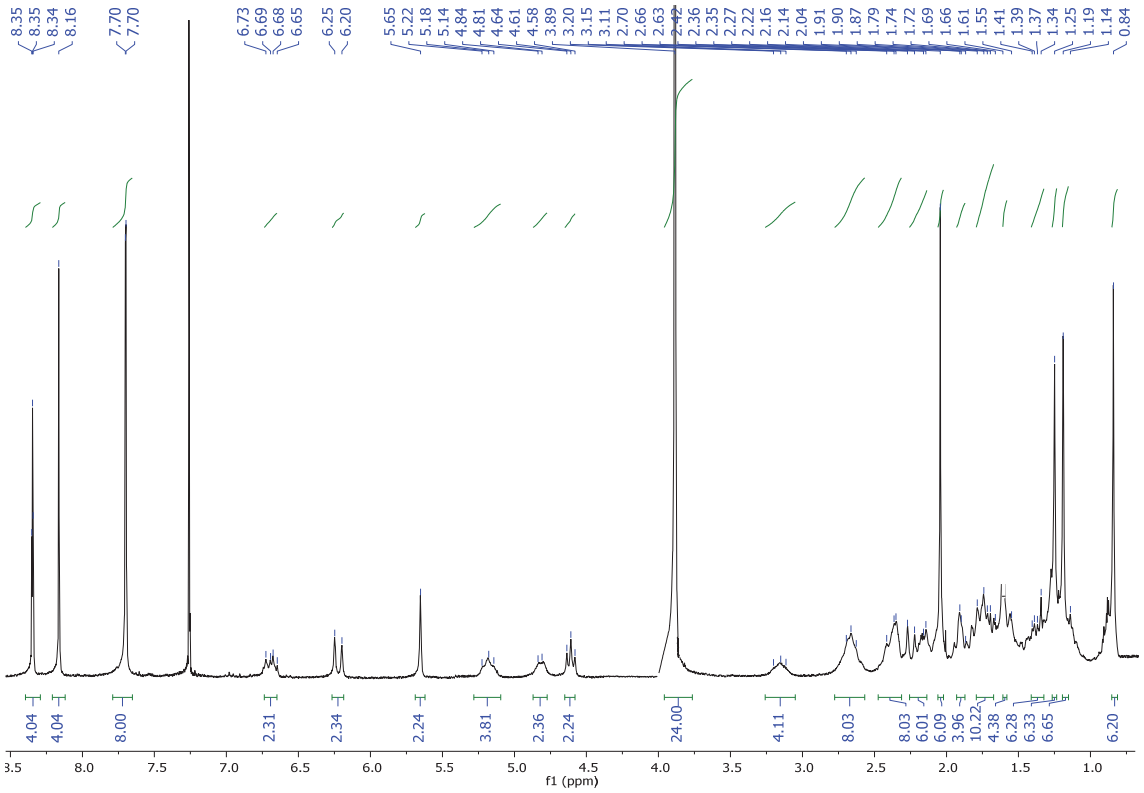

Figure 47. ^{1}H NMR (300 MHz, $CDCl_3$) of PC71

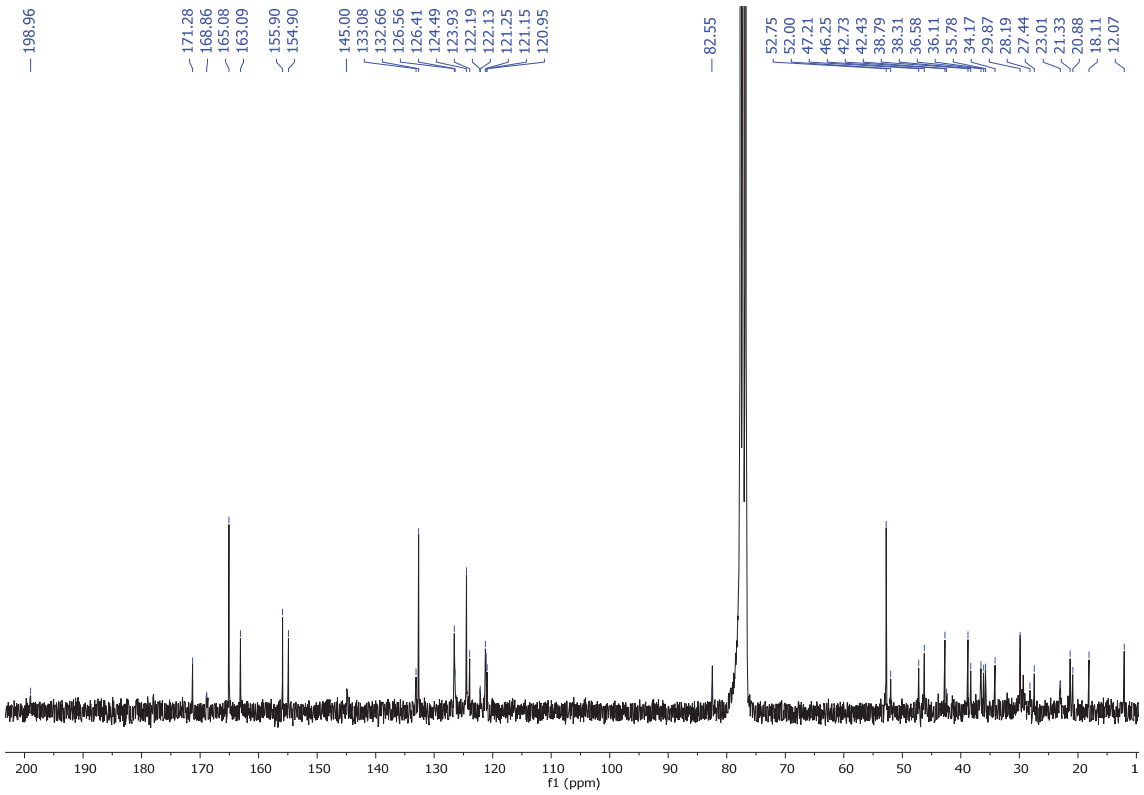

Figure 48. ^{13}C NMR (101 MHz, $CDCl_3$) of PC71

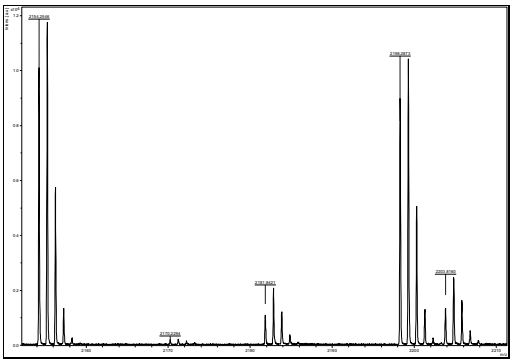

Figure 49. Mass spectrum (MALDI+, DCTB) of PC71

Solvatochromism: The concentration of **PC71** is $1 \cdot 10^{-5}$ M. The excitation wavelength is 432 nm. The absorption and emission spectra have been measured in the listed solvents below in the range between 200 to 900 nm. The used solvents are: MeOH, DMSO, DMF, MeCN, acetone, ethyl acetate, THF, $CHCl_3$, DCM and toluene.

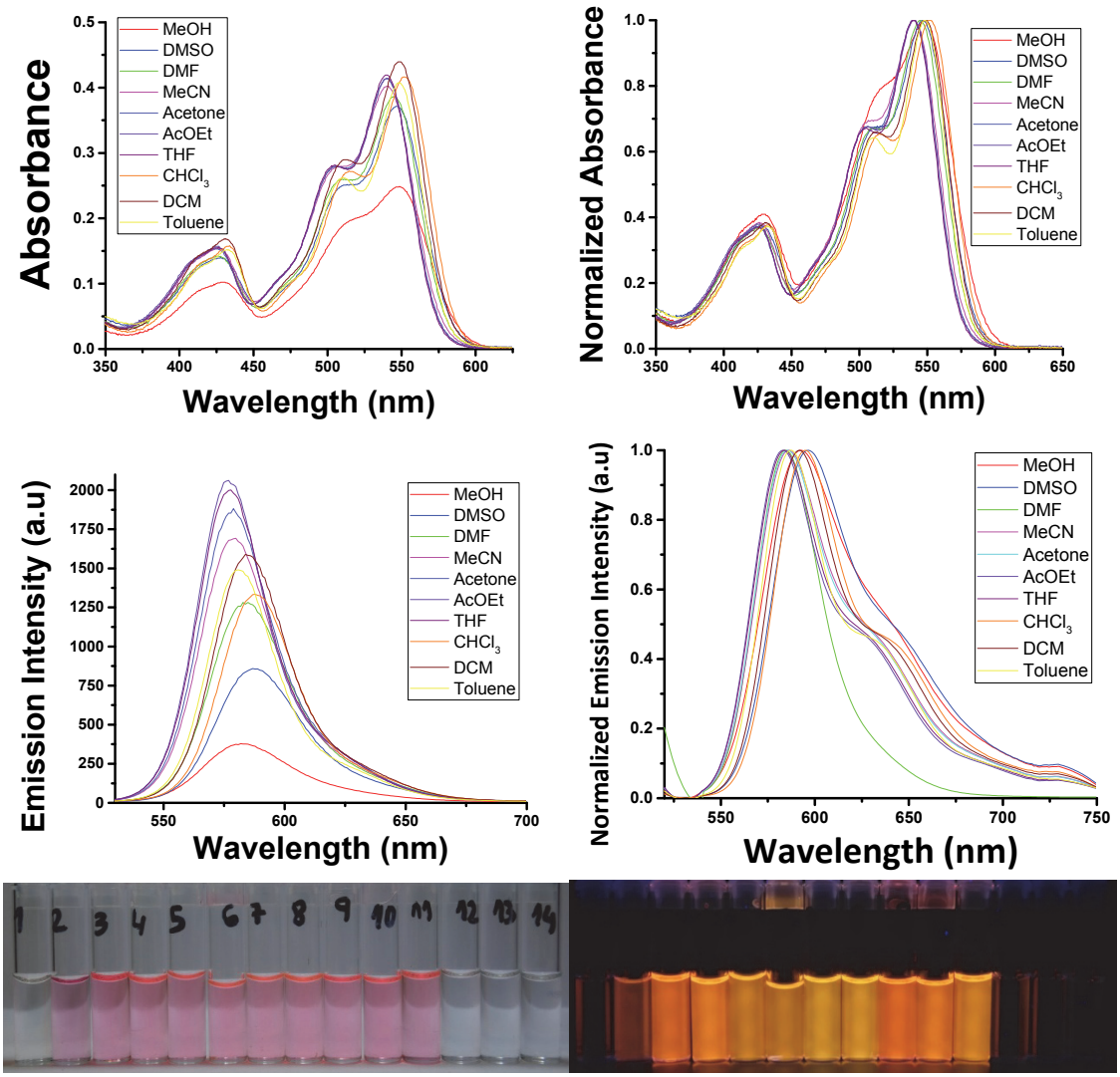

Solvents: 1: Water, 2: MeOH, 3: DMSO, 4: DMF, 5: MeCN, 6: acetone, 7: AcOEt, 8: THF, 9: $CHCl_3$, 10: DCM, 11: toluene, 12: diethyl ether, 13: hexane, 14: cyclohexane.

Figure 50. Upper. Absorbance spectra and Normalized absorbance spectra of PC71. Middle: Fluorescence spectra and Normalized and corrected fluorescence spectra of PC71. Lower. Solvatochromic effect of PC71 under white light and light of 366 nm.

1.14. Synthesis of *N,N'*-bis((1-(piperidin-1-yl)-4-androsten-17*β*-acetoxy-3-one-7*α*-yl)but-2-en-1-one))-1,6,7,12-tetrakis(3,5-bis(hydroxycarbonyl)phenoxy)perylene-3,4,9,10-tetracarboxylic diimide (PC79).

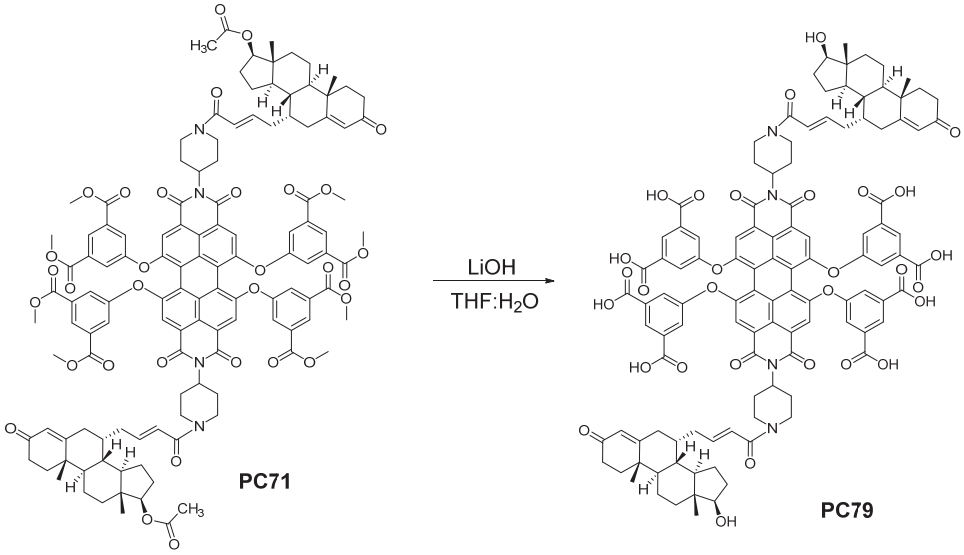

Lithium hydroxide (18 mg, 0.77 mmol) dissolved in H_2O (2 mL) were added to *N,N'*-bis-(1-(piperidin-1-yl)-4-androsten-17*β*-acetoxy-3-one-7*α*-yl)but-2-en-1-one)-1,6,7,12-tetrakis(3,5-bis(methoxycarbonyl)phenoxy)perylene-3,4,9,10-tetracarboxylic diimide **PC71** (21 mg, 0.01 mmol) dissolved in THF (8 mL). The mixture was stirred at 45 °C overnight. The solvents were removed under reduced pressure to obtain a brown oil-solid in 99 % yield (23.5 mg, 0.01 mmol). **R_f (MeOH):** 0. **Mp**: > 350 °C. **FT-IR (KBr, cm^{-1}):** 3428 (O-H), 2977 (C-H), 2954 (C-H), 2923 (C-H), 2854 (C-H), 1630 (CONH), 1545 (C_{Ar}-C_{Ar}), 1439 (CH_2), 1164, 1124, 1056, 993, 911, 860 (fingerprint region). **^{1}H NMR (300 MHz, D_2O) *δ*:** 8.46 (s, 16H, H_{Ar}), 3.99 – 3.92 (m, 10H, CH), 3.86 – 3.58 (m, 39H, CH+CH_2), 2.44 (t, *J* = 8.1 Hz, 4H, CH+CH_2), 2.26 – 2.18 (m, 8H, CH+CH_2), 2.14 (m, 5H, CH+CH_2), 2.05 – 1.80 (m, 39H, CH+CH_2).

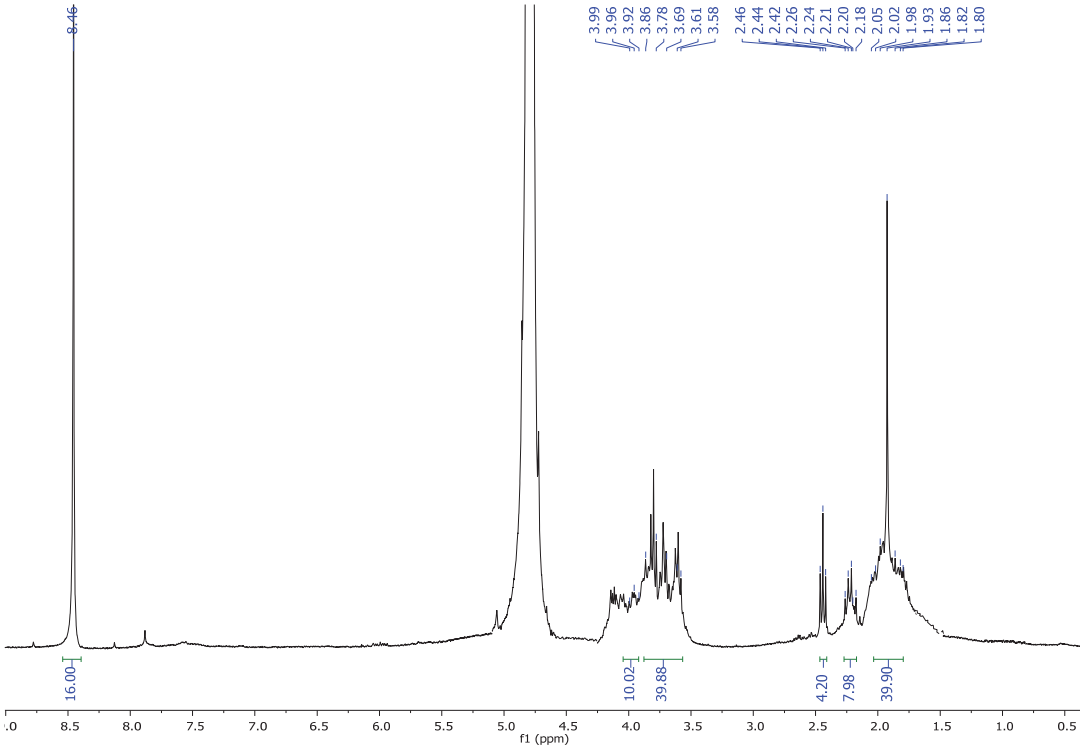

Figure 51. ^{1}H NMR (300 MHz, D_2O) of PC79

Solvatochromism:

The concentration of **PC79** is $1 \cdot 10^{-5}$ M. The excitation wavelength is 466 nm. The absorption and emission spectra have been measured in the listed solvents below in the range between 200 to 900 nm. The used solvents are: H_2O.

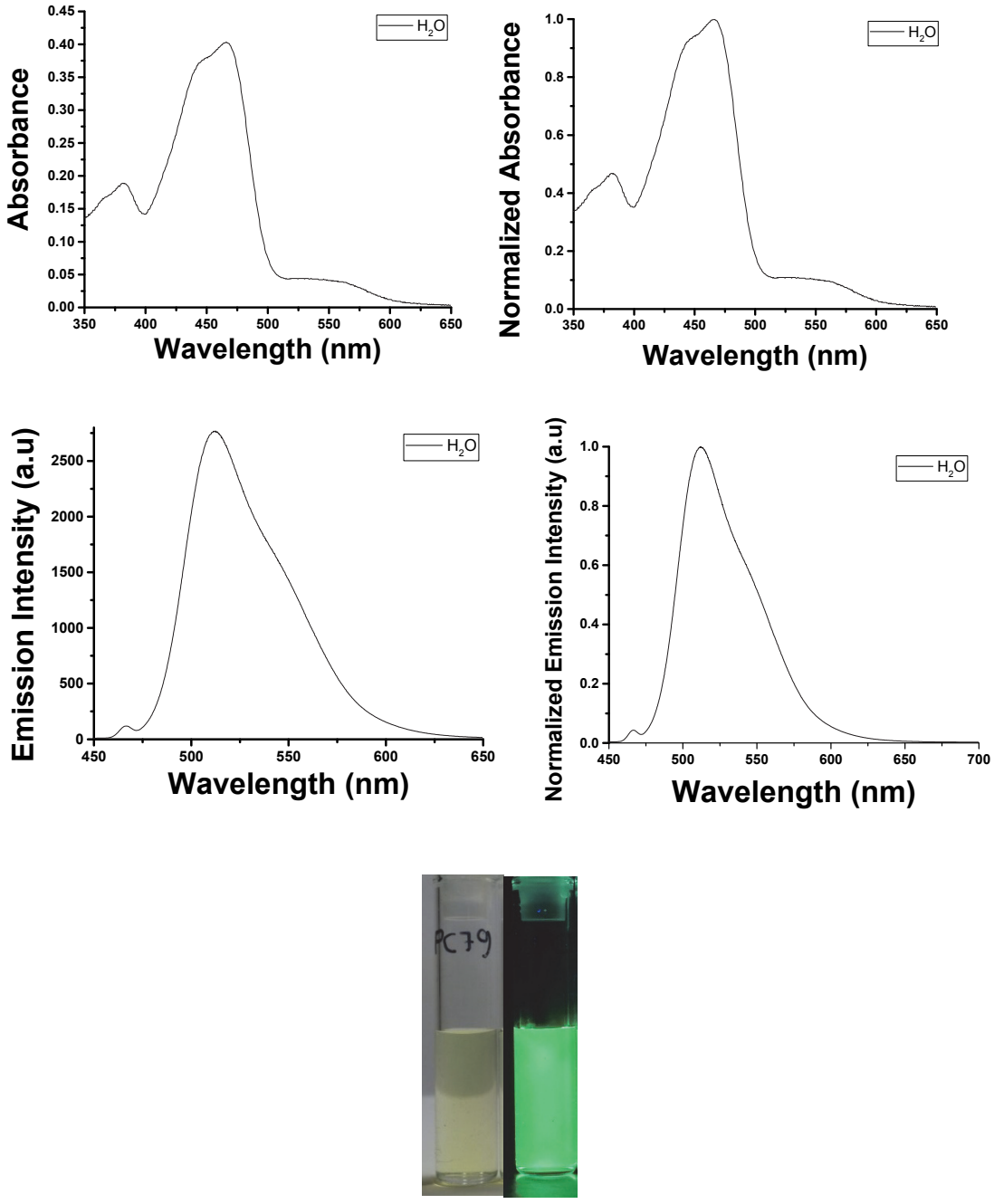

Solvents: 1: Water.

Figure 52. Upper. Absorbance and Normalized absorbance spectra of PC79. Middle: Fluorescence and Normalized fluorescence spectra of PC79. Lower. Solvatochromic effect of PC79 under white light and light of 366 nm.

1.15. Synthesis of *N*-(1-piperidine)-*N',N'-Bis*((1-(2-(2-methoxyethoxy)ethyl)piperidine)-1,6,7,12-tetrakis(3,5-bis(methoxycarbonyl)phenoxy)perylene-3,4,9,10-tetracarboxylic diimide (PC91).

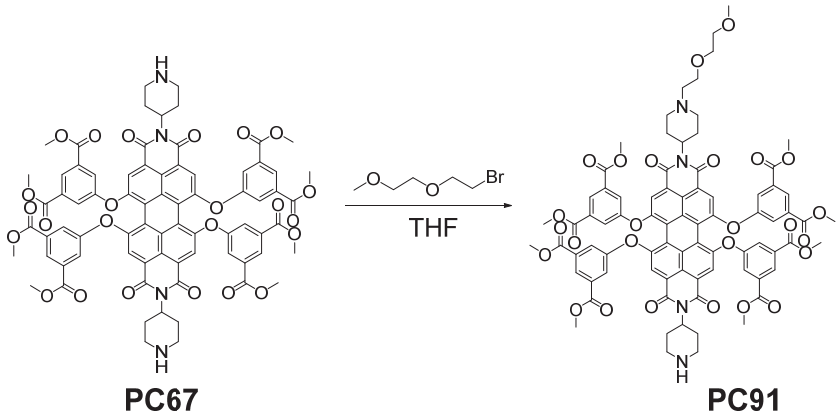

1-Bromo-2-(2-methoxyethoxy)eyhane (56.4 µL, 0.42 mmol) and DIPEA (10 µL, 0.04 mmol) were added under nitrogen to *N,N'*-bis-(1-piperidine)-1,6,7,12-tetrakis(3,5-bis(methoxycarbonyl)phenoxy)perylene-3,4,9,10-tetracarboxylic diimide **PC67** (30 mg, 0.02 mmol) dissolved in THF (10 mL). The purple-pink mixture was stirred at room temperature for 4 days until the reactant disappears in TLC. The solvent was removed under reduced pressure. Purification was carried out by silica gel flash chromatography using DCM:MeOH (XX:XX) as eluent to give compound **PC91** as a deep pink solid in 68 % yield (21 mg, 0.01 mmol). **R_f (DCM:MeOH 50:4):** 0.**Mp (°C):** > 350 °C. **^{1}H NMR (300 MHz, D_2O) *δ*:** 8.46 (s, 16H, H_{Ar}), 3.99 – 3.92 (m, 10H, C**H**), 3.86 – 3.58 (m, 39H, C**H**+CH_2), 2.44 (t, *J* = 8.1 Hz, 4H, C**H**+CH_2), 2.26 – 2.18 (m, 8H, C**H**+CH_2), 2.14 (m, 5H, C**H**+CH_2), 2.05 – 1.80 (m, 39H, C**H**+CH_2). **MS (MALDI+, DCTB):** m/z calcd. for $C_{79}H_{70}N_4O_{26}$ ([M]$^+$): 1491.4278; found: 1491.4223.

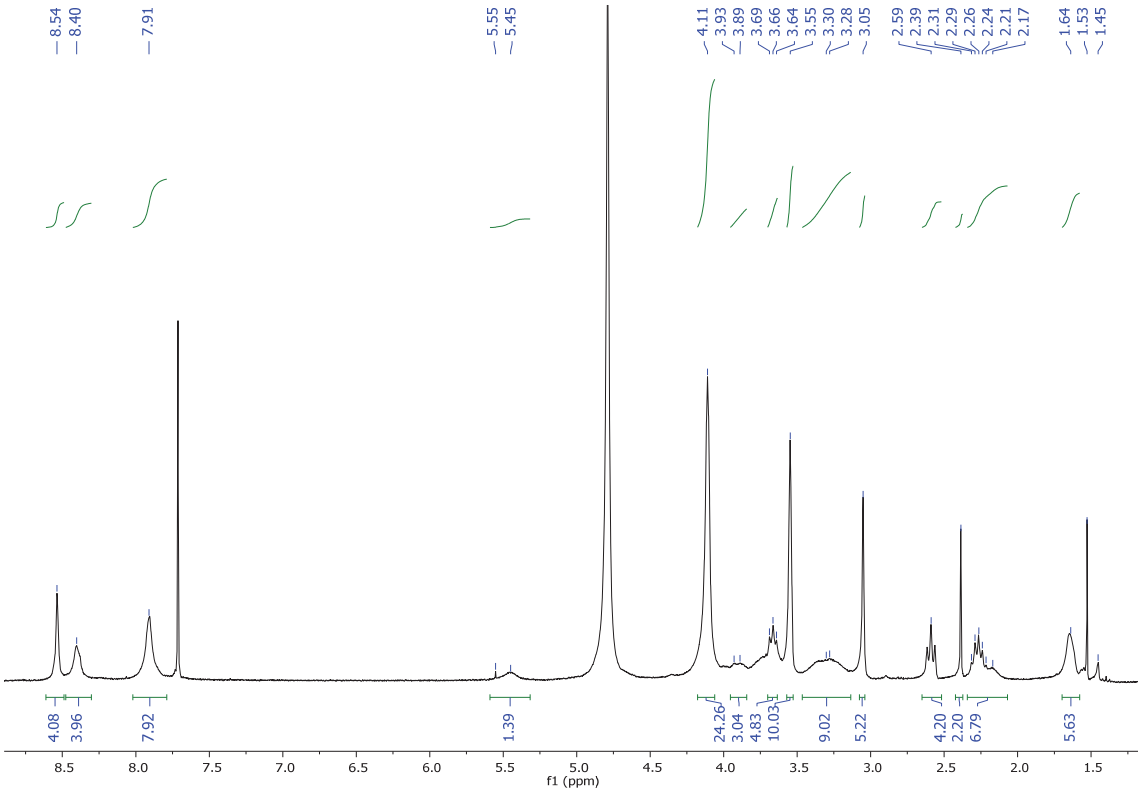

Figure 53. ^{1}H NMR (300 MHz, $CHCl_3$) of PC91

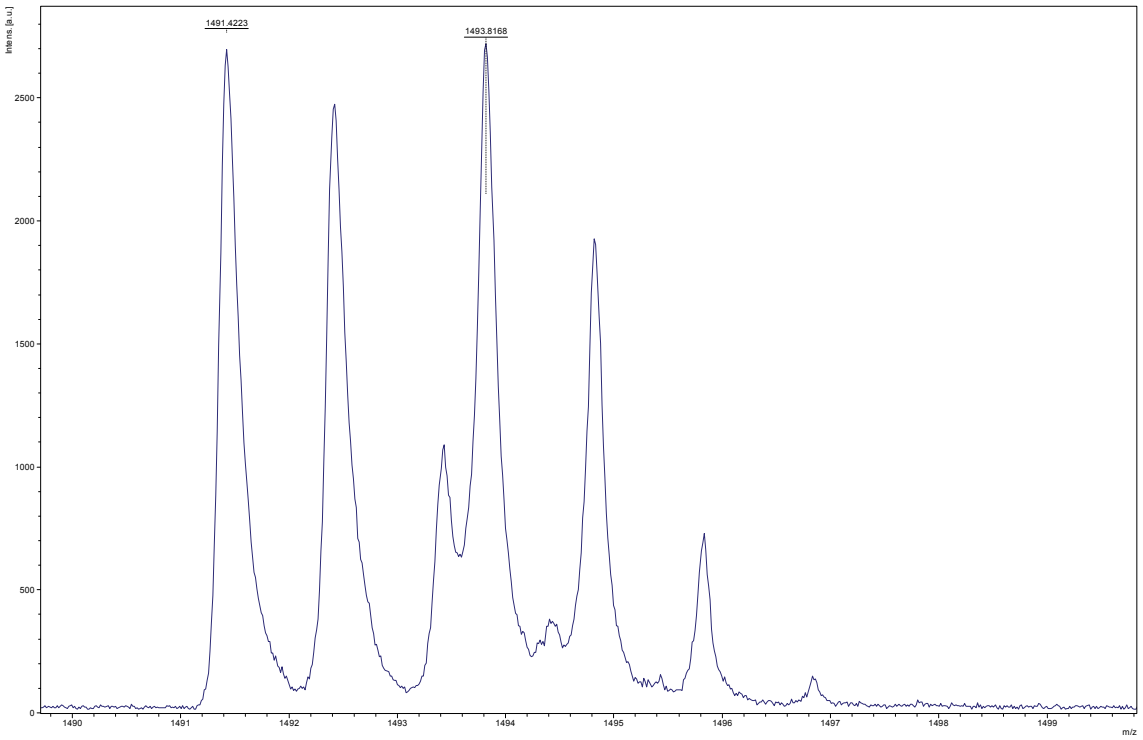

Figure 54. Mass spectrum (MALDI+, DCTB) of PC91

2. Confocal laser microscopy protocol.

Each PDI separately **PC51**, **PC66**, **PC67**, **PC71**, **PC73**, **PC79** and **PC80** (1 µM in water) were dissolved in a Standard Cell culture medium, mainly a saline solution that includes bovine serum proteins.

If the compound was soluble in this mixture, it would be added to HeLa cells. A culture of PDI-HeLa Cell was stained in-vivo, fixed with 4 % of paraformaldehyde and incubated at 37 °C for 20 minutes. The laser excitation wavelength was 488 nm, with violet filter.

3. Study of cytoxicity by MTT cell proliferation assay.

The cytotoxicity of each PDI (**PC66**, **PC71**, **PC73**, **PC79** and **PC80**) was carried out in SW480 colon adenocarcinoma cells after 24 hours of incubation time and it was evaluated by means of MTT cell proliferation assay. In this way, each value (IC_{50}) of cytoxicity will be given by comparison with the antitumor doxorubicin (IC_{50} = 65.3 ± 3.3 µM).

Approximately 5 10^3 SW480 colon adenocarcinoma cells were cultured in 200 µL culture medium per well (DMEM medium), supplemented with 10 % newborn calf serum and 1 % amphotericin-penicillin-streptomycin solution in 96-well plates and incubated at 37 °C under a 5% CO_2 atmosphere. The cells grew for 24 hours and then, they were exposed to different concentrations of the tested drugs (dissolved in culture medium) for 24 hours. Hydrogen peroxide was used as a positive control. The cells were washed with the culture medium and incubated with MTT (500 µg/ml) for a further period of 3 hours. At the end of the incubation, the medium was removed. After that they were carefully washed with PBS and 200 µl DMSO were added to each well. Absorbance was measured at 570 nm in a microplate reader. Four replicates per dose were included. The IC_{50} values, that was, the concentrations which produced 50% inhibition of cell viability, were calculated from MTT data using GraphPadPrism Software Inc. (version 6.01) (USA).

4. Synthesis and characterization of compounds of the globotriose series:

4.1. Synthesis of 4-methoxyphenyl-O-(2,3,4,6-Tetra-O-acetyl-*α*-D-galactopyranosyl)-(1-4)-O-(2,3,6-tri-O-acetyl-*β*-D-O-galactopyranosyl)-(1-4)-O-2,3,6-tri-O-acetyl-*β*-D-glucopyranoside (PC97).

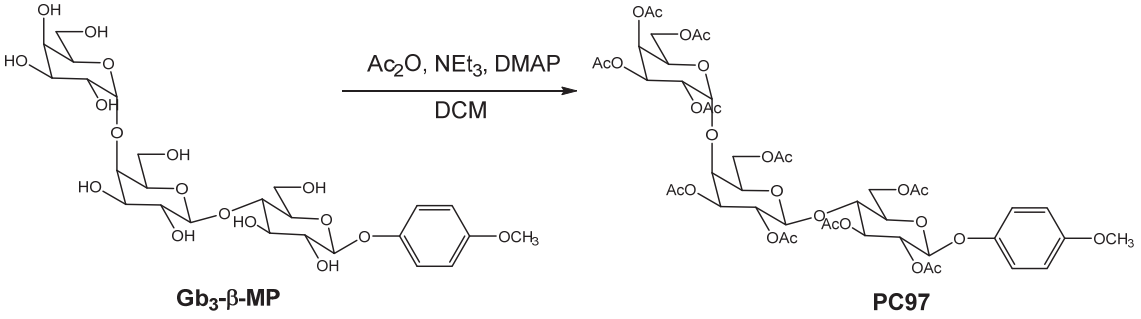

Acetic anhydride (0.8 mL, 10.4 mmol), triethylamine (1.46 mL, 10.4 mmol) and a catalytic amount of DMAP (19.3 mg, 0.96 mmol) were added under nitrogen to 4-methoxyphenyl-O-(*α*-D-galactopyranosyl)-(1,4)-O-(*β*-D-galactopyranosyl)-(1,4)-*β*-D-glucopyranoside **Gb_3-β-MP** (100 mg, 0.164 mmol) dissolved in DCM (12 mL). The mixture was stirred at room temperature overnight. Then, it was added to an aqueous solution of HCl 1M (3 x 20 mL) and extracted with dichloromethane (3 x 10 mL). The combined organic extracts were evaporated under reduced pressure to obtain a pale yellow foam in 99 % yield (167 mg, 0.162 mmol). **R_f (DCM:MeOH 50:4):** 0.2. **^{1}H NMR (300 MHz, $CDCl_3$) *δ*:** 6.90 (t, *J* = 8.4 Hz, 2H, H_{Ar}), 6.76 (d, *J* = 9.1 Hz, 2H, H_{Ar}), 5.53 – 5.50 (m, 1H, CH-O-MP), 5.31 (dd, *J* = 11.6 Hz and 3.5 Hz, 1H, CH-O_{gluc}), 5.21 (dd, *J* = 10.7 Hz and 3.4 Hz, 1H, CH-O_{galac}), 5.18 – 5.09 (m, 2H, CH), 4.90 – 4.88 (m, 1H, CH), 4.85 – 4.68 (m, 1H, CH), 4.48 – 4.40 (m, 3H, CH), 4.40 – 4.27 (m, 2H, CH_2-OAc), 4.12 – 4.05 (m, 4H, CH_2-OAc), 3.92 (d, *J* = 11.9 Hz, 2H, CH), 3.71 (s, 3H, O-$C_6H_4OC\mathbf{H}_3$), 3.61 – 3.40 (m, 2H, CH), 2.12 – 1.94 (m, 30H, OCOC$\mathbf{H}_3$). **^{13}C NMR (75 MHz, $CDCl_3$) *δ*:** 170.7 (O**C**OCH_3), 170.6 (O**C**OCH_3), 170.5 (O**C**OCH_3), 170.4 (O**C**OCH_3), 170.4 (O**C**OCH_3), 170.2 (O**C**OCH_3), 170.1 (O**C**OCH_3), 170.0 (O**C**OCH_3), 169.9 (O**C**OCH_3), 169.9 (O**C**OCH_3), 155.5 (C_{quat}), 151.1 (C_{quat}), 118.4 (Ar-**C**H), 114.5 (Ar-**C**H), 102.0 (AcOCH_2-CHO-**C**H-), 101.9 (AcOCH_2-CHO-**C**H-), 100.1 (AcOCH_2-CHO-**C**H-), 73.4 (CH), 72.8 (CH), 72.1 (CH), 71.9 (CH), 71.7 (CH), 68.3 (CH), 68.2 (CH), 67.9 (CH), 67.8 (CH), 67.5 (CH), 67.3 (CH), 67.0 (CH), 62.8 (**C**H_2OAc), 61.2 (**C**H_2OAc), 60.4 (**C**H_2OAc), 55.6 (-O-C_6H_4-O**C**H_3), 20.8 (OCO**C**H_3), 20.8 (OCO**C**H_3), 20.7 (OCO**C**H_3), 20.7 (OCO**C**H_3), 20.7 (OCO**C**H_3), 20.6 (OCO**C**H_3), 20.6 (OCO**C**H_3), 20.6 (OCO**C**H_3), 20.5 (OCO**C**H_3), 20.4 (OCO**C**H_3). **HRMS (ESI+):** m/z calcd. for $C_{45}H_{58}NaO_{27}$ ($[M+Na]^+$): 1053.3058; found: 1053.3056.

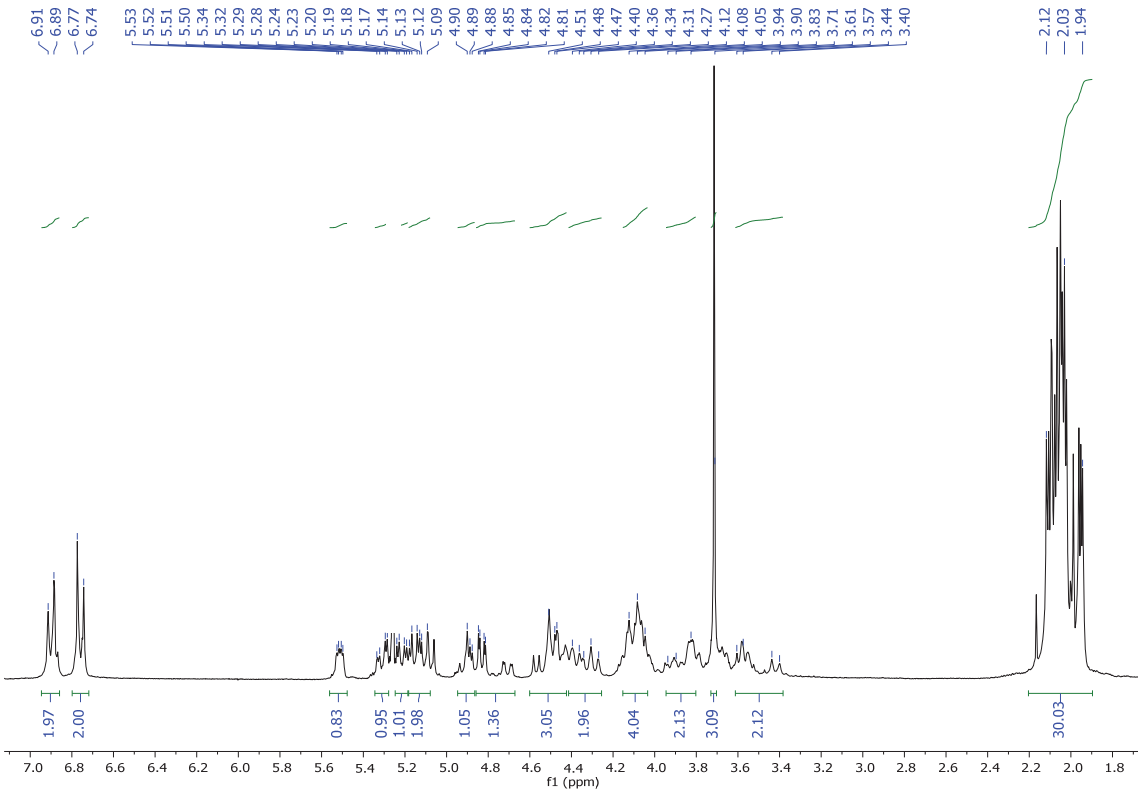

Figure 55. ^{1}H NMR (300 MHz, $CDCl_3$) of PC97

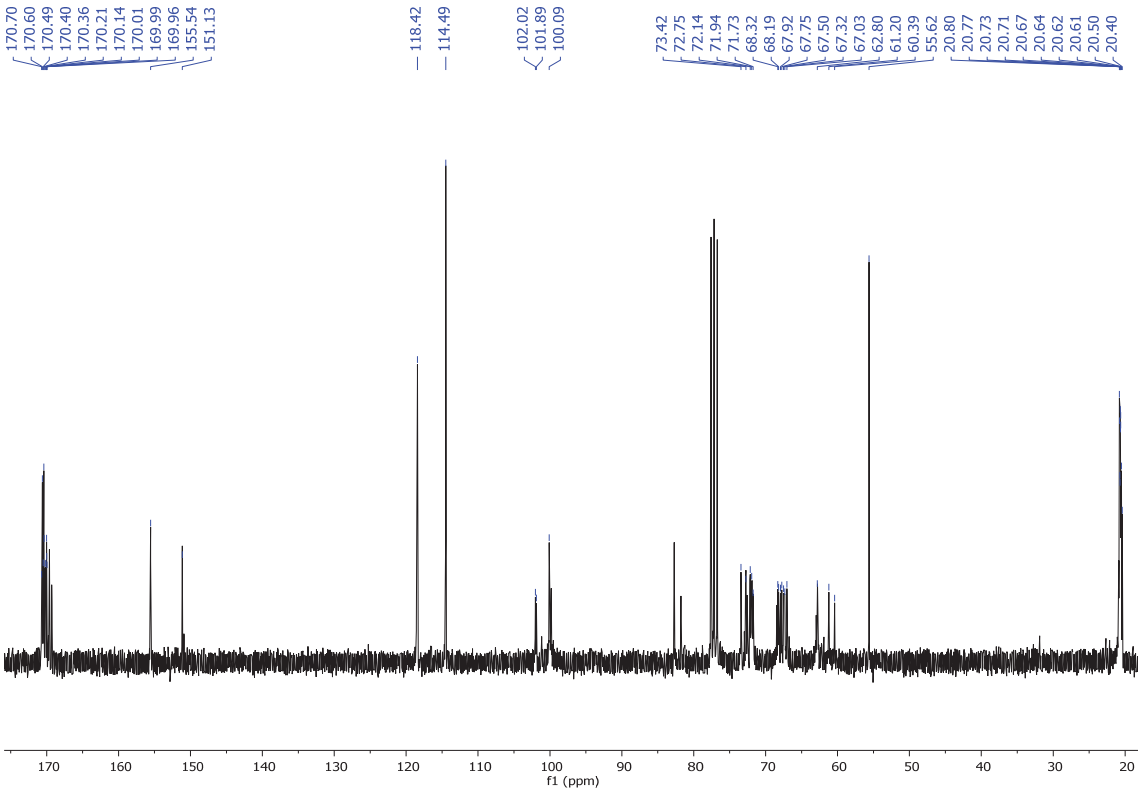

Figure 56. ^{13}C NMR (75 MHz, $CDCl_3$) of PC97

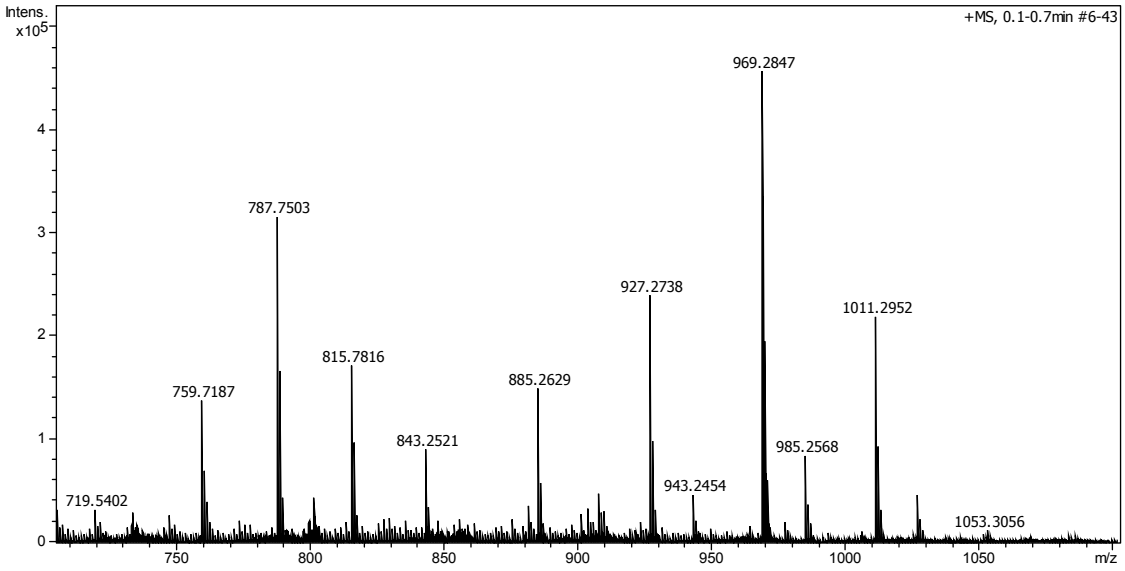

Figure 57. Mass spectrum (ESI+) of PC97

4.2. Synthesis of 4-hydroxyl-O-(2,3,4,6-Tetra-O-acetyl-*α*-D-galactopyranosyl)-(1-4)-O-(2,3,6-tri-O-acetyl-*β*-D-O-galactopyranosyl)-(1-4)-O-2,3,6-tri-O-acetyl-*β*-D-glucopyranoside (PC98).

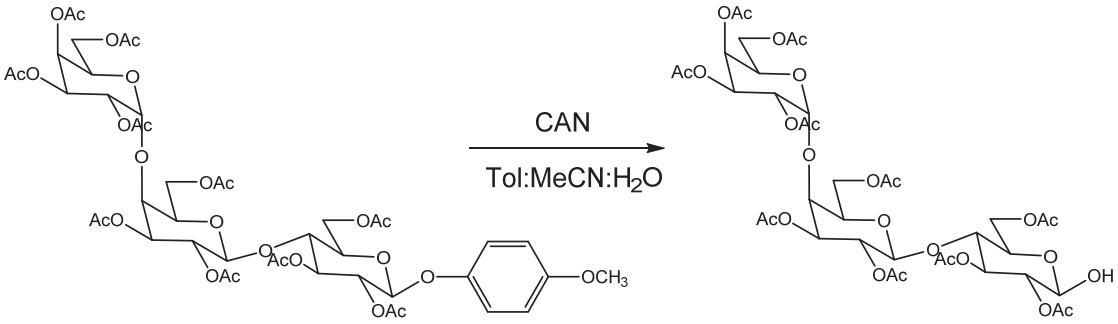

Cerium ammonium nitrate (414.8 mg, 0.75 mmol) was added to a solution of 4-methoxyphenyl-O-(2,3,4,6-tetra-O-acetyl-*α*-D-galactopyranosyl)-(1-4)-O-(2,3,6-tri-O-acetyl-*β*-D-O-galactopyranosyl)-(1,4)-O-2,3,6-tri-O-acetyl-*β*-D-glucopyranoside (130 mg, 0.126 mmol) dissolved in a mixture of toluene:MeCN:water (2:4:1, 5mL). The mixture was stirred at room temperature for 3 hours. The reaction was diluted with EtOAc (50 mL) and washed with H_2O (15 x 2 mL) and brine (15 mL). The obtained solid was purified by recrystallization in Ethyl acetate:Hex (5:95), as a pale yellow foam in 80 % yield (93 mg, 0.1 mmol). **R_f (DCM:MeOH 50:4):** 0.3. **^{1}H NMR (300 MHz, $CDCl_3$) *δ*:** 5.55 – 5.53 (m, 1H, CH-OH), 5.36 – 5.31 (m, 1H, CH-O_{gluc}), 5.26 – 5.16 (m, 2H, CH-O), 4.97 – 4.89 (m, 1H, CH), 4.82 – 4.65 (m, 2H, CH), 4.58 – 4.28 (m, 5H, CH), 4.20 – 4.06 (m, 6H, CH_2-OAc), 3.95 – 3.43 (m, 6H, CH), 2.14 – 1.97 (m, 30H, OCOC**H**$_3$). **^{13}C NMR (75 MHz, $CDCl_3$) *δ*:** 171.4 (O**C**OCH$_3$), 170.9 (O**C**OCH$_3$), 170.8 (O**C**OCH$_3$), 170.7 (O**C**OCH$_3$), 170.7 (O**C**OCH$_3$), 170.6 (O**C**OCH$_3$), 170.6 (O**C**OCH$_3$), 170.6 (O**C**OCH$_3$), 170.5 (O**C**OCH$_3$), 170.3 (O**C**OCH$_3$), 101.9 (AcOCH$_2$-CHO-**C**H-), 101.0 (AcOCH$_2$-CHO-**C**H-), 100.0 (AcOCH$_2$-CHO-**C**H-), 90.3 (CHOH), 72.9 (CH), 72.8 (CH), 72.3 (CH), 72.1 (CH), 69.4 (CH), 68.9 (CH), 68.5 (CH), 67.8 (CH), 67.4 (CH), 67.1 (CH), 62.8 (CH), 62.7 (CH), 61.4 (**C**H$_2$OAc), 60.5 (**C**H$_2$OAc), 60.3 (**C**H$_2$OAc), 21.1 (OCO**C**H$_3$), 21.0 (OCO**C**H$_3$), 20.9 (OCO**C**H$_3$), 20.9 (OCO**C**H$_3$), 20.9 (OCO**C**H$_3$), 20.8 (OCO**C**H$_3$), 20.7 (OCO**C**H$_3$), 20.6 (OCO**C**H$_3$), 20.6 (OCO**C**H$_3$), 20.5 (OCO**C**H$_3$).

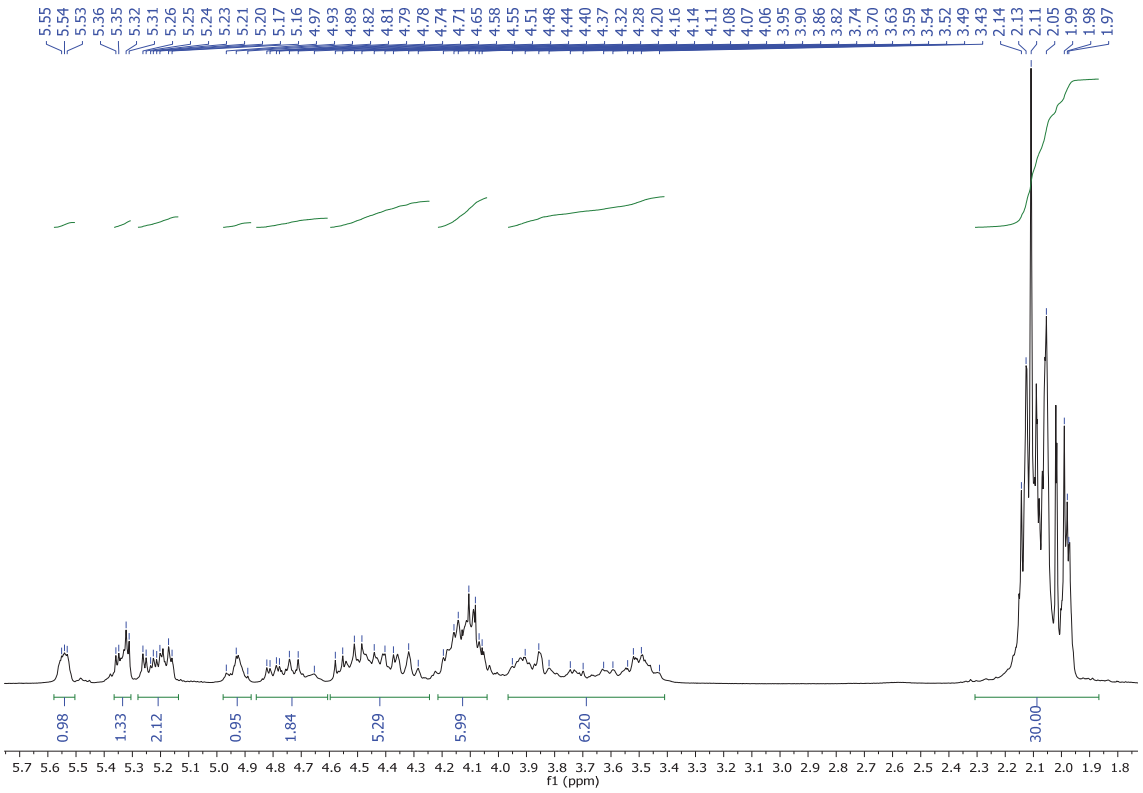

Figure 58. ^{1}H NMR (300 MHz, $CDCl_3$) of PC98

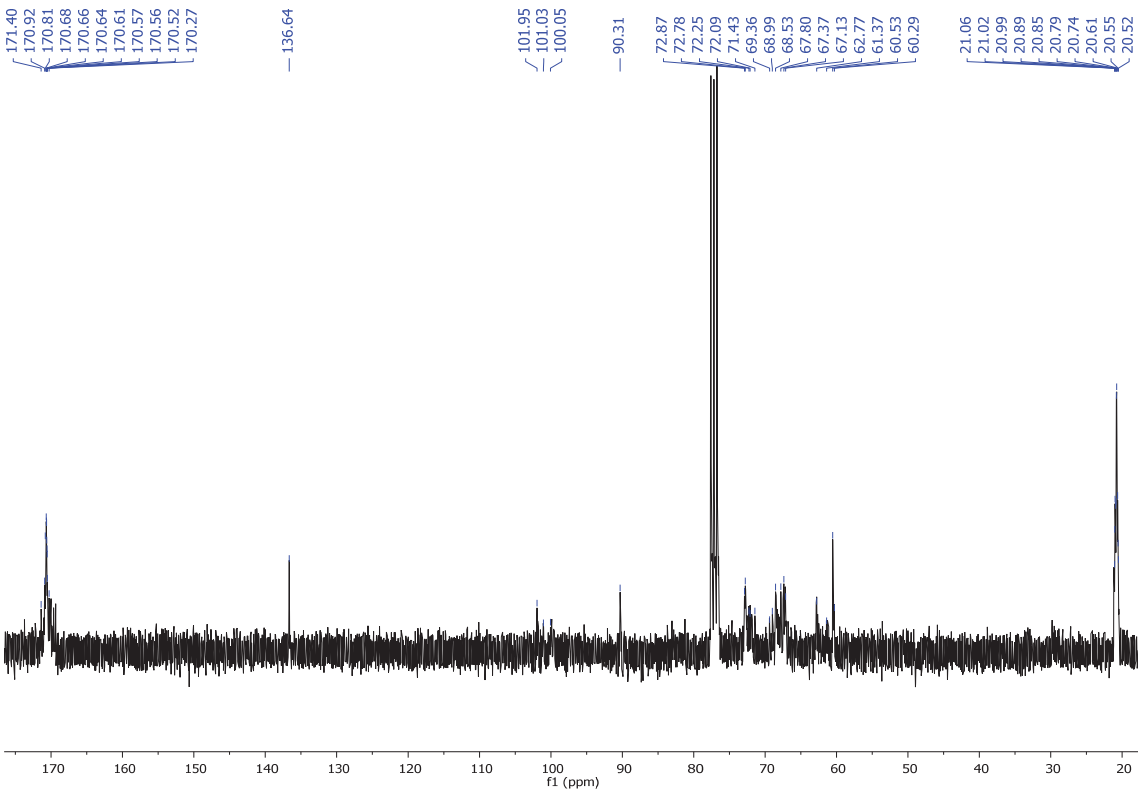

Figure 59. ^{13}C NMR (75 MHz, $CDCl_3$) of PC98

4.3. Synthesis of (2,3,4,6-tetra-O-acetyl-*α*-D-galactopyranosyl)-(1-4)-O-(2,3,6-tri-O-acetyl-*β*-D-O-galactopyranosyl)-(1-4)-O-2,3,6-tri-O-acetyl-*β*-D-glucopyranosyl fluoride (PC99).

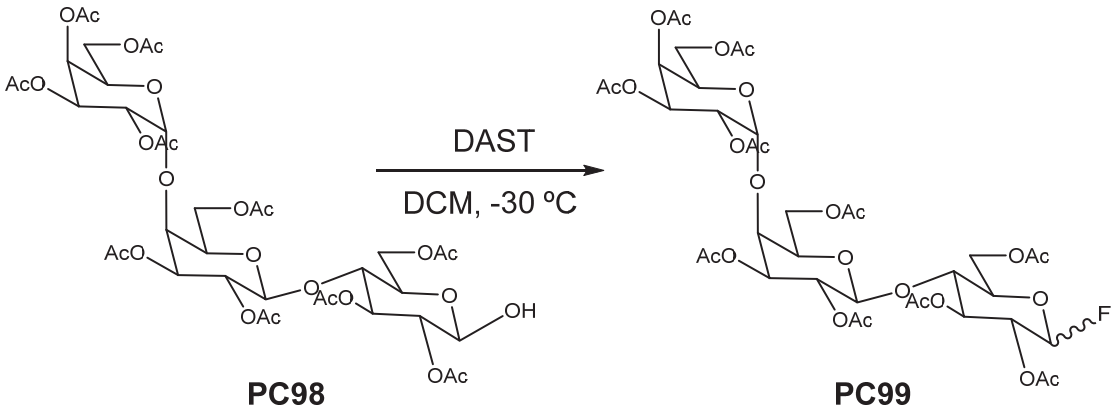

Diethylaminosulfur trifluoride (26.7 µl, 0.201 mmol) was added slowly to 4-Hydroxyl-O-(2,3,4,6-tetra-O-acetyl-*α*-D-galactopyranosyl)-(1,4)-O-(2,3,6-tri-O-acetyl-*β*-D-O-galactopyranosyl)-(1,4)-O-2,3,6-tri-O-acetyl-*β*-D-glucopyranoside (93 mg, 0.1 mmol) dissolved in DCM (5 mL) at -30 ^{o}C. The resulting mixture was stirred for 1-8 hours, maintaining the temperature below -10 ^{o}C, and the reaction was monitporized by TLC (ethyl acetate:toluene, 2:8). The crude was washed with $NaHCO_3$ (10 x 2 mL) and brine (10 mL). The combined organic extracts were dried over anhydrous sodium sulphate, filtered and evaporated under reduced pressure. Purification was carried out by silica gel flash chromatography using DCM:MeCN to DCM-MeOH 1:1 (50:50) as eluent to give compound **PC99** (α/β anomeric fluorine mixture) as a white foam 70 % yield (65.5 mg, 0.07 mmol). **R_f (DCM:MeOH 50:2):** 0.3. **^{1}H NMR (300 MHz, $CDCl_3$) *δ*:** 5.57 – 5.53 (m, 1H, CH-F), 5.37 – 5.34 (m, 1H, CH-O_{gluc}), 5.22 – 5.16 (m, 2H, CH-O), 5.13 – 5.00 (m, 1H, CH), 4.95 (dd, *J* = 16.4 Hz and 3.4 Hz, 1H, CH), 4.73 (dt, *J* = 10.9 Hz and 2.6 Hz, 1H), 4.57 (dd, *J* = 7.9 Hz and 3.1 Hz, 1H), 4.46 – 4.34 (m, 3H, CH), 4.19 – 3.98 (m, 6H, CH_2-OAc), 3.95 – 3.74 (m, 3H, CH), 3.68 – 3.62 (m, 1H, CH), 2.15 – 1.98 (m, 30H, OCOC**H**$_3$). **^{13}C NMR (75 MHz, $CDCl_3$) *δ*:** 171.0 (O**C**OCH$_3$), 170.8 (O**C**OCH$_3$), 170.7 (O**C**OCH$_3$), 170.6 (O**C**OCH$_3$), 170.5 (O**C**OCH$_3$), 170.3 (O**C**OCH$_3$), 170.2 (O**C**OCH$_3$), 170.1 (O**C**OCH$_3$), 169.8 (O**C**OCH$_3$), 169.6 (O**C**OCH$_3$), 109.9 (**C**H-F), 102.1 (AcOCH$_2$-CHO-**C**H-), 101.2 (AcOCH$_2$-CHO-**C**H-), 99.7 (AcOCH$_2$-CHO-**C**H-), 73.9 (CH), 72.9 (CH), 72.2 (CH), 72.1 (CH), 69.3 (CH), 68.7 (CH), 67.8 (CH), 67.5 (CH), 67.3 (CH), 67.1 (CH), 63.3 (CH), 62.9 (CH), 62.6 (**C**H$_2$OAc), 61.6 (**C**H$_2$OAc), 60.5 (**C**H$_2$OAc), 21.1 (OCO**C**H$_3$), 20.9 (OCO**C**H$_3$), 20.9 (OCO**C**H$_3$), 20.9 (OCO**C**H$_3$), 20.9 (OCO**C**H$_3$), 20.8 (OCO**C**H$_3$), 20.7 (OCO**C**H$_3$), 20.6 (OCO**C**H$_3$), 20.6 (OCO**C**H$_3$), 20.5 (OCO**C**H$_3$). **^{19}F NMR (282 MHz, $CDCl_3$) *δ*:** -132.6, -140.5 (DAST), -149.0. **HRMS (qTOF, ID):** m/z calcd. for $C_{38}H_{51}FNaO_{25}$ ([M+Na]$^{+}$): 949.2596; found: 949.2576.

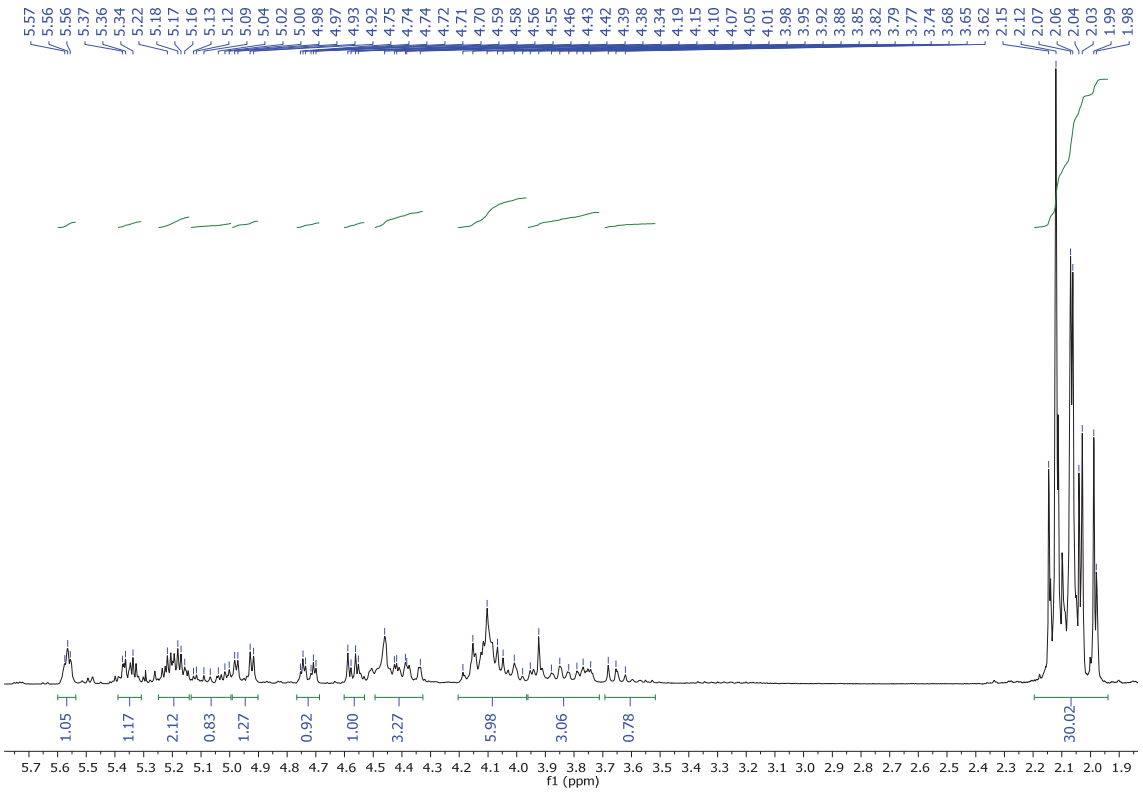

Figure 60. ^{1}H NMR (300 MHz, $CDCl_3$) of PC99

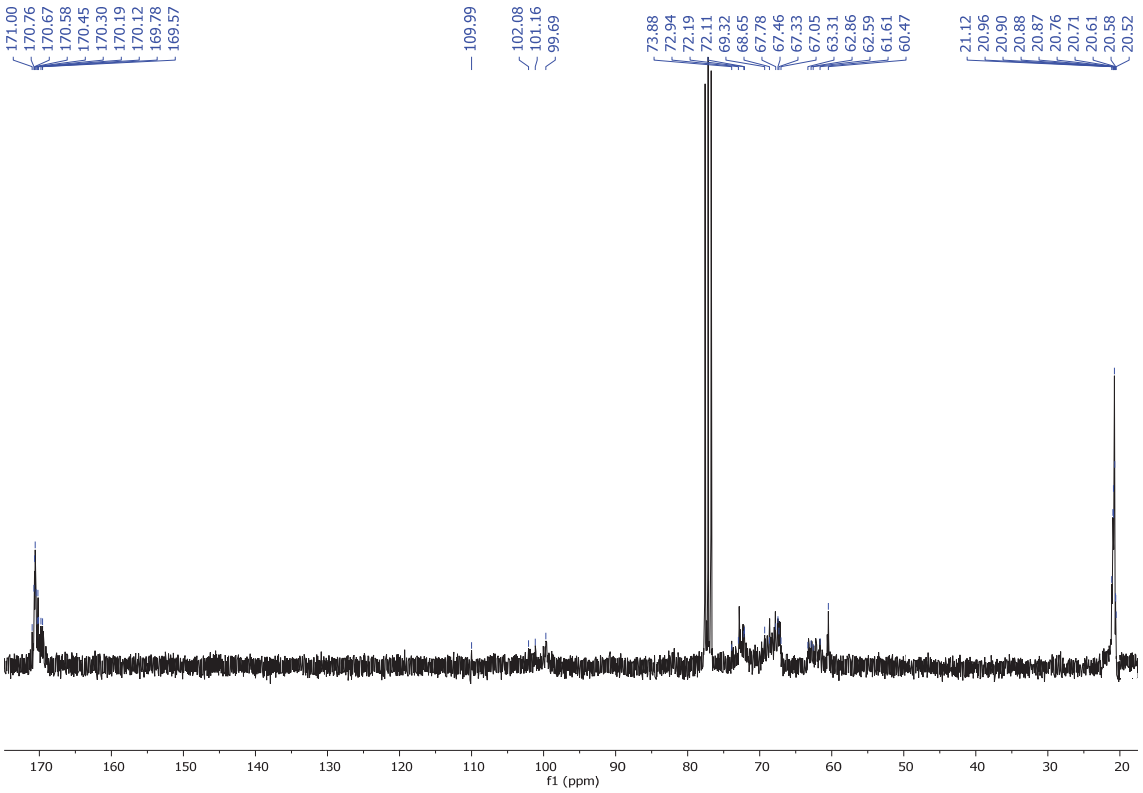

Figure 61. ^{13}C NMR (75 MHz, $CDCl_3$) of PC99

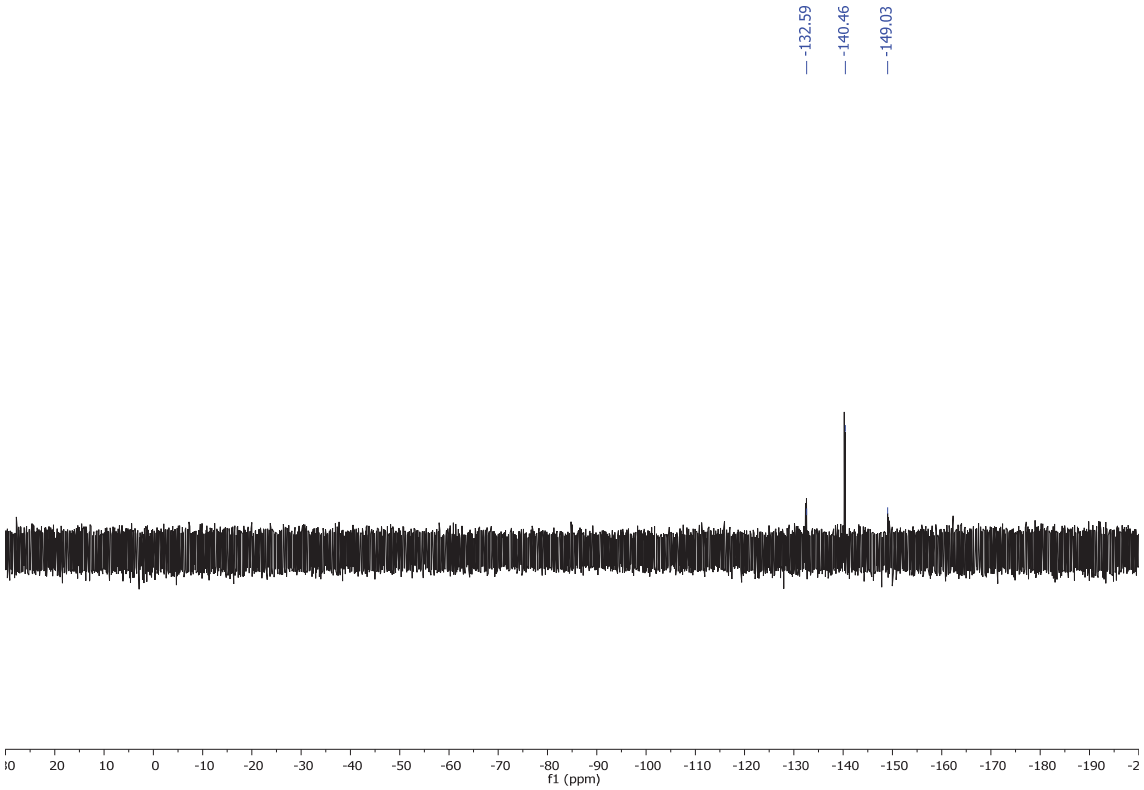

Figure 62. ^{19}F NMR (282 MHz, $CDCl_3$) of PC99

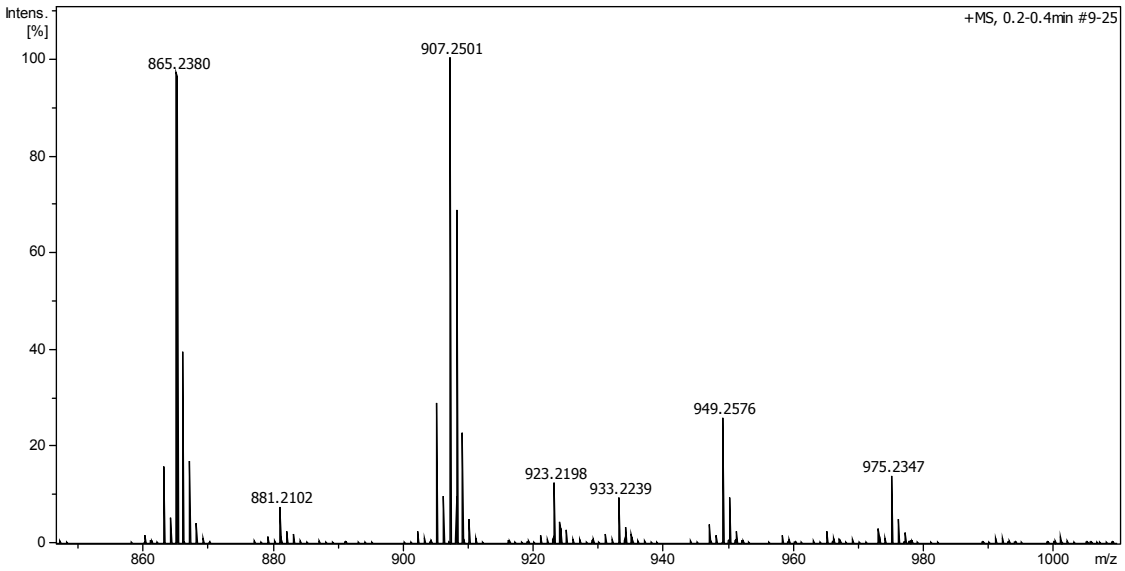

Figure 63. Mass spectrum (qTOF) of PC99

4.4. Synthesis of 2-(2-(2-(2-azidoethoxy)ethoxy)ethoxy)ethyl-O-(2,3,4,6-tetra-O-acetyl-*α*-D-galactopyranosyl)-(1-4)-O-(2,3,6-tri-O-acetyl-*β*-D-O-galactopyranosyl)-(1-4)-O-2,3,6-tri-O-acetyl-*β*-D-glucopyranosyl (PC100).

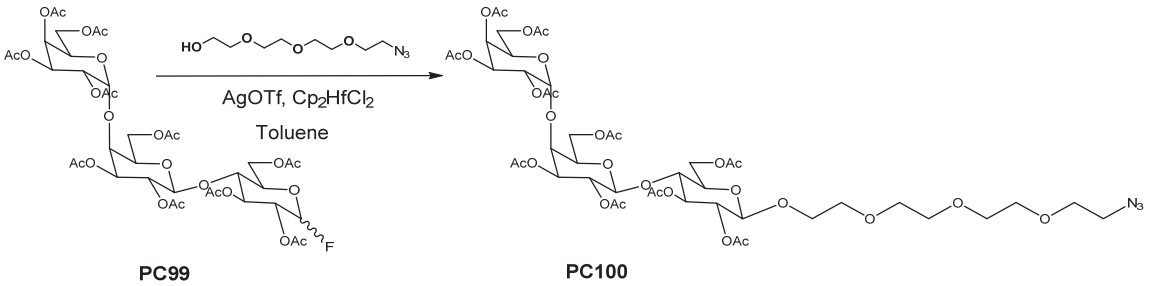

A mixture of silver triflate (97.1 mg, 0.38 mmol), bis(cyclopentadienyl) hafnium (IV) dichloride (92.2 mg, 0.24 mmol) and 4 Å activated molecular sieves in dry toluene (8 mL) was stirred at room temperature for one hour. The mixture was then cooled to -40 ^{o}C, a solution of (2,3,4,6-Tetra-O-acetyl-*α*-D-galactopyranosyl)-(1,4)-O-(2,3,6-tri-O-acetyl-*β*-D-O-galactopyranosyl)-(1,4)-O-2,3,6-tri-O-acetyl-*β*-D-glucopyranosyl fluoride **PC99** (60 mg, 0.064 mmol) and 2-(2-(2-(2-azidoethoxy)ethoxy)ethoxy)ethan-1-ol (12 mg, 0.054 mmol) in toluene (3.5 mL) were added. The mixture was stirred for 2 hours, quenched with NEt_3 (3 mL), diluted with DCM (10 mL) and filtered through celite. The filtrate was washed with aqueous $NaHCO_3$ (2 x 50 mL) and brine (50 mL) solutions. The combined organic extracts were dried over anhydrous sodium sulphate and evaporated under reduced pressure. Purification was carried out by silica gel flash chromatography using DCM to MeCN as eluents to give compound PC100 as a yellow oil in 97 % yield (70 mg, 0.061 mmol). **R_f (DCM:MeOH 50:2):** 0.2. **^{1}H NMR (300 MHz, $CDCl_3$) *δ*:** 5.58 – 5.54 (m, 1H, CH-O), 5.39 – 5.10 (m, 3H, CH-O), 5.00 – 4.74 (m, 2H, CH), 4.67 (s, 2H, CH), 4.59 – 4.30 (m, 4H, CH), 4.21 – 4.01 (m, 6H, CH_2-OAc), 3.93 – 3.82 (m, 2H, O-CH_2CH_2-O), 3.74 – 3.59 (m, 10H, O-CH_2CH_2-O), 3.50 – 3.40 (m, 2H, O-CH_2CH_2-O), 2.17 – 1.99 (m, 30H, OCOC**H**$_3$), 1.82 – 1.69 (m, 4H, CH_2CH_2-N_3). **^{13}C NMR (75 MHz, $CDCl_3$) *δ*:** 170.6 (O**C**OCH$_3$), 170.5 (O**C**OCH$_3$), 170.3 (O**C**OCH$_3$), 170.1 (O**C**OCH$_3$), 169.9 (O**C**OCH$_3$), 169.5 (O**C**OCH$_3$), 169.4 (O**C**OCH$_3$), 168.9 (O**C**OCH$_3$), 168.9 (O**C**OCH$_3$), 168.8 (O**C**OCH$_3$), 101.1 (AcOCH$_2$-CHO-**C**H-), 100.9 (AcOCH$_2$-CHO-**C**H-), 99.6 (AcOCH$_2$-CHO-**C**H-), 76.9 (CH), 75.9 (CH), 75.8 (CH), 73.4 (CH), 72.8 (CH), 71.9 (CH), 70.6 (CH_2), 70.6 (CH), 70.0 (CH_2), 69.8 (CH), 69.4 (CH), 69.1 (CH_2), 69.0 (CH), 68.9 (CH), 67.9 (CH), 67.2 (CH), 67.1 (CH), 63.6 (CH_2), 61.9 (**C**H$_2$), 61.7 (**C**H$_2$OAc), 61.4 (**C**H$_2$OAc), 60.3 (**C**H$_2$OAc), 50.7 (**C**H$_2$N$_3$), 20.9 (**C**H$_3$), 20.9 (**C**H$_3$), 20.8 (**C**H$_3$), 20.7 (**C**H$_3$), 20.7 (**C**H$_3$), 20.6 (**C**H$_3$), 20.6 (**C**H$_3$), 20.6 (**C**H$_3$), 20.5 (**C**H$_3$), 20.5 (**C**H$_3$). **HRMS (ESI+):** m/z calcd. for $C_{46}H_{67}N_3NaO_{29}$ ([M+Na]$^+$): 1148.3752; found: 1148.3748.

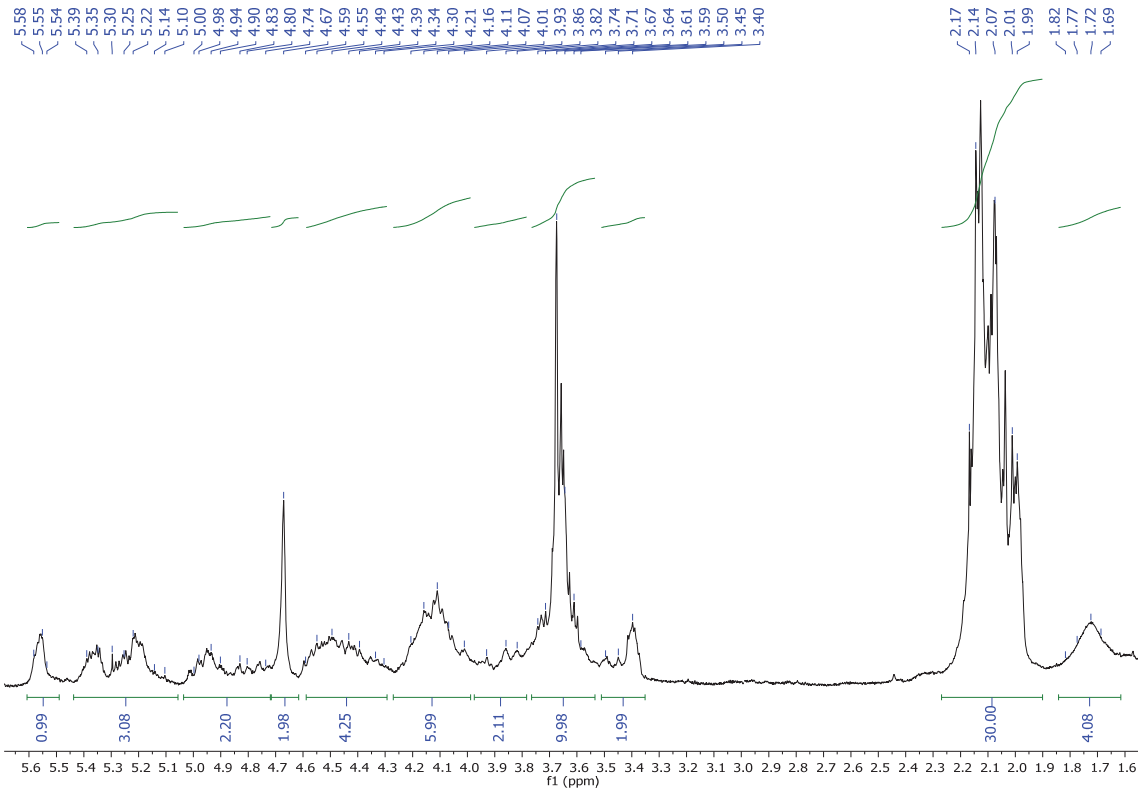

Figure 64. ^{1}H NMR (300 MHz, $CDCl_3$) of PC100

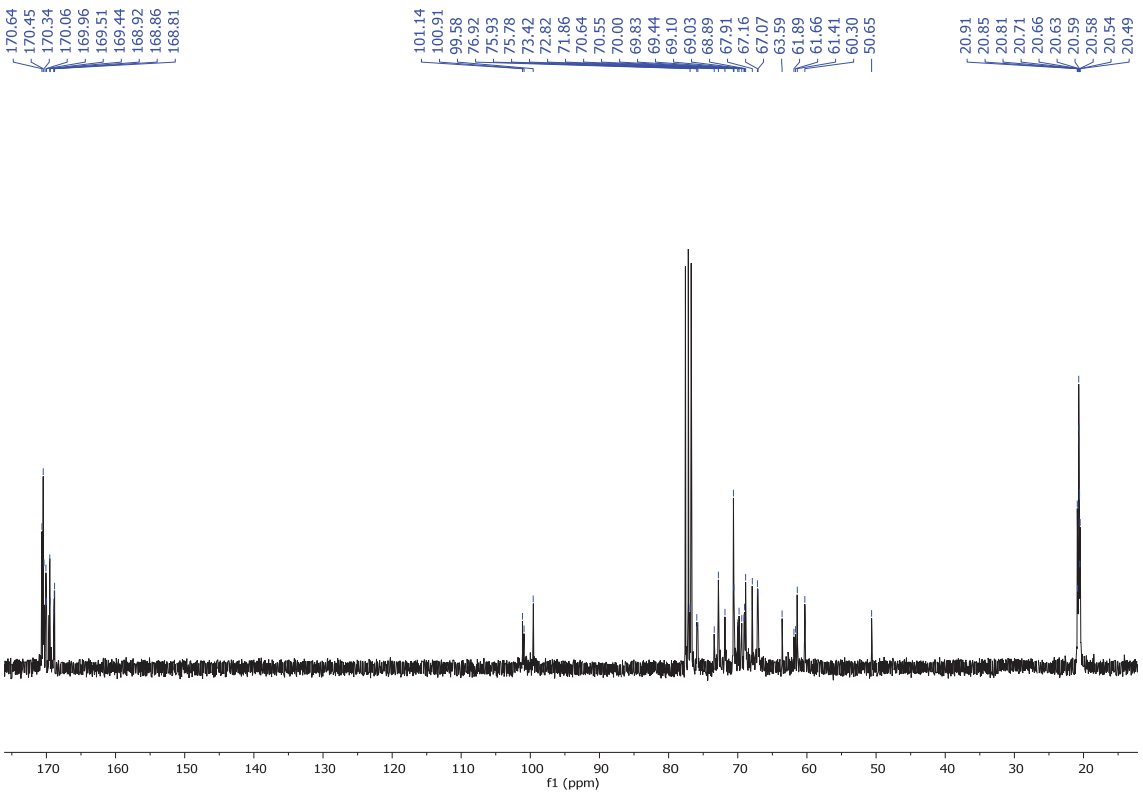

Figure 65. ^{13}C NMR (75 MHz, $CDCl_3$) of PC100

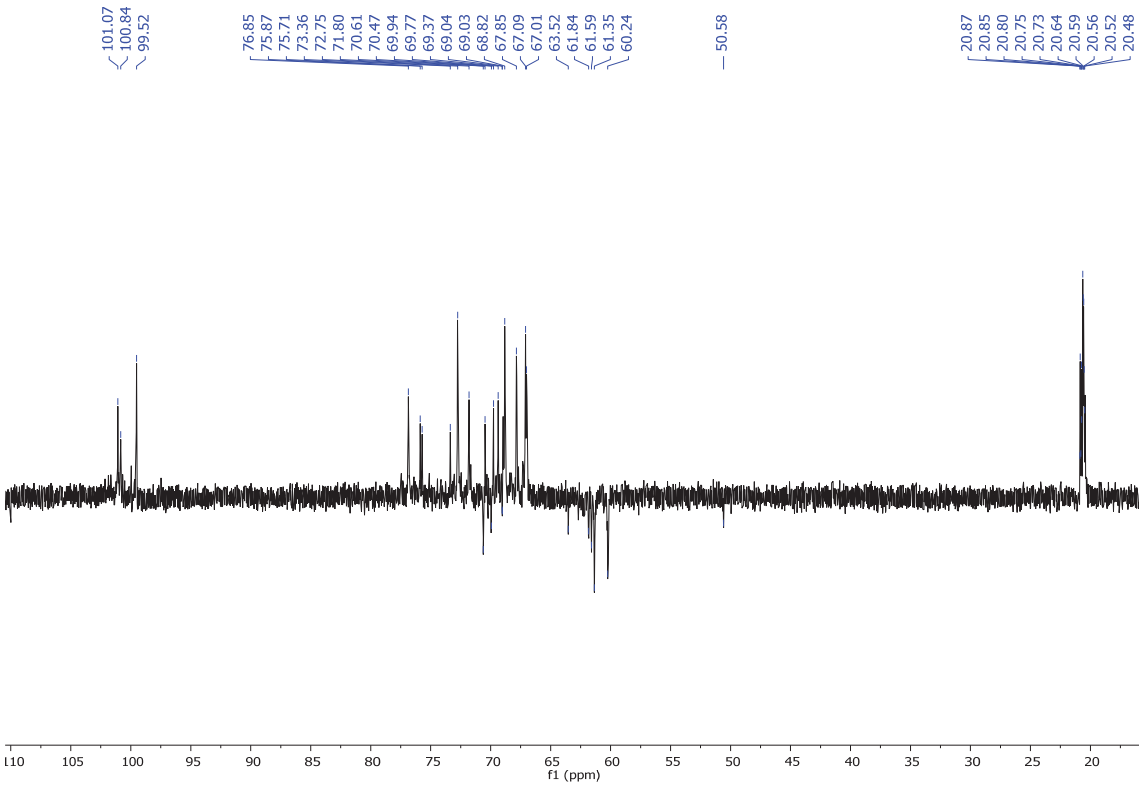

Figure 66. ^{13}C NMR-DEPT-135 (75 MHz, $CDCl_3$) of PC100

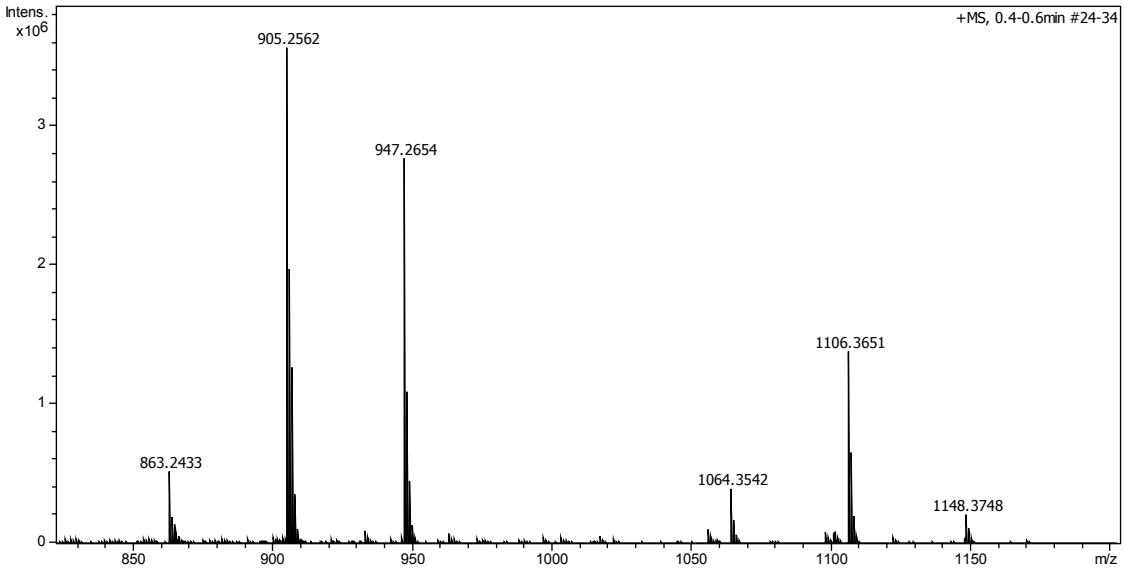

Figure 67. Mass spectrum (ESI+) of PC100

4.5. Synthesis of *N,N'*-bis((1-piperidin-1-yl)hex-5-yn-1-one)-1,6,7,12-tetrakis(3,5-bis(methoxycarbonyl)phenoxy)perylene-3,4,9,10-tetracarboxylic diimide (PC101).

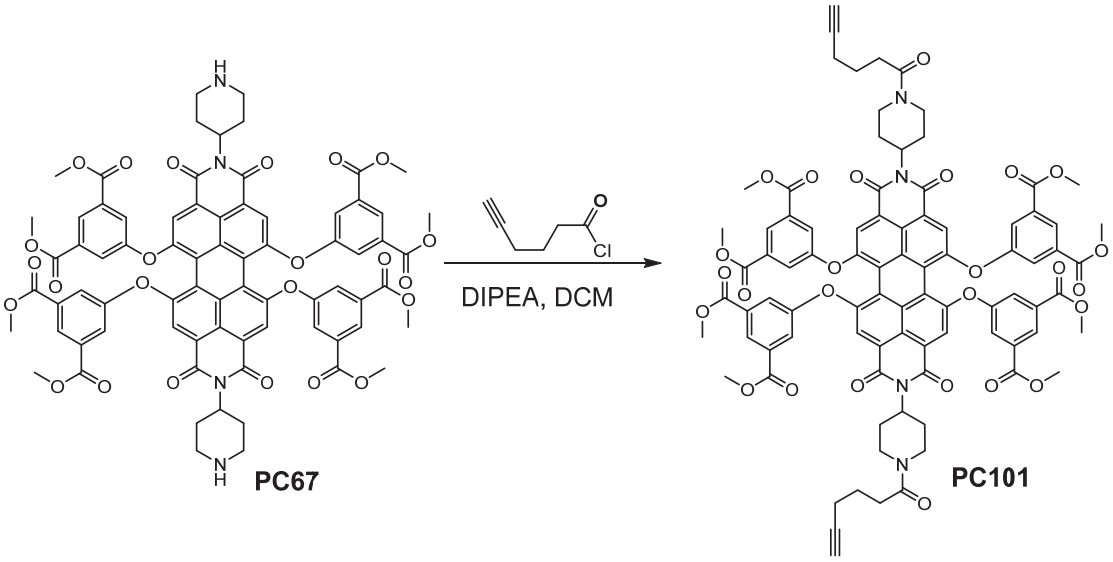

Hex-5-ynoyl chloride (9 mg, 0.07 mmol) was added dropwise under nitrogen to a solution of DIPEA (16.7 mg, 0.13 mmol) and *N,N'*-bis-(1-piperidine)-1,6,7,12-tetrakis(3,5-bis(methoxycarbonyl)phenoxy)perylene-3,4,9,10-tetracarboxylic diimide **PC67** (45 mg, 0.032 mmol) disolved in DCM (10 mL). The mixture was stirred at room temperature for 1.5 hours, then the solvent was evaporated under reduced pressure. Purification was carried out by silica gel flash chromatography using DCM to MeOH as eluents to give compound **PC101** as a pink solid in 40 % yield (20 mg, 0.01 mmol). **R_f (DCM:MeOH 50:2):** 0.5. **^{1}H NMR (400 MHz, $CDCl_3$) δ:** 8.33 (t, *J* = 1.4 Hz, 4H, H_{Ar}), 8.15 (s, 4H, H_{Ar}), 7.69 (d, *J* = 1.4 Hz, 8H, H_{Ar}), 5.18 – 5.12 (m, 2H, N-CH), 4.78 (d, *J* = 8.4 Hz, 2H, CH_2), 4.02 (d, *J* = 12.3 Hz, 2H, CH_2), 3.88 (s, 24H, $COOCH_3$), 3.10 (t, *J* = 12.8 Hz, 2H, CH_2), 2.72 – 2.55 (m, 6H, CH_2), 2.45 (t, *J* = 7.4 Hz, 4H, C**H**$_2$$CH_2CH_2$-C≡CH), 2.27 (td, *J* = 6.7 Hz and 2.6 Hz, 4H, CH_2CH_2C**H**$_2$-C≡CH), 1.94 (t, *J* = 2.6 Hz, 2H, -C≡C**H**), 1.85 – 1.82 (m, 4H, CH_2), 1.75 – 1.67 (m, 4H, 2xCH_2C**H**$_2$$CH_2$-C≡CH). **^{13}C NMR (101 MHz, $CDCl_3$) δ:** 170.6 (**C**$ON_{piperidine}$), 165.0 (**C**$OOCH_3$), 163.1 (**C**ON**C**O_{Imide}), 155.8 (-C_q-O-**C**$_{qPhenol}$), 154.8 (-**C**$_q$-O-$C_{qPhenol}$), 133.0 (C_{Ar}), 132.6 (C_{Ar}), 126.4 (CH), 124.4 (CH), 123.9 (C_{Ar}), 121.2 (C_{Ar}), 121.1 (C_{Ar}), 120.9 (CH), 83.9 (-**C**≡CH), 69.1 (-C≡**C**H), 52.7 (COO**C**H_3), 51.9 (**C**HN_{imide}), 45.6 (CH_2), 41.9 (CH_2), 31.7 (**C**$H_2CH_2CH_2$-C≡CH), 29.7 (CH_2), 28.8 (CH_2), 28.1 (CH_2), 23.9 (CH_2**C**H_2CH_2-C≡CH), 18.1 (CH_2CH_2**C**H_2-C≡CH). **HRMS (MALDI+, DCTB):** m/z calcd. for $C_{86}H_{72}N_4O_{26}$ ($[M+H]^+$): 1577.4508; found: 1577.4524.

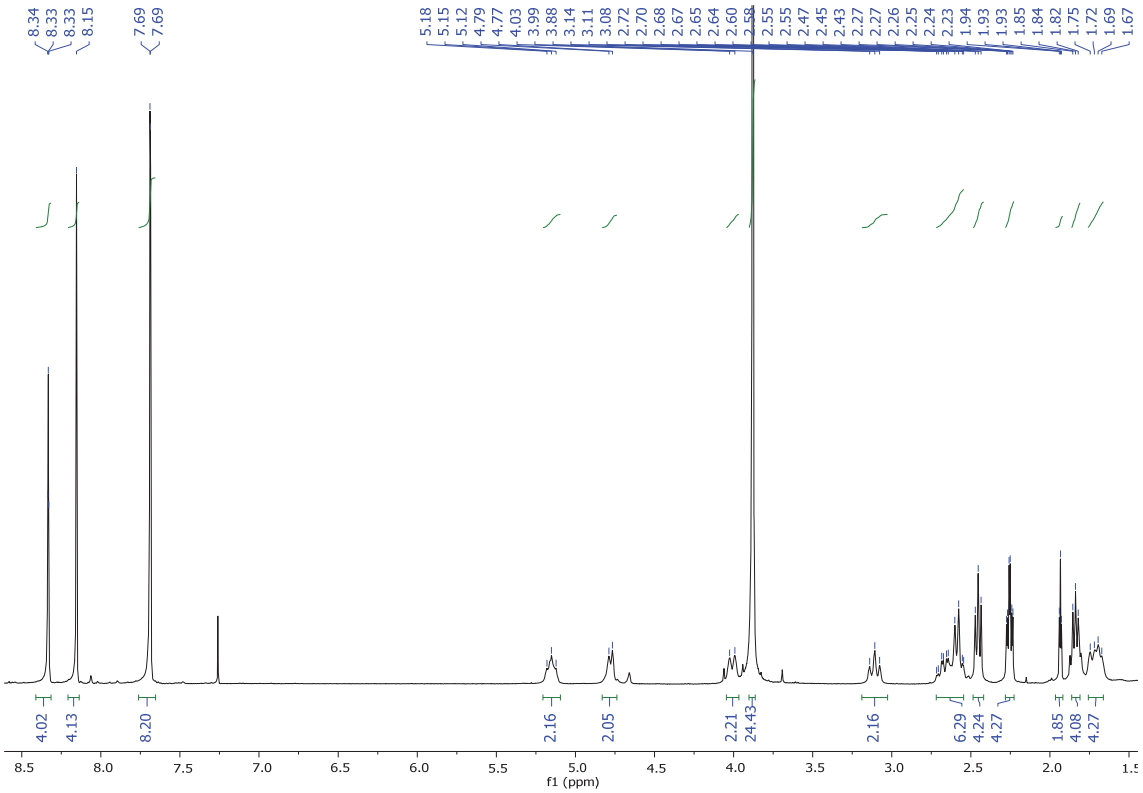

Figure 68. ^{1}H NMR (400 MHz, $CDCl_3$) of PC101

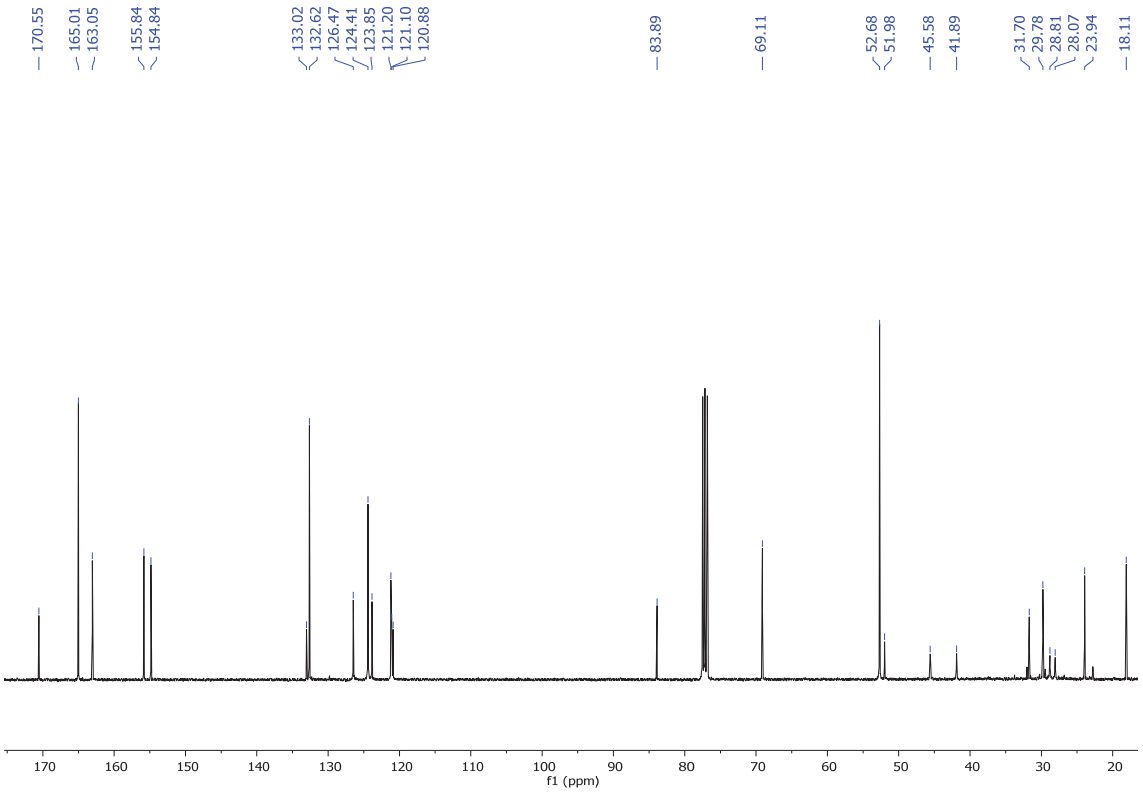

Figure 69. ^{13}C NMR (101 MHz, $CDCl_3$) of PC101

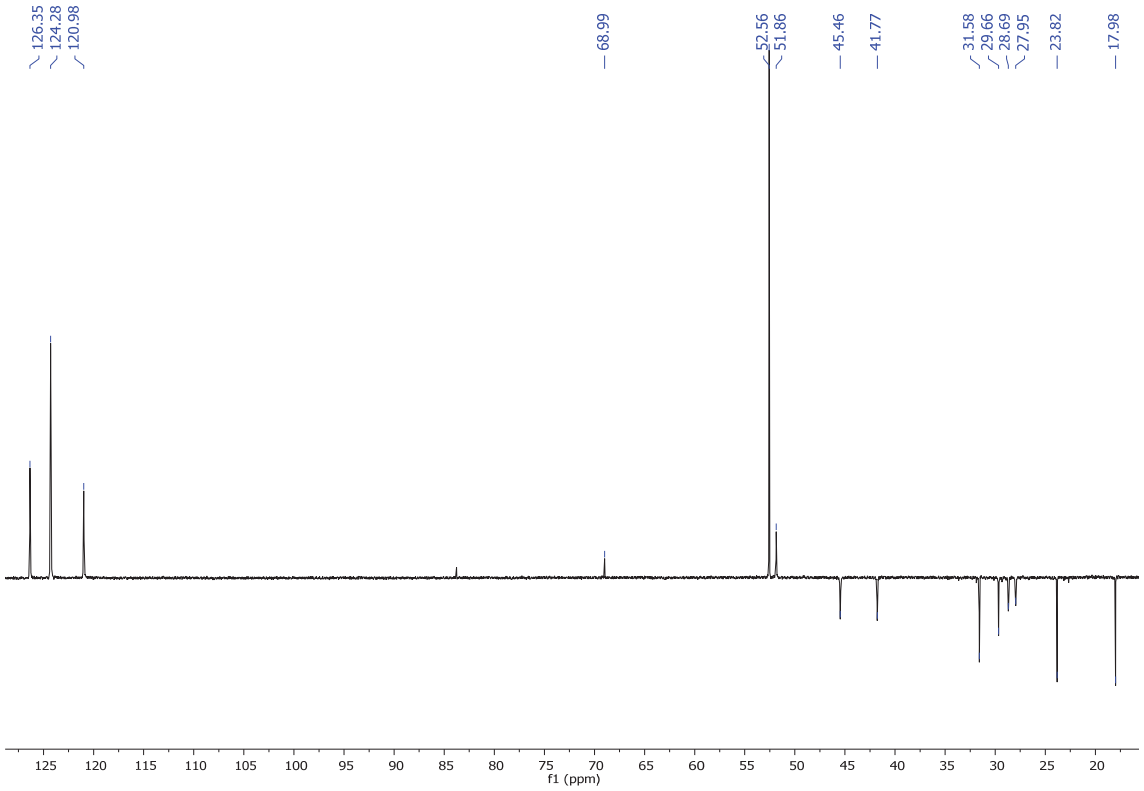

Figure 70. ^{13}C DEPT-135 NMR (101 MHz, $CDCl_3$) of PC101

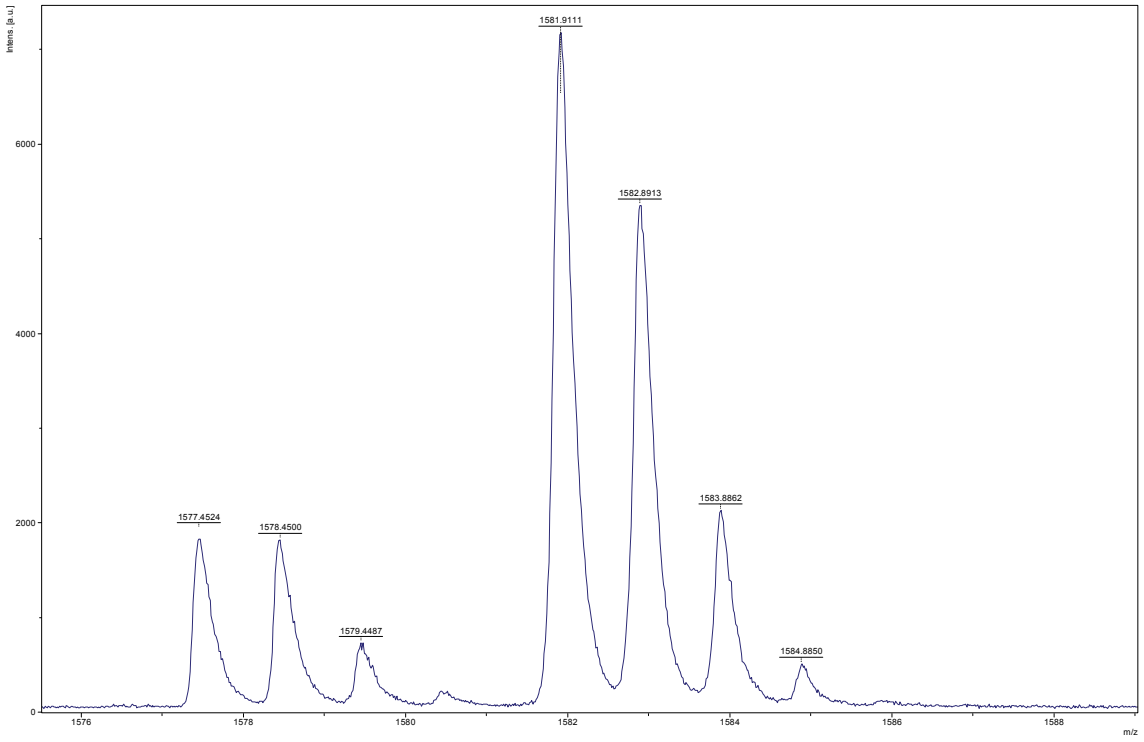

Figure 71. Mass spectrum (MALDI+, DCTB) of PC101

4.6. Synthesis of *N*-(1-piperidine)-*N'*-((1-piperidin-1-yl)hex-5-yn-1-one)-1,6,7,12-tetrakis(3,5-bis(methoxycarbonyl)phenoxy)perylene-3,4,9,10-tetracarboxylic diimide (PC103).

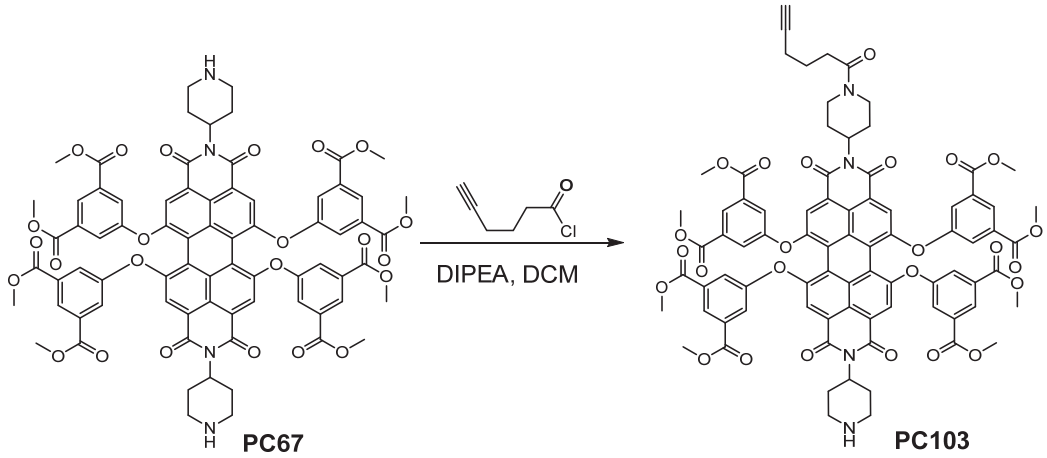

Hex-5-ynoyl chloride (9.4 mg, 0.07 mmol) disolved in DCM (50 mL) was added dropwise under nitrogen to a solution of DIPEA (18.6 mg, 0.14 mmol) and *N,N'*-bis-(1-piperidine)-1,6,7,12-tetrakis(3,5-bis(methoxycarbonyl)phenoxy)perylene-3,4,9,10-tetracarboxylic diimide **PC67** (100 mg, 0.07 mmol) dissolved in DCM (50 mL). The mixture was stirred at room temperature for 5 hours, then the solvent was evaporated under reduced pressure. Purification was carried out by silica gel flash chromatography using DCM to MeOH as eluents to give compound **PC103** as a pink solid in 21 % yield (22.3 mg, 0.015 mmol). **R_f (DCM:MeOH 50:2):** 0.7. **^{1}H NMR (300 MHz, $CDCl_3$) *δ*:** 8.35 (q, *J* = 1.2 Hz, 4H, H_{Ar}), 8.16 (d, *J* = 12.2 Hz, 4H, H_{Ar}), 7.68 (dd, *J* =3.8 Hz and 1.4 Hz, 8H, H_{Ar}), 5.19 – 5.12 (m, 2H, N-CH), 4.79 (d, *J* = 8.5 Hz, 1H, CH_2), 4.02 (d, *J* = 12.9 Hz, 1H, CH_2), 3.88 (s, 24H, $COOCH_3$), 3.17 – 3.04 (m, 6H, CH_2), 2.47 (t, *J* = 7.4 Hz, 2H, C**H**$_2$CH$_2$CH$_2$-C≡CH), 2.27 (td, *J* = 6.7 Hz and 2.6 Hz, 2H, CH$_2$CH$_2$C**H**$_2$-C≡CH), 1.94 (t, *J* = 2.6 Hz, 1H, -C≡C**H**), 1.87 – 1.83 (m, 4H, CH_2), 1.74 (d, *J* = 14.8 Hz, 2H, CH$_2$C**H**$_2$CH$_2$-C≡CH). **HRMS (MALDI, DCTB+):** m/z calcd. for $C_{80}H_{66}N_4O_{25}$ ([M+H]$^+$): 1483.4089; found: 1483.4134.

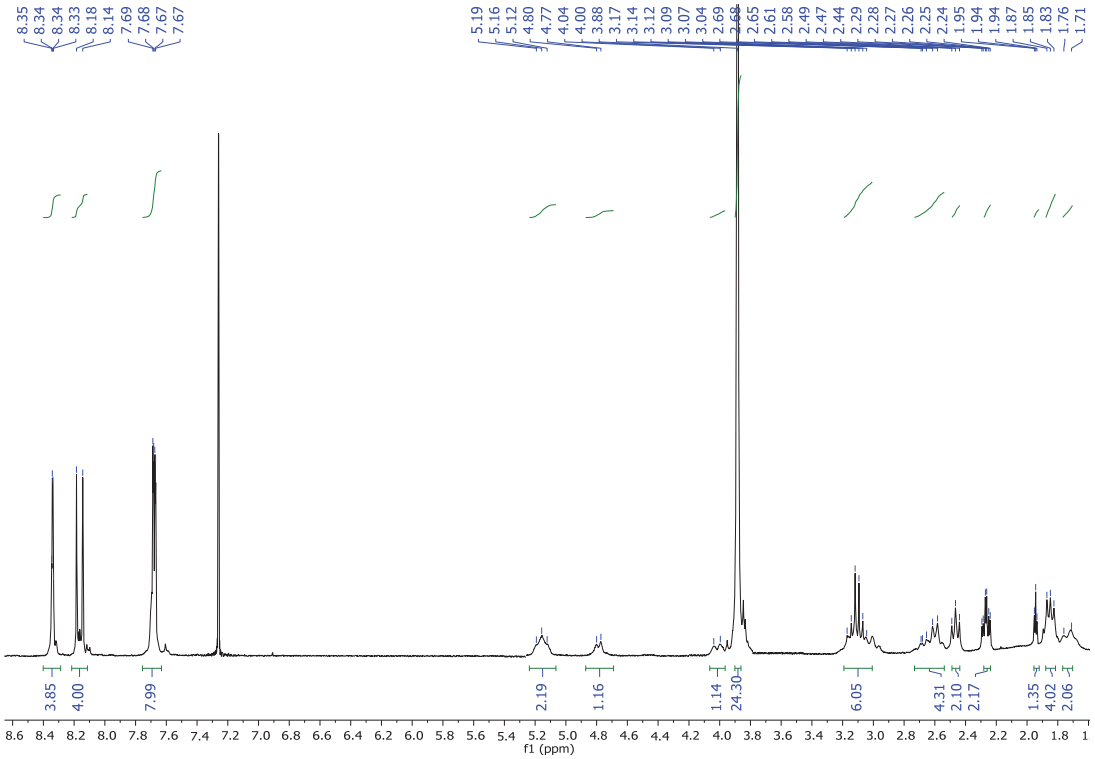

Figure 72. ^{1}H NMR (300 MHz, $CDCl_3$) of PC103

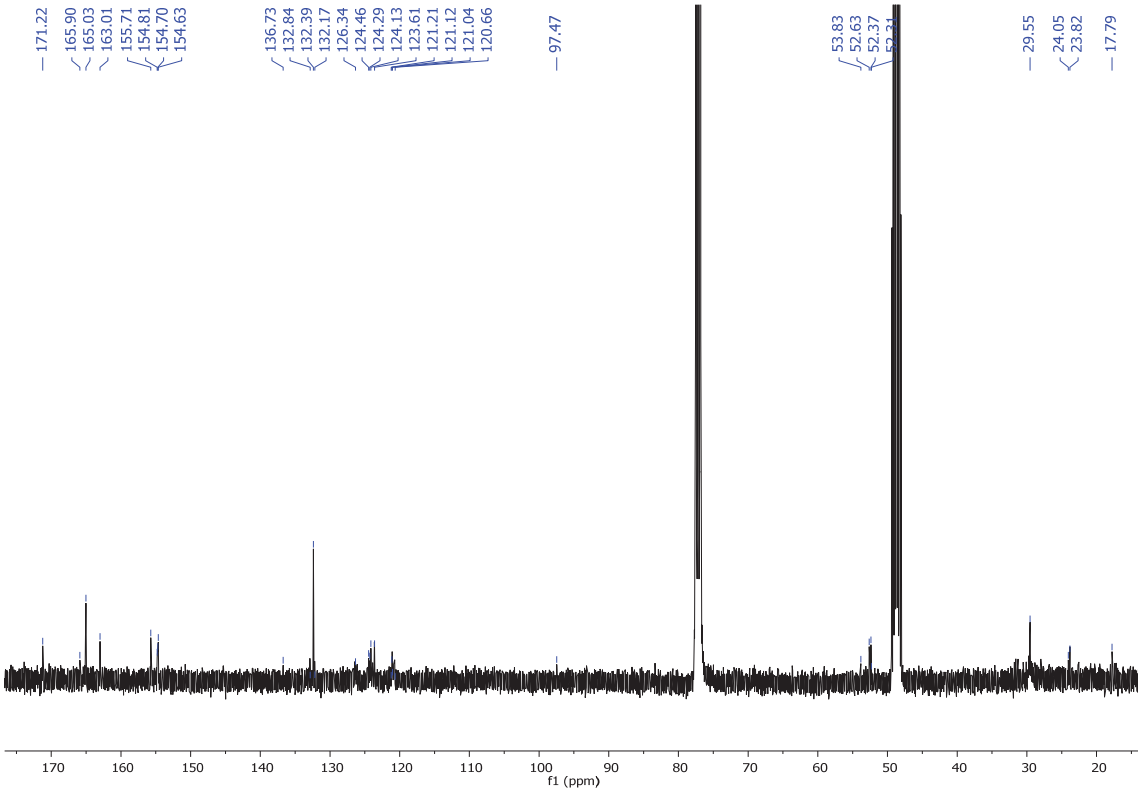

Figure 73. ^{13}C NMR (101 MHz, $CDCl_3$:MeOD) of PC103

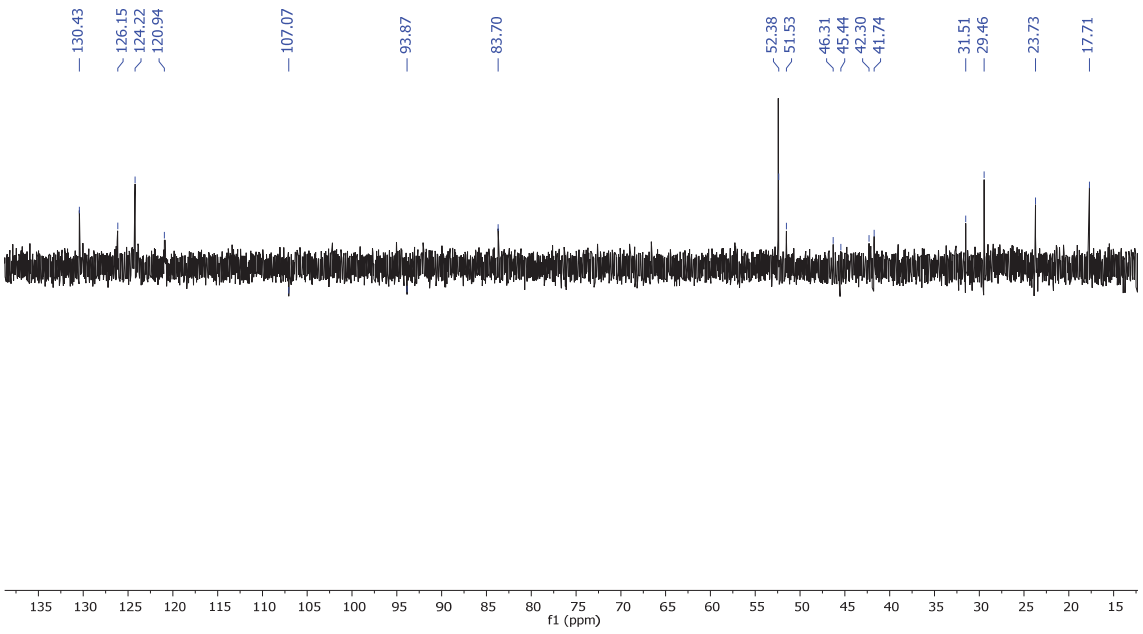

Figure 74. ^{13}C DEPT-135 NMR (101 MHz, $CDCl_3$:MeOD) of PC101

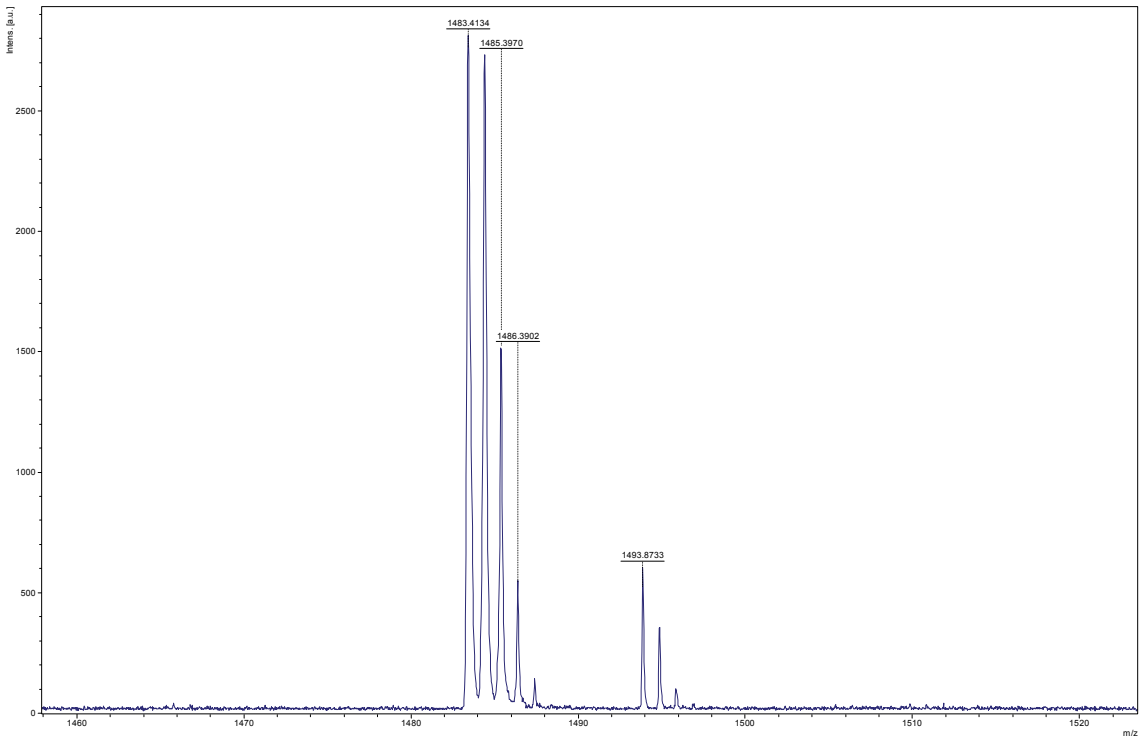

Figure 75. Mass spectrum (MALDI+, DCTB) of PC103

4.7. Synthesis of *N*-((1-piperidin-1-yl)-6-biotinamidohexan-1-one)-*N'*-((1-piperidin-1-yl)hex-5-yn-1-one)-1,6,7,12-tetrakis(3,5-bis(methoxycarbonyl)phenoxy)perylene-3,4,9,10-tetracarboxylic diimide (PC104).

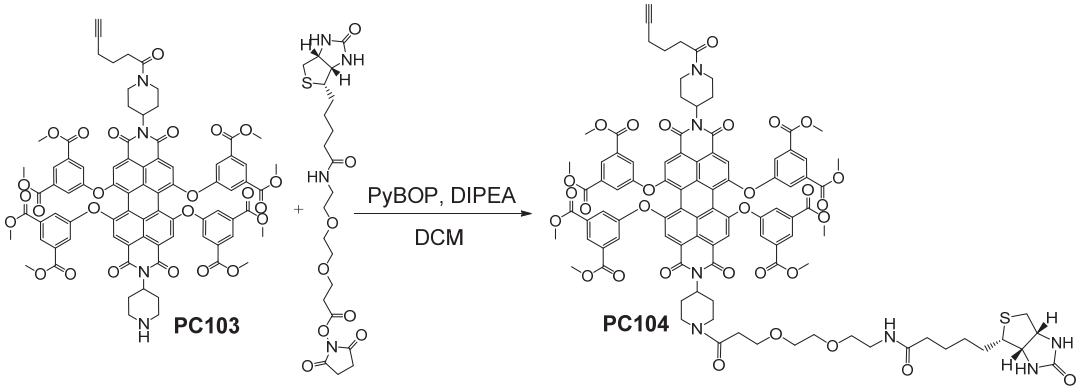

N-(1-piperidine)-*N'*-((1-piperidin-1-yl)hex-5-yn-1-one)-1,6,7,12-tetrakis(3,5-bis(methoxycarbonyl)phenoxy)perylene-3,4,9,10-tetracarboxylic diimide **PC103** (20 mg, 0.013 mmol) and PyBOP (6.8 mg 0.013 mmol) dissolved in DCM (4 mL) were added under nitrogen to *N*-succinimidyl 9-(biotinamido)-4,7-dioxanonanoate (6.5 mg, 0.013 mmol) and DIPEA (4.5 µL, 0.026 mmol) dissolved in DCM (0.7 mL). The purple-pink mixture was stirred at room temperature for 3 hours until the reactant disappears in TLC. The solvent was removed under reduced pressure and the residue was purified to flash chromatography (silica, DCM:MeOH) to obtain a deep pink solid in 54 % yield (13 mg, 0.012 mmol). **R_f (DCM:MeOH 50:2):** 0.8. **^{1}H NMR (400 MHz, $CDCl_3$) δ:** 8.34 – 8.33 (m, 4H, H_{Ar}), 8.15 (d, *J* = 3.1 Hz, 4H, H_{Ar}), 7.69 (t, *J* = 12.2 Hz, 8H, H_{Ar}), 6.82 (s, 0.5H, NHCO), 5.99 (s, 0.5H, NHCO), 5.21 – 5.10 (m, 2H, N-CH), 4.79 – 4.75 (m, 2H, CH_2), 4.48 – 4.45 (m, 1H, CHNHCO), 4.30 – 4.27 (m, 1H, CHNHCO), 4.03 – 3.97 (m, 2H, CH_2), 3.88 (s, 24H, $COOCH_3$), 3.67 (dt, *J* = 6.7 Hz and 3.4 Hz, 2H, CH_2S), 3.60 (s, 2H, CH_2S), 3.53 (t, *J* =

4.3 Hz, 2H, $CH_2NHCOCH_2$), 3.40 (s, 2H, $CH_2CON_{piperidine}$), 3.10 (tq, *J* = 7.4 Hz and 4.3 Hz, 4H, CH_2+$CONHCH_2$), 2.84 (d, *J* = 11.1 Hz, 1H, $SCHCH_2$), 2.72 – 2.54 (m, 9H, CH_2), 2.46 (t, *J* = 7.4 Hz, 2H, $CH_2CH_2CH_2$-C≡CH), 2.26 (td, *J* = 6.8 Hz and 2.7 Hz, 2H, $CH_2CH_2CH_2$-C≡CH), 2.21 (d, *J* = 7.8 Hz, 1H,), 1.94 (t, *J* = 2.6 Hz, 1H, -C≡CH), 1.85 (q, *J* = 7.2 Hz, 2H, CH_2), 1.75 – 1.68 (m, 4H, $CH_2CH_2CH_2$-C≡CH), 1.50 (d, *J* = 4.5 Hz, 6H, CH_2), 1.42 (d, *J* = 6.7 Hz, 4H, CH_2). **^{13}C NMR (101 MHz, $CDCl_3$:MeOD) *δ*:** 173.7 (2x**C**ONH), 170.6 (2x**C**$ON_{piperidine}$), 169.5, 165.1 (8x**C**$OOCH_3$), 163.7, 163.1 (2xN**C**=O), 155.9, 154.9, 133.1, 132.7, 126.6, 124.5, 123.9, 121.2, 121.2, 121.1, 121.1, 120.9, 120.9, 83.9, 70.3, 69.1, 67.3, 61.9, 60.4, 53.9, 53.6, 52.7, 52.0, 51.8, 45.6, 42.2, 41.9, 39.2, 35.8, 33.5, 31.7, 29.8, 25.6, 23.9, 17.8, 18.2, 18.6. **HRMS (MALDI, DCTB+):** m/z calcd. for $C_{97}H_{93}N_7O_{30}SNa$ ($[M]^+$): 1890.5580; found: 1890.5542.

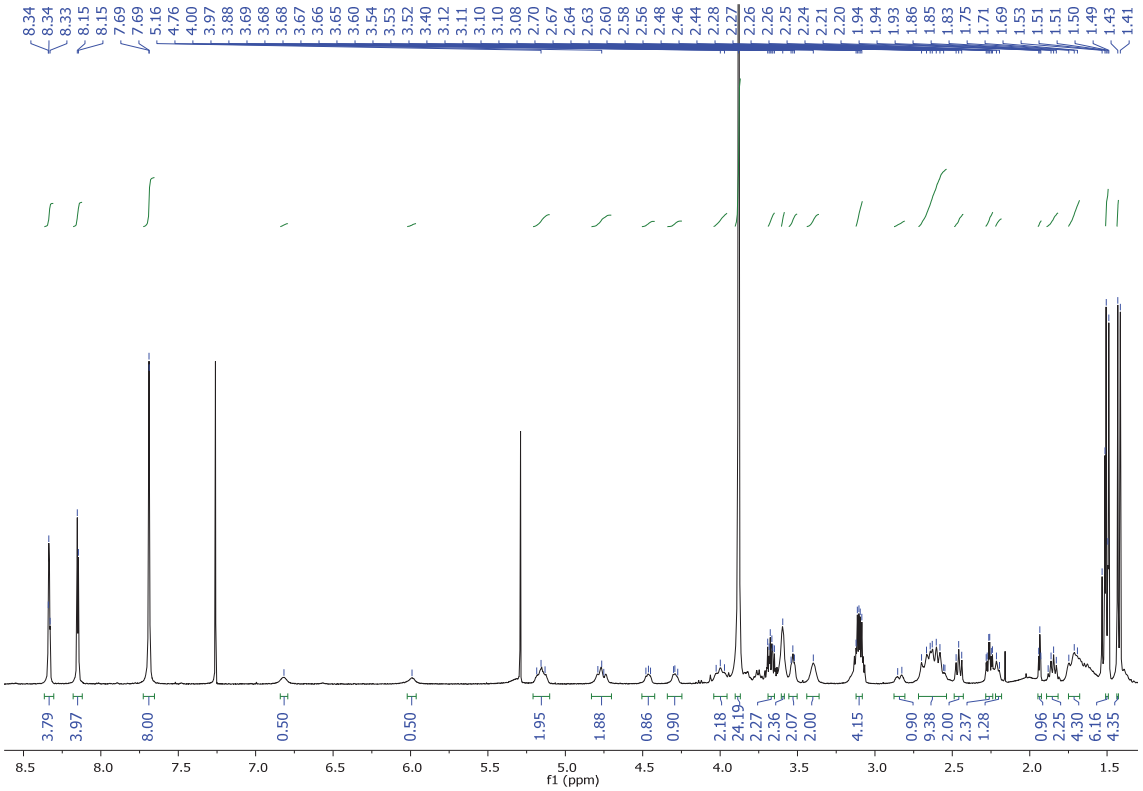

Figure 76. ^{1}H NMR (300 MHz, D_2O) of PC104

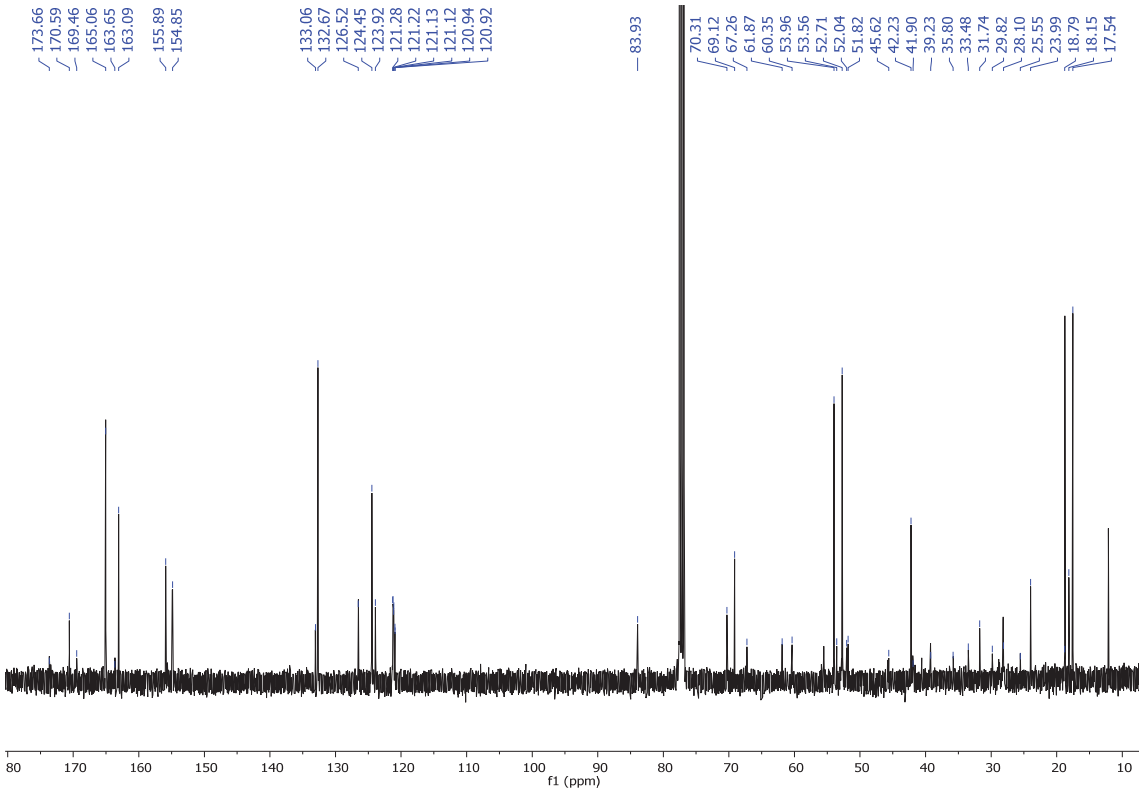

Figure 77. ^{13}C NMR (101 MHz, $CDCl_3$) of PC104

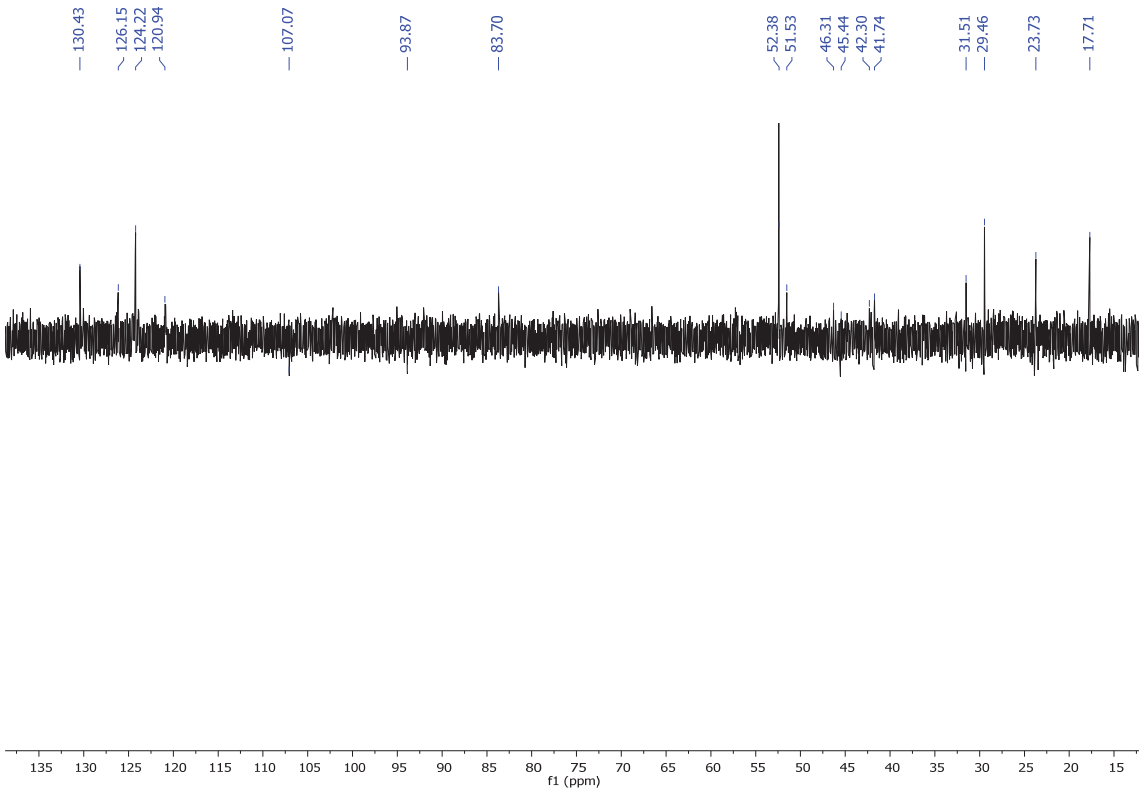

Figure 78. ^{13}C NMR-DEPT-135 (101 MHz, $CDCl_3$:MeOD) of PC104

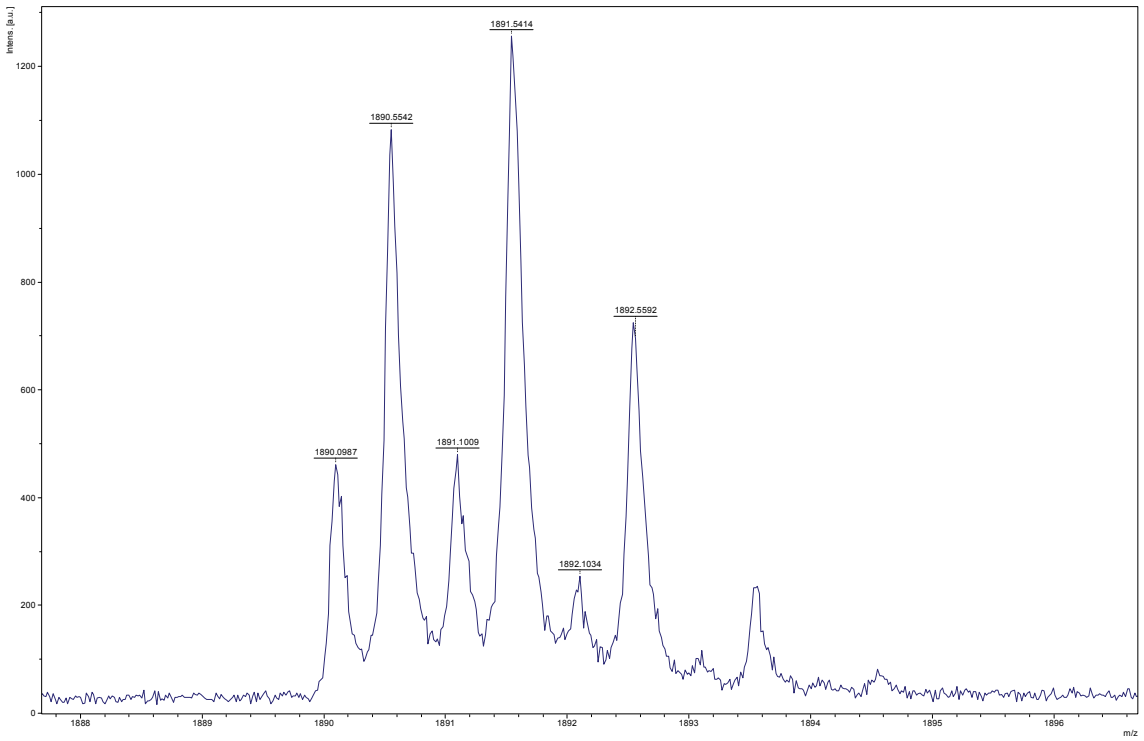

Figure 79. Mass spectrum (MALDI+, DCTB) of PC104

APPENDIX 1

1. Materials.

All materials and solvents were commercially available and used as received, unless otherwise indicated.

Multi walled carbon nanotubes were acquired from ALDRICH (carbon >98% (total metals impurities) prepared by chemical vapour deposition (CVD), diameter of the tube ranges between 6-13 nm and the average length 10 µm) and used as they were.

2. Apparatus.

Infrared spectra (FT-IR) were recorded with a JASCO FT/IR-4200 fitted with a JASCO "ATR PRO ONE" ATR. Transmission spectra were collected from pressed KBr pellets. The spectrum has been yielded at a resolution of 4 cm^{-1} and scan speed of 1 mm/s. All spectra represent an average of 500 scans.

Thermogravimetric analysis (TGA) data were recorded using a 4-6 mg sample under a nitrogen atmosphere on a TA Instrument Q50 TGA analyser at a scan rate of 10 °C min^{-1}.

Ultraviolet–visible (UV-Vis) and **fluorescence** spectra were recorded using a U-3900 Hitachi and F-7000 Hitachi Fluorescence spectrophotometer, respectively, in 1 cm UV quartz cuvette at 25 °C.

Scanning electron microscopy (SEM) images were obtained from the gold-sputtered membranes using a JEOL JSM-6460LV instrument with an Oxford Instruments INCA EDS (Energy-dispersive X-ray spectroscopy).

Transmission electron microscopy (TEM) was performed by dipping a holey carbon TEM grid into a colloidal suspension of the MWCNTs. Samples were imaged using two models: a) TEM JEOL JEM-FS2200 HRP) using Gatan Ultrascan camera of 2k x 2 with a range of accelerating voltage from 80 to 200 kV (UVA University) and b) TEM JEOL- model JEM 1011, images were collected using a Gatan digital camera of high resolution (IDIVAL institute); by the other hand the optical microscopy is a Nikon A1R confocal microscope and an Nikon Ti epifluorescence microscope designed to make time lapse.

Confocal. Confocal microscopy images were obtained using a NIKON A1R scanning confocal laser microscope equipped with TIRF module, laser lines 405 nm, 457 nm, 477 nm, 488 nm, 514 nm, 561 nm, 638 nm microscope. Images were processed with the NIS-Elements Advanced Research software.

NMR spectra were recorded in Varian Mercury-300 and Varian Unity Inova-400 machines, in $CDCl_3$, CD_3OD. Chemical shifts are reported in ppm with respect to residual solvent protons, coupling constants (JX-X ¢) are reported in Hz.

Elemental analyses of C, H and N were taken in a Leco CHNS 932.

Mass spectra were taken in a Micromass AutoSpec machine, by electronic impact at 70 eV.

Confocal Raman Microscope-Atomic Force Microscope (AFM) model Alpha300R – Alpha300A AFM Witec system with a power of 0.5 mW 532 nm He-Ne laser and magnification 10X (NA 0.25) and 785 nm Ti:Sapphire laser. Detailed scans from 500 to 3500 cm-1 were conducted on each MWCNT sample and the integration time and accumulation are 0.5 s and 10 respectively.

Ultrasonic bath Elma D-78224, singen/htw.

3. Methods.

The **quantum yield** and **several titrations** were recorded in Edinburgh Instruments FLS980.

Quantum yield. To measure as accurately as possible the fluorescence increase caused by TATP, the calculation of the quantum yield was measured. To do so in solids it is necessary to have a fluorometer provided with an integration sphere. The precision of this method is checking by repeating three times each sample obtaining an error always inferior to 2%.

Programme R. The limit of detection associated to the linear regression was calculated. In order to obtain a reliable limit, the values of false positive and false negative measurements were fixed as equal or inferior to 5%. The limit of detection calculated for TATP was 0.73 mg/mL ($3.3 \cdot 10^{-3}$ M) in a 5 μM solution of the **NZ29**, within 15 seconds after addition measurements.